Multi-component crystallisation routes to tuneable optical properties

Jones, Charlotte

Award date:
2016

Awarding institution:
University of Bath

Multi-component Crystallisation Routes to Tuneable Optical Properties

Charlotte Louise Jones

A thesis submitted for the degree of Doctor of Philosophy

University of Bath
Department of Chemistry

September 2015

Table of Contents

List of Figures

List of Tables

Acknowledgements

Chick and Lynne have to be the first two people that I thank. Chick, I am so grateful for the opportunity to do this PhD and to be able work in your group, and for all the fantastic opportunties that have come with it. Taking on this PhD is without a doubt one of the best decisions I have ever made. Lynne, I'm not entirely sure where to begin, because without your help and support along the way, I'm genuinely not sure where I'd be! For teaching me crystallography, the amazing ideas, the coffee and inevitable gossip, the pep talks, the scientific debates (typically lost by me) and the countless hours you have spent helping me - I will always be indebted to you.

Thank you to the Wilson and Raithby groups, past and present, for all the great times in and out of work (and for all the cake). I've thoroughly enjoyed working with everybody and have made some great friends. I have also been fortunate enough to have been involved in the Metastable Materials programme in Bath during my PhD, and some great ideas, support and collaborations have come through this involvement, so thank you to all of the M4 team.

During my PhD I have been lucky enough to have been able to carry out a number of experiments at Diamond Light Source, on Beamlines I19 and I11, and at the Advanced Light Source on Beamline 11.3.1, and I would like to thank all of the beamline scientists for their help in the studies. I must also thank my 'beamtime buddies' for making the often tough and sleep-deprived days and nights that much more bearable. Special thanks have to go to Lucy who has accompanied me on almost all of the experiments, for the singing (sorry, Lynne), the vending-machine trips, the midnight porridge and the organised napping.

Last, but definitely not least, thank you to my wonderful family for their endless support and encouragement over the years, and for always backing me in everything I've chosen to do; I am incredibly lucky. And to Richard - I'm probably not the easiest person to live with, but you've always been there to look after me and brighten my day with some awful jokes. The last six years have been the best and we have had some amazing adventures - here's to the next one!

Abstract

The application of multi-component crystallisation as a route to tuneable and switchable colour properties is investigated. Molecular complexes of haloanilines with nitro- and dinitro-substituted benzoic acid derivatives are presented, which enable determination of the crucial structural properties required for colour in these systems, in addition to demonstrating possible approaches to achieving tuneable and temperature-dependent colour. The findings offer a framework for future design and development of this class of functional materials.

Two possible mechanisms for thermochromism have been established in the series of molecular complexes. The first mechanism is disorder-facilitated structural rearrangement; molecular disorder prevails in many of the molecular complexes, due to competition between donor and acceptor sites, and inherently results in an inefficient crystal packing in the structures. In some of the molecular complexes, the increased crystal space surrounding the molecules facilitates a structural rearrangement, which is accompanied by a change in colour, and allows the phase transition to occur in a single-crystal to single-crystal manner. The thermochromic transition temperature is tuneable through modification of the haloaniline molecule, including the reversibility of the transition.

The second thermochromic mechanism is proton transfer, between the haloaniline and dinitrobenzoic acid components in metastable systems; the phase transition occurs with a distinct colour change but does not occur in a single-crystal to single-crystal manner. Similarly to the disorder-facilitated thermochromism, the transition temperature is tuneable through exchange of the halogen atom. One molecular complex combines the two thermochromic mechanisms, with the crystal space generated through disorder allowing proton transfer to occur with preservation of the single crystal. Proton transfer in the series of molecular complexes is key to the generation of both colour and switchable colour, with the transfer of a proton acting as a colour switch; a salt-cocrystal continuum region has been established for the series, based on ΔpKa values.

The colour in the solid-state is induced through formation of a mixed stack arrangement of aromatic electron-donor and electron-acceptor molecules, which themselves are colourless or pale-coloured. Where at least one of the molecular components is in their neutral form, colour prevails, ranging between red and yellow; a number of possible stoichiometries and stacking types of the donor and acceptor have been observed. Tuneable colour has been achieved through simple modifications of the molecular components, through exchange of the halogen substituent or introduction of a methyl group, for example.

Abbreviations

2-BrA	2-bromoaniline
2-ClA	2-chloroaniline
2-FA	2-fluoroaniline
2-IA	2-iodoaniline
2-IP	2-iodophenol
2-XA	2-haloaniline
2-Br-4-MA	2-bromo-4-methylaniline
2-Cl-4-MA	2-chloro-4-methylaniline
2-I-4-MA	2-iodo-4-methylaniline
2-X-4-MA	2-halo-4-methylaniline
2-NBA	2-nitrobenzoic acid
2,4-DNBA	2,4-dinitrobenzoic acid
2,5-DNBA	2,5-dinitrobenzoic acid
3-BrA	3-bromoaniline
3-IA	3-iodoaniline
3-XA	3-haloaniline
3,4-DNBA	3,4-dinitrobenzoic acid
3,5-DNBA	3,5-dinitrobenzoic acid
3,5-DNSA	3,5-dinitrosalicylic acid
4-BrA	4-bromoaniline
4-IA	4-iodoaniline
4-XA	4-haloaniline
4-Br-2-IA	4-bromo-2-iodoaniline
4-Br-2-MA	4-bromo-2-methylaniline
4-Br-3-MA	4-bromo-3-methylaniline
4-Cl-2-MA	4-chloro-2-methylaniline
4-I-2-MA	4-iodo-2-methylaniline
4-X-2-MA	4-halo-2-methylaniline
ADP	Anisotropic displacement parameter
CSD	Cambridge Structural Database
CT	Charge-transfer
DSC	Differential scanning calorimetry
HOMO	Highest occupied molecular orbital
HSM	Hot-stage microscopy
IR	Infrared
LUMO	Lowest occupied molecular orbital
NLO	Non-linear optical/optics
PXRD	Powder X-ray diffraction
SCSC	Single-crystal to single-crystal
SCXRD	Single crystal X-ray diffraction
UV	Ultraviolet

CHAPTER 1

Introduction

1 Introduction

1.1 Preamble

The work in this thesis describes a systematic investigation into the use of crystal engineering as a route to tuneable optical properties, with a focus on colour and temperature-dependent colour switching. Chapter 1 discusses the key concepts involved and provides background to previous work in related studies.

1.2 Crystal engineering

The field of 'crystal engineering',[1–3] a term first introduced by Schmidt in a 1971 paper concerning organic solid-state photochemistry,[4] is focused on the designed synthesis of functional solid-state materials, with the aim of controlling desirable physical and chemical properties. Crystal engineering has attracted attention across multiple scientific disciplines, with its principles having the potential to address a diverse range of structure-dependent properties; notable areas where impact has been made include pharmaceuticals,[5–7] non-linear optical (NLO) materials,[8,9] energetic materials,[10,11] and metal-organic frameworks (MOFs), which have potential applications in gas storage and catalysis.[12]

Central to crystal engineering are the interactions that direct the assembly of the molecules in the crystal. The two most commonly exploited interactions, which dictate much of the current research in the field, are hydrogen bonds and coordination bonds. The focus of the work presented herein is on organic molecular solids, which are composed of molecules held together by attractive forces of a range of strengths, from hydrogen bonds at the stronger end of the spectrum to van der Waals interactions at the weaker end. Intermolecular interactions are much weaker than the covalent bonds involved in the construction of the individual molecules, but have a substantial effect on the extended structure and properties of the solid materials. The ability to predict and design a crystal structure is the first step towards being able to fine tune properties, thus understanding the intermolecular interactions involved in the assembly of molecules, and the interplay between them, is crucial.[13–15]

Closely related to crystal engineering is the field of supramolecular chemistry, defined as "chemistry beyond the molecule".[16] Crystal engineering can be considered a solid-state form of supramolecular synthesis, and in this view, supramolecular synthons, which are structural units formed using known intermolecular associations, can be successfully utilised in the controlled design of extended solid-state architectures. Molecular self-assembly is central to crystal

engineering; hence for rational design of molecular solid-state structures, common synthons that are able to form specific and robust motifs are identified. The synthons can involve the same functional groups (homosynthons) or differing functional groups (heterosynthons) (Figure 1.1).[17]

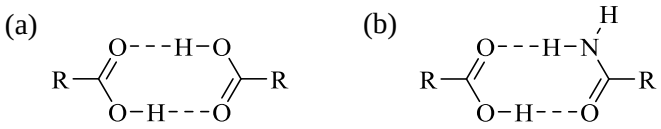

Figure 1.1 Two common supramolecular synthons used in crystal engineering: (a) acid-acid dimer (homosynthon); (b) acid-amide dimer (heterosynthon).

1.3 Intermolecular interactions

For the targeted design of functional organic crystals, it is necessary to understand the properties of the intermolecular interactions that form them. Of the crystal engineering tools available, hydrogen bonds[18–20] remain at the forefront due to their strength and directionality. However, a number of weaker intermolecular interactions, including halogen bonds[21–23] and π···π interactions,[24] are receiving increasing attention. Evidently, in order to predict and rationalise crystal structures, the combination of all of the different intermolecular interactions, and the competition between them, must be considered.[25–27]

1.3.1 Hydrogen bonding

The hydrogen bond is a key interaction across a vast range of scientific disciplines, and is vital to the structure and function of many important systems, with water and DNA being two of the most notable. Despite having been actively studied for around a century, hydrogen bonds remain a topic of keen interest in research, particularly with the rapid growth of crystal engineering over the last decade. The hydrogen bond is still the most important type of intermolecular interaction for molecular recognition; its directionality and strength have been exploited in numerous crystal engineering strategies, where molecules are commonly chosen for the compatibility of their hydrogen bond donor and acceptor sites.[20]

A hydrogen bond is a donor-acceptor interaction that specifically involves a hydrogen atom. According to the definition recommended by the IUPAC, "*the hydrogen bond is an attractive interaction between a hydrogen atom from a molecule or molecular fragment X-H in which X is more electronegative than H, and an atom or a group of atoms in the same or a different*

molecule, in which there is evidence of bond formation".[18] In this thesis, the donor group will be referred to as D-H and the acceptor as A, with the formation of a hydrogen bond depicted as D-H···A. In order for the donor, D-H, to interact with the acceptor, A, the acceptor must be electron rich and have lone pair electrons or polarisable π electrons. If the acceptor is on the same molecule as the donor, then an intramolecular hydrogen bond is formed, and if it is on a different molecule, this results in the formation of an intermolecular hydrogen bond.[18]

1.3.1.1 Classification of hydrogen bonds

Hydrogen bonding is a particularly complicated interaction to define, due to the wide range of bond strengths, geometries and types of donor and acceptor atoms that may be involved in such interactions.[28] The energies of hydrogen bonds range between values similar to those of covalent bonds and those of van der Waals forces, depending on the nature of the donor and acceptor atoms. A hydrogen bond can be classified according to a number of properties, with Jeffrey[19] making a well utilised classification of strong, moderate and weak (Table 1.1); however, it should be noted that while generally applicable, the boundaries are not strict and there are exceptions.[19]

Table 1.1 Classification of hydrogen bonds as strong, moderate and weak according to their properties.[19]

	Strong	**Moderate**	**Weak**
D-H···A interaction	Mostly covalent	Mostly electrostatic	Electrostatic
Bond lengths	D-H ≈ H···B	D-H < H···B	D-H << H···B
H···A (Å)	~ 1.2 - 1.5	~ 1.5 - 2.2	~ 2.2 - 3.2
D···A (Å)	2.2 - 2.5	2.5 - 3.2	3.2 - 4.0
Bond angles (°)	175 - 180	130 - 180	90 - 150
Bond energy (kcal mol^{-1})	14 - 40	4 - 15	< 4

Strong hydrogen bonds have short donor-acceptor distances (≤ 2.5 Å) and are typically close to linear; they may be considered to be quasi-covalent in nature, and consequently have been termed three-centre four-electron bonds.[29] Such bonds are formed when the donor atom has a deficiency of electron density (positively charged, resulting in a deshielding effect) or when the acceptor atom has an excess of electron density (negatively charged, increasing the interaction with the proton). Some examples include O-H···O$^-$ or N$^+$-H···N; when hydrogen bonds are formed between charged donor or acceptor groups, they are often termed charge-assisted or

ionic.[19,29,30] Strong hydrogen bonds may also occur when the donor and acceptor groups are necessarily close as a result of the molecular conformation.[19]

Moderate (or normal) hydrogen bonds are the most common class of hydrogen bond, with donor-acceptor distances of ~ 2.5 - 3.2 Å. They are generally formed between a neutral donor group and a neutral acceptor atom with a lone electron-pair; some common donor groups include $N^{+}(H_2)H$ and O-H, and common acceptor groups include C=O (e.g. carboxylic acids) and N=O (nitro groups).[19]

Weak hydrogen bonds are also relatively common and frequently play a role in crystal packing; they typically have donor-acceptor distances of ≥ 3.2 Å, and at the weakest end of the classification, the hydrogen bonds have energies similar to those of van der Waals interactions. They form when one or both of the donor and acceptor atoms have only moderate to low electronegativity, or the acceptor group has no lone pairs but has π-electrons.[19,31] Weak hydrogen bonds can be subdivided according to the strength of the donor and acceptor groups. The first division includes hydrogen bonds involving a weak donor and a strong acceptor, such as C-H···O and C-H···N, and this type of hydrogen bond has been most studied. The second division covers those hydrogen bonds involving a strong donor and a weak acceptor, for example O-H···π and O-H···C=C. The final division includes those hydrogen bonds that involve a weak donor and a weak acceptor, such as C-H···π.[31] Halogen atoms can also act as weak hydrogen bond acceptors i.e. D-H···X-C (where X = halogen), but the limit of hydrogen bond behaviour is being reached when considering interactions of this type, particularly for C-H···X-C interactions.[32]

While hydrogen bonds are most commonly simple two-centre interactions, involving just a single donor and acceptor (Figure 1.2, left), they can also be bifurcated. The term bifurcated has been used to describe two cases. In the first case, there are two simultaneous acceptor groups and a single donor group, and these can also be called three-centre hydrogen bonds (Figure 1.2, middle); the two H···A separations will often differ in magnitude, with one being the major component and one the minor component.[20,33] In the second case, there are two donor groups and a single acceptor group (Figure 1.2, right).[34]

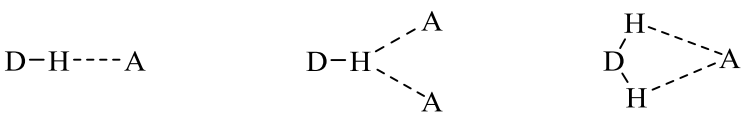

Figure 1.2 A two-centre hydrogen bond (left), a bifurcated hydrogen bond with a single donor group and two acceptor groups (middle) and a bifurcated hydrogen bond with two donor groups and a single acceptor group (right).

1.3.1.2 Potential energy surfaces and proton disorder

When a hydrogen bond, D-H···A is formed, the single well potential that describes the covalent D-H bond is accompanied by a second minimum, representing the H···A interaction; the resulting potential energy surfaces are normally represented as a function of the D-H distance (Figure 1.3). The usual situation is an asymmetric double-well potential (Figure 1.3, middle), where there is a significant energy difference between the two possible sites and the hydrogen atom resides on the donor atom. A symmetric double-well potential is also possible, where the energies of the two possible sites are very similar; in this case the hydrogen atom may reside on either the donor or the acceptor (Figure 1.3, right). In short strong hydrogen bonds or 'low-barrier' hydrogen bonds, the barrier is either very low or disappears; in a single-well potential there is no barrier and the hydrogen bond is symmetric (Figure 1.3, left).[19,35,36]

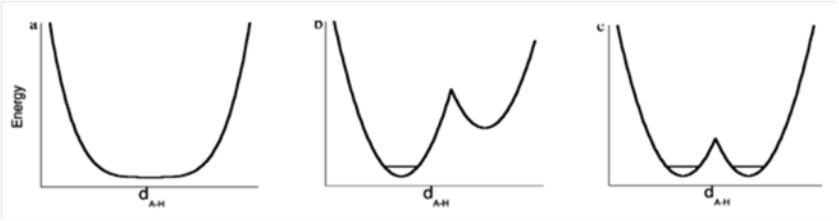

Figure 1.3 Potential energy surfaces for the motion of H-atoms in a hydrogen bond; single-well potential (left), asymmetric double-well potential (middle) and symmetric double-well potential (right). (Image taken from [35]).

In the case of the symmetric double-well potential, where the energies of the two sites are very similar or equivalent, the two sites may both be partially occupied, resulting in proton disorder which may be static or dynamic.[36] Proton disorder is frequently observed in benzoic acid dimers, where there are two possible dimer configurations due to the similarity in the energies of the two sites. Proton disorder is typically studied using neutron diffraction,[37,38] which allows the hydrogen atom positions to be elucidated with accuracy, but it has also been successfully studied using X-ray diffraction.[39] In the dimers where proton disorder has been observed, the disorder frequently has a temperature dependency;[38,39] at low temperature, the H-atom typically orders into a single configuration, but as the temperature is increased the relative occupancies of the two sites become more equally populated. This is also reflected in the C-O and C=O bond lengths of the carboxylic acid group, with the two bond lengths becoming closer to equal as the occupancies do.[37,38] The local crystalline environment around the dimer is known to affect the potential energy surface of the hydrogen bond; if the environment is more asymmetric then there is a greater asymmetry of the hydrogen bond, and the onset temperature of the population of the second site is higher. This has been demonstrated in combined neutron and X-ray diffraction studies on 3,5-dinitrobenzoic acid dimers.[39]

1.3.1.3 Hydrogen bond patterns in the solid-state

From a crystal engineering perspective, being able to predict which hydrogen bonds may form is key to the design strategy, especially in the design of multi-component crystals (§1.4). A set of rules proposed by Etter[40] allow many hydrogen bonding patterns to be predicted and rationalised:

1. All good proton donors and acceptors are used in hydrogen bonding.
2. Six-membered-ring intramolecular hydrogen bonds form in preference to intermolecular hydrogen bonds.
3. The best proton donors and acceptors remaining after intramolecular hydrogen bond formation form intermolecular hydrogen bonds to one another.

As a means of systematically defining hydrogen bonding patterns, Etter developed graph-set notation.[40] The graph-set symbol is assigned according to the motif generated by the intermolecular hydrogen bonding, which may be C (chain), R (ring) or D (dimer, or other finite set); intramolecular hydrogen bonds are denoted S. The notation also includes the number of donors (d) and acceptors (a) in the motif (assigned as subscripts and superscripts, respectively), and the number of atoms in the repeat motif. A benzoic acid dimer (Figure 1.1 (a)) is thus described using the graph-set notation $R_2^2(8)$; the 'R' refers to the formation of the hydrogen bonded ring motif, the subscript and superscript '2' refer to the number of hydrogen bond donor and acceptor groups, respectively, and the '(8)' refers to the number of atoms involved in the hydrogen bonded ring.

1.3.2 Halogen bonding

The halogen bond is emerging as a powerful and highly-directional non-covalent interaction; as a class of interaction they parallel hydrogen bonds closely in many ways,[41,42] which is reflected in the similarity of the IUPAC definition, "*a halogen bond occurs when there is evidence of a net attractive interaction between an electrophilic region associated with a halogen atom in a molecular entity and a nucleophilic region in another, or the same, molecular entity*".[43] Similarly to the hydrogen bond, a halogen bond can be denoted D-X···A, where the covalently bound D-X is the halogen bond donor group and A is the halogen bond acceptor. X is any halogen atom with an electron-poor region, which can be part of a dihalogen or a substituent on another molecule, and A is typically a molecular entity that has at least one electron-rich region. Some common donor moieties include dihalogen molecules, haloarenes, and haloalkanes, with some common acceptors being lone-pair possessing atoms such as N (e.g. in pyridine) or O (e.g. carbonyl group), or a π-system, such as an arene moiety. Halogen atoms may also form

halogen···halogen interactions. A halogen bond can be characterised by an interatomic distance X···A of less than the sum of the van der Waals radii of the two atoms.[21,43]

Covalently-bonded halogen atoms are usually viewed as being negative in character, so the existence of halogen bonding may seem counterintuitive since a halogen atom would not be expected to interact with an electron-rich region. The nature of the halogen bond has been a subject of many theoretical and experimental studies; it is generally considered to be a largely electrostatically-driven interaction, but the bonding contributions of polarisation, charge-transfer and dispersion all play a role.[44–48] One useful rationale for the existence of halogen bonding is based on the concept of the 'σ-hole',[45] which is valuable for the understanding of halogen bonds. Quantum mechanical calculations have shown that the charge distribution around a covalently-bonded halogen atom is anisotropic, and exhibits a positive region of electrostatic potential along the extension of the D-X bond (typically C-X), which has been denoted the 'σ-hole'. A computational study was conducted on CF_3X to show the effect of the halogen-substituent;[45] when X = F, each of the halogen surfaces has a negative potential, due to the high electronegativity of fluorine. When one fluorine atom was substituted for another halogen (X = Cl, Br and I), this resulted in a region of positive potential which increases in size as the halogen atom does (Figure 1.4). These positive regions, which result from an anisotropic distribution of charge, can interact favourably with a negative region on an acceptor molecule, giving rise to the halogen bond.

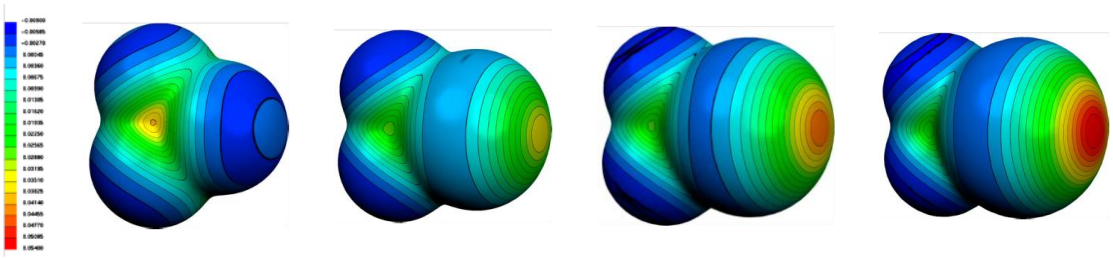

Figure 1.4 The molecular electrostatic potential, in Hartrees, at the 0.001 electrons $Bohr^{-3}$ isodensity surface of CF_3X, where X = F, Cl, Br, I (from left to right). Blue regions indicate electron-rich regions, and the red region indicates the positive region of the σ-hole. (Images taken from [45]).

More recently, halogen bonding has received increasing interest in the field of crystal engineering, and in the design of functional materials, as a result of their strength, directionality and tunability.[49–52] Both halogen···heteroatom and halogen···halogen interactions are utilised. For the former, where the acceptor is a Lewis base such as N or O, the interaction is often close to linear with the D-X bond (i.e. the D-X···A angle is close to 180°).[43] For the latter, studies have shown that there are two preferred geometries for the interaction, which can be designated type I and type II. Type I contacts occur when $\theta_1 = \theta_2$, where θ_1 is the D-X_1···X_2 angle and θ_2 is

the $X_1 \cdots X_2$-D angle (Figure 1.5, left); type II contacts have a perpendicular arrangement and arise when $\theta_1 = \sim 180°$ and $\theta_2 = \sim 90°$ (Figure 1.5, right).[53]

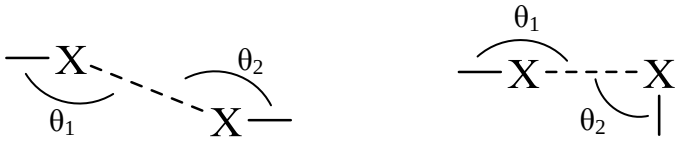

Figure 1.5 The geometry of type I (left) and type II (right) halogen···halogen interactions.

The type II contacts are electrostatic in nature, involving the approach of an electrophilic region of one halogen atom and the nucleophilic region of the second halogen atom, which agrees with the formal definition of a halogen bond. However, the type I contacts are not of the same character and are not halogen bonds, since at the point of interaction, the electrostatic potentials are equivalent. The interaction is considered to be van der Waals in nature, with the arrangement tending to minimise repulsion by interfacing the neutral regions of the two halogen atoms.[54,55] However, a study by Awwadi *et al.*[56] suggests that when the angle is in the range $140° < \theta_1 = \theta_2 < 160°$, the type I interaction (in this case C-X···X-C) is electrostatically attractive in nature; there is an energy minimum in this angle range, where the positive region of the halogen and a negative electrostatic potential ring of the other halogen are interfacing.

The strength of halogen bonds can vary in the range 10 - 200 $kJmol^{-1}$ making them comparable to a range of hydrogen bonds, and they are also highly directional as a consequence of the σ-hole;[57] however, due to the size of a halogen compared to a hydrogen atom, they can be more sensitive to steric hindrance than hydrogen bonds.[58] The strength of a halogen bond is related to the size of the σ-hole; the greater the polarisability of the halogen atom and the lower the electronegativity, the more positive the σ-hole. A more positive σ-hole results in the formation of a stronger halogen bond, thus halogen bond strength increases in the order $F << Cl < Br < I$.[21,57] Since fluorine is the least polarisable and the most electronegative of the halogen atoms, it is the least likely to function as a halogen bond donor; it may possess a σ-hole only in some cases, including F_2 or when the fluorine is bound to a suitably strong electron-withdrawing moiety.[59]

The strength of halogen bonds can be fine-tuned, and this tunability makes them valuable to crystal engineering. The size and charge of the σ-hole can be readily modulated through exchange of the halogen atom or through variation of the motif to which the halogen atom is bound. For example, halogen bonds involving aryl halides are typically quite weak (with X···A distances close to the sum of the van der Waals radii), but an electron-withdrawing group or positive charge on the aromatic ring can increase the halogen bond strength.[60,61]

1.3.3 π···π interactions

Another class of non-covalent interactions are aromatic···aromatic interactions, or π···π interactions, which are attractive interactions between aromatic π-systems. The term 'π···π interaction' is typically used to describe stacks of aromatic moieties that are approximately parallel and separated by ~ 3.3 - 3.8 Å.[62] There are several distinguishable arrangements that pairs of aromatic moieties can adopt, including parallel face-to-face, parallel offset, and edge-to-face (T-shaped) (Figure 1.6).[62–64] The T-shaped arrangement involves a C-H···π interaction.

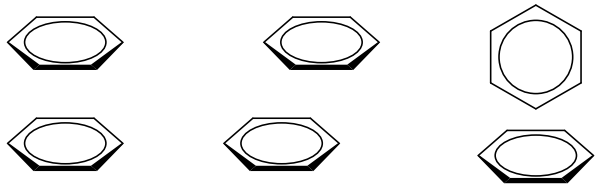

Figure 1.6 Possible geometries for aromatic···aromatic interactions, from left to right: parallel face-to-face, parallel offset, and edge-to-face (T-shaped).

In 1990, Hunter and Sanders proposed an electrostatic model for aromatic interactions,[24] based on the charge distribution in a π-system; the aromatic ring (i.e. benzene) is described as a positively-charged σ-framework sandwiched between two negatively-charged regions of electron density (Figure 1.7). The model is widely accepted and its associated rules can predict the geometries adopted by various aromatic molecules in the solid-state. In terms of the possible geometries and interactions, three rules state: (1) π-π repulsion dominates in a face-to-face π-stacked geometry; (2) π-σ attraction dominates in an edge-on or T-shaped geometry; (3) π-σ attraction dominates in an offset π-stacked geometry. The offset geometry minimises π-electron repulsion and maximises π-σ attraction.[24,63]

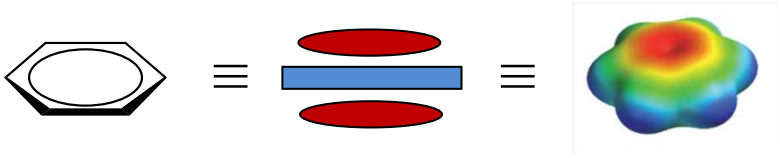

Figure 1.7 Representation of the charge distribution in benzene, where a positively-charged σ-framework is sandwiched between two negatively-charged regions of electron density. (Image on right taken from [64]).

However, the stacking interactions between aromatic molecules can be strongly influenced by ring substituents or ring heteroatoms which vary the π-polarisation. The addition of an electron-donating group (e.g. NH_2) to one of the molecules in the pair increases the electron density associated with the ring and increases the repulsion, whereas an electron-withdrawing group

(e.g. NO_2) has the opposite effect. If one aromatic molecule has an electron-donating group (and is therefore electron-rich) and one has an electron withdrawing group (and is therefore electron-deficient), then the unlike polarisations attract; this situation makes face-to-face stacking more favourable and may give rise to charge-transfer.[24,63,64]

There has been some debate over the use of the term π···π interaction and it is not particularly well-defined.[64,65] It has been suggested that the interactions between electron-rich (donor) and electron-deficient (acceptor) aromatic molecules may be better described as aromatic donor···acceptor interactions, but they are also often referred to as charge-transfer (CT) or electron-donor-acceptor (EDA) interactions.[64] This widely exploited interaction is discussed in more detail in the context of organic mixed stack charge-transfer complexes in §1.5.

1.3.4 Bond hierarchy

Establishing a hierarchy of intermolecular interactions, of the same type or different, is critical for successful crystal engineering design. Interactions are typically ranked according to their varying strengths, and the ranking of hydrogen bond interactions has been the focus of many co-crystallisation studies.[40,66,67] The hydrogen bond patterns in crystal structures can typically be rationalised based on the complementarity and varying strengths of the hydrogen bond donors and acceptors, such that the best hydrogen bond donor seeks out the best hydrogen bond acceptor (§1.3.1.3);[40] this is based primarily on electrostatics, where potential maxima and minima correspond to donor and acceptor sites, respectively.[68] Similar work has also been carried out to investigate the hierarchy in halogen bonding, which is also based on electrostatics.[69,70] Halogen bonds can be ranked according to the positive electrostatic potential of the σ-hole, which increases in the order F << Cl < Br < I and their strength can also be increased by the presence of electron-withdrawing groups on the donor molecule (§1.3.2). The studies in this area suggest that the 'best-donor best-acceptor' rule of hydrogen bonding is also generally applicable to halogen bonding.

In systems involving only one type of interaction, establishing a hierarchy can be relatively straightforward; however, when considering a combination of interactions, there is the potential for competition to arise. More recently, there have been a number of contributions investigating the competition between hydrogen and halogen bonds,[26,71,72] which can often have comparable strength and play similar roles in solid-state assembly. The competition between the two types of interaction is clearly dependent on the sets of molecular components being investigated; in addition, the fact that hydrogen and halogen bonds exhibit similar behaviour means that a large amount of data would be required to establish an exact relationship. In a multi-component

crystallisation study (§1.4), Aakeröy *et al.*[71] looked at the structure-directing balance between hydrogen bonds and halogen bonds using a set of bi-functional donor molecules equipped with one hydrogen bond donor and one halogen bond donor, including 4-iodotetrafluorobenzoic acid, 4-bromotetrafluorobenzoic acid, 4-iodotetrafluorophenol, 4-bromotetrafluorophenol, 4-iodotetrafluoroaldoxime and 4-bromotetrafluoroaldoxime. These molecules were co-crystallised with 3,3'- and 4,4'-azobipyridine; the study focused on the competition between the hydrogen bond and halogen bond donors for the pyridine N-atoms, and postulated the outcomes shown in Figure 1.8.

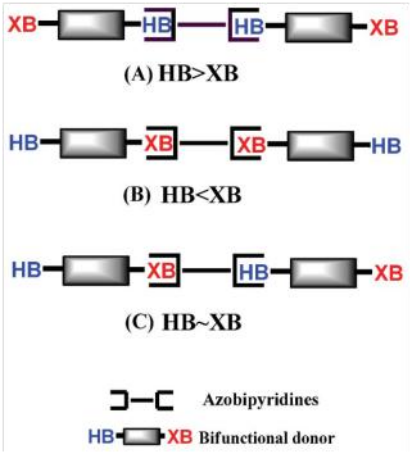

Figure 1.8 Postulated outcomes for the interactions between the donor and acceptor molecules. (Image taken from [71]).

It was established that the orientation of the binding site was highly influential; in the 3,3'-azopyridine co-crystals, hydrogen bonding was the driving force, whereas in the 4,4'-azobipyridine co-crystals, the hydrogen and halogen bonds contribute more or less equally in the assembly. It was also found that iodine functions as a better halogen bond donor than bromine, and that there was no distinction between the three hydrogen bond donor types in terms of binding in the presence of halogens. It was acknowledged that further work is necessary in order to understand the precise reasons for the observed patterns of behaviour.[71]

1.4 Multi-component crystallisation

One of the approaches used in crystal engineering is multi-component crystallisation (or co-crystallisation), which targets the formation of crystalline solids containing two or more molecular species;[3] in some cases the method is also used to achieve a desired solid form of a single component, known as templating.[73] The incorporation of a second component (co-former)

into the crystallisation will alter the crystal packing, thus providing a route to modifying or improving the properties of a solid compared to the individual parent molecule.

Multi-component crystals encompass a range of solids, including: those formed of neutral molecular components, ionic molecular components, solvates and hydrates (Figure 1.9); multi-component crystals with various stoichiometries of the components, or mixed neutral and ionic species, are possible. There is considerable debate about the nomenclature used to describe multi-component crystals, specifically regarding the definition and use of the term ‘co-crystal' (or 'cocrystal').[74–77] However, 'co-crystal' is typically used in relation to a multi-component solid in which the molecular components are neutral (in the absence of proton transfer), while 'salt' describes a multi-component solid in which the molecular components are ionic (where proton transfer is complete).[77–79] This is complicated further in pharmaceutical applications, where both components are required to be solids at room temperature to be termed 'co-crystal'.[7] In this work, the general terms 'neutral molecular complex' and 'ionic molecular complex' will be used to differentiate between the protonation states of the molecular components in the final crystal, with 'solvate' referring to those molecular complexes which incorporate a solvent molecule. Molecular complexes with mixed ionisation states are also reported, where neutral and ionic molecules co-exist.

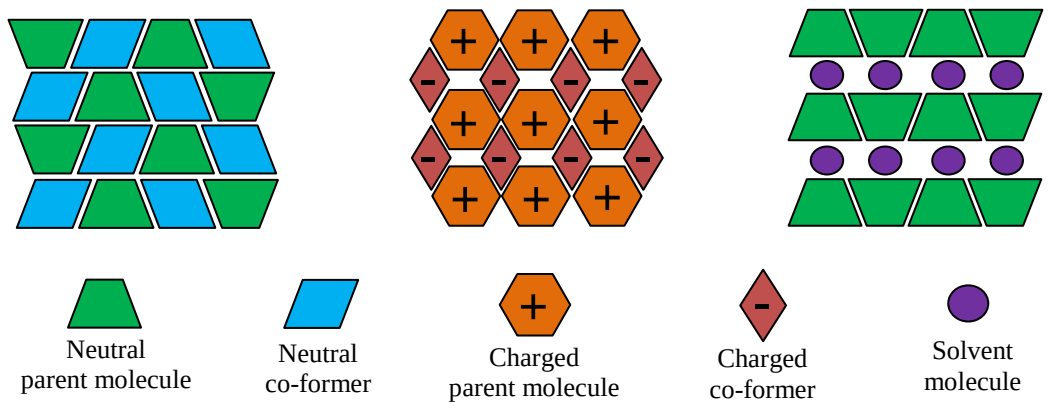

Figure 1.9 Schematic representations of possible multi-component crystal forms, including a neutral molecular complex (left), ionic molecular complex (middle) and solvate (right).

The driving force in the assembly of a multi-component crystal is the formation of intermolecular interactions between the components, using the concept of synthons to assemble the molecules in the solid-state. Some functional group combinations are particularly favoured in multi-component crystallisation studies, due to the preference to interact with each other rather than themselves, increasing the likelihood of forming a multi-component crystal;[80] for example, carboxylic acid functionalised molecules with suitable N-containing heterocycles

e.g. pyridine, are well known due to the robust and reliable nature of the synthon formed through hydrogen bonding.[74] The hydrogen bond has been utilised successfully in the design and formation of numerous multi-component crystals.[81–83]

The design of systems of higher complexity, for example those combining more than one type of non-covalent interaction, requires careful consideration of the relative strengths of the various intermolecular interactions. Aakeroy *et al.*[84] demonstrated how strong directional hydrogen and halogen bonds could be combined in a reliable strategy for the assembly of a 1:2 multi-component crystal of tetrafluorodiiodobenzene and *iso*-nicotinamide (Figure 1.10). N···I halogen bonds form between tetrafluorodiiodobenzene and *iso*-nicotinamide molecules, with hydrogen bonds between self-complementary *iso*-nicotinamide molecules, resulting in a 1D chain. The chains link *via* hydrogen bonds between amide dimers, resulting in a 1D ladder similar to that observed in a number of hydrogen bonded *iso*-nicotinamide carboxylic acid co-crystals.[85]

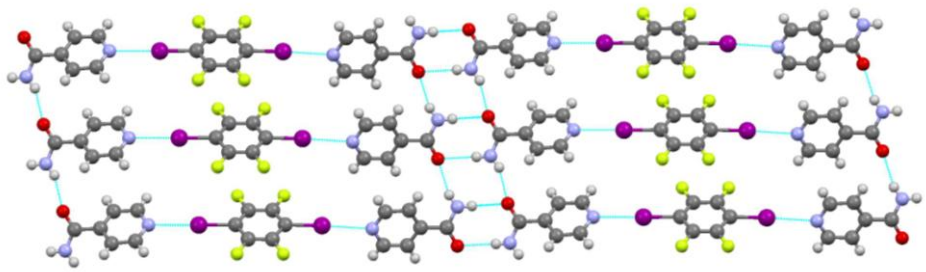

Figure 1.10 1D chains formed in the 1:2 multi-component crystal of tetrafluorodiiodobenzene and *iso*-nicotinamide (CSD[86] refcode: YIPCIK).[25]

The use of multi-component crystallisation in the field of crystal engineering has expanded rapidly in recent years, particularly due to its wide use and relevance in pharmaceutical research. The method of multi-component crystallisation has been used to form complexes, in either salt or co-crystal form, as a means of increasing the value of an API, by improving properties such as solubility and stability, without compromising the pharmaceutical activity.[6,7,87–89] The method has also been utilised for other applications, such as in the production of agrochemicals, where the aim is often to lower the solubility of the active ingredient to enable a more stable formulation so the active ingredient is not washed away too quickly.[90,91] It has also been employed in the design of energetic materials, for example to improve stability without compromising explosive power,[10,11,92,93] and in the development of organic ferroelectric materials.[94,95]

1.4.1 Proton transfer and the ΔpKa rule

An additional factor to consider in the design strategy for a multi-component complex is the likelihood of proton transfer occurring between the molecular components. Proton transfer is one of the simplest chemical reactions, forming the basis of acid-base chemistry, and involves the transfer of a hydrogen atom from one binding site to another, either within the same molecule (intramolecular) or between two molecular species (intermolecular).[19]

In the co-crystallisation of an acid-base system, there are two main possibilities: the molecular components will crystallise in their neutral forms (co-crystal) or in their ionic forms (salt), with the distinction between the two based on whether a proton has been transferred from the acid to the base. The two types of complex are situated at either end of a continuum, with proton transfer either absent or complete. However, there are also examples of systems with mixed protonation states, where neutral and ionic components co-exist, [79,96–98] or systems displaying proton disorder.[79] In some solid-state molecular complexes, dynamic proton transfer processes are known to occur, typically across hydrogen bonds; this may be in response to an external stimulus, such as temperature[99] or an electric field,[100] thus the location of the proton is dependent upon the external environment.

The difference in the pK_a values of the acid and base components is commonly used as a guide to determine whether a neutral or ionic molecular complex is likely to form. While strictly applicable to the solution state, a ΔpKa rule has been applied successfully in the prediction of proton transfer in multi-component solids,[83,101] but it should be treated as a guide and not as a fixed rule.[102] One general and commonly used rule is that proton transfer will occur if the difference in the pKa values (ΔpKa, where ΔpKa = pKa(base) - pKa(acid)) is greater than or equal to 3.[79] If the ΔpKa is less than or equal to zero, then a neutral molecular complex can be expected. However, there exists a significant intermediate region of uncertainty between 0 and 3 (the salt-cocrystal continuum),[79] in which it is difficult to predict whether proton transfer will occur. The crystallisation may result in a neutral or ionic molecular complex, or systems with mixed protonation states or proton disorder. For those molecular complexes that fall in the continuum, the location of the proton, and the extent of proton transfer, may be ambiguous.[79]

In some multi-component complexes the structural difference between a neutral or ionic form is often only in the location of the proton in the hydrogen bond. For example, in the case of the acid-pyridine synthon, the hydrogen bonds O-H···N and $O^-\cdots H\text{-}N^+$ would be expected for neutral and ionic molecular complexes, respectively (Figure 1.11); similar crystal structures

may be expected, and distinguishing between the neutral and ionic forms would be dependent on the ability to locate the proton.[103]

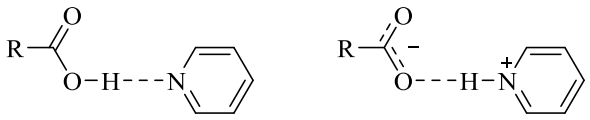

Figure 1.11 Location of the proton in a neutral acid-pyridine complex (left) and an ionic acid-pyridine complex (right).

However, the position of a proton can impact significantly on the intermolecular interactions that are formed in the structure; in addition, the occurrence of proton transfer has been shown in some cases to result in molecular complexes with an unexpected stoichiometric ratio of the molecular components, or solvates,[78,104] through a requirement to balance the number of hydrogen bond donors and acceptors. In ionic molecular complexes, the crystal packing is typically governed by the charge-assisted intermolecular interactions between the ions, whereas in a neutral molecular complex the interactions between the molecular components will generally be weaker in nature. The differences in the intermolecular interactions, and consequently the crystal packing, will alter the properties of the molecular complex.[13,78]

1.5 Organic mixed stack molecular complexes

The majority of organic multi-component crystals are assembled using hydrogen and halogen bonds; however, mixed stack crystalline complexes, formed *via* interactions between alternating π-donor and π-acceptor molecules, are also considered to be multi-component crystals. These molecular complexes may often be referred to as charge-transfer (CT) or electron-donor-acceptor (EDA) complexes, and have been reviewed in detail by Herbstein.[105] The driving force in the assembly of a mixed stack complex is the charge-transfer interaction between suitable electron-rich donor (D) and electron-poor acceptor (A) molecules, which are inherently complementary in nature (§1.3.3). The alternate stacking results in an association and partial overlap of the π-orbitals of the donor and acceptor molecules; an electron can be excited from the HOMO π-orbital of the donor molecule to the LUMO π-orbital of the acceptor molecule (π-π*). Charge-transfer complexes are often associated with the appearance of a new absorption band in the visible region and can therefore be strongly coloured, despite the individual components being colourless. This arises as a result of the electronic excitation between the donor and acceptor molecules, with the HOMO-LUMO energy gap between the donor and acceptor smaller than on either of the individual molecules.[64,106–108]

Charge-transfer from the donor to acceptor gives the composition $D^{Z+}A^{Z-}$, where $0 \leq Z \leq 1$. The degree of charge-transfer depends on the nature of the donor and acceptor molecules, with the difference between their energy levels and their organisation in the crystal determining the electronic properties of the complex. There are numerous types of π-donor and π-acceptor; theory suggests that a good donor has a low ionisation potential and a good acceptor has a high electron affinity, and they should also be planar in nature in order to maximise the interaction and the electron transfer.[105,108] Benzene derivatives with electron-donating groups (e.g. CH_3, NMe_2) are common π-donors and those with electron-withdrawing groups (e.g. CN, NO_2) are common π-acceptors; some representative examples are shown in Figure 1.12.

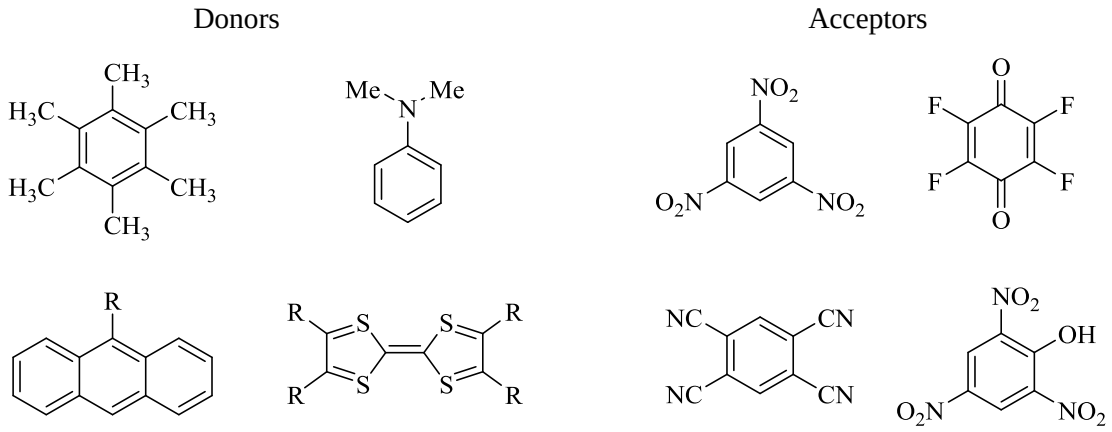

Figure 1.12 Typical π-donor and π-acceptor molecules.[109]

The majority of mixed stack donor···acceptor crystals have a 1:1 stoichiometric ratio of the donor and acceptor, although other stoichiometries, such as 2:1 and 1:2, are known, but less common. The intermolecular separation along the stack is typically 0.1 - 0.2 Å less than the "thickness" of the components (which is often around ~3.5 Å).[105] The molecular complex of anthracene and picric acid was one of the first to be prepared, and crystallises as red needles with a 1:1 ratio of the two components (Figure 1.13 (a));[110] another relatively early example, which provided the first direct evidence for a non-covalent interaction in this class of complexes, is the 1:1 molecular complex of 4-iodoaniline trinitrobenzene (Figure 1.13 (b)).[111]

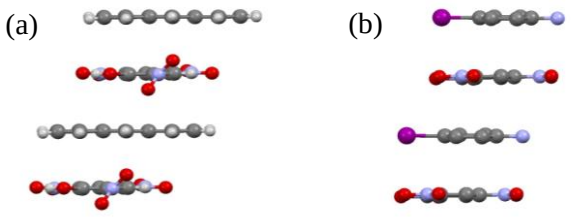

Figure 1.13 Mixed donor···acceptor stacks in the CT complexes of (a) anthracene picric acid (CSD[86] refcode: ANTPIC[110]) and (b) 4-iodoaniline trinitrobenzene (CSD[86] refcode: IANNOB[111]).

More recently, the formation of mixed stack complexes has been utilised in a number of crystal engineering studies;[112–114] this is particularly due to the realisation of the technologically-relevant properties of mixed stack charge-transfer crystals,[108] for example ferroelectricity.[95,115] There are also a few examples focused on tuning the colour of charge-transfer crystals, provided in §1.7.1 and §1.8.

An additional note of importance to the work presented in this thesis, is the orientational disorder (§1.9.1) that is known to occur in some organic mixed stack weak CT complexes.[105] The charge-transfer interactions and the formation of mixed stack columns take precedence over a close packing arrangement; the result of this is an orientational disorder of one of the molecules due to an inefficient packing arrangement.[115–117]

1.6 Polymorphism

Polymorphism is the ability of a material to exist in two or more chemically identical, but crystallographically distinct forms, with a widely accepted definition by McCrone of a polymorph being "a solid crystalline phase of a given compound resulting from the possibility of at least two crystalline arrangements of the molecules of that compound in the solid-state".[118] Differences between polymorphs may be changes in the molecular conformation, or conformationally equivalent molecules packing in different ways. Polymorphs have their own unique properties on account of their different crystal packing arrangements; as such, they represent a key branch of crystal engineering in terms of achieving optimum properties through control of the solid form.[119]

Polymorphism is encountered in the manufacturing of many important classes of crystalline materials, including pharmaceuticals (e.g. carbamazepine),[7,120] energetic materials (e.g. HMX, RDX),[119,121,122] and pigments (e.g. quinacridone).[123] While a polymorph can be favourable in terms of its properties, there can also be implications as polymorphism can affect many solid-state properties.[119] Polymorphism in pharmaceutical products has been widely documented; polymorphs of active pharmaceutical ingredients (APIs) can have distinct chemical and physical properties, including solubility, melting point and dissolution rates, and consequently the quality, safety and bioavailability of the drug can be affected.[121] In the field of energetic materials, the performance of a material is dependent on a number of factors including sensitivity to detonation, stability and density, all of which can be affected by the solid-state form.[119,121]

As a consequence of their different solid-state packing, polymorphs can display varying colours. A polymorphic system which clearly demonstrates this is 5-methyl-2-[(2-nitrophenyl)amino]-3-thiophene (Figure 1.14 (a)), more commonly known as ROY, which has at least seven known crystal structures, and at least three others forms for which the crystal structures have not been determined.[124] One of the most striking features of the system is the red, orange and yellow coloured crystals that are yielded depending on the particular polymorph (Figure 1.14 (b)), hence the abbreviation ROY (for red, orange, yellow). Each polymorph has a different visible absorption spectrum, and the variation in colour can be attributed to conformational differences in the molecule in the different solid-state forms. The largest conformational difference is seen in the torsion angle, θ, between the thiophenyl and phenyl aromatic rings (Figure 1.14 (a)), with variation in this torsion angle resulting in differing extents of π-conjugation between the rings.

Figure 1.14 (a) Chemical structure of 5-methyl-2-[(2-nitrophenyl)amino]-3-thiophene (ROY), showing the torsion angle, θ; (b) photographs of three of the polymorphs of ROY (left to right: red prisms, yellow needles and orange plates).[124]

The different forms in a polymorphic system have varying stabilities, dependent on their free energies, with the most stable form having the lowest free energy. At a certain temperature and pressure, only one polymorph is stable, with other polymorphs in that system therefore being metastable. Metastable forms have a tendency to reduce their free energy, and may transform to the more stable form over time or in response to a change in the environment (e.g. temperature). Thermodynamically, polymorphic systems can be classified as two types, enantiotropic or monotropic, depending on the polymorphic behaviour. In an enantiotropic system, one polymorph is most stable over one temperature and pressure range and another polymorph is most stable over a different temperature and pressure range; thus at a certain transition point where the free energies are equal, the two polymorphs can interconvert, with this being a reversible process. In a monotropic system, the polymorphs have the same ordering of relative stabilities at all temperatures, thus only one polymorph is stable below the melting point, and all other forms are always metastable.[119]

Controlling the polymorphic form obtained in crystallisation is not always an easy task. Different polymorphs may appear simultaneously under the same conditions, a phenomenon termed 'concomitant polymorphism'. For any material, there are a certain set of conditions under

which it will crystallise, known as the occurrence domain; sometimes these domains overlap, thus more than one form may be obtained.[125] There is also a phenomenon of 'disappearing polymorphs', which refers to the situation in which a previously existing form can no longer be obtained using the same procedure, and another form dominates.[126]

1.7 Tuning solid-state optical properties using crystal engineering strategies

1.7.1 Colour

Colour is a distinguishing property of any material, and the development of colour and the understanding of its origin have been important to the progression of chemistry. For an individual molecule, the origin of colour is attributed to its molecular electronic structure; however, in the solid-state, the absorption characteristics of the isolated chromophore are influenced by the crystal packing and the intermolecular interactions with neighbouring molecules. This effect has been clearly demonstrated in examples of polymorphic systems that display different colours depending on the form adopted.[123,124,127–129] The dependence of colour on different crystal packing arrangements has been termed crystallochromy[130] and has been observed and investigated for a number of single-component systems, predominantly pigments.[130–133] The effect is perhaps best shown by a series of perylene pigments, in early investigations on the correlation of molecular packing and pigment colour.[130] The basic chromophore for each is identical, a planar perylenetetracarboxylic diimide moiety, but exchanging the bulky substituent on the periphery of the chromophore alters the colour quite dramatically. Each of the pigments has the same absorption spectrum in solution, so the solid-state effect can be clearly attributed to the crystal packing. The perylene moieties stack in a parallel fashion but the bulky substituent on either side of the basic chromophore results in shifts in order to avoid unfavourable interactions between stacked molecules. The level of aromatic overlap thus differs between pigments, and it is to this effect that the different electronic transition energies can be attributed.

The method of multi-component crystallisation offers a route to the modification of properties in the solid-state, through introduction of a co-molecule to alter the crystal packing arrangement (§1.4). A small number of studies have investigated the origin of the colour in multi-component systems, including a zwitterionic co-crystal of acetaminophen and 2,4-pyridinedicarboxylic acid, which is red in colour upon forming the co-crystal,[134] and a series of hydrogensquarate and violurate systems.[135–137] In the latter systems, a red colour in the solid-state is attributed to shifting of disordered protons in infinite chains of the ionic fragment. However, whilst there are many examples of utilising multi-component crystallisation for the

modification of optical properties such as luminescence and non-linear optical properties, there are limited examples of systematic investigations into the tunability of colour. This is surprising, given the potential of crystal engineering in the field of pigments, not only in tuning colour, but also for modification of other important pigment properties, such as fastness and solubility.[138]

A study conducted by Bučar *et al.*[139] provided the first example of hydrogen-bond-based pigment co-crystals, in which the tunability of the colour of fluorescein by co-crystallisation was investigated. Fluorescein (fls) has three forms (i) flsQ, which is a red powder and has a quinoid structure (Figure 1.15 (a)), (ii) a yellow powder with a zwitterionic structure, and (iii) flsL, which is a white powder and has a lactoid structure (Figure 1.15 (a)). The red form, flsQ, was co-crystallised with the co-formers acridine (acr), phenanthridine (phi) and pyrazine (pyr), all chosen for their hydrogen bond acceptor sites (Figure 1.15 (a)); the stoichiometric ratio of flsQ and the co-former was selected based on the number of hydrogen bond acceptors in the co-former. Mechanochemical co-crystallisation was chosen as the primary crystallisation method, with crystallisation by slow evaporation of solvent also conducted for comparison.

Each product of the mechanochemical co-crystallisation was yielded as a different colour, with the acridine, phenanthridine and pyrazine co-crystals being ochre, yellow and pale green, respectively (Figure 1.15 (b)). The crystal structures were determined from powder X-ray data, and show that fluorescein is present in its lactoid form (flsL), thus a tautomeric transformation had occurred. Acridine and phenanthridine form 1:2 co-crystals (A and B, respectively) while pyrazine forms a 1:1 co-crystal (C). Co-crystals A and B display very similar crystal structures, with flsL and the co-former forming discrete three-molecule assemblies through N-H···O hydrogen bonds; the discrete assemblies stack *via* π···π interactions. Co-crystal C is comprised of 1D polymers formed through O-H···N hydrogen bonds, with the polymers assembled *via* O-H···O hydrogen bonds.

The same co-formers were also used in solution-based co-crystallisation experiments; the resultant co-crystals displayed different colours to the mechanochemically formed co-crystals, ranging from bright to dark yellow (Figure 1.15 (b)). The co-crystals were characterised by single crystal X-ray diffraction, revealing that the fluorescein was again present in its lactoid form (flsL); the co-crystals of acridine and phenanthridine (1 and 2) had stoichiometries of 1:2, while pyrazine forms a 1:1:1 co-crystal MeOH solvate (3). The crystal structure of 1 is different to that of the corresponding co-crystal, A, with two three-component assemblies forming a six-component aggregate, while the crystal structure of 2 matches that of the mechanochemically prepared co-crystal, B. In 3, the flsL, pyridine and disordered methanol form flat molecular tapes, which assemble into a 3D structure through O-H···O hydrogen bonds.

(a)

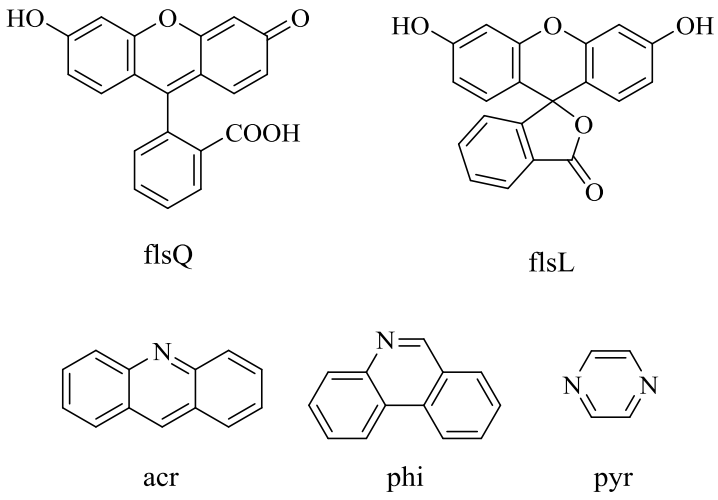

(b)

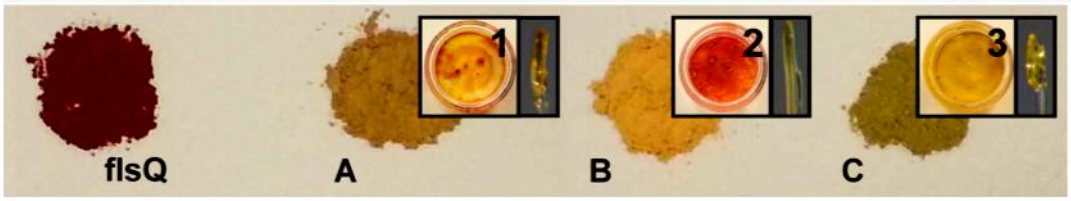

Figure 1.15 (a) Molecular structures of flsQ and flsL, and the co-formers acridine (acr), phenanthridine (phi) and pyridine (pyr); (b) photographs of a bulk sample of flsQ (left) and the mechanochemically prepared co-crystals of acridine (A), phenanthridine (B) and pyrazine (C), in addition to the solution-grown co-crystals of acridine (1), phenanthridine (2) and pyrazine (3). (Image taken from [139]).

In a further example, also using mechanochemical co-crystallisation, Kuroda *et al.* investigated the formation of a CT complex of racemic-bis-β-naphthol (*rac*-BN) (electron donor) and benzoquinone (BQ) (electron acceptor), which are white and yellow, respectively.[140] The study highlights how sensitive the colour of a CT complex is to its crystal structure, and how different crystallisation methods can result in different crystal forms. On grinding *rac*-BN and BQ, the colour gradually changed from very pale yellow to pink to red (Figure 1.16 (a)). Re-crystallisation of the sample yielded a very small number of red plate crystals, allowing the structure of the complex formed through grinding to be elucidated. This structure was compared with that formed through solution-based co-crystallisation, where the product was yielded as dark red block crystals. The crystal structures of the two were found to be different; in the crystals obtained from grinding, BQ is sandwiched between a racemic pair of BN molecules, while in the crystals obtained from solution the BQ is sandwiched between a homochiral pair of BN molecules.

In a follow-up paper,[141] the incorporation of a third co-molecule into the *rac*-BN-BQ crystallisation was investigated, forming three-component systems with biphenyl (BF), naphthalene (NP) and anthracene (AN). Similarly, co-grinding and solution-based

crystallisation were utilised for comparison. From solution, dark blue crystals were obtained with each of the guest molecules. Through co-grinding, bluish-black, dark blue and reddish-purple powders were obtained with BF, NP and AN, respectively (Figure 1.16 (b)), demonstrating the tunability of colour through changing the guest molecule.

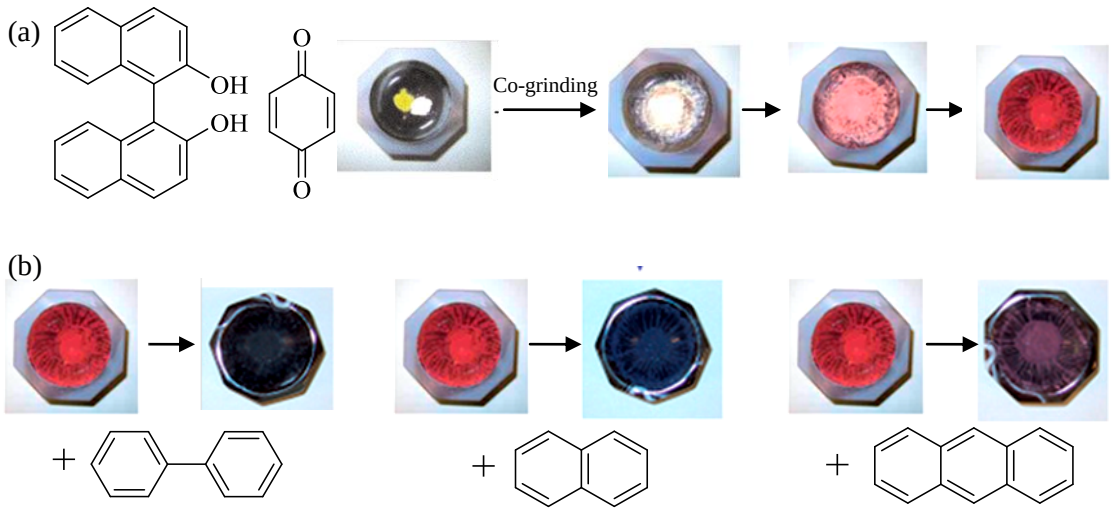

Figure 1.16 (a) Co-grinding *rac*-BN and BQ, forming a new red CT complex (*rac*-BN-BQ); (b) Formation of three-component CT complexes of rac-BN-BQ with BF (left), NP (middle) and AN (right). (Images taken from [140] and [141]).

The crystal structures of *rac*-BN-BQ-BF and *rac*-BN-BQ-AN differed depending on the method of formation, while the crystal structure obtained for *rac*-BN-BQ-NP is identical for the complexes formed from solution and co-grinding. With the exception of the BF crystal obtained from solution, all of the complexes have very similar crystal structures, with a triplet structure of BQ sandwiched between a racemic pair of BN molecules (BQ···BN···BQ), and similar orientation of the guest molecules; the BF crystal structure has a BN···BQ···BF triplet. The solid-state colour of each complex is attributed to charge-transfer between the donor (BN) and acceptor (BQ) molecules, but given the different colours evident, the intermolecular interactions between the donor···acceptor CT units must be influential.

1.7.2 Luminescence

Organic solid-state luminescent materials are widely studied for their promising optoelectronic applications in the areas of light-emitting diodes,[142,143] lasers[144] and sensors.[145] Tuneable luminescent materials are highly desirable for future applications in multi-colour light displays and optoelectronic devices.[146] The fabrication of multi-component solids has been shown to be a powerful strategy for tuning and tailoring luminescent properties, through selection of an

appropriate co-former to alter the packing arrangement.[147–151] Studies in this area have also provided key insights into the relationships between the molecular/crystal structure and the luminescent properties.[152]

In an exemplary study by Yan *et al.*,[150] modification of the luminescent properties of a stilbene-type molecule was achieved using a co-crystallisation strategy to control the stacking of molecules in the solid-state, and achieve variation in the fluorescence properties. 1,4-bis-p-cyanostyrylbenzene (A), a fluorescent model system, was co-crystallised with the following aromatic co-formers: 1,4-diiodotetrafluorobenzene (B), 1,4-diiodobenzene (C), resorcinol (D), 1,4-dibromotetrafluorobenzene (E), 4-bromotetrafluorobenzene carboxylic acid (F) and 2,3,4,5,6-pentafluorophenol (G) (Figure 1.17). Each co-former lacked visible solid-state fluorescence, and was selected due to the potential for its functional groups to interact with the cyano group of the stilbene *via* hydrogen and halogen interactions in a supramolecular fashion. Powder X-ray diffraction confirmed that new molecular complexes, 1 - 6, were formed with each of the co-formers B - G, respectively.

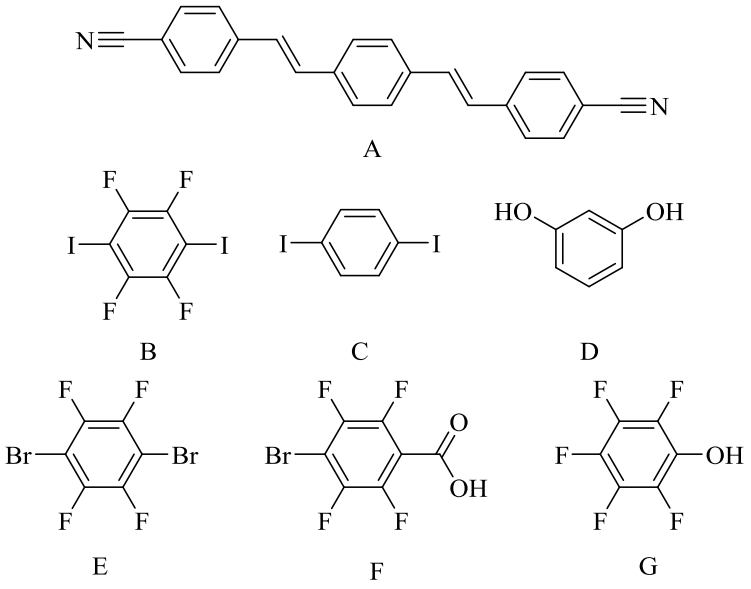

Figure 1.17 Chemical structures of the fluorescent stilbene molecule, 1,4-bis-p-cyanostyrylbenzene (A), and the co-formers 1,4-diiodotetrafluorobenzene (B); 1,4-diiodobenzene (C); resorcinol (D); 1,4-dibromotetrafluorobenzene (E); 4-bromotetrafluorobenzene carboxylic acid (F); 2,3,4,5,6-pentafluorophenol (G).

UV-visible spectra for A and the co-crystals showed that the co-crystals have different optical absorption characteristics to A. The powder samples under daylight exhibit different colours compared to that of A (Figure 1.18 (a)), and exhibit multi-colour luminescence, with colours ranging from blue to green to yellow, while A has yellow emission (Figure 1.18 (b)). The co-crystals also exhibit strong two-photon fluorescence (Figure 1.18 (e)). To enable

structure-property relationships to be determined, crystals were obtained to allow single-crystal X-ray diffraction to be carried out; the single crystals also exhibit tuneable emission (Figure 1.18 (c)).

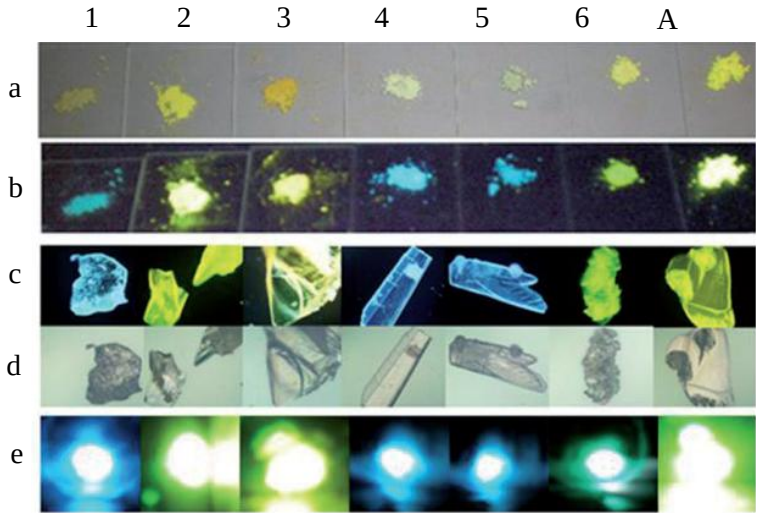

Figure 1.18 Photographs of co-crystals 1 - 6 and a sample of A. (a) and (b): powder samples under daylight and UV (365 nm), respectively; (c) and (d): single crystal sample under UV (365 nm) and daylight; (e) two-photon luminescence under 800 nm laser.

In the case of pure A, the molecular arrangement is ladder-like, with two of the molecules acting as the rungs, whilst the third molecule interacts with the rungs via C-H···C≡N hydrogen bonds. When A is co-crystallised with co-former B, for example, C≡N···I halogen bonds are formed, resulting in an increased separation between molecules of A compared to that in the pure crystal, and molecules of A are no longer stacked directly on top of one another. Similar observations related to different types of molecular stacking and their correlation to colour were made for the other co-crystals. For example, the co-crystal that shows a near identical stacking arrangement to that found in pure A also has a yellow emission. It can therefore be concluded that the major contributing factor to a change in the solid-state luminescent properties is an alteration in the stacking fashion of the chromophore.

1.7.3 Non-linear optical properties

Non-linear optics (NLO) is the study of the interaction of light with various media where the response to the applied electromagnetic field is non-linear; typically laser light is required for observation of NLO phenomena.[153] Possible organic NLO materials have received special interest due to their advantages over inorganic systems, including high molecular polarisability and fast response time.[154] The search for new organic crystals possessing important NLO

properties remains a challenge; to this end, multi-component crystallisation strategies have been applied in attempts to achieve desirable NLO properties.[101,155,156]

In the field of non-linear optics, second harmonic generation (SHG) is the most readily understood and widely used phenomenon; materials that display SHG have the ability to double the frequency of the incident light, so laser light can be produced that is of higher energy than the initial source.[153] SHG in the solid-state is dependent on both the molecular hyperpolarisability and the macroscopic non-linearity, i.e. the orientation and organisation of the molecules in the crystal lattice; for a non-zero macroscopic non-linearity, crystallisation in a non-centrosymmetric space group is a prerequisite.[157,158] Multi-component crystallisation strategies have been employed in the design of NLO materials, to increase the likelihood of crystallisation in a non-centrosymmetric space group.[101,159,160] This is demonstrated in a number of cyanophenol-pyridine and nitrophenol-pyridine complexes, utilising a combination of ionic and hydrogen bonding interactions; four of the molecular complexes that formed had non-centrosymmetric crystal structures and all exhibited positive SHG activity.[101] Multi-component crystallisation has also been utilised to enhance the NLO effects by the co-crystallisation of two components which themselves are NLO materials, as in the molecular complex of melamine barbital.[161]

1.8 Thermochromism

Materials which undergo a colour change in response to an external stimulus are important for their potential applications as imaging and sensing materials;[162] the colour changes in these smart materials are known to be driven by a variety of stimuli, including temperature,[163] light[164] and pressure.[165] The temperature-dependent colour change of a material is known as thermochromism,[163] and can occur in both the solution[166] and solid-states[167,168] in a range of materials, both inorganic[169] and organic. Thermochromism in single-component organic materials has a limited number of known origins, and typically involves an equilibrium between two molecular species (e.g. *cis-trans* isomerisation or intramolecular proton transfer).[163] A well known class of crystalline organic thermochromic systems are salicylideneanilines, where the thermochromic mechanism is a tautomerism between the OH and NH forms.[170]

Multi-component crystallisation as a route towards solid-state thermochromic materials is currently under-explored, despite the method offering potential for tuning properties *via* variations in the intermolecular interactions between the assembled molecular components. Of the multi-component crystals known to undergo single-crystal to single-crystal (SCSC) thermochromic phase transitions, the colour change is commonly attributed to the transfer of a

proton between the two molecular components. 2-iodoanilinium picrate[171] is a complex of 2-iodoaniline and picric acid, and has two stable forms at ambient temperature, which are yellow and green in colour; crystal structure analysis reveals a hydrogen bonded 2-iodoanilinium cation and picrate anion pair in each. Upon heating both forms above 60 °C, a colour change to red is observed; spectroscopic characterisation of the high-temperature form attributes the thermochromic transition to a proton transfer from the NH_3^+ group to the hydroxyl group O-atom (Figure 1.19), resulting in a neutral charge-transfer complex.

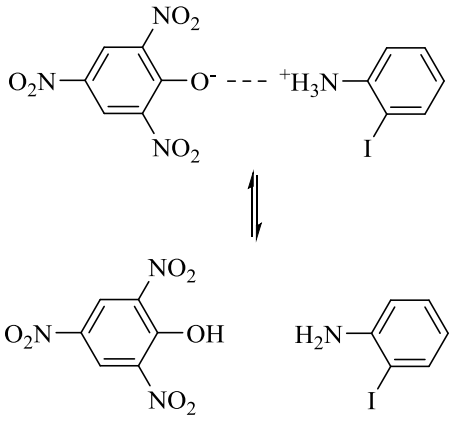

Figure 1.19 Mechanism of the thermochromism in 2-iodoanilinium picrate, with transfer of a proton between the amine and hydroxyl groups of 2-iodoaniline and picric acid, respectively.[171]

Another system which undergoes a thermally-induced reversible SCSC phase change associated with a proton transfer is the squaric acid 4,4'-bipyridine adduct.[99,172] At room temperature, the crystals are pale yellow in colour. On heating to 180 °C, a colour change from yellow to red is observed; the colour change starts at one end of the crystal and moves along the length of the block. On cooling below 150 °C, the crystal changes back to the pale yellow form. A number of experimental methods identify that the yellow to red colour change occurs when a proton is transferred to give the doubly protonated 4,4'-bipyridine cation and the squarate dianion.

In addition to these two proton transfer systems, Kinuta *et al.* reported thermochromism in the charge-transfer complexes of 1,1'-bi-2-naphthol (BN) and the viologens 1,1'-dimethyl-4,4'-bipyridinium dichloride ($MVCl_2$) and 1,1'-dibenzyl-4,4'-bipyridinium dichloride ($BVCl_2$) (Figure 1.20 (a)).[173] At 298 K, the molecular complex of $MVCl_2$ is dark red in colour but on cooling to 80 K, the colour gradually lightens, becoming light red (Figure 1.20 (b)); the complex is heated and cooled several times, with the same effect observed each time, thus suggesting reversible thermochromism. Crystal structure analysis of the high and low temperature forms shows that the crystal packing is the same at both temperatures. However, on cooling, the unit cell volume decreases and the distances of all of the intermolecular interactions

also decrease, in particular those between the viologen cations; in addition there is a change in the donor-acceptor dihedral angles. The results suggest that the thermochromism can be attributed to these small structural variations, due to a change in the unit cell volume. A similar effect was also observed in the $BVCl_2$ complex, but the colour change was less dramatic, with a smaller change in the intermolecular distances and donor-acceptor dihedral-angles.

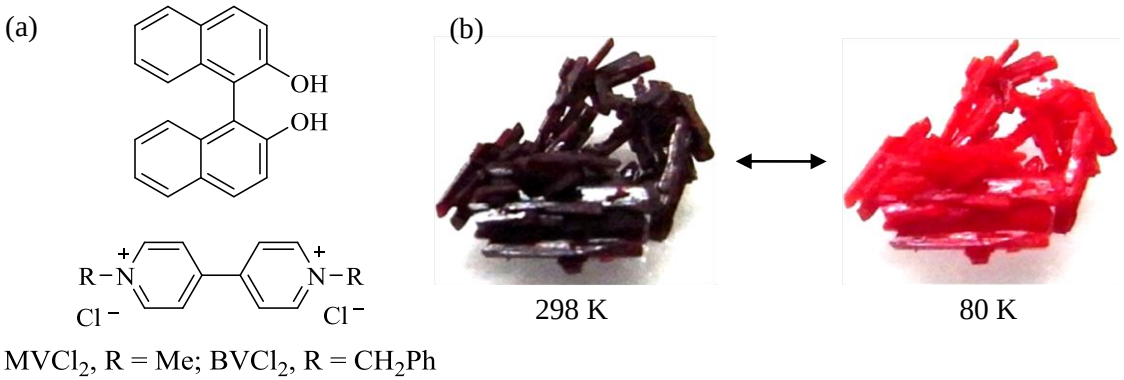

Figure 1.20 (a) Molecular structures of BN, $MVCl_2$ and $BVCl_2$; (b) crystals of the molecular complex of BN and $MVCl_2$ at 298 K and 80 K, showing the reversible colour change upon heating and cooling.

1.9 Disorder

The crystalline state is defined as a regular arrangement of atoms, but in reality crystals often exhibit some imperfections, such as disorder, in which case the unit cells throughout the crystal are no longer identical. The crystal structure that is determined from the Bragg peaks of the diffraction pattern will be the spatial average over the entire crystal. For a disordered system, where a molecule or part of a molecule is disordered over two positions, the overall crystal structure contains a certain percentage of each of the positions (i.e. the disordered moiety occupies different positions in different unit cells), and a superposition of the two is observed as the averaged model. Disorder in a crystal structure can often be apparent during the collection of single-crystal X-ray diffraction data, due to the presence of diffuse scattering in the diffraction pattern. During crystal structure refinement, residual electron density around atoms or molecules, distorted geometry, and poorly shaped and sized anisotropic displacement parameters (ADPs) can be a good indication of the presence of disorder. Refinement of a structure based on a single atomic position can make the ADPs large and elongated in shape, as the ellipsoid is being used to describe more than the one atom position;[174] the size and shape of ADPs also provides information on thermal vibrational disorder and it can sometimes be difficult to distinguish between the disorder types.[175] For many cases of disorder (including those described in this work), the refinement requires two (or more) sets of atomic coordinates for the two (or more) positions, along with the relative percentage occupancies of the two sites.

1.9.1 Types of disorder

Disorder can be categorised into three main types: static disorder, dynamic disorder and orientational disorder.[176] Static disorder refers to the situation where there is no additional motion of the atoms in the crystal, and covers many types of defect. It can describe the case where a molecule may possess more than one well-defined conformation, as well as where the same atomic site in the crystal is occupied by different atom types (substitutional disorder).[174]

Dynamic disorder refers to disorder which is time-dependent and typically involves vibration, libration or rotation of atoms or groups of atoms; it can occur, for example, when a group of atoms (e.g. *tert*-butyl group) is rotating virtually freely as each rotational angle is energetically similar. Dynamic disorder often has a temperature-dependency, and at low temperature the disorder may be frozen out.[174] Atomic vibrational motion is a type of dynamic disorder which refers to the vibrations of atoms about their equilibrium positions. This type of disorder is temperature-dependent, with greater motion at higher temperature; the ADPs reveal the extent and direction of the vibration.[175]

Finally, orientational disorder refers to the situation where a molecule can adopt more than one orientation; this may be static in nature, such that different unit cells have the molecule in different fixed orientations, or it can be dynamic if the molecule has sufficient energy to rotate.[176] Orientational disorder can also have a temperature-dependence, with rotation of the molecule more likely to occur at higher temperatures; on cooling, disorder-order phase transitions may occur.[105]

1.9.2 Properties of disordered materials

The properties of many materials are not dependent purely on the average structure, but can often be a result of the presence of disorder. In inorganic systems, defects have been extensively studied and exploited as a means of engineering desirable properties, such as conductivity and ferroelectricity, which are often directly related to the disordered nature of the structure.[177] However, disorder in organic molecular materials has not been similarly exploited, likely due to the difficulty in controlling the nature of such defects, and the understanding of the role of disorder in the properties of organic materials is limited.

In some recent examples, disorder has been found to impact the properties of some pharmaceutical materials. In crystalline aspirin, single crystals can contain domains of two polymorphs I and II; the diffraction pattern is a superposition of the diffraction patterns of the

two polymorphs and there is diffuse scattering observable which is indicative of stacking faults. Importantly, the intergrowth of the two polymorphs can lead to different properties compared to either of the pure polymorphs. The intergrown aspirin crystals have a melting point of up to 20 °C lower and a dissolution rate of up to five times higher; the origin of this effect lies in the disorder.[178,179] A similar phenomenon has also been observed in the case of felodipine, with the diffraction pattern revealing a disordered layer stacking sequence.[179]

1.9.3 Diffuse scattering

Diffuse scattering is present in the diffraction patterns of most materials, but is much weaker than the Bragg scattering, with intensities around 10^3 - 10^4 times lower, and as a result it can often be overlooked or classified as part of the background scattering. In the case of random disorder, e.g. uncorrelated thermal motion, there will be no structure to the diffuse scattering and it is effectively indistinguishable from the background scattering. While interpretation of the Bragg scattering provides the average structure of a material, diffuse scattering contains information about deviations from the average structure and about correlations of molecules over short length scales. Different types of disorder give rise to particular diffraction effects, so the diffuse scattering can vary in type and intensity, and may be the result of a complex combination of disorder effects. If the diffuse scattering is strong enough and has structure, then interpretation is possible. Structured diffuse scattering can only be observed if there are correlations of molecules over short length scales (short-range order) and so its presence indicates that the disorder is not random.[175,180]

Many properties of crystalline materials can be dependent upon the disorder or short-range order in the structure. Thus, understanding the diffuse scattering and the local crystalline structure, rather than the average, can aid in the understanding of properties. The development of methods to measure, interpret and analyse diffuse scattering has been slow compared to those of conventional structure determination which is due to a combination of two main factors which make the interpretation and analysis quite demanding. Firstly, there are difficulties in the collection of high quality diffuse scattering measurements due to diffuse scattering being so weak compared to the Bragg scattering; diffuse scattering is also spread widely across reciprocal space. Secondly, structural models to explain the diffuse scattering are difficult to construct, especially considering the number of different types of disorder that can be present.[177] However, there have been considerable advances more recently in both the measurement of diffuse scattering and its interpretation. Computer simulations, such as Monte Carlo simulation, are a powerful technique for the interpretation of diffuse scattering. The method involves the construction of different possible models using the average structure and chemical knowledge;

the occupancies and molecular orientations can be varied, and the different models tested. Diffraction patterns can be calculated from the models and compared with the experimental diffraction patterns; the model can be adjusted iteratively until a satisfactory agreement is obtained.[177,180] The most obvious local ordering, however, does not necessarily reproduce the diffuse scattering and multiple models will often need to be tested. An example of the interpretation of diffuse scattering using a Monte Carlo simulation was provided by a study on pentachloronitrobenzene (PCNB).[181] In each molecular site in the crystal, PCNB can adopt one of six different orientations (Figure 1.21 (a)); strong, structured diffuse scattering is observed around and between the Bragg peaks in the diffraction pattern. This diffuse scattering suggests that any disorder is not random and it remains at low temperature implying that it is static in nature. The PCNB molecules are arranged in layers, and in some combinations of orientations, the nitro group can adopt positions where there is a steric repulsion between molecules in parallel planes. A Monte Carlo simulation was used to interpret and model the diffuse scattering, reproducing the experimental diffraction patterns in detail with excellent agreement (Figure 1.21 (b)). The first model which was tested, looked at short range ordering between molecules in parallel planes, disfavouring situations where the nitro groups were present in close proximity. No satisfactory solution was found using this model, indicating that the relative positions of molecules between planes was random. Instead, the distinct diffraction pattern was found to be a result of tilting of the molecules in parallel planes where close steric contacts were made between nitro groups; these tilts increase the intermolecular distances between two neighbouring NO_2 groups or neighbouring NO_2 and Cl groups, but reduce the distances between neighbouring Cl groups, thus allowing the molecules to reduce the strong repulsive forces. A model such as this was also indicated in the atomic displacement parameters which were elongated out of the plane of the molecule.[181]

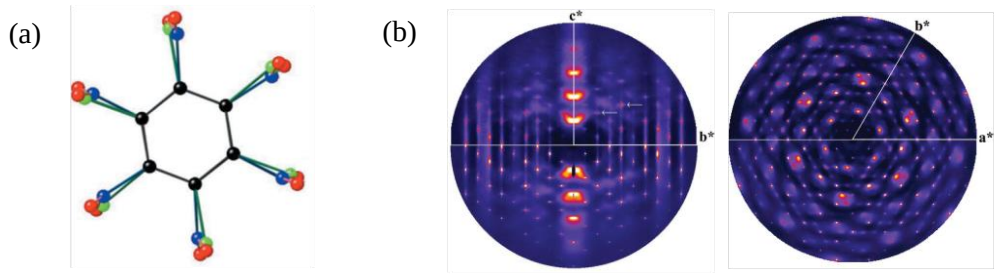

Figure 1.21 (a) Six-fold orientational disorder of pentachloronitrobenzene; (b) agreement between the experimental diffraction patterns (lower semi-circle) and the calculated diffraction patterns (upper semi-circle). (Images taken from [181]).

1.10 Aims and objectives

The research aims of this thesis are to investigate multi-component crystallisation as a means of inducing and tuning colour and switchable colour in the solid-state. Taking inspiration from the thermochromic molecular complex 2-iodoanilinium picrate, a systematic study is conducted using a series of haloanilines and nitro-substituted benzoic acid derivatives, with the key objectives being identification of the structural features necessary for colour and tuneable colour in the multi-component materials, in addition to the development of new mechanisms for thermochromism.

In order to investigate possible routes to tuning colour in the solid-state, systematic modifications are made to the molecular components, for example exchange of the halogen or introduction of an additional substituent. For potential routes to thermochromism in the materials, focus is placed on utilising proton transfer as a colour switch and incorporating molecular disorder in mixed stack charge-transfer systems; it is anticipated that molecular disorder may provide the crystal space necessary to allow solid-state rearrangements. The effect of the substituent nature and its position on the colour, transition types and transition temperatures will be discussed.

CHAPTER 2

Theory

2 Theory

2.1 Principles of crystallography

Crystallography is the study of the structure and properties of crystalline materials, primarily by diffraction methods, which exploit the periodic nature of crystalline solids. Diffraction experiments most commonly use X-rays, but neutrons and electrons can also be used depending on the nature of the study; in this work, all of the crystal structures were determined using single crystal X-ray diffraction. X-ray diffraction is a particularly powerful technique, used across a range of scientific disciplines, which reveals a three-dimensional image of the material being studied. This shows the precise spatial arrangement of atoms in the solid-state, but also provides information on thermal motion, connectivity, molecular geometry and molecular packing arrangement, which are all fundamental to the properties of the material.

2.1.1 The crystalline state

2.1.1.1 The lattice and unit cell

A perfect crystal is a highly ordered solid material in which some basic structural pattern is repeated in a precise and regular way throughout the solid in three dimensions; the repeating pattern, or motif, may be a single atom, but can also be a molecule, a number of ions, or an assembly of a few molecules. Each motif is repeated essentially infinitely by translational symmetry, and this translational symmetry is defined by the lattice of the structure; the lattice can be constructed by selecting any single point along with all other identical points in the crystal to generate an infinite array of lattice points (Figure 2.1 (a)). Translation between lattice points can be defined by vectors, with three basis vectors required to describe the complete lattice geometry. The smallest repeating volume of the lattice that is representative of the crystal as a whole is called the unit cell, which is formed by connecting lattice points, and can be considered the building block of the crystal structure. The unit cell is characterised by six parameters based on the basis vectors of the lattice: three cell lengths (a, b, c) and the three angles between them (α, β, γ) (Figure 2.1 (b)). For any lattice there is more than one choice of unit cell, but by convention the smallest possible unit cell that reflects the symmetry within the structure is usually chosen.[182,183]

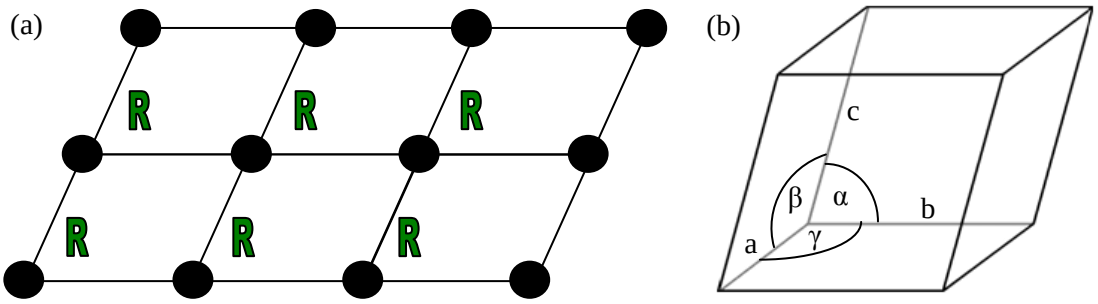

Figure 2.1 (a) The lattice and repeating motif (R) shown in two dimensions, with each parallelogram representing a two-dimensional unit cell; (b) a unit cell, described by three lengths, *a*, *b*, *c*, and three angles, *α*, *β*, *γ*.

Rotation and reflection symmetry in the structure (§2.1.1.2) imposes restrictions and special values on the unit cell parameters, for example the presence of a two-fold rotation axis makes two of the angles 90° but places no restrictions on the third angle. By full consideration of the possible symmetries for the lattice, unit cells can be classified into a total of seven crystal systems (Table 2.1), and these can be further classified by lattice types, of which there are four (Figure 2.2). The unit cell with the smallest number of lattice points is the primitive cell (P), which has a lattice point on each corner; each lattice point contributes ⅛ to each unit cell and therefore there is a total of one lattice point per unit cell. It is always possible to choose a primitive cell, but sometimes it is optimal to select a larger unit cell that contains more than one lattice point in order to best exploit the symmetry of the structure. These non-primitive unit cells include those where additional lattice points are centred on two opposing faces (A, B or C, depending on which faces are centred), at the body centre of the cell (I), or centred on all of the faces (F). When the seven crystal systems are combined with the four possible lattice types this gives a total of fourteen lattices, termed the Bravais Lattices (Table 2.1). Some lattice types are missing for particular crystal systems, as they can be reduced to a lattice with a different centering; for example, in the monoclinic crystal system the body-centred (I) lattice can be converted to the standard monoclinic C-type lattice.[182,183]

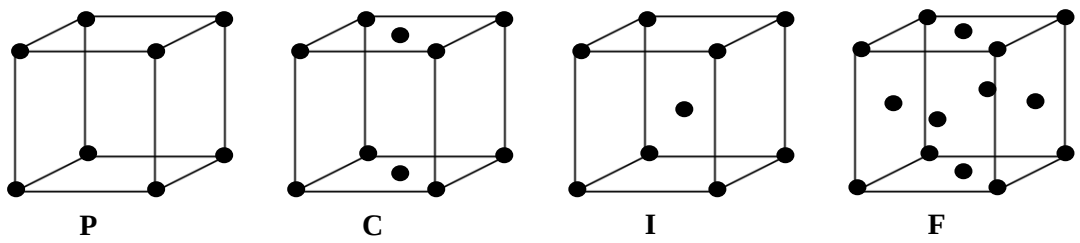

Figure 2.2 The four lattice types: **P** (primitive), **C** (face centred), **I** (body centred) and **F** (all-face centred).

Table 2.1 The unit cell restrictions for each of the crystal systems, and the distribution of the fourteen Bravais Lattices into the seven crystal systems.[184]

Crystal system	Unit cell restrictions		Lattice types
Triclinic	$a \neq b \neq c$	$\alpha \neq \beta \neq \gamma$	P
Monoclinic	$a \neq b \neq c$	$\alpha = \gamma = 90°, \beta \neq 90°$	P, C
Orthorhombic	$a \neq b \neq c$	$\alpha = \beta = \gamma = 90°$	P, C, I, F
Tetragonal	$a = b \neq c$	$\alpha = \beta = \gamma = 90°$	P, I
Trigonal	$a = b = c$	$\alpha = \beta = \gamma \neq 90°$	P
Hexagonal	$a = b \neq c$	$\alpha = \beta = 90°, \gamma = 120°$	P
Cubic	$a = b = c$	$\alpha = \beta = \gamma = 90°$	P, I, F

2.1.1.2 Symmetry and space groups

Symmetry plays an essential part in all aspects of crystallography; it has already been shown that every perfect crystalline solid is an assembly of unit cells which are related to one another by translational symmetry, defining the lattice of the structure. However, to describe the crystal structure fully it is also necessary to establish the internal symmetry within the unit cell, and thus how the molecules in the unit cell are related to each other. The smallest unique structural unit of the crystal structure is the asymmetric unit, from which the contents of the unit cell can be generated by application of the internal symmetry. Symmetry properties can be described in terms of the presence of symmetry elements and their associated symmetry operations; while symmetry elements are a physical point, line or plane, symmetry operations perform a certain transformation upon an object about the symmetry element. There are six possible types of symmetry element in crystallography, which can be divided into two categories: non-translational and translational. Non-translational symmetry elements leave the position of one point unchanged, and include: (i) inversion centre, (ii) rotation axis (2-, 3-, 4- or 6-fold), (iii) mirror plane, and (iv) roto-inversion axis, which couples a rotation axis with an inversion centre (Figure 2.3). For a particular finite object, the combination of these non-translational symmetry elements, all passing through a common point, is described by a point group, of which there are 32 relevant to crystallography.[183]

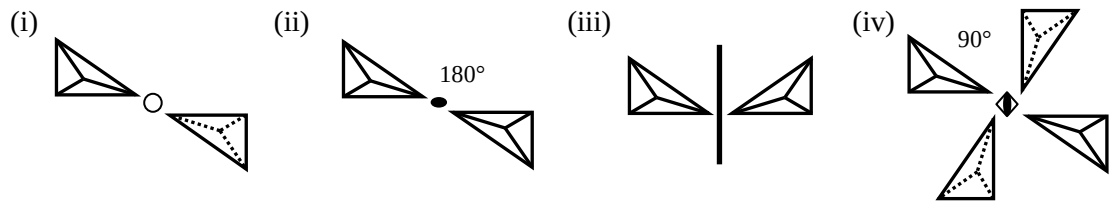

Figure 2.3 Non-translational symmetry elements and the associated operations: (i) inversion centre, (ii) rotation axis (2-fold), (iii) mirror plane, (iv) roto-inversion axis (4-fold).

Due to the presence of translational symmetry, crystals can also have translational symmetry elements present, which arise from the coupling of translation with rotation and reflection. Screw axes involve rotation about an axis followed by translation along the direction of the rotation axis; glide planes involve reflection in a mirror plane followed by translation parallel to the plane of reflection (Figure 2.4).

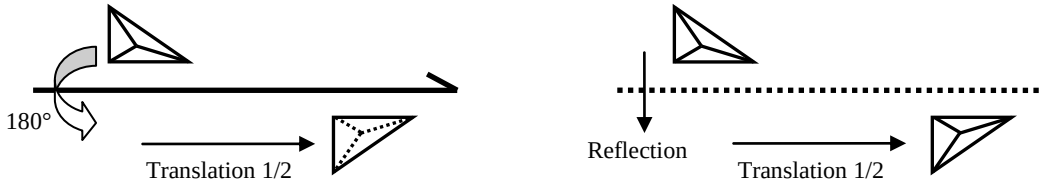

Figure 2.4 Translational symmetry elements and the associated operations: (i) screw axis (2_1) and (ii) glide plane.

Just as non-translational symmetry elements can be combined to give the point group, the combination of symmetry elements for an infinite three-dimensional lattice can be defined in a similar way. Combination of the allowable combinations of the translational and non-translational symmetry elements, together with the fourteen possible lattice types, results in 230 possible descriptions, which are the known as the crystallographic space groups.[185] The space group for the crystal structure describes all of the symmetry elements and their locations. The relevant symmetry operations of the space group are applied to the asymmetric unit to generate the unit cell; in turn, translation of the unit cell in three dimensions generates the entire crystal structure.[183]

2.1.2 X-ray diffraction

The technique of X-ray diffraction has been of the greatest importance in revealing the structures of crystalline materials, with its discovery dating back over a century. The important properties of X-rays were first described by Röntgen in 1896;[186] however, it was not until several years later in 1912, that von Laue showed that if X-rays were passed through a crystal then diffraction would take place.[187] This proved that X-rays behaved like waves, with wavelengths of a comparable magnitude to lattice spacings (in the order of Å). X-ray diffraction originates from the interaction of X-rays with the electron clouds of atoms in the sample; in diffraction, only elastic scattering is considered, meaning the energy of the scattered photon is unchanged. If one were to consider interaction with a single electron, the direction and polarisation of the X-ray photon would be unchanged by the scattering angle, 2θ; X-rays would be scattered with equal intensities in all directions. except for a simple polarisation factor dependent on 2θ. However, when this is extended to interaction with more than one electron,

interference of diffracted beams will occur; if the waves are in phase then the interference is constructive, and if the waves are out of phase then the interference is destructive.[184]

2.1.2.1 The Laue Equations

To understand the geometry of diffraction, a very simple model can be considered which consists of a one-dimensional row of equivalent atoms along the direction of the crystallographic *a*-axis (Figure 2.5). For the waves of diffracted beams to be in phase, and for interference to be constructive, then the path difference (OQ - PR, Figure 2.5) must be equal to whole numbers (n_1) of wavelengths (λ). The condition for constructive interference from two adjacent points in the one-dimensional lattice, with a lattice spacing of *a*, is given in Equation 2.1; the path difference is related to the angle of incidence (μ) and angle of scattering (ν).

$$path\ difference = a\ (cos\nu - cos\mu) = n_1\lambda \qquad \textbf{Equation 2.1}$$

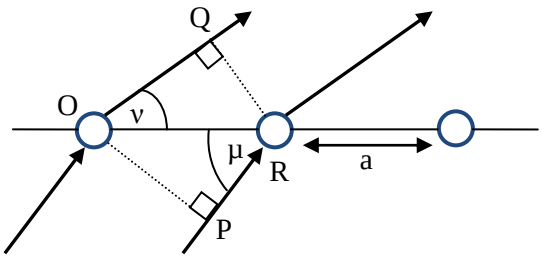

Figure 2.5 Scattering of X-rays from a one-dimensional row of equivalent atoms, where a is the spacing of atoms, μ is the angle of incidence and ν is the angle of scattering.

When this is extended to a three-dimensional lattice, with axes *a*, *b* and *c*, there are three equations of the same type to consider (Equations 2.2 - 2.4), where n_1, n_2 and n_3 are integer numbers. These are the Laue equations, and for diffraction to be observed they must be fulfilled simultaneously.[183]

$$a\ (cos\nu_1 - cos\mu_1) = n_1\lambda \qquad \textbf{Equation 2.2}$$

$$b\ (cos\nu_2 - cos\mu_2) = n_2\lambda \qquad \textbf{Equation 2.3}$$

$$c\ (cos\nu_3 - cos\mu_3) = n_3\lambda \qquad \textbf{Equation 2.4}$$

2.1.2.2 Bragg's Law

In 1913, W.L. Bragg first used X-ray diffraction as a means of establishing the arrangement of atoms in three-dimensions.[188,189] This need to describe the geometry of X-ray diffraction led to the formulation of Bragg's Law, which provides an equivalent, but more convenient way of

visualising how diffraction takes place in a crystal and is used as the basis for X-ray diffraction geometry (Figure 2.6). Although not physically rigorous, it assumes that X-rays are reflected from planes in the crystal, known as lattice planes, defined simply as two dimensional slices through the crystal. A set of parallel planes is indexed using a Miller index *hkl* and each plane is separated by a characteristic spacing '*d*', denoted d_{hkl}. The intercepts of the plane with the *a*-, *b*- and *c*-axes of the unit cell are 1/*h*, 1/*k* and 1/*l*; for example, a plane intercepting the *a*- and *b*-axes at ⅓ and 1, respectively, with no intercept of the *c*-axis (effectively intercepting at ∞), would have a Miller index *hkl* of (3,1,0). Bragg's Law provides the geometrical conditions under which constructive interference of waves is achieved. For the diffracted waves to be in phase, the difference in path length (XY + YZ) must be equal to an integral multiple of the wavelength, and the angles of incident radiation and reflected radiation (θ) must also be equal. Simple trigonometry gives rise to Bragg's Law (Equation 2.5), where n is an integer and λ is the wavelength of the incident radiation.[183]

$$2d_{hkl}sin\theta = n\lambda \qquad \textbf{Equation 2.5}$$

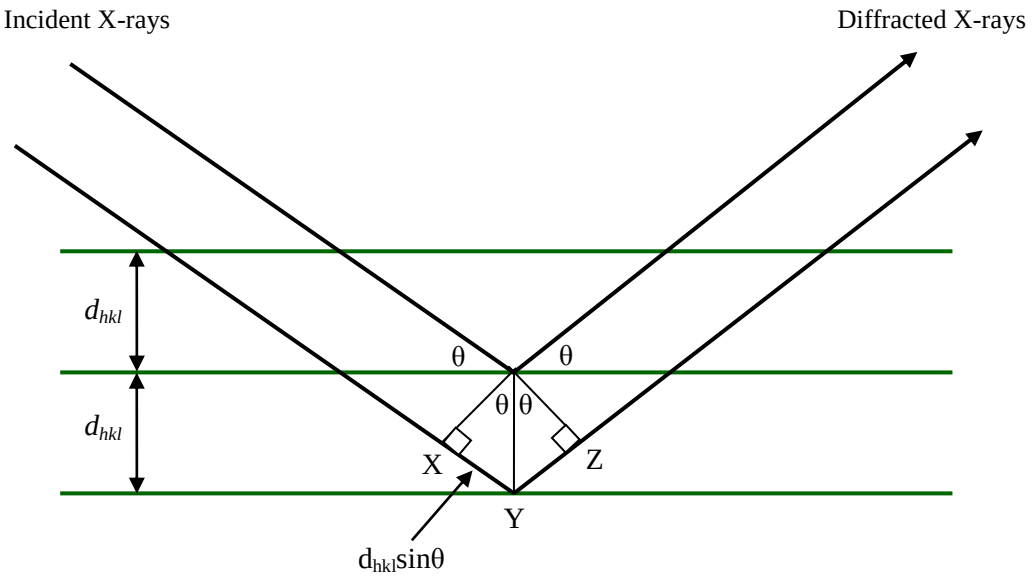

Figure 2.6 The Bragg construction for diffraction, showing the difference in path length between the incoming and reflected radiation (XY + YZ), the spacing between the sets of planes (d) and the angle of incident and diffracted X-rays (θ).

2.1.3 The diffraction pattern and reciprocal space

Scattering from single molecules is very weak, but diffraction from a macroscopic crystal which has a regular array of a huge number of molecules, produces a measurable diffraction pattern. The diffraction pattern consists of an array of spots, or Bragg reflections, with varying positions

and intensities; each individual reflection can be uniquely labelled with an index, *hkl*, and is observed when the Bragg condition is fulfilled for a set of lattice planes of the same index. To observe all of the possible Bragg reflections, it is necessary to rotate the crystal appropriately in the beam to achieve the value of θ for which constructive interference will occur. The diffraction pattern obtained has three main properties relating to the crystal structure. The positions of the spots relate to the crystal lattice and unit cell geometry; the symmetry of the pattern is very closely related to the symmetry of the unit cell so the crystal system and space group can be determined; the intensities of the various diffraction spots hold all of the information about the arrangement of the atoms in the unit cell.

The lattice of the three dimensional diffraction pattern is known as the reciprocal lattice; whilst crystal lattices occupy real space, reciprocal lattices occupy reciprocal space. To construct the reciprocal lattice, each set of real space planes is described by a vector where the direction is normal to the planes and whose magnitude is related to the spacing between planes (d_{hkl}); the reflection observed in the diffraction pattern is at the end of this vector. By rearrangement of Bragg's Law (Equation 2.6), it can be seen that the scattering angle, θ, is related to the reciprocal of the *d*-spacing ($1/d_{hkl}$), thus the end-points of the vectors (which are known as scattering vectors, d*) are a distance of $1/d_{hkl}$ from a single origin. If we take all of the scattering vectors and start them from the same origin, the ends of the vectors are the reciprocal lattice points.[183]

$$\sin\theta = \frac{n\lambda}{2}.\frac{1}{d_{hkl}} \qquad \textbf{Equation 2.6}$$

Just as the lattice in real space can be defined by three vectors **a**, **b** and **c**, the reciprocal lattice can be described in a similar way using vectors **a***, **b*** and **c***. The relationship between the reciprocal and real space lattices is shown by Equation 2.7; dividing by the volume, V, gives dimensions of reciprocal length.

$$\mathbf{a}^* = \frac{\mathbf{b} \times \mathbf{c}}{\mathrm{V}} \qquad \mathbf{b}^* = \frac{\mathbf{a} \times \mathbf{c}}{\mathrm{V}} \qquad \mathbf{c}^* = \frac{\mathbf{a} \times \mathbf{b}}{\mathrm{V}} \qquad \textbf{Equation 2.7}$$

A useful construction that can be used to visualise a diffraction experiment is the Ewald construction (Figure 2.7), which combines reciprocal space with the Ewald sphere, and shows how the crystal must be oriented to observe particular reflections. The Ewald sphere has a radius of 1/λ (where λ is the wavelength of radiation), and at the centre is the crystal (C). A set of direct lattice planes (with spacing *d*) is arranged such that there is an angle of θ to the incident

beam; if θ satisfies Bragg's Law for that set of planes, then a reflection is observed at an angle of 2θ to the incident beam (vector CP). The origin of the reciprocal lattice is placed at the point O on the edge of the Ewald sphere. Reflection is observed when a node of the reciprocal lattice, P (and the end of the scattering vector OP) intercepts the Ewald sphere, fulfilling Bragg's Law. The scattering vector OP is normal to the direct lattice planes and has a magnitude of $1/d_{hkl}$. The crystal and its reciprocal lattice can be rotated about O in order to pass each reciprocal lattice point *hkl* through the edge of the sphere and allow the observation of reflections from each set of lattice planes.[183,184]

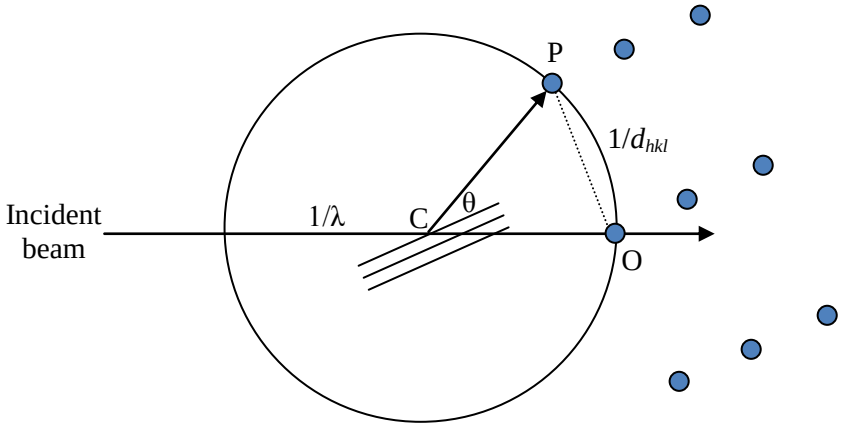

Figure 2.7 The Ewald construction showing diffraction from a set of planes with spacing d_{hkl} at an angle of θ to the incident beam.

2.1.4 Structure factors and Fourier transforms

The spatial distribution of the reflections, and how they relate to the direct lattice, is understood using the concept of reciprocal space; however, in order to determine the locations of the atoms in the unit cell, the intensities of the reflections are required. Each diffracted wave has an amplitude ($|F|$) and phase (ϕ) which can be represented by *F*, which is a complex number; each individual reflection with indices *h*, *k* and *l* can be represented by *F(hkl)* (Equation 2.8). *F*(*hkl*) is called the structure factor and is proportional to the square root of the intensity of the reflection, *I*(*hkl*) (Equation 2.9) which is obtained from the diffraction experiment. Although many factors, such as crystal quality and absorbance, affect the intensity of X-rays in the diffraction pattern, the structure factor depends purely on the crystal structure.

$$F(hkl) = |F(hkl)|.\,exp\,[i\phi(hkl)] \qquad \textbf{Equation 2.8}$$

$$F(hkl) \propto \sqrt{I(hkl)} \qquad \textbf{Equation 2.9}$$

The diffraction pattern is the Fourier transform of the electron density (or crystal structure); the mathematical relationship is given by Equation 2.10. This equation is applied at different stages of a crystal structure determination to each reflection in the diffraction pattern to obtain a set of calculated structure factors, $F_c(hkl)$. The structure factor for each reflection in the diffraction pattern is expressed as the Fourier summation of the electron density of all individual atoms (j, with coordinates x_j, y_j and z_j), expressed in the form of atomic scattering factors, f_j.[182]

$$F(hkl) = \sum_{j}^{N} f_j \,.\, exp[2\pi i(hx_j + hy_j + hz_j)] \qquad \textbf{Equation 2.10}$$

The atomic scattering factor is a measure of the scattering strength of an isolated atom, and is dependent on the atom type and the Bragg angle, θ (Figure 2.8). The scattered intensity is proportional to the square of the atomic number, thus heavier atoms are easier to identify than lighter atoms. When 2θ = 0°, all of the X-rays scattered by the electrons of the atom are in phase, and the atomic scattering factor is equal to the atomic number; however at higher scattering angles destructive interference effects mean that the intensity falls off rapidly.[183,184]

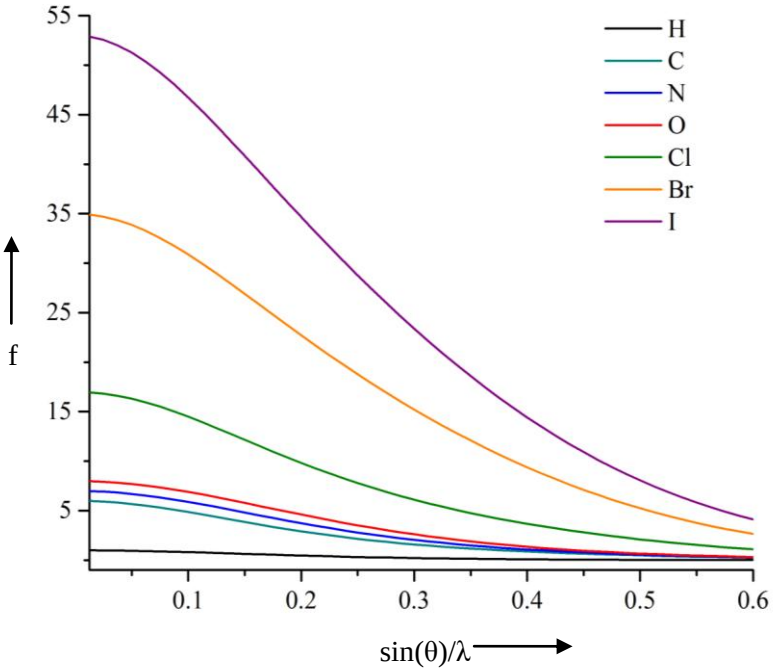

Figure 2.8 A plot of the atomic scattering factors, f, as a function of the scattering angle, θ, shown for selected elements.

Atomic scattering factors are also modified by atomic vibrations, which result in a weakening of the scattering strength; atoms are generally vibrating about their mean position, and the effect of motion is described by the atomic displacement parameters (ADPs). If the vibration is equal in

all directions, then the atom is isotropic, and the atomic scattering factor (*f*) is modified according to Equation 2.11, where *U* is the square of the mean vibration amplitude. The factor $8\pi^2U$ increases in value with temperature, and is often termed the Debye-Waller factor, B.[183]

$$f' = f.\exp\left(-\frac{8\pi^2 U sin^2\theta}{\lambda^2}\right) \qquad \textbf{Equation 2.11}$$

If the vibration is unequal in the different directions, then the atom is said to be anisotropic (i.e. it has anisotropic ADPs). The description of anisotropic vibrations is much more complicated, with the shape and orientation of the vibrations described by six U_{ij}-parameters; the resulting 3D locus of the vibrations is often represented by an ellipsoid, termed the thermal ellipsoid.

Just as the diffraction pattern is the forward Fourier transform of the electron density, the electron density is the inverse Fourier transform of the diffraction pattern, and can be expressed in terms of the structure factors (Equation 2.12). This shows how electron density in the unit cell can be obtained from a diffraction pattern by carrying out a Fourier summation of the structure factors corresponding to all *h*, *k*, *l* values for many different coordinates *x*, *y*, *z*.[182]

$$\rho(xyz) = \frac{1}{V}\sum_{hkl}|F(hkl)|\exp\left[i\phi(hkl)\right].exp\left[-2\pi i(hx+ky+lz)\right] \qquad \textbf{Equation 2.12}$$

2.1.5 Structure solution: the Phase Problem

To solve a crystal structure and obtain an electron density map, the value of *F*(*hkl*) is required, which includes both the amplitude and the phase as shown in Equation 2.12. Experimentally, a set of observed structure factors is obtained, but we only know the amplitude; the phase information has been lost, and this constitutes the phase problem of X-ray structure analysis. In order to solve the structure, the phases must be determined, and various methods have been developed to do this. The Patterson method and Direct Methods are the two most common, but more recently developed methods, such as Charge Flipping, are becoming increasingly used.

2.1.5.1 The Patterson method

The Patterson method is most typically used when there are heavy atoms present in the structure, and makes use of a Fourier synthesis in which the Fourier coefficients are effectively the observed intensities. The structure factors, *F(hkl)*, are replaced by the product of each one with its complex conjugate, to give a real number (Equation 2.13); this means that the Patterson function (Equation 2.14) uses the squared amplitudes, $|F_o(hkl)^2|$. The Patterson function uses a

three dimensional grid in Patterson space with *u*, *v*, *w* coordinates which are fractions of the unit cell edges, but are not directly related to atomic coordinates *x*, *y*, *z*.

$$F(hkl).F^*(hkl) = |F(hkl)|^2 \qquad \textbf{Equation 2.13}$$

$$P(uvw) = \frac{1}{V}\sum_{hkl}|F_o(hkl)|^2.exp[-2\pi i(hu + kv + lw)] \qquad \textbf{Equation 2.14}$$

The result of the function is a Patterson map which is very similar to an electron density map, in that there are peaks of positive density in various positions; however, instead of the peaks referring to the positions of atoms in the structure, the maxima correspond to ends of interatomic vectors. For each pair of atoms in the structure with coordinates (x_1, y_1, z_1) and (x_2, y_2, z_2), there will be two peaks observed with coordinates in Patterson space (u, v, w) corresponding to (x_1-x_2, y_1-y_2, z_1-z_2) and (x_2-x_1, y_2-y_1, z_2-z_1). For this reason, the map always has an inversion centre at the origin. The heights of the peaks in the map are proportional to the product of the atomic numbers of the two atoms concerned. The highest peak in the map will always be at the origin, and is due to the vector of every atom with itself; its height is proportional to the sum of the squares of the atomic numbers for every atom in the unit cell. Aside from this peak, the next largest peaks will correspond to vectors between the heaviest atoms in the structure; by using the internal unit cell symmetry this can reveal the positions of these atoms. Knowledge of the location of these heavy atoms gives an initial model, allowing approximate phases to be calculated which can then be used to develop the structure further.[182]

2.1.5.2 Direct methods

Direct methods is a trial and error technique, that attempts to derive the phases by mathematical means from a single set of X-ray diffraction intensities, without prior knowledge of the crystal structure. The methods make use of the fact that the structure factor amplitudes and phases are not independent of one another, and are linked through a knowledge of the electron density. Certain constraints are imposed on the electron density, with the two most important being (i) electron density must be concentrated into discrete regions (representing atoms), and (ii) electron density must always be positive. These fundamental properties restrict the relationships between the phases of the different Fourier components, and have led to the development of a range of probability relationships among the structure factor phases based upon the structure factor amplitudes.

Using the first constraint, that electron density is concentrated into discrete regions corresponding to atoms, the effects of atomic shape can be removed and the structure factors,

$F_o(hkl)$, can be modified to give normalised structure factors, $E(hkl)$, which are used in direct methods. Normalisation removes the θ-dependence of the atomic scattering factor (fall off of intensity at high angles) and makes the structure factors comparable.

Sayre developed a relationship which combines the two constraints of discrete atoms and positive electron density with an assumption that crystals are composed of multiple equal atoms. The relationship states that the structure factor for any reflection, *hkl*, can be calculated by summing the products of the structure factors of all pairs of reflections whose indices add up to the values of *h*, *k* and *l* (Equation 2.15).[190] As an example, the structure factor E_{321} could be calculated according to Equation 2.16. Initially, pairs of reflections where one or both components are weak are ignored, as stronger reflections contribute more to the summation. If the reflections in a pair are strong, and the structure factor to be calculated is strong, then the probability of determining the phase using this relationship alone is high.

$$F_{hkl} = k \sum_{h'k'l'} F_{h'k'l'} \cdot F_{h-h',k-k',l-l'} \qquad \textbf{Equation 2.15}$$

$$E_{321} = E_{100} \cdot E_{221} + E_{110} \cdot E_{211} + E_{111} \cdot E_{210} + \cdots \qquad \textbf{Equation 2.16}$$

Karle and Hauptman extended Sayre's equation and developed the triplet relationship. This uses the knowledge that if two E-values are known, then a third E-value can be determined from the relationship of the three; the stronger the reflections used, the higher the probability that the relationship is accurate. The vectors associated with the triplet of reflections form a closed triangle in reciprocal space, and the indices of the three reflections sum to zero. The set of three structure factors can be termed *E(h)*, *E(k)* and *E(h-k)*, where *E(h)* = E_{hkl}, *E(k)* = $E_{h'k'l'}$ and *E(h-k)* = $E_{h-h',k-k',l-l'}$. A reflection, *E(h)*, may be involved in a number of triplet relationships, which allows extension beyond the starting set.

In the case of centrosymmetric structures, the phase problem is really a 'sign problem', such that only the correct signs (+ or -) have to be assigned to the reflections. The relationship for a triplet of reflections is given in Equation 2.17, where S is the sign. If the signs of *E(k)* and *E(h-k)* are both positive or both negative, then it is highly probable that *E(h)* will be positive; however, if *E(k)* and *E(h-k)* have opposite signs then *E(h)* is likely to be negative.

$$S(h) \approx S(k) \,.\, S(h-k) \qquad \textbf{Equation 2.17}$$

In the case of non-centrosymmetric structures, the phase angle, ϕ, must be determined, rather than just the sign; a similar phase relationship can be derived (Equation 2.18):

$$\phi(h) \approx \phi(k) + \phi(h-k) \qquad \textbf{Equation 2.18}$$

The tangent formula (Equation 2.19) was derived by Karle and Hauptman, and allows a phase, $\phi(h)$, to be obtained from a large number of triplet relationships:

$$\tan\phi(h) \approx \frac{\sum_k |E(k)E(h\text{-}k)| \sin\left(\phi(k)+\phi(h\text{-}k)\right)}{\sum_k |E(k)E(h\text{-}k)| \cos\left(\phi(k)+\phi(h\text{-}k)\right)} \qquad \textbf{Equation 2.19}$$

In the structure determination process, normalised structure amplitudes, $|E|$, are first calculated from the experimental amplitudes. Phase relationships (triplets) are set up, and a starting set of reflections are chosen for phase determination, focusing on those relating reflections with large *E*-values, as these phases can be estimated with greater reliability, and those *E*-values involved in many triplet relationships. The initial trial phases for the reflections are assigned randomly. An iterative process is carried out, whereby a weighted tangent formula is applied successively to expand and refine the phases. After each iteration, the best phase sets, based on the triplet relationships, are retained; a figure of merit is used as an indication of their quality. The number of phase sets used is reduced after each iteration, until only a few remain. Electron density maps are produced using the best phase sets and the experimental amplitudes, and this gives a series of peaks from which a recognisable part of the structure may be observed, and from this, knowing that the selected phases are correct, the model can then be improved.[183,184]

2.1.5.3 Charge flipping

More recently, a new class of structure solution methods have been developed, called dual-space iterative methods; these methods place constraints in both real and reciprocal space. Charge flipping is the best known of these methods.[191] The charge flipping algorithm requires no knowledge of the structure, and all that is needed is a set of experimental $|F_o|$ values; initially all $|F_o|$ values are assigned random starting phases. A Fourier transform using these random phases results in an electron density map, ρ_1. Next is the charge flipping stage, where the signs of all density points with a value below a certain small, positive threshold, δ, are inverted, giving ρ_2. A set of temporary structure factors are calculated from this, and the phases of the calculated structure factors, F_c, are used along with the experimental $|F_o|$ values in the next iteration to generate ρ_3. This iterative process continues until there is convergence, which is judged according to several criteria. Charge flipping needs no symmetry information and essentially solves the structures in the space group P1; the symmetry can be determined following structure solution using the diffraction pattern intensities along with the electron density reconstructed using the charge flipping algorithm.[191]

2.1.6 Structure completion and refinement

Following structure solution by one of the described methods, a trial structure is obtained where approximate positions have been determined for many of the atoms, but the structure is incomplete. In some cases, some of the atoms may not have been located, and in all cases the trial model is only a first approximation of the real structure. At this stage of the crystal structure determination process, structure refinement is carried out, which involves developing and optimising the trial model to achieve the best possible fit with the experimental data. Refinement is carried out for a number of reasons including: to identify atoms missing from the structure; improvement of the phasing; to assess the validity of a structure; and to obtain the best possible values for structural parameters in the model. Refinement strategies include both Fourier and least-squares methods.

Fourier methods are important for completing the structure, allowing missing atoms to be located. Using the trial model from structure solution, a set of structure factors, F_c, can be calculated using the forward Fourier transform (Equation 2.10), which gives values for both $|F_c|$ and ϕ_c. The calculated structure factor phases, ϕ_c, are used along with the observed structure factor amplitudes, $|F_o|$, to generate Fourier maps (using Equation 2.12); this leads to atoms that are missing in the structure appearing as peaks in the map, resulting in a new model structure. The structure can be further developed in this way (Fourier recycling) and with each cycle the model improves. As the structure nears completion, difference Fourier maps can be generated, where $|F| = |F_o|-|F_c|$ and $\phi = \phi_c$.

Structure refinement by the method of least-squares is most common; the principle asserts that the best fit of $|F_o|$ and $|F_c|$, thus the optimal values of the parameters, minimises the function shown in Equation 2.20, where Y_{obs} is either F_o, F_o^2 or I, and Y_{calc} is either F_c or F_c^2 (to match Y_{obs}). Refinement against F^2 is currently slightly more common, but there are arguments for and against the choice of F or F^2. The weights, w, are chosen to represent the relative influence a particular reflection should have on the results, and typically include a term that represents the statistical error of the data.[184]

$$M = \sum w(Y_{obs} - Y_{calc})^2 \qquad \textbf{Equation 2.20}$$

In a crystal structure determination, the 'refinable parameters' are those which can be varied to improve the fit; the most important parameters are those that describe the positions and vibrations of the atoms, which are the atomic coordinates (x, y, z) and the atomic displacement

parameters (*U* isotropic or six $U_{i,j}$ anisotropic). In addition, there is an overall scale factor, and site occupancies can be refined. For each anisotropic atom there are commonly nine parameters to refine, which include *x*, *y*, *z* and six $U_{i,j}$ values (one for each axis and three cross-terms).

In a typical refinement, the least-squares refinement and Fourier difference map generation is repeated until all non-hydrogen atoms have been located and there is convergence of the positional parameters. Once all of the non-hydrogen atoms have been located, anisotropic displacement parameters can be introduced. At this point, depending on the quality of the data, further peaks may appear in the difference maps, which correspond to hydrogen atom positions; in which case, these can be assigned and refined with isotropic displacement parameters. Sometimes this may require the use of restraints (e.g. distance restraints), resulting in a semi-free refinement. If a hydrogen atom cannot be located or refines poorly then it can be placed in a calculated position and refined as riding on the atom (X) to which it is bound; this fixes the bond distance X-H to a standard value and fixes the isotropic displacement parameters of H to be proportional to X. The riding model means that in the refinement, any shifts are applied to both H and X, thus the bond length and angles remain constant.

Sometimes, the number of parameters that are included in the refinement needs to be decreased or increased. This can be achieved by restricting the refinement, and introducing constraints and/or restraints, which are often necessary in cases where disordered fragments of a structure must be modelled (§2.1.7). Constraints result in the reduction of the number of parameters and are rigid mathematical rules that must be adhered to. There are different types of constraints, including rigid group constraints or constraints for atoms on special positions; riding hydrogen atoms are also constrained. Restraints have the effect of increasing the number of observations. Unlike constraints they are not rigid, and may include restricting bond lengths or angles to expected values based on prior knowledge, or restraining two chemically equivalent bonds to be equal.[174,184]

The refinement process should lead to convergence as the agreement between the model and the experimental data improves. In order to assess how well the model agrees, an R-factor, or residual factor, is used. Since we do not have phases from experiment, the comparison of data is done using the amplitudes of the observed structure factors, $|F_o|$, and calculated structure factors, $|F_c|$ (Equation 2.21). The R-factor is calculated after each refinement cycle, and its value should decrease as the model progresses. Another residual factor used very commonly in crystal structure determination is the weighted R-factor (wR_2), which incorporates weighting factors (Equation 2.22).[183]

$$R = \frac{\sum ||F_o| - |F_c||}{\sum |F_o|}$$ **Equation 2.21**

$$wR_2 = \sqrt{\frac{\sum w(F_o^2 - F_c^2)^2}{\sum w(F_o^2)^2}}$$ **Equation 2.22**

An additional index used to indicate of the quality of the model is the goodness of fit (GooF) (Equation 2.23), where n = the number of reflections and p = the number of parameters. For a correctly modelled structure, the value of S should be close to 1.[184]

$$S = \sqrt{\frac{\sum w(F_o^2 - F_c^2)^2}{n - p}}$$ **Equation 2.23**

In terms of a final model, there are a number of points to consider, some of which are described here. Firstly, the value of R is a good indication that a good model has been achieved; if this is the case then its value should be < 0.05 (Equation 2.21). The model must make chemical sense, with bond lengths and angles taking expected values according to the literature, and atomic displacement parameters should be a sensible size and shape; non-spherical or large ellipsoids may suggest disorder. The final difference electron density map, which will show residual electron density, should have no significant peaks or troughs.

2.1.7 Refinement of molecular disorder

Many of the crystal structures presented in this thesis have molecular disorder present, typically with the molecules disordered over two positions; the disorder can be either symmetry-independent or a result of the molecule being situated on a special position that has higher symmetry than the molecule possesses. There are some good general indicators that point towards disorder in a structure during the refinement stage; these include significant residual electron density, poorly shaped and sized atomic displacement parameters, and distorted geometry. The refinement of disorder is, in theory, relatively simple, in that two sets of atomic coordinates are required for the two positions, along with the relative occupancies of the two sites. From the difference electron density map, it is usually possible to identify one of the molecular conformations with relative ease, but to find the second site can often prove more challenging, especially if the site has a low occupancy. Sometimes a second set of peaks will appear in the map or, if an atom is strongly anisotropic, the output from the refinement program may suggest splitting to give the two possible sites. The atoms of the disordered fragment

should be refined with isotropic displacement parameters prior to the formulation of the disorder, as this makes it easier to locate additional atomic positions from the residual electron density peaks.[174]

In SHELXL,[192] the refinement of disorder makes use of PARTs and the introduction of free variables. PARTs split the atomic coordinates of the disorder into two groups, with each group of atoms corresponding to each component. It is also necessary to refine the occupancies of the two sites and to do this a second free variable is introduced. The site occupancy factors are changed to correspond to the free variable, with the value of the free variable corresponding to the occupancy of the site in PART 1; for example, if the two sites are disordered in a 70:30 ratio, then the free variable will have a value of 0.7. The sum of the occupancies across both sites must be equal to unity. Where the disorder is due to symmetry then the occupancies are given; for example, if the molecule is situated on an inversion centre, then the site occupancy factors are set to 0.5.[174]

The refinement of disorder often requires the introduction of restraints and/or constraints, primarily to ensure a chemically meaningful model; their introduction can also improve the data to parameter ratio. Similarity restraints can be used on chemically equivalent bond lengths and angles to make them take similar values; bond lengths and angles can also be restrained to take expected values. The anisotropic refinement of atoms can often be problematic for the disordered fragments, so similarity restraints can make the ADPs more reasonable. Sometimes, it is necessary to also include constraints in the refinement of the disorder. Some useful constraints include those which force two or more atoms to take the same coordinates or to have equal ADPs; in addition, it is also possible to constrain a set of atoms to take a standard geometry, for example a regular hexagon in the case of a benzene ring. With the aid of restraints and/or constraints, it should be possible to obtain a chemically-sensible and plausible model for the structure; at this stage, it should be possible to refine the atoms of the disordered components with anisotropic displacement parameters. The hydrogen atoms of the disordered fragments should be included, which is usually done by placing them in geometrically calculated positions and refining as riding on the atoms to which they are bound.[174,184]

2.2 Powder X-ray diffraction

While the focus of this work was the determination of crystal structures from single crystal X-ray diffraction data, powder X-ray diffraction (PXRD) was also conducted on some of the samples. The principles and geometry of X-ray diffraction discussed in §2.1.2 also apply to diffraction from polycrystalline powders. In single crystal X-ray diffraction, there is one crystal

and therefore one orientation; to observe diffraction from different sets of planes, the crystal has to be rotated so that the angle, θ, satisfies Bragg's Law. An ideal polycrystalline powder, on the other hand, consists of a very large number of very small crystallites which are randomly orientated with respect to each other, and every possible crystallite orientation should be represented equally (although, in reality, preferred orientation often occurs which is undesirable). At an angle of θ_1, there should be a number of crystallites in the correct orientation for diffraction to occur from a set of planes with lattice spacing, d_1; this gives rise to a cone of diffraction which has a semi-vertex angle of $2\theta_1$. Simultaneously in the sample, at an angle of θ_2 there should be a number of crystallites that are in the correct orientation for diffraction to occur from a set of planes with lattice spacing d_2; these crystallites give rise to a second cone of diffraction with a semi-vertex angle of $2\theta_2$. This applies for every angle over a specified 2θ range, and the result is a set of diffraction cones, with each corresponding to diffraction from different lattice planes.[193]

While the diffraction pattern of a single crystal consists of distinct Bragg reflections, the diffraction cones that result from a powder give rise to a diffraction pattern which consists of a series of concentric rings. If the crystallites are randomly orientated then the rings are uniform in width and intensity. PXRD data is presented as a plot of 2θ against intensity, with each peak corresponding to a particular *d*-spacing; the three-dimensional diffraction data is therefore effectively compressed into one-dimension. The peak positions (2θ) contain information on the crystal class, lattice type and lattice parameters; it is important to note that the peak positions are dependent on the wavelength, and are also shifted depending on the temperature of the sample during the measurement. The peak intensities contain information on the atom types and atom positions in the unit cell; the intensities can be affected by large crystallite sizes and non-random crystallite orientations (preferred orientation).[193]

In this work, powder X-ray diffraction was used as a means of sample identification and to study and follow phase transitions. It is possible to solve crystal structures from powder diffraction data, but there are a number of difficulties associated with this. The main problem is that the data has been compressed into one-dimension in the powder diffraction pattern; this means that there is considerable peak overlap, resulting in a loss of structural information.

2.3 Diffuse scattering

As previously discussed, when X-rays are diffracted from a crystalline solid, discrete Bragg peaks are observed due to the periodic nature of the material; the locations and intensities of these peaks allow us to obtain a crystal structure. However, in reality, crystals are not perfect,

and there can be a departure from periodicity, such that the translational symmetry breaks down. When this is the case, weak diffuse scattering is also observed in the diffraction pattern, between the Bragg peaks. Where diffuse scattering is present, there is often a reduction in the intensities of the Bragg reflections. Diffuse scattering in a diffraction pattern can arise from a variety of sources, and often it is due to a combination of effects making its interpretation highly complex. It may arise as a result of thermal motions, where atoms and molecules are displaced from their average positions; the scattering from this source is termed thermal diffuse scattering. In this work, the diffuse scattering of interest is that which results from static disorder, where different unit cells have different arrangements of the time-averaged atomic positions. If there are correlations of molecules over short length scales (short range order), then structured diffuse scattering is observed. Diffuse scattering contains information about pairs of sites, and thus how atoms and molecules interact; different types of disorder give rise to particular diffraction effects, so the diffuse scattering can vary in type and intensity.[177,180]

Many properties of crystalline materials are often a result of, and dependent upon, the deviations from ideality, thus understanding the diffuse scattering can aid understanding of properties. However, the interpretation and analysis of diffuse scattering features is non-trivial. Most commonly, a Monte Carlo computer simulation is used; utilising chemical knowledge and the average structure, different possible models are constructed where the occupancies and molecular orientations can be varied. The different models can be tested and the calculated diffraction patterns compared with the experimental diffraction patterns; the process is repeated iteratively until a good agreement is obtained. However, this type of analysis is highly complex and requires very high quality diffraction data; diffuse scattering presented in this work is thus interpreted qualitatively.[177,180]

2.4 Differential scanning calorimetry

Differential scanning calorimetry (DSC) is a technique used to study how the heat capacity of a sample changes with temperature. This is determined by measuring the difference in the amount of heat required to maintain a sample pan and reference pan at the same temperature; both pans are heated at a constant rate throughout the experiment using a specified temperature programme. DSC can be used to detect a range of thermal events including melts, crystallisations, phase transitions and glass transitions; the measurements provide both qualitative and quantitative information about changes in the sample. The principle of the technique is that when the sample undergoes a transformation, a different amount of heat will need to be flowed to it than the reference pan in order to maintain both at the same temperature. For an exothermic event such as crystallisation, less heat is required to flow to the sample in

order to increase the temperature; for an endothermic event such as a melt, more heat is required to flow to the sample than the reference. The result of a DSC experiment is a thermogram of heat flow against temperature, with endothermic and exothermic changes corresponding to thermal events (Figure 2.9); where a heat flux instrument is used, as in this work, exothermic events are plotted with a positive heat flow (Exo Up).[194]

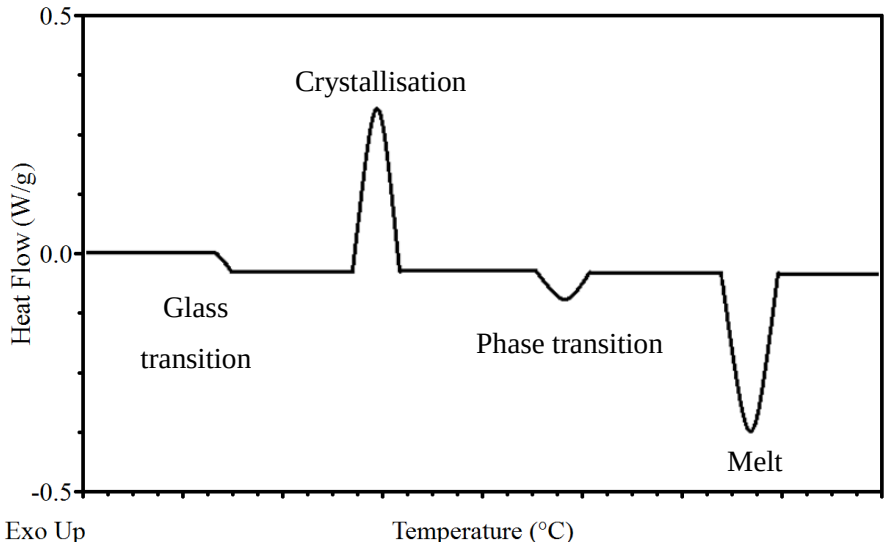

Figure 2.9 Example of a DSC thermogram showing the types of thermal transitions observed in differential scanning calorimetry experiments: a glass transition, crystallisation, phase transition and melt.

2.5 Colour

Visible light is in the region of the electromagnetic spectrum corresponding to the narrow wavelength range of around 380-720 nm; colour is observed when a material absorbs light at a wavelength in this range. When a material absorbs light of a particular colour, it is the complementary colour that is observed, which is a result of the remaining wavelengths of the incident light being scattered.

In organic molecules, which are the focus of this work, an electron can be promoted from a bonding or non-bonding molecular orbital to a higher energy anti-bonding orbital when light of the correct wavelength is absorbed for a particular electronic excitation; possible electronic excitations are shown in Figure 2.10. Of the transitions shown, only two are important with regards to colour, as they typically have energies that are within the wavelength range of the visible spectrum; these are n-π* and π-π*, which are of the smallest energy (and therefore at a longer wavelength). For a π-π* transition, the π-orbital is the highest occupied molecular orbital (HOMO) and the π*-orbital is the lowest unoccupied molecular orbital (LUMO).

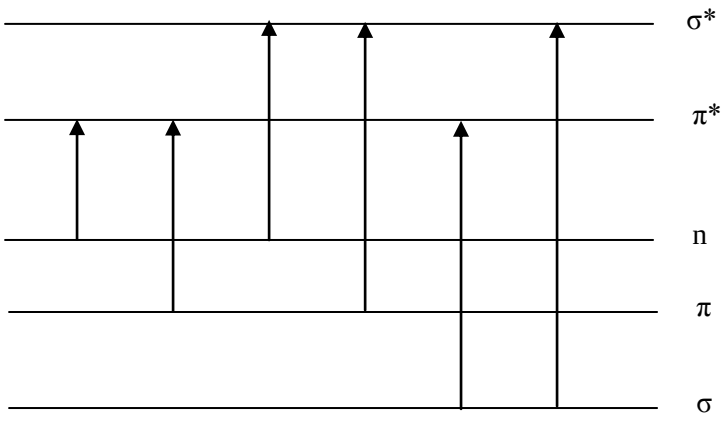

Figure 2.10 Possible electronic transitions in an organic molecule.

The part of a molecule which can be considered responsible for the colour is known as the chromophore; in organic molecules the chromophores are unsaturated linkages, or normally a number of unsaturated linkages. Organic molecules exhibiting colour are conjugated systems so have a number of unsaturated linkages in conjugation resulting in a delocalised system. As the amount of conjugation in a system increases, the energy gap between the HOMO and LUMO decreases, and therefore the spectrum shifts to a longer wavelength and the molecule will be more likely to absorb a wavelength in the visible region of the spectrum. For example, hexa-1,3,5-triene absorbs at a higher wavelength than ethene which only has a single isolated carbon-carbon double bond. The conjugated systems are not limited to linear hydrocarbons; many conjugated π-systems can act as chromophores and absorb in the visible region, including aromatic molecules. As for linear conjugated systems, as the number of aromatic rings in conjugation increases, for example from benzene to anthracene, the spectrum shifts to a longer wavelength.[195]

In binary systems of suitable neutral electron-donor and electron-acceptor molecules, mixed stacks often form. When this occurs, a new charge-transfer (CT) band is often observed in the visible region which is due to electronic excitation from the HOMO π-orbital of the electron-rich component to the LUMO π*-orbital of the electron-deficient component (Chapter 1, §1.5).

CHAPTER 3

Techniques and Instrumentation

3 Techniques and Instrumentation

Chapter 3 details the range of experimental techniques and instruments that were employed in the preparation and characterisation of the materials studied; more specific experimental details will be provided in subsequent chapters where appropriate.

3.1 Crystallisation and crystal evaluation

Due to the nature of the research being undertaken, the main focus of the sample preparation in this work was the growth of good quality single crystals of target molecular complexes, to enable the collection of single-crystal X-ray diffraction data. There are a range of methodologies for the synthesis of single crystals of multi-component materials, with the most flexible and widely used being solution-based methods including slow evaporation, slow cooling and diffusion (liquid-liquid and vapour). All of the molecular complexes studied in this work were obtained *via* slow evaporation of solvent which is probably the most widely used method of crystal growth. Although this is a relatively simple technique there are a number of factors to take in to consideration, including solvent choice, evaporation temperature, and quantities of compound, all of which can be varied to achieve synthesis of the required complex, including its stoichiometry, and optimum crystal growth. Finding the right conditions for obtaining good single crystals of a particular material often involves a certain amount of trial and error.

The same general slow evaporative crystallisation procedure (Figure 3.1, left) was employed for forming each of the molecular complexes. Stoichiometric molar quantities of the two molecular components (typically 10-50 mg of each) were weighed into clean 7 ml glass vials and dissolved using the minimum amount of solvent to form a saturated solution; around 1-3 ml of solvent was normally required. Typically, stoichiometric molar ratios of 1:1 and 2:1 were used, although this did not always dictate that a molecular complex was formed in the same ratio. It was important that the starting materials were completely dissolved, and in some cases it was necessary to gently heat the solutions or use a sonicator to facilitate dissolution. Once dissolved, a plastic lid was used to seal the vial, and perforated to allow the solvent to evaporate slowly; the number of perforations could be altered to control the rate of evaporation. Sample solutions were then left to evaporate free from agitation, as disturbance tends to lead to poorer quality crystals; vials were either kept at ambient temperature or at some other controlled, fixed temperature. Over a period of time, the concentration of the solution increases and supersaturation is achieved resulting in nucleation and, hopefully, single crystal growth. Once product had formed and the solvent had evaporated, the vials were stored at ambient temperature ready for analysis.

The two main variables in the experiments were the solvent and the temperature. Selection of a suitable solvent plays an important role in the outcome of a crystallisation. Prior to setting up the crystallisations, the solubilities of the two starting materials were assessed in a wide range of solvents. Ideal solvents are those in which both components are moderately soluble; sometimes solvent mixtures can be used for manipulation of the solubility. Crystallisation trials employed a range of solvents, including methanol, ethanol, acetonitrile, acetone, isopropanol, diethyl ether and ethyl acetate. The solvent choice is not only important with regards to the solubility of the materials, but can also influence the rate of evaporation due to differences in volatility. It may also affect the product of the co-crystallisation; solvents are sometimes incorporated in the crystal, forming a solvate, and different solvents may also result in different polymorphs of a particular system.

It was also possible to vary the temperature of the sample solution to control the rate of evaporation, which can affect both the crystal size and the crystallisation product; crystallisation trials always employed a range of evaporation temperatures in addition to ambient temperature. To achieve elevated temperatures, crystallisation vessels were placed in specially designed hot-plates (Figure 3.1, right), which were held at fixed temperatures of 30 °C, 40 °C or 50 °C; sample vials could also be placed in the fridge to achieve a temperature of 4 °C and slow the rate of evaporation. Samples were removed from the hot-plates once all the solvent had evaporated, as prolonged heating of the product can result in degradation of the crystals.

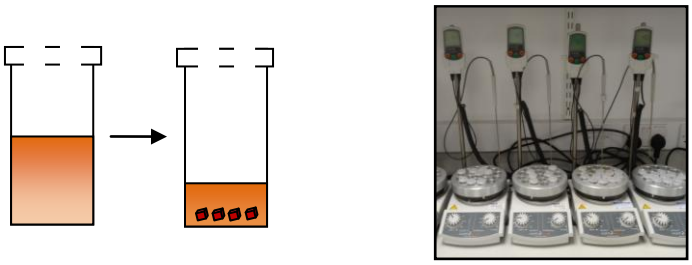

Figure 3.1 Left: Schematic of the crystallisation method of slow evaporation.
Right: Temperature-controlled hot-plates for slow evaporation.

Where single crystals of a target molecular complex were not formed through slow evaporation, other co-crystallisation techniques were explored, including slow cooling and vapour diffusion (Figure 3.2). The method of slow cooling is based on solubility decreasing with temperature. Experiments were carried out in the laboratory using two different instruments, a ReactArray Microvate crystalliser and a Cambridge Reactor Design Polar Bear Plus,[196] which are both programmable for controlled heating and cooling. Near-saturated solutions were prepared, sealed and placed in the crystalliser. Slow cooling experiments were started at a high

temperature and the solution was allowed to cool slowly according to a specified temperature programme. Vapour diffusion uses a binary solvent system; the molecular components were dissolved in a suitable, relatively non-volatile solvent in a small vial. This was placed into a larger vial which contained a volatile anti-solvent in which the molecular components do not dissolve. This larger vial was sealed, and the anti-solvent diffuses through the vapour phase into the solution, thereby reducing the solubility of the molecular complex and causing nucleation and thus crystal growth to occur.

Figure 3.2 Schematics of the solvent crystallisation methods of slow cooling (left) and vapour diffusion (right).

Once the solvent had evaporated it was necessary to assess the result of the crystallisation trial. Evaluation began with a simple visual assessment of the contents of the vial using optical microscopy which can not only determine whether crystals had grown and their general quality, but also whether a new complex had formed or whether there were multiple phases present. Sometimes no single crystals had formed and the vial contained only powder or oil. Different crystalline phases can often be distinguished by their shape and colour. If a single crystalline product has formed then the crystals should all appear uniform; in particular for the research described in this thesis, the individual molecular components are colourless or pale in colour so a coloured material was a good first indication that a new product had formed. If the vial contents are not uniform, and multiple phases are observed, then there are a number of possibilities; most commonly a molecular complex has not formed and the molecular components have instead crystallised separately, or due to the stoichiometry of the crystallisation there are crystals of a new molecular complex alongside crystals of excess starting material. Additionally, sometimes a reaction product had formed or two polymorphs had crystallised concomitantly under the same crystallisation conditions.

After visual assessment of the vial contents, unit cell screening was carried out on suitable single crystals and the unit cell parameters were compared against starting materials and existing molecular complexes in the Cambridge Structural Database (CSD).[86] Where necessary, powder X-ray diffraction was employed to assess the bulk sample, and the diffraction patterns could be compared against those of starting materials or known complexes. If the desired

product had not formed, or not as single crystals, then at this stage the crystallisation conditions or method could be varied to optimise crystal growth. Altering the conditions also allowed investigation of other possible products, for example alterative stoichiometries.

3.2 X-ray diffraction

X-ray diffraction was the principal method of sample characterisation in this work as it provides the most definitive structural information. A combination of single-crystal X-ray diffraction (SCXRD) and powder X-ray diffraction (PXRD) was used, utilising both laboratory and synchrotron sources.

3.2.1 Generation of X-rays

X-rays that are of a suitable wavelength for crystallography can be generated by X-ray tubes (standard sealed and microfocus), rotating anode generators, and synchrotrons. Most routine diffraction experiments are conducted on laboratory instruments, the majority of which are equipped with standard sealed X-ray tubes. In the X-ray tube, a heated tungsten filament (cathode) produces electrons which are accelerated in a vacuum by an electric field towards a metal target (anode). The accelerated electrons collide with the metal target and, if the energy is sufficient, an electron can be ejected from the inner electron shells of the metal atoms. An electron from a higher level can then drop down to fill the vacancy, emitting an X-ray photon. Microfocus sources work in a similar way to conventional X-ray tubes, but the accelerated electrons are focused on a much smaller spot on the anode and a much lower power is required, thus more usable X-rays are produced. This can significantly reduce data collection times and makes it possible to collect data on smaller single crystals in-house.

The X-rays generated (K_α and K_β emissions, depending on the energy level from which the electron drops to fill the inner shell vacancy) are characteristic of the metal target. Laboratory diffractometers typically have either a molybdenum target (Kα Mo, $\lambda = 0.71073$ Å) or a copper target (Kα Cu, $\lambda = 1.54184$ Å), although some diffractometers are dual-source which allows switching between the two types of radiation to suit the sample and experiment. For single-crystal X-ray diffraction, molybdenum radiation is often the wavelength of choice for chemical crystallography for a number of reasons, including lower absorption coefficients, higher resolution data, and more compact diffraction patterns. Copper radiation is preferred if the crystals are small and weakly diffracting, as copper gives stronger diffracted intensities, or if the unit cell is particularly large because the longer wavelength can help to resolve the reflections. Copper radiation is also used for determining the absolute configuration of a light atom

structure. For PXRD, copper radiation is by far the most common for routine analysis due its wavelength being above 1Å; shorter wavelengths (e.g. Mo, Ag) scatter more weakly and result in contraction of the diffraction pattern towards low 2θ, thus more peak overlap.

Synchrotrons are particle accelerators which produce high intensity electromagnetic radiation, whose energy and wavelength ranges between the infrared and X-ray regions. They are far less accessible than laboratory sources, and the cost of generating synchrotron radiation is much greater, but they do offer a number of advantages over laboratory sources. The most important characteristic is the higher brightness; the light is more intense and more highly collimated. Synchrotron radiation is also more coherent, tuneable, highly polarised, has a broader energy spectrum and has a pulsed nature. The process of X-ray generation begins at the electron gun where electrons are produced by thermionic emission; a metal plate (cathode) is heated under vacuum which results in electrons effectively evaporating from the surface. The electrons are packed into 'bunches' which are first fed into the linear accelerator (linac), followed by the booster ring, which both work to accelerate the electrons so they are travelling at close to the speed of light (Figure 3.3). When they have attained a sufficiently high energy (the electrons must be relativistic in order to produce the desired synchrotron radiation), the electrons are injected into the storage ring, made up of alternating straight sections and curved sections to form a ring. In the curved sections, bending magnets force the electrons to follow a circular path. When the moving electrons are deflected from their straight path by the magnets, they produce synchrotron light which is emitted tangentially to the plane of the electron beam. Third-generation synchrotrons (e.g. Diamond Light Source[197]) also use insertion devices (undulators and wigglers) along the straight sections; these are an array of magnets which cause the beam to follow an undulating or wiggling path. The result is an more intense and focused light; in addition, the insertion devices can also be used to fine-tune the wavelength for particular applications. Beamlines are positioned to capture the synchrotron light emitted from the storage ring. A beamline typically has four major sections: the front end (where the light is extracted and channeled into the beamline), the optics hutch (where the beam is filtered and focused), the experimental hutch (where the experimental equipment is housed and the X-rays interact with the sample), and the control cabin (where the experiment is monitored and controlled).

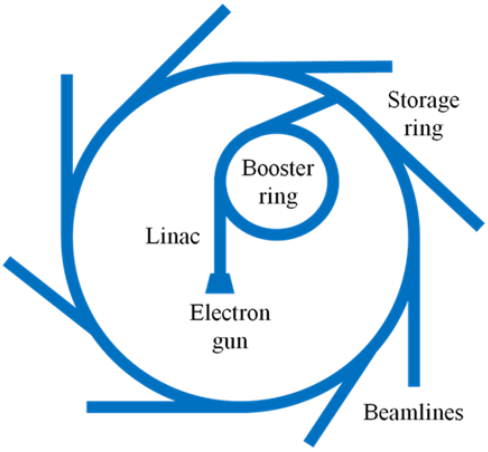

Figure 3.3 Schematic of a synchrotron.

Whether a laboratory instrument or a synchrotron facility is used, the generated X-ray photons have a range of different energies (and wavelengths). Thus before the X-rays reach the sample, X-ray optics produce a focused beam that has a single appropriate wavelength; this can be done using a filter, monochromator or mirrors. In this work, each of the laboratory instruments and synchrotron beamlines were equipped with a monochromator. This uses a crystal mounted in such a way that diffraction from it selects a defined wavelength, λ, according to Bragg's Law. Once a monochromatic beam is achieved, it is passed along a collimator which controls the beam size and ensures the beam is parallel.

3.2.2 Single-crystal X-ray diffraction

All of the crystal structures presented were determined using single-crystal X-ray diffraction, which was conducted primarily using laboratory diffractometers, but synchrotron sources were also used depending on the experimental requirements. The experimental procedure was generally the same for both sources.

Sample selection

A single crystal was selected using polarised light microscopy. For laboratory diffraction experiments, the crystal should ideally be ~0.1-0.4 mm in all three dimensions, although it is possible to work with crystals outside of this size range; at a synchrotron much smaller crystals are used (typically 50-100 μm). If the crystals are significantly larger than required then they can be cut to a smaller size. The crystal should have well defined faces and edges, be free from cracks or defects and uniformly extinguish polarised light with each 90° rotation; if the light is not extinguished throughout the crystal then it is not single. Once a suitable crystal has been selected, it is mounted on the tip of a glass fibre or on a loop attached to the goniometer head

using a perfluoropolyether oil. The chosen sample temperature for the experiment is set and the goniometer head is then placed on the diffractometer; the crystal is carefully centred, by adjustment of the horizontal and vertical positions, to ensure that it does not move out of the X-ray beam as it is rotated during the data collection.

Screening, data collection and data processing

Once the crystal has been selected, mounted and centred on the diffractometer, the process of obtaining crystal data can begin. The first step is the screening of the crystal (or pre-experiment) which involves collecting an initial set of images (typically up to ten frames on a laboratory diffractometer). This allows the quality of the diffraction from the crystal to be assessed, for example whether there is any splitting of reflections and whether the diffraction is strong enough. Using the reflections from the screening images, the orientation matrix and initial unit cell dimensions, Bravais lattice and crystal system can be determined through an indexing procedure; this information is used to decide on the experimental parameters and data collection strategy. The unit cell can also be checked against starting materials and existing complexes. Once the crystal has been deemed suitable, a data collection strategy is then computed to collect the most complete and highest quality data possible in the most efficient way; a number of experimental conditions can be altered as required to achieve specific targets, including resolution (normally 0.8Å) and redundancy (preferably 3-5). Various factors influence the data collection time such as the crystal size, crystal symmetry and X-ray source; the vast majority of experiments are complete within 24 hours, with some collections complete within as little as two hours.

Once the data collection has finished, the data are processed. First, a peak hunting tool is used which locates all of the Bragg reflections across all of the specified frames of data; the peaks are then indexed, whereby the Miller indices of each of the Bragg reflections are determined, and from this the unit cell with the best fit can be assigned. An integration process is then conducted, which adds up all of the pixel counts that are associated with each reflection to give an intensity for each *hkl*; background counts are estimated and subtracted, and initial corrections are applied to the data. The result is a list of Miller indices and their associated intensities, which is the information required to complete the next steps towards obtaining a crystal structure.

Structure solution and refinement

The theory of the crystal structure solution and refinement processes was described in §2.1.5 and §2.1.6. In this work all of the crystal structures of the molecular complexes were solved by

direct methods using the program SHELXS (-97 or -2013).[192] Crystal structures were refined using the least-squares refinement program SHELXL-2014;[198] PLATON[199] was used where necessary to check the space group assignment. All of the programs were used within the WinGX program suite.[200] In general, non-hydrogen atoms were freely refined with anisotropic thermal parameters; hydrogen atoms were treated by a mixture of independent and constrained refinement and always refined with isotropic displacement parameters. Specific refinement details, including disorder modeling and hydrogen atom treatment, are described in the experimental details in subsequent chapters. Crystal structures were viewed and analysed using the structure visualisation program Mercury.[201]

3.2.2.1 Laboratory diffractometers

During the course of the research four different in-house diffractometers were employed for SCXRD experiments: (1) Rigaku Oxford Diffraction[202] (formerly Agilent Technologies) Gemini A Ultra diffractometer, which has a four-circle kappa goniometer and is equipped with an Atlas CCD detector. The diffractometer has a dual sealed tube source (Mo and Cu radiation) and uses a graphite monochromator. (2) Rigaku Oxford Diffraction[202] Xcalibur diffractometer which has a four-circle kappa goniometer and is equipped with an Eos S2 CCD detector. The diffractometer has a sealed tube source (Mo radiation) and uses a graphite monochromator. (3) Rigaku Oxford Diffraction[202] SuperNova diffractometer which has a four-circle kappa goniometer and is equipped with an Eos S2 CCD detector. The diffractometer has dual Mo and Cu high-flux microfocus sources with almost instantaneous switching between the two types of radiation, and uses a graphite monochromator. (4) Rigaku[203] R-AXIS/RAPID diffractometer, which has a four-circle goniometer and is equipped with an image plate detector. The diffractometer has a standard sealed tube source (Mo radiation) and uses a graphite monochromator.

Although each of the diffractometers is slightly different, the general experimental set-up is the same. A typical set-up is shown in Figure 3.4 for the Rigaku Oxford Diffraction[202] Gemini A Ultra diffractometer. The four-circle goniometer with kappa geometry (2θ, φ, ω, κ) allows the crystal to be moved precisely to all the positions required to collect a complete set of diffraction data; the detector can also move which allows the sample-to-detector distance to be altered. For data collection and processing procedures the Gemini, Xcalibur and SuperNova diffractometers use the Rigaku Oxford Diffraction *CrysAlisPro* software package[204] and the R-AXIS/RAPID diffractometer uses the Rigaku *CrystalClear*^{TM} software package.[205] Each diffractometer is equipped with a liquid nitrogen flow device (Oxford Cryosystems Cryostream 700 or Oxford Instruments CryojetXL),[206] which is aligned with the crystal and allows control over the sample

temperature. Standard data collections are routinely carried out at low temperature, normally between 100 and 150 K. However, whilst liquid nitrogen flow devices are predominantly used to cool the sample, they can also be used to heat the sample to carry out variable and high temperature studies.

One of the main differences between the Rigaku Oxford Diffraction[202] Gemini Ultra, Xcalibur and SuperNova diffractometers and the Rigaku[203] R-AXIS/RAPID diffractometer is the detector type; the detector measures an area of diffraction from the crystal. The Gemini, Xcalibur and SuperNova diffractometers are all equipped with a Charge-Coupled-Device (CCD) area detector, while the R-AXIS/RAPID diffractometer is equipped with an image plate detector. The two detector types have advantages and disadvantages, but the CCD area detector is the most common in current laboratory diffractometers.

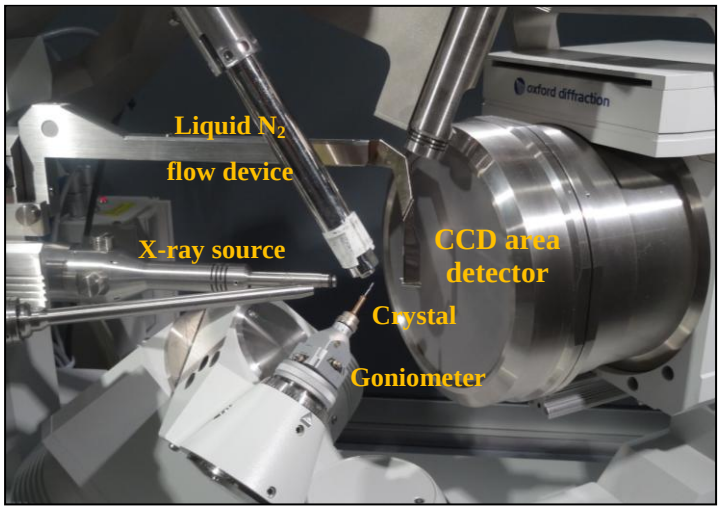

Figure 3.4 Experimental set-up for a laboratory single-crystal X-ray diffraction experiment (shown for the Rigaku Oxford Diffraction[202] Gemini A Ultra diffractometer).

A CCD area detector uses a semiconductor chip that contains an array of many individual photon detectors, or pixels, which are used to build up an image. The first step, after passing the diffracted X-rays through a protective beryllium window, is the conversion of the X-rays to light which is achieved with a phosphor. The light must then be detected, which typically requires a fibre optic taper to reduce the size of the light pattern on the phosphor to match the size of the CCD chip. The chip collects the incoming photons, which are converted to electrons and stored; the number of electrons collected by each pixel is proportional to the intensity of the incoming radiation at each pixel. The information is next converted to a digital format, with the final process being the readout of the associated charge of each pixel, which occurs pixel-wise from the corners of the CCD chip. Although the dynamic range of a CCD area detector is not as

great as that of an image plate detector, CCD area detectors have much faster readout times which is their main advantage.

The main part of an image plate detector is a storage phosphor screen, typically a barium fluorohalide; the plate contains trace amounts of Eu^{2+} and when X-rays are incident on the phosphor this results in the loss of an electron to give Eu^{3+}. The released electrons are captured by F-centres, which are halogen ion vacancies. Once the X-ray exposure is complete, the readout process involves a He-Ne laser scanning across the phosphor which stimulates the release of visible photons from the F-centres; this is known as photostimulated luminescence (PSL). The number of photons released in this process is proportional to the number of F-centres populated by electrons, and thus proportional to the diffracted X-rays reaching the detector. The luminescence is detected by a photomultiplier tube and converted to a digital signal for processing. The readout process is not particularly efficient, so the plate has to be erased by exposure to a light source. The time associated with the readout and erasing process is the main drawback of image plate detectors; however they usually have a large curved active area, a relatively low cost, and a large dynamic range, which makes them useful for measuring weak and strong diffraction simultaneously without saturation of the detector.

3.2.2.2 Synchrotron sources

During this work, two synchrotron facilities were used for the collection of single-crystal X-ray diffraction data: Diamond Light Source[197] on Beamline I19[207] and the Advanced Light Source,[208] Lawrence Berkeley National Laboratory on Beamline 11.3.1. For SCXRD, synchrotrons are often utilised for their high intensity radiation which enables the study of crystals which are very small and of insufficient quality for structure determination on a laboratory source, as well as structurally complex systems where greater detail is required. They are also used for specific types of experiments for example: structural studies using variable temperature or high pressure, studies of metastable species, gas uptake and exchange experiments, charge density studies, and diffuse scattering measurements. Depending on the specific study, the tunability and pulsed nature of synchrotron radiation can be exploited, in addition to the high intensity.

At the synchrotron sources, the experiments carried out in this work utilised either a complementary metal-oxide-semiconductor (CMOS) detector or a hybrid pixel array detector. The CMOS Active Pixel Sensor (APS) detector (e.g. Bruker AXS[209] PHOTON 100), works similarly to CCD detectors, in that a phosphor converts the incident X-rays to light and a chip then converts the light photons to electrons. However, each of the pixels has its own readout

amplifier and therefore the readout is fast and continuous, compared to a CCD detector where the charge is shifted from pixel to pixel until it reaches the readout amplifier. CMOS APS detectors can also be run in shutterless mode, so the sample is constantly exposed to X-rays and continuously rotated, which maximises the efficiency of data acquisition. The second type of detector is the hybrid pixel array detector (e.g. DECTRIS[210] PILATUS 300K), which combines an array of silicon sensor pixels and an array of readout channels which use CMOS technology. X-rays are detected directly without the need for a phosphor and each readout channel is connected to the corresponding pixel, so each photon is detected and counted individually. A hybrid pixel array detector has many advantages including a very high dynamic range, high sensitivity, excellent signal-to-noise ratio, short readout times and shutterless operation.

Beamline I19, Diamond Light Source - Diffuse Scattering

The development of methods to measure, interpret and analyse diffuse scattering has been slow compared to those of conventional structure determination. Diffuse scattering is very weak in comparison to the Bragg peaks which makes the collection of high quality diffuse scattering measurements difficult. Structural models to explain the diffuse scattering are also difficult to construct, and these two factors in combination make the interpretation and analysis quite demanding. However, the inherently low background and high intensity of a synchrotron source enhances the weak diffuse scattering features; in combination with this, the use of a hybrid pixel detector offers a number of advantages. Of particular importance is the very high dynamic range which enables the weak diffuse scattering and the strong Bragg scattering to be collected simultaneously, without the low resolution reflections becoming saturated. Additionally due to the fast readout times and shutterless operation, a whole sphere of data can be collected relatively quickly enabling greater regions of reciprocal space to be measured.

Diffuse scattering measurements were conducted on Beamline I19[207] at Diamond Light Source,[197] which uses Si (111) monochromated radiation (λ = 0.6889 nm). Data were collected in Experimental Hutch 2 (EH2) using a four-circle diffractometer with a DECTRIS[210] PILATUS 300K hybrid pixel detector. The sample temperature was controlled using an Oxford Cryosystems Cryostream Plus.[206] Measurements were conducted at 100 K, unless high temperature phases were being studied, and data were collected over a full sphere at 0.1° or 0.2° oscillations. The data collection process was controlled though the in-house General Data Acquisition (GDA) software. Diffraction images were converted into an Esperanto format and read into the Rigaku Oxford Diffraction software package *CrysAlisPro*[204] which was used for indexing and integration procedures. Using *CrysAlisPro*,[204] reconstructed reciprocal space layers were created to study the diffuse scattering.

Beamline 11.3.1, Advanced Light Source

Variable temperature experiments were conducted on Beamline 11.3.1 at the Advanced Light Source,[208] Berkeley, which uses Si (111) monochromated radiation (λ = 0.7749 nm). Data were collected using a Bruker AXS[209] D8 diffractometer equipped with a Bruker AXS[209] PHOTON 100 CMOS detector; the sample temperature was controlled using an Oxford Cryosystems Cryostream Plus.[206] Data collection and processing procedures were completed using the Bruker AXS APEX2 software.[211]

3.2.2.3 *In situ* heating experiments

Crystals of some molecular complexes had to be heated *in situ* on the diffractometer in order to collect data at high temperature. *In situ* heating experiments were carried out using both laboratory and synchrotron sources, and samples were heated using a liquid nitrogen flow device. A crystal was mounted on a glass fibre using oil only. In some cases it was necessary to protect the crystal from the liquid nitrogen flow. A 0.7 mm borosilicate glass capillary was carefully placed over the mounted crystal, and secured on the goniometer head using wax. The goniometer head was mounted on the goniometer at room temperature, and the crystal was centred as normal. The technique of mounting the crystal in the capillary was also successfully transferred to single-crystal UV-visible absorption heating experiments (§3.4.1).

3.2.3 Powder X-ray diffraction

Powder X-ray diffraction (PXRD) is a rapid, non-destructive solid-state characterisation technique used for both qualitative and quantitative analysis; it can provide a wealth of information and requires very minimal sample preparation. Sometimes powders are the product of a slow evaporation crystallisation and therefore PXRD is necessary for characterisation, but single crystals can also be ground to form a powder for analysis, depending on the purpose of the study. PXRD has a number of applications, but as the diffraction pattern obtained is characteristic of the crystalline material it is most widely used as a means of phase identification (fingerprinting). By comparison against the diffraction patterns of known materials, it can be used to determine whether a new molecular complex has formed or whether the sample contains a mixture of phases (assessment of phase purity), and can distinguish between two or more polymorphs of a system; quantitative analysis of phases in a mixture can also be carried out using the relative peak intensities if the data is of good quality, as can refinement of known structural models using the Rietveld method. PXRD is also used for *in situ* experiments to follow phase transitions and study sample behaviour which is done by collecting diffraction patterns whilst varying the sample environment (e.g. temperature, pressure). Diffraction patterns

can be indexed using specialised software which allows determination of the unit cell lattice parameters of the material. Although challenging, it is possible to solve crystal structures using powder diffraction data. SCXRD is the optimum method for determining the detailed structure of crystalline material, but if suitable single crystals are not formed then the method is not applicable. If PXRD data is of high enough quality and resolution (a synchrotron source is often required), *ab initio* structural elucidation may be successful. The process is non-trivial and far from routine, but considerable advances in more recent years are making it more accessible.

Although powder X-ray diffraction is a powerful technique for the characterisation of materials, with the advantage of using a polycrystalline powder sample, there are some limitations. Compared to SCXRD, a relatively large amount of material is required for the experiment. For identification of an unknown sample, homogeneous and single phase materials are ideal; however, crystallisation trials can often result in a mixture of phases. For fingerprinting, it is necessary to have reference patterns for comparison but this is not always possible.

In this work, PXRD was used to determine whether a new molecular complex had formed, to distinguish between polymorphs, or to study and follow phase transitions (and potentially index unknown phases); no crystal structures were solved or refined from PXRD data. Experiments were conducted on both laboratory and synchrotron sources depending on the experimental requirements, but the general procedures were the same. A sample representative of the bulk was ground using a pestle and mortar to obtain a polycrystalline powder containing a very large number of very small crystallites, ideally randomly orientated. The sample preparation is important as the proportional intensities can be affected when samples contain large crystallites or crystallites with non-random orientations (preferred orientation). The sample was placed in a capillary or prepared for flat-plate analysis, mounted on the diffractometer and centred to ensure the sample stayed in the path of the collimated X-ray beam. The sample remained stationary relative to the incident X-ray beam, but was continuously rotated to minimise preferred orientation effects, and the detector was moved through a defined 2θ range.

3.2.3.1 Laboratory source

Laboratory PXRD experiments were conducted using either capillary or flat-plate mode. Capillary experiments used borosilicate glass capillaries with a diameter of between 0.3-0.7 mm, depending on the sample type and amount of sample available, filled to approximately 40 mm depth and sealed using a flame. For flat-plate experiments a small amount of sample was pressed onto a glass slide ensuring the powder was densely-packed with a smooth, flat surface covering an area of approximately 10 mm^2. Samples were analysed at room temperature with a

Bruker AXS[209] D8 Advance powder diffractometer equipped with a Vantec-1 detector, using graphite-monochromated copper radiation (Cu Kα λ = 1.54184 Å). The capillary or glass slide was mounted on the diffractometer and centred; data were typically collected over the range 2θ = 5-50° with data collections taking approximately 20 minutes (scan rate of ~2°/minute). Qualitative analysis of the powder diffractions patterns was carried out through simple pattern-matching against the powder diffraction patterns of the starting materials, previously analysed samples, and simulated powder diffraction patterns of the structurally characterised molecular complexes. This was done both visually, by simply overlaying the patterns, and through use of the PolySNAP software package[212] which is a suite of cluster analysis and visualisation tools capable of automated high-throughput analysis, and ranks how well patterns match.

3.2.3.2 Synchrotron source

PXRD experiments were carried out at Diamond Light Source[197] on Beamline I11 to study phase transitions in the molecular complexes described in §4.1; full experimental details are given in §4.1.6.1. For PXRD the synchrotron source offers a number of advantages over the laboratory source including, but not limited to, higher intensity X-rays, higher angular resolution, very high signal-to-noise and signal-to-background ratios, faster data acquisition, and greater accessibility to different sample environments. For the study of these particular molecular complexes, the use of the synchrotron meant high resolution diffraction patterns could be collected in combination with variable temperature measurements, with a view to following the phase transitions and indexing the diffraction patterns.

Experiments were conducted on Beamline I11, which uses Si (111) monochromated radiation with an optimised energy of 15 keV (λ ~ 0.826 Å). Powdered samples were loaded into borosilicate glass capillaries with diameters of 0.5 mm or 0.7 mm depending on the sample; the capillaries were filled to between 40-50 mm depth and sealed with glue. The capillary was then placed in a brass holder and secured using glue, and the brass holder screwed into a holder base ready for the data collection (Figure 3.5). Up to 200 samples can be loaded onto the carousel for automated sample changing by the robotic arm, enabling high throughput measurements. For data collection, the magnetic sample holders fit directly to magnetic spinners mounted at the centre of the θ circle face plate. There are two cameras in the experimental hutch with crosshairs to check the alignment of the sample in the X-ray beam. The diffractometer has three co-axial, high precision rotary stages (θ, 2θ and δ), and there are two types of detector available on the beamline (Figure 3.5). The first is a wide angle position sensitive detector (PSD) which is based on Mythen-2 Si strips and is mounted on the δ-circle; this detector is used for high speed scans with an angular coverage of 2θ = 2-100°. The typical collection time for a powder pattern is

milliseconds to minutes. The second type is the multi-analysing crystal detectors (MACs) which are used for high resolution scans. There are five MAC arms located around the large 2θ circle; each consists of nine Si crystals, totaling 45 crystals and photomultiplier based detectors. This results in an angular coverage of 2θ = 0-150°, with a typical collection time for a powder pattern of between 30-60 minutes. The sample temperature is controlled using an Oxford Cryosystems Cryostream Plus,[206] which enables temperatures between 80 - 500 K to be achieved. Control scripts can be written as appropriate, with sequences of commands to ramp the temperature, collect at specified temperatures, move the capillary position, and change the sample.

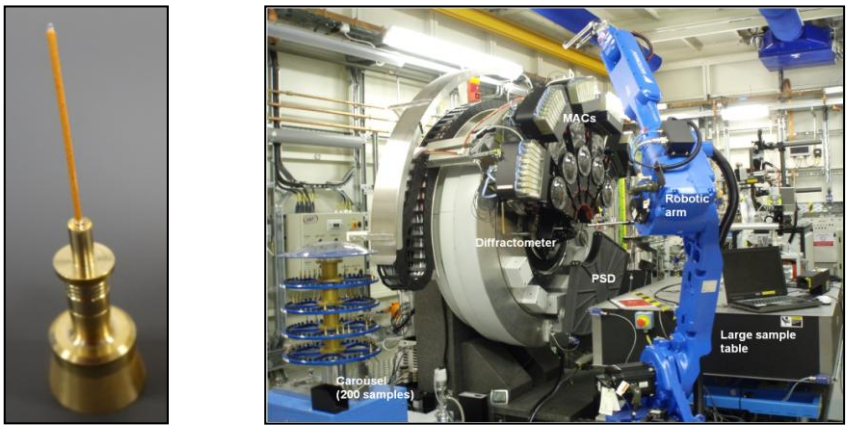

Figure 3.5 A loaded capillary attached to the sample holder and base (left); I11 experimental hutch showing the diffractometer, sample carousel, sample table, robotic arm, PSD and MACs.[197]

3.3 Thermal analysis

Thermal analysis was conducted on the molecular complexes primarily to study temperature-dependent behaviour, but also as a means of quickly identifying the presence of new molecular complexes through determination of a melting point. A combined approach of hot-stage microscopy (HSM) and differential scanning calorimetry (DSC) was used in this work; the information obtained from DSC is greatly enhanced by carrying out simultaneous HSM measurements, and vice-versa. As a visual technique, HSM is particularly useful for confirming the nature of thermal events observed in DSC measurements at a specific temperature, for example distinguishing a phase transition from a melt.

3.3.1 Hot-stage microscopy

Hot-stage microscopy combines microscopy and thermal analysis which enables the study of the physical properties of a material as a function of temperature and time, through visual observations during heating and cooling. The general set-up for the experiment includes a

heating stage and sample chamber, coupled with an optical microscope and a camera which allows videos to be recorded during the heating and cooling processes. Hot-stage microscopy has a number of applications including co-crystal screening, investigation of polymorphism, melting point determination, study of crystallisation processes, and phase transition determination. In this work, HSM was a vital tool for studying the phase transitions and temperature-dependent optical properties of the molecular complexes.

HSM analysis was conducted using a Mettler Toledo[213] FP82 hot stage equipped with a Leica DM1000 microscope. A single crystal of the sample was placed on a slide in the sample chamber and subjected to a temperature program using the FP90 Central Processor. An Infinity 2 camera was mounted on the microscope which allowed the experiment to be recorded. A software package by Studio86Designs[214] enabled video and image capturing using *Studio Capture*, and playback of the recorded videos using *Studio Player* which allowed control of the playback frame rate. In initial screening experiments samples were typically heated using a ramp rate of 5 °C/minute from a start temperature of 30 °C until the sample had melted. To study specific phase transitions the sample was heated and cooled between 30 °C and an end temperature approximately 10 °C above the phase transition temperature.

3.3.2 Differential scanning calorimetry

Differential scanning calorimetry (DSC) experiments were carried out primarily to study phase transitions; the technique was also used to determine melting points, identify new molecular complexes and distinguish between polymorphs. DSC experiments were conducted using a TA Instruments[215] Q20 differential scanning calorimeter. Samples were ground very gently and 1-3mg of the sample was weighed into a Tzero™ aluminium pan and sealed with a Tzero™ aluminium lid using a press; an empty, sealed Tzero™ aluminium pan was used as the reference. Prior to the experiments, the thermal behaviour of the material was analysed using HSM, and a melting point was determined to guide the DSC experiment. In a standard DSC experiment, the sample was heated at a rate of 5 °C/minute; the temperature was allowed to equilibrate at the start temperature (typically between 20 - 40 °C) and kept isothermal for two minutes at the end temperature (~10 °C above the melting point of the sample). The sample was then cooled at a rate of 5 °C/minute back to the start temperature. DSC was also a very useful technique for studying the reversibility or irreversibility of phase transitions, by conducting consecutive heating and cooling cycles on the same sample. The onset temperatures of observed transitions in the sample were determined using the TA Universal Analysis software;[216] the onset temperature is the temperature at which a change in the DSC thermogram occurs and is defined as the intersection of the tangents of the peak with the extrapolated baseline.

3.4 Spectroscopy

3.4.1 Single-crystal UV-visible spectroscopy

Single-crystal UV-visible spectroscopic measurements were carried out on many of the molecular complexes, in particular those that formed as coloured crystals. Absorption spectra were collected using a Hamamatsu UV-Vis light source (tungsten-halogen lamp) and J&M Analytik TIDAS 1 spectrometer. A single crystal of the sample was cut into a thin plate with approximate dimensions of 0.3 mm x 0.3 mm x 0.1 mm. The crystal was mounted, using oil, on a UV-transparent thin film mount inserted into a magnetic goniometer base; this was then placed on a goniometer head and the crystal position was adjusted using a goniometer key to align the crystal in the beam, aided by the use of a camera (Figure 3.6). The orientation of the crystal was adjusted to yield the cleanest and strongest spectroscopic signal. Standard data collections were conducted at ambient temperature using the software Bio-Kine32[217] with absorbance measured in the range 350 - 800nm; thirty spectra were collected and averaged for each sample measurement. For heating experiments, a single crystal was mounted on a glass fibre using oil, and a glass capillary was placed over the crystal to avoid crystal degradation (§3.2.2.3). The sample was mounted at room temperature and heating was controlled using an Oxford Cryosystems Cryostream Plus.[206]

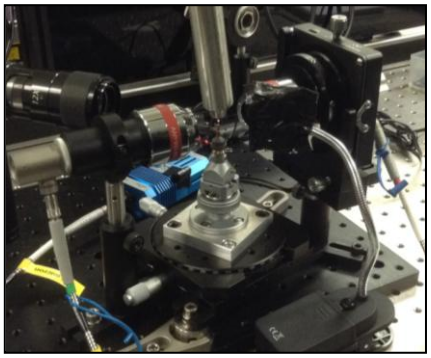

Figure 3.6 Single crystal UV-visible spectroscopy set-up.

3.4.2 FT-IR spectroscopy

FT-IR spectroscopy was conducted on some of the starting materials and complexes, as necessary. Spectra were recorded at room temperature on a Perkin Elmer[218] Spectrum 100 FT-IR spectrometer, using a Universal ATR accessory for sampling; data were collected and processed using Perkin Elmer software Spectrum.

CHAPTER 4

Molecular disorder and thermochromism in haloaniline complexes

4 Molecular disorder and thermochromism in haloaniline complexes

4.1 Introduction

Chapter 4 is concerned with the introduction of molecular disorder as a design tool in multi-component molecular complexes, with a focus on the colour and the thermal behaviour that such disorder facilitates. A series of 2-haloaniline (2-XA) and 2-halo-4-methylaniline (2-X-4-MA) complexes with 3,4-dinitrobenzoic acid (3,4-DNBA) are reported, all of which display molecular disorder of the aniline component. The molecular complexes crystallise in their neutral forms with mixed stack packing arrangements, and are all strongly coloured which is attributed to charge-transfer. Four of the molecular complexes are observed to undergo phase transitions in response to a change in temperature, two of which are thermochromic. This switchable behaviour may be attributed to the additional space available in the packing arrangement due to the presence of molecular disorder, which facilitates the structural rearrangement.

4.1.1 Thermochromism and phase transitions

Thermochromism is the temperature-dependent change in the colour of a material, and can occur in both the solution and solid-states in various types of materials. As discussed in Chapter 1 (§1.8), there are limited examples of organic multi-component thermochromic materials; however, they are ideal systems, with multi-component crystallisation offering potential for tuning properties *via* variations in the intermolecular interactions between the assembled molecular components.

Of the multi-component crystals known to undergo single-crystal to single-crystal (SCSC) thermochromic phase transitions, the colour change is commonly attributed to the transfer of a proton between the two molecular components; two notable examples include the complex of 2-iodoanilinium picrate,[171] upon which this work was based, and the 1:1 adduct formed between squaric acid and 4,4'-bipyridine[99,172] (Chapter 1, §1.8). 2-iodoanilinium picrate has two stable forms at ambient temperature (yellow and green in colour), which are both ionic. Upon heating both forms above 60 °C, a proton is transferred from the NH_3^+ group to the hydroxyl group O-atom, resulting in a neutral charge-transfer complex, which is red in colour. The squaric acid 4,4'-bipyridine adduct also undergoes a thermally induced reversible SCSC phase change associated with a proton transfer across a hydrogen bond. At room temperature, the crystal is pale yellow, but on heating to 180 °C, a colour change from yellow to red is observed which is

the result of proton transfer to give the doubly protonated 4,4'-bipyridine cation and the squarate dianion.

The mobility of molecules within a crystal tends to be limited, but molecules can undergo conformational changes or translational motion, which may result in, for example, topochemical solid-state reactions[219] or polymorphic transitions.[119] In order to preserve the integrity of the single crystal, the overall changes in the crystal structure are typically small, with minimal disruption of the packing arrangement.[220,221] There are very few examples of large structural rearrangements occurring in a single-crystal to single-crystal manner.[222,223]

4.1.2 Molecular disorder

As discussed in Chapter 1 (§1.9.2), disorder can impact the properties of some organic materials, with this suggesting that there is significant scope for utilising disorder as an additional approach for modification of properties. In relation to the work presented here, some organic mixed stack weak charge-transfer (CT) complexes, composed of planar aromatic donors and acceptors, have been reported to incorporate orientational disorder. The CT interactions take precedent over a close packing arrangement, resulting in inefficient packing and orientational disorder of one of the molecules.[105,116,117,224]

In a recent study,[115] a weak CT complex was designed to allow planar molecules to reorient and exhibit a dielectric response to an external electric field. The CT crystals were prepared using tetrabromophthalic anhydride (TBPA) as the electron-acceptor and aromatic hydrocarbons as electron-donors. With the co-former hexamethylbenzene, no orientational disorder of the TBPA molecule was observed; this was rationalised through the formation of a halogen bond, making a single orientation favourable. With the co-formers coronene and perylene, there were no significant intermolecular interactions other than the CT interactions, and the TBPA molecule exhibited dynamic orientational disorder at room temperature, with exchange between the two orientations giving a significant dielectric response. On cooling the perylene complex to 100 K, the TBPA disorder disappeared, and a phase transition characteristic of an order-disorder transition was observed. It was suggested that the dynamic nature of the TBPA molecules in the coronene and perylene complexes at room temperature was a result of the additional free space in the CT crystals, and that the larger donor molecules typically allowed increased mobility and orientation.

There are further examples in which space has been designed into crystalline materials to achieve molecular switching. This concept has been implemented through a supramolecular

approach in the design of ferroelectric molecular materials, where one of the most important design elements is creating sufficient crystal space for molecular rotations. Close-packed systems are clearly favoured in lattice formation, thus careful design of the constituents is necessary in order to design space into the system. Liu *et al.* reported a ferroelectric crystal of (*m*-fluoroanilinium^{+})-(dibenzo[18]crown-6) [Ni(dmit)$_2$] (dmit^{2-} = 2-thioxo-1,3-dithiole-4,5-dithiolate), whose flip-flop motion of the *m*-fluoroanilinium rotator component caused an inversion of the dipole moment in the solid-state.[225] In a follow-up study,[226] a strategy was applied to reduce the energy barrier for the flip-flop motion. [Ni(dmit)$_2$]$^{-}$) salts with supramolecular cations of dibenzo[18]crown-6 and 4-methylanilinium derivatives were synthesised; the introduction of the methyl substituent in the *para*-position resulted in an expansion of the space, reducing the potential energy barrier for the 180° molecular flip-flop motion in the solid-state compared to the *m*-fluoroanilinium derivative.[226]

Investigations into molecular motions with the aim of developing functional materials with desirable properties are so far limited. With suitable choice of molecular components, molecular disorder could be used as a design feature in multi-component organic molecular materials to increase crystal space and freedom to rearrange; with sufficient space, there is the potential for significant molecular movement in response to external stimuli, such as temperature changes.

4.1.3 Design strategy

The thermochromic CT complex of 2-iodoanilinium picrate provided the inspiration for this work; derivatives of the two molecular components were explored, with all retaining similar functional groups (i.e. halogen, NH_2 and NO_2), that are expected to be important for generating the desired optical properties. A search of the Cambridge Structural Database (CSD)[86] was conducted for organic structures containing 2-haloaniline. There are only five reported molecular complexes of 2-haloanilines (2-XA), three of which are 2-haloanilinium picrate complexes, and in each case the molecules are in their ionic forms; there are no structures containing the 2-haloaniline molecules in their neutral forms. Additionally there are no examples of molecular complexes of 2-X-4-MA. In terms of the choice of co-former, the search was focused on dinitrobenzoic acids. There are no known multi-component molecular complexes utilising 3,4-dinitrobenzoic acid (3,4-DNBA); the structure of pure 3,4-DNBA consists of a hydrogen bonded herringbone arrangement of the molecules.

A series of co-crystallisation experiments were conducted on 2-haloanilines (2-XA, where X = I, Br, Cl, F), 2-halo-4-methylanilines (2-X-4-MA, where X = I, Br, Cl) and 2-iodophenol

(2-IP), with the co-former 3,4-dinitrobenzoic acid (3,4-DNBA) (Figure 4.1). The molecular components are all colourless or pale-coloured in their single component forms.

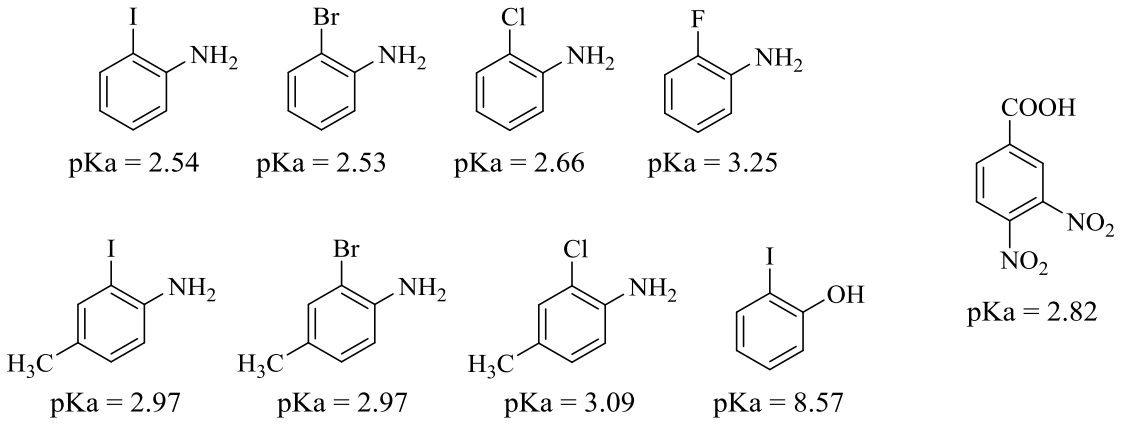

Figure 4.1 Chemical structures of the molecular components used in the multi-component crystallisation experiments in Chapter 4, and their pKa values.[227,228] Top (left to right): 2-IA, 2-BrA, 2-ClA and 2-FA; bottom (left to right): 2-I-4-MA, 2-Br-4-MA, 2-Cl-4-MA and 2-IP; right: 3,4-DNBA.

The ΔpKa values for 3,4-DNBA with the aniline components are either negative or close to zero, which suggests a likelihood of forming neutral molecular complexes. In their neutral forms, the aniline components can all act as aromatic electron-donors, due to the NH_2 substituent being strongly electron-donating; the 3,4-DNBA molecule can act as an aromatic electron-acceptor, due to the nitro groups and carboxylic acid group being strongly electron-withdrawing. This gives the possibility of forming mixed stack CT complexes. In a neutral complex, the 3,4-DNBA molecules would be expected to form homodimers, according to Etter's rules,[40] as the strongest hydrogen bond donors and acceptors are the hydroxyl and carbonyl groups of the carboxylic acid group. Such an interaction would leave only the nitro group O-atoms of 3,4-DNBA available to act as hydrogen/halogen bond acceptors; the O-atoms of nitro groups are relatively poor acceptors when compared to O-atoms bound to carbon.[229,230] The 2-XA and 2-X-4-MA molecules are all bi-functional hydrogen and halogen bond donors, providing the potential for competition between the NH_2 and halogen substituents for the acceptors; furthermore, through simple exchange of the halogen, the strength of the halogen bond interaction can be tuned. The combination of hydrogen bonds and halogen bonds is becoming increasingly important in crystal engineering, and several studies have been carried out concerning the competition between the two. The strength of the hydrogen and halogen bonds is comparable in many cases and they can contribute equally in the assembly of a molecular complex.[26,71]

4.2 Phase transitions in 2-haloaniline 3,4-dinitrobenzoic acid complexes

4.2.1 Experimental details

Molecular complexes **1** - **6** were obtained *via* the method of slow evaporation (§3.1) or upon heating; a 1:2 stoichiometric molar ratio of the 2-haloaniline and 3,4-dinitrobenzoic acid was used. Co-crystallisations were also set up using a 1:1 ratio of the two components, but only 1:2 molecular complexes were obtained. Crystallisation trials employed a range of solvents and evaporation temperatures; the conditions which resulted in growth of the crystals used for collection of SCXRD data are reported here. Single crystal X-ray diffraction experiments were carried out according to the procedures outlined in §3.2.2; crystallographic data are given in Table 4.1 and refinement details are reported in Appendix A4.

2-iodoaniline 3,4-dinitrobenzoic acid, Form I (1)

Molecular complex **1** was synthesised from ethanol at room temperature; dark red block crystals were obtained. Single crystal X-ray diffraction data were collected at 100 K using a Rigaku R-AXIS/RAPID image plate diffractometer. The structure was solved by direct methods using SHELXS-97[192] and refined using SHELXL-2014,[198] both within the WinGX program suite.[200]

2-iodoaniline 3,4-dinitrobenzoic acid, Form II (2)

Molecular complex, **2**, was obtained upon heating; the crystal colour and morphology was very similar to **1**. A single crystal of **1** was heated to 55 °C using a Mettler Toledo FP82 hot stage and, following the conversion to **2**, the single crystal was mounted and flash-cooled to 100 K on the diffractometer. Single crystal X-ray diffraction data were collected using a Rigaku R-AXIS/RAPID image plate diffractometer. Molecular complex **2** was also synthesised by slow evaporation from acetonitrile at 40 °C. Under these conditions the molecular complex grew concomitantly with **1**, but in extremely small quantities and not reproducibly. Single crystal X-ray diffraction data were collected at 100 K using a Rigaku R-AXIS/RAPID image plate diffractometer. The structure was solved by direct methods using SHELXS-97[192] and refined using SHELXL-2014,[198] both within the WinGX program suite.[200]

2-iodoaniline 3,4-dinitrobenzoic acid, Form III (3)

Molecular complex **3** was obtained upon heating; a large crystal of **1** was heated to 90 °C using a Mettler Toledo FP82 hot stage and, following the conversion to **3**, the sample was removed from the hot stage and cooled to room temperature. A smaller single crystal of suitable size and quality was cut, mounted and flash-cooled to 100 K; single crystal X-ray diffraction data were

collected using a Rigaku Oxford Diffraction Gemini Ultra diffractometer (Mo Kα radiation). The structure was solved by direct methods using SHELXS-97[192] and refined using SHELXL-2014,[198] both within the WinGX program suite.[200] Further data collections were also conducted using: Rigaku Oxford Diffraction XCalibur diffractometer at room temperature (no N_2 flow); Rigaku Oxford Diffraction Supernova (Cu Kα radiation) at room temperature (no N_2 flow); Agilent Technologies Supernova (Cu Kα radiation) at 200 K.

2-bromoaniline 3,4-dinitrobenzoic acid, Form I (4)

Molecular complex **4** was synthesised from ethyl acetate at room temperature; dark red block crystals were obtained. Single-crystal X-ray diffraction data were collected at 100 K using a Rigaku R-AXIS/RAPID image plate diffractometer. The structure was solved by direct methods using SHELXS-97[192] and refined using SHELXL-2014,[198] both within the WinGX program suite.[200]

2-bromoaniline 3,4-dinitrobenzoic acid, Form II (5)

Molecular complex **5** was synthesised from acetonitrile at room temperature, with crystal colour and morphology identical to **4**. Crystals of molecular complex **5** grew concomitantly with **4** in extremely small quantities and not reproducibly. Single-crystal X-ray diffraction data were collected at 100 K using a Rigaku R-AXIS/RAPID image plate diffractometer. The structure was solved by direct methods using SHELXS-97[192] and refined using SHELXL-2014,[198] both within the WinGX program suite.[200]

2-chloroaniline 3,4-dinitrobenzoic acid, Form I (6)

Molecular complex **6** was synthesised from acetonitrile at room temperature; dark red block crystals were obtained. Single-crystal X-ray diffraction data were collected at 100 K using a Bruker AXS D8 diffractometer equipped with a PHOTON100 CMOS detector on Beamline 11.3.1 at the Advanced Light Source, Berkeley, USA. The structure was solved by direct methods using SHELXS-2013[192] and refined using SHELXL-2014,[198] both within the WinGX program suite.

Table 4.1 Crystallographic data for molecular complexes **1** - **6**

	1	**2[a]**	**2[b]**	**3**	**4**	**5**	**6**
Formula	(C_6H_6IN) $2(C_7H_4N_2O_6)$	(C_6H_6IN) $2(C_7H_4N_2O_6)$	(C_6H_6IN) $2(C_7H_4N_2O_6)$	(C_6H_6IN) $2(C_7H_4N_2O_6)$	(C_6H_6BrN) $2(C_7H_4N_2O_6)$	(C_6H_6BrN) $2(C_7H_4N_2O_6)$	(C_6H_6ClN) $2(C_7H_4N_2O_6)$
M/g mol^{-1}	643.26	643.26	643.26	643.26	596.27	596.27	551.81
T/K, radiation	100(2), Mo Kα	100(2), Mo Kα	100(2), Mo Kα	100(2), Mo Kα	100(2), Mo Kα	100(2), Mo Kα	150(2), λ 0.7749
Space Group	$P\bar{1}$	$P\bar{1}$	$P\bar{1}$	$P2_1$	$P\bar{1}$	$P\bar{1}$	$P\bar{1}$
a/Å	7.6665(4)	7.7402(6)	7.7254(15)	7.4478(3)	7.6494(7)	7.6563(13)	7.6015(3)
b/Å	12.4731(7)	13.7231(12)	12.688(3)	18.8907(7)	12.9817(15)	7.7638(11)	13.0062(6)
c/Å	13.7392(7)	21.9905(18)	22.024(4)	8.5618(4)	17.434(2)	21.880(4)	17.4679(8)
α	116.045(4)	91.984(7)	91.663(7)	90	91.724(7)	92.400(7)	91.773(3)
β	91.955(3)	91.917(7)	91.836(7)	97.758(4)	94.451(7)	90.266(6)	94.407(3)
γ	98.794(2)	101.475(7)	101.278(7)	90	100.836(7)	118.379(8)	100.700(3)
V/Å	1158.9(1)	2285.8(3)	2281.3(8)	1193.57(9)	1693.4(3)	1142.8(3)	1690.2(2)
Z	2	4	4	2	3	2	3
ρ_{cal}/ g cm^{-3}	1.843	1.869	1.867	1.790	1.754	1.733	1.626
μ/mm^{-1}	1.459	1.480	1.483	1.417	1.900	1.877	0.249
θ Range/°	2.991 - 27.484	3.113 - 27.484	3.037 - 27.485	3.228 - 26.370	3.051 - 27.479	3.025 - 27.484	1.935 - 26.370
Ref Collected	27725	48130	56424	9554	38961	25457	23144
Independent	5283	10374	10384	4173	7697	5188	6909
Observed>2σ	3996	5941	6182	3633	5281	4244	4579
Rint	0.0327	0.0676	0.0563	0.0581	0.0644	0.0588	0.0632
Completeness %	99.8	99.7	99.8	99.7	99.8	99.7	99.8
Parameters	317	635	636	312	483	390	475
Flack parameter	-	-	-	0.516(19)[c]	-	-	-
GooF	1.094	1.094	1.139	1.059	1.113	1.116	1.019
R_1 (obs)	0.0710	0.0816	0.0747	0.0679	0.0525	0.0494	0.0657
R_1 (all)	0.0888	0.1327	0.1145	0.0780	0.0819	0.0624	0.1105
wR2 (all)	0.2086	0.2550	0.2544	0.1787	0.1547	0.1321	0.1678
$\rho_{max,min}$/e Å^{-3}	2.094, -2.470	4.215, -1.059	4.407, -1.719	2.936, -0.894	1.817, -0.605	0.878, -0.811	1.027, -0.652

a = obtained upon heating above the phase transition; b = grown evaporatively; c = the Flack parameter is likely to be unreliable due to the presence of disorder.

4.2.2 Form I: Molecular complexes 1, 4 and 6

Form I of the molecular complexes 2-IA 3,4-DNBA (**1**), 2-BrA 3,4-DNBA (**4**) and 2-ClA 3,4-DNBA (**6**) were all grown reproducibly in large quantities by slow evaporation at room temperature; each generally formed using all of the solvent and temperature combinations. The molecular components of the complexes are all pale in colour; 2-iodoaniline, 2-bromoaniline and 2-chloroaniline are light grey, light brown and light yellow, respectively, and the co-former 3,4-dinitrobenzoic acid is light yellow. Dissolution of the 2-haloaniline and 3,4-DNBA gave solutions that were yellow in colour, with the resulting crystalline molecular complexes all red in colour; the origin of this colour therefore lies solely in the solid-state. Single crystal UV-visible absorption spectra were collected, as outlined in §3.4.1, for Form I of each molecular complex at room temperature. The absorption bands are all very similar in shape and indicative of $\pi\cdots\pi^*$ charge-transfer; there is a very small shift in the band to longer wavelength from **1** to **4** to **6** with absorption below ~570 nm, ~590 nm and ~610 nm, respectively (Figure 4.2).

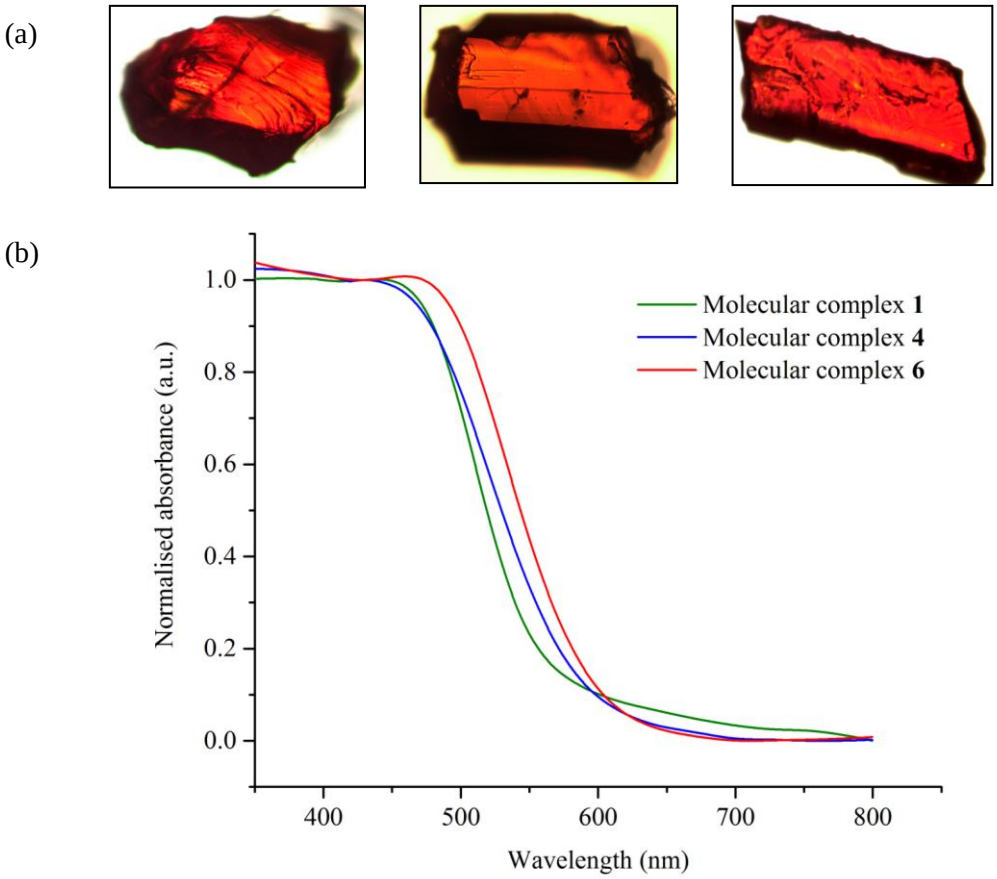

Figure 4.2 (a) Photographs of single crystals of (from left to right) molecular complexes **1**, **4** and **6**; (b) single crystal UV-visible absorption spectra for molecular complexes **1**, **4**, and **6** collected at room temperature.

The molecular complexes crystallise in the triclinic space group $P\bar{1}$; the molecular components are all present in their neutral forms as predicted from the negative ΔpKa values (−0.28, −0.29 and −0.16 for 2-IA 3,4-DNBA, 2-BrA 3,4-DNBA and 2-ClA 3,4-DNBA, respectively). The 2-haloaniline and 3,4-dinitrobenzoic acid crystallise in a 1:2 ratio. Under ambient conditions, molecular complexes **1**, **4** and **6** are isostructural, with the 2-BrA and 2-ClA complexes isomorphous, differing only by the halogen substituent. The asymmetric unit of **1** contains two independent molecules of 3,4-DNBA and two half-occupied 2-IA molecules. The asymmetric units of **4** and **6** contain three independent molecules of 3,4-DNBA, one fully occupied 2-BrA/2-ClA molecule and one half-occupied 2-BrA/2-ClA molecule.

The molecules of 3,4-DNBA form dimers *via* O-H···O hydrogen bonds of moderate strength between the carboxylic acid groups (**a** and **b**, Figure 4.3, Table 4.2); this acid dimer synthon ($R_2^2(8)$ graph-set motif) is commonly observed for carboxylic acids.[40] The C-O bond lengths (1.264(6)/1.273(5) Å and 1.266(6)/1.272(5) Å for molecular complex **1**; 1.269(4)/1.263(4) Å, 1.285(4)/1.247(4) Å and 1.282(4)/1.253(4) Å for molecular complex **4**; 1.252(4)/1.276(4) Å, 1.271(4)/1.258(4) Å and 1.268(4)/1.252(4) Å for molecular complex **6**) are intermediate between distances expected for single and double bonds, which may indicate the presence of proton disorder.[37,39] However, due to the significant molecular disorder of the 2-XA molecules in the complexes, the H-atom positions cannot be reliably determined, thus a model was employed with a single proton position. In each case, the hydrogen atom was located in Fourier difference maps and bound to the C-O group with the longer bond distance; the O-H distance was restrained to be 0.9 Å and the H-atom displacement parameters constrained to $1.5U_{eq}$ of the O-atom to which it is bonded.

In molecular complex **1**, the two 3,4-DNBA molecules of the dimer are not coplanar, with an angle of ~15° between the mean ring planes. In molecular complexes **4** and **6**, two of the independent 3,4-DNBA molecules form a dimer and are close to coplanar, with an angle of less than 1° between the mean ring planes; the third 3,4-DNBA molecule forms a dimer with a symmetry equivalent molecule. The carboxylic acid groups in the molecular complexes are all close to coplanar with the ring planes, with torsion angles of less than 10° (~2°/6° in molecular complex **1**, ~3°/7°/8° in molecular complex **4**, and ~4°/6°/8° in molecular complex **6**). Due to steric effects all of the nitro groups are twisted significantly out of the ring planes (*m*-NO_2 groups by ~14°/29° in molecular complex **1**, ~43°/39°/52° in molecular complex **4**, and ~44°/41°/54° in molecular complex **6**; *p*-NO_2 groups by ~83°/55° in molecular complex **1**, ~44°/41°/28° in molecular complex **4**, and ~40°/44°/29° in molecular complex **6**). The tilt direction of neighbouring *m*- and *p*-NO_2 substituents is always the same, allowing close contacts

to be avoided; variations in the torsion angles across the series do not significantly affect the crystal packing or optical properties.

The 3,4-DNBA dimers are linked through weak C-H···O hydrogen bonds (**c** - **f**, Figure 4.3, Table 4.2) to form an ordered hydrogen bonded tape, as seen in the crystal structure of 3,4-DNBA (CSD[86] refcode: YADKOF).[231] Due to the dimer molecules of **1** being twisted with respect to each other, the C-H···O hydrogen bonds are generally longer than the equivalent bonds in the 2-BrA and 2-ClA complexes. There is also a large difference between the strength of hydrogen bonds **c** and **f** in molecular complex **1**, whereas the two bonds are equal or very close to equal in molecular complexes **4** and **6** (Table 4.2).

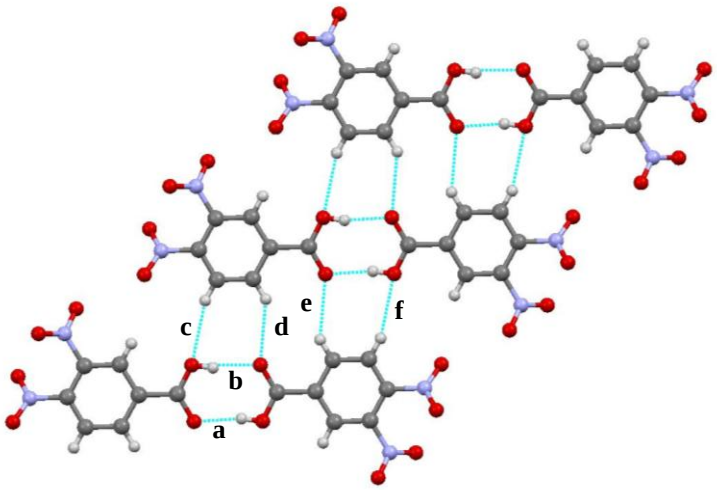

Figure 4.3 Hydrogen bonded tape of 3,4-dinitrobenzoic acid dimers in **1**, **4** and **6**. 3,4-DNBA molecules form dimers through moderate strength O-H···O hydrogen bonds (**a** and **b**); dimers are connected through weak C-H···O hydrogen bonds (**c** - **f**). Hydrogen bond data for **a** - **f** are given in Table 4.2.

Each molecular complex contains two crystallographically independent 2-haloaniline molecules, both of which show whole-molecule disorder over two well-defined positions. In terms of the average structure, the molecular disorder is identical in **4** and **6**; however the disorder in **1** differs in terms of the relative orientations of the 2-IA molecules. The disorder models for each of the 2-haloaniline molecules are average models (Figure 4.4), and in each independent site in the crystal the molecule adopts one of the possible molecular orientations. Single-crystal X-ray diffraction data were collected at 100 K and 295 K on each of the complexes, as well as at a range of temperatures in-between; the models fit the data well at all temperatures, which implies that the disorder is static in nature, rather than dynamic.

Table 4.2 Hydrogen bond data for the 3,4-DNBA network in molecular complexes **1**, **4** and **6** (refer to Figure 4.3 for labels **a** - **f**).

Bond type	D-H···A	D-H	H···A	D···A	<(DHA)
Molecular complex **1**					
a	O8-H8···O1	0.91(2)	1.72(2)	2.628(4)	177(5)
b	O2-H2···O7	0.91(2)	1.72(2)	2.622(4)	175(6)
c	C6-H6···O2_#1	0.93	3.10	3.830(5)	137
d	C7-H7···O7_#1	0.93	2.78	3.561(6)	142
e	C14-H14···O1_#2	0.93	2.56	3.392(6)	145
f	C13-H13···O8_#2	0.93	2.60	3.492(5)	161
Molecular complex **4**					
a, b	O1-H1···O2_#1	0.88(2)	1.76(2)	2.631(3)	171(4)
c, f	C4-H4···O1_#3	0.93	2.60	3.479(4)	158
d, e	C3-H3···O2_#4	0.93	2.57	3.365(4)	143
a	O7-H8···O13_#4	0.91(2)	1.70(2)	2.603(3)	176(4)
b	O14-H9···O8_#4	0.88(2)	1.74(2)	2.616(3)	171(4)
c	C20-H20···O14_#5	0.93	2.56	3.462(4)	162
d	C21-H21···O8_#6	0.93	2.56	3.345(4)	142
e	C14-H14···O13_#6	0.93	2.57	3.357(4)	142
f	C13-H13···O7_#5	0.93	2.56	3.452(4)	162
Molecular complex **6**					
a, b	O14-H14A···O13_#1	0.90(2)	1.73(2)	2.625(3)	179(4)
c, f	C18-H18···O14_#2	0.93	2.56	3.441(4)	15
d, e	C17-H17···O13_#3	0.93	2.56	3.361(4)	144
a	O2-H2···O7	0.93(2)	1.68(2)	2.610(3)	175(4)
b	O8-H8···O1	0.90(2)	1.71(2)	2.606(3)	177(4)
c	C11-H11···O8_#4	0.93	2.53	3.420(4)	161
d	C10-H10···O1_#2	0.93	2.54	3.343(4)	144
e	C7-H7···O7_#5	0.93	2.55	3.343(4)	144
f	C6-H6···O2_#5	0.93	2.54	3.436(4)	161

Molecular complex **1**: #1 x+1,y,z #2 -x+1,-y,-z+1

Molecular complex **4**: #1 -x+2,-y,-z+1 #2 x+1,y,z #3 -x+3,-y,-z+1 #4 -x+2,-y+2,-z #5 x-1,y,z #6 -x+1,-y+2,-z

Molecular complex **6**: #1 -x+2,-y+1,-z+1 #2 x+1,y,z #3 -x+3,-y+1,-z+1 #4 x+1,y,z #5 x-1,y,z

Note: Aromatic H-atoms were placed in calculated positions.

In **1**, the two independent 2-IA molecules lie on inversion centres and therefore the ratio of the occupancies of the two possible orientations is 50:50 in each case; the relative positions for the disorder in both sites are very similar (Figure 4.4 (a)). In **4** and **6**, the two independent 2-haloaniline molecules have different disorder models. One molecule of 2-BrA/2-ClA has symmetry-independent disorder with occupancies of 0.905(1):0.095(1) in **4** and 0.876(2):0.124(2) in **6** (shown in green and pink, respectively, Figure 4.4 (b)); the second molecule of 2-BrA/2-ClA lies on an inversion centre and the ratio of the occupancies is 50:50 (shown in orange and blue, Figure 4.4 (b)). There are also significant peaks in the electron density map observable in the region of the second 2-BrA molecule in **4**, suggesting a more complex disorder model, however it has not been possible to resolve this due to the very low occupancy (approximately 7%).

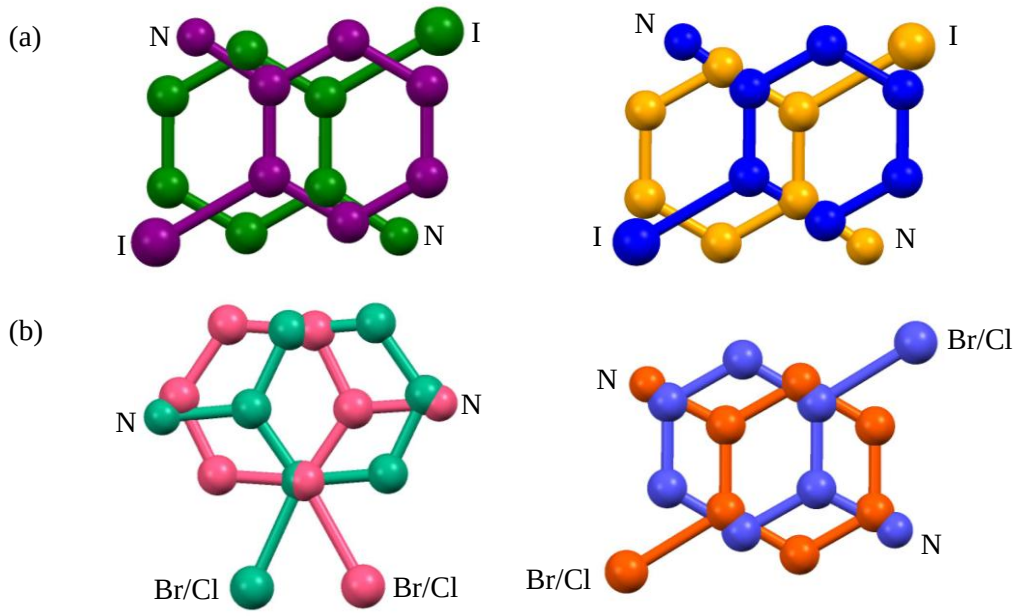

Figure 4.4 The molecular disorder of the two independent 2-haloaniline molecules in (a) molecular complex **1**, where disorder occupancies are 50:50 for both, and (b) molecular complexes **4** and **6**, where disorder occupancies are ~90:10 (green/pink) and 50:50 (blue/orange). Hydrogen atoms have been omitted for clarity.

The ordered 3,4-DNBA tapes form a framework which contains channels that are occupied by the disordered 2-haloaniline molecules. The 2-XA molecules interact with the dimers *via* a combination of hydrogen and halogen bonding interactions; the formation of these favourable interactions for the two orientations further implies the static nature of the disorder. The interactions vary depending on the nature of the halogen and the orientation of the 2-haloaniline molecule within the channel (Figure 4.5). Due to the high level of disorder in the complexes, only the donor-acceptor distances are reported (Table 4.3).

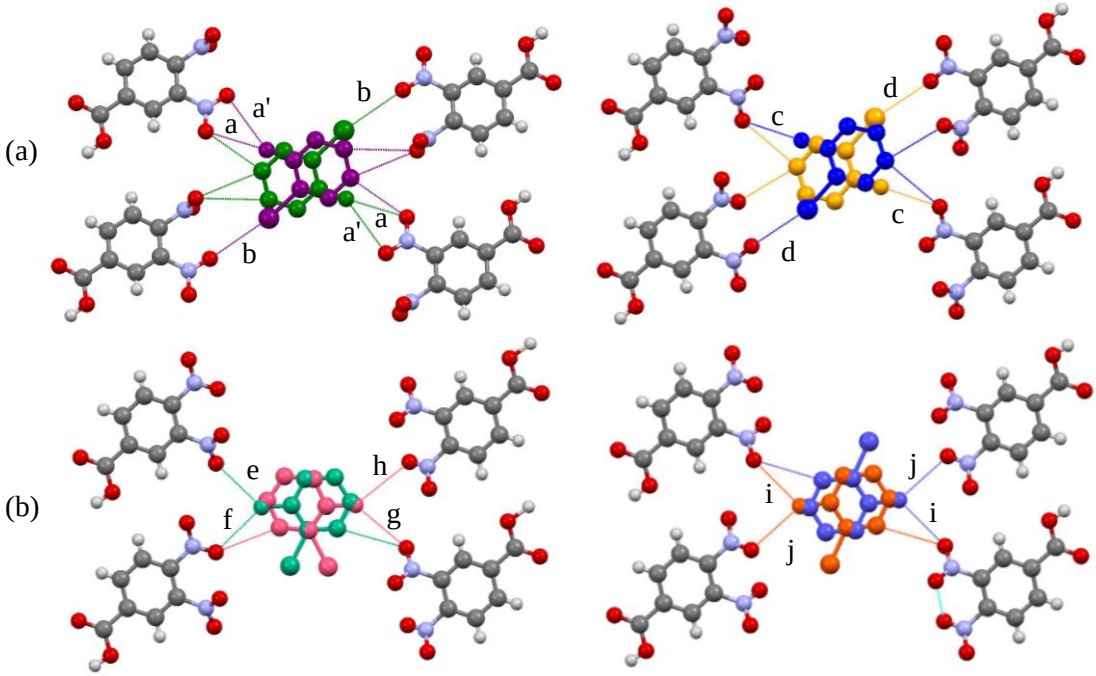

Figure 4.5 Selected intermolecular interactions between the 2-haloaniline molecules and the 3,4-dinitrobenzoic acid molecules in (a) molecular complex **1** and (b) molecular complexes **4** and **6**. Hydrogen atoms of 2-XA molecules have been omitted for clarity. Donor-acceptor distances for **a**-**j** are given in Table 4.3.

In molecular complex **1**, in each site the interactions are identical for the two possible orientations of 2-IA as the molecules are situated on inversion centres. The amine groups interact with oxygen atoms of the *m*-nitro group of one of the 3,4-DNBA molecules through moderate strength hydrogen bonds (**a**, **a'** and **c**, Figure 4.5 (a), Table 4.3). Iodine atoms interact with an oxygen atom of another *m*-nitro group through C-I···O halogen bonds (**b** and **d**, Figure 4.5 (a), Table 4.3), with I···O distances of 3.15(4) Å and 3.34(4) Å (c.f. the sum of the van der Waals radii of I and O of 3.53 Å). There are also weak C-H···O hydrogen bonds between aromatic H-atoms of 2-IA and the nitro group O-atoms of 3,4-DNBA (C···O distances range between ~3.3 and ~3.5 Å). There are no interactions between 2-IA molecules within the channels.

In molecular complexes **4** and **6**, the interactions are very similar for the two molecular sites and for both orientations (Figure 4.5 (b)). The amine groups interact with oxygen atoms of the *m*- and *p*-nitro groups of 3,4-DNBA molecules through moderate strength hydrogen bonds (**e**-**j**, Figure 4.5 (b), Table 4.3). The strength of these interactions are the same in **4** and **6**. For the orientation with the minor occupation (shown in green), hydrogen bond **h** is weak in comparison to **e** and **f** (major occupation), which is a possible explanation for the difference in occupancies. There are also weak C-H···O hydrogen bonds between aromatic H-atoms of the

2-XA and the nitro group O-atoms of 3,4-DNBA (C···O distances range between ~3.3 and ~3.4 Å). Due to the Br/Cl atoms being directed within the channel, there are no interactions between the halogen atoms and the 3,4-DNBA network. For the molecule shown in green/pink, there are C-H···X hydrogen bonds within the channels, between the aromatic hydrogen atoms and the halogen atom; the C···X distances range between ~3.45 Å and ~3.75 Å. For the molecule shown in orange/blue, there are no interactions within the channel; adjacent molecules must have the same orientation to avoid close halogen contacts (Br···Br = 2.567(4) Å, Cl···Cl = 2.658(3) Å).

Table 4.3 Bond donor-acceptor distances for selected intermolecular interactions between the 2-haloaniline molecules and the 3,4-DNBA framework in molecular complexes **1**, **4** and **6** (refer to Figure 4.5 for labels **a**-**j**).

Bond type	**D-H···A or D···A**	**d(D···A)/ Å**
Molecular complex **1**		
a, a'	N-H···O	3.13(2), 3.18(2)
b	I···O	3.34(4)
c	N-H···O	2.95(2)
d	I···O	3.15(4)
Molecular complex **4**		
e	N-H···O	3.20(5)
f	N-H···O	3.14(5)
g	N-H···O	2.94(3)
h	N-H···O	3.57(3)
i	N-H···O	3.02(1)
j	N-H···O	3.21(1)
Molecular complex **6**		
e	N-H···O	3.19(5)
f	N-H···O	3.13(5)
g	N-H···O	2.93(3)
h	N-H···O	3.57(3)
i	N-H···O	3.08(1)
j	N-H···O	3.19(1)

The disordered 2-XA molecules and the ordered 3,4-DNBA tapes form a two-dimensional sheet structure. In molecular complex **1**, a single sheet type is formed, which incorporates both of the independent 2-IA molecules in alternating channels across the sheet (Figure 4.6 (a)). In molecular complexes **4** and **6**, there are two sheet types formed, A and B, with each sheet incorporating channels of one of the independent disordered 2BrA/2ClA molecules (Figure 4.6 (b)). Sheet A contains the 2-BrA/2-ClA with symmetry-independent disorder (shown in green and pink), whilst sheet B contains the 2-BrA/2-ClA disordered by inversion (shown in orange and blue). In each molecular complex, the sheets are stacked forming a layered structure. The two independent sheets in **4** and **6** have an AABAAB stacking arrangement; there are twice as many of sheet A than sheet B.

In each molecular complex, a mixed stack structure is formed. The sheets are staggered such that stacking occurs between alternating 2-haloaniline molecules and 3,4-DNBA dimers, due to the 1:2 ratio of the molecules i.e. one 2-XA to each 3,4-DNBA dimer (Figure 4.6). The stacked 2-XA molecules and 3,4-DNBA dimers are close to parallel, with an angle of ~1° between the mean planes. The 2-XA molecules and 3,4-DNBA dimers stack through aromatic donor···acceptor interactions and halogen···π interactions; there are also $O_{nitro}\cdots O_{nitro}$ and $O_{nitro}\cdots$ π interactions between 3,4-DNBA molecules in adjacent sheets. There are very similar approximate stacking distances of ~3.40 Å, ~3.35 Å and ~3.35 Å between stacked 2-IA molecules and 3,4-DNBA dimers in **1**, **4** and **6**, respectively.

In molecular complex **1**, there are two types of stacking and molecular overlap (**i** and **ii**, Figure 4.7 (a)); the stacking is the same above and below each independent 2-IA molecule, and for both molecular orientations, as they are situated on inversion centres (the stacking is shown for one of the orientations for each site, Figure 4.7 (a), right). In molecular complexes **4** and **6**, there are three types of stacking and molecular overlap (shown by stacking types **iii**, **iv** and **v**, Figure 4.7 (b)); for the molecule with symmetry-independent disorder (green and pink), the stacking is different above and below the molecule, and differs with molecular orientation (**iii** and **iv**, Figure 4.7 (b), right). For the molecule disordered by inversion (orange and blue), the stacking is the same above and below each 2-BrA/2-ClA molecule, and for both orientations (**v**, Figure 4.7 (b), right; the stacking is therefore only shown for one of the orientations).

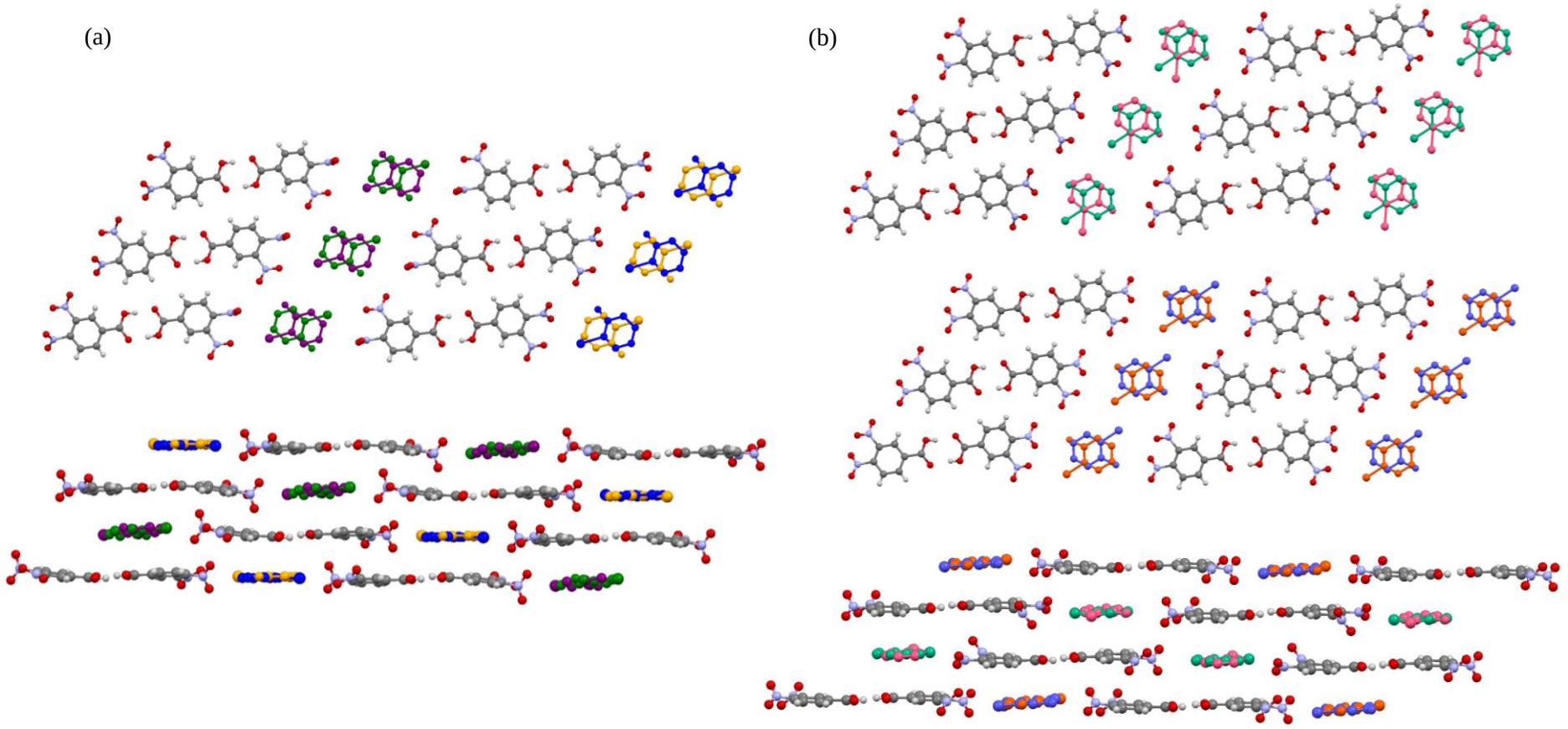

Figure 4.6 Two dimensional sheet structures (top) and stacking of sheets (bottom) in (a) molecular complex **1**, where a single sheet incorporates channels of both of the independent 2-IA molecules and (b) molecular complexes **4** and **6**, where there are two sheet types, with each incorporating a single 2-BrA/2-ClA molecule.

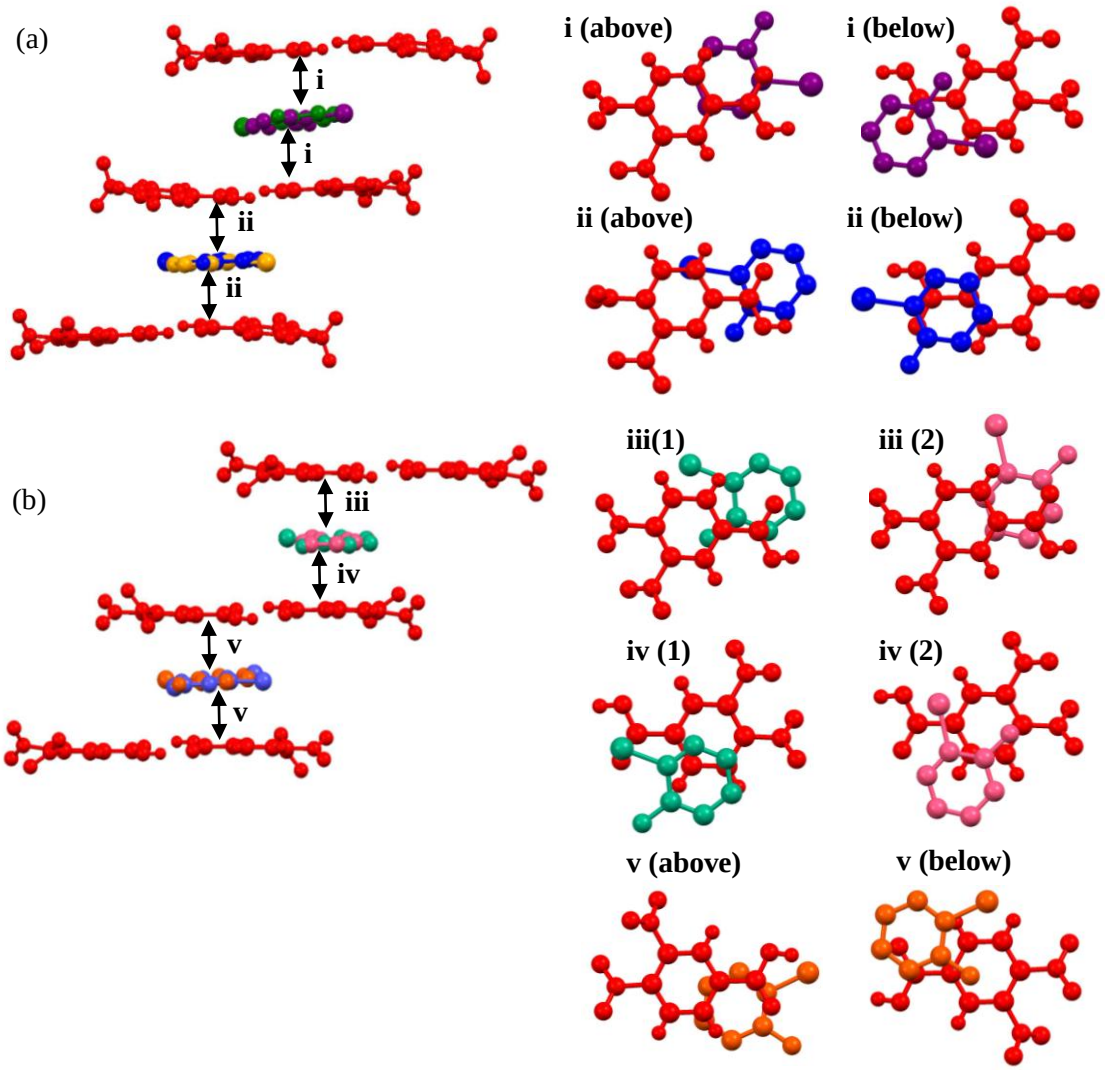

Figure 4.7 (a) Stacking in molecular complex **1** (**i** and **ii**); the molecular overlap is the same for both possible orientations in each site and is therefore only shown for one orientation above and below. (b) Stacking in molecular complexes **4** and **6** (**iii**, **iv** and **v**); the molecular overlap differs for the two orientations (1 and 2) shown in green and pink but is the same for both possible orientations shown in orange and blue and is therefore only shown for one orientation above and below. 3,4-DNBA molecules are shown in red and the disordered 2-XA molecules are shown in the colours according to Figure 4.4.

In all three molecular complexes, the stacking distances are very similar (3.35 Å to 3.40 Å) and the rings of the stacked 2-XA and 3,4-DNBA molecules are offset, with very little ring overlap. Additionally, the amount of molecular overlap for each 2-XA site is similar or the same for both possible orientations of the disordered molecule. In molecular complex **1**, there is significant overlap of either the 2-IA ring or the I-atom with the centre of the 3,4-DNBA dimer; the molecular overlap is very similar for both of the 2-IA sites (Figure 4.7 (a)). In molecular complexes **4** and **6**, the 2-XA molecules are slightly more aligned with the 3,4-DNBA rings, particularly for the site with symmetry-independent disorder (shown in green and pink), but the most significant overlap is still with the carboxylic acid groups. The halogen atoms only overlap with the dimer centres in the site with symmetry-independent disorder.

The colours of the three molecular complexes are very similar, as observed visually and in the visible absorption spectra (Figure 4.2). The red colour in the solid-state can be attributed to $\pi\cdots\pi^*$ charge-transfer between the stacked molecules. The crystal packing in the complexes is dominated by the aromatic donor⋯acceptor interactions, with the amount of molecular overlap similar for both possible orientations of the disordered 2-XA molecules; the hydrogen bonding between 2-XA and 3,4-DNBA in the sheets is only moderate to weak in nature.

4.2.3 Thermal behaviour and optical properties

Molecular complexes **1**, **4** and **6** all exhibit significant temperature-dependent behaviour, undergoing a series of phase transitions on heating. The transitions were identified through a combination of hot-stage microscopy (HSM) and differential scanning calorimetry (DSC) experiments, carried out according to the procedures detailed in §3.3. High resolution powder X-ray diffraction experiments were also conducted on the molecular complexes, which allowed the phase transitions to be followed *in situ* as they occur (§4.2.6). The thermal behaviour is similar in all three complexes and directly related to the exchange of the halogen coupled with molecular disorder. The phase transition temperatures increase with decreasing formula mass i.e. from **1** to **4** to **6**; this must be due to the halogen type (size and intermolecular interactions) as this is the only difference between the complexes. Consequently, molecular complexes **1** and **4** exhibit two phase transitions prior to the melt, while in molecular complex **6** there is just a single phase transition before melting.

The first phase transition in each molecular complex can be observed by HSM, and is a single-crystal to single-crystal transition; this second phase will be referred to as Form II. The transition corresponds to a jump in the crystal position and a very small change in the shape of the crystal, although the change in **6** is very small. The transition temperatures for **1**, **4** and **6** are 52 °C, 65 °C and 90 °C, respectively. Upon further heating, molecular complexes **1** and **4** undergo a second phase transition, at 85 °C and 95 °C respectively, which occurs with survival of the single crystal; this third phase will be referred to as Form III. For 2-IA 3,4-DNBA, **1**, the second transition is thermochromic, and is associated with a distinct change in colour from red to yellow (Figure 4.8) which was observed by HSM; additionally, there is a significant jump in the crystal position and change in crystal shape. Visually, there is no apparent change in colour in 2-BrA 3,4-DNBA, **4**, but there is a jump in the crystal position and a change in the crystal shape. No further transitions were observed in molecular complex **6** prior to melting. The crystals of the 2-IA, 2-BrA and 2-ClA complexes were observed to melt at 107 °C, 114 °C and 110 °C, respectively.

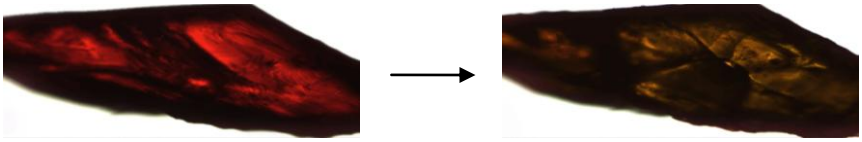

Figure 4.8 Thermochromic phase transition observed in the molecular complex of 2-IA 3,4-DNBA (Form II to Form III) upon heating to 85 °C using hot-stage microscopy.

Despite the apparent similarities in the thermal behaviour of the three molecular complexes, the reversibility of the phase transitions differs considerably. The two phase transitions in molecular complex **1** are both irreversible, and the molecular complex therefore remains in the new phase(s) on cooling to room temperature. In molecular complexes **4** and **6** the phase transitions occur reversibly and repeatedly over multiple heating and cooling cycles, with conversion back to Form I on cooling back to room temperature. This behaviour was determined through a combination of thermal analysis and X-ray diffraction.

DSC cycling experiments clearly demonstrate the irreversible (**1**) and reversible (**4** and **6**) nature of the phase transitions. Experiments were conducted on a TA Instruments Q20 DSC, as outlined in §3.3.2 with a ramp rate of 5 °C/minute; in each experiment the final temperature was chosen to be above the temperature of the final phase transition but below the melting point. Molecular complex **1** was heated and cooled between 20 °C and 93 °C for a total of two cycles (Figure 4.9 (a)). In the first cycle there are two endothermic events corresponding to the phase transitions to Form II and Form III with onset temperatures of 52.7 °C and 84.9 °C, respectively; the transition temperatures closely match those observed in HSM experiments. In Cycle 2 there are no thermal events on heating and cooling within the same temperature range, which indicates that there was no transition back to Form I, and the molecular complex remained as Form III. A similar experiment was also carried out with a final temperature of 60 °C, to investigate the first phase transition only. The same irreversible behaviour was observed and the molecular complex remained as Form II on cooling, with no thermal events observed in the second heating and cooling cycle.

Molecular complex **4** was heated and cooled between 20 °C and 100 °C for a total of four cycles (Figure 4.9(b)). On heating, two endothermic events are observed in each of the four cycles, corresponding to the first and second phase transitions, demonstrating the reversible behaviour of the phase transitions. There is a slight hysteresis with the forward transitions, with the onset temperatures of the phase transitions in Cycle 1 slightly higher than in cycles thereafter. In the first cycle, the onset temperatures for the transitions to Form II and Form III are 66.4 °C and 91.7 °C, respectively; this compares to 61.5 °C and 89.9 °C in subsequent cycles. Exothermic events are also observed on cooling with onset temperatures of 66.1 °C and 25.8 °C

corresponding to the reverse transitions back to Form II and Form I, respectively. A similar experiment was also carried out to investigate the first phase transition only, with two heating and cooling cycles between 20 °C and 80 °C. The same reversible behaviour was observed and the molecular complex converted back to Form I on cooling.

Molecular complex **6** was heated and cooled between 20 °C and 93 °C, for a total of two cycles (Figure 4.9 (c)). The single phase transition in **6** is fully reversible and there is a slight hysteresis evident. On the first cycle, the phase transition to Form II occurs at an onset temperature of 90.7 °C, compared to 86.6 °C in the second cycle. In addition, there is an exothermic peak on cooling, with an onset temperature of 49.4 °C, which corresponds to the transition back to Form I.

SCXRD experiments were used to confirm which phase was present following a single heating and cooling cycle. A single crystal of each complex was heated using the hot-stage to just above each phase transition temperature; the single crystals were then cooled back to room temperature and mounted on the diffractometer at 100 K. One single crystal of molecular complex **1** was heated to 57 °C and a second single crystal to 90 °C; the unit cell parameters corresponded to the new phases, Form II and Form III, respectively. Single crystals of molecular complex **4** were heated to 70 °C and 100 °C; a single crystal of **6** was heated to 95 °C. The unit cell parameters matched Form I after heating and cooling, demonstrating the reversibility of the transitions. For all molecular complexes, the unit cell screening experiments also confirmed that the phase transitions occurred in a single-crystal to single-crystal manner, with strong diffraction and clear spots observed after heating and cooling *via* HSM.

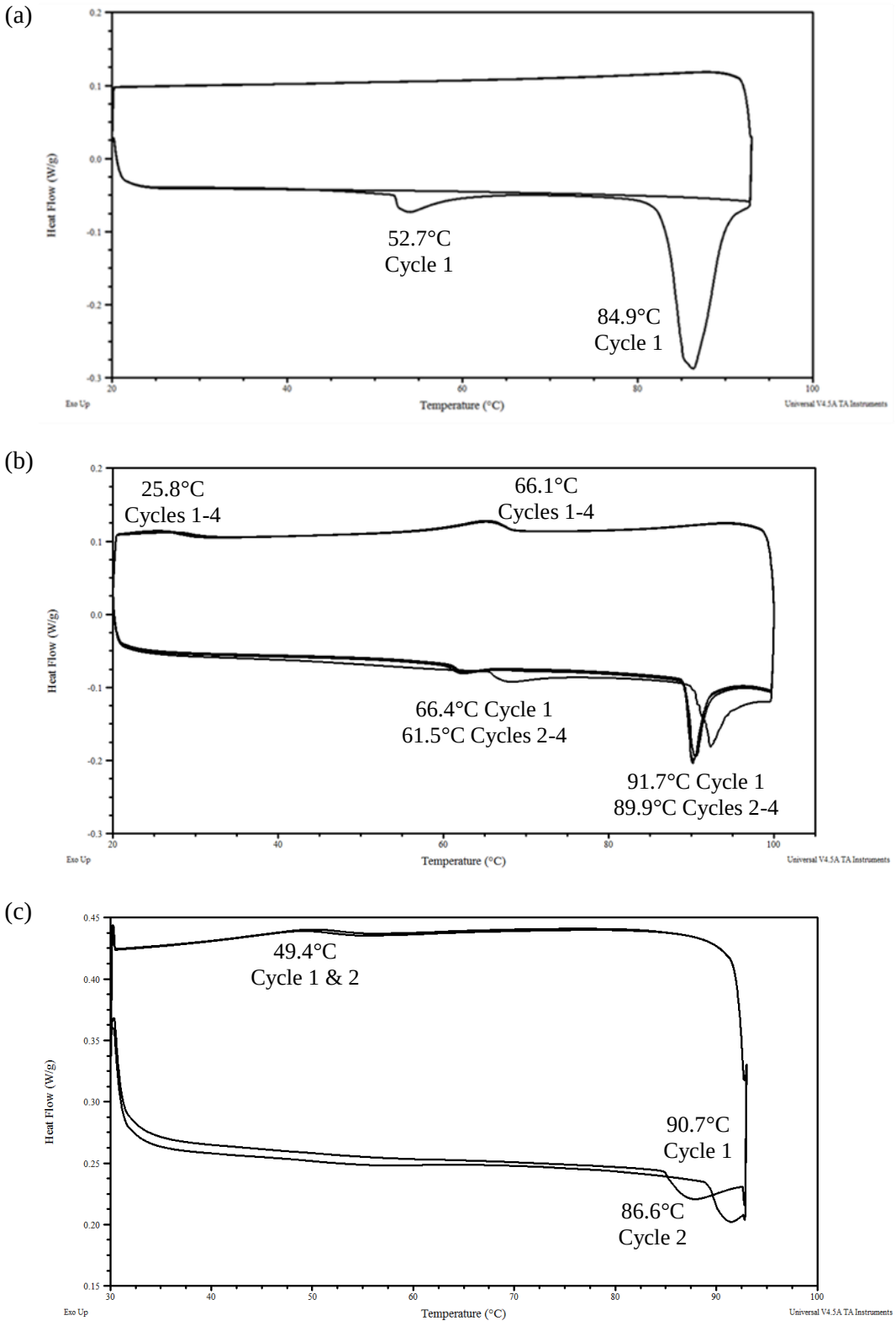

Figure 4.9 DSC thermograms for (a) molecular complex **1**, showing the endothermic peaks corresponding to transitions to the two irreversible phase transitions; (b) molecular complex **4**, showing the endothermic and exothermic peaks corresponding to the two forward and reverse phase transitions; (c) molecular complex **6**, showing the endothermic and exothermic peak corresponding to the single forward and reverse phase transitions. Reported temperatures are the onset temperatures of the phase transitions.

Single-crystal UV-visible spectroscopy was carried out, as outlined in §3.4.1, on molecular complexes **1** and **4**. The close proximity of the phase transition and melt in molecular complex **6** meant that it was not possible to record UV-visible absorption spectra after the phase transition had occurred. Single crystals of **1** and **4** was heated using a cryostream and spectra were collected every 5 K from 300 K to a final temperature of 380 K. In **1**, there is only a small change in the spectrum following the first phase transition (measurement at 340 K, Figure 4.10); however, on undergoing the phase transition to Form III, there is a significant shift of the charge-transfer absorption band to shorter wavelength, with absorption below 540 nm, which is consistent with the colour change from red to yellow observed in the hot-stage microscopy experiment (measurement at 370 K, Figure 4.10).

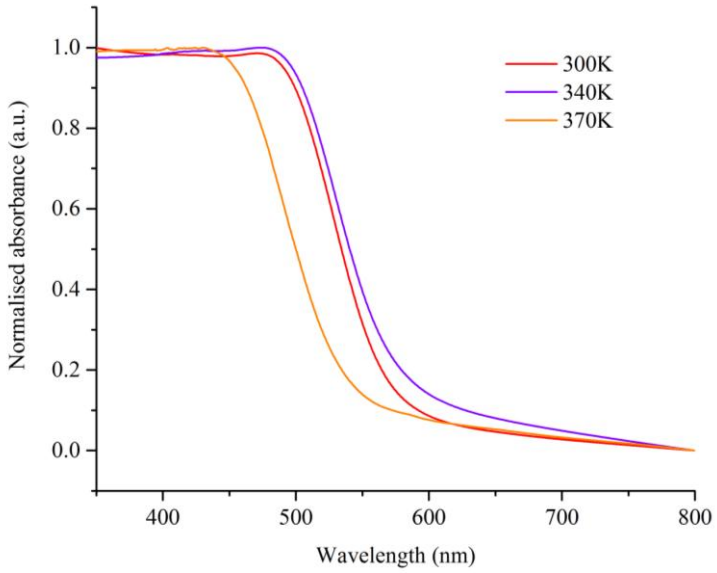

Figure 4.10 Normalised single-crystal UV-visible absorption spectra for **1**, collected at 300 K, 340 K and 370 K

The same experiment was carried out on molecular complex **4**; comparison of the UV-visible absorption spectra collected at 300 K and 350 K show that there is no significant change in the absorption band on going to Form II and Form III, and thus no evidence of thermochromism (Figure 4.11). Visual inspection of the crystal following the experiment showed there had been a loss of crystallinity, and small changes in the absorption band upon heating are attributed to this. The same crystal degradation was observed in single crystal X-ray diffraction experiments, where the crystals were heated *in situ* with the use of a cryostream (§4.2.4.3).

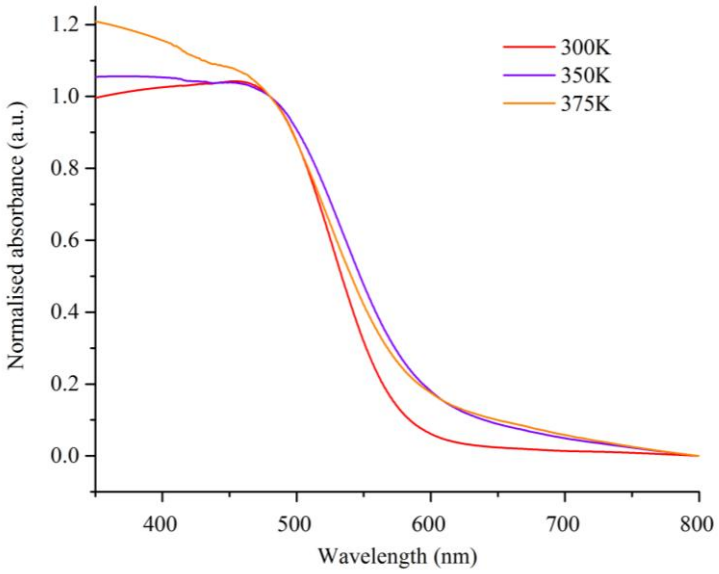

Figure 4.11 Normalised single-crystal UV-visible absorption spectra for **4**, collected at 300 K, 350 K and 375 K

4.2.4 Forms II and III: Structural rational

In order to understand the nature of the phase transitions, single-crystal X-ray diffraction was used, where possible, to structurally characterise the new phases. Some difficulties were encountered in the data collections, particularly where the phase transitions were reversible. It was possible to fully characterise each form of the 2-IA 3,4-DNBA complexes, **1**, **2** and **3**; crystal structures were obtained for only Forms I and II of 2-BrA 3,4-DNBA (**4** and **5**) and Form I of 2-ClA 3,4-DNBA (**6**).

4.2.4.1 Obtaining the crystallographic data

Form II

As discussed in §4.2.1, Form II of 2-IA 3,4-DNBA, **2**, was obtained by slow evaporation, and also upon heating to 52 °C. A single crystal of **1** was heated to 55 °C *via* HSM and the phase transition to Form II was observed. The irreversible nature of the phase transition allowed the single crystal to be cooled, with the crystal remaining as Form II. The single crystal was mounted at 100 K on the diffractometer and unit cell screening revealed new unit cell parameters. Single crystal X-ray diffraction data were collected and a crystal structure for **2** was obtained. Single crystal X-ray diffraction data were also collected at 100 K on a single crystal grown by slow evaporation and an identical crystal structure was obtained.

A second form of 2-BrA 3,4-DNBA, Form II, **5**, was obtained by slow evaporation from acetonitrile at room temperature; this polymorph grew concomitantly with **4**, in extremely small quantities and not reproducibly. Single crystal X-ray diffraction data were collected at 100 K; the crystal structure of molecular complex **5** is isostructural with Form II of 2-IA 3,4-DNBA, **2**. Experiments were conducted to ascertain whether molecular complex **5** was also obtained upon heating i.e. upon observation of the phase transition to Form II. However, the characterisation of this phase was problematic, with the reversible nature of the phase transitions meaning that experiments could not be conducted easily. A single crystal of **4** was heated to 68 °C using the hot-stage microscope, and the phase transition to Form II was observed by the jump in position. The single crystal was flash cooled to 100 K on the diffractometer in an attempt to prevent the reverse transition; however this was not possible and the reverse transition occurred, with unit cell parameters corresponding to those of **4**.

As such, single crystals of molecular complex **4** had to be heated *in situ* on the diffractometer in order to try and collect crystal data. A single crystal was mounted at 300 K, under N_2 flow, and the temperature was ramped to 345 K (72 °C), which was just above the temperature of the phase transition to Form II. A number of different ramp rates were tried, ranging between 120 K/hour and 360 K/hour. However, in each experiment there was little or no diffraction on collection of the first diffraction image, with complete degradation of the single crystal by the end of the unit cell screening. Multiple experiments were carried out on laboratory diffractometers, on Beamline I19 at Diamond Light Source, and on Beamline 11.3.1 at the Advanced Light Source, with the same result in each experiment. It should also be noted that *in situ* heating experiments were also carried out for 2-IA 3,4-DNBA both in-house and at Diamond Light Source, but these crystals did not survive this process either.

As it was possible to heat single crystals *via* HSM and for the single crystals to survive, it was probable that the nitrogen flow, in combination with high temperature and radiation damage, might be responsible for the rapid degradation of the single crystals when heated *in situ*. To shield the sample from the N_2 flow, a single crystal of **4** was mounted inside a glass capillary on a Rigaku Oxford Diffraction SuperNova diffractometer at 300 K (§3.2.2.3), as this diffractometer allows rapid data collection. The temperature of the cryostream was increased to 345 K (72 °C) at a ramp rate of 120 K/hour, and the crystal was screened. There was strong diffraction and new unit cell parameters were obtained. However, over the duration of a full data collection the diffraction gradually weakened, with complete crystal degradation within approximately one hour. The capillary experiment was carried out multiple times but the crystals only survived for approximately half of the time required for complete data to be collected. The capillary heating method has not yet been transferred to a synchrotron source.

Peak hunting over the frames which were successfully collected before complete degradation of the crystal gave a unit cell similar to that of molecular complex **5**, but with an approximate doubling of the length of the crystallographic *b*-axis. This was not the highest ranked unit cell, with only ~40% of peaks matched over successful frames, however there was significant splitting and damage to the crystal and structure solution was not possible. The doubled unit cell also had unit cell lengths very similar to Form II of 2-IA 3,4-DNBA, molecular complex **2**. Due to the structural similarity of molecular complex **5** to molecular complex **2** (§4.2.4.2), and the similarity of the thermal behaviour, it is probable that molecular complex **5** is also 'Form II', obtained upon heating past the first phase transition. Unit cell parameters for molecular complexes **2** and **5**, and the unit cell parameters from *in situ* heating experiments, are given in Table 4.4. It was not possible to investigate Form II of molecular complex **6**, 2-ClA 3,4-DNBA, by single crystal X-ray diffraction due to the phase transition being so close to the melting point of the complex.

Table 4.4 Data collection temperatures and unit cell parameters for molecular complex **2** and **5**

	Molecular complex **2**		Molecular complex **5**	
Obtained by:	**Evaporation**	**Heating**[a]	**Evaporation**	**Heating**[b]
Data collection T / K	100	100	100	345
a / Å	7.7254(15)	7.7402(6)	7.6563(13)	7.721(2)
b / Å	13.688(3)	13.7231(12)	7.7638(11)	14.856(8)
c / Å	22.024(4)	21.9905(18)	21.880(4)	22.256(4)
α / °	91.663(7)	91.984(7)	92.400(7)	106.07(3)
β / °	91.836(7)	91.917(7)	90.266(6)	93.45(2)
γ / °	101.278(7)	101.475(7)	118.379(8)	102.72(3)
Volume / Å^3	2281.3(8)	2285.8(3)	1142.8(3)	2393(2)

[a] Single crystal of **1** heated to 58 °C *via* HSM, cooled to room temperature and then flash-cooled to 100 K on the diffractometer.
[b] Single crystal of **4** mounted inside a glass capillary and heated *in situ* on the diffractometer to 345 K (72 °C). The single crystal did not survive a full data collection so the unit cell parameters could only be determined using the frames where diffraction was observed.

Form III

A single crystal of Form III of 2-IA 3,4-DNBA, molecular complex **3**, was obtained by heating. A large single crystal of molecular complex **1** was heated to 87 °C using the hot-stage microscope. The phase transition was clearly observed by a jump in the crystal position and a strong change in the colour of the crystal from red to yellow. As the phase transition is irreversible, the crystal was removed from the hot-stage and cooled to room temperature; a single crystal of suitable size was cut, mounted and flash-cooled to 100 K on a Rigaku Oxford

Diffraction Gemini Ultra diffractometer. Visually, it was apparent that the crystal remained in its new phase on cooling, with unit cell screening confirming this. New unit cell parameters were obtained and single crystal X-ray diffraction data were collected on Form III of 2-IA 3,4-DNBA, molecular complex **3**, using Mo Kα radiation. Due to uncertainty in the space group, attempts were also made to collect data using Cu Kα radiation, but crystal degradation occurred on each attempt.

It was not possible to collect single crystal X-ray diffraction data for Form III of 2-BrA 3,4-DNBA. Due to the reversible transition, the crystal had to be heated *in situ*; heating to 368 K (95 °C) resulted in complete degradation of the single crystal, even when the crystal was mounted inside a capillary.

4.2.4.2 Form II: Molecular complexes 2 and 5

For 2-IA 3,4-DNBA, the transition from molecular complex **1** to **2** results in an increase in the density. In comparison, for 2-BrA 3,4-DNBA the transition from molecular complex **4** to **5** results in a decrease in the density. It is likely that this plays a role in the reversibility of the phase transition in 2-BrA 3,4-DNBA, with the crystal packing in molecular complex **5** being less efficient than in molecular complex **4**. In both the 2-IA and 2-BrA molecular complexes, the structures are very similar. Both Form II structures are in the space group $P\bar{1}$, with all components still present in their neutral forms. The overall layered packing arrangement is maintained, with the main difference being a reorientation of the disordered 2-haloaniline molecules in the molecular plane. The asymmetric unit of molecular complex **2** consists of four independent 3,4-DNBA molecules and two independent disordered 2-IA molecules; the asymmetric unit of molecular complex **5** contains two independent 3,4-DNBA molecules and one disordered 2-BrA molecule.

The 3,4-DNBA molecules form dimers through moderate strength O-H···O bonds between carboxylic acid groups (Table 4.5), as observed in Form I. The C-O bond lengths (1.263(7)/1.268(6) Å, 1.263(7)/1.260(8) Å, 1.249(8)/1.293(7) Å and 1.244(8)/1.288(8) Å for molecular complex **2**; 1.261(4)/1.269(5) Å and 1.265(5)/1.271(4) Å for molecular complex **5**) are intermediate between distances expected for single and double bonds, which may indicate the presence of proton disorder.[37,39] However, due to the significant molecular disorder of the 2-XA molecules in the complexes, the H-atom positions cannot be reliably determined, thus a model was employed with a single proton position. In each case, the hydrogen atom was located using Fourier difference maps and bound to the C-O group with the longer bond distance; the O-H distance was restrained to be 0.9 Å and the H-atom displacement parameters constrained to

1.5U_{eq} of the O-atom to which it is bonded. The hydrogen bonded 3,4-DNBA dimer network is maintained from Form I to Form II, with weak C-H···O hydrogen bonds connecting dimers (as shown in Figure 4.3); hydrogen bond data for molecular complexes **2** and **5** are given in Table 4.5.

Table 4.5 Hydrogen bond data for the 3,4-DNBA network in molecular complexes **2** and **5** (refer to Figure 4.3 for labels **a** - **f**)

Bond type	**D-H···A**	**D-H**	**H···A**	**D···A**	**<(DHA)**
Molecular complex **2**					
a	O8-H8···O1	0.91(2)	1.71(2)	2.610(6)	171(7)
b	O2-H2···O7	0.91(2)	1.70(2)	2.617(6)	178(7)
c	C6-H6···O2_#1	0.93	2.73	3.578(7)	153
d	C7-H7···O7_#1	0.93	2.69	3.414(8)	136
e	C14-H14···O1_#2	0.93	2.64	3.411(7)	141
f	C13-H13···O8_#2	0.93	2.67	3.555(7)	159
a	O14-H15···O19_#3	0.89(2)	1.82(3)	2.661(5)	157(7)
b	O20-H20···O13_#3	0.90(2)	1.75(3)	2.629(6)	165(8)
c	C25-H25···O20_#2	0.93	2.63	3.506(8)	158
d	C24-H24···O13_#4	0.93	2.628	3.354(8)	135
e	C17-H17···O19_#4	0.93	2.640	3.348(8)	133
f	C18-H18···O14_#2	0.93	2.65	3.508(7)	153
Molecular complex **5**					
a	O1-H5···O8	0.90(2)	1.71(2)	2.610(3)	175(4)
b	O7-H6···O2	0.90(2)	1.75(2)	2.633(3)	165(4)
c	C4-H4···O2_#1	0.93	2.62	3.497(4)	157
d	C3-H3···O7_#1	0.93	2.587	3.309(5)	135
e	C14-H14···O1_#2	0.93	2.587	3.358(5)	141
f	C13-H13···O8_#2	0.93	2.678	3.561(5)	159

Molecular complex **2**: #1 x+1,y,z #2 x-1,y,z #3 -x+2,-y+1,-z+1 #4 -x+1,-y+1,-z+1

Molecular complex **5**: #1 x,y-1,z #2 x,y+1,z

Note: aromatic H-atoms are placed in calculated positions.

In molecular complex **2**, the molecules of the dimers are close to coplanar with angles of ~3° and ~5° between the mean ring planes. There is a single dimer in molecular complex **5**, with an angle of ~3° between the mean ring planes of the 3,4-DNBA molecules. In molecular complexes **2** and **5**, the carboxylic acid groups are all close to coplanar with the benzene ring (torsion angles of less than 4° in **1** and less than 2° in **5**). In molecular complex **2**, the *m*-NO_2

groups are twisted out of the ring planes by ~14°, ~38°, ~25° and ~37°; the *p*-NO_2 groups are twisted out of the ring planes by ~68°, ~46°, ~63° and ~30°. In molecular complex **5**, the *m*- and *p*-nitro groups of one of the 3,4-DNBA molecules are disordered over two positions, approximately 50:50. Due to steric effects, the positions adopted by the two nitro groups are influenced by each other resulting in just two possible combinations of arrangements. For the 3,4-DNBA molecule with ordered nitro groups, the *m*- and *p*-NO_2 groups are twisted out of the ring plane by ~28° and ~58°, respectively. In the 3,4-DNBA molecule with disordered nitro groups, one of the arrangements has the *m*- and *p*-NO_2 groups twisted out of the ring plane by ~32° and ~40°, respectively; the second arrangement has the *m*- and *p*-NO_2 groups twisted out of the ring plane by ~42° and ~44°, respectively. The torsion angles of the nitro groups in **2** and **5** are comparable to those in **1** and **4**, respectively, with any slight differences having no apparent impact on the colour.

Each independent 2-haloaniline molecule has whole molecule disorder over two well-defined positions, but with a change in the relative molecular orientations compared to Form I (Figure 4.12); this is the main difference between Forms I and II. The molecular disorder is surprisingly similar in the Form II molecular complexes, **2** and **5**, despite the differences in the molecular orientations in the Form I complexes. In molecular complex **2** there are still two independent 2-IA molecules; however, these are no longer situated on inversion centres and are instead disordered over two non-symmetry-related positions (Figure 4.12). The disorder proportions shift from the symmetry-constrained 50:50 for both molecular sites in Form I, to proportions of 0.768(2):0.231(2) (shown in purple and green, respectively - right, Figure 4.12 (a)) and 0.526(1):0.474(1) (shown in blue and yellow, respectively - right, Figure 4.12(a)) in Form II. In molecular complex **5** there is just a single independent 2-BrA molecule which is also disordered over two non-symmetry-related positions with proportions of approximately 0.923(2):0.077(2) (shown in blue and pink, respectively - right, Figure 4.12(b)).

The 2-IA and 2-BrA molecules interact with the ordered 3,4-DNBA hydrogen bonded tapes through a combination of hydrogen and halogen bonds; the reorientation of the 2-XA molecules in the phase transition means the interactions are different to those in the Form I molecular complexes (**1** and **4**). Due to the identical disorder models for the 2-XA molecules in **2** and **5**, the types of interaction are the same in both (summarised in Figure 4.13). In each 2-XA site, the interactions depend on the molecular orientation adopted by the 2-XA molecule. In both orientations, the halogen atom interacts with the O-atoms of 3,4-DNBA nitro groups through C-X···O contacts (**a**, **b** and **d**, Figure 4.13); in both orientations, the amine group interacts with the O-atoms of 3,4-DNBA nitro groups through N-H···O hydrogen bonds (**c**, **e** and **f**, Figure 4.13). The donor-acceptor distances for the interactions are given in Table 4.6.

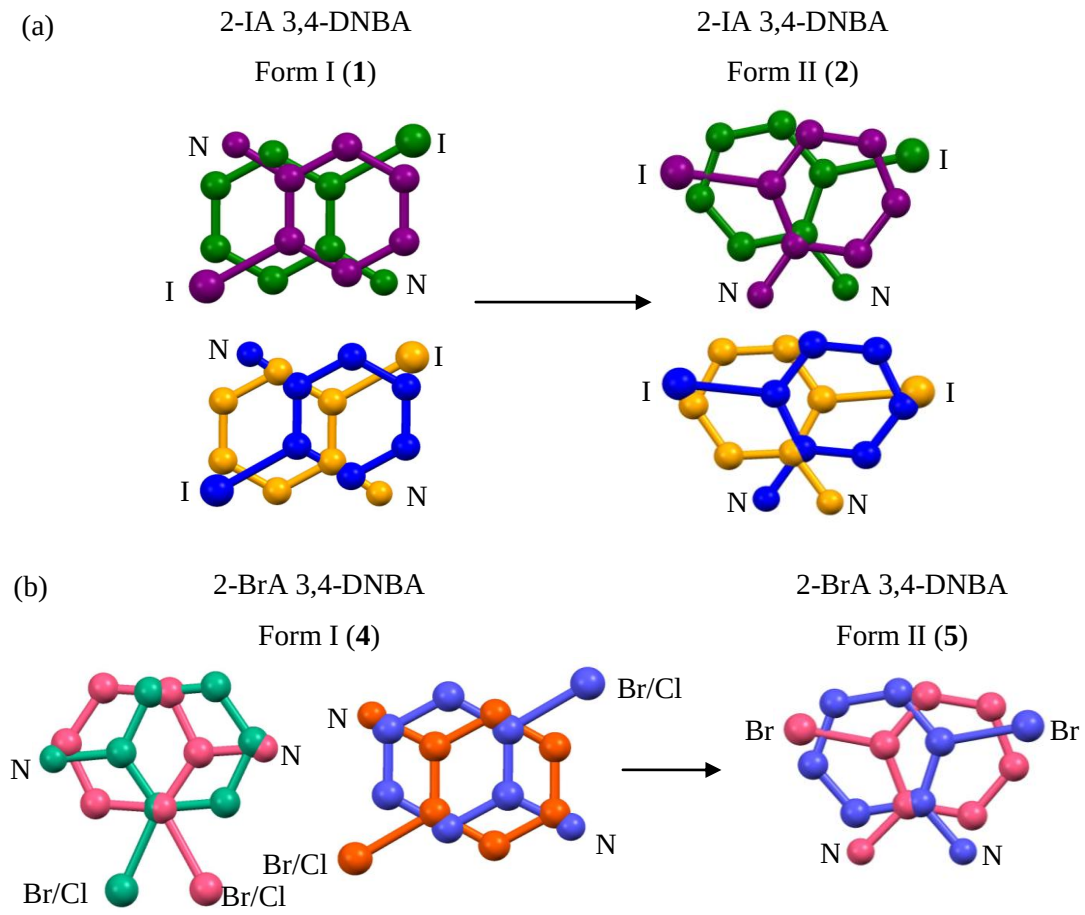

Figure 4.12 Comparison of the molecular disorder in Forms I (left) and II (right) of the 2-IA and 2-BrA molecular complexes. (a) Left: the 50:50 disorder of the 2-IA molecules over inversion centres in **1**; Right: the symmetry-independent disorder of the 2-IA molecules in molecular complex **2**, where occupancies are ~77:23 (purple/green) and ~52:48 (blue/yellow). (b) Left: the two disordered 2-BrA molecules in **4** (symmetry-independent ~90:10 in green/pink, and 50:50 over an inversion centre in orange/blue; Right: the symmetry-independent disorder of the 2-BrA molecule in molecular complex **5**, where the disorder occupancy is ~90:10 (blue/pink) . Hydrogen atoms have been omitted for clarity.

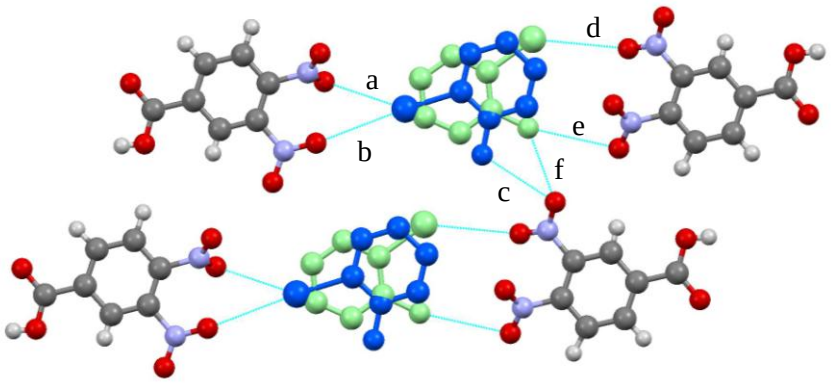

Figure 4.13 The intermolecular interactions between the 2-XA molecules and the 3,4-dinitrobenzoic acid molecules in molecular complexes **2** and **5**. Hydrogen atoms on the 2-XA molecules have been omitted for clarity. Donor-acceptor contact distances (labelled **a-f**) are given in Table 4.6.

Table 4.6 Donor-acceptor distances (X = I, Br) for the intermolecular interactions between the 2-XA molecules and the 3,4-DNBA framework in molecular complexes **2** and **5** (refer to Figure 4.13 for labels **a** - **f**).

		d(D···A)/ Å Molecular complex 2		**d(D···A)/ Å Molecular complex 5[a]**
Label	**D···A or D-H···A**	**2-IA (Site 1)**	**2-IA (Site 2)**	**2-BrA**
a	X···O	3.384(4)	3.350(4)	3.306(7)
b	X···O	3.441(4)	3.382(4)	3.572(8)[b]
c	N-H···O	3.39(1)	3.37(1)	3.49(4), 3.37(5)
d	X···O	3.537(4)[b]	3.342(5)	3.460(5) [b], 3.564(5)[b]
e	N-H···O	3.42(2)	3.44(1)	3.13(7), 3.28(6)
f	N-H···O	3.14(1)	3.03(1)	3.22(7), 3.004(7)

a: Two values are given for **c** -**f** for molecular complex **5** due to the nitro groups being disordered over two positions.

b: Note, these distances are longer than the sum of the van der Waals radii of X and O and are reported for comparison.

The orientation with the major occupancy differs between molecular complexes **2** and **5**. In molecular complex **2**, the molecule shown in blue (Figure 4.13) is the majorly occupied orientation in both of the 2-IA sites (77% and 52% occupancies). In this orientation, the 2-IA molecules are involved in two C-I···O halogen bonds (**a** and **b**) (3.384(4) Å, 3.350(4) Å, 3.441(4) Å, 3.382(4) Å c.f. the sum of the van der Waals radii of I and O = 3.50 Å). In the orientation with the minor occupancy (shown in green, Figure 4.13, 23% and 48% occupancies), there is only a single C-I···O halogen bond (**d**), and in one of the 2-IA sites this is longer than the sum of the van der Waals radii (3.537(4) Å). In molecular complex **5**, the orientation shown in green (Figure 4.13) has the higher occupancy (90%). In this orientation, the molecule is involved in two N-H···O hydrogen bonds (**e** and **f**); the hydrogen bonds are significantly stronger than in the alternate orientation (shown in blue, Figure 4.13, 10% occupancy). With the exception of one halogen bond (**a**), the Br···O distances are greater than the sum of the van der Waals radii of 3.37 Å.

The combination of interactions results in a very similar two-dimensional sheet structure to the Form I complexes, with the only difference being the relative orientations of the 2-haloaniline molecules in the channels. In molecular complex **2** there are two independent sheet types, A and B, with each sheet incorporating one of the 2-IA molecules. In molecular complex **5** there is just a single independent sheet. Due to the similarity of the disorder models in molecular complexes **2** and **5**, the sheets are identical (Figure 4.14).

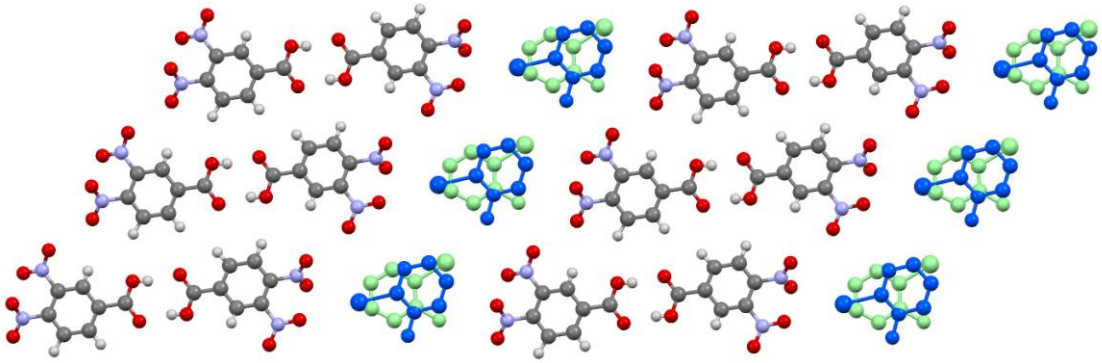

Figure 4.14 Two-dimensional sheet structure in molecular complexes **2** and **5**.

The two-dimensional sheets stack to form a layered structure similar to that of Form I. In molecular complex **2**, the two-dimensional sheets have an AABBAABB stacking arrangement in the direction of the crystallographic *b*-axis; in molecular complex **5**, the sheets stack in the direction of the crystallographic *a*-axis. The alternate stacking of 2-haloaniline molecules and 3,4-DNBA dimers is maintained during the phase transition; however there is a slight slipping of the stacked layers, with alternate layers more aligned in Form II (Figure 4.15). The stacked 2-XA molecules and 3,4-DNBA dimers are close to parallel, with an angle of ~6° between the mean planes. There are aromatic donor···acceptor and halogen···π interactions between stacked 2-XA molecules and 3,4-DNBA dimers, as well as $O_{nitro}\cdots O_{nitro}$ and $O_{nitro}\cdots\pi$ interactions between 3,4-DNBA molecules in adjacent sheets. There are equivalent interlayer distances of ~3.35 Å and ~3.34 Å in molecular complexes **2** and **5**, respectively. These distances are approximately the same as those in the Form I molecular complexes.

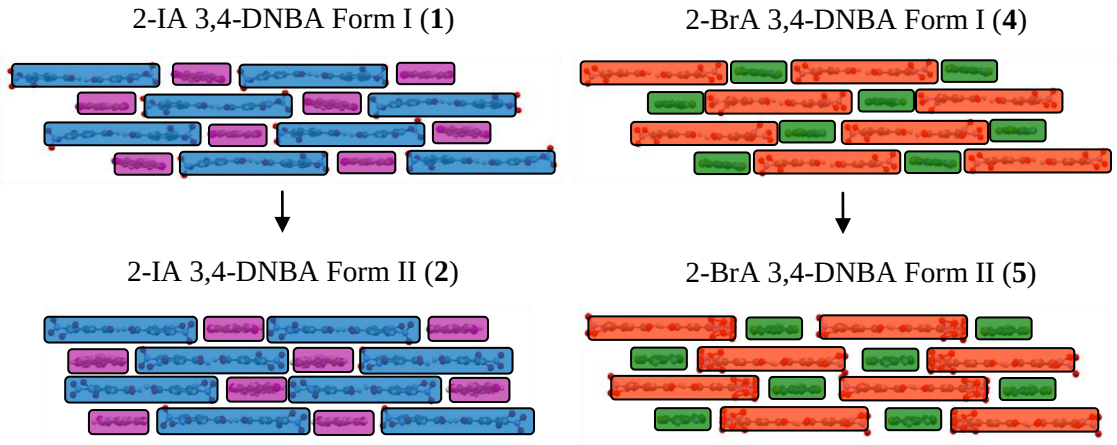

Figure 4.15 Slipping of the layers on going from Form I to Form II in 2-IA 3,4-DNBA (left) and 2-BrA 3,4-DNBA (right). 2-IA and 2-BrA molecules are highlighted in purple and green, respectively; 3,4-DNBA dimer units are highlighted in blue and orange.

In molecular complex **4**, there are four types of stacking (**i** - **iv**, Figure 4.16 (a)) with the molecular overlap differing according to the 2-IA site and the molecular orientation adopted. In molecular complexes **5**, there are two types of stacking (**v** and **vi**, Figure 4.16 (b)) and the molecular overlap depends on the molecular orientation.

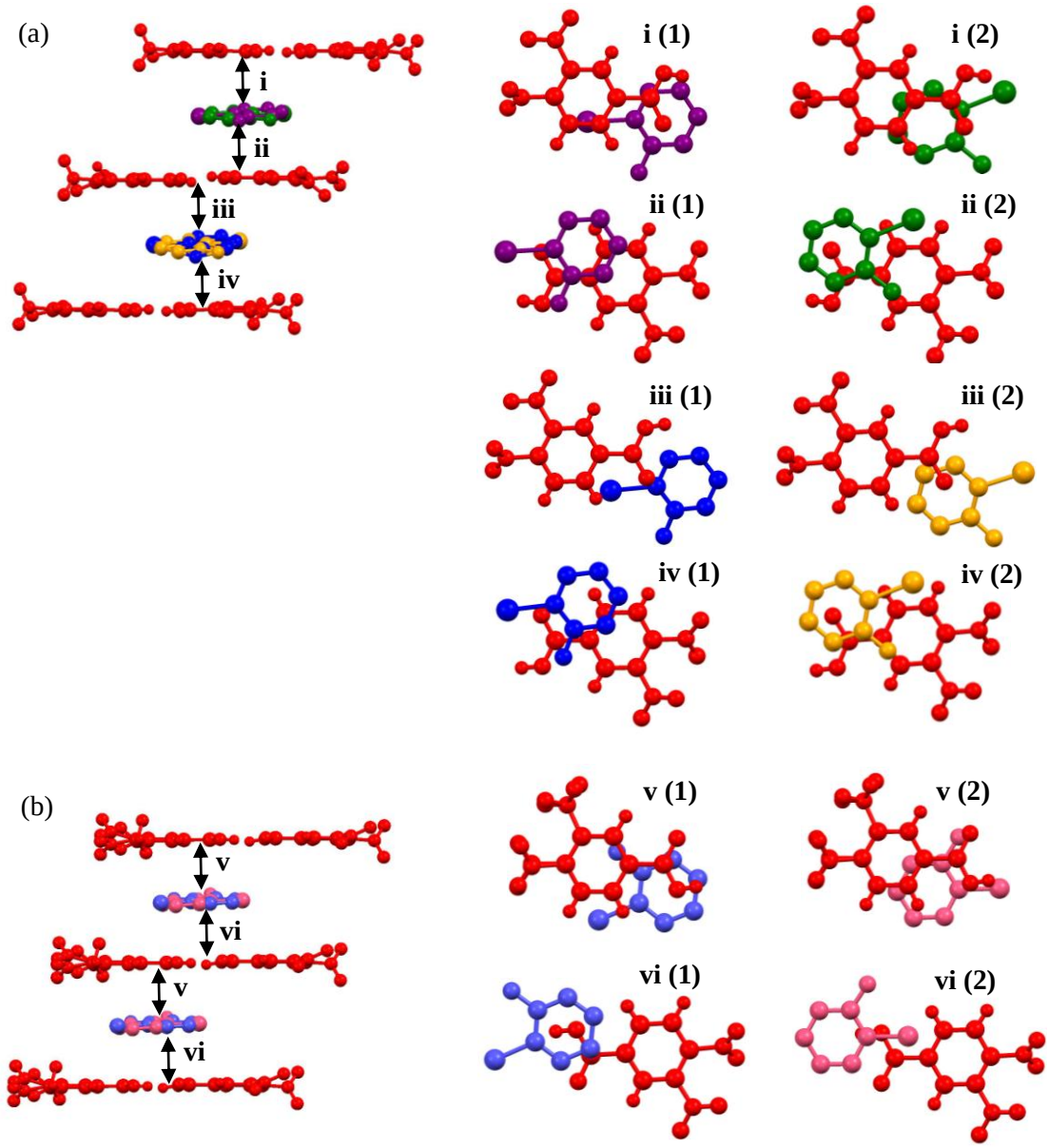

Figure 4.16 (a) Stacking in molecular complex **2**, where there are four types of stacking (**i** - **iv**); the molecular overlap differs for the two orientations (1 and 2); (b) Stacking in molecular complex **5**, where there are two types of stacking (**v** and **vi**); the molecular overlap differs for the two orientations (1 and 2). 3,4-DNBA molecules are shown in red and the disordered 2-XA molecules are shown in the colours according to Figure 4.12.

As for Form I, the crystal packing is dominated by the aromatic donor···acceptor interactions. The slight shift in the layers during the phase transition does not result in a change in the colour of either complex thus $\pi\cdots\pi^*$ charge-transfer absorbance must be similar. This is reflected in the

similarity of the interlayer spacing and the molecular overlap in Forms I and II. As observed in the Form I molecular complexes, there is very little overlap between the rings of stacked 2-XA and 3,4-DNBA molecules. Molecular overlap remains to be predominantly between the 2-XA ring or halogen atom and the centre of the 3,4-DNBA dimer and the amount of molecular overlap is similar for both possible orientations of the disordered 2-XA molecules (Figure 4.16).

4.2.4.3 Form III: Molecular complex 3

For 2-IA 3,4-DNBA, on going through the phase transition to Form III there is a significant change in the unit cell parameters, with molecular complex **3** adopting a monoclinic space group, therefore of higher symmetry than the two lower temperature molecular complexes (**1** and **2**). There was some ambiguity in the space group, but the best model for the molecular complex was obtained in the non-centrosymmetric space group $P2_1$. In the absence of the 2-IA molecules, the 3,4-DNBA components have symmetry consistent with the centrosymmetric space group $P2_1/n$; however, it was not possible to resolve the 2-IA molecules in this higher symmetry space group and it was best modelled in $P2_1$ with the 2-IA molecules breaking the symmetry.

On going through the phase transition to Form III, the molecular complex undergoes a massive structural rearrangement, going from the layered and planar structure adopted in Forms I and II, to a herringbone structure (Figure 4.17); this structural rearrangement is accompanied by a colour change from red to yellow, observed in HSM, and the phase transition is therefore thermochromic. Such a large structural rearrangement was unexpected, given that the single crystal survived the phase transition.

The asymmetric unit of **3** contains two independent 3,4-DNBA molecules and a single 2-IA molecule. The 3,4-DNBA molecules form a hydrogen bonded dimer through moderate strength O-H···O hydrogen bonds between the carboxylic acid groups (Table 4.7); an angle of ~7° was calculated between the mean ring planes of the dimer molecules, similar to that in Forms I and II. The C-O bond lengths (1.25(1)/1.26(1) Å and 1.25(1)/1.27(1) Å) are intermediate between distances expected for single and double bonds, which may indicate the presence of proton disorder.[37,39] However, due to the molecular disorder present, the H-atom positions cannot be reliably determined, thus a model was employed with a single proton position. In each case, the hydrogen atom was located using the Fourier difference maps and bound to the C-O group with the longer bond distance; the O-H distance was restrained to be 0.9 Å and the H-atom displacement parameters constrained to $1.5U_{eq}$ of the O-atom to which it is bonded. The hydrogen bonded 3,4-DNBA tapes (Figure 4.3) are maintained through the transition, with the

same weak C-H···O hydrogen bonds linking the dimers; the linking hydrogen bonds (**c** - **f**) are generally shorter than in Forms I and II (Table 4.7). The carboxylic acid groups of the two 3,4-DNBA molecules are very close to coplanar with the benzene rings, with torsion angles of less than ~1°. The *m*- and *p*-nitro groups in both 3,4-DNBA molecules are twisted out of the ring plane; the *m*-nitro groups have torsions of ~37° and ~39° and the *p*-nitro groups have torsions of ~54° and ~56°. Despite the significant rearrangement of the structure, the torsion angles are comparable to those of Forms I and II, and there are no significant changes in the conformations of the molecular components.

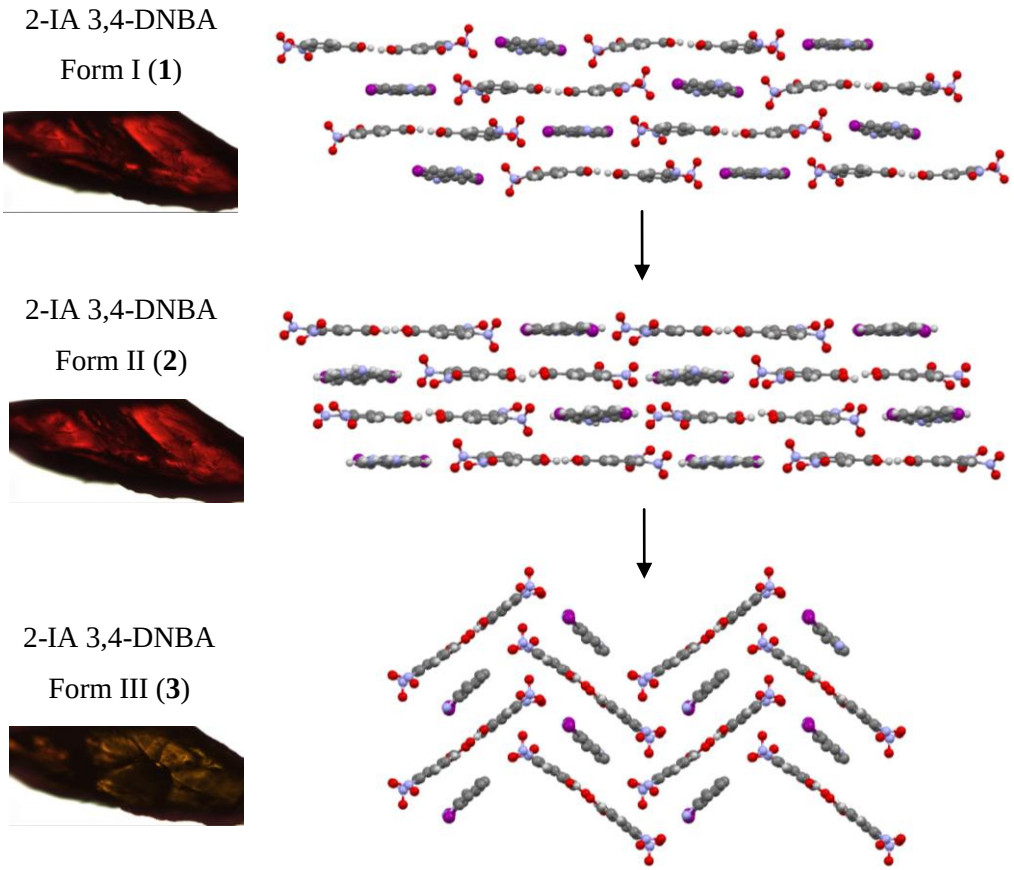

Figure 4.17 A comparison of the overall crystal packing in Forms I, II and III of 2-IA 3,4-DNBA (**1**, **2** and **3**), showing the massive structural rearrangement on going to Form III, with survival of the single crystal. This rearrangement is associated with a colour change from red to yellow.

The 2-IA molecule remains disordered, with whole molecule disorder over two well-defined positions with occupanices of 0.56(2) and 0.44(2) (purple/pink in Figure 4.18). In terms of the average structure, the disorder is quite different to that seen in Forms I and II, with the iodine atom and rings in approximately the same position in both possible molecular orientations (Figure 4.18).

Table 4.7 Hydrogen bond data for the 3,4-DNBA network in molecular complex **3** (refer to Figure 4.3 for labels **a** - **f**)

Bond type	D-H···A	D-H	H···A	D···A	<(DHA)
a	O1-H1···O7 #1	0.90(3)	1.69(4)	2.587(10)	171(14)
b	O8-H8···O2 #2	0.89(3)	1.76(6)	2.620(10)	161(14)
c	C11-H11···O8 #3	0.93	2.46	3.330(11)	156
d	C10-H10···O2 #4	0.93	2.50	3.33(1)	149
e	C3-H3···O7 #5	0.93	2.54	3.37(1)	149
f	C4-H4···O1 #3	0.93	2.65	3.260(12)	124

#1 -x+1,y+1/2,-z+1 #2 -x+1,y-1/2,-z+1 #3 x-1,y,z #4 -x,y-1/2,-z+1 #5 -x, y+1/2 ,-z+1

Note: aromatic H-atoms are placed in calculated positions.

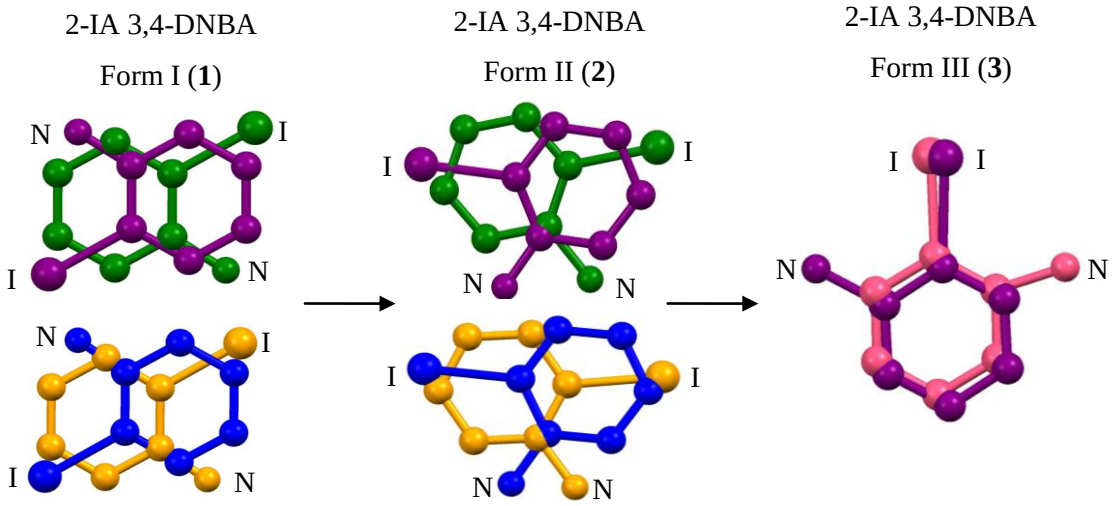

Figure 4.18 The molecular disorder of the single 2-IA molecule in molecular complex **3** (right), with occupancies of 56:44 (shown in purple and pink, respectively), compared with the disordered molecules in **1** (left) and **2** (middle). Hydrogen atoms have been omitted for clarity.

As in Forms I and II of the complex, channels of the disordered 2-IA molecules interact with the 3,4-DNBA network *via* a combination of hydrogen and halogen bonds, which are similar for both possible molecular orientations; donor-acceptor distances are given in Table 4.8. When in the orientation shown in purple, the amine group interacts with the *m*-nitro group through a single weak N-H···O hydrogen bond (**a**, Figure 4.19), and when in the orientation shown in pink, there are two N-H···O hydrogen bonds (one moderate and one weak) formed between the amine group and O-atoms of the *m*- and *p*-nitro groups of one 3,4-DNBA molecule (**b** and **c**, Figure 4.19); in both cases this is a weak N-H···O hydrogen bond. In both orientations, the iodine atom interacts with the *m*-nitro group through a C-I···O halogen bond (**d**, Figure 4.19); the interaction is of the same strength for both orientations of the 2-IA molecule.

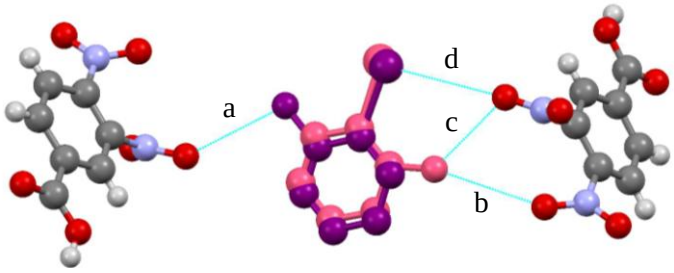

Figure 4.19 (a) Intermolecular interactions between the disordered 2-iodoaniline molecules and the 3,4-DNBA molecules. Hydrogen atoms on the 2-IA molecule are omitted for clarity.

Table 4.8 Donor-acceptor distances for the intermolecular interactions between the 2-IA and the 3,4-DNBA framework in molecular complex **3** (refer to Figure 4.19 for labels **a** - **c**).

Label	D-H···A or D···A	d(D···A)/ Å
a	N-H···O	3.47(2)
b	N-H···O	3.68(3)
c	N-H···O	3.05(3)
d	I···O	3.24(2) (purple), 3.26(2) (pink)

The combination of the interactions results in a zigzag sheet structure (Figure 4.20) rather than the planar sheets formed in **1** and **2**. The 2-IA and 3,4-DNBA molecules are tilted with respect to each other, with an angle of ~74° between the mean ring planes of 2-IA and 3,4-DNBA molecules in the same zigzag sheet. The zigzag sheets stack to give a herringbone packing arrangement, forming columns of alternately stacked 2-IA molecules and 3,4-DNBA dimers (Figure 4.20 (b));

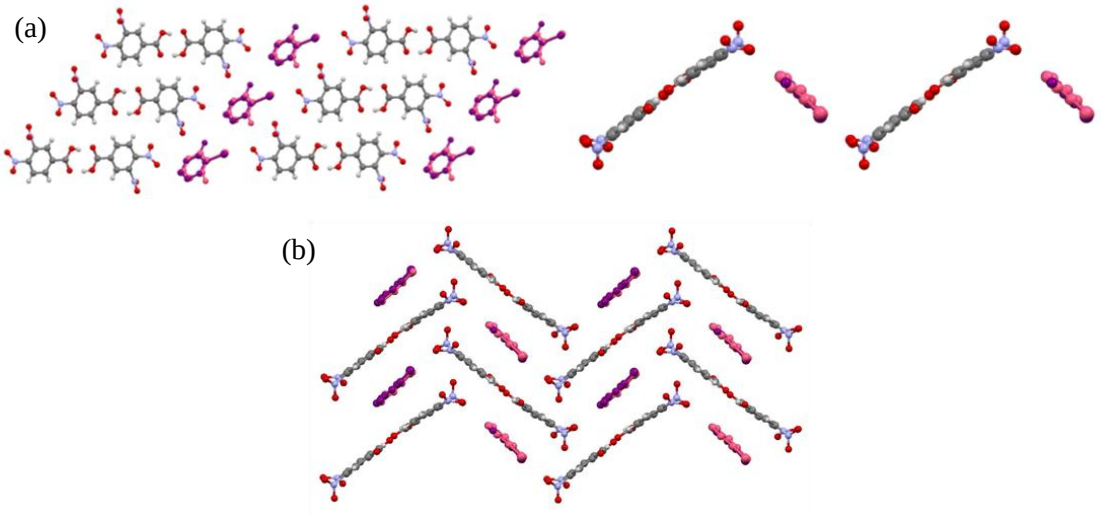

Figure 4.20 (a) A single zigzag sheet viewed from above (left) and along the sheet (right); (b) herringbone packing arrangement and stacking of alternate 2-IA molecules and 3,4-DNBA dimers.

There are aromatic donor···acceptor and halogen···π interactions between stacked 2-IA and 3,4-DNBA molecules; there are also O···π interactions between 3,4-DNBA molecules in adjacent columns, formed between the nitro groups of one 3,4-DNBA molecule and the aromatic ring of a second 3,4-DNBA molecule. Due to the herringbone arrangement the interactions between the stacked 2-IA and 3,4-DNBA molecules occur only within a three molecule 3,4-DNBA/2-IA/3,4-DNBA (A-D-A) unit (Figure 4.21, left); thus, unlike Forms I and II, the stacks are not formed through continuous aromatic donor···acceptor interactions. There are two types of stacking within each three-molecule unit (**i** and **ii**, Figure 4.21) and the molecular overlap differs with the molecular orientation adopted by the 2-IA molecule; there is an approximate molecular separation of ~3.38 Å between the stacked molecules which is equivalent to the separation in Forms I and II.

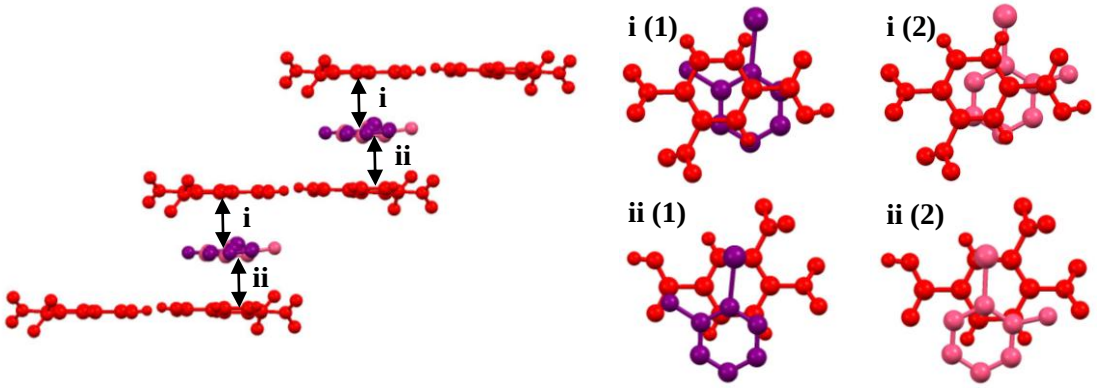

Figure 4.21 Stacking in molecular complex **3**, where stacking is within a three-molecule 3,4-DNBA/2-IA/3,4-DNBA unit, with two types of stacking (i and ii); molecular overlap differs for the two orientations (1 and 2). 3,4-DNBA molecules are shown in red and the disordered 2-XA molecules are shown in the colours according to Figure 4.12.

The molecular overlap is quite different to molecular complexes **1** and **2**; there is more significant overlap between the 2-IA and 3,4-DNBA rings in molecular complex **3**, and no overlap of the 2-IA ring or halogen atom with the carboxylic acid group or the centre of the 3,4-DNBA dimer. The change in colour from red to yellow upon the transition was observed in the variable-temperature UV-visible absorption spectra (Figure 4.10), with a broad charge-transfer absorption band still observed in the visible region for **3**. The change in colour is attributed to the change in stacking and molecular overlap, altering the nature of the charge-transfer. It is possible that the significant change in the orientations of the disorder also plays a role; in **3**, the two orientations of the disordered molecule adopt almost equivalent positions, differing only by the flipping of the amine group, whereas in **1** and **2** the two positions of the aromatic rings of the disordered molecules are quite different. However, although the structural

analysis provides a good indication, a full understanding of the charge-transfer interactions, disorder effects, and differences in the optical properties requires further work.

4.2.5 Diffuse scattering and local order

The crystal structures of molecular complexes **1 - 6** are a space and time average over the whole crystal, determined using the strong Bragg peaks in the diffraction pattern. Electron density maps were used to assign the atomic sites of the two possible molecular orientations, aided by the presence of the heavier halogen atoms; site occupancy factors were either given (where disorder was over an inversion centre), or refined with the use of a second free variable. In each 2-haloaniline site, the molecule has been modelled as disordered over two positions. For all of the disordered molecules, similar, or in some cases identical, type and strength interactions are observed for both molecular orientations, and it is the competition between these that is likely to give rise to the disorder.

Understanding the structure beyond the average unit cell is vital in determining the relationship between the structure and function, particularly if theory is to be successfully applied. To investigate the molecular disorder and local ordering in the molecular complexes, and changes in local ordering through the phase transitions, diffuse scattering data were collected at Diamond Light Source on beamline I19 using single-crystal X-ray diffraction; details of the experimental set-up are given in §3.2.2.2. Data were collected on molecular complexes **1**, **2** and **4** (all obtained through slow evaporation); diffuse scattering measurements have not been obtained for molecular complex **6**. Crystals of **1** and **4** were also heated *in situ* in an attempt to obtain diffuse scattering measurements for the higher temperature forms (**3** and **5**). However, the single crystals did not survive the heating process, which was likely to be due to a combination of thermal stress and the higher intensity of the synchrotron radiation; it is also possible that the glue used to hold the crystal resulted in degradation at higher temperatures.

Diffuse scattering was observed in the diffraction patterns of each of the molecular complexes, indicating there that is some short-range order present; the disorder is thus not random. In each case, it is possible that additional diffuse scattering was present to that reported, but missed in the analysis of the patterns due to it being weak. Due to difficulties in the processing of data using the Pilatus detector on I19, it was not possible to conduct a full analysis and interpretation of the diffuse scattering. However, it is possible to achieve a basic understanding of the diffuse scattering by relating it to the average crystal structure of the material. Using crystal engineering principles, possible favourable local configurations, and the interactions of neighbouring molecules, can be explored; for example, the orientation of a molecule could affect the

orientation of adjacent molecules due to steric effects. In molecular complexes **1** - **6**, orientational correlations could be along the channels of disordered 2-haloaniline molecules or in the stacking direction. Although it is possible that there are correlations of 2-haloaniline molecules across the sheets, it is likely that the individual 2-haloaniline channels are independent of one another, since the orientation of the 2-haloaniline molecules has no influence upon the ordered 3,4-DNBA network that separates the channels.

4.2.5.1 2-iodoaniline 3,4-dinitrobenzoic acid

Molecular complex 1

In molecular complex **1**, both independent 2-IA molecules are situated on inversion centres; the intermolecular interactions are identical in both orientations and there is an equal chance of the molecule being in either orientation. There are no interactions between 2-IA molecules within a channel, thus the orientation of a 2-IA molecule in the channel imposes no restriction on the orientation of the adjacent 2-IA molecules. It is therefore possible for adjacent molecules to be in the same orientation or in alternating orientations, leading to short-range order (Figure 4.22 (a)). In terms of the stacking direction, it is possible for the stacks to include 2-IA molecules with the same orientation, or alternating orientations (Figure 4.22 (b)).

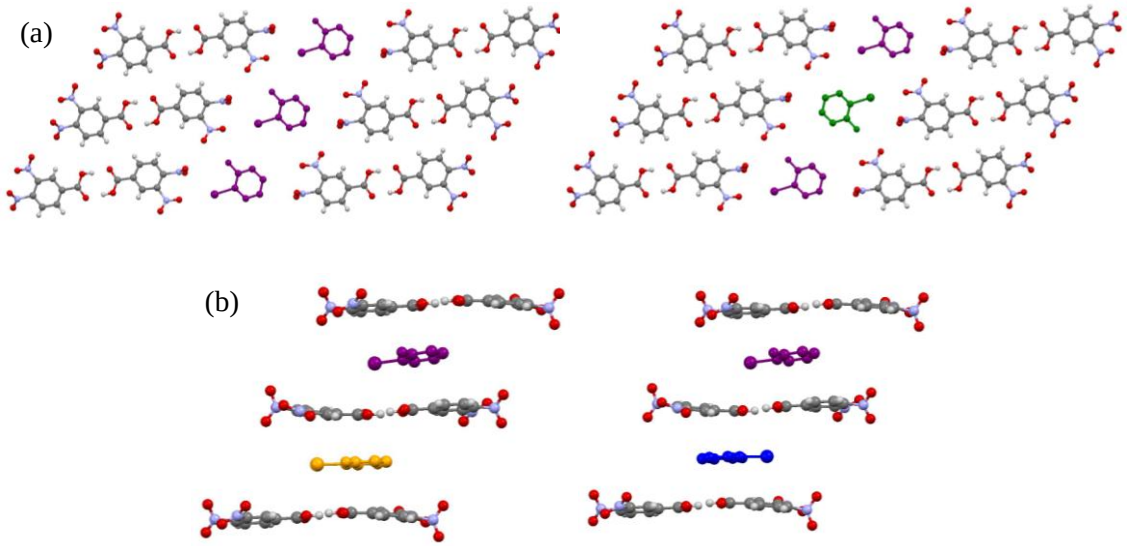

Figure 4.22 Molecular complex **1**: 2-IA molecules (a) within a channel in the same orientation (left) and alternating orientations (right); (b) within stacks in the same orientation (left) and alternating orientations (right).

To obtain diffuse scattering measurements for **1**, single crystal X-ray diffraction data were collected at 100 K. Diffuse scattering was observed in the diffraction pattern, indicating that there is short-range order in the structure; this scattering is quite broad which suggests that there

are correlations extending over fairly short length scales. The diffuse scattering is observed between Bragg peaks of changing *k*, changing *l*, and simultaneously changing *k* and *l* (Figure 4.23(a)), which corresponds to the directions of the crystallographic *b*- and *c*-axes, and the direction diagonally between *b* and *c* (Figure 4.23 (b)). The strongest diffuse scattering corresponds to the stacking direction (diagonally between the *b*- and *c*-axes) and the dominant local ordering could therefore be within the stacks.

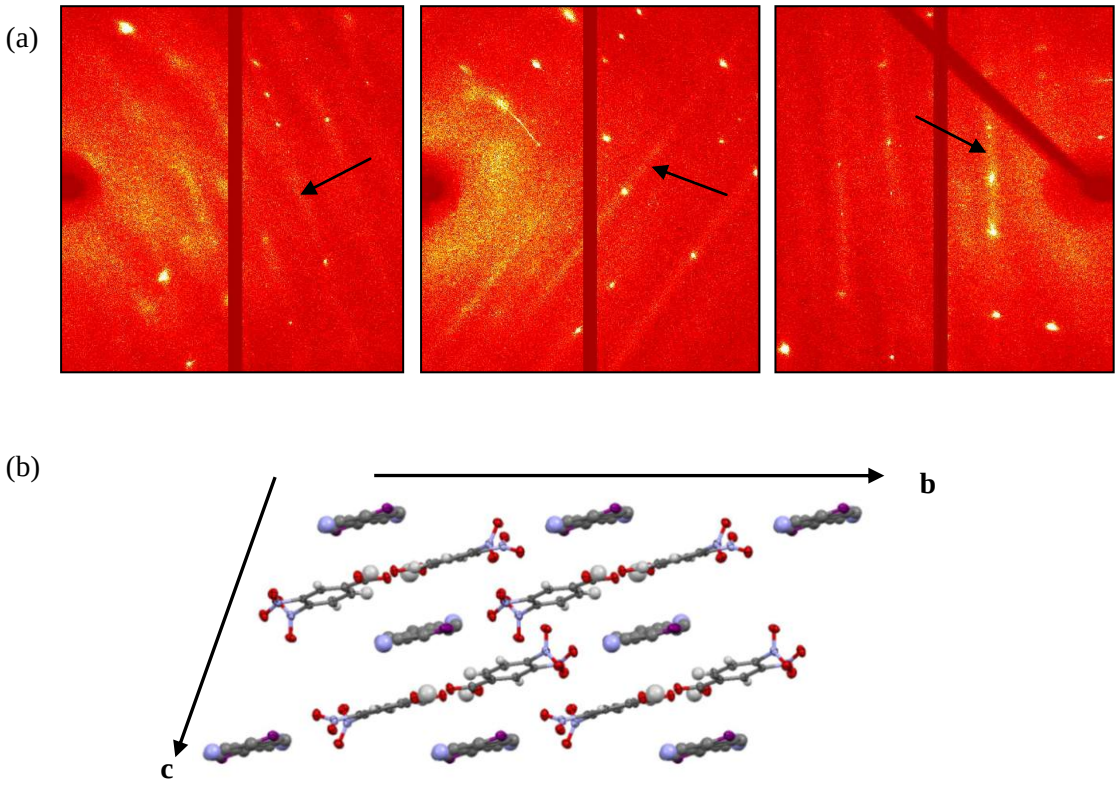

Figure 4.23 (a) Diffuse scattering features in the diffraction pattern of molecular complex **1**, showing the broad streaks between Bragg peaks of changing *k* (left), changing *l* (middle) and changing *k* and *l* (right). (b) Packing in molecular complex **1**, showing the directions of the crystallographic *b*- and *c*-axes.

Molecular complex 2

In molecular complex **2**, the molecular disorder is the same in each of the 2-IA sites. It is possible for adjacent 2-IA molecules in the channels to be in the same orientation or to be in alternating orientations (Figure 4.24 (a)). If they are in alternating orientations, this results in a weak N-H···I hydrogen bond between the two molecules. In the first of the 2-IA sites (molecules shown in green/purple, Figure 4.12) the N···I distance is ~3.3 Å and in the second site (molecules shown in blue/yellow, Figure 4.12) the N···I distance is ~3.7 Å. Similarly to molecular complex **1**, there could also be correlations of molecules in the stacking direction,

with no restrictions imposed on the orientations in either direction, and the possibility of stacks including 2-IA molecules with the same orientation, or alternating orientations (Figure 4.24 (b)).

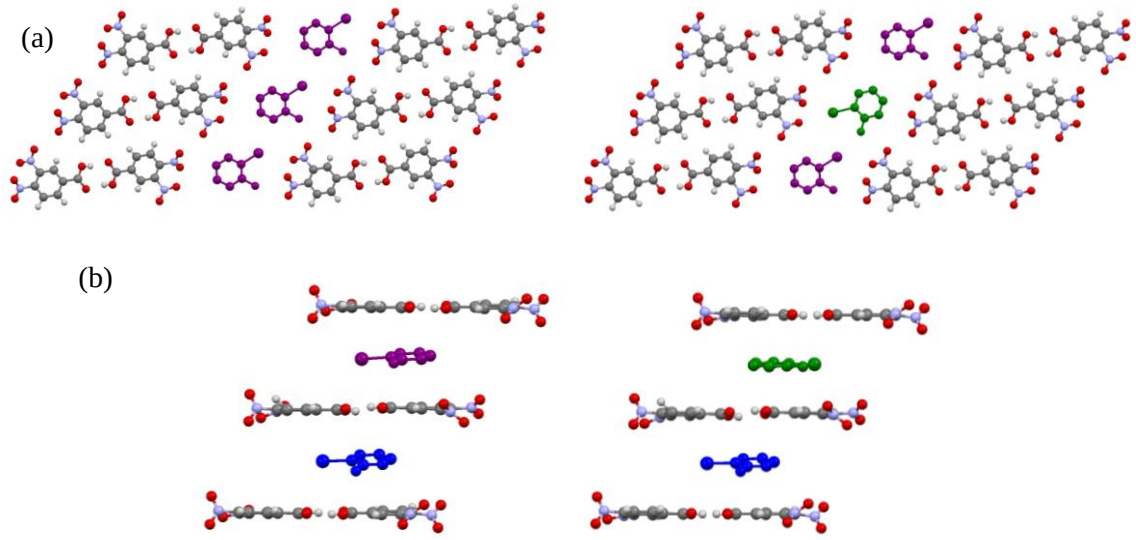

Figure 4.24 Molecular complex **2**: 2-IA molecules (a) within a channel in the same orientation (left) and opposite orientations (right); (b) within stacks in the same orientation (left) and alternating orientations (right).

Diffuse scattering measurements were collected at 100 K on a single crystal of molecular complex **2** that was obtained through slow evaporation. The only diffuse scattering observed in the diffraction pattern of molecular complex **2** runs between Bragg peaks of changing *k*, and is much sharper than that observed in molecular complex **1** (Figure 4.25). The sharpness of the diffuse scattering indicates that there are correlations over longer length scales than in **1**. The direction of the diffuse scattering corresponds to the crystallographic *b*-axis (direction of stacking), and is therefore likely to be due to correlations of molecules within the stacks.

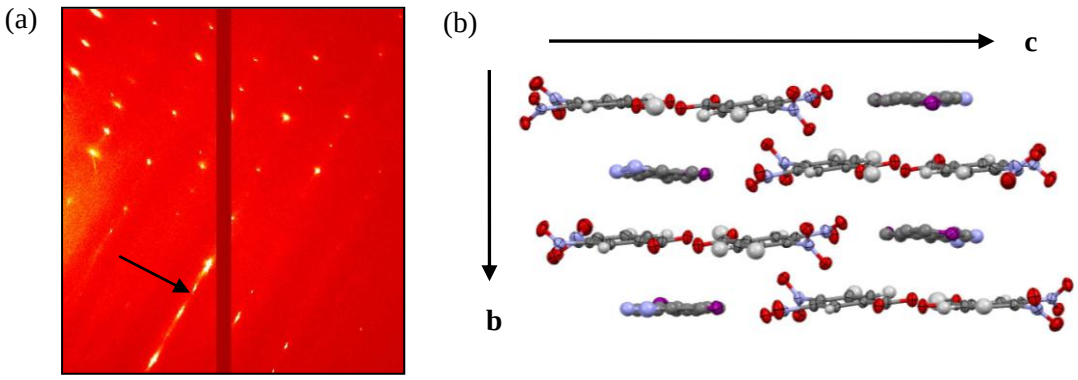

Figure 4.25 (a) Sharp diffuse scattering in the diffraction pattern of molecular complex **2**, between Bragg peaks of changing *k*. (b) Packing in molecular complex **2**, showing the directions of the crystallographic *b*- and *c*-axes.

Molecular complex 3

In molecular complex **3**, there is an approximately equal chance of adopting the two possible orientations. Due to the positions of the two orientations relative to each other there are no interactions between adjacent 2-IA molecules, so molecules in the channels can be in the same orientation or in alternating orientations (Figure 4.26). Similarly to molecular complexes **1** and **2**, there could also be correlations of molecules in the stacks of 2-IA molecules and 3,4-DNBA dimers, with no restrictions imposed.

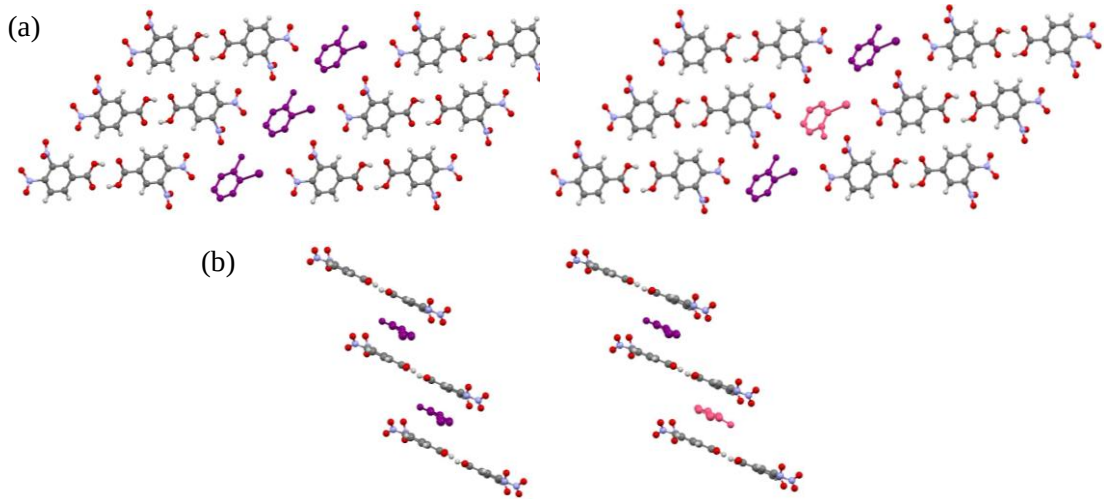

Figure 4.26 Molecular complex **3**: 2-IA molecules (a) within a channel in the same orientation (left) and alternating orientations (right); (b) within stacks in the same orientation (left) and alternating orientations (right).

In order to try and collect diffuse scattering measurements, a single crystal of **1** was mounted at room temperature and heated to 365 K (92 °C) using a ramp rate of 60 K/hour; the crystal was held at this temperature for 5 minutes, and then cooled to 100 K for data collection. However, powder rings were evident from the start of the experiment, with complete degradation of the single crystal before the data collection was complete, thus it was not possible to obtain diffuse scattering measurements for molecular complex **3**.

4.2.5.2 2-bromoaniline 3,4-dinitrobenzoic acid

Molecular complex 4

In molecular complex **4**, one of the independent 2-BrA molecules is disordered over an inversion centre. In contrast to the 2-IA complexes, these molecules must be oriented in the same way and this must be propagated along the channel (Figure 4.27(a), left). If adjacent 2-BrA molecules were in alternating orientations (Figure 4.23 (a), right), the Br atoms would be

too close to each other, with a Br···Br distance of ~2.57 Å (c.f. sum of the van der Waals radii of 3.60 Å). Thus, there must be local order along the channels, but individual channels do not have to be the same; however, there must be short-range order or a superstructure would be identifiable. The second 2-BrA molecule has symmetry-independent disorder in a 90:10 ratio, and therefore 90% of these molecules in the crystal adopt the orientation shown in green. In these channels, the orientation of a molecule in the channel impose no restriction on the adjacent molecules, meaning it is possible for molecules to be in the same orientation (Figure 4.27 (b), left) or alternating orientations (Figure 4.27 (b), right). There could also be correlations of molecules in the molecular stacks, with the halogen atoms pointing in the same direction or in different directions (Figure 4.27(c))

It should be noted that the molecular disorder in 2-ClA 3,4-DNBA, **6**, is the same as that in **4**; therefore, the same restrictions apply to the channels of molecules with symmetry independent disorder. If adjacent 2-ClA molecules were in alternating orientations, the Cl atoms would be too close to one another, with a Cl···Cl distance of ~2.66 Å (c.f. sum of the van der Waals radii = 3.50 Å). Therefore there has to be local order in the individual channels as for **4**.

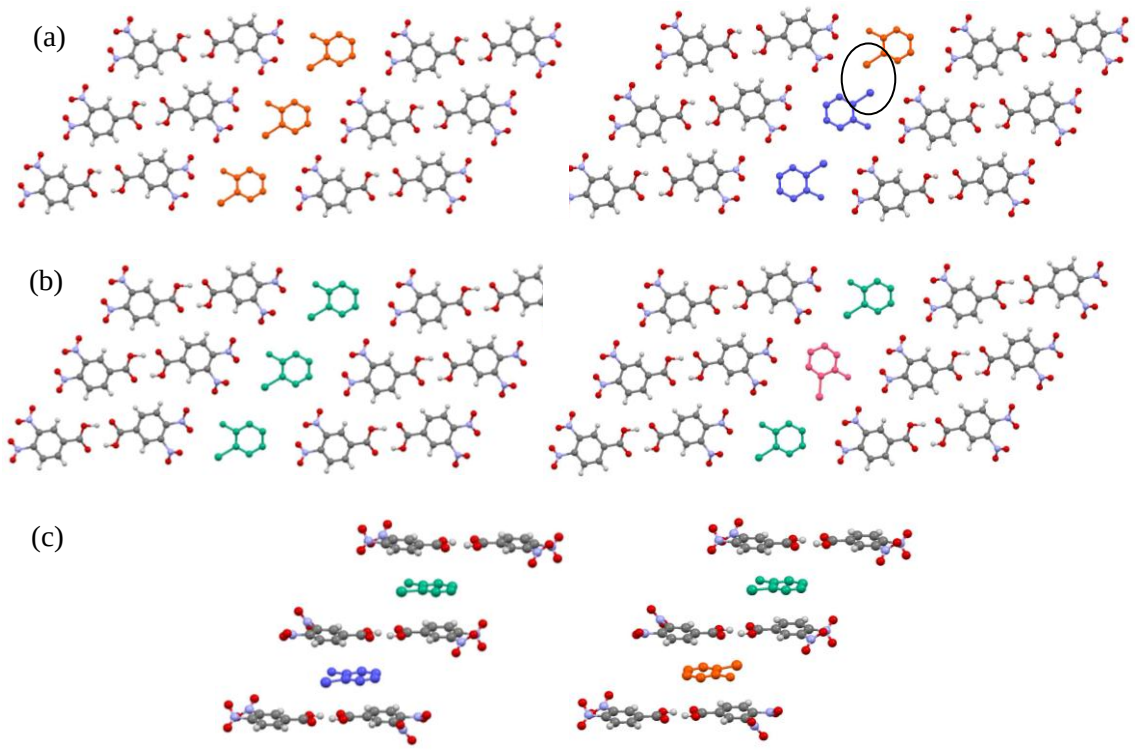

Figure 4.27 Molecular complex **4** (and **6**): (a) Channels of 2-BrA molecules disordered by inversion all in the same orientation (left), and in alternating orientations (right); the close halogen (circled) atoms disallow this; (b) channels of 2-BrA molecules with symmetry-independent disorder, all in the same orientation (left) and alternating orientations (right); (c) molecular stacks of 2-BrA molecules and 3,4-DNBA dimers, with the same and alternate orientations possible.

To collect diffuse scattering measurements for **4**, single crystal X-ray diffraction data were collected at 100 K. Very sharp diffuse scattering is observed between Bragg peaks of changing *k* and *l* in the diffraction pattern (Figure 4.28). The direction of the diffuse scattering observed corresponds to that diagonally between the crystallographic *b*- and *c*- axes, which is the direction in which the molecules stack, and therefore there are likely to be correlations of molecules in the stacks. The sharp diffuse scattering indicates local order over longer length scales.

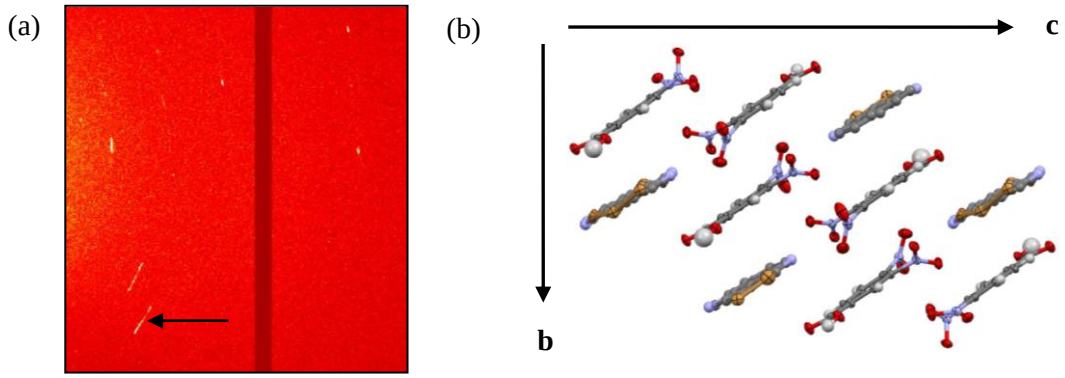

Figure 4.28 (a) Sharp diffuse scattering in the diffraction pattern of molecular complex **4**, between Bragg peaks of changing *k* and *l*. (b) Packing in molecular complex **4**, showing the directions of the crystallographic *b*- and *c*-axes.

Molecular complex 5

The disorder in molecular complex **5** is identical to that in molecular complex **2** (discussed in §4.2.5.1), but there is only one independent 2-BrA molecule; it is possible for adjacent 2-BrA molecules in the channel to be in the same orientation or to be in alternating orientations (Figure 4.24). If they are in alternating orientations, this results in a weak N-H···Br hydrogen bond between the two molecules (N···Br = ~ 3.3 Å). There could also be correlations of molecules in the stacking direction.

In an attempt to obtain diffuse scattering measurements for **5**, single crystals of molecular complex **4** were heated *in situ*. Crystals were mounted at room temperature and then heated using a ramp rate of 60 K/hour. A number of data collection temperatures were tried on different crystals, including 340 K, 345 K and 350 K. The data collection at 345 K (72 °C) was the most successful, however powder rings were evident from the start and data quality was very poor; it was therefore not possible to collect diffuse scattering measurements for **5**.

4.2.6 High resolution powder diffraction studies (I11, Diamond Light Source)

Due to the difficulties encountered in the single crystal X-ray diffraction experiments, it was not possible to structurally characterise some of the new phases, specifically the higher temperature forms of 2-BrA 3,4-DNBA and 2-ClA 3,4-DNBA. High resolution powder diffraction was employed using Beamline I11 at Diamond Light Source. This was the ideal technique for looking at the multi-component systems, with the higher intensity of the synchrotron source enabling high resolution data to be collected in combination with variable temperature measurements. This allowed the phase changes to be followed as well as accurate determination of the phase transition temperature or temperature range. In addition, with data of suitable quality there was the potential of determining lattice parameters, and possibly the crystal structure, of the unknown phases where a single crystal would not survive. This was of particular interest for confirming the structure of Form II of 2-BrA 3,4-DNBA, as well as establishing the Form III structure. Variable temperature experiments were carried out on molecular complexes **1**, **4** and **6** to follow the phase transitions *in situ*. In addition, samples of each of the molecular complexes were pre-heated past each of the phase transitions prior to the experiments and single scans were carried out at room temperature.

4.2.6.1 Experimental details

A full description of the sample preparation and experimental set-up is given in §3.3.2. For variable temperature experiments (λ = 0.825698 nm), data were collected using both detector types (PSD and MAC); the sample temperature was controlled using an Oxford Cryosystems cryostream. Preliminary data were collected with the PSD Mythen-2 detector (2θ = 2°-100°), taking 10 second diffraction patterns every 5 K, in order to identify the temperature range of the phase transitions. A fresh sample was then studied using the MAC detector (2θ = 0°-150°) for higher resolution data, recording patterns for 1800 seconds (30 minutes). Data were collected either side of the phase transitions, and then over the temperature range of interest using smaller temperature increments of 2 K. After each temperature ramp, the temperature was held for five minutes before diffraction patterns were collected to ensure equilibration of temperature across the length of the capillary. For experiments on pre-heated samples of the molecular complexes (λ = 0.825682 nm) a single 10 second diffraction pattern was collected using the PSD Mythen-2 detector (2θ = 2°-100°) at room temperature.

2-IA 3,4-DNBA

0.7 mm (internal diameter) borosilicate capillaries were used for all experiments. *Variable temperature experiments* - PSD: The sample of molecular complex **1** was heated and cooled

between 295-375 K and a diffraction pattern was collected every 5 K. MAC: Diffraction patterns were collected at 295 K, every 2 K between 320-330 K (phase transition 1), at 340 K (midway between phase transitions), every 2 K between 355-365 K (phase transition 2), and at 375 K. The sample was cooled and a final diffraction pattern was collected at 295 K. During the experiment, the capillary position was translated perpendicular to the beam after every two measurements to prevent radiation damage. *Pre-heated samples* - Powdered samples of molecular complex **1** were heated to 55 °C and 87 °C using a hot-plate to obtain Form II (molecular complex **2**) and Form III (molecular complex **3**), respectively. The samples were cooled and stored in sealed vials until beamtime. Using the PSD detector, single diffraction patterns were collected at room temperature on each of the pre-heated samples.

2-BrA 3,4-DNBA

0.5 mm (internal diameter) borosilicate capillaries were used for all experiments. *Variable temperature experiments* - PSD: The sample of molecular complex **4** was heated and cooled between 295-375 K and a diffraction pattern was collected every 5 K. MAC: On heating, diffraction patterns were collected at 295 K, every 2 K between 335-345 K (phase transition 1), every 2 K between 355-365 K (phase transition 2) and at 375 K. On cooling, diffraction patterns were collected every 5 K between 335-320 K and finally at 295 K. During the experiment, the capillary position was translated perpendicular to the beam after every two measurements to prevent radiation damage. *Pre-heated samples*- Powdered samples of molecular complex **4** were heated to 67 °C and 97 °C using a hot-plate to transform the molecular complex to Form II and Form III, respectively. The samples were cooled and stored in sealed vials until beamtime. Using the PSD detector, single diffraction patterns were collected at room temperature on each of the pre-heated samples.

2-ClA 3,4-DNBA

0.5 mm (internal diameter) borosilicate capillaries were used for all experiments. *Variable temperature experiments* - PSD: The sample of molecular complex **6** was heated and cooled between 295-385 K and a diffraction pattern was collected every 5 K . MAC: On heating, diffraction patterns were collected at 295 K and every 2 K between 375-385 K. On cooling, diffraction patterns were collected every 2 K between 360-350 K and finally at 295 K. During the experiment the capillary position was translated perpendicular to the beam after every two measurements to prevent radiation damage. *Pre-heated samples* - A powdered sample of molecular complex **6** was heated to 100 °C using a hot-plate, to transform the molecular complex to Form II. The sample was cooled and stored in a sealed vial until beamtime. Using the PSD detector, a single diffraction pattern was collected at room temperature on the pre-heated sample.

4.2.6.2 Following the phase transitions

In each case, the room temperature diffraction patterns of Form I of each of the complexes (**1**, **4** and **6**) matched the simulated diffraction patterns, thus no changes occurred to the sample upon grinding (Appendix A4, Figure A4.1). Using the high speed PSD detector, diffraction patterns were collected every 5 K on each molecular complex which enabled the approximate temperature range for each of the phase transitions to be established quickly. The MAC experiments then focused on these temperature ranges, collecting high resolution diffraction patterns every 2 K, as well as recording diffraction patterns either side of the phase transitions to ensure high resolution data were collected for each of the pure phases. At present, the analysis of the diffraction patterns and phase transitions has been carried out using simple peak matching across the range of temperatures.

2-IA 3,4-DNBA

In the diffraction patterns collected using the PSD detector, the first phase transition in 2-IA 3,4-DNBA occurred between 320 - 330 K (47 - 57 °C); this matched that expected from the thermal analysis (~52 °C). At 320 K (47 °C), the diffraction pattern matched that of Form I and at 325 K (52 °C) there was a mixture of Form I and a new phase; by 330 K (57 °C) the peaks corresponding to the original phase had disappeared. Thus, data were collected using the MAC detector over this range (320 - 330 K) in 2 K increments. The first phase transition occurred between 322 - 324 K (49 - 51 °C); at 322 K all peaks corresponded to the first phase, and by 324 K new peaks had emerged and peaks present at 322 K had disappeared (Figure 4.29 (a)).

According to the PSD data, the second phase transition occurred between 355 - 365 K (82 - 92 °C); this matched that expected from the thermal analysis (~85 °C). At 360 K (87 °C) there was a mixture of phases present, with a single new phase having emerged by 365 K (92 °C). Therefore, diffraction patterns were collected using the MAC every 2 K over the temperature range 355-365 K. A diffraction pattern was also collected at 340 K (67 °C), which was mid-way between the two phase transitions. In the diffraction patterns collected at 355 K (82 °C) and 357 K (82 °C), there was a slight loss of crystallinity (Figure 4.29 (b)), either due to radiation damage to the sample or due to being mid-way through the phase transition. The two diffraction patterns appeared to be a mixture of the Forms II and III. The diffraction pattern collected at 359 K (86 °C) corresponded to Form III (Figure 4.29 (b)). For both the PSD and MAC experiments, final diffraction patterns were collected at 375 K; the sample was cooled back to room temperature and a diffraction pattern was collected at 295 K. The patterns at 375 K and at 295 K (after cooling) matched well, confirming that the phase transition is not reversible (Figure 4.29 (c)).

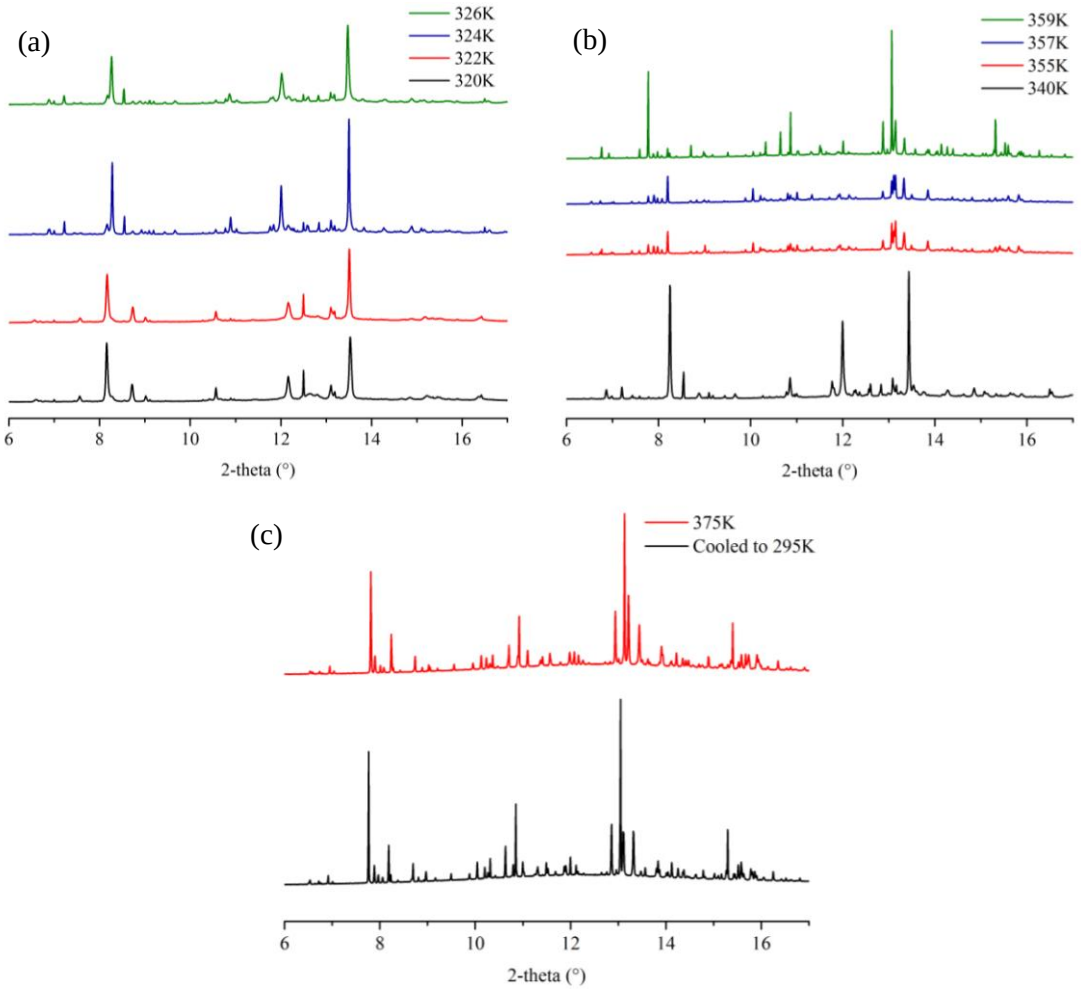

Figure 4.29 2-IA 3,4-DNBA: (a) Diffraction patterns (MAC) between 320 K and 326 K, showing the first phase transition occurring between 322 K and 324 K. (b) Diffraction patterns (MAC) at 340 K (mid-way between phase transitions 1 and 2), at 355 K and 357 K (loss of crystallinity and mixture of phases) and the new phase at 359 K. (c) Diffraction patterns (MAC) at 375 K and after cooling to 295 K. There is no change on cooling, confirming the irreversible phase transition.

Prior to beamtime, samples of molecular complex **1** were also heated to above each of the phase transition temperatures using a hot-plate, to 57 °C and 90 °C to obtain Forms II and II, respectively. This eliminated the possibility of having only partial conversion which was possible in the variable temperature experiments as a temperature gradient was present along the capillary. A single diffraction pattern was collected on each of the pre-heated forms at room temperature, allowing them to be compared directly, with no peak shifts due to temperature. The pre-heated samples (expected to be molecular complexes **2** and **3**) were plotted against the room temperature diffraction pattern of molecular complex **1** (Figure 4.30).

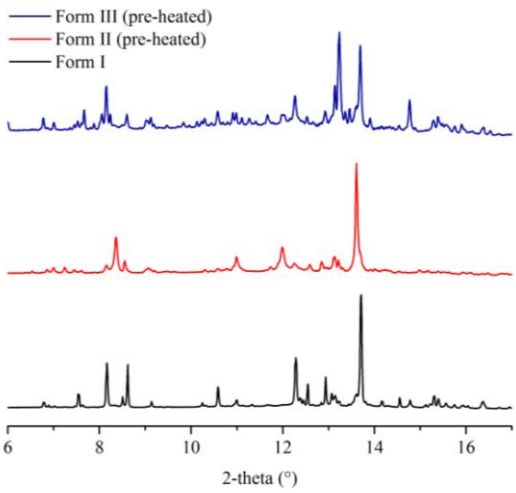

Figure 4.30 Room temperature diffraction patterns (PSD) of molecular complex **1**, and of the samples pre-heated to Forms II (**2**) and III (**3**).

The diffraction patterns of the samples heated to beyond the first phase transition (Form II), both *in situ* and on the hot-plate, are consistent with the simulated pattern of **2** (Appendix A4, Figure A4.2), with some shifts in peak positions reflecting the temperature differences and some preferred orientation effects affecting the intensities in the *in situ* temperature scan patterns. Form III gives a more complex picture, with a less good match to the simulated powder pattern of **3** (Appendix A4, Figure A4.3); this, however, may reflect the poorer quality of the model used to calculate the simulated pattern (due to the disorder), and may also be due to preferred orientation effects. There may also be a mixture of phases present in the Form III samples, possibly due to a temperature gradient across the capillary, or due to the balance between obtaining pure Form III and the proximity of the transition to the melting point of the sample. However, there is an associated colour change from red to yellow on passing through the phase transition to Form III; this supports the conclusion that the bulk powder sample and the single crystal Form III are the same.

2-BrA 3,4-DNBA

Diffraction patterns collected using the PSD detector showed an extremely subtle change in two peak intensities (~2θ = 8.5) between 335 - 345 K (62 - 72 °C), which was assumed to be the first phase transition (thermal analysis had shown the transition to occur at ~65 °C). A second change in the diffraction pattern was observed between 355 - 365 K (82 - 92 °C); although this was at a lower temperature than expected (thermal analysis had shown the transition to occur at ~95 °C), it was thought to correspond to the second phase transition (Figure 4.31 (a)). Therefore, MAC data were collected in 2 K steps over the two temperature ranges of 335 - 345 K and 355 - 365 K. The subtle change in the peak at ~2θ = 8.5 was still observed at 340 K

(67 °C); however, two significant changes in the diffraction pattern were observed above this temperature, as opposed to only a single change in the PSD experiment.

The first transition was between 355 - 357 K (82 - 84 °C), and corresponded to the changes observed in the diffraction pattern in the PSD experiment over the range 355 - 365 K (82 - 92 °C) (Figure 4.31 (b)). The small changes observed between phases I and II are consistent with the small differences in the simulated pattern of **4** and the simulated pattern of the proposed Form II structure, **5** (obtained evaporatively) (Appendix A4, Figure A4.4). Furthermore, this suggests small structural changes which is consistent with the subtle structural differences between molecular complexes **4** and **5**. The simulated pattern of **5** and the diffraction pattern of phase II are reasonably consistent (Appendix A4, Figure A4.4), with some shifts in peak positions reflecting the temperature differences and some preferred orientation effects affecting the intensities in the *in situ* temperature scan patterns. This further suggests that the phase transition corresponds to the transition from **4** to **5**. As for the 2-IA 3,4-DNBA complexes, there may be preferred orientation effects and it is possible there is a mixture of phases present.

The second major transition in the MAC data was very clear, between 363-365 K (90 - 92 °C) (Figure 4.31 (c)). This suggested that this final transition was actually missed in the PSD experiment, possibly due to the presence of a temperature gradient across the capillary; the temperature was held for a much longer period of time in the MAC experiments, allowing the temperature to be equilibrated across the whole sample. It is probable that in the MAC data, the transitions at 355-357 K (82 - 84 °C) and 363 - 365 K (90 - 92 °C) corresponded to the first and second phase transitions, respectively. The temperature of the first phase transition of 357 K (84 °C) is slightly higher than expected according to thermal analyses (~66 °C), but the temperature of the second phase transition of 365 K (92 °C) is in the expected temperature range according to thermal analyses. It is possible that the very subtle change observed in the peak intensities, at ~2θ = 8.5, could be due to a change in the proportions of the disorder, but the only way to confirm this would be by single crystal data.

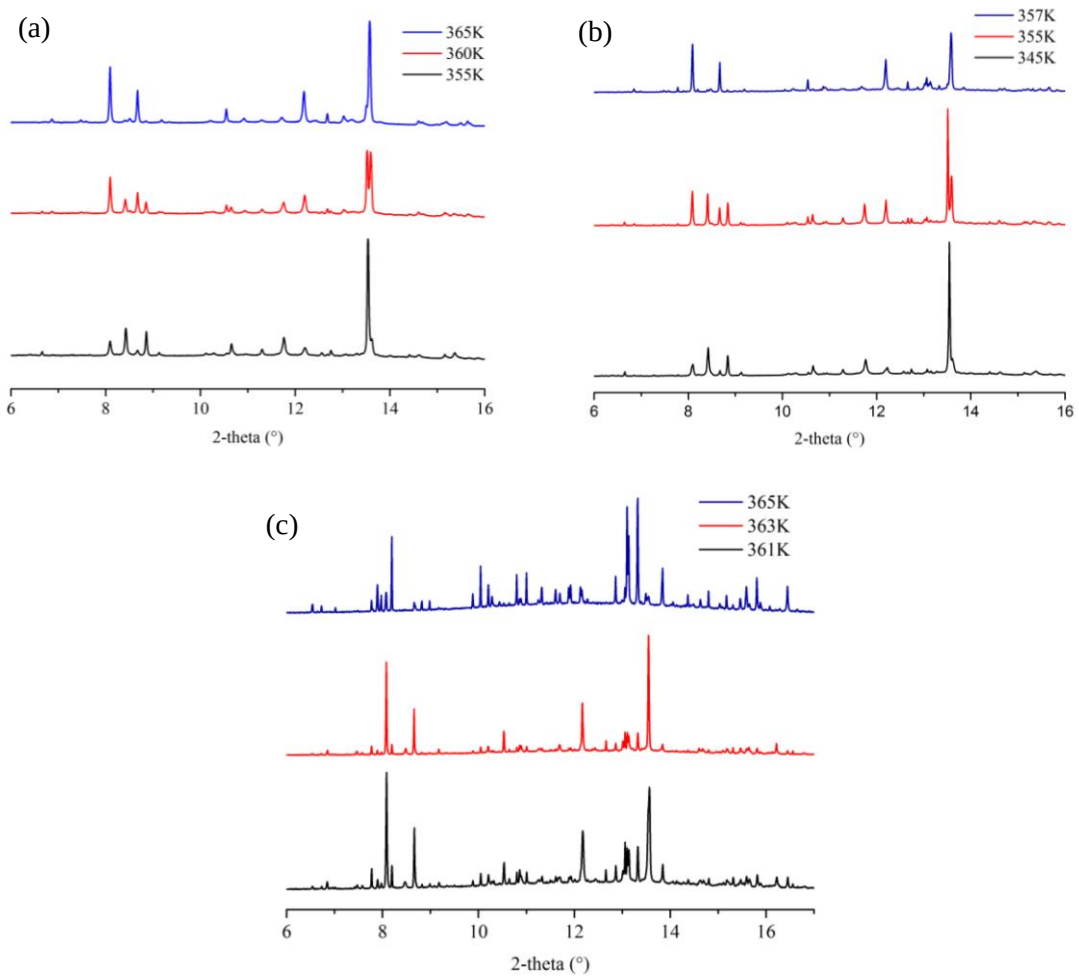

Figure 4.31 2-BrA 3,4-DNBA: (a) Phase transition in the temperature range 355-365 K in PSD data; (b) phase transition between 355-357 K in MAC data; (c) phase transition observed in the MAC data between 363 - 365 K.

In the PSD and MAC experiments, the samples were heated to a final temperature of 375 K and then cooled to 295 K. In the PSD experiment, diffraction patterns were collected every 5 K on cooling back to room temperature; a very small change was observed between 330 K (57 °C) and 320 K (47 °C), and MAC collections therefore focused on this temperature range. High resolution diffraction patterns were collected every 5 K between 335 K (62 °C) and 320 K (47 °C), with a final collection at 295 K. There were no significant changes in the diffraction patterns over this range, with just two small peaks emerging at 2θ = 8.7° and 13.8°. The diffraction patterns collected at 375 K and 295 K (after cooling) matched very closely, with no apparent conversion back to Form I (shown for MAC data, Figure 4.32 (a)). There was no significant change in the diffraction patterns on cooling in the PSD experiments either. It is possible that this is due to a temperature gradient across the capillary, or the greater sample size used in comparison to that used in the thermal analyses. It is also possible that due to holding the temperature at 375 K for 30 minutes, melting and recrystallisation occurred, resulting in an

unexpected phase (N.B. the diffraction patterns at 375 K and at 295 K after cooling do not correspond to the starting materials).

To investigate the reversibility further, samples of molecular complex **4** were heated prior to beamtime using a hot-plate, to 70 °C and 100 °C to obtain Forms II and III, respectively. The samples were allowed to cool back to room temperature and were stored in sealed vials. A single diffraction pattern was collected on each of the pre-heated samples at room temperature, using the PSD detector, and compared to the room temperature diffraction pattern of Form I. The diffraction patterns are all consistent with that of Form I, confirming that each of the samples had converted back to Form I, as expected from the thermal analyses (Figure 4.32 (b)).

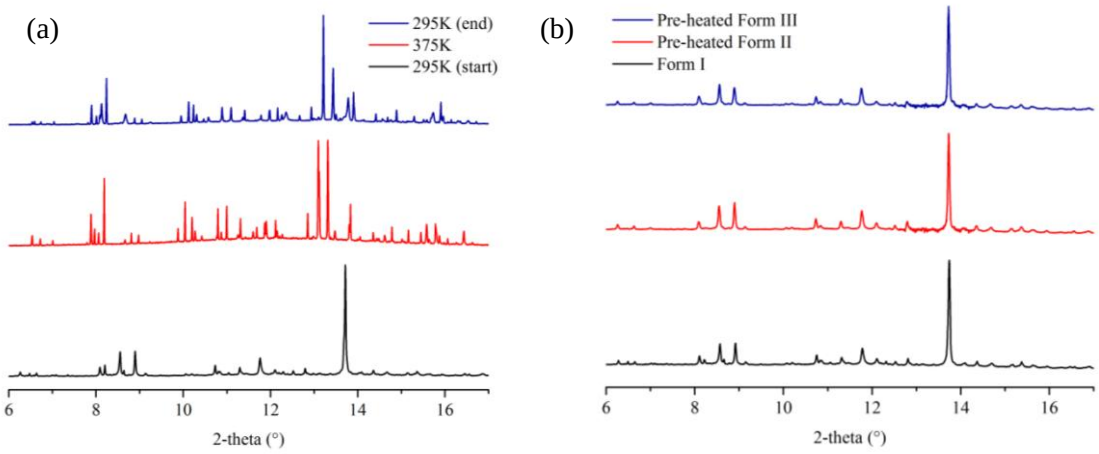

Figure 4.32 (a) Diffraction patterns (MAC) comparing the first collection at 295 K with the diffraction patterns collected before and after cooling back to 295 K. (b) Room temperature diffraction patterns (PSD) of molecular complex **4**, and the samples pre-heated (to Forms II and III) and cooled.

2-ClA 3,4-DNBA

Diffraction patterns collected using the PSD detector showed that the single phase transition in molecular complex **6** occurred between 375 - 385 K (102 - 112 °C); thermal analysis showed the phase transition occurred at ~90 °C and the sample melts at 110°C. At 380 K (107 °C), a mixture of two phases were present, with the transition complete by 385 K (112 °C) (Figure 4.33 (a)). MAC data was collected every 2 K over this temperature range, with an initial diffraction pattern collected at 295 K. However, the transition had taken place during the temperature ramp to 375 K, with the diffraction pattern collected at 375 K (102 °C) matching the new phase (Figure 4.33 (b)).

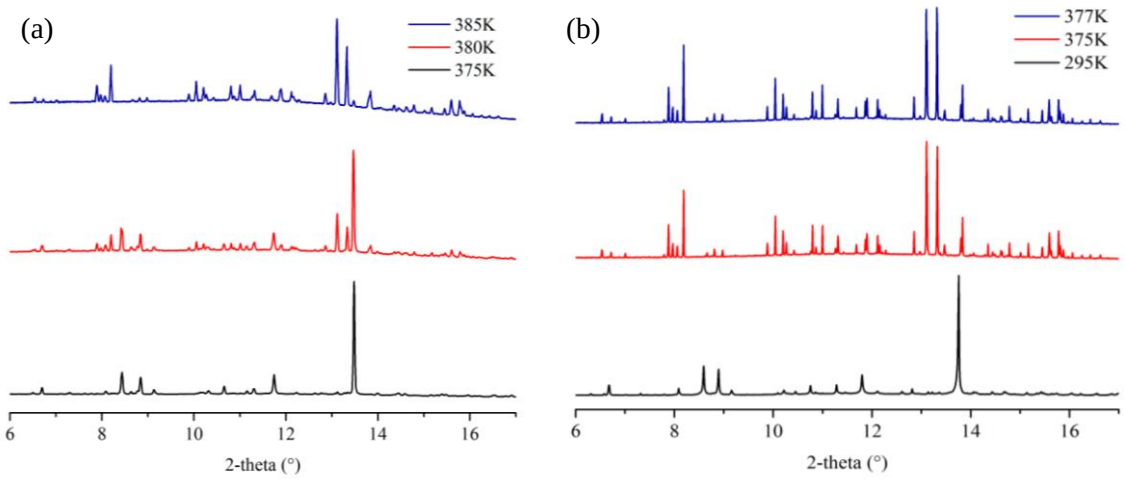

Figure 4.33 Diffraction patterns collected using (a) the PSD between 375 K and 385 K, and (b) the MAC at 295 K, 375 K and 377 K. Note, the phase transition had occurred prior to reaching 375 K.

PSD data showed that on cooling, the reverse phase transition occurred between 360 K (87 °C) and 350 K (77 °C). The final data collection after cooling to 295 K matched that of Form I, clearly showing that the reverse transition had occurred (Figure 4.34 (a)). Diffraction patterns were collected using the MAC every 2 K on cooling over the same temperature range. However, in this data there was no significant change in the diffraction pattern on cooling; although there are small changes, the final pattern collected at 295 K is very similar to that collected prior to cooling (Figure 4.34 (b)). In order to observe the phase transition in the PXRD experiments, the sample temperature had to be held very close to the melting point of the molecular complex for 30 minutes to collect MAC data. It is possible that there was a melt and recrystallisation as a different form, thus the reverse transition was not observed (N.B. the diffraction patterns at 375 K and at 295 K after cooling do not correspond to the starting materials).

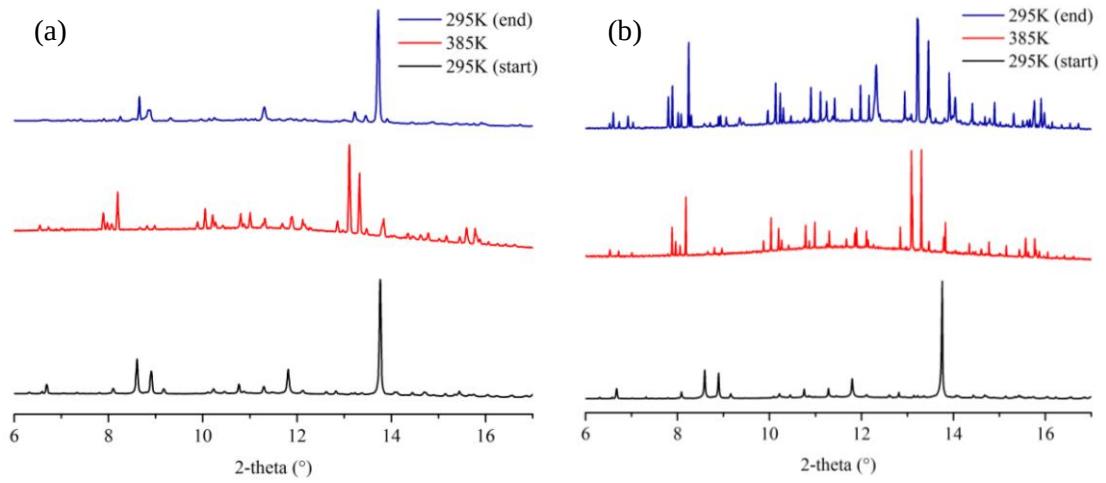

Figure 4.34 Diffraction patterns of 2-ClA 3,4-DNBA collected at 295 K, at 385 K and at 295 K (after cooling) using (a) PSD and (b) MAC. The reverse transition is observed in PSD data but not MAC data.

To investigate the reversibility further, a sample of molecular complex **6** was heated using a hot-plate prior to beamtime to 95 °C, which was just past the transition temperature observed in thermal analysis; the sample was cooled and stored in a sealed vial. A room temperature diffraction pattern was collected on the sample using the PSD detector, and compared with the room temperature diffraction pattern of Form I (**6**). Unlike the 2-BrA 3,4-DNBA complexes, there are additional, unexpected peaks in the pre-heated sample compared to Form I (Figure 4.35). The reason for this unknown, but it is possible that heating to a high temperature on the hot-plate, in order to go through the transition, led to a melt and recrystallisation of part of the sample, resulting in a small amount of a second phase being present.

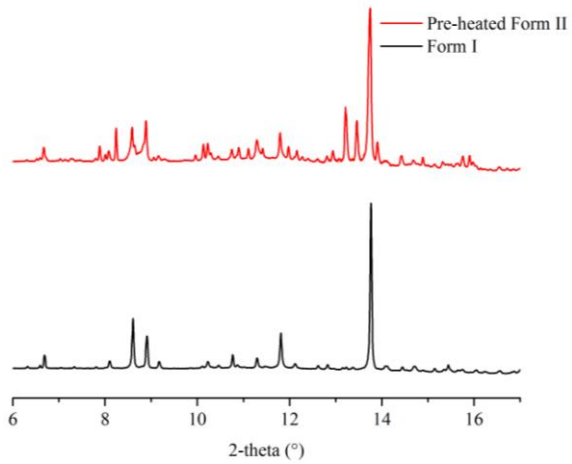

Figure 4.35 Room temperature diffraction patterns (PSD) of Form I (molecular complex **6**) and the sample pre-heated to Form II and cooled.

4.2.6.3 Summary

The room temperature diffraction patterns of Form I of each of the complexes (**1**, **4** and **6**) matched the simulated diffraction patterns, and therefore no changes occurred during the sample preparation. For each of the molecular complexes, the phase transitions that were expected to occur were observed, and in general the phase transition temperatures observed correlated well with those expected from the thermal analyses. In addition, the diffraction patterns of each of the new phases were generally consistent with the simulated diffraction patterns for each of the forms. However, the experiments were challenging and there were a number of issues to consider. Of particular note are the discrepancies in some of the transition temperatures between the PSD and MAC experiments; there were evidently problems with temperature gradients across the capillaries. In the PSD experiments, the sample was held at each temperature for only 30 seconds, compared to 30 minutes in the MAC experiments; it is possible that in the PSD experiments this did not allow the whole capillary to be heated to the recorded temperature

across the whole capillary. In the case of the 2-BrA 3,4-DNBA experiments, this led to the second phase transition being missed in the PSD data collection. In addition, due to the expected problem with temperature gradients, it is possible that there are also mixtures of phases present in the diffraction patterns.

In 2-IA 3,4-DNBA, the irreversibility of the phase transitions was confirmed through cooling in the variable temperature experiments (PSD and MAC), and through data collection on pre-heated samples. However, for 2-BrA 3,4-DNBA and 2-ClA 3,4-DNBA, there were problems with the consistency of the reversible behaviour across the PSD experiments, MAC experiments and pre-heated sample experiments. The reversible phase transitions were not always observed as expected according to the thermal analyses. This was the case for 2-BrA 3,4-DNBA in both the variable temperature experiments (MAC and PSD). However, the pre-heated samples did all convert back to Form I. For 2-ClA 3,4-DNBA, the reverse transition was only observed in cooling in the PSD experiments. It is possible that upon heating of some samples, there was a melt and recrystallisation of all, or part of, the sample; this was most probable in the MAC experiments due to subjecting the sample to a temperature very close to the melting point for 30 minutes. On removing the capillary, parts of the sample did appear to of melted and recrystallised, with larger crystallites present; this may also have led to preferred orientation effects being observed.

4.2.7 Mechanism for the phase transitions

The molecular disorder is a major structural feature in each of the molecular complexes and their associated phase transitions, thus its effect on the crystal packing and structural rearrangement was investigated. For each 2-haloaniline site in the crystals of **1** - **6**, there are two possible molecular orientations which partially overlap. It was therefore expected that this would result in a greater volume of crystal space available for the 2-haloaniline molecules in the molecular complexes compared to that in an ordered crystal. Although the average structure shows two possible molecular positions, only one of these is occupied in any one site, which means there is likely to be space around this molecule. This concept can be understood using the 'molecular fish' which is disordered over two positions, shown in purple and green (Figure 4.36); it can only be in one of the positions at any one time, and the structure surrounding the fish is static. Thus, when the fish is in the position shown in purple, the part shown in green is void space.

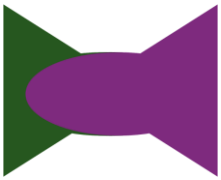

Figure 4.36 'Molecular fish' disordered over two positions; when the fish in the position shown in purple, the part shown in green is void space.

In order to measure this potential additional crystal space in the molecular complexes, the 2-haloaniline molecules were removed from the model and the void space was calculated to determine the volume of crystal space available to the 'guest' 2-haloaniline molecules in the ordered 3,4-dinitrobenzoic acid network. This was calculated using Mercury,[201] with a probe radius of 1.2 Å and a grid spacing of 0.1 Å; an example of the space available to the 2-haloaniline molecule is shown in Figure 4.37 for molecular complex **3**. The volumes occupied by ordered 2-haloaniline molecules were obtained from data for the single-component crystal structures in the Cambridge Structural Database (CSD)[86]: RALTOO (2-iodoaniline),[232] IGEHIM (2-bromoaniline)[233] and IGEHEI (2-chloroaniline).[233] Table 4.9 details the relevant volumes and void calculations for molecular complexes **1** - **6**.

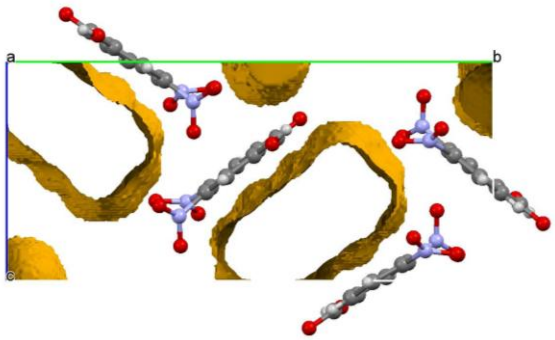

Figure 4.37 Example of the calculation of the volume of space associated with the 2-IA molecules (shown for molecular complex **3**); calculations were conducted by removing the 2-IA molecules from the model.

The void space calculations show that the average volume of crystal space attributed to each 2-haloaniline site is increased in all of the disordered molecular complexes, in comparison to the fully ordered 2-haloaniline molecules. In **1**, **4** and **6**, there is a 19.40%, 16.36% and 20.09% increase in the volume of crystal space associated with the 2-haloaniline molecules, respectively, compared to the ordered 2-haloaniline molecule in each case. In general, crystal packing is driven to produce the most efficient and densely packed arrangement of molecules in a solid. However, in mixed stack CT complexes, molecular disorder can occur due to inefficient packing, in particular where there are no strong interactions to favour a single position.

Table 4.9 Relevant volumes and results of void space calculations for molecular complexes **1** - **6**

	Molecular complex 1	**Molecular complex 2**	**Molecular complex 3**
Formula unit (Z)	C_{20} H_{14} N_5 O_{12} I (2)	C_{20} H_{14} N_5 O_{12} I (4)	C_{20} H_{14} N_5 O_{12} I (2)
Unit cell volume (Å^3)	1158.91(11)	2285.8(3)	1193.57(9)
Density (g/cm^3)	1.843	1.870	1.790
Void/unit cell with 2-XA removed (Å^3)	398.63	728.91	409.52
Average volume/ disordered 2-XA site (Å^3)	199.32	182.23	204.76
Volume of ordered 2-XA site (Å^3)	166.930	166.930	166.930
% increase in volume for disordered 2-XA site	19.40%	9.17%	22.66%
	Molecular complex 4	**Molecular complex 5**	**Molecular complex 6**
Formula unit (Z)	C_{20} H_{14} N_5 O_{12} Br (3)	C_{20} H_{14} N_5 O_{12} Br (2)	C_{20} H_{14} N_5 O_{12} Cl (3)
Unit cell volume (Å^3)	1693.4(3)	1142.8(3)	1690.15(13)
Density (g/cm^3)	1.754	1.733	1.626
Void/unit cell with 2-XA removed (Å^3)	552.25	344.79	563.15
Average volume/ disordered 2-XA site (Å^3)	184.08	172.40	187.72
Volume of ordered 2-XA site (Å^3)	158.195	158.195	156.317
% increase in volume for disordered 2-XA site	16.36%	8.98%	20.09%

In each of the 2-XA 3,4-DNBA complexes, there is significant empty crystal space surrounding each of the 2-XA molecules. Due to the 1:2 ratio of the 2-XA and 3,4-DNBA molecules, there is only a single 2-XA molecule to each 3,4-DNBA dimer. To form a mixed stack complex, the stacking must occur between 2-XA molecules and the centres of the dimers. The formation of the ordered and robust 3,4-DNBA dimer host network very effectively increases the size of the 'acceptor part' of the stack, and the volume of space available to the donor (Figure 4.38).

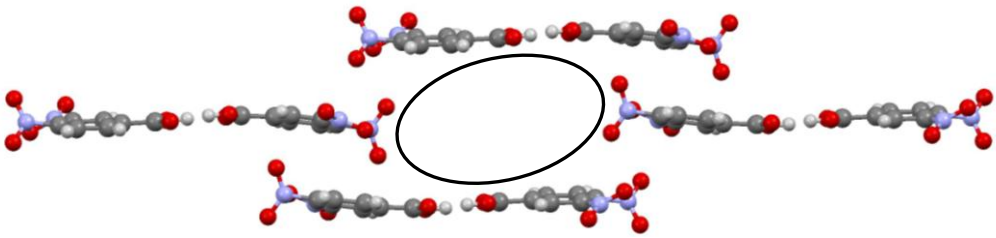

Figure 4.38 The space available (circled) to the donor 2-XA molecules in the 2-XA 3,4-DNBA dimer mixed stack arrangement.

The greater volume of crystal space (or 'reorientation pockets') associated with each 2-haloaniline molecule may allow the structure the flexibility to rearrange, thereby allowing the massive structural rearrangement to Form III to occur in a single-crystal to single-crystal manner. For 2-IA 3,4-DNBA, the thermochromic properties can therefore also be attributed to the disorder present in the system and the structural changes which the disorder facilitates.

In terms of the crystallisation of 2-IA 3,4-DNBA, based on the higher density and smaller amount of void crystal space, Form II would be expected to be the most stable and most likely to be formed. However, Form II was only obtained in very small quantities. Comparison of the intermolecular interactions (N-H···O and C-I···O) between 2-IA molecules and the 3,4-DNBA tapes in **1** and **2**, shows that the interactions within the sheets are generally stronger in molecular complex **1**. It is possible that the greater strength of the interactions between the disordered guest 2-IA molecules and the ordered 3,4-DNBA network results in the formation of **1** being more favourable.

With regards to the phase transitions, the higher density of Form II compared to Form I provides a possible explanation for the irreversibility of the first phase transition, despite Form I appearing to be more favourable upon crystallisation. For the second transition, although Form III is the least dense, the structure remains as the herringbone form and does not convert back, despite the more efficient packing in Forms I and II. It is possible that this is due to the rearrangement being too large.

In 2-BrA 3,4-DNBA and 2-ClA 3,4-DNBA, the phase transitions are all reversible. The transition temperatures are also higher than those of the equivalent transitions in 2-IA 3,4-DNBA. Despite the similarities of the Form II structures of 2-IA 3,4-DNBA (**2**) and 2-BrA 3,4-DNBA (**5**), in the 2-BrA complex the transition is associated with a decrease in density; this decrease in density is a possible explanation for the reversibility of the phase transition in 2-BrA 3,4-DNBA compared to 2-IA 3,4-DNBA. In addition, in Form I, the N-H···O hydrogen bonds formed between the disordered 2-BrA molecules and the 3,4-DNBA network are stronger than those formed in Form II.

It was not possible to obtain a crystal structure, or unit cell parameters, for Form III of 2-BrA 3,4-DNBA, but it is probable that the second phase transition was also associated with a decrease in density; the same may be true for the single phase transition observed in 2-ClA 3,4-DNBA. It is also possible that rearrangement to Form III in 2-BrA 3,4-DNBA is not as significant as observed in the 2-IA molecular complex. A smaller rearrangement would also provide an explanation for the lack of thermochromic properties in 2-BrA 3,4-DNBA.

4.2.8 Summary and discussion

In the first section of this chapter, six molecular complexes of 2-haloaniline 3,4-dinitrobenzoic acid have been reported. The molecular complexes have the same 1:2 stoichiometry and include the same ordered hydrogen bonded 3,4-DNBA tape network; there is whole molecule disorder of the 2-haloaniline molecules over two well-defined positions in each of the complexes. Forms I and II of the complexes are all yielded as red crystals, with the origin of the colour lying in the solid-state. Due to the 1:2 stoichiometry, there is only one 2-XA molecule to each 3,4-DNBA dimer. The crystal packing is dominated by aromatic donor···acceptor interactions between alternately stacked 2-XA and 3,4-DNBA dimers. The molecular separation of the stacked molecules is the same in each complex, and the predominant overlap is between the 2-XA ring/halogen and the centre of the 3,4-DNBA dimer; the colour can be attributed to charge-transfer, with a broad band observed in the solid-state UV-visible absorption spectra. In Form III of 2-IA 3,4-DNBA, which is yellow in colour, the crystal packing has a herringbone arrangement rather than planar. The stacking is not continuous between aromatic donor and acceptor molecules and is predominantly between the 2-IA and 3,4-DNBA rings, with no overlap with the centre of the dimer; this may provide an explanation for the change in colour.

The disorder in the complexes is likely to be due to competition between the similar strength N-H···O hydrogen bonds and halogen bonds that can be formed between the 2-XA and 3,4-DNBA molecules. The molecular complexes are all neutral, thus carboxylic acid dimers

form through the strongest hydrogen bond donors and acceptors; this leaves nitro group O-atoms for the 2-XA molecules to interact with, with a mismatch of the number of hydrogen/halogen bond donor and acceptor atoms. The disordered molecules act as 'guests' in the ordered 3,4-DNBA hydrogen bonded host network, and form channels within the planar sheets. It is apparent that disorder is a prerequisite to form a stable lattice; diffuse scattering measurements indicate local ordering in the complexes, predominantly in the stacking direction.

Each of the molecular complexes undergo phase transitions upon heating; the phase transitions were studied by DSC, HSM, UV-visible spectroscopy, single crystal X-ray diffraction and powder X-ray diffraction. 2-IA 3,4-DNBA and 2-BrA 3,4-DNBA both undergo two transitions prior to melting, while 2-ClA 3,4-DNBA undergoes only a single transition. The phase transition temperatures increase with decreasing molecular weight of the halogen, which must reflect the nature of the halogen. In the 2-IA 3,4-DNBA complex, the phase transitions are both irreversible (as shown in the DSC and PXRD experiments). However, in 2-BrA 3,4-DNBA and 2-ClA 3,4-DNBA the phase transitions are both reversible, although the PXRD results showed this somewhat ambiguously. Characterisation of the higher temperature forms by SCXRD proved challenging, with *in situ* heating typically resulting in crystal degradation. It is likely that Form II of 2-BrA 3,4-DNBA is equivalent to molecular complex **5** (obtained evaporatively).

The first phase transition in 2-IA 3,4-DNBA and 2-BrA 3,4-DNBA is associated mainly with a reorientation of the disordered 2-haloaniline molecules. Despite the different disorder in Form I of the two complexes, the Form II molecular complexes (**2** and **5**) are isostructural and have identical disorder. However, in 2-BrA 3,4-DNBA, the complex converts back to Form I upon cooling. It is possible that this is due to Form I having a higher density than Form II; In 2-IA 3,4-DNBA, the opposite is true. The second phase transition in 2-IA 3,4-DNBA, to Form III, involves a massive structural rearrangement, going from the layered structure of Form II to a herringbone structure. This transformation occurs with survival of the single crystal, which is very surprising given the very dramatic change in the structure. This transition is also thermochromic, and is associated with a clear change in colour from red to yellow, as identified through hot-stage microscopy and UV-visible spectroscopy. Although Form III of 2-BrA 3,4-DNBA could not be structurally characterised, it is likely that the transition from Form II to III is associated with a further decrease in density and the rearrangement is much less significant than for the 2-IA 3,4-DNBA complex; this would provide an explanation for both the reversible behaviour and for the lack of thermochromic properties.

Analysis of the crystal structures shows that there is an significant increase in the volume of crystal space available to accommodate each 2-haloaniline molecule compared to a fully

ordered case, with the presence of molecular disorder inherently resulting in less efficient packing. It is likely that the molecular orientations and large structural rearrangement are therefore disorder-facilitated, with the greater volume of crystal space available to the disordered molecules allowing the structure significant flexibility to rearrange. The thermochromic properties of 2-IA 3,4-DNBA can therefore also be attributed to the disorder present in the systems and the structural changes which the disorder allows. The structures presented in §4.2, strongly suggest that the introduction of disorder in the crystalline state can lead to favourable properties on application of an external stimulus.

4.3 Molecular complexes of 2-fluoroaniline and 3,4-dinitrobenzoic acid

Following the successful multi-component complex formation of 2-IA, 2-BrA and 2-ClA with 3,4-DNBA (§4.2), experiments were conducted using 2-fluoroaniline (2-FA) as the co-former. This was primarily to investigate whether molecular complexes would form, and additionally whether the potential molecular complexes displayed similar temperature-dependent behaviour. The ΔpKa value for 2-FA and 3,4-DNBA is 0.43 which lies in the salt-cocrystal continuum, thus proton transfer may or may not occur. This compares to the negative values of ΔpKa for the other 2-haloaniline complexes, where the components remained in their neutral states as expected. From a crystal engineering perspective, fluorine typically behaves very differently to the other halogens (I, Br, Cl); fluorine is the least polarisable and most electronegative of the halogen atoms, and much less likely to acts as a halogen bond donor with the strength of the halogen bond donor decreasing in the order I>Br>Cl>>F (Chapter 1, §1.3.2). Due to the differences between the roles of fluorine and the other halogens in crystal engineering, and the greater ΔpKa value, formation of a molecular complex similar to those obtained from the other 2-haloaniline co-formers was not necessarily expected.

4.3.1 Experimental details

Molecular complexes **7** and **9** were obtained *via* the method of slow evaporation (§3.1); molecular complex **8** was obtained upon cooling **7**. A 1:2 stoichiometric molar ratio of the 2-fluoroaniline and 3,4-dinitrobenzoic acid was used; crystallisation trials employed a range of solvents and evaporation temperatures. The quantities of the molecular components were varied, in addition to the type of crystallisation vessel, to optimise molecular complex growth. Some vapour diffusion crystallisations were also set up, but were unsuccessful. The conditions which resulted in growth of the crystals used for collection of SCXRD data are reported here; more details on the crystallisation conditions are provided in §4.3.2. Single crystal X-ray diffraction

experiments were carried out according to the procedures outlined in §3.2; crystallographic data are given in Table 4.10 and refinement details are reported in Appendix A4.

2-fluoroaniline 3,4-dinitrobenzoic acid (7)

Molecular complex **7** was synthesised from methanol, dissolving the components in the minimum amount of solvent; the crystallisation was carried out in a glass beaker on a larger scale than standard crystallisations (0.5 mmol (0.056 g) 2-FA, 1 mmol (0.216 g) 3,4-DNBA). The beaker was covered in parafilm and four small perforations were made; evaporation was carried out in the fridge at 4 °C. Red block crystals were obtained after two days and single crystal X-ray diffraction data were collected at ambient temperature using a Rigaku Oxford Diffraction Gemini Ultra diffractometer (Mo Kα radiation). The structure was solved by direct methods using SHELXS-2013[192] and refined using SHELXL-2014,[198] both within the WinGX program suite.[200] N.B. Larger crystals were grown, but still in relatively small quantities, when the crystallisation was carried out in a sealed vial at 4 °C; crystals were obtained after approximately six weeks.

2-fluoroanilinium 3,4-dinitrobenzoate 3,4-dinitrobenzoic acid (8)

Molecular complex **8** was obtained by slow-cooling (120 K/hour) a single crystal of molecular complex **7** from ambient temperature to 220 K *in situ* on the diffractometer. Single crystal X-ray diffraction data were collected at 220 K using a Rigaku Oxford Diffraction Gemini Ultra diffractometer (Mo Kα radiation). Following data collection at 220 K, the same crystal was further cooled to 150 K *in situ* and data were collected at 150 K. The structures (at 220 K and 150 K) were solved by direct methods using SHELXS-2013[192] and refined using SHELXL-2014,[198] both within the WinGX program suite.[200]

2-fluoro-4-[(1E)-2-(2-fluorophenyl)diazenyl]-benzenamine 3,4-dinitrobenzoic acid (9)

The reaction product, molecular complex **9**, was synthesised from methanol at both 4 °C and ambient temperature, and was yielded as small, dark red triangular plate crystals. Single crystal X-ray diffraction data were collected at 100 K using a Rigaku Oxford Diffraction Gemini Ultra diffractometer (Mo Kα radiation). The structure was solved by direct methods using SHELXS-2013[192] and refined using SHELXL-2014,[198] both within the WinGX program suite.[200]

Table 4.10 Crystallographic data for molecular complexes **7** - **9**

	7	**8**	**8**	**9**
Formula	(C_6H_6FN) $2(C_7H_4N_2O_6)$	$(C_6H_7FN)^+$ $(C_7H_3N_2O_6)^-$ $(C_7H_4N_2O_6)$	$(C_6H_7FN)^+$ $(C_7H_3N_2O_6)^-$ $(C_7H_4N_2O_6)$	$(C_{12}H_9F_2N_3)$ $2(C_7H_4N_2O_6)$
M/g mol^{-1}	535.36	535.36	535.36	657.46
T/K, radiation	297(2), Mo Kα	220(2), Mo Kα	150(2), Mo Kα	100(2), Mo Kα
Space Group	$P\bar{1}$	$P\bar{1}$	$P\bar{1}$	C2/c
a/Å	7.6425(4)	7.7279(5)	7.6618(6)	13.8428(6)
b/Å	13.9342(6)	11.1134(5)	11.1022(6)	7.2799(3)
c/Å	16.2419(8)	13.6352(10)	13.6067(12)	52.755(2)
α	87.270(4)	84.617(5)	84.743(6)	90
β	87.188(4)	85.492(6)	85.879(7)	90.652(3)
γ	86.355(4)	70.905(5)	70.877(6)	90
V/Å	1722.34(14)	1100.29(12)	1087.88(15)	5316.0(4)
Z	3	2	2	8
ρ_{cal}/ g cm^{-3}	1.548	1.616	1.634	1.643
μ/mm^{-1}	0.136	0.141	0.143	0.141
θ Range/°	2.853 - 25.027	3.081 - 26.369	3.106 - 25.025	2.943 - 26.372
Ref Collected	14073	10064	7197	32495
Independent	6059	4485	3459	5431
Observed>2σ	2252	2414	2274	3635
Rint	0.0669	0.0534	0.0366	0.0819
Completeness %	99.9	99.7	89.9	99.9
Parameters	459	365	365	418
GooF	0.972	1.013	1.013	1.027
R_1 (obs)	0.0972	0.0601	0.0517	0.1074
R_1 (all)	0.2224	0.1325	0.0937	0.1499
wR2 (all)	0.3554	0.1562	0.1445	0.2819
$\rho_{max,min}$/e Å^{-3}	0.614, -0.544	0.361, -0.337	0.409, -0.258	2.437, -1.248

4.3.2 Crystallisation and sample analysis

In the co-crystallisation trials, two multi-component complexes, **7** and **9**, were formed through slow evaporation of solvent. Molecular complex **7** is a 1:2 molecular complex of 2-FA and 3,4-DNBA, with similar crystal packing to molecular complexes **1**, **4** and **6**. On cooling, molecular complex **7** undergoes a phase transition to molecular complex **8**; molecular complex **8** could not be obtained *via* slow evaporation. Molecular complex **9** is a 1:2 molecular complex containing a single molecule of the product of a reaction between two 2-FA molecules and two molecules of 3,4-DNBA.

2-FA is a dark yellow liquid and 3,4-DNBA is a pale yellow solid; dissolution of the two components gave pale yellow solutions. Molecular complex **7** formed as red crystals, transforming to pale yellow crystals upon transformation to **8**; molecular complex **9** formed as dark red crystals. The outcome of the crystallisations was complicated; a number of phases were

identified with various colours and morphologies. However, the bulk samples consisted of mainly colourless crystals, with very few coloured crystals of **7** and **9**; analysis of the samples has shown that the colourless phase is likely to be the starting material 3,4-DNBA.

A number of difficulties were encountered in the growth of the desired 1:2 molecular complex of 2-FA 3,4-DNBA (**7**). A very small number of crystals were yielded from methanol when crystallisations were performed at 4 °C in a sealed, or almost sealed, vessel, which inhibited evaporation of the liquid 2-fluoroaniline component and aided molecular complex formation. The synthesis was not reproducible, and the same crystallisation conditions did not always result in crystals of the molecular complex forming. Additionally the crystals were unstable and degraded quite quickly at room temperature once exposed to air, typically within 24 hours, likely to be due to loss of 2-FA; however if the sample was kept in a sealed vial at 4 °C the crystals of the molecular complex remained stable for at least three months.

Powder X-ray diffraction experiments were conducted on the bulk samples at room temperature, using a Bruker AXS D8 Advance diffractometer in flat-plate mode; the diffraction patterns that were obtained matched the diffraction pattern of 3,4-dinitrobenzoic acid exactly, with no additional phases apparent (Appendix A4, Figure A4.5). A number of the colourless crystals were also screened by single-crystal X-ray diffraction. The diffraction patterns were poor, but the unit cell that was obtained corresponded to that of the starting material 3,4-DNBA.

Hot-stage microscopy was conducted on samples of the colourless crystals obtained in the crystallisations, and also on a crystal of molecular complex **7** that remained sufficiently stable. Experiments were conducted using a Mettler Toledo FP82 hot stage equipped with a Leica DM1000 microscope, according to the procedure outlined in §3.3.1. A colourless crystal from the bulk sample was heated between 30 °C and 170 °C at a rate of 5 °C /minute. On heating, the crystal unexpectedly turned red in colour at ~162 °C, immediately prior to melting (at ~166 °C, which corresponds to the melting point of 3,4-DNBA). A second identical crystal was heated to 162 °C, and the same colour change was observed; the temperature was held at 162 °C to prevent melting, and the sample was cooled rapidly back to 30 °C with loss of the red colour observed at ~140 °C (Figure 4.39). The sample was heated and cooled in the same manner over four cycles, and the reversible colour change was observed each time. Crystals of pure 3,4-DNBA were heated in the same way but no colour change was observed. The melting point and X-ray diffraction analysis suggests that the colourless crystals are starting material (3,4-DNBA), thus the colour change and nature of the crystals is not yet fully understood. It is possible that it is due to a coating on the crystals.

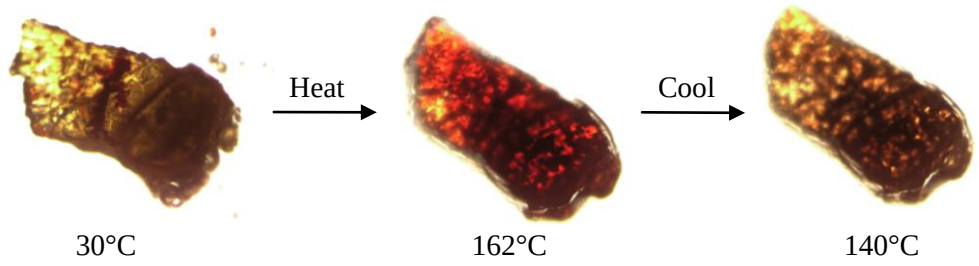

Figure 4.39 Hot-stage microscopy analysis of a sample of the colourless crystals obtained in the crystallisation of 2-FA and 3,4-DNBA, showing the reversible colour change upon heating to 162 °C.

HSM analysis was also conducted on a red block crystal of the 1:2 molecular complex 2-FA 3,4-DNBA, **7**. The crystal was heated between 30 °C and 170 °C at a rate of 5 °C/minute. The 2-FA 3,4-DNBA complex does not exhibit a phase transition upon heating. At 68 °C, there is a melt and recrystallisation of the sample, giving colourless needle crystals; this new phase melts at ~166 °C, which corresponds to the melting point of 3,4-DNBA. It is therefore probable that the melt at 68 °C was due to loss of 2-FA from the structure, leaving 3,4-DNBA.

DSC experiments were conducted on the bulk samples using a TA Instruments Q20 differential scanning calorimeter, according to the procedure outlined in §3.3.2; samples were ground very gently prior to being placed in a Tzero™ pan. It was not possible to obtain enough crystals of molecular complex **7** to conduct DSC analysis on the pure sample. The bulk samples were heated and cooled between 40 °C and 170 °C, at a rate of 5 °C/minute. The DSC thermograms were similar to that of pure 3,4-DNBA, with a melt at ~164 °C (compared to ~166 °C for 3,4-DNBA) and a sharp recrystallisation at ~93 °C (compared to ~103°C for 3,4-DNBA). In general, the DSC experiments indicated that there was predominantly a single component (probably 3,4-DNBA) present in the bulk sample. However, in some of the samples an additional small endothermic peak at ~66 °C was observed in the thermograms. The temperature of this thermal event corresponds to the temperature at which the melt of molecular complex **7** was observed in the HSM analysis, and may be due to loss of remaining 2-FA in the sample (Appendix A4, Figure A4.6).

4.3.3 2-fluoroaniline 3,4-dinitrobenzoic acid (7)

Molecular complex **7** is yielded as red block crystals (Figure 4.40), of the same colour and morphology as molecular complexes **1**, **4** and **6**. A single crystal was mounted on a Rigaku Oxford Diffraction Gemini diffractometer at 100 K and screened, however the diffraction images were poor and indicative of crystal degradation, assumed to be due to flash-cooling and the low stability of the crystals. Crystal screening at ambient temperature resulted in much

higher quality diffraction images, and therefore data were collected at ambient temperature (without N_2 flow), with survival of the single crystal over the period of data collection.

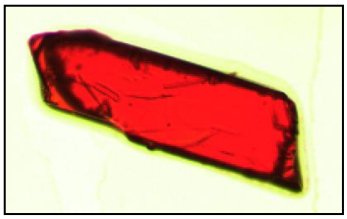

Figure 4.40 Photograph of a crystal of molecular complex **7**.

2-fluoroaniline and 3,4-dinitrobenzoic acid crystallise in a 1:2 ratio in the triclinic space group $P\bar{1}$, and all molecular components are present in their neutral forms. The crystal structure of **7** is very similar to those of Form I of the previously described 2-haloaniline molecular complexes, with the unit cell parameters closely matching those of the 2-BrA and 2-ClA molecular complexes, **4** and **6**. The asymmetric unit contains three independent molecules of 3,4-DNBA, one fully occupied 2-FA molecule (disordered over two symmetry-independent positions) and one half-occupied 2-FA molecule (disordered over an inversion centre).

The molecules of 3,4-DNBA form dimers *via* moderate strength O-H···O hydrogen bonds between the carboxylic acid groups. Weak C-H···O hydrogen bonds connect 3,4-DNBA dimers, forming the same hydrogen bonded tape as observed in **1** - **6** (Figure 4.3); hydrogen bond data are given in Table 4.11. As in molecular complexes **4** and **6**, two of the independent 3,4-DNBA molecules form a dimer with an angle of ~5° calculated between the mean ring planes of the dimer molecules, and the third 3,4-DNBA molecule forms a dimer with a symmetry-equivalent coplanar molecule. The C-O bond lengths of the carboxylic acid groups (1.263(9)/1.248(8) Å, 1.265(8)/1.265(8) Å, 1.256(8)/1.263(8) Å) are intermediate between distances expected for single and double bonds, which may indicate the presence of proton disorder.[37,39] However, due to the molecular disorder in the complexes, a model was employed with a single proton position, with the hydrogen atom located using the Fourier difference maps and bound to the C-O group with the longer bond distance. The carboxylic acid groups all lie close to coplanar with the ring planes (~3°, ~1°, ~1°), whilst the *m*- and *p*-nitro groups of the 3,4-DNBA molecules are twisted out of the planes of the rings due to steric effects (*m*-NO_2 groups by ~32°, ~40°, ~44° and *p*-NO_2 by ~55°, ~37°, ~48°) similarly to **1**, **4** and **6**.

Table 4.11 Hydrogen bond data (3,4-DNBA) for molecular complex **7** (refer to Figure 4.3 for labels **a** - **f**)

Bond type	D-H···A	D-H	H···A	D···A	<(DHA)
a, b	O14-H14A···O13 #1	0.91(2)	1.70(2)	2.601(2)	173(9)
c, f	C20-H20···O14 #2	0.93	2.75	3.596(8)	152.6
d, e	C21-H21···O13 #3	0.93	2.76	3.537(8)	141.1
a	O7-H2···O2	0.90(2)	1.77(4)	2.636(6)	161(9)
b	O1-H1···O8	0.91(2)	1.74(3)	2.632(6)	165(9)
c	C13-H13···O8 #4	0.93	2.56	3.434(7)	155.9
d	C14-H14···O1 #4	0.93	2.59	3.324(8)	135.8
e	C3-H3···O7 #2	0.93	2.57	3.339(9)	139.6
f	C4-H4···O2 #2	0.93	2.55	3.439(7)	160.5

#1 -x+2,-y,-z+1 #2 x-1,y,z #3 -x+1,-y,-z+1 #4 x+1,y,z

Note: aromatic H-atoms are placed in calculated positions.

As observed in the other 2-XA molecular complexes, **7** contains two crystallographically independent 2-FA molecules which are both disordered. Due to fluorine having a much lower molecular weight than I, Br and Cl, and by the fact that low temperature single crystal X-ray diffraction data were not accessible, the modeling of the disordered 2-FA atoms was less straightforward; it is therefore possible that there is more complex disorder present than that which was able to be modelled. It is also possible that the disorder at room temperature is dynamic rather than static; low temperature data could not be collected to investigate this. The model reported is the best that could be obtained from the data, and consists of two 2-FA molecules with whole molecule disorder over two positions. The two 2-FA molecules have different disorder models; one 2-FA molecule has symmetry-independent disorder with relative occupancies of 0.568(8) and 0.432(8) (purple and green, Figure 4.41) and the other 2-FA molecule is disordered 50:50 over an inversion centre (pink and blue, Figure 4.41).

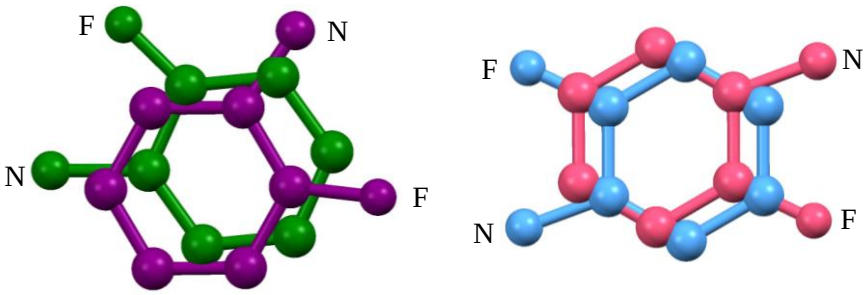

Figure 4.41 The molecular disorder of the two independent 2-fluoroaniline molecules in molecular complex **7**. Disorder occupancies are ~57:43 for the molecule shown in purple/green (symmetry-independent disorder), and 50:50 for the molecule shown in pink/blue (disordered over inversion centre). Hydrogen atoms are omitted for clarity.

The ordered hydrogen bonded 3,4-DNBA tape incorporates channels of the disordered 2-FA molecules. The amine groups of the 2-fluoroaniline molecules interact with the 3,4-DNBA molecules through N-H···O hydrogen bonds (**a** - **e**, Figure 4.42). For the molecule with symmetry-independent disorder (shown in purple/green) there are two hydrogen bonds formed (**a** and **b**, Figure 4.42) when in the orientation with the slightly higher occupancy (shown in purple); there is also a weak C-H···O bond between an aromatic H-atom and nitro group O-atom (C···O = 3.24(1) Å). This compares to a single hydrogen bond in the opposite orientation (shown in green). For the molecule disordered over an inversion centre (shown in pink/blue), a bifurcated N-H···O hydrogen bond (d and e, Figure 4.42) is formed in each orientation. The donor-acceptor distances are reported in Table 4.12. The F-atoms are not involved in any interactions, thus the disorder in this complex must arise through a mismatching of donor and acceptor atoms. There are no interactions between 2-FA molecules in the channels.

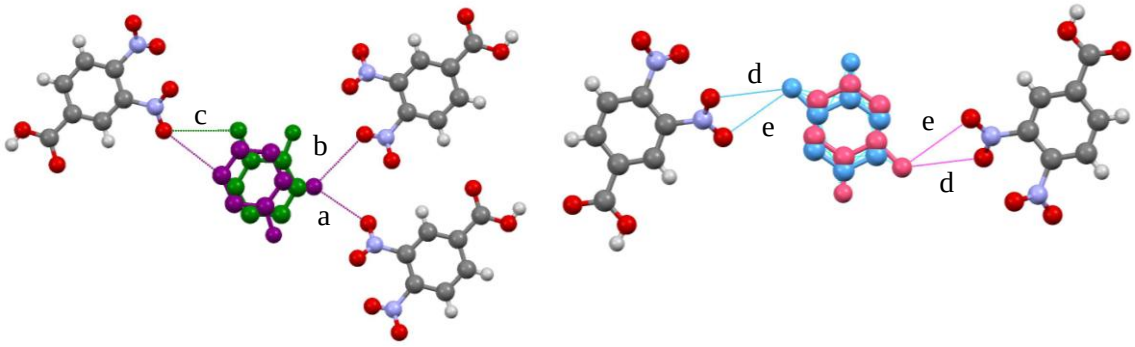

Figure 4.42 Intermolecular interactions between the 2-fluoroaniline molecules and the 3,4-dinitrobenzoic acid molecules. Hydrogen atoms have been omitted for clarity. Donor-acceptor distances for **a**-**e** are given in Table 4.12.

Table 4.12 Donor-acceptor distances for selected intermolecular interactions between the 2-fluoroaniline molecules and the 3,4-DNBA framework (refer to Figure 4.5 for labels **a**-**e**).

Bond type	D-H···A	d(D···A)/ Å
a	N-H···O	2.96(2)
b	N-H···O	3.29(2)
c	N-H···O	3.26(2)
d	N-H···O	3.32(2)
e	N-H···O	3.25(2)

A two-dimensional sheet structure is formed in the same way as in the 2-haloaniline complexes **1**, **4** and **6**. Similarly to the 2-BrA and 2-ClA complexes, there are two sheet types, A and B, with each incorporating one of the independent 2-fluoroaniline molecules (Figure 4.43 (a)). Sheet A contains the 2-FA with symmetry-independent disorder and sheet B contains the 2-FA

disordered over the inversion centre; the sheets stack with an AABAAB arrangement, with stacking occurring between alternating 2-FA molecules and 3,4-DNBA dimers (Figure 4.43 (b)). The mean planes of the stacked 2-FA molecules and 3,4-DNBA dimers are tilted by ~12° with respect to each other.

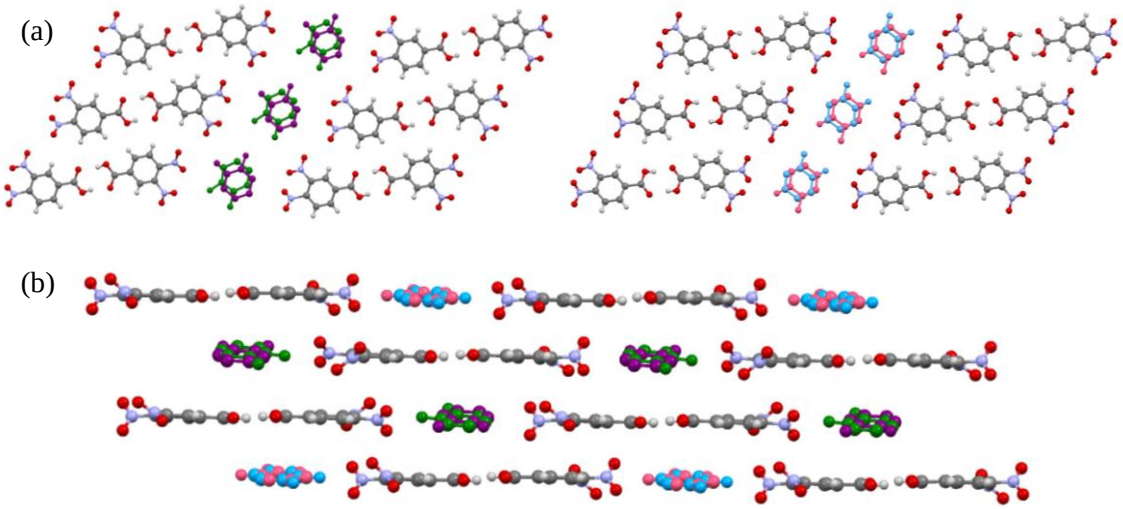

Figure 4.43 (a) Two-dimensional sheets A (left) and B (right) formed in molecular complex **7**; (b) stacking of two-dimensional sheets.

A separation of ~3.35Å was calculated between stacked molecules, which is the same as that observed in the other 2-haloaniline complexes. The 2-FA and 3,4-DNBA molecules stack *via* aromatic donor···acceptor interactions; there are also interactions between 3,4-DNBA molecules in adjacent layers, including $O_{nitro}\cdots O_{nitro}$ and $O_{nitro}\cdots\pi$ interactions. There are three types of stacking and molecular overlap (shown by stacking types **i**, **ii** and **iii**, Figure 4.44); for the 2-FA molecule with symmetry-independent disorder (shown in purple and green), the stacking is different above and below the molecule, and differs with molecular orientation (**i** and **ii**, Figure 4.44, right). For the molecule disordered by inversion (shown in pink and blue), the stacking is the same above and below the 2-FA molecule, and for both molecular orientations (**iii**, Figure 4.44, right; the stacking is therefore only shown for one of the orientations).

As for Forms I and II of the 2-IA, 2-BrA and 2-ClA complexes, the crystal packing is dominated by the aromatic donor···acceptor interactions. Molecular complex **7** has the same red colour in the solid-state as **1** - **5**, thus the $\pi\cdots\pi^*$ charge-transfer absorbance must be similar. This is reflected in the similarity of the interlayer spacing and the molecular overlap. There is no overlap between the rings of stacked 2-FA and 3,4-DNBA molecules. The molecular overlap occurs predominantly between the 2-XA ring or halogen atom and the centre of the 3,4-DNBA

dimer, as for the other red 2-XA 3,4-DNBA complexes. Additionally, the amount of molecular overlap is similar or the same for both possible orientations of the disordered molecules.

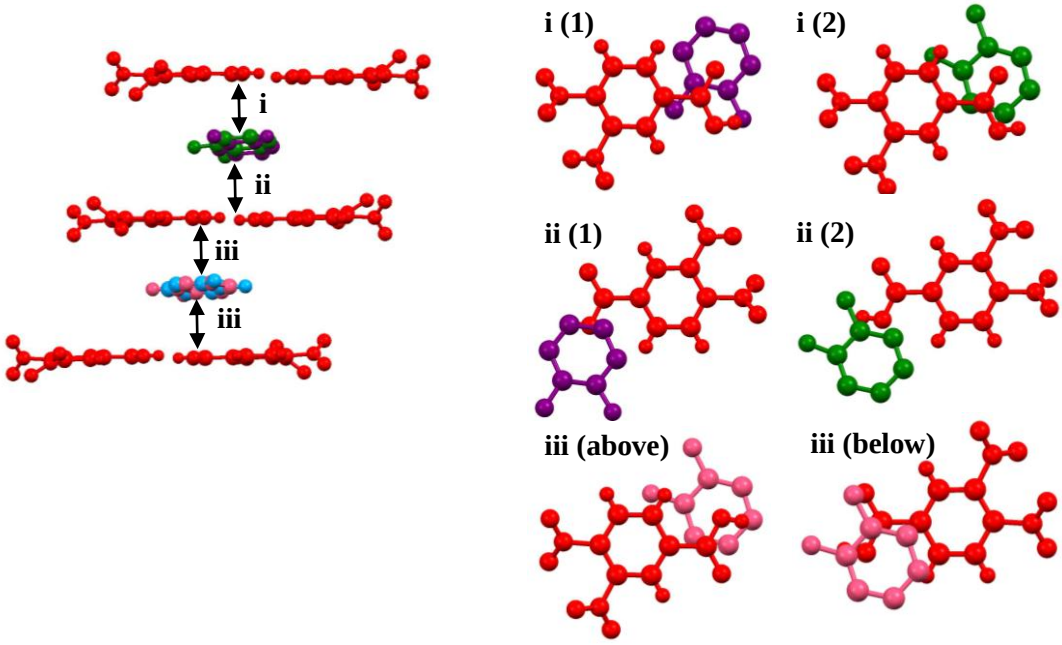

Figure 4.44 Stacking in molecular complex **7**, where there are three types of stacking (**i**, **ii** and **iii**); the molecular overlap differs for the two orientations (1 and 2) shown in purple and green but is the same for both possible orientations shown in pink and blue. 3,4-DNBA molecules are shown in red and the disordered 2-XA molecules are shown in the colours according to Figure 4.41.

In the same way as for molecular complexes **1** - **6** (§4.2.7), the volume of crystal space available in each 2-fluoroaniline site was calculated by removing the disordered 2-FA molecules from the model. An average volume of 187.64 $Å^3$ was calculated for each 2-fluoroaniline, which contrasts with 139.18 $Å^3$ for each molecule in the structure of 2-FA (CSD[86] refcode: IDAHOL).[234] This equates to a significant 34.82% increase in the space available to each 2-fluoroaniline site in molecular complex **7** compared to the crystal structure of 2-FA, which is a significantly greater percentage increase than in molecular complexes **1** - **6**. The 3,4-DNBA dimer framework and stacking-type remains identical to that in **1** - **6**, with the same approximate volume of crystal space therefore available for the 2-FA molecules to accommodate; however, the 2-FA molecules are much smaller in size. It is therefore unsurprising that molecular complex **7** is only formed in very small quantities and was quite unstable.

4.3.4 2-fluoroanilinium 3,4-dinitrobenzoate 3,4-dinitrobenzoic acid (8)

Following completion of the ambient temperature data collection on molecular complex **7**, the same single crystal was slowly cooled *in situ*, initially to 220 K, using a ramp rate of

120 K/hour, in order to see if the crystal survived to allow a low temperature data collection. However, during the process of slow cooling to 220 K, the crystal was observed to change colour from red to colourless; screening revealed new unit cell parameters. Molecular complex **7** therefore undergoes a phase transition to molecular complex **8**, but the exact temperature of the transformation is unknown. Data were collected at 220 K, and the crystal was then cooled to 150 K, and data were collected again. The same unit cell parameters were obtained at 150 K and 220 K; data are presented from the collection at 220 K as these data were complete.

Molecular complex **8** adopts the triclinic space group $P\bar{1}$, with the molecular components 2-FA and 3,4-DNBA present in a 1:2 ratio, as in **7**. The phase transition involves the transfer of a proton from the carboxylic acid group of one of the 3,4-DNBA molecules to the amine group of the 2-FA molecule; the asymmetric unit contains a 2-fluoroanilinium cation, a 3,4-dinitrobenzoate anion and a neutral 3,4-dinitrobenzoic acid molecule. The phase transition is therefore a transformation between the neutral charge-transfer complex and an ionic form, induced upon cooling. Despite the transfer of a proton, the phase transition results in a relatively small change in the overall packing arrangement, but there is a significant change in the intermolecular interactions; the structure is dominated by the charge-assisted hydrogen bonds involving the protonated 2-FA molecule. The two 3,4-DNBA molecules are linked to form a dimer through a single charge-assisted O-H···O^- hydrogen bond of moderate strength between the carboxylic acid and carboxylate groups (**a** in Figure 4.45 (a), Table 4.13); the hydrogen bond is significantly stronger than in the standard hydrogen bonds in **1** - **6**. The proton resides on one of the 3,4-DNBA molecules and was assigned easily from the electron density map. In the 3,4-dinitrobenzoate anion, the C-O bonds of the carboxylate group show character intermediate between single and double bonds, and are approximately equidistant which is consistent with the delocalised charge (1.236(5) Å and 1.279(5) Å). In the neutral 3,4-DNBA molecule, the two C-O bonds of the carboxylic acid group show clear single and double bond character (1.219(5) Å and 1.308(4) Å).

In terms of their relative orientations, the 3,4-DNBA molecules remain in positions similar to those of the neutral dimer, thus the 3,4-DNBA network is essentially maintained. However, the two molecules twist away from each other by ~10° due to the loss of the proton. The carboxylate group twists out of the ring plane by ~29° (Figure 4.45 (a)); the carboxylic acid group remains close to coplanar with the ring plane (torsion angle of ~4°). The nitro groups are all rotated out of the ring planes due to steric effects. The torsion angles for nitro groups of the 3,4-dinitrobenzoate anion are ~22° and 57° for the *meta* and *para* positions, respectively; for the 3,4-dinitrobenzoic acid molecule the corresponding torsion angles are 31° and 60°. The torsions of the *m*-NO_2 groups are generally slightly smaller than in **7**, while the torsions of the

p-NO_2 groups are slightly greater. Weak C-H···O hydrogen bonds link the 3,4-DNBA dimer units to form a very similar hydrogen bonded tape to that observed in molecular complexes **1** - **7** (**b** - **g** in Figure 4.45 (b), Table 4.13). Due to the carboxylate group being twisted out of the ring plane, there are no C-H···O bonds to the second O-atom of the carboxylate group.

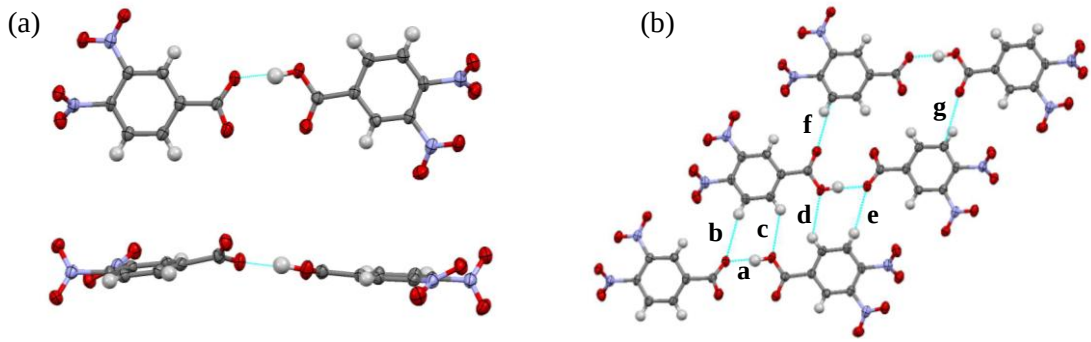

Figure 4.45 (a) Top: Moderate strength charge-assisted O-H···O hydrogen bond linking the 3,4-DNBA molecules; Bottom: Slight twisting of the 3,4-DNBA molecules relative to each other. (b) Hydrogen bonded tape of 3,4-DNBA molecules showing charge-assisted O-H···O hydrogen bonds (**a**) and weak C-H···O hydrogen bonds (**b** - **g**).

The 2-fluoroanilinium cation remains disordered following the phase transition, but the disorder model is much simpler, and can be described with more confidence due to the availability of low temperature data. The benzene ring and protonated amine group adopt a single well-defined position; the disorder is simply associated with the fluorine substituent in the *ortho*-position, likely due to the small size of the fluorine atoms and the similar crystal environment for both orientations. The two fluorine sites have 70:30 occupancies for the atoms shown in purple and green, respectively (Figure 4.46). Upon protonation, the 2-FA cation is effectively locked into place in the structure, with the phase transition therefore associated with a significant flipping of the 2-FA molecules within the channels (Figure 4.46). It is probable that the increase in crystal space due to disorder in **7** facilitates this molecular reorientation.

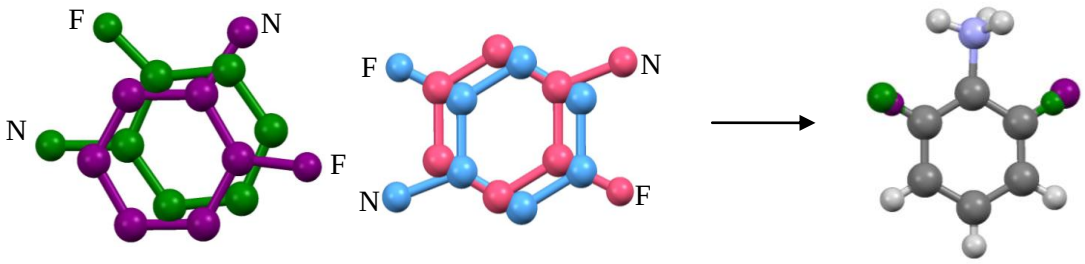

Figure 4.46 Comparison of the molecular disorder in the two independent 2-FA molecules in **7** (left) and the simpler molecular disorder of the fluorine substituents in the 2-fluoroanilinium cation in molecular complex **8** (right) with occupancies of 70:30 for the atoms shown in purple and green respectively. The two possible H-atoms sites in the *ortho* positions are also shown in purple and green.

The 2-fluoroanilinium cation is involved in a number of intermolecular interactions with 3,4-DNBA molecules (Figure 4.47), with the strongest of these interactions being three moderate strength charge-assisted N-H···O hydrogen bonds between the NH_3^+ group and oxygen atoms of adjacent 3,4-DNBA molecules, resulting in a three-dimensional hydrogen bonding geometry (**h** - **j**, Figure 4.47 (a), Table 4.13); these hydrogen bonds dominate the crystal packing arrangement. The two strongest hydrogen bonds (**h** and **i**) form between the protonated amine group and carboxylate group oxygen atoms in layers above and below. The weakest of the hydrogen bonds (**j**) forms between the amine group hydrogen that lies in the plane of the 2-FA ring and the *meta* nitro group of an adjacent 3,4-dinitrobenzoate anion in the same layer. The 2-fluoroanilinum cation is also involved in either C-F···O interactions or weak C-H···O hydrogen bonds with nitro group oxygen atoms within the layer (Figure 4.47 (b)). For the fluorine site with the highest occupancy, shown in purple, there is an F···O distance of 2.625(3) Å (compared to the sum of the van der Waals radii of fluorine and oxygen of 3.05 Å); for the fluorine site with the lower occupancy, shown in green, F···O = 2.859(8) Å, 2.886(7) Å, 2.881(7) Å). For both possible H-atom sites, in the *ortho* positions, the C···O distances for the weak hydrogen bonds are in the range 3.5 - 4.0 Å. Despite the F···O distances being less than the sum of the van der Waals radii, halogen bonds involving fluorine typically only occur when fluorine is bound to a strongly electron-withdrawing moiety, which is not the case here; it is possible that the short F···O distance is a consequence of the crystal packing.

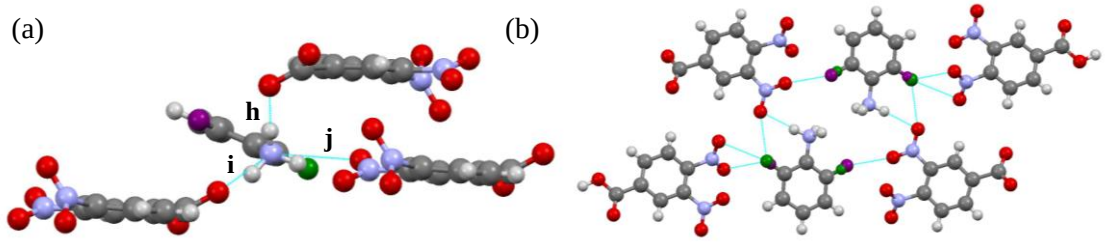

Figure 4.47 (a) Hydrogen-bonding interactions of the NH_3^+ group. (c) Interactions between the disordered 2-fluoroanilinium cations and nitro groups of the 3,4-DNBA molecules in the same layer.

There is a similar two-dimensional sheet structure to that formed in the other 2-XA 3,4-DNBA complexes, where the disordered 2-FA molecules form channels in the hydrogen bonded 3,4-DNBA network (Figure 4.48 (a)); there are no interactions between adjacent 2-fluoroanilinum anions within the chains. The strongest N-H···O hydrogen bonds involving the NH_3^+ group of 2-FA direct the stacking of the sheets (Figure 4.48 (b)); there are a number of short contacts (O···O, N···O and O···π) between the 3,4-DNBA components in adjacent layers. This packing arrangement contrasts with molecular complex **7** where the stacking is dominated by interactions between aromatic donor and acceptor molecules. The sheets stack to form a

layered structure, with alternating 2-FA and 3,4-DNBA dimers in the stacking direction (Figure 4.48 (c)); the layers are more rippled and less planar than in molecular complex **7**. An approximate interlayer distance of ~3.48 Å was calculated between mean sheet planes.

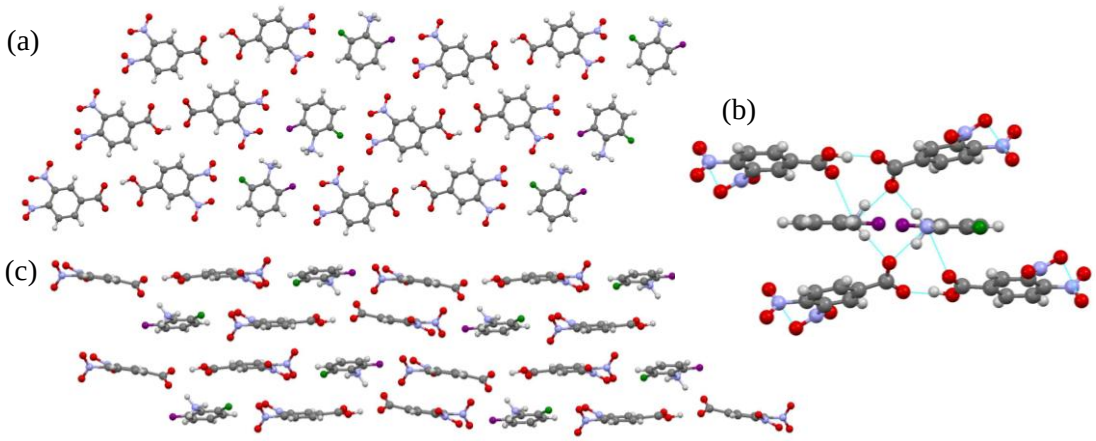

Figure 4.48 (a) Two-dimensional sheet structure in molecular complex **8** formed through a combination of hydrogen bonds and C-F...O interactions. (b) Stacking of the sheets, showing the non-coplanarity of the 2-FA cations and 3,4-DNBA dimers; (c) Hydrogen-bonding interactions between 2-FA and 3,4-DNBA molecules in adjacent layers, which direct the stacking.

Table 4.13 Hydrogen bond data for molecular complex **8** (refer to Figure 4.45 for labels **a** - **g** and Figure **4.47** (b) for labels **h** - **j**).

Bond type	D-H···A	D-H	H···A	D···A	<(DHA)
a	O7-H7A···O1	0.98(4)	1.61(4)	2.585(3)	172(3)
b, e	C13-H13A···O1_#1	0.93	2.73	3.624(3)	161.9
c, d	C14-H14···O7_#1	0.93	2.71	3.369(4)	128.6
f, g	C4-C4···O8_#2	0.93	2.33	3.197(4)	154.9
h	N8-H12···O2_#3	1.01(4)	1.73(4)	2.694(3)	159(3)
i	N5-H11···O2_#4	0.97(5)	1.82(5)	2.789(4)	175(4)
j	N5-H13···O6_#5	0.94(4)	2.19(4)	3.046(3)	152(3)

#1 -x,-y+1,-z+2 #2 -x+1,-y+1,-z+1 #3 -x,-y+1,-z+1 #4 x,y+1,z #5 -x,-y+2,-z+1

The 2-FA cations and 3,4-DNBA molecules are tilted by ~25° with respect to each other. Due to the tilt, there are no π···π interactions between molecules. Furthermore, the protonation of the electron-rich 2-FA molecule means it cannot act as an electron donor, and has changed in nature due to the strongly withdrawing NH_3^+ group. Thus the aromatic donor···acceptor type interactions in the neutral 2-XA 3,4-DNBA molecular complexes are not observed; the π···π* charge-transfer absorbance is diminished and thus proton transfer in this system switches off colour.

As for molecular complexes **1** - **7**, the volume of crystal space available in each 2-fluoroaniline site was calculated by removing the disordered 2-FA molecules from the model. An average volume of 147.46 $Å^3$ was calculated for each 2-fluoroaniline molecule in **8**, which is very close to the volume of 139.18 $Å^3$ calculated for each molecule in the crystal structure of 2-FA (which also has similar disorder fluorine atom disorder). The proton transfer upon cooling results in a loss of whole molecule disorder, and is accompanied by more efficient packing, with less space available in the 3,4-DNBA network to accommodate the 2-FA molecules.

4.3.5 Molecular complex 9

In addition to the red block crystals of molecular complex **7**, a second coloured molecular complex, **9**, was also formed from methanol, but in very small quantities. The molecular complex was yielded as very small dark red, triangular plate crystals. Analysis of the crystal structure showed that a diazotization reaction had occurred between two molecules of 2-fluoroaniline to form 2-fluoro-4-[(1E)-2-(2-fluorophenyl)diazenyl]-benzenamine (2-F-4-BA) (Figure 4.49 (a)). The reaction product 2-F-4-BA crystallises with 3,4-dinitrobenzoic acid in a 1:2 ratio, in the monoclinic space group C2/c, and each of the molecular components are present in their neutral forms. The same 3,4-DNBA tape is formed as in molecular complexes **1** - **7**. However, rather than the 3,4-DNBA network acting as a host to disordered 2-haloaniline molecules, the 2-F-4-BA molecules are an ordered part of the sheet structure (Figure 4.49 (b)).

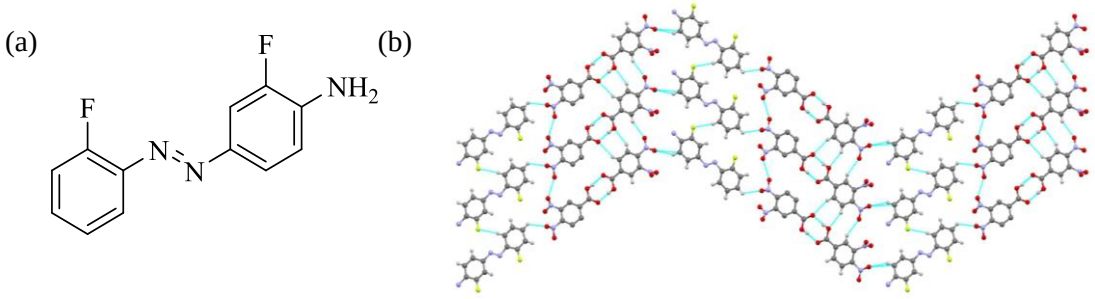

Figure 4.49 (a) 2-fluoro-4-[(1E)-2-(2-fluorophenyl)diazenyl]-benzeneamine, the product of a diazotization reaction between two molecules of 2-FA; one molecule crystallises with two molecules of 3,4-DNBA to give molecular complex **9**; (b) Planar two-dimensional sheet structure formed in **9**.

4.3.6 Summary and discussion

A number of difficulties were encountered in the crystallisation of the desired molecular complex, with the bulk of the samples appearing to be the starting material 3,4-DNBA. However, a 1:2 molecular complex of 2-FA 3,4-DNBA, **7**, was formed in very small quantities, along with small amounts of a molecular complex containing the product of a reaction between

two 2-FA molecules (**9**). Molecular complex **7** is structurally very similar to those of the Form I complexes presented in §4.2, and the crystals that are yielded are of the same colour and morphology. The molecular complex contains the same hydrogen bonded 3,4-DNBA tapes, which incorporate disordered 2-FA molecules in the channels to form sheets. However, unlike the equivalent 2-IA, 2-BrA and 2-ClA complexes, no phase transitions are observed upon heating. The red colour in the solid-state can be attributed to charge-transfer due to aromatic donor···acceptor interactions between the electron-rich 2-FA molecules and electron-poor 3,4-DNBA molecules. It is also possible that the molecular disorder plays a role in the colour.

It was not possible to collect low-temperature data on molecular complex **7**, as on cooling from room temperature to 220 K, the molecular complex undergoes a phase transition to give molecular complex **8**, resulting in a colour change from red to colourless; the exact temperature of the transition is unknown. The phase transition involves the transfer of a proton from one of the 3,4-DNBA molecules to the amine group of 2-FA. The ΔpKa value for the 2-FA 3,4-DNBA pair lies in the salt-cocrystal continuum, thus it was possible that proton transfer could occur. Molecular complex **8** is the only system presented in this chapter in which proton transfer has occurred, and the molecules are not all in their neutral states. Despite the loss of a proton from the dimer, the hydrogen bonded 3,4-DNBA tape is essentially maintained; this is enabled through the 1:2 stoichiometry of the components, with the one of the acidic protons remaining on the 3,4-DNBA. The benzene ring and protonated amine group of the 2-fluoroanilinium cation adopt a single well-defined position, with the protonation of the amine group therefore locking the 2-FA moiety in place; however, there is disorder of the fluorine substituent over the two *ortho*-positions.

There is a large volume of space available to the 2-FA molecules in molecular complex **7**. The 3,4-DNBA dimer network and stacking arrangement remains identical to the 2-IA, 2-BrA and 2-ClA complexes, but the space occupied by the 2-FA molecule is much smaller in size. It is highly probable that this large amount of extra space due to the disorder facilitated the rearrangement of the 2-FA molecules upon the proton transfer on cooling, allowing the transition to occur in a single-crystal to single-crystal manner. The sheets of **8** are similar to those of **7**, incorporating the 3,4-DNBA tapes and channels of 2-FA cations, but the layers are more rippled due to the change in the hydrogen bonding arrangement from planar to three-dimensional. The 2-FA and 3,4-DNBA molecules are tilted significantly with respect to each other, and consequently there are no π-π interactions. The protonation of the 2-FA means it can no longer function as an electron donor, thus there are no aromatic donor···acceptor type interactions, which are likely to give rise to the strong red colour in the neutral 2-XA 3,4-DNBA molecular complexes; therefore, the proton transfer switches off colour. The proton transfer

mechanism of the phase transition, in combination with disorder, or without disorder (Chapter 5), could provide an alternative route to thermochromic properties in multi-component organic complexes.

4.4 Molecular complexes of 2-halo-4-methylaniline and 3,4-dinitrobenzoic acid

Keeping the amine group and the halogen atom in adjacent ring positions, starting materials were selected with a methyl substituent in the *para* position of the 2-haloaniline to give 2-halo-4-methylaniline (2-X-4-MA, where X = I, Br, Cl), and a series of co-crystallisation experiments were conducted with 3,4-DNBA to investigate the effect on the crystal packing, molecular disorder and optical properties. The ΔpKa values for 2-I-4-MA 3,4-DNBA, 2-Br-4-MA 3,4-DNBA and 2-Cl-4-MA 3,4-DNBA are 0.15, 0.15 and 0.27, respectively. These values lie in the salt-cocrystal continuum, although close to the lower boundary, thus proton transfer may or may not occur. The values compare to the negative values of ΔpKa for the 2-IA, 2-BrA and 2-ClA complexes, where the components remained in their neutral states.

4.4.1 Experimental details

Molecular complexes **10** - **12** were obtained *via* the method of slow evaporation (§3.1) using a 1:2 stoichiometric molar ratio of the 2-halo-4-methylaniline and 3,4-dinitrobenzoic acid. Crystallisation trials employed a range of solvents and evaporation temperatures; the conditions which resulted in growth of the crystals used for collection of SCXRD data are reported here. Single crystal X-ray diffraction experiments were carried out according to the procedures outlined in §3.2; crystallographic data are given in Table 4.14 and refinement details are reported in Appendix A4.

2-iodo-4-methylaniline 3,4-dinitrobenzoic acid (10)

Molecular complex **10** was synthesised from acetonitrile at 40 °C; yellow/orange block shaped crystals were obtained. Single crystal X-ray diffraction data were collected at 150 K using a Rigaku Oxford Diffraction SuperNova diffractometer (Cu Kα radiation). The structure was solved by direct methods using SHELXS-2013[192] and refined using SHELXL-2014,[198] both within the WinGX program suite.[200]

2-bromo-4-methylaniline 3,4-dinitrobenzoic acid (11)

Molecular complex **11** was synthesised from 2-propanol at ambient temperature; yellow/orange block shaped crystals were obtained. Single crystal X-ray diffraction data were collected at 150 K using a Rigaku Oxford Diffraction Xcalibur diffractometer. The structure was solved by

direct methods using SHELXS-2013[192] and refined using SHELXL-2014,[198] both within the WinGX program suite.[200]

2-chloro-4-methylaniline 3,4-dinitrobenzoic acid (12)

Molecular complex **12** was synthesised from methanol at 40 °C; yellow/orange block shaped crystals were obtained. Single crystal X-ray diffraction data were collected at 150 K using a Rigaku Oxford Diffraction Xcalibur diffractometer. The structure was solved by direct methods using SHELXS-2013[192] and refined using SHELXL-2014,[198] both within the WinGX program suite.[200]

Table 4.14 Crystallographic data for molecular complexes **10** - **12**

	10	**11**	**12**
Formula	(C_7H_8NI) $2(C_7H_4N_2O_6)$	(C_7H_8NBr) $2(C_7H_4N_2O_6)$	(C_7H_8NCl) $2(C_7H_4N_2O_6)$
M/g mol^{-1}	657.29	610.30	565.84
T/K, radiation	150(2), Mo Kα	150(2), Mo Kα	150(2), Mo Kα
Space Group	$P2_1/n$	$P2_1/n$	$P2_1/n$
a/Å	7.5367(1)	7.5249(4)	7.5111(4)
b/Å	18.5672(3)	18.5150(8)	18.5699(9)
c/Å	8.9534(2)	8.8256(4)	8.7549(6)
α	90	90	90
β	98.942(2)	98.466(5)	98.256(5)
γ	90	90	90
V/Å	1237.67(4)	1216.22(10)	1208.48(12)
Z	2	2	2
ρ_{cal}/ g cm^{-3}	1.764	1.667	1.555
μ/mm^{-1}	10.845	1.766	0.235
θ Range/°	4.763 - 71.976	3.325 - 29.291	3.345 - 29.347
Ref Collected	15699	10197	9574
Independent	2418	2971	2900
Observed>2σ	1996	1463	1197
Rint	0.0346	0.0397	0.0698
Completeness %	100.0	99.8	99.7
Parameters	162	157	157
GooF	3.187	2.324	1.645
R_1 (obs)	0.2545	0.2533	0.1952
R_1 (all)	0.2657	0.3405	0.3167
wR2 (all)	0.6269	0.6453	0.5416
$\rho_{max,min}$/e Å^{-3}	2.102, -0.738	1.994, -1.325	1.484, -0.555

4.4.2 Molecular complexes 10, 11 and 12

2-I-4-MA is a light grey solid, 2-Br-4-MA and 2-Cl-4-MA are light brown liquids, and 3,4-dinitrobenzoic acid is a light yellow solid; dissolution of the two components resulted in yellow solutions in each case. The 2-halo-4-methylaniline 3,4-dinitrobenzoic acid molecular

complexes, **10** - **12**, were all yielded as yellow/orange block crystals with identical morphologies (Figure 4.50); the majority of the sample crystallised as powders, with only a small number of single crystals available for SCXRD experiments. The molecular complexes were also studied using hot-stage microscopy, but no temperature-dependent effects were observed.

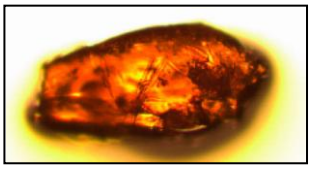

Figure 4.50 Photograph of a single crystal of molecular complex **10**; the crystals of molecular complexes **11** and **12** are similar.

Attempts were made to model the structure in both $P2_1$ and $P2_1/n$; it was difficult to resolve the 2-IA molecules in both space groups, but the best model was obtained in the centrosymmetric space group $P2_1/n$. Structural analysis revealed that molecular complexes **10** - **12** are all isostructural; furthermore, the introduction of the methyl group substituent results in a herringbone packing arrangement like that of 2-IA 3,4-DNBA Form III (**3**).

The asymmetric units of the three complexes contain one independent 3,4-DNBA molecule and one half-occupied 2-X-4-MA molecule situated on an inversion centre; the molecular components are all in their neutral forms. The 3,4-DNBA molecules are fully ordered but the 2-X-4-MA component is highly disordered in each case. Due to the complexity of disorder, it was not possible to resolve all of the atoms despite the data being of good quality; the current model is the best that could be achieved and is incomplete. It was possible to identify and assign the heavy halogen substituents in the Fourier difference map due to the greater electron density associated with them. However, it was not possible to locate the amine and methyl substituents reliably due to overlapping regions of electron density and the low occupancies of each of the atomic sites. Hydrogen atoms have been placed in calculated positions on the 3,4-DNBA molecules, but have not been assigned on the 2-X-4-MA molecules. A significant number of constraints and restraints had to be applied in the refinement to the disordered molecules to achieve chemically-sensible molecular geometries (Appendix A4); in addition, the atoms of the 2-X-4-MA molecules could only be refined isotropically.

In the current model, there are four positions for each 2-X-4-MA combining 50:50 disorder over the inversion centre with symmetry-independent disorder over two positions (Figure 4.51) (giving approximate occupancies of 39:39:11:11 in **10** and 34:34:16:16 in **11** and **12**). The two

orientations shown in dark and light blue are related by inversion the two orientations shown in dark and light purple are also related by inversion.

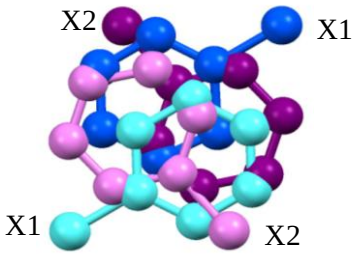

Figure 4.51 The disordered 2-halo-4-methylaniline molecule in molecular complexes **10**, **11** and **12**, where X = I, Br, Cl. The molecule has symmetry-independent disorder over two positions and is also disordered over an inversion centre. The molecules shown in dark and light blue are related by inversion and the molecules shown in dark and light purple are related by inversion. Only the halogen substituents could be modelled reliably; the amine and methyl substituents could not be located.

As observed in all of the complexes in this chapter, the same 3,4-DNBA hydrogen bonded tape is formed (Figure 4.3); the independent 3,4-DNBA molecule forms a dimer with an equivalent molecule through moderate-strength O-H···O hydrogen bonds which are linked *via* a number of weak C-H···O hydrogen bonds (Table 4.15). The C-O bond lengths (1.24(1)/1.25(1) Å in **10**; 1.22(1)/1.28(1) Å in **11**; 1.24(1)/1.27(1) Å in **12**) are intermediate between distances expected for single and double bonds, which may indicate the presence of proton disorder.[37,39] However, due to the significant molecular disorder present, the H-atom positions cannot be reliably determined, thus a model was employed with a single proton position. In each case, the hydrogen atom was located using the Fourier difference maps and bound to the C-O group with the longer bond distance; the O-H distance was restrained to be 0.9 Å and the H-atom displacement parameters constrained to $1.5U_{eq}$ of the O-atom to which it is bonded. Similarly to **3**, in each molecular complex the carboxylic acid groups are close to coplanar with the benzene ring (torsion angles of less than 5°); the *m*- and *p*-NO_2 groups have torsions of ~50° and ~51°, ~52° and ~48°, and ~45° and ~48°, in molecular complexes **10**, **11** and **12**, respectively.

Due to the high level of disorder, and the incomplete model, it is not possible to analyse the interactions between 2-X-4-MA molecules and 3,4-DNBA dimers. However, in terms of the packing, the molecular complexes have a herringbone structure similar to **3**; the ordered 3,4-DNBA dimer network incorporates channels of the disordered 2-X-4-MA molecules, forming zigzag sheets (Figure 4.52 (a)). Angles of ~85°, 83° and ~84° were calculated between the mean ring planes of 3,4-DNBA and 2-X-4-MA molecules in molecular complexes **10**, **11** and **12**, respectively.

Table 4.15 Hydrogen bond data (3,4-DNBA dimers) in molecular complexes **10** - **12** (refer to Figure 4.3 for labels **a** - **f**)

Bond type	D-H···A	D-H	H···A	D···A	<(DHA)
Molecular complex **10**					
a, b	O1-H1···O2 #1	0.82	1.83	2.634(8)	168.0
c, f	C4-H4···O2 #2	0.93	2.63	3.48(1)	153.0
d, e	C3-H3···O1 #3	0.93	2.59	3.41(1)	146.7
Molecular complex **11**					
a, b	O2-H2···O1 #1	0.82	1.80	2.612(9)	168.1
c, f	C4-H4···O2 #2	0.93	2.59	3.46(1)	155.1
d, e	C3-H3···O1 #3	0.93	2.549	3.37(1)	147.0
Molecular complex **12**					
a, b	O1-H1···O2 #1	0.82	1.79	2.601(7)	168.7
c, f	C4-H4···O2 #2	0.93	2.57	3.442(9)	156.0
d, e	C3-H3···O1 #3	0.93	2.53	3.35(1)	147.5

#1 -x+2,-y+1,-z+2 #2 x-1,y,z #3 -x+1,-y+1,-z+2

The sheets stack in the same way as reported for molecular complex **3**, resulting in segregated stacks of alternating electron-rich 2-X-4-MA molecules and electron-poor 3,4-DNBA molecules, with the stacking dominated by the aromatic donor···acceptor interactions (Figure 4.52 (b)). There is an approximate stacking distance of ~3.40 Å in **10**, **11** and **12**, which is equivalent to those in **3**. Similarly to **3**, the aromatic donor···acceptor interactions occur within a three-molecule 3,4-DNBA/2-X-4-MA/3,4-DNBA unit, with molecular overlap appearing to be between the planar rings.

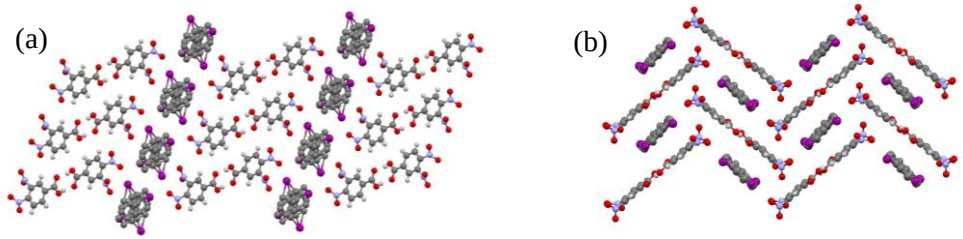

Figure 4.52 (a) Zigzag sheets, shown for molecular complex **10**, with alternating 2-I-4-MA channels and 3,4-DNBA networks; the sheets are the same in **11** and **12**. (b) Stacking of zigzag sheets resulting in segregated stacks of alternate 2-X-4-MA molecules and 3,4-DNBA dimers.

The crystals of **10** - **12** are slightly more orange in colour than the yellow crystals of **3**; the colour can be attributed to charge-transfer between the donor and acceptor molecules. The colours of charge-transfer complexes are dependent upon, and sensitive to, the electronic

properties of the donor and acceptor and upon their relative orientations and overlap. It is possible that the introduction of the electron donating methyl group to the donor molecule may have had an impact on the optical properties by altering the nature of the donor molecule; in addition, the different disorder in the structure may be influential. Due to the uncertainty in the model, it is not possible to assess the exact orientations of the 2-X-4-MA molecules.

As for molecular complexes **1** - **8**, the volume of crystal space available to each 2-X-4-MA molecule was calculated by removing the disordered molecules from the model. Average volumes of 225.24 $Å^3$, 216.39 $Å^3$ and 210.87 $Å^3$ were calculated for the crystal sites of 2-I-4-MA, 2-Br-4-MA and 2-Cl-4-MA, respectively. This is a similar volume to that in the herringbone structure of **3** (204.76 $Å^3$). The crystal structures of the pure components were not available to calculate the volume occupied by an ordered molecule. However, these molecules differ from 2-IA, 2-BrA and 2-ClA by a methyl group only; using the rule of 18 $Å^3$ for each non-hydrogen atom, this gives approximate volumes of 184.93 $Å^3$, 176.20 $Å^3$ and 174.32 $Å^3$ for 2-I-4-MA, 2-Br-4-MA and 2-Cl-4-MA, respectively. This equates to an estimated 21 - 23% increase in crystal space in the disordered structure when compared to an ordered molecule.

4.4.3 Summary and discussion

The introduction of a methyl group in the *para* position of the 2-haloaniline component results in a very different structure to the molecular complexes of 2-XA 3,4-DNBA formed at room temperature. The ΔpKa values lie in the salt-cocrystal continuum, but only neutral crystals are formed. The haloaniline component and 3,4-DNBA still crystallise in a 1:2 stoichiometric ratio; furthermore, the haloaniline component remains disordered. However, the 2-X-4-MA molecules in **10**, **11** and **12** are significantly more disordered than in the 2-XA complexes. The disorder is over at least four possible positions, and it is not possible to locate all of the atoms of the 2-X-4-MA in the structure; it is also likely that the disorder is actually more complex than it was possible to model. The model reported is the best that could be achieved from the data.

Rather than the layered, planar structures observed in **1**, **4** and **6**, the crystal structures have an identical herringbone packing arrangement to molecular complex **3**. It is not fully understood why there is such a change in the crystal packing with the introduction of a methyl group, especially as it was not possible to fully model the disordered components. In the 2-IA 3,4-DNBA molecular complexes, **1**, **2** and **3**, the herringbone structure of **3** had a greater amount of crystal space accommodating the 2-IA molecules (~205 $Å^3$) than the planar structures of **1** and **2**. It is possible that, with the CT interactions dominating the packing and the greater size of the methyl-substituted haloaniline, the herringbone structure is required in order to

accommodate the 2-X-4-MA molecules. In a related argument, it is also possible that the introduction of the methyl group results in additional bond competition, leading to the significant disorder that results in the requirement of extra crystal space; this may force the formation of the herringbone structure.

The yellow/orange colour of the crystals can be attributed to charge-transfer between the planar aromatic donor and acceptor molecules, and the CT interactions dominate the packing. It is apparent that infinite stacks of the donor and acceptor molecules are not a requirement for the colour, with overlap occurring within a three-molecule A-D-A unit. The slight difference in the colours of the 2-X-4-MA 3,4-DNBA complexes and molecular complex **3** may be due to alteration of the donor molecule by introduction of the electron-donating methyl group; charge-transfer is very sensitive to the nature of the donor and acceptor molecules, their separation and their relative orientations. It is not possible to accurately assess the molecular overlap due to the uncertainties in the model and the complicated disorder; the nature of the disorder may also affect the optical properties.

4.5 Switching off colour and disorder: 2-iodophenol 3,4-dinitrobenzoic acid

To investigate the role of the hydrogen bond donor in the molecular disorder, the amine group of the 2-iodoaniline co-former was exchanged for a hydroxyl group, to give 2-iodophenol (2-IP). Co-crystallisation experiments were conducted in the same way as for the previously described 2-haloaniline complexes, using a 1:2 stoichiometry of 2-iodophenol and 3,4-dinitrobenzoic acid.

It was expected that in the formation of a molecular complex, the stronger hydrogen bond donor (O-H) would eliminate the presence of molecular disorder, with the molecular components 2-iodophenol and 3,4-dinitrobenzoic acid forming an ordered structure. As a ring substituent, the hydroxyl (OH) group is still electron-donating, but is a poorer donor than NH_2 due to the greater electronegativity of oxygen than nitrogen; charge-transfer is highly sensitive to the nature of the donor and acceptor molecules, and exchanging the NH_2 group for an OH group will alter the interactions that take precedent in the formation of a molecular complex.

4.5.1 Experimental details

2-iodophenol 3,4-dinitrobenzoic acid (13)

Molecular complex **13** was synthesised *via* slow evaporation (§3.1) from ethyl acetate at ambient temperature using a 1:2 stoichiometric molar ratio of the 2-iodophenol and 3,4-dinitrobenzoic acid; colourless plate crystals were obtained. Single crystal X-ray diffraction data were collected at 150 K, according to the procedures outlined in §3.2, using a Rigaku Oxford Diffraction SuperNova diffractometer (Cu Kα radiation).The structure was solved by direct methods using SHELXS-2013[192] and refined using SHELXL-2014,[198] both within the WinGX program suite;[200] crystallographic data are given in Table 4.16 and refinement details are reported in Appendix A4.

Table 4.16 Crystallographic data for molecular complex **13**

Formula	(C_6H_5IO) $_2(C_7H_4N_2O_6)$
M/g mol^{-1}	644.24
T/K, radiation	150(2), Cu Kα
Space Group	$P\bar{1}$
a/Å	7.6204(1)
b/Å	7.6644(2)
c/Å	43.5424(7)
α	89.758(2)
β	85.625(1)
γ	63.472(2)
V/Å	2267.48(8)
Z	4
ρ_{cal}/ g cm^{-3}	1.887
μ/mm^{-1}	11.846
θ Range/°	4.075 - 66.599
Ref Collected	31751
Independent	8007
Observed>2σ	7416
Rint	0.0439
Completeness %	100
Parameters	703
GooF	1.043
R_1 (obs)	0.0422
R_1 (all)	0.0468
wR2 (all)	0.1171
$\rho_{max,min}$/e Å^{-3}	1.321, -1.014

4.5.2 Crystal structure analysis: comparison with molecular complex 1

The molecular components 2-iodophenol and 3,4-dinitrobenzoic acid are white and light yellow solids, respectively, with dissolution of the two giving very pale yellow solutions. The

molecular complex 2-IP 3,4-DNBA, **13**, is yielded in small quantities as colourless plate crystals; this compares to the red crystals of the disordered molecular complex 2-IA 3,4-DNBA, **1**. A single crystal UV-visible spectrum was collected, as outlined in §3.4.1, for molecular complex **13** at room temperature (Figure 4.53, with a comparison against molecular complex **1**); substituting the amine group of 2-iodoaniline for a hydroxyl group results in a significant shift of the absorption band to shorter wavelength, with absorption below 450 nm compared to 570 nm. Thus, absorption characteristic of aromatic donor···acceptor charge-transfer is not observed.

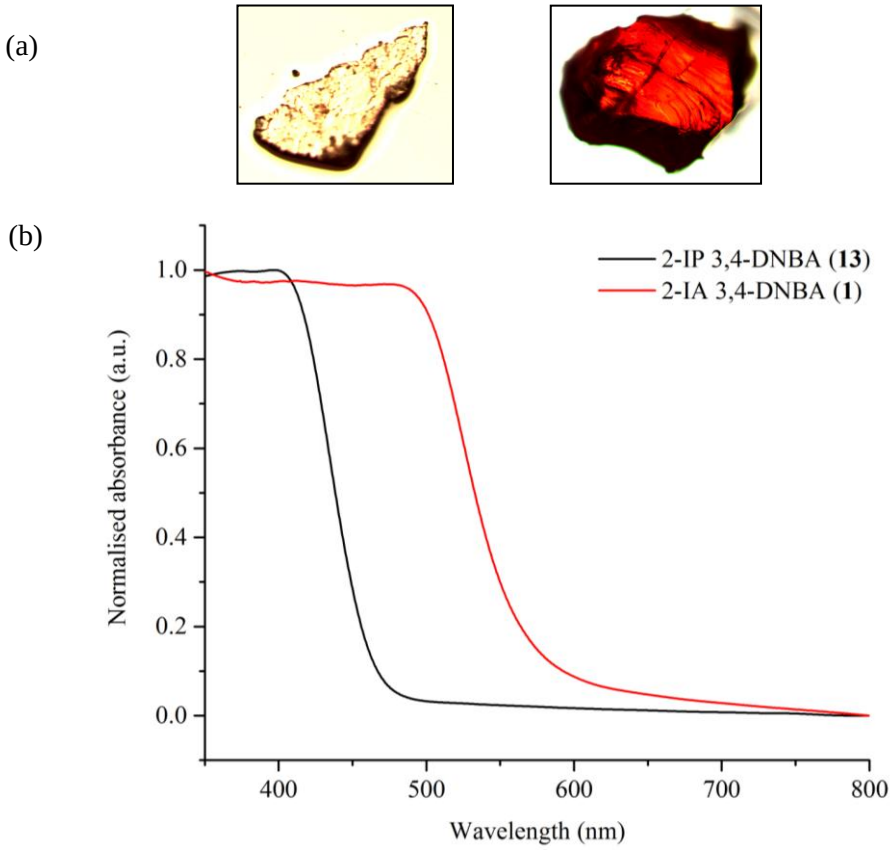

Figure 4.53 (a) Photographs of crystals of molecular complexes **13** (left) and **1** (right); (b**)** single crystal UV-visible absorption spectrum for molecular complex **13** (black) compared against the spectrum for molecular complex **1** (red); both were collected at room temperature.

Despite the difference in the optical properties, the overall packing of 2-IP 3,4-DNBA is very similar to Form I of 2-IA 3,4-DNBA. Molecular complex **13** crystallises in the triclinic space group $P\bar{1}$; the molecular components are present in their neutral forms, with 2-IP and 3,4-DNBA crystallising in a 1:2 ratio. The asymmetric unit of **13** contains four independent molecules of 3,4-DNBA and two fully ordered 2-IP molecules. The four independent molecules of 3,4-DNBA form two dimers via O-H···O hydrogen bonds of moderate strength between the carboxylic acid groups (Table 4.17). Each of the C-O bond lengths of the carboxylic acid groups

are intermediate between distances expected for single and double bonds (1.269(4) and 1.252(6)Å, 1.264(5) and 1.256(6) Å, 1.267(6) and 1.255(4) Å, 1.264(6) and 1.260(4) Å) which may indicate the presence of proton disorder.[37,39] Due to the presence of a heavy atom in the structure, a model was employed with a single proton position, with the hydrogen atom located using Fourier difference maps and bound to the C-O group with the longer bond distance; the O-H distance was restrained to be 0.9 Å and the H-atom displacement parameters constrained to $1.5U_{eq}$ of the O-atom to which it is bonded. Each dimer interacts with another equivalent dimer through weak C-H···O hydrogen bonds (Table 4.17) to generate ordered hydrogen bonded tapes identical to those observed previously in the 2-haloaniline complexes (Figure 4.3). Similarly to molecular complex **1**, the dimer molecules are not coplanar, with an angle of ~6° calculated between the mean ring planes of the 3,4-DNBA molecules in the first dimer, and ~14° in the second dimer. The carboxylic acid groups are all close to coplanar with the ring planes, with torsion angles of less than 10° (~0° and 8° in first dimer; ~5° and ~8° in second dimer). Due to steric effects, all of the nitro groups are twisted significantly out of the ring planes (*m*-NO_2 groups by ~28°/47° in first dimer and ~27°/41° in second dimer; *p*-NO_2 groups by ~30°/57° in first dimer and ~30°/58° in second dimer); the tilt direction of neighbouring *m*- and *p*-NO_2 substituents is always the same, allowing close contacts to be avoided.

Unlike the disordered 2-IA 3,4-DNBA complex, **1**, the two independent 2-IP molecules are fully ordered. The average volume of crystal space occupied by the ordered 2-IP molecules is 169.46 $Å^3$, which is very similar to the volume of 162.93 $Å^3$ for the molecule in the crystal structure of pure 2-IP.[235] The average space occupied by the disordered 2-IA molecules in the charge-transfer complex of **1** is 199.32 $Å^3$ which is approximately 30 $Å^3$ greater than that in **13**. Therefore, there is a change in the 3,4-DNBA network on substitution of the 2-IP for 2-IA, with less volume of space in the 'donor' site. This is also accompanied with the switching off of molecular disorder.

A two-dimensional sheet structure is formed that is very similar to that of **1** (Figure 4.54). There is a single sheet type which incorporates both 3,4-DNBA dimers and both independent 2-IP molecules. The hydroxyl group of each 2-IP molecule forms a moderate-strength hydrogen bond to the *m*-NO_2 group of an adjacent 3,4-DNBA molecule (**g** and **h**, Table 4.17). The iodine atoms of the two 2-IP molecules also form halogen bonds with *m*-NO_2 group oxygen atoms of adjacent 3,4-DNBA molecules (I···O = 3.369(3) Å and 3.354(3) Å, compared to the sum of the van der Waals radii of I and O of 3.50 Å). The hydroxyl group is a strong hydrogen bond donor, and it is probable that the strength of the O-H···O hydrogen bond in **13**, compared to the weaker N-H···O hydrogen bonds in **1**, removes the competition between hydrogen and halogen bond formation that resulted in the molecular disorder of 2-IA. Thus, the formation of a moderate

strength O-H···O hydrogen bond locks in the orientation of the 2-IP molecules, so each only adopts a single position. Comparison of the sheets in **1** and **13** shows that the position of the electron donating NH_2/OH groups in the channels differs between the two complexes (Figure 4.54); however, the benzene ring and halogen atom of the 2-iodophenol is in a similar position to one of the molecular orientations of the 2-iodoaniline molecules (purple and blue).

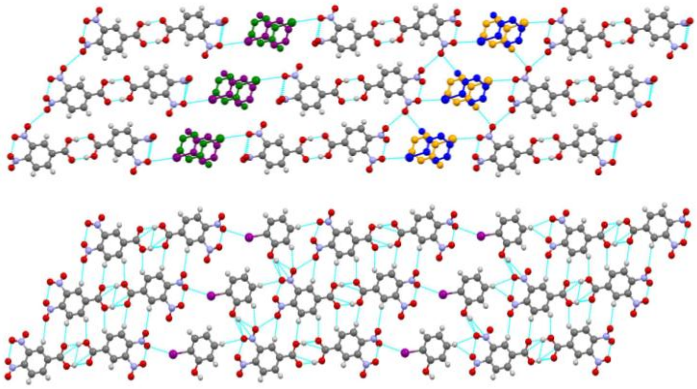

Figure 4.54 Comparison of the two-dimensional sheet structures formed in the ordered molecular complex of 2-iodophenol 3,4-dinitrobenzoic acid, **13** (top) and the disordered molecular complex of 2-iodoaniline 3,4-dinitrobenzoic acid, **1** (bottom).

Table 4.17 Hydrogen bond data for molecular complex **13** (refer to Figure 4.3 for labels **a**- **f; g** and **h** are O-HO bonds formed through the hydroxyl group).

Bond type	D-H···A	D-H	H···A	D···A	<(DHA)
a	O7-H7A···O2 #1	0.93(2)	1.76(2)	2.665(3)	166(5)
b	O1-H1···O8 #1	0.93(2)	1.68(2)	2.603(3)	176(4)
c	C19-H19···O8 #2	0.93	2.51	3.395(4)	159.8
d	C20-H20···O1 #3	0.93	2.61	3.282(5)	129.6
e	C7-H7···O7#3	0.93	2.57	3.279(5)	133.1
f	C6-H6···O2 #2	0.93	2.58	3.435(4)	152.5
a	O13-H13A···O19 #4	0.93(2)	1.69(2)	2.613(3)	175(5)
b	O20-H20A···O14 #4	0.92(2)	1.76(2)	2.659(3)	164(4)
c	C24-H24···O13 #5	0.93	2.52	3.423(4)	163.7
d	C23-H23···O19 #6	0.93	2.54	3.308(5)	140.0
e	C36-H36···O14 #6	0.93	2.58	3.274(5)	132.4
f	C37-H37···O20 #5	0.93	2.55	3.416(4)	154.4
g	O25-H16···O17 #5	0.89(2)	2.20(4)	2.980(4)	145(5)
h	O26-H17···O10 #7	0.93(2)	2.02(3)	2.859(4)	149(5)

#1 -x+1,-y,-z #2 x,y+1,z #3 -x+1,-y+1,-z #4 -x+1,-y+2,-z+1 #5 x,y-1,z #6 -x+1,-y+1,-z+1 #7 x,y+1,z

The sheets stack to form a layered structure, although the layers are slightly rippled (Figure 4.55 (a)). The sheets are staggered in a similar way to **1**, such that 2-IP molecules stack alternately with 3,4-DNBA dimers. There are π···π interactions between aromatic rings but the stacking appears to be dominated by an O···π interaction between the lone pair of the hydroxyl group O-atom and the aromatic ring of a 3,4-DNBA molecule, which shift the rings to form the interaction. There are two types of stack, with each containing one of the independent 2-IP molecules; there are approximates stacking distances of ~3.40 Å (Figure 4.55 (b), Stack 1) and ~3.45 Å (Figure 4.55 (b), Stack 2), with the separation therefore equal to that in molecular complex **1** (~3.40 Å). In each stack, the overlap differs above and below the 2-IP molecules (Figure 4.55 (b), right).

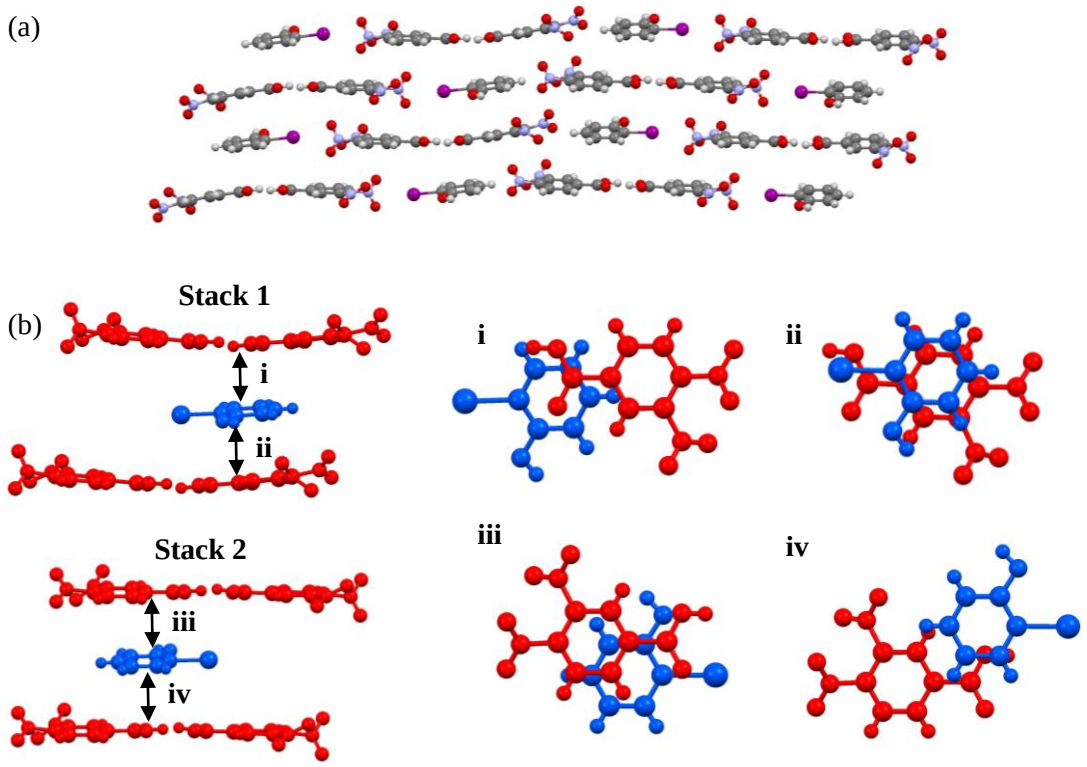

Figure 4.55 (a) Stacking of two-dimensional sheets in molecular complex **13** to form a layered structure; (b) The two types of stack and associated molecular overlap of 2-IP (shown in blue) and 3,4-DNBA (shown in red).

In both of the stacks, there is significant overlap of the 2-IP and 3,4-DNBA rings (**ii** and **iii**, Figure 4.55 (b)) as well as overlap with the carboxylic acid group and centre of the 3,4-DNBA dimer (**i** and **iv**, Figure 4.55 (b)). This contrasts with the molecular complex of 2-IA 3,4-DNBA, **1**, where there is very little ring overlap and the overlap is predominantly between the 2-IA ring and the carboxylic acid group of 3,4-DNBA or the centre of the dimer. Unlike the 2-XA 3,4-DNBA complexes, where the aromatic donor···acceptor interactions dominate the stacking,

the major interaction directing the stacking of the sheets in **13** appears to be the O···π interaction; this occurs between the lone pair of the hydroxyl group O-atom and the aromatic ring of a 3,4-DNBA molecule, thus shifting the aromatic molecules in the stacks to accommodate the interaction.

4.5.3 Summary and discussion

Using crystal engineering principles, it was expected that substituting the amine group of 2-iodoaniline for a hydroxyl group, to give 2-iodophenol, would switch off the disorder by exploiting the strength of the hydroxyl group as a hydrogen bond donor. This was observed in the formation of a 1:2 molecular complex of 2-iodophenol and 3,4-dinitrobenzoic acid, **13**, in which the 2-IP molecules were fully ordered. The hydroxyl group is a stronger hydrogen bond donor than the amine group, and the formation of a hydrogen bond involving this group resulted in only a single possible orientation, locking the 2-IP molecule in place. However, 2-IP 3,4-DNBA has a very similar overall packing arrangement as 2-iodoaniline 3,4-dinitrobenzoic acid, although there is a smaller volume of space in the 'donor' site. In both molecular complexes the molecular components are in their neutral states; both structures are made up of two-dimensional sheets consisting of alternating channels of 3,4-DNBA dimers and 2-IA/2-IP molecules. This demonstrates the robustness of the 3,4-DNBA framework even with a different 'host' molecule. However, the 3,4-DNBA framework differs slightly, since there is a smaller volume of space is available to the 2-IP than the 2-IA. A layered structure is formed, with the stacking distance in molecular complex **1** equal to the stacking distance in **13**. However, in **13**, an O···π interaction between the lone pair of the hydroxyl group and the aromatic ring of a 3,4-DNBA molecule appears to dominate the stacking, rather than aromatic donor···acceptor interactions.

Despite the structural similarities between the molecular complexes, the crystals have very different optical properties; while **1** crystallises as red block crystals, **13** is yielded as colourless plate crystals. In **13**, there is no absorbance characteristic of π···π* charge-transfer; this will be due to the differences in the interactions between the alternating molecules. Charge-transfer between aromatic molecules depends on the molecular overlap of the HOMO (of the donor) and LUMO (of the acceptor), and is very sensitive to the electronic properties of the donor and acceptor moieties and to the relative orientations of the overlapping donor and acceptor molecules. The molecular overlap and relative orientations of the stacked molecules differ between the 2-IA and 2-IP complexes, with greater ring overlap in the 2-IP 3,4-DNBA complex. In addition, aromatic donor···acceptor interactions may be obscured if other intermolecular interactions take precedence; this is observed here, through both the strong O-H···O hydrogen

bonds within the sheets, and the interaction of the hydroxyl O-atom with the aromatic ring of 3,4-DNBA in the stacks. Furthermore, the NH_2 and OH groups have different donating strengths, with the higher electronegativity of the OH group making it a weaker donor. The strength and type of the hydrogen bonding involving the NH_2 and OH substituents may also have an effect; it has been shown for aniline and phenol derivatives that the effect of hydrogen bonding is transferred to the aromatic ring and can induce changes in the π-electron delocalisation.[236] It is also possible in this particular case that the molecular disorder, or lack of, is playing a role in determining the colour in the solid-state, with the substitution for the OH group effectively switching disorder off and locking the 2-IP molecule in place through the formation of a single moderate strength O-H···O hydrogen bond. A full understanding of the differences in the electronic transitions in the molecular complexes and the influences of the disorder on the optical properties requires further work, including calculations that are still very challenging for computational chemistry capabilities for solid-state molecular crystals.

The pair of molecular complexes, **1** and **13**, provide valuable insight into how crystal engineering principles, and the knowledge of intermolecular interactions, may be applied to designing disorder into molecular complexes. This may be useful not only in terms of inducing and tuning colour, but also in facilitating phase transitions, as described in detail in §4.2.

4.6 Conclusions

Twelve molecular complexes of 2-haloanilines, 2-halo-4-methylanilines and 2-iodophenol with 3,4-dinitrobenzoic acid have been synthesised and characterised. In each of the molecular complexes, the halogenated component and 3,4-dinitrobenzoic acid crystallise in a 1:2 ratio and, with the exception of the 2-FA 3,4-DNBA complex, **8**, which was obtained upon cooling, all of the components are present in their neutral forms. The ΔpKa values for the 2-haloaniline complexes (where X = I, Br, Cl) are all negative, thus proton transfer was not expected. For the 2-fluoroaniline and 2-halo-4-methylaniline complexes, the ΔpKa values are all in the salt-cocrystal continuum (but close to zero), and all formed as neutral complexes at ambient temperature; proton transfer in the 2-FA complex on cooling resulted in a mixed ionisation state complex (Table 4.18). The neutral molecular complexes are all strongly coloured, ranging between red and yellow, with the exception of the 2-iodophenol complex which is colourless.

Table 4.18 ΔpKa values for the multi-component crystallisations of the anilines with 3,4-DNBA and the type of molecular complex(es) formed.

Co-molecule 1	ΔpKa	Neutral (N), ionic (I) or mixed ionisation (M) complex
2-iodoaniline	-0.28	N
2-bromoaniline	-0.29	N
2-chloroaniline	-0.16	N
2-fluoroaniline	0.43	N, M (on cooling)
2-iodo-4-methylaniline	0.15	N
2-bromo-4-methylaniline	0.15	N
2-chloro-4-methylaniline	0.27	N

Each of the molecular complexes features the same 3,4-DNBA tape, in which the neutral 3,4-DNBA molecules form dimers through moderate strength O-H···O hydrogen bonds, and these are connected through weak C-H···O hydrogen bonds. The majority of the C···O distances of the hydrogen bonds are between 3.3 - 3.4 Å and there is very little change in this hydrogen bonded network across the complexes. The robustness of the network would allow 3,4-dinitrobenzoic acid to be used in the design of future complexes; this persists even with the introduction of the strong hydrogen bonding character of 2-iodophenol.

All of the aniline complexes feature disorder of the aniline molecule over at least two positions, and it is apparent that disorder is a prerequisite to form a stable lattice. The disordered molecules interact with 3,4-DNBA through hydrogen and halogen bonds, resulting in a competition for the acceptor atoms. The disordered molecules are incorporated as guests into the ordered 3,4-DNBA host system. The crystal packing in the complexes can be divided into two types: planar and herringbone.

The 2-haloaniline complexes formed by solvent evaporation all form the same planar sheet structure, with the only major difference between the structures being the orientation of the 2-haloaniline component in the channels. Due to the formation of a 1:2 complex, there is only one 2-XA molecule to each 3,4-DNBA dimer. In all of the planar complexes (which are red in colour), the neutral aromatic donor (aniline) and acceptor (3,4-DNBA) dimers stack alternately; overlap is typically between the aniline molecule and the carboxylic acid groups of the 3,4-DNBA dimer, with intermolecular separations of approximately 3.4 Å. The colour can be attributed to $\pi\cdots\pi^*$ charge-transfer between donor and acceptor moieties. The planar complexes all display temperature-dependent behaviour. 2-IA 3,4-DNBA, 2-BrA 3,4-DNBA and 2-ClA

3,4-DNBA all undergo phase transitions on heating, with the transition temperature increasing with decreasing molecular weight, which must be due to the nature of the halogen (size and intermolecular interactions). This demonstrates the possibility of tuning temperature-dependent effects through interchanging the halogen. The reversibility of the phase transitions also differs, with the transitions in 2-IA 3,4-DNBA both irreversible, compared to the fully reversible transitions in 2-BrA 3,4-DNBA and 2-ClA 3,4-DNBA. This is attributed to differences in the interactions within the structures, as well as density changes on the transitions.

The first phase transition in the 2-IA and 2-BrA complexes involves a reorientation of the disordered molecules in the channels. The second transition in 2-IA 3,4-DNBA, however, involves a massive structural rearrangement from a planar to a herringbone structure, which the crystals surprisingly survive; this transition is thermochromic and is associated with a distinct colour change from red to yellow. It is probable that the rearrangement in the second phase transition of 2-BrA 3,4-DNBA is less significant as the transition is reversible. In the herringbone complex, the stacking is between rings, with a similar separation to the planar complexes, but the stacking is not continuous along the stack. The colour can be attributed to a charge-transfer between the aromatic donor and acceptor, with the change in colour on the transition likely due to changes in the stacking type and molecular overlap.

Conversely, 2-FA 3,4-DNBA undergoes a phase transition upon cooling. In this case the mechanism involves the transfer of a proton from a 3,4-DNBA carboxylic acid group to the 2-FA amine group, and is associated with a change in colour from red to colourless. This is the only disordered molecular complex in which some of the molecular components are in their ionic states, and is also the only molecular complex in the haloaniline series which is colourless. It is probable that this is due to the significant change in the hydrogen bonding from planar to three-dimensional, with the loss of charge-transfer upon protonation of the amine group. NH_3^+ is strongly electron-withdrawing, thus there is a considerable change in the molecular orbitals and the donating ability of the molecules, making donor···acceptor interactions not possible. This molecular complex highlights the switching of colour in multi-component complexes depending on the protonation states of the molecules, which is explored further in subsequent chapters.

The molecular complexes of 2-halo-4-methylaniline 3,4-dinitrobenzoic acid all adopt the same herringbone structure as the high temperature form of 2-IA 3,4-DNBA (**3**). The 2-X-4-MA molecules are highly disordered and it was not possible to resolve all of the atoms or analyse the interactions between the 3,4-DNBA network and the disordered channels. It is possible that the herringbone arrangement must be adopted in the case of larger 'guest' molecules as the

3,4-DNBA network affords more space to accommodate the molecules. There is no temperature-dependent behaviour observed in these complexes.

The structure adopted by 2-IP 3,4-DNBA provides key insights into the possible role of disorder in phase transitions and in determining solid-state colour. The molecular complex adopts a very similar planar sheet structure to the equivalent 2-IA complex, despite the difference in the hydrogen bond donor (OH). The molecular complex forms as colourless crystals compared to the red crystals of the 2IA complex. The structure is fully ordered, due to a strong O-H···O hydrogen bond formed between the 2-IP molecules and the 3,4-DNBA network, which locks the 2-IP molecule in place. Although the molecular complex is composed of alternately stacked 2-IP molecules and 3,4-DNBA dimers, the 2-IP has different donating properties compared to 2-IA. In addition, the dominant interaction in the stacking is an O···π interaction between the lone pair of the hydroxyl group O-atom and the aromatic ring of 3,4-DNBA, and there are no aromatic donor···acceptor type charge-transfer interactions.

In the molecular complexes of 2-IA 3,4-DNBA, 2-BrA 3,4-DNBA and 2-ClA 3,4-DNBA, the disorder remains the same at 100 K and 300 K, and is therefore likely to be static in nature rather than dynamic; this is further corroborated in the formation of the favourable interactions with the 3,4-DNBA network when in the two possible molecular orientations. The disorder is not likely to be random as strong, localised diffuse scattering is observed in the diffraction images; it is indicative of dominant ordering in the stacking direction, which will have the greatest impact on the charge-transfer interactions. It is clear that a more detailed understanding of the molecular disorder is required to understand fully the optical properties of the disorder.

The results presented in this chapter introduce several key concepts. Firstly, all of the neutral disordered complexes reported are strongly coloured; the dominant interactions in the formation of the complexes are the aromatic donor···acceptor interactions and the colour can therefore be attributed to charge-transfer between the donor aniline component and the acceptor 3,4-DNBA. Upon proton transfer or loss of disorder, the crystals are colourless and colour is therefore switched off. Secondly, each aniline molecule has an increased volume of crystal space available in comparison to the fully ordered molecule in each case; this is further evidenced in the smaller amount of space in the ordered 2-IP site in 2-IP 3,4-DNBA. Combining the effects of the dominant CT interactions in the mixed stacks, and, he presence of molecular disorder, inefficient packing is inherent. With the formation of a 1:2 complex, there is only one donor molecule to each 'acceptor dimer'. Stacking occurs between 2-XA and the centre of the dimer and this results in increased crystal space surrounding each of the molecules. It is suggested that this additional space is facilitating the phase transitions in the 2-IA, 2-BrA and 2-ClA

3,4-DNBA complexes, and in particular allowing the massive structural rearrangement to Form III in 2-IA 3,4-DNBA to occur in a single crystal to single crystal manner. Such large rearrangements are not typically known to occur with survival of the single crystals. It is likely that this additional space due to disorder allows the proton transfer to occur in 2-FA 3,4-DNBA upon cooling, with survival of the single crystal.

Thus, the presence of disorder and the inherent additional crystal space in these mixed stack complexes has been shown to facilitate phase transitions on application of an external stimulus, which in this case is variable temperature; this provides a route to designing functional materials with desirable properties i.e. thermochromism. With suitable molecular components, it may be possible to introduce disorder into further molecular complexes, using similar crystal engineering principles and the knowledge of competition between interactions.

CHAPTER 5

Proton transfer and thermochromism in haloaniline complexes

5 Proton transfer and thermochromism in haloaniline complexes

5.1 Introduction

Chapter 5 is concerned with the formation of distinct neutral and ionic forms of the same molecular complex (in aniline-dinitrobenzoic acid systems) with the same 1:1 stoichiometry; the ΔpKa values for the multi-component systems all fall in the salt-cocrystal continuum. The different (neutral/ionic) forms were often obtained under the same evaporative crystallisation conditions thus it was not possible to predict which form would be obtained. The neutral form is metastable and transformation to the more stable ionic form occurs under thermal activation but also spontaneously at room temperature over time; the transformation is associated with a proton transfer but the crystal structures do not simply differ in the location of the proton, but instead show significantly different intermolecular interactions and crystal packing. Consequently, the neutral and ionic forms have very different optical properties, with the neutral forms strongly coloured and the ionic forms colourless. The proton transfer mechanism thus provides a route to thermochromism in aniline-dinitrobenzoic acid systems.

5.1.1 Neutral or ionic molecular complex?

In the multi-component crystallisation of an acid-base pair, a proton may be transferred between the acid and base components, forming an ionic molecular complex (or salt), or the molecular components may remain in their neutral forms, resulting in a neutral molecular complex (or co-crystal); there is also the possibility of solvates or hydrates forming, and for the multi-component crystal to have more than one possible crystal form (polymorphs) (§1.4). The difference in pKa values (ΔpKa) between the acid and base is commonly used as a guide to determine whether a neutral or ionic molecular complex is likely to form (§1.4.1).[79]

In many multi-component complexes, for example those that include the acid-pyridine synthon, the structural difference between a neutral or ionic form is often only in the location of the proton in the hydrogen bond. In this case, the hydrogen bonds O-H···N and $O^{-}\cdots H\text{-}^{+}N$ would be expected for neutral and ionic molecular complexes, respectively; similar crystal structures may be expected, and the distinction between the neutral and ionic forms would be dependent on the ability to locate the proton.[103] However, the protonation state can have a significant impact on the intermolecular interactions that form and often on the material properties.[78] The effect on properties is also evident in a number of processes where proton transfer occurs in the solid-

state, often in response to external stimuli, with an associated change in properties, such as those discussed with regards to thermochromism (§1.8).[99,171,172]

Many multi-component crystallisation studies have been conducted where the primary aim is to investigate whether a neutral or ionic complex is formed with a specific type of parent molecule and a range of co-formers.[98,104,237] In each of these studies, either a neutral or an ionic molecular complex was formed which could be rationalised according to the ΔpKa values. Literature precedence for systems where both neutral and ionic molecular complexes are formed which are stable under ambient conditions is very rare. Mootz and Wiechert[238] isolated two molecular complexes of pyridine and formic acid, with different stoichiometric ratios. In the neutral 1:1 co-crystal there was no proton transfer, while in the 1:4 molecular complex there were N^+-H$\cdots O^-$ interactions observed. Haynes *et al.*[96] obtained a salt and a co-crystal of lutidine with fumaric acid, with 1:2 and 2:1 stoichiometries of the base and acid in the salt and co-crystal, respectively. However, in both of these examples, the stoichiometries of the molecular components in the two complexes differed, and the salt complexes comprised co-existing neutral and ionic components. To the best of our knowledge, there are no examples of isolating and structurally characterising a neutral and an ionic complex formed from identical parent and co-former molecules, in the same stoichiometric ratio, under the same crystallisation conditions; the two forms are distinct, with very different structures, with complete proton transfer in the neutral form and absent proton transfer in the ionic form.

5.1.2 Polymorphism and metastable forms

In this chapter, the neutral and ionic pairs of the molecular complexes should not be described as polymorphs (§1.6) since the chemistry of the molecular species differs between the two, however, they do display behaviour similar to that of polymorphs. They also offer the opportunity to study structure-property relationships, with the crystal forms easily distinguished by their strikingly different colours.

The relative stabilities of polymorphic forms depends on their free energies, with the most stable form having the lowest free energy. As discussed in §1.6, at a fixed temperature and pressure, only one polymorph is stable, with other polymorphs in that system therefore metastable. Metastable forms can coexist with the thermodynamically stable form, but have a finite existence, and may sometimes transform to the more stable form over time or in response to a change in environment.[119] Polymorphs may also appear simultaneously under the same conditions, termed concomitant polymorphism. For any material, there are a certain set of conditions under which it will crystallise, known as the occurrence domain; sometimes these

domains overlap, and more than one form may be obtained in the same experiment at conditions which are common to more than one domain.[125]

5.1.3 Design strategy

Building on the study discussed in Chapter 4, which utilised 2-haloanilines, a multi-component crystallisation study was conducted on 4-haloanilines (4-XA, where X = I, Br) and 4-halo-2-methylanilines (4-X-2-MA, where X = I, Br, Cl) (which are more basic than the corresponding 2-haloanilines) with the co-former 3,5-dinitrobenzoic acid (3,5-DNBA) (Figure 5.1). Some of the results of this study have been recently published.[239]

There are no previously reported molecular complexes of 4-haloanilines with dinitrobenzoic acids in the CSD.[86] The molecular components are colourless or pale-coloured in their single component forms. The ΔpKa values for 3,5-DNBA with the aniline components all fall in the salt-cocrystal continuum, thus there is the possibility of neutral or ionic complexes forming. In their neutral forms, the aniline components can act as aromatic electron donors, due to the strongly donating NH_2 substituent, and the 3,5-DNBA can act as an aromatic electron acceptor, due to the strongly withdrawing NO_2 and carboxylic acid group substituents.

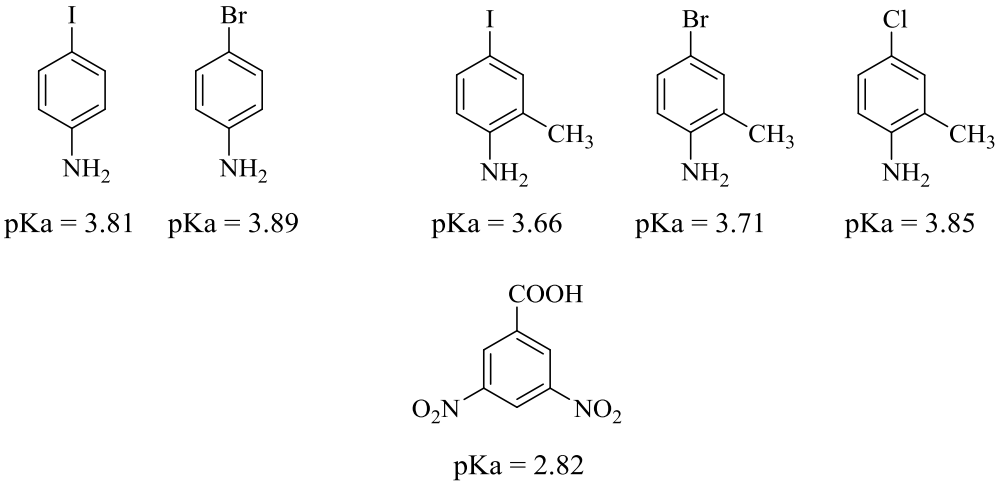

Figure 5.1 Chemical structures of the molecular components used in the multi-component crystallisation experiments in Chapter 5, and their pKa values.[228,240] Top (left to right): 4-IA, 4-BrA, 4-I-2-MA, 4-Br-2-MA and 4-Cl-2-MA; bottom: 3,5-DNBA.

For these multi-component crystallisations, there is the possibility of a proton being transferred between the proton donor (3,5-DNBA) and the proton acceptor (aniline) to form a salt, or ionic molecular complex. In the latter, hydrogen bonds would be expected to form between the protonated amine (NH_3^+) and carboxylate groups (COO^-). However, in the case of a neutral

complex, according to Etter's rules,[40] the 3,5-DNBA molecules would be expected to form homodimers through the strongest hydrogen bond donors and acceptors (hydroxyl and carbonyl groups of the carboxylic acid group). In this case, the difference in the neutral and ionic structures would thus not simply be in the location of the acidic proton, and therefore significant structural consequences would be anticipated.

This is demonstrated in this study where, unusually, both neutral and salt forms of the same two-component complex for each parent/co-molecule system were formed under the same conditions (with the exception of 4-Cl-2-MA); the neutral molecular complexes are metastable forms. The structures of the neutral and ionic molecular complexes differ greatly, and the colour of the molecular complex is dependent on the ionisation states of the molecular components.

5.2 Molecular complexes of 4-haloaniline and 3,5-dinitrobenzoic acid

5.2.1 Experimental details

Molecular complexes **14 - 19** were obtained *via* the method of slow evaporation (§3.1), using a 1:1 stoichiometric molar ratio of the 4-haloaniline and 3,5-dinitrobenzoic acid. Crystallisation trials employed a range of solvents and temperatures. The crystallisation conditions which resulted in growth of the crystals used for collection of SCXRD data are reported here; more details on the crystallisation conditions are provided in §5.2.2. Single crystal X-ray diffraction experiments were carried out according to the procedures outlined in §3.2. Crystallographic data are given in Table 5.1 and refinement details are reported in Appendix A5.

4-iodoanilinium 3,5-dinitrobenzoate Form I (14)

Molecular complex **14** was synthesised from ethanol at ambient temperature; colourless needle crystals were obtained. Single crystal X-ray diffraction data were collected at 100 K using a Rigaku Oxford Diffraction Gemini Ultra diffractometer (Mo Kα radiation). The structure was solved by direct methods using SHELXS-2013[192] and refined using SHELXL-2014,[198] both within the WinGX program suite.[200]

4-iodoanilinium 3,5-dinitrobenzoate Form II (15)

Molecular complex **15** was synthesised from acetonitrile at ambient temperature; colourless block crystals were obtained. Single crystal X-ray diffraction data were collected at 100 K using a Rigaku R-AXIS/RAPID image plate diffractometer. The structure was solved by direct

methods using SHELXS-97[192] and refined using SHELXL-2014,[198] both within the WinGX program suite.[200]

4-iodoaniline 3,5-dinitrobenzoic acid (16)

Molecular complex **16** was synthesised from ethyl acetate at 40 °C; small red block crystals were obtained. Crystals of **16** were also obtained from ethanol and acetonitrile. Single crystal X-ray diffraction data were collected at 150 K using a Rigaku Oxford Diffraction Gemini Ultra diffractometer (Mo Kα radiation). The structure was solved by direct methods using SHELXS-2013[192] and refined using SHELXL-2014,[198] both within the WinGX program suite.[200]

4-iodoaniline 3,5-dinitrobenzoic acid methanol solvate (17)

Molecular complex **17** was synthesised from methanol at ambient temperature; large red block crystals were obtained. Single crystal X-ray diffraction data were collected at 100 K using a Rigaku R-AXIS/RAPID image plate diffractometer. The structure was solved by direct methods using SHELXS-97[192] and refined using SHELXL-97,[198] both within the WinGX program suite.[200] There is significant crystallographic disorder in molecular complex **17**, and significant restraints and constraints had to be applied in the refinement (Appendix A5).

4-bromoanilinium 3,5-dinitrobenzoate (18)

Molecular complex **18** was synthesised from ethanol at room temperature; colourless needle crystals were obtained. Single crystal X-ray diffraction data were collected at 150 K using a Rigaku Oxford Diffraction SuperNova diffractometer (Mo Kα radiation). The structure was solved by direct methods using SHELXS-2013[192] and refined using SHELXL-2014,[198] both within the WinGX program suite.[200]

4-bromoaniline 3,5-dinitrobenzoic acid (19)

Molecular complex **19** was synthesised from acetonitrile at 40 °C; yellow/orange block crystals were obtained. Single crystal X-ray diffraction data were collected at 100 K using a Rigaku R-AXIS/RAPID image plate diffractometer. The structure was solved by direct methods using SHELXS-97[192] and refined using SHELXL-2014,[198] both within the WinGX program suite.[200]

Table 5.1 Crystallographic data for molecular complexes **14** - **19**

	14	**15**	**16**	**17**	**18**	**19**
Formula	$(C_6H_7NI)^+$ $(C_7H_3N_2O_6)^-$	$(C_6H_7NI)^+$ $(C_7H_3N_2O_6)^-$	(C_6H_6NI) $(C_7H_4N_2O_6)$	$2(C_6H_6NI)$ $2(C_7H_4N_2O_6)$ (CH_3OH)	$(C_6H_7NBr)^+$ $(C_7H_3N_2O_6)^-$	(C_6H_6NBr) $(C_7H_4N_2O_6)$
M/g mol^{-1}	431.14	431.14	431.14	894.32	384.15	384.15
T/K, radiation	100(2), Mo Kα	100(2), Mo Kα	150(2), Mo Kα	100(2), Mo Kα	150(2), Cu Kα	100(2), Mo Kα
Space Group	$P2_12_12_1$	$P2_12_12_1$	$P\bar{1}$	$P\bar{1}$	$P2_12_12_1$	$P\bar{1}$
a/Å	6.7588(1)	6.0536(7)	7.2766(3)	9.947(7)	6.7937(1)	7.3332(10)
b/Å	12.0929(2)	10.5285(16)	7.3862(3)	12.823(9)	11.9574(1)	13.937(2)
c/Å	36.4619(5)	24.444(3)	14.2883(5)	13.020(10)	35.8729(3)	15.611(2)
α	90	90	99.348(3)	94.249(16)	90	65.133(5)
β	90	90	103.7125(4)	91.739(16)	90	82.758(6)
γ	90	90	90.271(3)	90.493(19)	90	83.330(6)
V/Å	2980.16(8)	1558.0(4)	735.39(5)	1655(2)	2914.13(5)	1432.5(3)
Z	8	4	2	2	8	4
ρ_{cal}/ g cm^{-3}	1.922	1.838	1.947	1.730	1.751	1.781
μ/mm^{-1}	2.185	2.090	2.214	1.967	4.205	2.907
θ Range/°	3.065-26.366	3.16-27.47	2.798-27.484	2.99-27.48	4.444-66.600	3.045-27.485
Ref Collected	15628	10999	10639	38785	14999	34237
Independent	6082	3552	3391	7522	5107	6545
Observed>2σ	5960	3349	2740	4315	4983	5473
Rint	0.0159	0.0299	0.0574	0.0586	0.0345	0.0408
Completeness %	99.6	99.7	99.9	99.2	99.9	99.8
Parameters	433	220	217	344	433	433
Flack parameter	-0.016(5)	-0.02(2)	-	-	-0.028(7)	-
GooF	1.071	1.154	1.081	1.075	1.044	1.143
R_1 (obs)	0.0205	0.0211	0.0460	0.0791	0.0390	0.0324
R_1 (all)	0.0213	0.0249	0.0633	0.1317	0.0397	0.0403
wR2 (all)	0.0476	0.0449	0.1099	0.1856	0.1067	0.0879
$\rho_{max,min}$/e Å^{-3}	1.172, -0.902	0.560, -0.357	0.876, -0.585	1.831, -0.695	1.205, -0.690	0.878, -0.652

5.2.2 Crystallisation discussion

4-iodoaniline (4-IA) and 4-bromoaniline (4-BrA) are light purple and beige crystalline solids, respectively, and 3,5-dinitrobenzoic acid (3,5-DNBA) is a light yellow solid; dissolution of the two components (3,5-DNBA with 4-XA) resulted in pale orange and yellow solutions for 4-IA and 4-BrA, respectively. The ΔpKa values for 3,5-DNBA with 4-IA and 4-BrA are 0.99 and 1.07, respectively, thus falling in the salt-cocrystal continuum. From the 1:1 co-crystallisation of 4-IA and 3,5-DNBA, four molecular complexes (**14** - **17**) were obtained *via* slow evaporation of solvent; the products include two polymorphic salt forms, one neutral form and a methanol solvate. From the co-crystallisation of 4-BrA and 3,5-DNBA, two molecular complexes (**18** and **19**) were obtained *via* slow evaporation of solvent; the products included one salt form and one neutral form. In each of the products, the 4-haloaniline and 3,5-DNBA are present in the same relative 1:1 stoichiometry; the ionic molecular complexes were yielded as colourless crystals, whereas the crystals of the neutral and solvate forms were strongly coloured (red or orange). An extensive set of co-crystallisation experiments were carried out for each system, and a combination of optical microscopy, single crystal X-ray diffraction, thermal analysis and powder X-ray diffraction was used to assess the crystallisation products.

4-iodoaniline 3,5-dinitrobenzoic acid

With the exception of **17**, the 4IA 3,5-DNBA molecular complexes were obtained under a range of crystallisation conditions but not reproducibly, and single crystals were difficult to grow; repeat crystallisation trials would often result in the formation of a different form of the molecular complex to that obtained under the same conditions in a previous trial. In addition, mixtures were often obtained, either due to concomitant growth or spontaneous interconversion, making the characterisation of the products difficult.

Single crystals of molecular complex **14**, one of the salt polymorphs, were grown reproducibly from 2-propanol at all temperatures, and were yielded as colourless needle crystals; this molecular complex was the only product formed from this solvent and the crystals were uniform. Below 30°C, crystallisation from ethanol, acetonitrile and ethyl acetate also yielded molecular complex **14**, but not reproducibly. In some crystallisation trials using these conditions (acetonitrile and ethanol, 4 °C and ambient temperature), the other salt polymorph, molecular complex **15**, was obtained. However, growth of **15** was less common and single crystals were only grown in very small quantities; this can be attributed to the lower density of the complex compared to **14** (Table 5.1).

Single crystals of molecular complex **16**, a neutral molecular complex, could be obtained from ethanol, acetonitrile and ethyl acetate, with evaporation carried out between 30 °C and 60 °C. The complex formed as red block crystals, making it easily distinguishable from the two salt polymorphs. However, molecular complex **16** is metastable, and preservation of the crystals in this form was problematic; the stability of the crystals also appeared to vary across the samples. Many of the crystals were observed to transform spontaneously to a colourless phase, which was polycrystalline. In the majority of samples, the red crystals of **16** transformed immediately upon exposure to the ambient environment, but in some cases the samples contained a mixture of red and colourless phases upon initial inspection of the vial. It is possible that the two phases had grown concomitantly, or that the sample had partially transformed, immediately following crystallisation; however, the nature of the polycrystalline colourless phase suggested rapid transformation had occurred prior to inspection of the vial. Conversely, some single crystals of molecular complex **16** were stable for significant periods of time (up to one year at the time of writing); in general, the most stable crystals were obtained from ethanol and ethyl acetate, with evaporation between 40 - 60 °C. However, no cases were observed where the whole sample remained as molecular complex **16**. Given the lack of colour, it was considered possible that molecular complex **16** was transforming to one of the known colourless salt polymorphs (**14** and **15**) or an unknown salt (§5.2.6.1).

Molecular complex **17** (a methanol solvate) was the only product formed when using methanol as the solvent and was always yielded as large red block single crystals, across the range of evaporation temperatures. In each case, the crystals were uniform and a single product was formed, confirmed by powder X-ray diffraction.

4-bromoaniline 3,5-dinitrobenzoic acid

The ionic form of the molecular complex, **18**, was grown *via* slow evaporation at ambient temperature from all solvents; the highest quality single crystals were obtained from ethanol. The molecular complex was yielded as colourless needle crystals, and the morphology was identical to the equivalent 4-IA 3,5-DNBA molecular complex (**14**).

Molecular complex **19**, a neutral form, was obtained *via* slow evaporation above room temperature; single crystals suitable for single crystal X-ray diffraction were obtained from acetonitrile at 40 °C. The complex formed as orange block crystals, which were easily distinguishable from the salt form. However, similarly to 4-IA 3,5-DNBA, molecular complex **19** was highly metastable and preservation of the form was problematic, with spontaneous conversion to a polycrystalline colourless phase, generally immediately upon exposure to the

ambient environment. Crystals of molecular complex **19** appeared much less stable than the equivalent neutral 4-IA 3,5-DNBA complex; single crystal X-ray diffraction data was collected at low temperature on one crystal of the molecular complex, but any remaining crystals transformed to the colourless phase before further analysis could be conducted.

Generally, evaporation carried out between 30 °C - 60 °C resulted in the polycrystalline colourless phase, or a mixture of this phase and a very small amount of **19**. Visually, the colourless phase matched that of the phase obtained upon spontaneous transformation, which suggested that rapid conversion of **19** had occurred prior to inspection of the vial. A number of repeat co-crystallisations were conducted but it was not possible to obtain any more crystals of molecular complex **19** for further analysis; the crystallisations always resulted in the same polycrystalline colourless phase. Given the lack of colour, it is possible that the colourless phase is an ionic form of the complex, either **18** or an unknown form (§5.2.6.2).

5.2.3 4-haloanilinium 3,5-dinitrobenzoate (14, 15 and 18)

Two polymorphs of 4-iodoanilinium 3,5-dinitrobenzoate, **14** and **15**,[239] and a single complex of 4-bromoanilinium 3,5-dinitrobenzoate, **18**, were formed; molecular complexes **14** and **18** are isomorphous. In all of the molecular complexes the components are ionic, with full proton transfer from the carboxylic acid group of 3,5-DNBA to the amine group of 4-XA, with the cations and anions in a 1:1 ratio. All form as colourless crystals (Figure 5.2) and crystallise in the orthorhombic space group $P2_12_12_1$. The asymmetric units of molecular complexes **14** and **18** contain two independent 4-iodoanilinium cations and two independent 3,5-dinitrobenzoate anions; this compares to the one of each of the cation and anion in the asymmetric unit of molecular complex **15**.

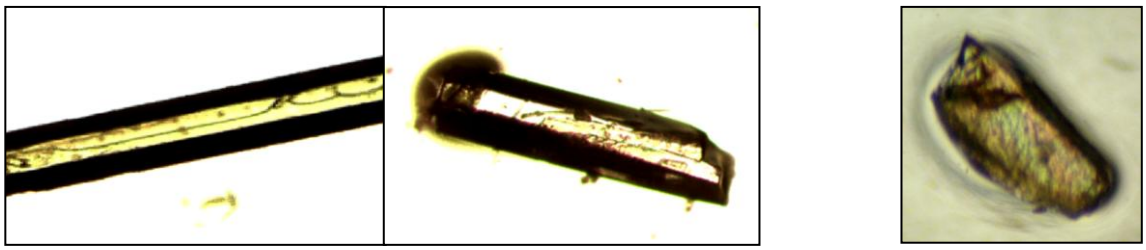

Figure 5.2 Photographs of colourless needle crystals of the isomorphous molecular complexes **14** and **18** (left) and a colourless block crystal of molecular complex **15** (right).

In the isomorphous molecular complexes, **14** and **18**, the C-O distances of the carboxylate groups of the 3,5-DNBA molecules are approximately equal, which is consistent with deprotonation and a delocalisation of the charge across the group (1.251(4)/1.251(4) Å and

1.249(4)/1.265(4) Å for molecular complex **14**; 1.243(6)/1.265(6) Å and 1.247(5)/1.272(5) Å for molecular complex **18**). The 3,5-DNBA molecules are approximately planar; each nitro group is twisted out of the ring plane by less than 10°, and the carboxylate groups by ~°1 and ~16° in molecular complex **14**, and ~2° and ~15° in molecular complex **18**. Each hydrogen atom of the tetrahedral NH_3^+ group of the 4-iodoanilinium cations is involved in a hydrogen bond to a carboxylate group oxygen atom of an adjacent 3,5-dinitrobenzoate anion; the charge-assisted hydrogen bonds direct the hydrogen bonding into a three-dimensional network. Hydrogen bonding data for **14** and **18** are given in Table 5.2.

Table 5.2 Hydrogen bonding data (Å, °) for molecular complexes **14** and **18**

D-H···A	**D-H**	**H···A**	**D···A**	**<(DHA)**
Molecular complex **14**				
N1-H1A···O1_#1	0.92(5)	1.87(5)	2.776(4)	171(4)
N1-H1B···O8	0.90(5)	1.94(5)	2.828(4)	167(4)
N1-H1C···O7_#2	0.90(5)	1.85(5)	2.739(4)	171(5)
N2-H2A···O2_#1	0.95(5)	1.76(5)	2.696(4)	169(5)
N2-H2B···O1_#3	0.86(5)	1.89(5)	2.706(4)	157(4)
N2-H2C···O8	0.95(5)	1.73(5)	2.668(4)	172(4)
Molecular complex **18**				
N1-H1A···O1_#1	0.74(7)	2.06(7)	2.789(5)	168(7)
N1-H1B···O8_#1	0.88(7)	1.98(7)	2.841(5)	165(6)
N1-H1C···O7	0.81(7)	1.94(7)	2.741(5)	167(6)
N2-H2A···O2	0.79(8)	1.91(8)	2.689(6)	169(7)
N2-H2B···O1_#1	0.77(8)	1.95(8)	2.689(6)	159(7)
N2-H2C···O8	0.75(7)	1.93(7)	2.673(5)	168(7)

Molecular complex **14**: #1 -x+3,y+1/2,-z+1/2 #2 x+1,y,z #3 -x+2,y+1/2,-z+1/2

Molecular complex **18**: #1 x+1, y, z

There are similar angles of ~58°/~65° and ~53°/63° between the mean ring planes of the 4-XA and 3,5-DNBA ions in **14** and **18**, respectively. Both 3,5-DNBA anions interact with both 4-IA cations *via* moderate strength N-H···O hydrogen bonds between the NH_3^+ and carboxylate groups (Table 5.2). The carboxylate group oxygen atoms, O1, O2, O8, act as hydrogen bond acceptors (with O8 accepting two hydrogen bonds), forming a $R_4^3(10)$ hydrogen bonded ring that includes two H-atoms of each independent NH_3^+ group (Figure 5.3(a)). The four-molecule units extend along the direction of the crystallographic *a*-axis through two further hydrogen bonds to form a continuous hydrogen bonded chain; a stack of parallel 4-haloanilinium cations

form the backbone of the chain (Figure 5.3(b)). The two independent cations stack alternately, with a separation of ~3.26 Å between stacked molecules; the two cations are almost coplanar, with angles of ~1.6° and ~1.7° calculated between the mean ring planes in **14** and **18**, respectively. The halogen atom of one cation forms a short contact with one of the nitro group oxygen atoms in an adjacent 3,5-DNBA chain (I···O = 3.312(3) Å and Br···O = 3.184(4) Å, compared to the sum of the van der Waals radii of the two atoms of 3.50 Å and 3.37 Å, respectively). There are also $O_{nitro}\cdots O_{nitro}$ and $O_{nitro}\cdots\pi$ interactions between 3,5-DNBA anions. Overall, the three-dimensional hydrogen bonding arrangement results in non-layered crystal structures, and there are no $\pi\cdots\pi$ stacking interactions between 4-XA and 3,5-DNBA molecules. Projection down the crystallographic *b*-axis shows the alternating sections of 4-XA and 3,5-DNBA molecules (Figure 5.3 (c)).

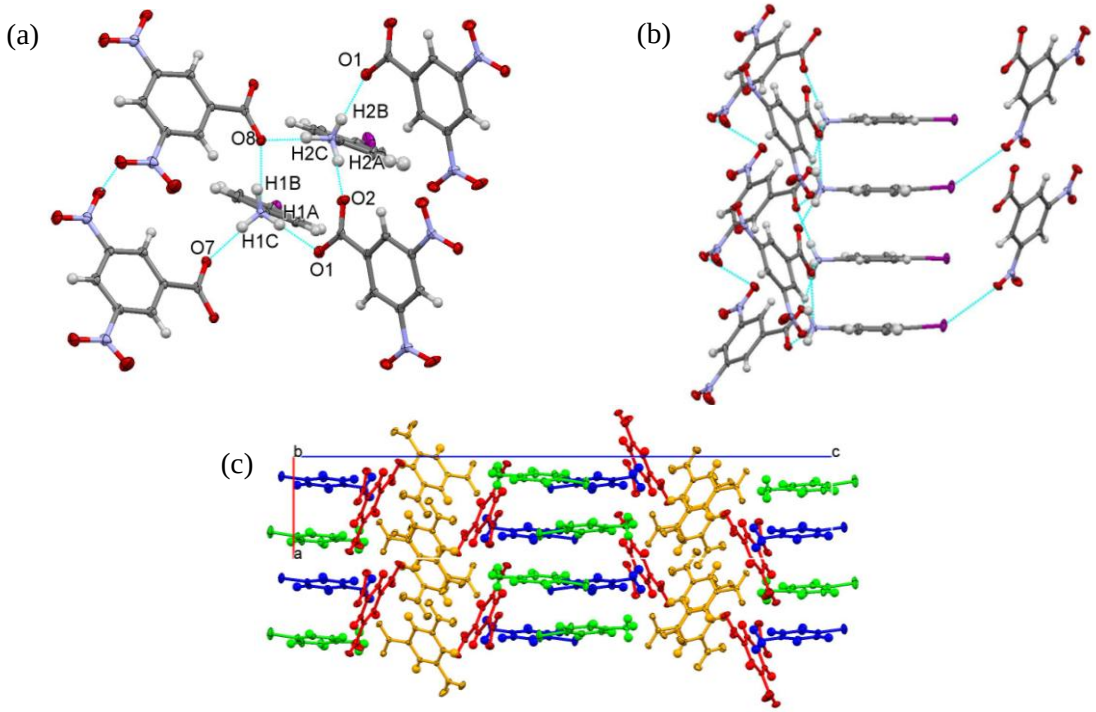

Figure 5.3 (a) Moderate strength N-H···O hydrogen bonds linking the two independent 4-XA cations and four 3,5-DNBA anions; (b) Hydrogen bonded chain with a backbone of stacked 4-XA cations, connecting adjacent chains *via* short C-X···O contacts; (c) the overall packing in molecular complexes **14** and **18**, with stacked 4-XA molecules shown in green and blue and 3,5-DNBA molecules shown in red and orange. (Note: Images (a) - (c) show molecular complex **14**).

The crystal structure of the second 4-IA 3,5-DNBA polymorph, molecular complex **15**, is very similar. The C-O distances of the carboxylate groups of the 3,5-DNBA molecules are approximately equidistant, which is consistent with a delocalisation of the charge across the group (1.266(3)/1.248(3) Å). The 3,5-DNBA molecules are all approximately planar; each nitro group is twisted out of the ring plane by less than 10°, and the carboxylate groups by ~1°. Each

hydrogen atom of the tetrahedral NH_3^+ group of the 4-iodoanilinium cations is involved in a hydrogen bond to a carboxylate group oxygen atom of an adjacent 3,5-dinitrobenzoate anion; the charge-assisted hydrogen bonds direct the hydrogen bonding into a three-dimensional network. Hydrogen bonding data are given in Table 5.3.

Table 5.3 Hydrogen bonding data (Å, °) for molecular complex **15**

D-H···A	**D-H**	**H···A**	**D···A**	**<(DHA)**
N1-H1A···O2 #1	0.93(4)	1.80(4)	2.727(4)	172(3)
N1-H1B···O1	0.94(4)	1.75(4)	2.681(4)	167(4)
N1-H1C···O2 #2	0.94(5)	1.84(5)	2.763(4)	168(4)

#1 x+1, y, z #2 x +1/2, y+5/2, -z;

The mean ring planes of the 4-IA and 3,5-DNBA ions are twisted by ~77° with respect to each other. A very similar hydrogen bonded network to the first polymorph is formed between 4-IA cations and 3,5-DNBA anions *via* moderate strength N-H···O hydrogen bonds (Figure 5.4). Both oxygen atoms of the carboxylate group, O1 and O2, act as hydrogen bond acceptors, with O2 accepting two hydrogen bonds, and the same $R_4^3(10)$ hydrogen bonded ring is formed (Figure 5.4 (a)). Similarly to **14**, this extends along the crystallographic *a*-axis to form a hydrogen bonded chain; however there is no stacking of 4-IA molecules, and instead the cations are oriented away from each other and on opposing sides of the chain. The iodine atoms form halogen bonds with one of the carboxylate oxygen atoms with an I···O distance of 2.987(2) Å, which is significantly shorter than the sum of the van der Waals radii of the two atoms (3.5 Å) and weaker than the halogen bond in **14**; this interaction links the individual hydrogen bonded chains along the direction of the crystallographic *b*-axis (Figure 5.4 (b)). The 3,5-DNBA anions interact with one another *via* $O_{nitro}\cdots O_{nitro}$ and $O_{nitro}\cdots\pi$ interactions, and with 4-IA cations in adjacent chains *via* $O_{nitro}\cdots\pi$ interactions and weak C-H···O contacts. Overall the crystal packing is quite similar to the other polymorph, with alternating sections of 4-IA and 3,5-DNBA molecules observed with projection down the crystallographic *b*-axis (Figure 5.4 (c)).

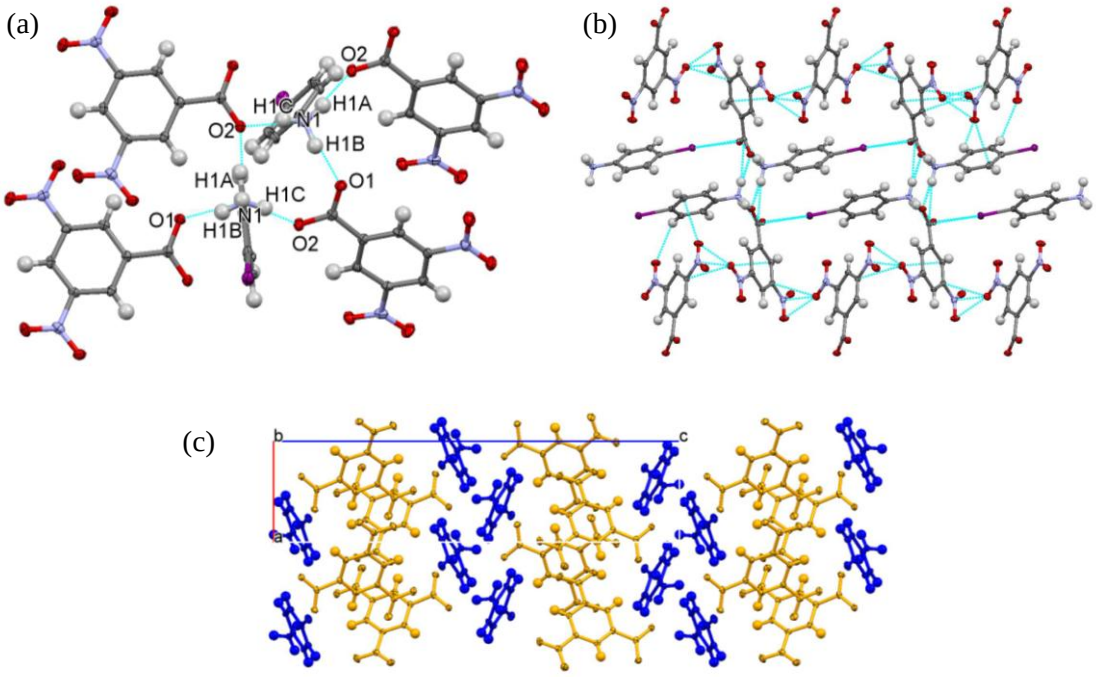

Figure 5.4 (a) Moderate strength N-H···O hydrogen bonds in molecular complex **15**, formed between the 4-IA and 3,5-DNBA ions, generating a hydrogen bonded chain in the direction of the crystallographic *a*-axis; (b) hydrogen bonded chains linked connected by short I···O contacts in the direction of the crystallographic *b*-axis; (c) The non-layered crystal packing, with 4-IA molecules shown in blue and 3,5-DNBA molecules shown in orange.

5.2.4 4-haloaniline 3,5-dinitrobenzoic acid (16 and 19)

The neutral molecular complexes of 4-iodoaniline 3,5-dinitrobenzoic acid, **16**, and 4-bromoaniline 3,5-dinitrobenzoic acid, **19**, are metastable, and only a few crystals remained sufficiently stable for analysis. Both of the neutral complexes are strongly coloured, compared to the pale colours of the individual components and the solution, with the origin of the colour therefore lying in the solid-state arrangement. Molecular complex **16** forms as red block crystals (Figure 5.5 (a)); a single crystal UV-visible absorption spectrum was collected at room temperature (Figure 5.5 (b)) according to the procedure outlined in §3.4.1. The absorbance is characteristic of a π···π* charge-transfer between the donor 4-IA and acceptor 3,5-DNBA molecules, with absorbance below ~600 nm. Molecular complex **19** forms as bright yellow/orange block crystals (Figure 5.5 (a)), but the transformation was more rapid in the 4-BrA complex, and it was not possible to preserve the crystals to conduct UV-visible spectroscopy.

(a)

(b)

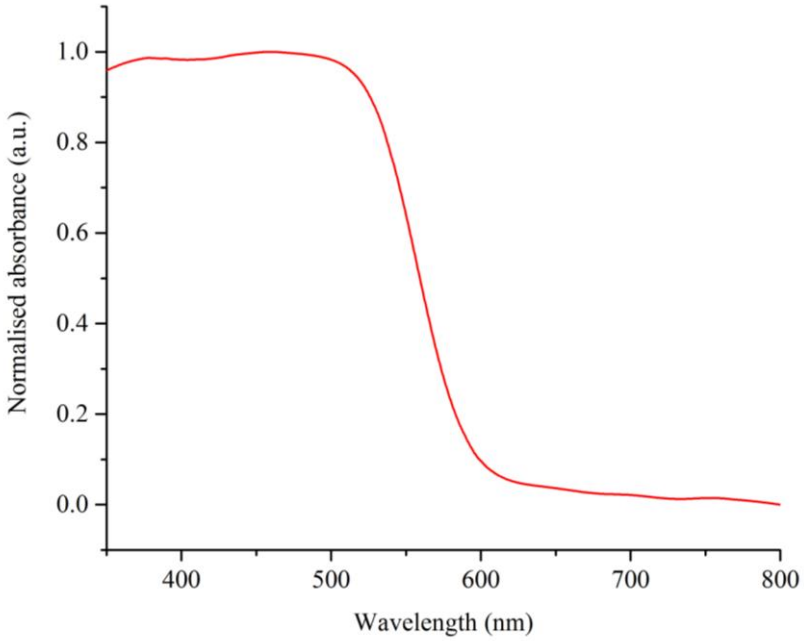

Figure 5.5 (a) Photographs of single crystals of molecular complex **16** (left) and molecular complex **19** (right); (b) single crystal UV-visible absorption spectrum for molecular complex **16** collected at room temperature.

The neutral molecular complexes are not isostructural but the overall crystal packing in each is similar. Both **16** and **19** crystallise in the triclinic space group $P\bar{1}$; the molecular components are neutral and crystallise in a 1:1 ratio. The asymmetric unit of **16** contains one molecule of each component, while the asymmetric unit of **19** contains two independent molecules of each component. In both complexes, the carboxylic acid groups of 3,5-DNBA are close to coplanar with the benzene ring with a torsion angle of ~1° in **16**, and torsion angles of ~2° and ~12° in **19**; all of the nitro groups are rotated out of the ring plane by less than 15°.

3,5-DNBA molecules form dimers through moderate strength O-H···O hydrogen bonds between the strongest hydrogen bond donors and acceptors, resulting in $R_2^2(8)$ hydrogen bonded rings; the dimers are formed between equivalent, coplanar molecules. Hydrogen bonding data for **16** and **19** are given in Table 5.4. The C-O bond lengths (1.243(6)/1.270(5) Å for molecular complex **16**; 1.256(3)/1.276(2) Å and 1.252(3)/1.277(3) Å for molecular complex **19**) are intermediate between distances expected for single and double bonds, which may indicate the presence of proton disorder.[37,39] A model was employed with a single proton position, with the hydrogen atom located using the Fourier difference maps, bound to the C-O group with the

longer bond distance; the O-H distance was restrained to be 0.9 Å and the H-atom displacement parameters constrained to $1.5U_{eq}$ of the O-atom to which it is bonded.

In both molecular complexes, alternating rows of the 4-haloaniline molecules and 3,5-DNBA dimers interact to form planar two-dimensional sheets, however the intermolecular interactions and molecular orientations of the 4-XA molecules within the chains differ between the two complexes (Figure 5.6). In **16**, pairs of 4-IA molecules are in opposite orientations, whereas in **19** the 4-BrA molecules are in similar orientations across the chain.

In molecular complex **16**, 3,5-DNBA dimers interact with one another through weak C-H···O hydrogen bonds between an aromatic H-atom (H11) and a nitro group O-atom (O4) to form a hydrogen bonded chain of 3,5-DNBA molecules (Figure 5.6 (a), Table 5.4). The 4-IA molecules form moderate to weak N-H···O hydrogen bonds through both H-atoms (H1A and H1B) to nitro group O-atoms of the 3,5-DNBA molecules; H1A interacts with O5 and O6 in a bifurcated manner and H1B interacts with O6 of the same nitro group (Figure 5.6 (a), Table 5.4). The iodine atoms are not involved in any halogen interactions.

In molecular complex **19**, each sheet incorporates both independent 4-BrA molecules and both 3,5-DNBA molecules. Unlike molecular complex **16**, there are no interactions between adjacent 3,5-DNBA dimers in the chains. The H-atoms of the amine groups on both 4-BrA molecules (H1A, H1B, H2A and H2B) are involved in moderate to weak N-H···O hydrogen bonds with nitro group O-atoms (O6, O12, O9 and O3, respectively) (Figure 5.6 (b), Table 5.4). In addition, each of the bromine atoms, Br1 and Br2, is involved in a short C-Br···O halogen bond with nitro group oxygen atoms O9 and O6, respectively (Br1···O9 = 3.261(1) Å and Br2···O6 = 3.368(2) Å, compared to the sum of the van der Waals radii of Br and O of 3.37 Å). There are also further weak C-H···O hydrogen bonds between the aromatic hydrogen atoms of 4-BrA molecules and nitro/carboxylic acid group oxygen atoms (C···O = ~3.3 - 3.5 Å).

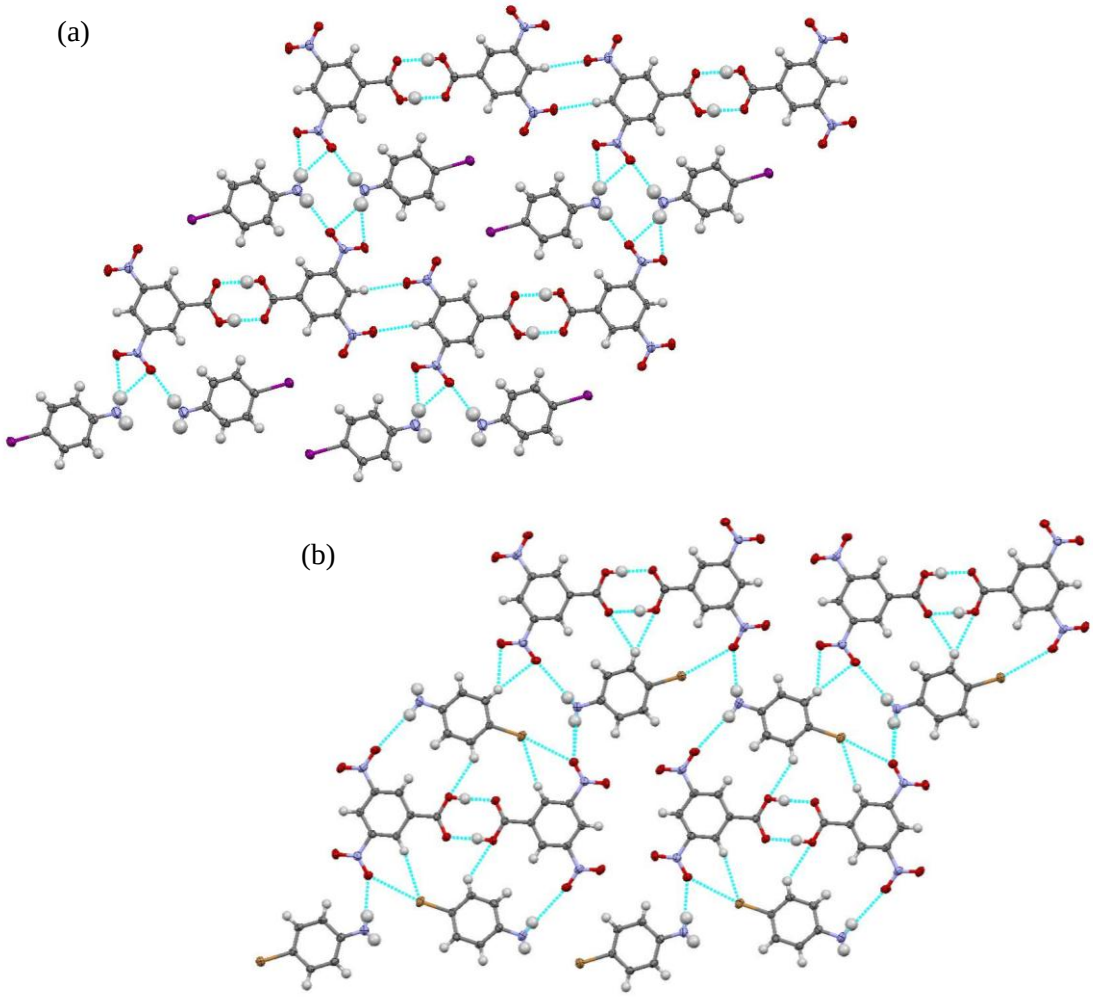

Figure 5.6 Two-dimensional planar sheets in (a) molecular complex **16** showing the N-H···O and C-H···O hydrogen bonds and (b) molecular complex **19**, showing the N-H···O and C-H···O hydrogen bonds and C-Br···O halogen interactions.

Within the sheets, the interactions between the 4-XA molecules and the hydrogen bonded 3,5-DNBA dimers are all weak or close to weak in nature (i.e. on the borderline between moderate and weak hydrogen bonds, and close to the sum of the van der Waals radii for halogen bonds); this highlights the poor hydrogen bond donating ability of the NH_2 donor groups. This may also explain why the neutral complex is the least stable form. In general, however, the hydrogen bonds in **16** are slightly stronger than those in **19**. In both complexes, the planar sheets stack to form a layered structure, with alternately stacked 4-XA (electron-donor) and 3,5-DNBA (electron-acceptor) molecules forming mixed stack columns; it is these aromatic donor···acceptor interactions that dominate the packing arrangement in the structures. There are very similar intermolecular separations of ~3.36 Å and ~3.32 Å between stacked 4-XA and 3,5-DNBA molecules in **16** and **19**, respectively.

Table 5.4 Hydrogen bonding data (Å, °) for molecular complexes **16** and **19**

D-H···A	**D-H**	**H···A**	**D···A**	**<(DHA)**
Molecular complex **16**				
O1-H1···O2_#1	0.86(7)	1.78(7)	2.627(5)	169(7)
C11-H11···O4_#2	0.93	2.48	3.405(5)	171.0
N1-H1A···O5_#3	0.86(8)	2.55(8)	3.353(7)	156(7)
N1-H1A···O6_#3	0.86(8)	2.41(8)	3.154(6)	145(7)
N1-H1B···O5_#4	0.82(8)	2.39(8)	3.191(7)	165(7)
Molecular complex **19**				
O1-H1···O2_#1	0.91(2)	1.71(2)	2.621(2)	178(3)
O7-H7···O18_#2	0.90(2)	1.70(2)	2.596(2)	176(3)
N1-H1A···O6_#3	0.71(3)	2.53(3)	3.219(3)	167(3)
N1-H1B···O12_#4	0.92(3)	2.75(3)	3.637(3)	162(2)
N2-H2A···O9	0.80(3)	2.36(3)	3.120(3)	160(3)
N1-H2B···O3_#5	0.77(3)	2.73(3)	3.467(3)	161(3)

Molecular complex **16**: #1 -x, -y-1, -z+1 #2 -x, -y, -z #3x-1, y-1, z #4 -x, -y, -z+1

Molecular complex **19**: #1 -x+1, -y+1, -z #2 -x+1, -y, -z+2 #3 x-1, y, z #4 x+1, y, z-1 #5 x+1, y, z

The mixed stacks in **16** and **19** are slightly different in terms of the orientations of the molecules and the molecular overlap; in addition, the stacked molecules are closer to coplanar in **16** than they are in **19** (~2° compared to ~5°). In **16**, there are two types of stacking and molecular overlap (**i** and **ii**, Figure 5.7 (a)); in **19** there are four types of stacking (**i - iv**, Figure 5.7 (b)) due to two independent molecules of each of 4-BrA and 3,5-DNBA.

In molecular complex **16**, for both **i** and **ii** there is partial ring overlap, and the halogen atom is directed away from the carboxylic acid group while the amine group sits above the carboxylic acid group or centre of the dimer. In molecular complex **19**, the overlap of **i** and **ii**, for the first 4-BrA molecule, is almost identical to that of **16**; however, the two independent 4-BrA molecules in the linear stack differ in orientation resulting in differing molecular overlap in the stacking direction. For **iii** and **iv**, there is a similar amount of aromatic ring displacement, but the halogen is directed towards or over the carboxylic acid group.

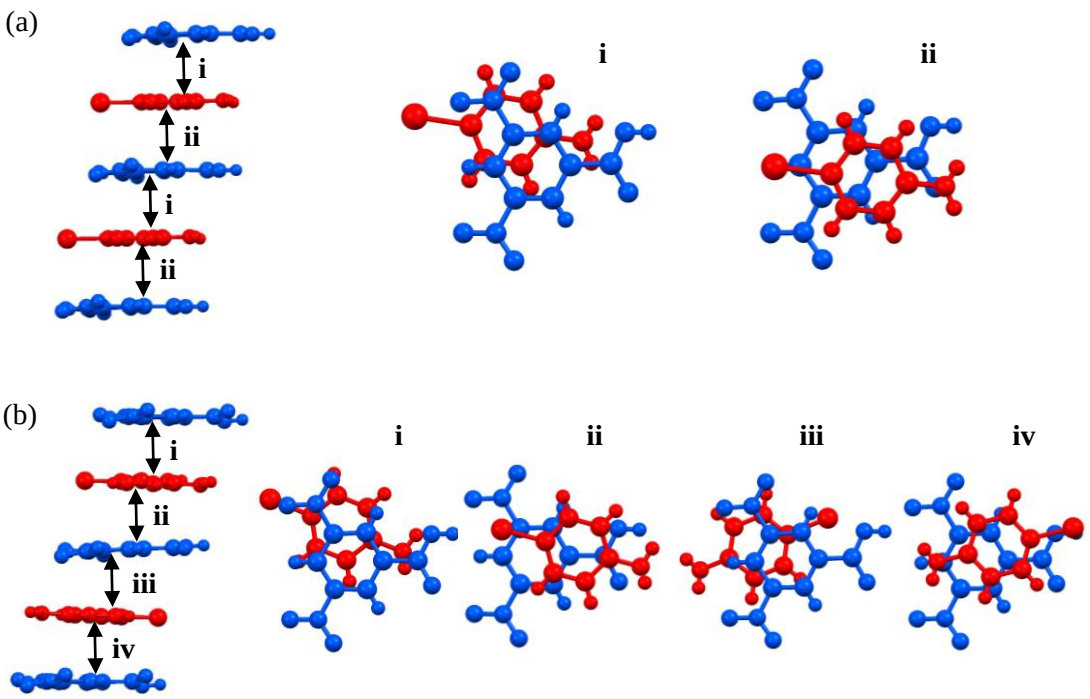

Figure 5.7 (a) Stacking of alternate 4-IA and 3,5-DNBA molecules and molecular overlap in **16**; (b) Stacking of alternate 4-BrA and 3,5-DNBA molecules and molecular overlap in **19**. The 4-XA is shown in red, and the 3,5-DNBA in blue.

The colour in both molecular complexes may be attributed to $\pi\cdots\pi^*$ charge-transfer between the aromatic donor and acceptor molecules in the mixed stacks. Charge-transfer depends on the molecular overlap of the HOMO (of the donor) and LUMO (of the acceptor), and is thus very sensitive to the electronic properties of the donor and acceptor moieties and to the relative orientations of the overlapping donor and acceptor molecules. The nature of the halogen substituent will alter the electron-donating properties of the 4-XA, and the differences in coplanarity and orientations in the stacks will also contribute to the differences in the optical properties of the two complexes. In addition, the hydrogen bonds involving the amine group, and between 3,5-DNBA dimers, are stronger in **16** than **19**, which may also play a role in the colour. The pair of complexes has demonstrated how simple exchange of the halogen substituent can tune the colour properties, however, further work is required in order to understand the electronic transitions involved.

5.2.5 4-iodoaniline 3,5-dinitrobenzoic acid MeOH (17)

The co-crystallisation experiments of 4-IA and 3,5-DNBA also resulted in a solvate form;[239] an equivalent solvated molecular complex was not formed with 4-BrA. Molecular complex **17** grew reproducibly in large quantities by slow evaporation from methanol at a range of

temperatures, forming as large red block crystals; this compares to the pale colours of the individual components and the solution, with the origin of the colour therefore lying in the solid-state. A single crystal UV-visible absorption spectrum was collected on **17** at room temperature (Figure 5.8) according to the procedure outlined in §3.4.1. The absorbance is characteristic of a $\pi\cdots\pi^*$ charge-transfer, with absorbance below ~540 nm. This is shifted to shorter wavelength by ~60 nm compared to the neutral 4-IA 3,5-DNBA complex (§5.2.4).

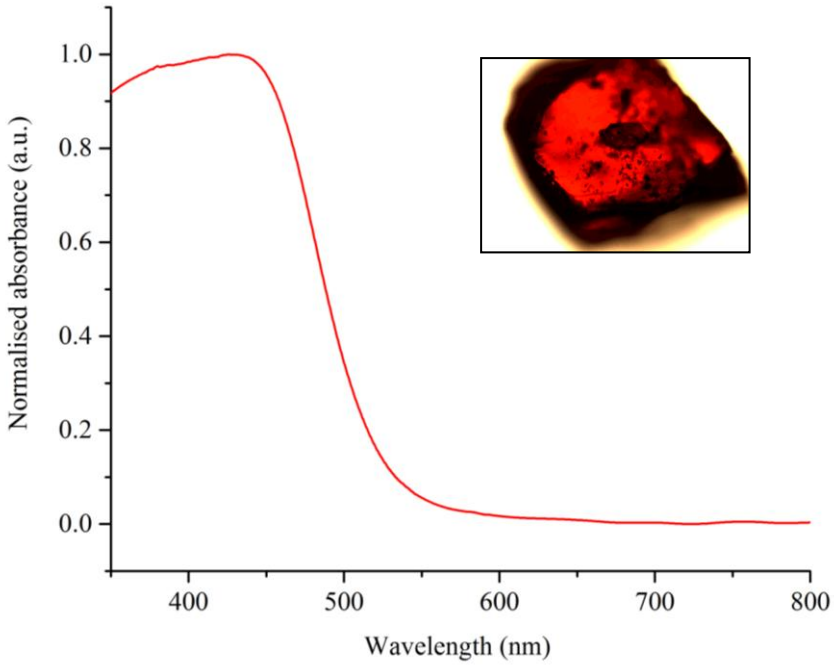

Figure 5.8 Single crystal UV-visible absorption spectrum for molecular complex **17** collected at room temperature, and a photograph of a single crystal of molecular complex **17**

Molecular complex **17** crystallises in the triclinic space group $P\bar{1}$, with 4-iodoaniline, 3,5-dinitrobenzoic acid and methanol in a 2:2:1 stoichiometric ratio. The crystal structure is very complex, with significant molecular disorder and ambiguity in the protonation states of the constituent moieties. The asymmetric unit contains two ordered molecules of 4-IA, two molecules of 3,5-DNBA, which are both disordered over two positions, and a molecule of methanol which is also disordered over two positions.

The two 4-IA molecules are generally well-described, although they do show slight elongation of the thermal parameters out of the ring plane when the molecules are refined anisotropically. However, when the two 3,5-DNBA molecules were freely refined anisotropically as a single position, both independent molecules showed identical significant elongation of the anisotropic displacement parameters about a pivot of a single NO_2 group (left, Figure 5.9). The pivot group can clearly be assigned as a nitro group due to the C-N distance (~1.46(1) Å) and N-O distances

(1.21(1) and 1.21(1) Å; 1.20(1) and 1.23(1) Å) which are consistent with the equivalent bond lengths in the neutral, unsolvated 4-IA 3,5-DNBA complex, **16**. However, when modelled in a single position, the other two ring substituents of 3,5-DNBA have bond lengths which show character between that of a nitro group and a carboxylic acid (or carboxylate) group, with regards to the C-C and C-N bonds. The two 3,5-DNBA molecules were therefore more appropriately modelled as disordered over two positions, about the pivot nitro group, corresponding to a flipping of the carboxylic acid (or carboxylate) group and second nitro group. The molecules therefore have two possible orientations (middle, Figure 5.9), which is viable due to the similar size and shape of a carboxylic acid group and a nitro group. Superimposition of these in the crystal structure results in an average structure (right, Figure 5.9) which accounts well for the significant elongation of the anisotropic displacement parameters observed in the initial anisotropic refinement, and results in an improvement in the refinement statistics. The two 3,5-DNBA molecules are disordered approximately 50:50 over the two possible orientations (shown in green/purple and blue/pink, Figure 5.10).

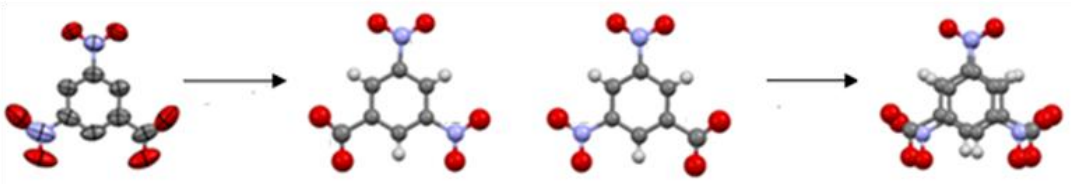

Figure 5.9 Molecular disorder in the 3,5-dinitrobenzoic acid molecules in molecular complex **17**. Left, the elongated anisotropic displacement parameters arising from a free refinement of a single position. Middle, the two possible orientations for the 3,5-dinitrobenzoic acid molecule. Right, the model where the two positions are superimposed.

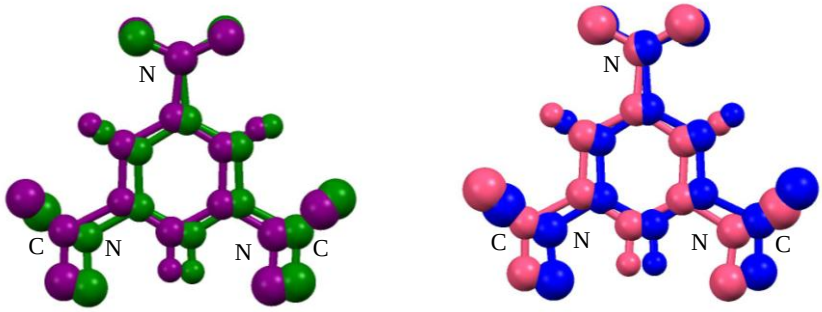

Figure 5.10 The molecular disorder of the two independent 3,5-DNBA molecules, with approximately 50:50 occupancies for the two possible molecular orientations.

The significant molecular disorder and residual electron density makes interpretation of the detailed crystal structure difficult, and it was not possible to assign hydrogen atom positions from the diffraction data; there is therefore some ambiguity in the protonation states of the 4-IA and 3,5-DNBA molecules i.e. whether proton transfer had occurred between the COOH and NH_2 groups of the molecules. In addition, significant restraints and constraints had to be applied

to the 3,5-DNBA molecules to ensure that approximately standard bond lengths and angles were obtained for the disordered carboxylic acid/carboxylate group and nitro group, so it was not possible to use the C-O bond lengths to confirm protonation or deprotonation of the carbonyl group. However, some information about the possible protonation states can be inferred from the interactions between 3,5-DNBA molecules. In addition, IR spectroscopy was conducted, according to the procedure outlined in §3.4.2, to investigate the protonation states of the 4-IA molecules. The IR spectrum of molecular complex **17** shows changes in the N-H stretching region when compared to the spectrum of pure 4-iodoaniline; this includes shifts and splitting of some of the peak positions which is indicative of changes in the amine group. The IR spectrum of **17** was also compared with the IR spectra of **31,** where there are fully resolved neutral and ionic 4-IA species, and **33**, where the 4-IA molecules are ionic (Chapter 6). The peaks do not match those of **33**, but are consistent with those of **31**, which may therefore support a model where the 4-IA molecules are present in both neutral and ionic forms. The IR spectra are provided in Appendix A5.

The 3,5-DNBA molecules are arranged into two independent one-dimensional chains along the direction of the crystallographic *a*-axis. The arrangement of the molecules in the chains is not consistent with either entirely deprotonated or entirely neutral 3,5-DNBA molecules. Firstly, neutral 3,5-DNBA molecules tend to form hydrogen bonded carboxylic acid dimers, with $R_2^2(8)$ graph-set notation, according to Etter's rules[40] and this is not observed in the structure. Conversely, if the 3,5-DNBA molecules were fully deprotonated (i.e. the substituent was always a carboxylate group), then there would be no significant interactions between 3,5-DNBA molecules to hold the chains together. It is important not to over-interpret the reliability of the bond lengths, and therefore intermolecular interactions, involving the atoms in these substituent groups due to the restraints and constraints used in the model. However, the O···O distance between neighbouring carboxylic acid/carboxylate groups in the chains is consistent with a short, charge-assisted hydrogen bond between neighbouring carboxylic acid and carboxylate groups (2.45(3) Å or 2.53(3) Å) (Figure 5.11 (a)). Additionally, the O···O distances between neighbouring carboxylic acid/carboxylate and nitro groups, or neighbouring nitro groups, are also consistent with either a moderate strength hydrogen bond or van der Waals interactions (Figure 5.11 (b) and (c)), with O···O distances ranging between ~2.9 Å and 3.3 Å. Considering these interactions and the arrangement of the molecules, it is most likely that there is approximately 50:50 disorder between a carboxylate and a carboxylic acid group.

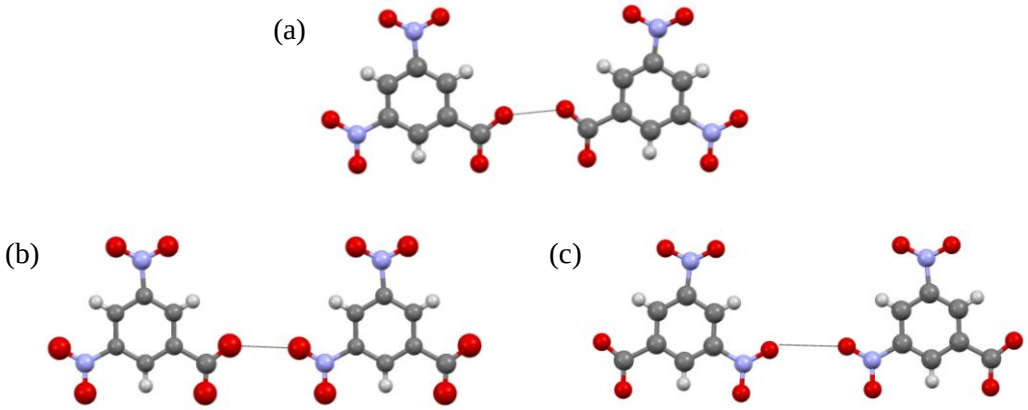

Figure 5.11 Possible interactions depending on the orientation of adjacent 3,5-DNBA molecules in the chain: (a) O-H···O hydrogen bond between a carboxylic acid and carboxylate group; (b) O-H···O hydrogen bond between adjacent carboxylic acid and nitro groups, or short O···O contact between adjacent carboxylate and nitro groups, depending on the protonation state; (c) short O···O contact between adjacent nitro groups.

The chains of 3,5-DNBA molecules interact with 4-IA molecules through N-H···O hydrogen bonds, between the amine group of 4-IA and the carboxylic acid/carboxylate and nitro groups of the 3,5-DNBA; the N···O distances range between ~2.7 Å and ~3.2 Å. The interactions occur irrespectively of the orientation adopted by the 3,5-DNBA molecules in the chain (Figure 5.12).

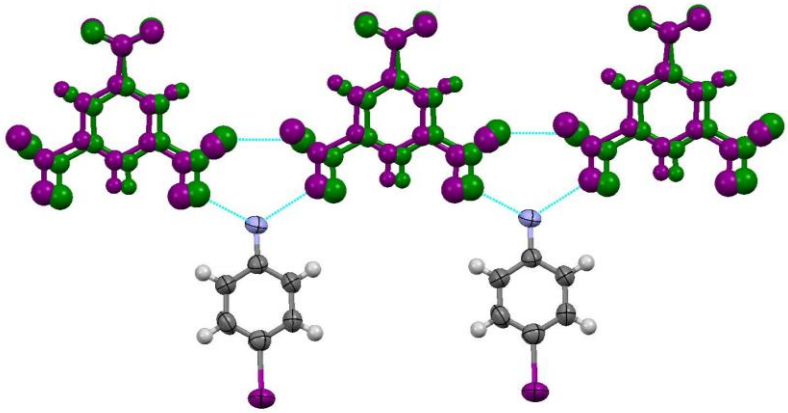

Figure 5.12 N-H···O hydrogen bonds between the amine groups of 4-IA molecules and the oxygen atoms of carboxylate/carboxylic acid/nitro groups of 3,5-DNBA molecules in one of the chains; both chain types are the same.

The single molecule of methanol incorporated in the structure is also approximately 50:50 disordered over two positions, and is situated between the two independent molecules of 4-IA (Figure 5.13). It is predicted that the inclusion of the molecule of methanol in the structure can be attributed to the imbalance of hydrogen bond donors and acceptors in the molecular complex. The two possible positions of the methanol relative to the 4-IA molecule provides further evidence for mixed protonation, through analysis of the possible intermolecular interactions and

bond angles. A model is proposed where the 4-iodoaniline can be present in the crystal structure in its neutral, NH_2, and protonated, NH_3^+, states.

When the methanol molecule is in the position shown in green, the H-atom bound to O15A acts as a hydrogen bond donor to N1 (Figure 5.13), with a C-O-N angle of ~115°. Therefore, to accept the hydrogen bond from the methanol molecule, N1 cannot be protonated and must be the neutral amine. When this is the case, the nitrogen atom of the other 4-IA molecule, N8, can be protonated and form a hydrogen bond to atom O15A; if N8 was also neutral then no additional hydrogen bond would be formed to the lone pairs of O15A. The opposite is true when the methanol molecule is in the yellow position. In this position N8 must be neutral in order to accept a hydrogen bond from the H-atom bound to O15B, with a C-O-N angle of ~116°. In this case, N1 is more likely to be in its protonated NH_3^+ state and form a hydrogen bond to the lone pairs of O15B. All of the N···O distances between N1/N8 and O15A/O15B are approximately 2.8Å, which are consistent with a moderate strength N-H···O or O-H···N hydrogen bond.

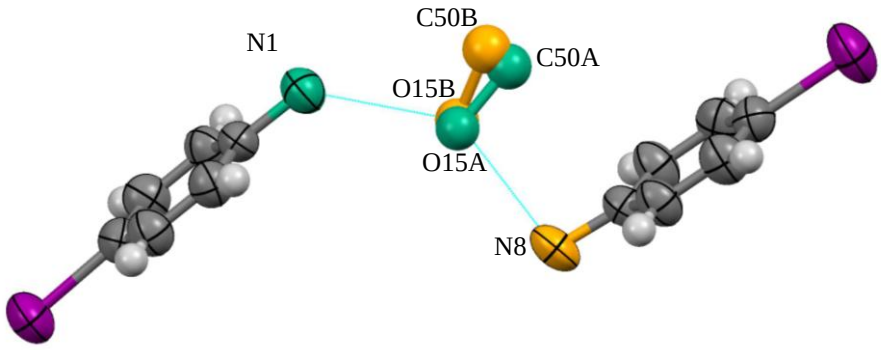

Figure 5.13 The disordered methanol in **17** showing the two possible hydrogen bonds to the two independent 4-IA molecules. When the methanol molecule is in the orientation shown in green, it acts as a hydrogen bond donor to N1. When the methanol molecule is in the orientation shown in orange, it acts as a hydrogen bond donor to N8.

The change in the protonation state of the amine groups is likely to result in small changes in the position of the 4-IA molecules in order to enhance the hydrogen bonding interactions; this is evident in the large size of the thermal parameters of these molecules in the direction of the hydrogen bonds, and from the intermolecular interactions (Figure 5.14). When the 4-IA molecules are neutral, the 4-IA molecules would be expected to be more coplanar with the 3,5-DNBA molecules to form the hydrogen bonds *via* the NH_2 group. When the 4-IA molecules are protonated, the NH_3^+ group would take a tetrahedral shape, and the 4-IA molecule may tilt slightly to act has a hydrogen bond donor to the 3,5-DNBA molecules and to the methanol molecule. In the global crystal structure, there is a statistical averaging of these two cases. This

results in the slightly elongated anisotropic thermal parameters out of the plane of the benzene ring for all of the atoms in the two 4-IA molecules.

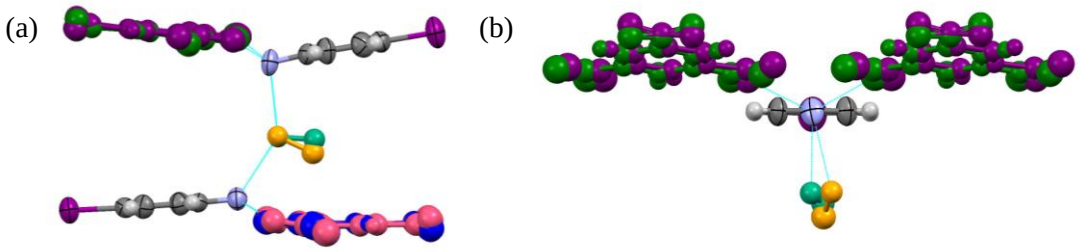

Figure 5.14 The intermolecular interactions of the amine groups (a) viewed along the 3,5-DNBA chains and (b) viewed perpendicular to the 3,5-DNBA, showing one of the 4-IA molecules. A model is proposed where the aniline can be present in both its neutral and protonated states. When neutral, the molecules may shift to become more coplanar with the 3,5-DNBA molecules such that the NH_2 group is coplanar with the rest of the 4IA molecule and the hydrogen bonds are still formed. When it is protonated, the molecule may shift down to forms three hydrogen bonds from the NH_3^+ group (two to the 3,5-DNBA molecules and one to a methanol O atom).

The crystal structure consists of two types of layers, A and B. Layer A contains the 3,5-DNBA molecule shown in green/purple, one of the independent 4-IA molecules and the molecule of methanol; layer B contains the 3,5-DNBA molecule shown in pink/blue and the second independent 4-IA molecule (Figure 5.15). In layer B, the iodine atom of 4-IA forms C-I···O halogen bonds to the oxygen atoms of the disordered carboxylic acid/carboxylate/nitro groups of two 3,5-DNBA molecules within the same layer, with I···O distances of ~3.4 Å (compared to the sum of the van der Waals radii of 3.5 Å). In layer A, there are no similar weak C-I···O interactions, but significant conclusions cannot be drawn from this as there is dependence on the local structure rather than the average structure. In both layers there are also weak C-H···O hydrogen bonds between the aromatic hydrogen atoms of 4-IA and the oxygen atoms of the pivot nitro groups (Figure 5.15).

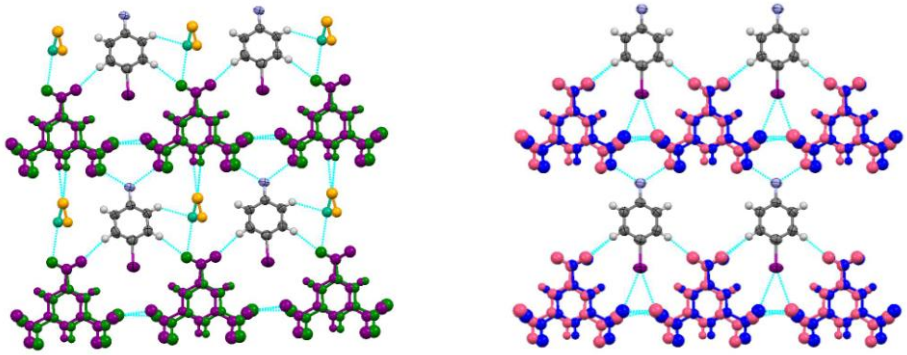

Figure 5.15 Layers A (left) and B (right) in molecular complex **17**, showing the C-I···O interactions in layer B.

The two layers have an AABBAABB stacking arrangement (Figure 5.16 (a)). The molecules of methanol in layer A interact with the amine groups in the layers directly above and below (as shown in Figure 5.13). There are π···π interactions between alternately stacked 4-IA and 3,5-DNBA molecules (Figure 5.16 (b)), with an approximate intermolecular separation of ~3.3 Å in the stacking direction. There are also π···π interactions between staggered molecules of 3,5-DNBA in adjacent layers. It is possible that the red colour in the solid-state can be attributed to charge-transfer between alternately stacked 4-IA and 3,5-DNBA molecules, which may occur when the molecules are neutral and consequently closer to coplanar. It is also possible that the presence of disorder may play a role. However, the system is very complicated and significant further work would be necessary in order to understand the nature of the disorder and the electronic transitions in relation to the optical properties.

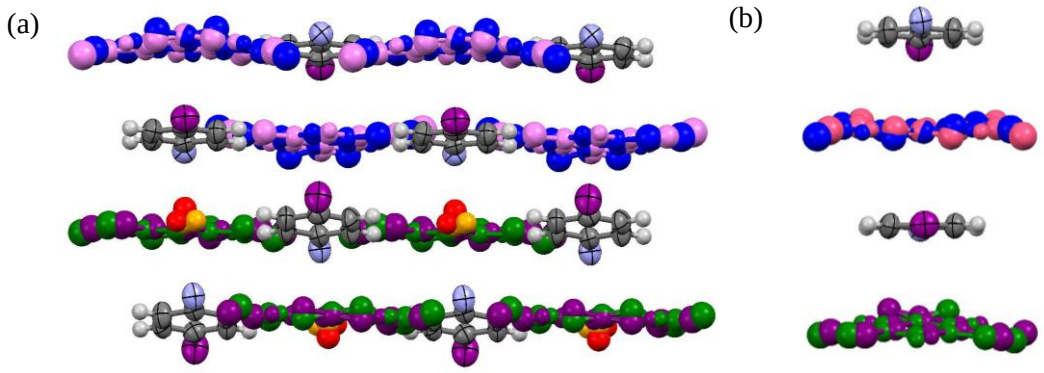

Figure 5.16 (a) Crystal packing in molecular complex **17**, with an AABBAABB stacking arrangement of the layers; (b) A single stack of alternating 4-IA and 3,5-DNBA molecules.

Diffuse scattering measurements

To investigate the significant molecular disorder in molecular complex **17**, diffuse scattering measurements were carried out at Diamond Light Source[197] using single crystal X-ray diffraction on Beamline I19. Single crystal X-ray diffraction data were collected at 100 K using a DECTRIS PILATUS 300K hybrid pixel detector; a full description of the experimental set-up is given in §3.2.2.2. The diffraction data show significant diffuse scattering, indicating that the molecular disorder is characteristic of the molecular complex, and therefore not due to twinning or poor crystal quality.

In the diffraction patterns, there are a number of different diffuse scattering features, of varying type and intensity. The diffuse scattering is very clear in the individual frames of data. The strongest diffuse scattering features are located between Bragg reflections of changing *l*; the diffuse scattering is sharp and connects diffraction spots (labelled A, Figure 5.17). There are

also broader, fuzzier diffuse features observable, perpendicular to the strong lines (A), which results in crossing streaks of diffuse scattering (labelled B, Figure 5.17); this weaker diffuse scattering extends out from Bragg peaks in the direction corresponding to either changing *h*, or changing *h* and *k*. There are also diffuse lines midway between rows of Bragg reflections (labelled C, Figure 5.17), and small tails to some Bragg peaks (labelled D, Figure 5.17).

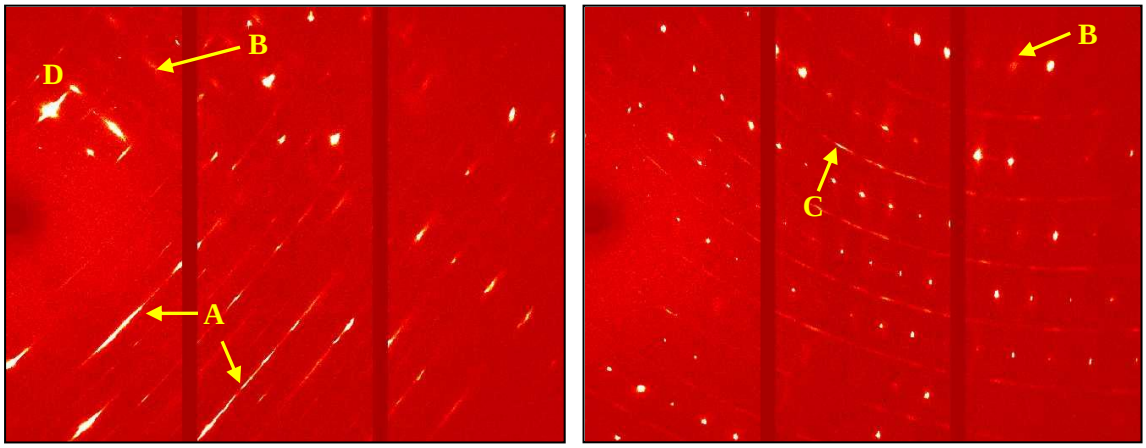

Figure 5.17 Main diffuse scattering features in the diffraction images: A: sharp streaks connecting Bragg peaks of changing *l*; B: fuzzy diffuse features extending from Bragg peaks; C: diffuse lines midway between rows of Bragg peaks; D: Bragg peak tails.

Reciprocal lattice layer reconstructions were generated for the *hk*n, *h*n*l* and n*kl* (n = 0 - 5) layers of reciprocal space using the Unwarp feature in the *CrysAlisPro* software package[204] (shown in Figure 5.18 for n = 0 and n = 3). The *hk*n, *h*n*l* and n*kl* layer-types are equivalent to projections down the *c**-, *b**- and *a**-axes, respectively. The most significant features of the reciprocal space slices are vertical streaks of diffuse scattering that run in a single direction parallel to the *l*-direction, linking lattice points, observed in the n*kl* and *h*n*l* layers. This is particularly clear in the *h*3*l* and 3*kl* layers and corresponds to the sharp diffuse scattering connecting Bragg peaks of changing *l* in the diffraction images. Although much weaker, in some regions of the slices there are diffuse scattering streaks parallel to the *h* and *k* directions, observable in the *h*3*l* and 3*kl* layers, respectively. In the *hk*n layers, faint lines of diffuse scattering are present parallel to the *h*-direction, midway between rows of reciprocal lattice points.

The diffuse scattering measurements clearly indicate that there is short-range order in the structure; the disorder is therefore not entirely random, and the diffuse scattering is probably due to a combination of disorder effects. The sharper diffuse scattering indicates ordering over larger length scales, whereas broad, fuzzy diffuse scattering indicates that there are correlations extending possibly over only a few unit cells.

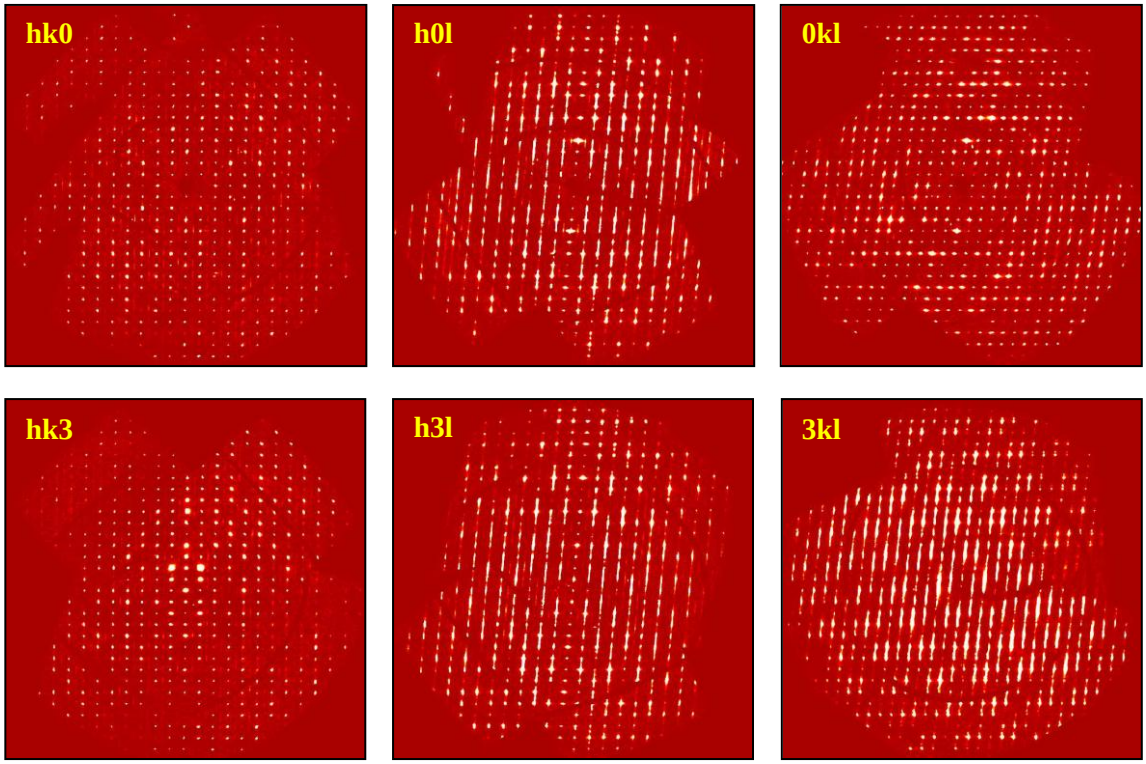

Figure 5.18 Reciprocal space slices of the layers *hk*n, *h*n*l* and n*kl* where n = 0 (top) and n = 3 (bottom), reconstructed from the diffraction data collected on molecular complex **17** at 100 K.

Using crystal engineering principles, it is possible to achieve a basic understanding of the diffuse scattering by relating it to the average crystal structure of the material. In molecular complex **17**, looking at the average structure, it may seem likely that the orientational disorder of the 3,5-DNBA molecules along the chains parallel to the crystallographic *a*-axis would be the most significant type of disorder in the structure. However, the strongest vertical streaks of diffuse scattering run parallel to the *c**-axis and are indicative of stacking faults along the direction of the crystallographic *c*-axis, which corresponds to the stacking direction in the crystal structure of molecular complex **17** (top, Figure 5.19). Therefore, it is possible that this strong diffuse scattering is due to the shifting of the 4-IA and methanol molecules in and out of the plane of the layers, depending on the protonation state. There may also be short-range order corresponding to the molecular shifts of 4-IA/methanol across the layers, as well as in the stacking direction. Furthermore, the protonation state of the 4-IA molecules would also affect the protonation state and orientation of the 3,5-DNBA molecules, which may result in short-range order of the molecules along individual 3,5-DNBA chains. The weaker diffuse features that are parallel to the *a**- and *b**-axes in the reciprocal space slices would correspond to local order in the directions of the crystallographic *a* and *b* axes, which relates to the direction of the chains and the direction across the layers, respectively (bottom, Figure 5.19). Considering the directions and types of diffuse scattering, the measurements provide further evidence for tilting

of the methanol molecules and the 4-IA molecules in the layers due to the probable mixed protonation states of the 4-IA/3,5-DNBA molecules.

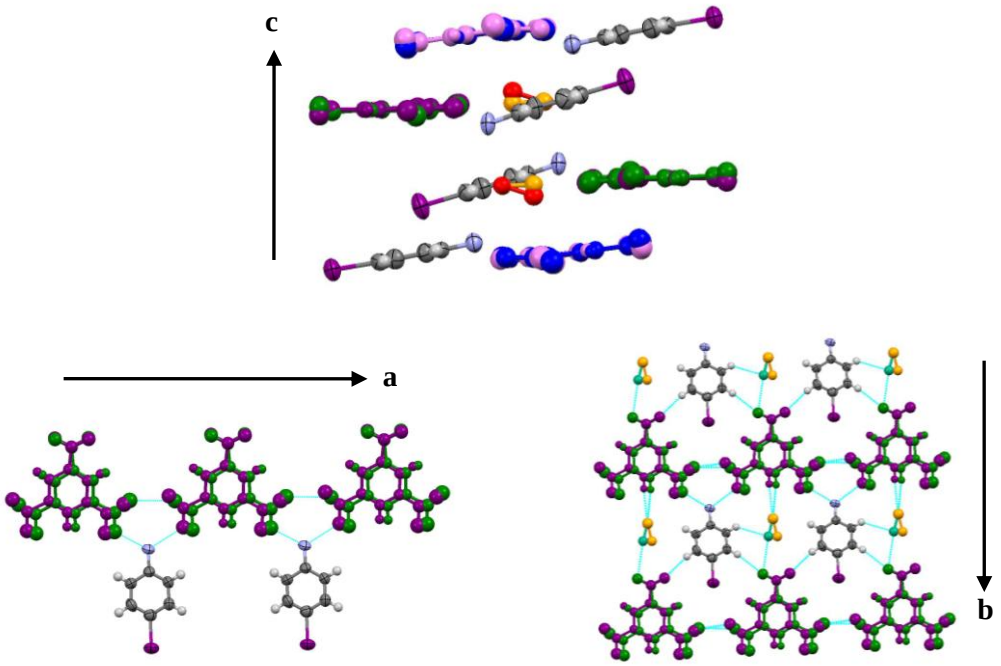

Figure 5.19 Possible short-range order based on the average structure and diffuse scattering features. Top: Stacking faults in the direction of the crystallographic c-axis. Bottom: Orientational disorder of the 3,5-DNBA molecules along the direction of and perpendicular to the crystallographic a-axis.

5.2.6 Sample analysis and phase transformations

As discussed in §5.2.2, the coloured, neutral forms of the 4-IA 3,5-DNBA and 4-BrA 3,5-DNBA molecular complexes, **16** and **19**, are both metastable, with the crystals undergoing spontaneous transformation to a polycrystalline colourless phase. In some cases, either part of or the entire sample appeared to have transformed prior to sample inspection. While some crystals of **16** remained stable for a significant period of time, the crystals of **19** were less stable; furthermore, it was not possible to obtain any more crystals of **19** in repeat crystallisation trials. Given the loss of colour, it was possible that the solid-state transformation corresponded to a conversion to an ionic form of the molecular complex. Hot-stage microscopy, differential scanning calorimetry and powder X-ray diffraction were carried out on samples of the molecular complexes, as well as on the transformed, or partially transformed, samples. Hot-stage microscopy experiments were conducted using a Mettler Toledo FP82 hot stage equipped with a Leica DM1000 microscope, as outlined in §3.3.1. Differential scanning calorimetry experiments were conducted using a TA Instruments Q20 differential scanning calorimeter, as outlined in §3.3.2. Powder X-ray diffraction experiments were conducted at room temperature

using a Bruker AXS D8 Advance powder diffractometer in flat-plate mode, as outlined in §3.2.3.1.

5.2.6.1 4-iodoaniline 3,5-dinitrobenzoic acid (14 - 17)

Thermal analysis

Hot-stage microscopy was carried out on a stable single crystal of molecular complex **16** (Figure 5.20 (a)), with heating conducted between 30 °C and 210 °C at a rate of 5 °C/minute. At approximately 98 °C, a colour change from red to colourless was observed, occurring as a wave across the crystal (Figure 5.20 (b)). This shows that the phase transition is cooperative over relatively long time-frames. The solid-to-solid transformation was complete by ~108 °C, and resulted in a colourless polycrystalline phase, with the shape of the original crystal retained (Figure 5.20(c)). At 118 °C, the crystal appeared to begin melting, forming an orange liquid which matched the colour of the sample solutions prior to crystallisation, and probably corresponds to the melt of the new phase of the molecular complex. At 140 °C, colourless needle crystals recrystallise from the melt, and this phase melts at ~200 °C. It is probable that the recrystallised phase is 3,5-DNBA, which has a melting point of 204 °C.

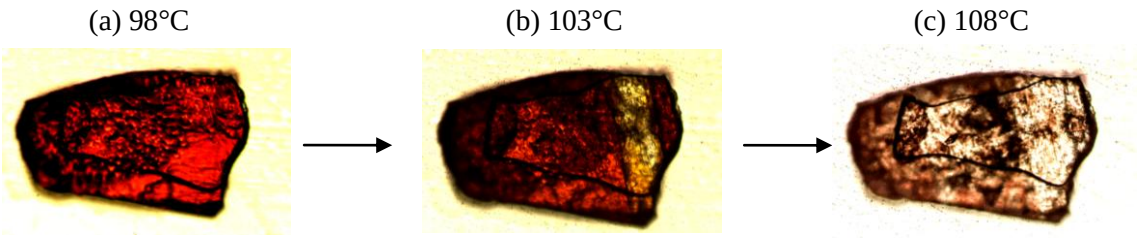

Figure 5.20 HSM analysis on a single crystal of molecular complex **16** obtained from ethanol, showing (a) the crystal immediately prior to the phase transformation at 98 °C; (b) the crystal during the phase transformation at 103 °C; (c) the crystal immediately after the phase transformation at 108 °C.

The same hot-stage microscopy experiment was also conducted on single crystals of **14**, **15** and **17**. Above 100 °C, the thermal behaviour matches that of molecular complex **16** in each case. In molecular complex **14**, no changes were observed to occur in the sample below 118 °C. In molecular complex **15**, there was a slight darkening and small jump of the single crystal at ~97 °C. In the methanol solvate form, **17** (Figure 5.21 (a)), a darkening of the crystal was observed at 70 °C, and this was accompanied by small bubbles in the oil surrounding the crystal, likely to be due to release of methanol (Figure 5.21 (b)). At ~90 °C, the number and size of the bubbles increases (Figure 5.21 (c)), and there is a gradual change in colour from red to colourless, which moves across the crystal, with the sample becoming polycrystalline. In the HSM experiments

for each of the samples (**14 - 17**), the melt forms an orange liquid at 118 °C, which may suggest that they have all transformed to the same phase prior to melting.

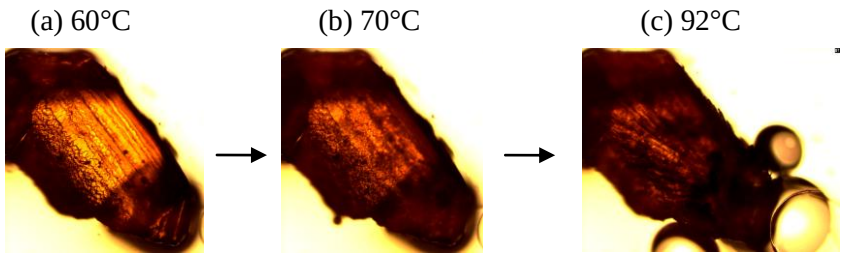

Figure 5.21 HSM analysis on a single crystal of molecular complex **17**, showing: (a) the crystal prior to any changes occurring; (b) darkening of the crystal and formation of small bubbles at 70 °C; (c) larger bubbles and phase transformation at 92 °C.

Differential scanning calorimetry experiments were conducted on samples of molecular complexes **14** - **17**. For the experiment on **16**, red crystals were selected from the partially-transformed samples to ensure a pure sample. For each experiment, samples were heated between 30 °C and 210 °C at a rate of 5 °C/minute. The DSC thermograms of molecular complexes **15**, **16** and **17** all show small endothermic peaks prior to 120 °C (circled in red, Figure 5.22 (b) - (d)); there are no thermal events observed for **14** prior to this temperature (Figure 5.22(a)). In molecular complexes **15** and **16**, the small peaks have onset temperatures of 98.4 °C and 93.7 °C, respectively. The nature of these peaks suggest a phase transformation, and the temperatures correlate reasonably well with those observed in the HSM experiments. In molecular complex **17**, the methanol solvate, the thermogram slopes downwards from ~65 °C, which probably corresponds to loss of methanol from the structure, and there is an additional small endothermic peak following this, with an onset temperature of 85.24 °C. This peak corresponds to the phase transformation observed by hot-stage microscopy, following the solvent loss.

Above 100 °C the thermograms of all four molecular complexes are very similar. In each case, there is a large, sharp endothermic peak, with very similar onset temperatures of 116.49 °C, 114.8 °C, 116.7 °C and 114.2 °C for the samples of molecular complexes **14**, **15**, **16** and **17**, respectively (Figure 5.22 (a)-(d)). This temperature corresponds to the first melt observed in hot-stage microscopy experiments, and is likely to be due to the melt of the molecular complex. Between 130 °C and 190 °C, there are a number of events which may be due to decomposition of the component molecules and/or recrystallisation of single phases; there is a final endothermic peak with an onset temperature of ~200 °C in each case, corresponding to the melt of the recrystallised phase (possibly 3,5-DNBA), as observed in the HSM experiments.

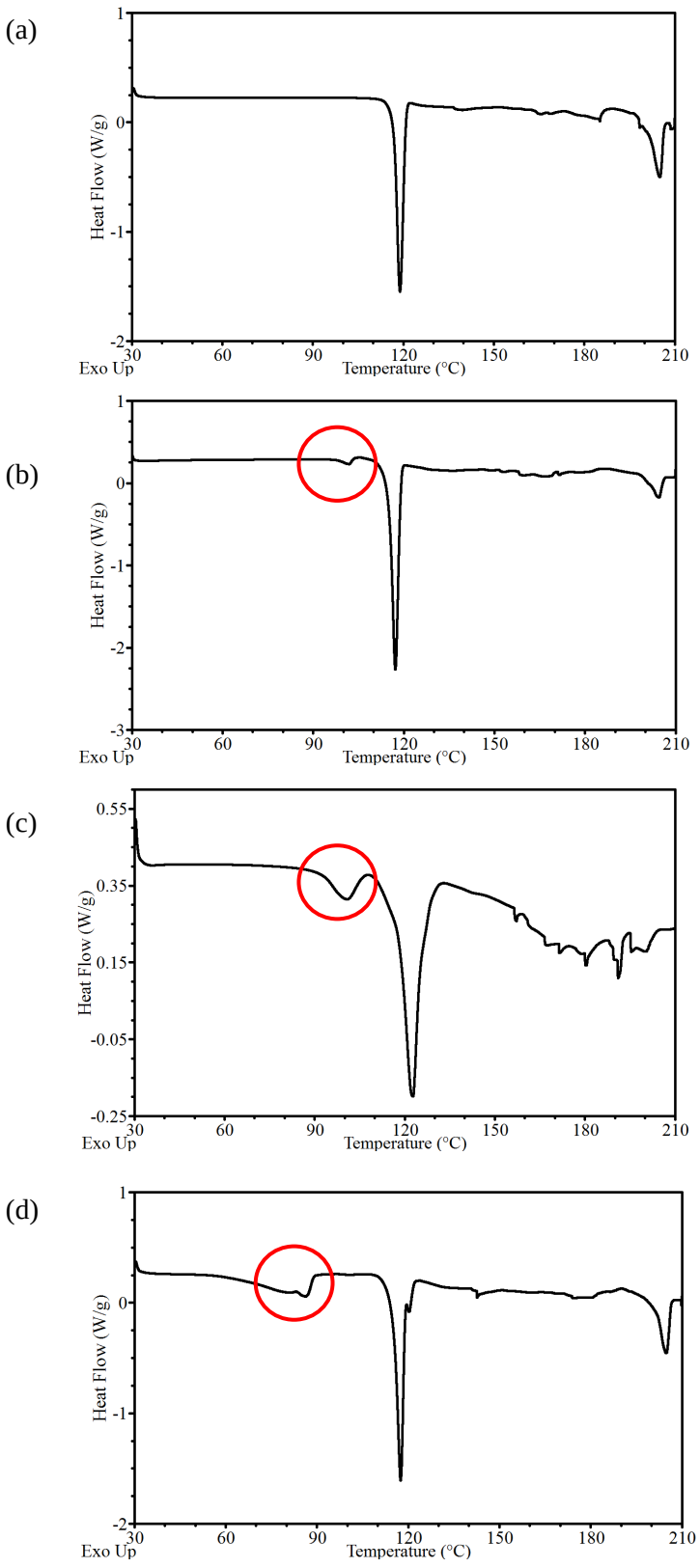

Figure 5.22 DSC thermograms of samples of (a) molecular complex **14**, (b) molecular complex **15**, (c) molecular complex **16** and (d) molecular complex **17**. The possible phase transformations are circled in red.

Powder X-ray diffraction

A selection of the samples of each molecular complex, formed under various crystallisation conditions, were analysed by powder X-ray diffraction. The powder diffraction patterns were compared against each other, against the simulated powder diffraction patterns for molecular complexes **14** - **17**, and against the simulated powder diffraction patterns for the two starting materials, 4-IA and 3,5-DNBA. The program PolySNAP[212] was used to determine the similarity of powder patterns and aid interpretation of the results.

The powder diffraction patterns of pure samples of **14**, **15** and **17** (shown in green, Table 5.5) matched the simulated powder patterns of the molecular complexes very well, with just a small peak shift due to the difference in data collection temperature for PXRD (ambient) and SCXRD (100 K). However, the analysis of **16** was more complicated. It was not possible to analyse a pure sample of molecular complex **16** by PXRD due to the mixtures of phases present, and in each case, prior to grinding, the bulk sample consisted partially of red crystals of **16** and partially of a colourless phase. The powder diffraction patterns of the some of the red/colourless mixtures (blue, Table 5.5) matched the diffraction patterns of one of the known colourless, ionic forms of the molecular complex, **14** or **15** (Figure 5.23 (a) and (b)), although there were a few peaks that did not match, as well as some preferred orientation effects. It appears, therefore, that the crystals of **16** in the sample transformed to one of the ionic forms (**14** or **15**), in the time between removing the sample from the crystallisation vessel and starting the PXRD experiment. However, the diffraction patterns of the majority of the red/colourless mixtures (shown in red, Table 5.5), are much more complicated, and do not match either **14** or **15**. In addition, the diffraction patterns of these samples are poorer quality, in terms of sample crystallinity, which is possibly due to going through a phase transition (Figure 5.23 (c)). There are also preferred orientation effects, which makes the analysis of the patterns very difficult. It is probable that the peaks correspond to a mixture of **16** and a colourless phase (either **14** or **15**, or an unknown form), but higher quality diffraction patterns would need to be obtained to confirm this.

Table 5.5 Summary of the characterisation of transformed samples by PXRD, detailing the crystallisation conditions. Pure samples grown evaporatively are shown in green, fully transformed samples of **16** are shown in blue, and mixtures are shown in red.

	Crystallisation conditions		
Sample	**Solvent**	**Temperature (°C)**	**PXRD pattern match**
1	Acetonitrile	4	Molecular complex **14**
2	Acetonitrile	RT	Molecular complex **14**
3	Ethanol	RT	Molecular complex **14**
4	Ethyl acetate	4	Molecular complex **14**
5	2-propanol	RT	Molecular complex **14**
6	Ethanol	40	Molecular complex **14**
7	Ethanol	4	Molecular complex **15**
8	Ethanol	30	Molecular complex **15**
9	Ethanol	30	Molecular complex **15**
10	Methanol	4	Molecular complex **17**
11	Methanol	RT	Molecular complex **17**
12	Acetonitrile	40	Mixture
13	Ethanol	40	Mixture
14	Ethanol	50	Mixture
15	Ethyl acetate	40	Mixture
16	Ethyl acetate	60	Mixture

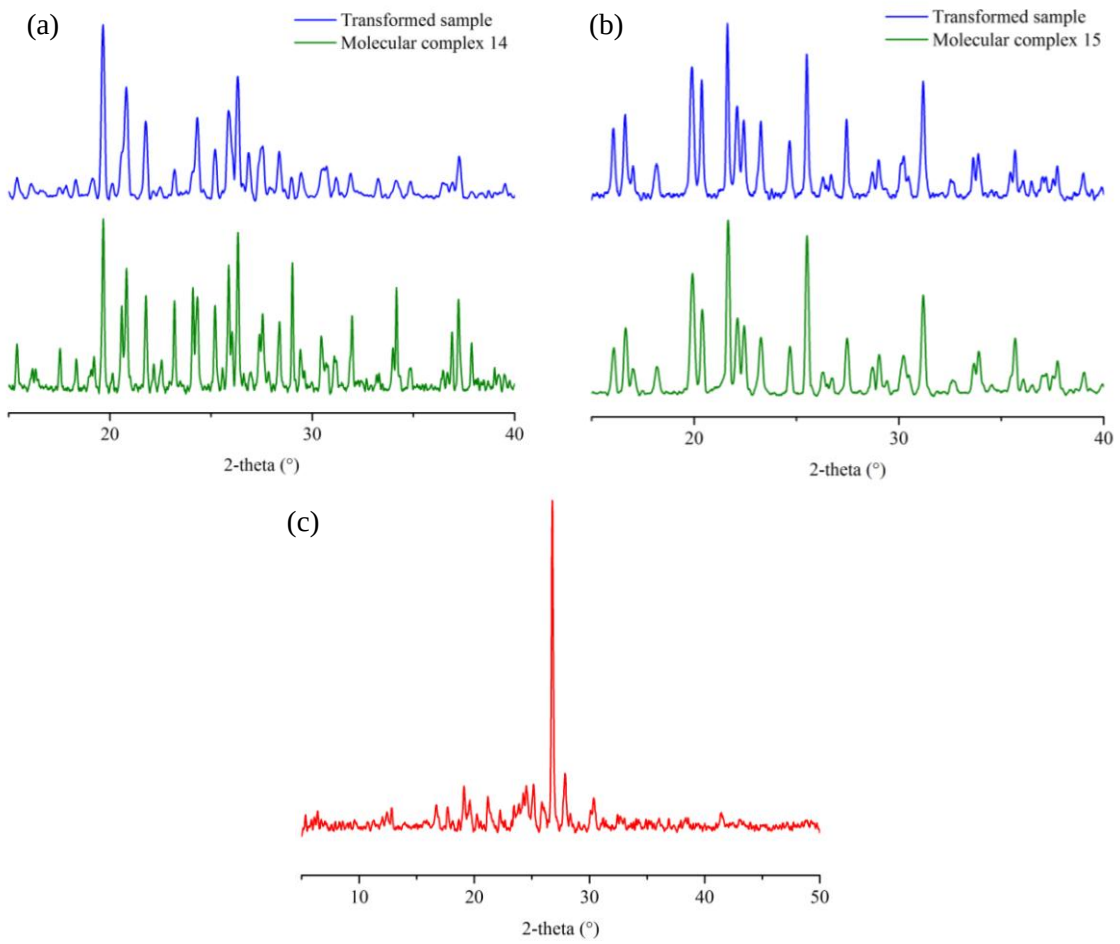

Figure 5.23 Powder diffraction patterns collected on some of the samples containing mixtures of red and colourless phases; the sample number refers to Table 5.5. (a) Pure molecular complex **14** (Sample 1) shown in green, transformed sample (Sample 6) shown in blue; (b) pure molecular complex **15** (Sample 7) shown in green, transformed sample (Sample 8) shown in blue; (c) an example of a diffraction pattern obtained for mixed phases, shown for Sample 13.

Summary of thermal and PXRD analyses

The thermal behaviour of the molecular complexes is quite complicated; however, the results of hot-stage microscopy and differential scanning calorimetry experiments match well. No thermal events were observed in molecular complex **14** prior to 100 °C, whereas the other complexes all appear to undergo solid-to-solid transformations. In the case of **16**, the loss of colour on undergoing the phase transformation may suggest conversion to an ionic form of the molecular complex, either known (**14** and **15**) or unknown. In each sample, there is a melt at ~120 °C which suggests that each of the complexes has transformed to the same phase prior to this temperature. PXRD experiments suggest that, at least in some cases, molecular complex **16** transforms to one of the known colourless molecular complexes, **14** and **15**. However, this is only observed over a very limited number of samples, with many of the diffraction patterns showing mixtures of phases which cannot be identified. In order to fully understand the thermal

behaviour of the complexes, it would be necessary to collect high resolution powder data for each of the pure molecular complexes in combination with *in situ* variable temperature measurements, on a larger range of samples. For this, pure samples of the metastable molecular complex, **16**, would need to be grown in sufficient quantities and preserved.

5.2.6.2 4-bromoaniline 3,5-dinitrobenzoic acid (18 and 19)

Thermal analysis

Hot-stage microscopy was conducted on samples of the ionic molecular complex, **18**, and a sample of the transformed phase; all crystals of **19** had transformed and HSM could therefore not be conducted on this phase. Heating was carried out between 30 °C and 210 °C at a rate of 5 °C/minute. In the single crystal of **18**, there is a very small shift in position at 105 °C, followed by a small jump at 115 °C. At 127 °C, there is a significant jump of the crystal, and simultaneous change in colour from colourless to orange, as the sample begins to melt. Between 132-135 °C, there is a loss of colour across the sample and recrystallisation of a colourless polycrystalline phase; this phase melts at ~200 °C. The sample of the polycrystalline colourless phase showed similar thermal behaviour. The sample appears to undergo a phase transition, with darkening and large cracks appearing across the sample between 100-112 °C. At 126 °C, the sample begins to melt, forming a pale orange liquid, followed by recrystallisation of a polycrystalline colourless phase between 132-140 °C. This phase melts at ~203 °C. It is possible that the final melt in each experiment corresponds to the melt of recrystallised starting material, 3,5-DNBA.

A sample of pure molecular complex **18** and a sample of the polycrystalline transformed phase were also analysed by DSC, with heating carried out between 30 °C and 210 °C at a rate of 5 °C/minute. There are a number of endothermic peaks observed in each of the samples. In the DSC thermogram of **18** (Figure 5.24 (a)), the first two endothermic peaks observed have onset temperatures of 102.1 °C (**i**, Figure 5.24) and 116.6 °C (**ii**, Figure 5.24 (a)), which match the temperatures of the jumps in crystal position in HSM analysis, and possibly correspond to phase transitions. There is a third significant peak with an onset temperature of 127.1 °C (**iii**, Figure 5.24 (a)), which is likely to be due to the melt of the complex. There are two further endothermic events, with onset temperatures of 135.6 °C and 141.4 °C (**iv** and **v**, Figure 5.24 (a)), followed by decomposition of the sample up to 200 °C. In the DSC thermogram of the transformed sample (Figure 5.24 (b)), there is a small endothermic peak over the approximate range 102-113 °C (**i**, Figure 5.24 (b)). This is followed by a sharp peak with an onset temperatures of 123.2 °C (**ii**, Figure 5.24 (b)) which is likely to correspond to the melt of the complex. There is a further endothermic peak with an onset temperature of 134.9 °C (**iii**, Figure

5.24 (b)), and an additional event with an onset temperature of 146.83 °C (**iv**, Figure 5.24). The DSC thermograms suggest that both samples are in the same phase upon melting.

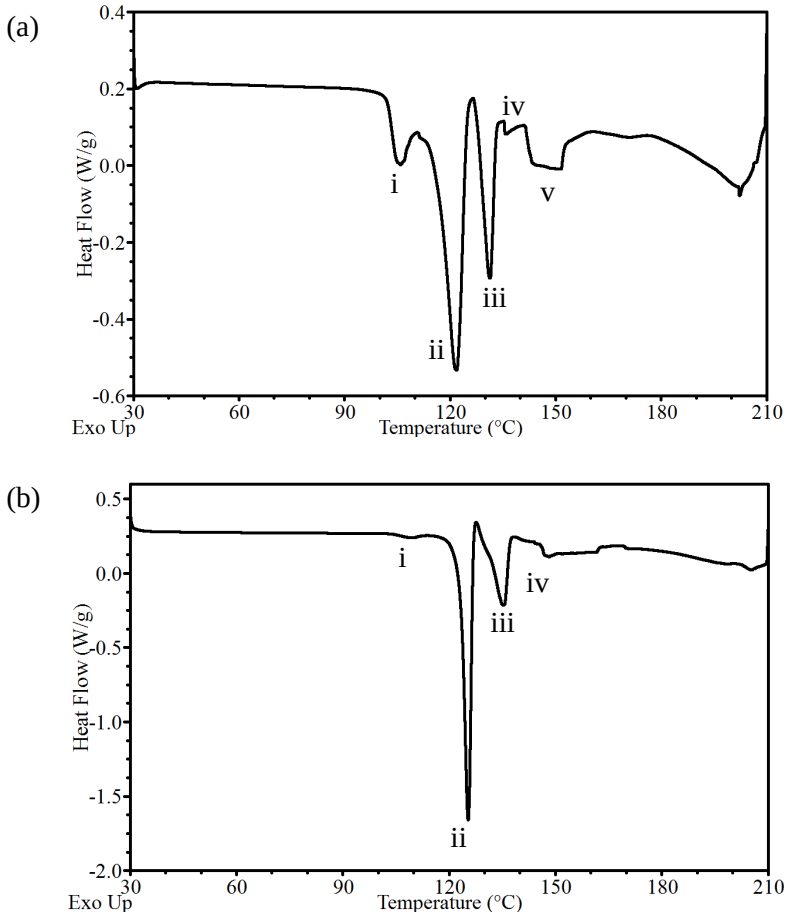

Figure 5.24 DSC thermograms of samples of (a) molecular complex **18** (b) the colourless polycrystalline phase obtained following transformation of molecular complex **19**. Labels **i-v** correspond to thermal events.

Powder X-ray diffraction

PXRD analysis was conducted on pure samples of molecular complex **18** and the transformed samples. The powder diffraction patterns were compared against each other, against the simulated powder diffraction patterns for molecular complexes **18** and **19**, and against the simulated powder diffraction patterns for the two starting materials, 4-BrA and 3,5-DNBA. The program PolySNAP[212] was used to determine the similarity of powder patterns and aid interpretation of the results.

In the 4-IA 3,5-DNBA series of molecular complexes, some of the samples of the neutral molecular complex were observed to transform to one of the known ionic forms. It was possible, therefore, that a similar transformation was occurring in the 4-BrA 3,5-DNBA

molecular complexes. However, the powder diffraction patterns of the transformed samples did not match the powder diffraction patterns of the ionic molecular complex **18** (Figure 5.25), or the simulated powder diffraction patterns for either of the structurally characterised complexes, or the powder diffraction patterns of either of the starting materials. Due to the colour change, it was possible that the transformation in 4-BrA 3,5-DNBA was to an unknown ionic form of the molecular complex.

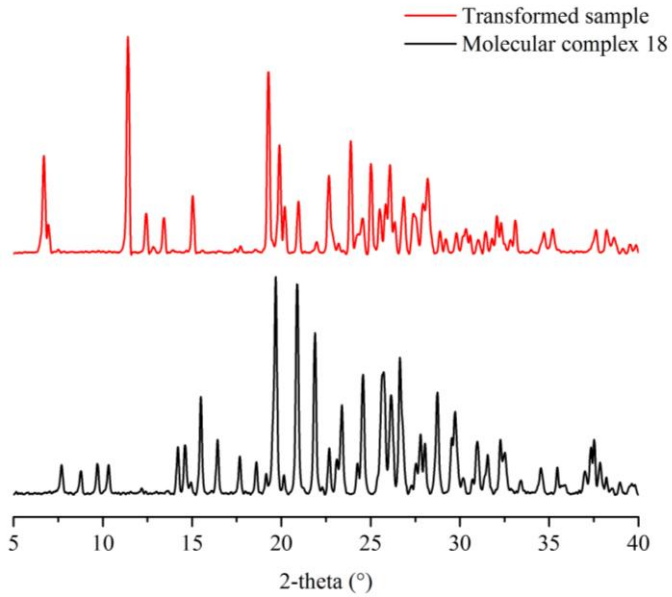

Figure 5.25 Powder diffraction patterns collected on a sample of molecular complex **18** (shown in black) and the polycrystalline colourless phase obtained following transformation of **19** (shown in red).

Summary of thermal and PXRD analyses

The hot-stage microscopy and differential scanning calorimetry experiments revealed complicated thermal behaviour. Prior to the melt at ~126 °C in HSM, molecular complex **18** appears to undergo two phase transitions (at 105 °C and 115 °C), while the transformed sample appears to undergo only a single transition (112 °C). This difference in thermal behaviour suggests that the spontaneous transformation of molecular complex **19** does not result in the known ionic complex **18**. However, the melt occurs at approximately 126 °C in both samples, which suggests that, upon heating, both convert to the same phase prior to melting.

The results of the PXRD experiments agree with the thermal analysis, showing that the transformed sample does not match that of the ionic molecular complex, **18**. However, given the colourless nature of the sample, it is probable that the transformation is to an unknown ionic form of the molecular complex. In order to fully understand the thermal behaviour of the complexes, it would be necessary to collect high resolution powder data for each of the pure

molecular complexes in combination with *in situ* variable temperature measurements. For this, pure samples of molecular complex **19** would need to be grown in sufficient quantities and preserved. Furthermore, a broader range of crystallisation trials should be conducted to investigate crystallisation of possible additional ionic forms of the molecular complex.

5.2.7 Summary and discussion

A total of six molecular complexes combining 4-iodoaniline and 4-bromoaniline with 3,5-dinitrobenzoic acid were obtained *via* slow evaporation, and structurally characterised by single crystal X-ray diffraction. All of the molecular complexes have a 1:1 stoichiometry of the 4-XA and 3,5-DNBA. Unexpectedly, it was possible to obtain both neutral and ionic molecular complexes; in the case of 4-IA, a methanol solvate with mixed protonation states was also formed. The ΔpKa values for 4-IA and 4-BrA with 3,5-DNBA are 0.99 and 1.07, respectively, which are in the salt-cocrystal continuum; this means that proton transfer may or may not occur. Typically, under the same crystallisation conditions either a neutral or an ionic molecular complex would be obtained for a particular system, making these 4-IA 3,5-DNBA and 4-BrA 3,5-DNBA systems unusual.

The neutral and ionic molecular forms of the two multi-component systems were easily distinguishable visually, as the solid-state colour is dependent on the crystal packing which is in turn dependent on the protonation states of the molecules. Where the components were fully ionic (**14**, **15** and **18**), the crystals were always colourless, and in each case the crystal structures were non-layered. Where the components were neutral (**16** and **19**), or there was mixed protonation (**17**), the crystals were always strongly coloured and the structures were layered. In the neutral molecular complexes, mixed stacks of alternating electron-donors (4-XA) and electron-acceptors (3,5-DNBA) were formed, with the aromatic donor···acceptor interactions dominating the packing arrangements; the interactions between the 4-XA and 3,5-DNBA molecules within the layers were only moderate to weak in strength.

The nature of the halogen had limited effect in the ionic forms, with molecular complexes **14** and **18** isostructural; in the three ionic molecular complexes, the charge-assisted hydrogen bonds involving the NH_3^+ group were most influential in terms of the packing arrangement. In the neutral forms of the molecular complexes, **16** and **19**, the crystal packing was similar but the two complexes were not isostructural. The relative molecular orientations and intermolecular interactions within the planar sheets and within the mixed stacks differed. In addition, the N-H···O hydrogen bonds involving the amine group are stronger in the 4-IA complex than in the 4-BrA complex; furthermore, there are hydrogen bonds between dimers in the 4-IA

complex, but not in the 4-BrA complex. In terms of solid-state colour, 4-IA 3,5-DNBA and 4-BrA 3,5-DNBA were red and orange respectively; the colour may be attributed to $\pi\cdots\pi^*$ charge-transfer between the aromatic donor and acceptor. The intermolecular separation of the donor and acceptor in the stacking direction is approximately the same in the two complexes, thus, the difference in colour must be due to the nature of the halogen and the relative orientations of the 4-XA and 3,5-DNBA molecules in the stacks. The difference in hydrogen bond strength may also play a role, with particular reference to those involving the amine group, and those that occur between 3,5-DNBA dimers. The pair of complexes demonstrates how the simple exchange of the halogen substituent allows the solid-state colour to be tuned.

In the case of **17**, the intermolecular interactions and overall crystal packing are very different to any of the unsolvated forms, with the introduction of methanol resulting in a disordered complex with mixed ionisation states of the molecular components. The layered structure results in red crystals, of similar colour to the layered structure of the neutral 4-IA 3,5-DNBA complex, and can be attributed to charge-transfer; the absorbance is shifted to shorter wavelength by ~60 nm compared to **16**. The nature of the charge-transfer interaction is not fully understood due to the complex nature of the system. It is possible that the presence of molecular disorder is a favourable attribute in terms of colour in the solid-state.

The crystallisation of the molecular complexes is complicated due to the number of obtainable possible forms, and it was not always possible to predict which product would result based on the crystallisation conditions. Both of the neutral molecular complexes are metastable, and transform to a colourless phase; typically, this occurred spontaneously under ambient conditions, but the same colour change was also observed upon heating crystals of molecular complex **16** that remained sufficiently stable. Molecular complex **19** was much less stable than **16**, with all of the crystals transforming spontaneously over a significantly shorter period of time. The stability of the neutral forms appears to decrease with decreasing molecular weight i.e. I to Br, with the concomitant increase in the stability of the ionic form. This is reflected in the higher melting point of the ionic form of the Br complex over that of the I complex, and thus reflects the strength of the halogen bonds formed.

For the 4-IA 3,5-DNBA system, the combination of thermal analysis and powder X-ray diffraction experiments all provide evidence that suggest that the neutral form of the complex, **16**, is transforming to a salt form; in some cases, PXRD has shown that this is to one of the structurally characterised forms, **14** and **15**. For 4-BrA 3,5-DNBA, the transformation of the neutral complex, **19**, does not appear to be to the known ionic form, **18**; however, given the similarity of the behaviour to 4-IA 3,5-DNBA, it is expected that the transformation is to an

ionic form. The phase transformation would therefore be propagated by a proton transfer from the carboxylic acid group of 3,5-DNBA to the amine group of 4-IA, corresponding to a significant structural arrangement. The difference between the neutral and ionic forms is not simply in the location of the acidic proton in a hydrogen bond, and the transformation does not occur in a single crystal to single crystal manner.

5.3 Molecular complexes of 4-halo-2-methylaniline and 3,5-dinitrobenzoic acid

5.3.1 Experimental details

Molecular complexes **20** - **24** were synthesised *via* the method of slow evaporation (§3.1), using a 1:1 stoichiometric molar ratio of the 4-halo-2-methylaniline and 3,5-dinitrobenzoic acid. Crystallisation trials employed a range of solvents and temperatures. The crystallisation conditions which resulted in growth of the crystals used for collection of SCXRD data are reported here; more details on the crystallisation conditions are provided in §5.3.2. Single crystal X-ray diffraction experiments were carried out according to the procedures outlined in §3.2. Crystallographic data are given in Table 5.6 and refinement details are reported in Appendix A5.

4-iodo-2-methylanilinium 3,5-dinitrobenzoate (20)

Molecular complex **20** was synthesised from ethanol at 4 °C; colourless block crystals were obtained. Single crystal X-ray diffraction data were collected at 100 K using a Rigaku R-AXIS/RAPID image plate diffractometer. The structure was solved by direct methods using SHELXS-97[192] and refined using SHELXL-2014,[198] both within the WinGX program suite.[200]

4-iodo-2-methylaniline 3,5-dinitrobenzoic acid (21)

Molecular complex **21** was synthesised from acetonitrile at ambient temperature; red block crystals were obtained. Single crystal X-ray diffraction data were collected at 100 K using a Rigaku R-AXIS/RAPID image plate diffractometer. The structure was solved by direct methods using SHELXS-97[192] and refined using SHELXL-2014,[198] both within the WinGX program suite.[200]

4-bromo-2-methylanilinium 3,5-dinitrobenzoate (22)

Molecular complex **22** was synthesised from methanol at ambient temperature; colourless block crystals were obtained. Single crystal X-ray diffraction data were collected at 150 K using a Rigaku Oxford Diffraction Gemini Ultra diffractometer (Mo Kα radiation). The structure was

solved by direct methods using SHELXS-2013[192] and refined using SHELXL-2014,[198] both within the WinGX program suite.[200]

4-bromo-2-methylaniline 3,5-dinitrobenzoic acid (23)

Molecular complex **23** was synthesised from methanol at 40 °C; orange block crystals were obtained. Single crystal X-ray diffraction data were collected at 150 K using a Rigaku Oxford Diffraction Gemini Ultra diffractometer (Mo Kα radiation). The structure was solved by direct methods using SHELXS-2013[192] and refined using SHELXL-2014,[198] both within the WinGX program suite.[200]

4-chloro-2-methylanilinium 3,5-dinitrobenzoate (24)

Molecular complex **24** was synthesised from acetonitrile at ambient temperature; colourless block crystals were obtained. Single crystal X-ray diffraction data were collected at 150 K using a Rigaku Oxford Diffraction Gemini Ultra diffractometer (Mo Kα radiation). The structure was solved by direct methods using SHELXS-2013[192] and refined using SHELXL-2014,[198] both within the WinGX program suite.[200]

5.3.2 Crystallisation discussion

4-iodo-2-methylaniline (4-I-2-MA), 4-bromo-2-methylaniline (4-Br-2-MA) and 4-chloro-2-methylaniline (4-Cl-2-MA) are light purple, light brown and light purple, respectively, and 3,5-dinitrobenzoic acid (3,5-DNBA) is a light yellow solid. Dissolution of the two components (3,5-DNBA with 4-X-2-MA) resulted in pale pink, yellow and orange solutions for 4-I-2-MA, 4-Br-2-MA and 4-Cl-2-MA, respectively. The ΔpKa values for 3,5-DNBA with 4-I-2-MA, 4-Br-2-MA and 4-Cl-2-MA are 0.84, 0.89 and 1.03, respectively, thus fall in the salt-cocrystal continuum. From the 1:1 co-crystallisation of the aniline with 3,5-DNBA, both neutral and salt forms were obtained for 4-I-2-MA (**20** and **21**) and 4-Br-2-MA (**22** and **23**), similarly to the 4-XA co-crystallisations in §5.2, but only a salt complex of 4-Cl-2-MA (**24**) was formed. In each case the two molecular components are present in the same relative 1:1 stoichiometry. Colourless crystals were yielded in the case of the ionic molecular complexes, whereas the crystals of the neutral molecular complexes were strongly coloured (red or orange). An extensive set of co-crystallisation experiments were carried out for each system, and a combination of optical microscopy, single crystal X-ray diffraction, thermal analysis and powder X-ray diffraction were used to assess the crystallisation products.

Table 5.6 Crystallographic data for molecular complexes **20** - **24**

	20	**21**	**22**	**23**	**24**
Formula	$(C_7H_9NI)^+$ $(C_7H_3N_2O_6)^-$	(C_7H_8NI) $(C_7H_4N_2O_6)$	$(C_7H_9NBr)^+$ $(C_7H_3N_2O_6)^-$	(C_7H_8NBr) $(C_7H_4N_2O_6)$	$(C_7H_9NCl)^+$ $(C_7H_3N_2O_6)^-$
M/g mol^{-1}	445.17	445.17	398.18	398.18	353.72
T/K, radiation	100(2), Mo Kα	100(2), Mo Kα	150(2), Mo Kα	150(2), Mo Kα	150(2), Mo Kα
Space Group	$P2_1$	$P\bar{1}$	$P2_1$	$P\bar{1}$	$P2_1$
a/Å	10.7563(9)	8.534(3)	10.4081(4)	7.1802(4)	10.2583(6)
b/Å	5.7898(4)	8.769(3)	5.8338(2)	7.2420(4)	5.8537(3)
c/Å	13.3632(9)	11.882(8)	13.2672(5)	14.7292(6)	13.2818(9)
α	90	111.035(8)	90	87.048(4)	90
β	107.858(8)	101.327(7)	107.035(4)	88.078(4)	106.933
γ	90	95.273(7)	90	89.926(5)	90
V/Å	792.12(10)	800.9(7)	770.23(5)	764.46(7)	762.98(8)
Z	2	2	2	2	2
ρ_{cal}/ g cm^{-3}	1.866	1.846	1.717	1.730	1.540
μ/mm^{-1}	2.058	2.036	2.706	2.727	0.288
θ Range/°	3.203 - 27.473	3.209 - 27.483	2.949 - 29.514	2.816 - 30.410	2.969 - 27.461
Ref Collected	18081	18691	7649	11434	5839
Independent	3620	3661	3622	4107	3155
Observed>2σ	3583	3500	3192	3061	2630
Rint	0.0206	0.0189	0.0361	0.0452	0.0321
Completeness %	99.7	99.8	99.8	99.9	99.8
Parameters	230	230	230	230	230
Flack parameter	-0.011(4)	-	0.003(7)	-	0.05(6)
GooF	1.095	1.135	1.033	1.068	1.044
R_1 (obs)	0.0131	0.0175	0.0385	0.0490	0.0431
R_1 (all)	0.0133	0.0185	0.0488	0.0766	0.0589
wR2 (all)	0.0332	0.0462	0.0613	0.1058	0.0785
$\rho_{max,min}$/e Å^{-3}	0.412, -0.246	0.515, -0.234	0.515, -0.389	1.339, -0.839	0.193, -0.224

4-iodo-2-methylaniline 3,5-dinitrobenzoic acid

The 4-I-2-MA 3,5-DNBA molecular complexes, **20** and **21**,[239] formed as colourless and red block crystals, respectively, making the two forms easily distinguishable visually. It was not possible to predict which molecular complex would form under a particular set of conditions, with both often forming under the same conditions. Both **20** and **21** were obtained from multiple solvents at each of the evaporation temperatures, and repeat crystallisation trials would often result in the formation of a different molecular complex to the previous trial. Furthermore, molecular complex **21** is metastable and preservation of the form was difficult, similarly to the corresponding 4-IA 3,5-DNBA complex; the stability of the crystals also varied across the samples. Many of the red crystals of **21** were observed to transform spontaneously to a polycrystalline colourless phase upon exposure to the ambient environment. Conversely, some crystals of **21** were stable for significant periods of time (up to one year at time of writing); typically, the most stable crystals were obtained *via* crystallisation above 30 °C. Given the similarity to the 4-IA 3,5-DNBA system, and the loss of colour upon transformation, it was possible that molecular complex **21** was transforming to the known ionic form (**20**).

4-bromo-2-methylaniline 3,5-dinitrobenzoic acid

The molecular complexes of 4-Br-2-MA 3,5-DNBA, **22** and **23**, formed as colourless and orange block crystals, respectively. Similarly to 4-I-2-MA 3,5-DNBA, it was not possible to predict which form would result based on the crystallisation conditions; each molecular complex was obtained from a range of solvent/temperature systems and many repeat crystallisation trials often resulted in a different form to a previous trial. However, single crystals of **23** were only obtained in one crystallisation trial (methanol, 40 °C); in all other cases the form was obtained as a powder only. Furthermore, molecular complex **23** is metastable, thus maintaining the form was difficult; the samples were typically observed to transform spontaneously to a colourless phase upon exposure to the ambient environment. However, it was possible to collect single crystal X-ray diffraction data and carry out HSM analysis on a single crystal of the molecular complex (obtained from methanol at 40 °C) prior to transformation.

4-chloro-2-methylaniline 3,5-dinitrobenzoic acid

In the co-crystallisations experiments of 4-Cl-2-MA 3,5-DNBA, it was only possible to obtain an ionic molecular complex, **24**; the molecular complex formed reproducibly as large single crystals in each of the crystallisation trials. Numerous repeats crystallisations were conducted, but no additional phases were formed.

5.3.3 4-halo-2-methylanilinium 3,5-dinitrobenzoate (20, 22 and 24)

The 4-halo-2-methylanilinium 3,5-dinitrobenzoate molecular complexes, **20**,[239] **22** and **24**, are isomorphous. They form as colourless block crystals (Figure 5.26) and crystallise in the triclinic space group $P\bar{1}$. The components of the molecular complexes are ionic, with full proton transfer from the carboxylic acid group of 3,5-DNBA to the amine group of 4-X-2-MA; the two components crystallise in a 1:1 ratio, with one molecule of each component in the asymmetric unit.

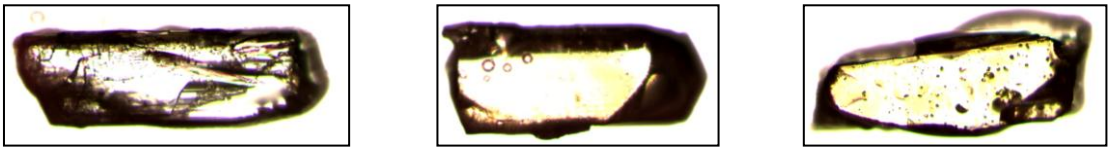

Figure 5.26 Photographs of single crystals of molecular complexes **20** (left), **22** (middle) and **24** (right)

The C-O distances of the carboxylate groups of the 3,5-DNBA molecules are approximately equal, which is consistent with deprotonation and a delocalisation of the charge across the group (1.246(3)/1.272(2) Å, 1.248(5)/1.266(4) Å, and 1.244(4)/1.269(4) Å for **20**, **22** and **24**, respectively). In each molecular complex the carboxylate group is twisted out of the ring plane by ~16°, and each of the nitro groups by less than 13°. Each hydrogen atom of the tetrahedral NH_3^+ group of the 4-halo-2-methylanilinium cation forms a hydrogen bond with a carboxylate group oxygen atom of an adjacent 3,5-dinitrobenzoate anion; hydrogen bonding data for the three molecular complexes are given in Table 5.7.

Similarly to the ionic forms of 4-XA 3,5-DNBA, moderate strength N-H···O hydrogen bonds form between the NH_3^+ group of 4-X-2-MA and the oxygen atoms of the 3,5-DNBA carboxylate groups, resulting in $R_4^3(10)$ hydrogen bonded rings in which both of the carboxylate group oxygen atoms, O1 and O2, act as hydrogen bond acceptors (with O1 accepting two hydrogen bonds) (Figure 5.27). The N1-H1B···O2 hydrogen bond is supported by a weak C-H···O hydrogen bond involving an aromatic C-H group adjacent to the NH_3^+ group (C···O = 3.307(3) Å (molecular complex **20**), 3.334(5) Å (molecular complex **22**), 3.360(4) Å (molecular complex **24**)). In addition, N1-H1A···O1 is supported by a weak C-H···O hydrogen bond from one of methyl C-H groups (C···O = 3.354(3) Å (molecular complex **20**), 3.352(6) Å (molecular complex **22**), 3.364(5) Å (molecular complex **24**); this is the only interaction in which the methyl group substituent is involved.

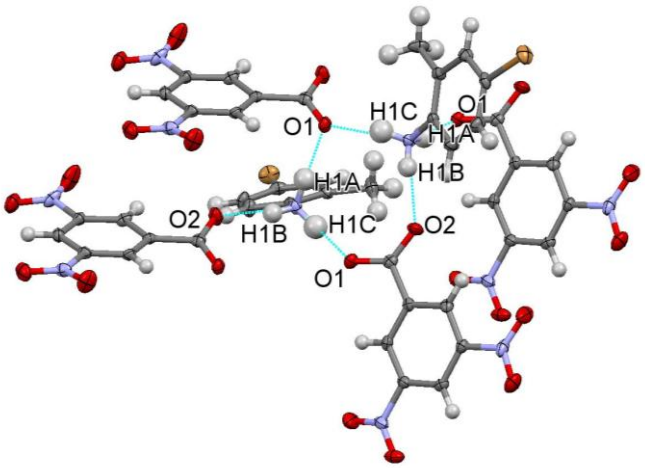

Figure 5.27 The hydrogen bonded ring (shown for molecular complex **22**) formed through moderate strength N-H···O hydrogen bonds between the hydrogen atoms of NH_3^+ and carboxylate group oxygen atoms. The interactions are identical across the three complexes.

Table 5.7 Hydrogen bonding data (Å, °) for molecular complexes **20**, **22** and **24**

D-H···A	**D-H**	**H···A**	**D···A**	**<(DHA)**
Molecular complex **20**				
N1-H1A···O1_#1	0.92(3)	1.86(3)	2.755(3)	164(3)
N1-H1B···O2_#2	0.79(4)	1.94(4)	2.720(3)	165(3)
N1-H1C···O1_#3	0.92(4)	1.87(4)	2.770(3)	168(3)
Molecular complex **22**				
N1-H1A···O1	1.00(7)	1.78(7)	2.764(5)	168(6)
N1-H1B···O2_#1	0.88(7)	1.85(7)	2.726(5)	169(5)
N1-H1C···O1_#2	0.85(6)	1.91(6)	2.747(5)	165(6)
Molecular complex **24**				
N1-H1A···O1_#1	0.97(4)	1.82(4)	2.771(4)	166(3)
N1-H1B···O2_#2	0.91(5)	1.83(5)	2.737(4)	171(4)
N1-H1C···O1_#3	0.96(4)	1.80(4)	2.742(4)	165(3)

Molecular complex **20**: #1 x-1, y, z-1 #2 -x, y-1, -z+1 #3 -x, y+1/2, -z+1

Molecular complex **22**: #1 x, y+1, z #2 -x+1, y+1/2, -z+2

Molecular complex **24**: #1 x+1, y, z #2 x+1, y+1, z #3 -x+1, y+1/2, -z+1

The halogen atom of the 4-X-2-MA cation forms a short X···O contact to the O-atom of one of the nitro groups (I···O = 3.204(2) Å, Br···O = 3.160(3) Å, Cl···O = 3.170(3) Å, compared to the sum of the van der Waals radii of the two atoms of 3.50 Å, 3.37 Å and 3.27 Å, respectively). In addition, there are $O_{nitro}\cdots O_{nitro}$ interactions between adjacent 3,5-DNBA anions and O···π interactions involving nitro and carboxylate group O-atoms. Overall, the hydrogen bonding

interactions of the tetrahedral anilinium group leads to a non-layered structure similar to the ionic 4-IA 3,5-DNBA molecular complex, **15**, with alternating sections of 4-X-2-MA and 3,5-DNBA molecules (Figure 5.28).

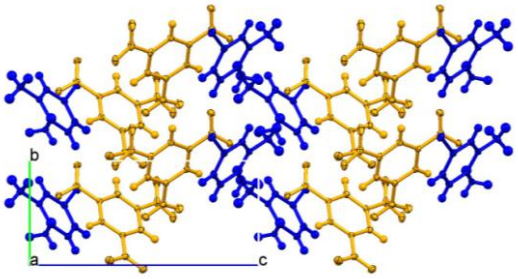

Figure 5.28 The non-layered crystal packing in molecular complexes **20**, **22** and **24**. 4-X-2-MA molecules are shown in blue and 3,5-DNBA molecules are shown in yellow.

5.3.4 4-halo-2-methylaniline 3,5-dinitrobenzoic acid (21 and 23)

The neutral molecular complexes of 4-I-2-MA 3,5-DNBA, **21**,[239] and 4-Br-2-MA 3,5-DNBA, **23**, form as red and orange block crystals, respectively (Figure 5.29 (a)); it was not possible to obtain a corresponding neutral form of 4-Cl-2-MA 3,5-DNBA. The colours of the two forms are very similar to the corresponding neutral 4-XA 3,5-DNBA molecular complexes (**16** and **19**). **21** and **23** are both metastable and the majority of the crystals spontaneously transformed to a polycrystalline colourless phase upon exposure to the ambient environment. However, crystals of **21** were sufficiently stable to allow a single crystal UV-visible absorption spectrum to be recorded, at room temperature (Figure 5.29 (b)), according to the procedure outlined in §3.4.1. The absorbance is characteristic of a $\pi\cdots\pi^*$ charge-transfer between the donor (4-I-2-MA) and acceptor (3,5-DNBA), with absorbance below ~620 nm. This compares to ~600 nm in the neutral 4-IA 3,5-DNBA complex. This difference may be attributed to the additional donating methyl substituent. Due to the rapid transformation of the 4-Br-2-MA complex (**23**), it was not possible to preserve the crystals to conduct UV-visible spectroscopy.

(a)

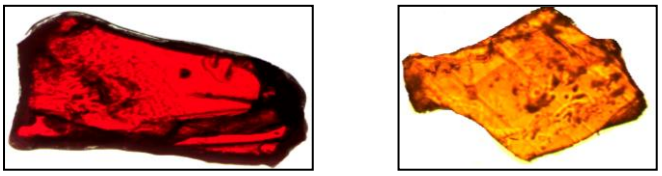

(b)

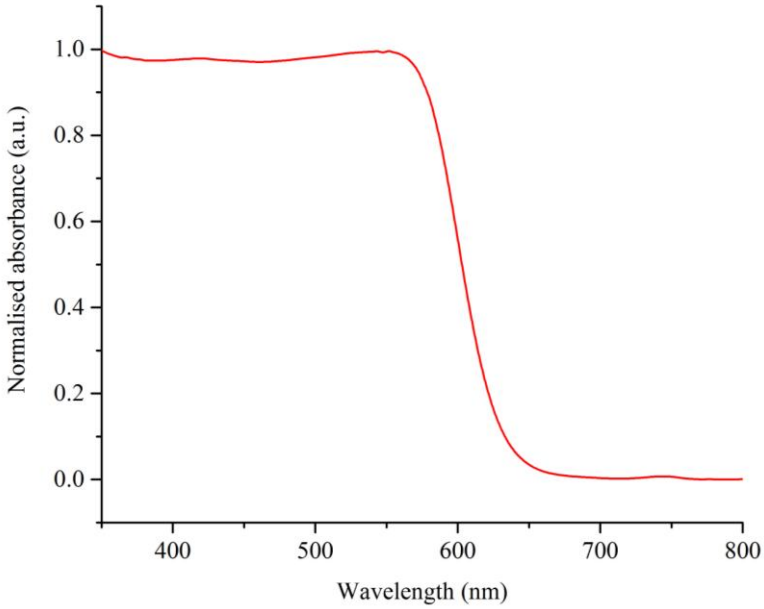

Figure 5.29 (a) Photographs of single crystals of molecular complexes **21** (left) and **23** (right); (b) Single crystal UV-visible absorption spectrum for molecular complex **21** collected at room temperature.

Molecular complexes **21** and **23** both crystallise in the triclinic space group $P\bar{1}$, with the neutral molecular components in a 1:1 ratio; the asymmetric unit contains one molecule of each of the neutral molecules. Similarly to the pair of neutral 4-XA 3,5-DNBA molecular complexes, the overall crystal packing in **21** and **23** is similar, but the complexes are not isostructural.

In both molecular complexes, the two components are close to coplanar, with an angle of only ~4° calculated between the mean ring planes of the two molecules. Furthermore, the carboxylic acid groups are both coplanar with the benzene rings, and the nitro group substituents in both complexes are all rotated out of the plane of the ring by less than 8°. Two molecules of 3,5-DNBA form a hydrogen bonded homodimer through moderate strength O-H···O hydrogen bonds, forming $R_2^2(8)$ rings (Figure 5.30); hydrogen bonding data for **21** and **23** is given in Table 5.8. The C-O bond lengths for the two molecular complexes (1.230(2) Å and 1.305(2) Å (molecular complex **21**), 1.224(4) Å and 1.301(3) Å (molecular complex **23**) are characteristic of single and double bonds, unlike the intermediate C-O bond lengths observed in the other neutral complexes reported in this chapter; this may be explained by the asymmetric environment around the hydrogen bond dimer.[39]

Alternating rows of the haloaniline molecules and 3,5-DNBA dimers interact to form planar two-dimensional sheets, however the intermolecular interactions and molecular orientations within the sheets differ between the two complexes (Figure 5.30). In each case, 4-X-2-MA molecules alternate in orientation along the sheet, but the relative orientations of the molecules with respect to the 3,5-DNBA dimers differs between the two complexes, which must be due to the nature of the halogen. In **23**, the rotation of the aniline has the effect of pushing the 3,5-DNBA dimer units apart.

In 4-I-2-MA 3,5-DNBA, **21** (Figure 5.30 (a)), the 3,5-DNBA dimers interact with one another through weak C-H···O hydrogen bonds (C···O = 3.614(2) Å) between an aromatic hydrogen (H12) and a nitro group oxygen (O5), forming a hydrogen bonded chain; the same chain was observed in the neutral 4-IA 3,5-DNBA complex, **16**. The H-atoms of the amine group, located in the Fourier difference maps, lie slightly out of the 4-I-2-MA ring plane, with approximate torsion angles of ~21° and ~10°, respectively. Weak N-H···O hydrogen bonds form between the amine group H-atoms, H1A and H1B, and nitro group O-atoms (Figure 5.30 (a), Table 5.8); In addition, two weak C-H···O hydrogen bonds are formed; the first is between one of the C-H groups of the methyl substituents (H7A) and a nitro group oxygen atom, O3 (C···O = 3.353(3) Å), and the second is between an aromatic C-H group of 4-I-2-MA (H6) and a nitro group oxygen atom, O6 (C···O = 3.386(2) Å) (Figure 5.30 (b)). The iodine atom of 4-I-2-MA is not involved in any interactions within the sheets.

In 4-Br-2-MA 3,5-DNBA, **23** (Figure 5.30 (b)), there are no interactions between the 3,5-DNBA dimers; the distance between adjacent nitro group O-atoms is slightly greater than the sum of the van der Waals radii (3.126(3) Å c.f. 3.1 Å). The H-atoms of the amine group, located in the Fourier difference maps, lie slightly out of the 4-I-2-MA ring plane, with approximate torsion angles of ~31° and ~13°, respectively, due to the close proximity of neighbouring NH_2 groups. Weak N-H···O hydrogen bonds form between only one of the amine group H-atoms, H1B, and a nitro group oxygen atom, O3 (Figure 5.30 (b), Table 5.8). A weak C-H···O hydrogen bond is formed between an aromatic C-H group of 4-Br-2-MA (H5) and a nitro group oxygen atom, O6 (C···O = 3.386(2) Å). In addition, the bromine atom of 4-Br-2-MA is involved in a C-Br···O interaction to a nitro group O-atom, O6 (Br···O = 3.120(2) Å, compared to the sum of the van der Waals radii of 3.37 Å) (Figure 5.30); the methyl group substituent is not involved in any interactions within the sheet.

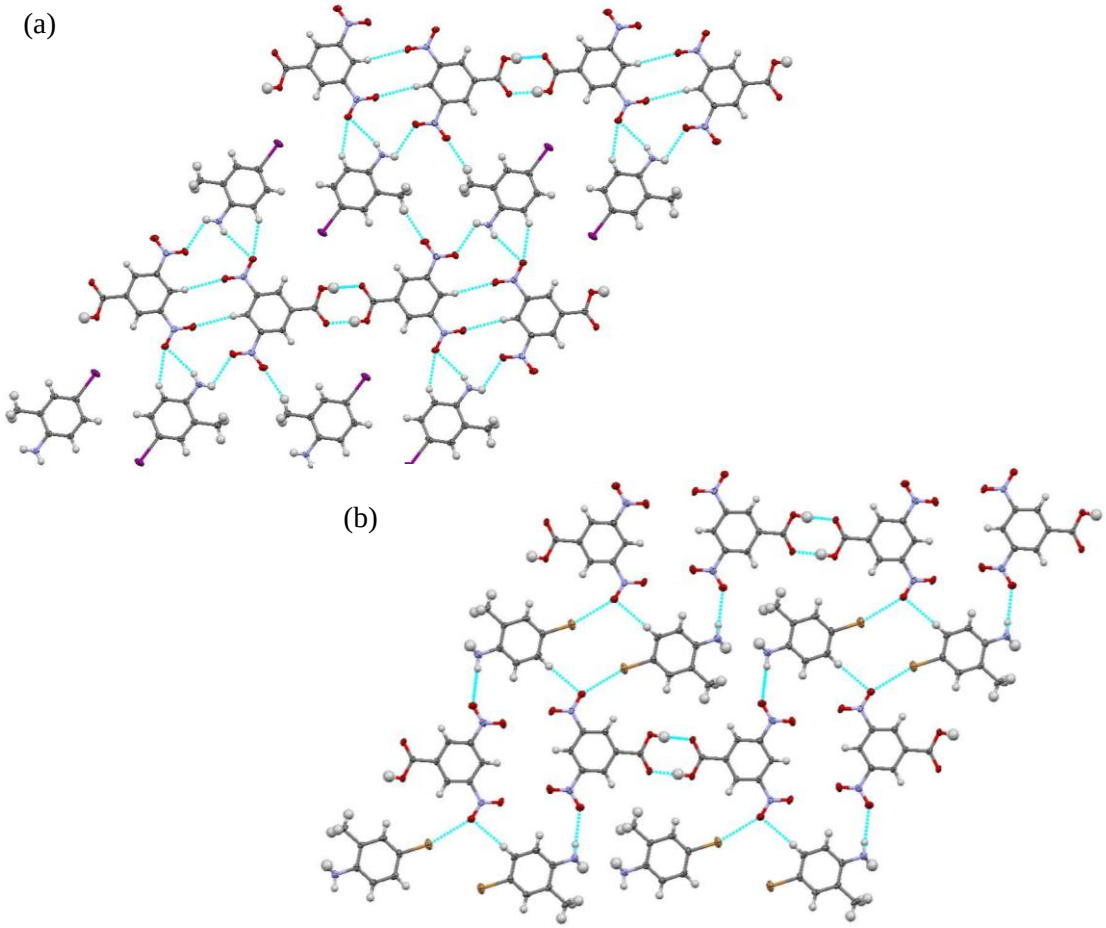

Figure 5.30 Two-dimensional sheet formed in (a) molecular complex **21**, showing the 3,5-DNBA dimers interacting with 4-I-2-MA molecules and adjacent 3,5-DNBA dimers through weak N-H···O and C-H···O hydrogen bonds and (b) molecular complex **23**, showing the bonded 3,5-DNBA dimers interacting with 4-Br-2-MA molecules through weak N-H···O and C-H···O hydrogen bonds, and short C-Br···O halogen bonds.

Table 5.8 Hydrogen bonding data (Å, °) for molecular complexes **21** and **23**

D-H···A	**D-H**	**H···A**	**D···A**	**<(DHA)**
Molecular complex **21**				
N1-H1A···O4 #1	0.82(2)	2.48(2)	2.921(2)	116(2)
N1-H1B···O6 #2	0.77(2)	2.56(2)	3.258(2)	152(2)
O1-H1···O2 #3	0.80(2)	1.83(2)	2.625(2)	178(3)
Molecular complex **23**				
N1-H1B···O6 #1	0.85(3)	2.31(3)	3.136(4)	164(3)
O1-H1···O3 #2	0.87(2)	1.77(2)	2.641(3)	172(4)

Molecular complex **21**: #1 x, y-1, z #2 -x, -y, -z+2 #3 -x, -y-1, -z+1

Molecular complex **23**: #1 -x+2, -y+1, -z #2 -x+3, -y, -z+1

Similarly to the neutral 4-XA 3,5-DNBA complexes, the interactions within the sheets are all weak or close to weak (i.e. on the borderline between moderate and weak hydrogen bonds, and close to the sum of the van der Waals radii for halogen bonds); this highlights the poor hydrogen bond donating ability of the N-H donor groups. This may also explain why the neutral complex is the least stable form. In general, the hydrogen bonds in **21** are stronger than in **23**. The planar sheets stack to form a layered structure, with alternately stacked 4-X-2-MA (donor) and 3,5-DNBA (acceptor) molecules forming mixed stack columns. In 4-I-2-MA 3,5-DNBA, there are aromatic donor···acceptor interactions between pairs of 4-I-2-MA and 3,5-DNBA, and there are π···π interactions between offset 3,5-DNBA molecules in adjacent layers. In 4-Br-2-MA 3,5-DNBA, there are aromatic donor···acceptor interactions continuously along the stack, but there are no offset π···π interactions between 3,5-DNBA molecules.

There are very similar intermolecular separations of ~3.23 Å and ~3.30 Å between stacked 4-X-2A and 3,5-DNBA molecules in **21** and **23**, respectively; the stacked molecules are close to coplanar in each case with ~4° between the ring planes of 4-X-2-MA and 3,5-DNBA in each complex. In **21** and **23**, there are two types of stacking and molecular overlap (**i** and **ii**, Figure 5.31), however, the mixed stacks in the two complexes are slightly different in terms of the orientations of the molecules and the type and amount of molecular overlap. In molecular complex **21**, the stacked molecules are offset, and there are only π···π interactions between the pair of molecules represented by stacking type '**ii**' (Figure 5.31 (a)), where there is a small amount of ring overlap and the amine group overlaps with the carboxylic acid group. There is very little overlap between molecules for **i**, with the nitro group sitting above the 4-I-2-MA ring (Figure 5.31 (a)). In molecular complex **21** there is a greater amount of ring overlap, and the halogen atom sits above the carboxylic acid group in **ii** (Figure 5.31 (b)).

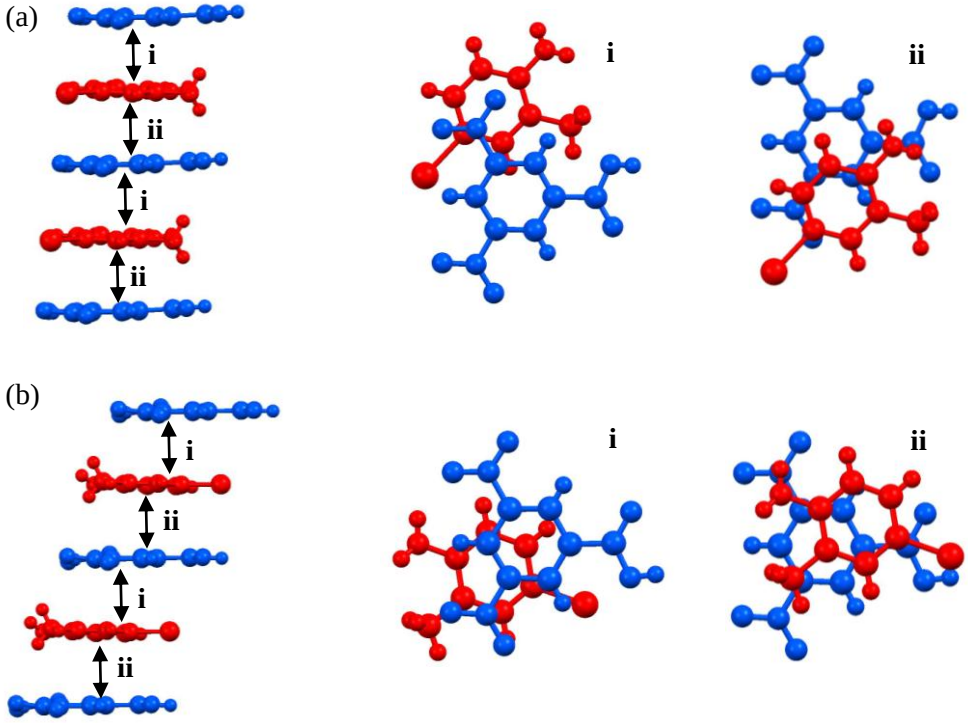

Figure 5.31 (a) Stacking of alternate 4-I-2-MA and 3,5-DNBA molecules and molecular overlap in **21**; (b) Stacking of alternate 4-Br-2-MA and 3,5-DNBA molecules and molecular overlap in **23**. The 4-X-2-MA is shown in red, and the 3,5-DNBA in blue.

The colour in both molecular complexes may be attributed to $\pi\cdots\pi^*$ charge-transfer between the neutral aromatic donor and acceptor molecules in the mixed stacks. Charge-transfer depends on the molecular overlap of the HOMO (of the donor) and LUMO (of the acceptor), and is thus very sensitive to the electronic properties of the donor and acceptor moieties and to the relative orientations of the donor and acceptor molecules in the mixed stack. Similarly to the neutral 4-XA 3,5-DNBA complexes, the nature of the halogen substituent will affect the electron donating properties of the 4-I-2-MA, and the differing orientations and overlap will also contribute to the differences in the optical properties of the two complexes. In addition, the hydrogen bonds involving the amine and methyl groups are stronger in **21** than **23**, which may also play a role in the colour; there are also hydrogen bonds between 3,5-DNBA dimers in **21**, but not in **23**. This pair of complexes has further demonstrated how simple exchange of the halogen substituent can tune the colour properties; the addition of the electron donating methyl group has minimal influence on the crystal packing, but shifts the absorbance in the visible region to longer wavelength. However, further work is required in order to understand fully the electronic transitions involved.

5.3.5 Sample analysis and phase transformation

As discussed in §5.3.2, the neutral forms of the 4-X-2-MA 3,5-DNBA molecular complexes, **21** and **23**, are metastable, with the crystals undergoing spontaneous transformation to a polycrystalline colourless phase. It was not possible to obtain a neutral form of 4-Cl-2-MA 3,5-DNBA, which may be associated with the higher ΔpKa value. Many red crystals of **21** remained stable for significant periods of time, but the transformation of crystals of molecular complex **23** was more rapid. Given the loss of colour upon transformation, it was possible that the solid-state transformation corresponded to conversion to the stable ionic forms of the molecular complexes, **20** and **22**. Where possible, hot-stage microscopy, differential scanning calorimetry and powder X-ray diffraction were carried out on samples of the ionic and neutral forms of the molecular complexes. Hot-stage microscopy experiments were conducted using a Mettler Toledo FP82 hot stage equipped with a Leica DM1000 microscope, as outlined in §3.3.1. Differential scanning calorimetry experiments were conducted using a TA Instruments Q20 differential scanning calorimeter, as outlined in §3.3.2; samples were ground very gently prior to being placed in a Tzero^{TM} pan. Powder X-ray diffraction experiments were conducted at room temperature using a Bruker AXS D8 Advance powder diffractometer in flat-plate mode, as outlined in §3.2.3.1.

5.3.5.1 4-iodo-2-methylaniline 3,5-dinitrobenzoic acid (20 and 21)

Thermal analysis

A number of crystals of **21** remained stable for a sufficient period of time for thermal analysis *via* hot-stage microscopy and differential scanning calorimetry. For the HSM analysis, a red single crystal of molecular complex **21** was heated between 30 °C and 130 °C at a rate of 5 °C/minute. A colour change from red to colourless was observed over the temperature range 77 - 84 °C; the transition moves across the crystal in a wave, with loss of single-crystallinity (Figure 5.32). Thus, the transformation occurs both spontaneously and upon heating. Following the transformation, the colourless phase melts starts to melt at ~117 °C, forming a red liquid, and there is immediate recrystallisation of colourless needles. Hot-stage microscopy was also carried out on a single crystal of the colourless, ionic form of the molecular complex, **20**. The crystal began to melt at ~117 °C, forming a red liquid, with recrystallisation of colourless needles observed from the melt.

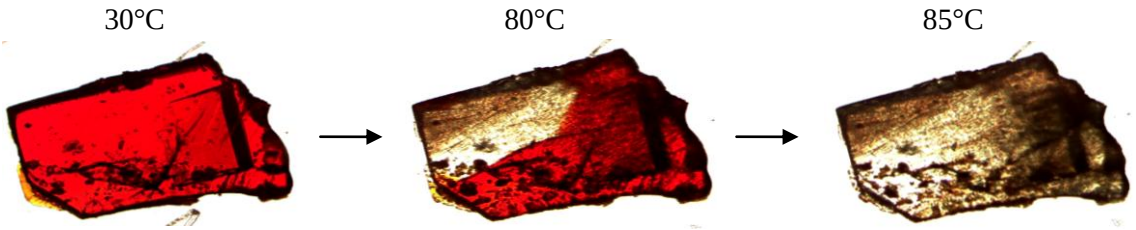

Figure 5.32 The thermally induced colour change in a crystal of molecular complex **21**, occurring as a wave across the crystal, shown at the start of the experiment (left), during the colour change (middle) and immediately following the transformation (right).

DSC experiments were also conducted on pure samples of **20** (ionic) and **21** (neutral); samples were heated between 40 °C and 130 °C at a rate of 5 °C/minute. The DSC thermogram obtained for the ionic form, **20**, has a sharp endothermic peak corresponding to the melt, with an onset temperature of 114.01 °C (Figure 5.33 (a)). DSC measurements on the neutral molecular complex, **21**, show a small exothermic event between 43 - 65 °C, which probably corresponds to the phase transformation to the colourless phase; the slight discrepancy between the phase transition temperatures in HSM and DSC may be due to a crystal size effect. This is followed by a large, sharp endothermic peak, with an onset temperature of 113.98 °C, corresponding to the melt (Figure 5.33 (b)).

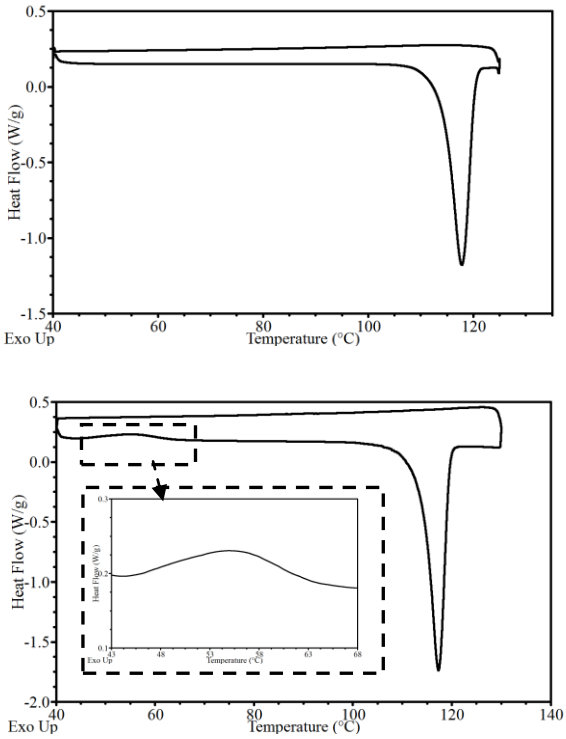

Figure 5.33 DSC thermograms of (a) molecular complex **20**, showing a large endothermic melt peak with an onset temperature of ~114 °C, and (b) molecular complex **21**, showing a small exothermic event between 43 - 65 °C (inset), corresponding to the colour change observed in HSM, and a melt with the same onset temperature as **20**.

Powder X-ray diffraction

PXRD was carried out on samples of the ionic molecular complex, **20**, samples of the neutral molecular complex, **21**, that remained sufficiently stable for analysis, and samples of **21** that had spontaneously transformed to the polycrystalline colourless phase. In addition, samples of molecular complex **21** were heated to 80 °C, which was just above the phase transition temperature, in order to convert the sample to the colourless form and investigate the phase transformation associated with the thermally induced colour change. Powder diffraction patterns were compared against each other and against the simulated patterns for the molecular complexes, using the program PolySNAP[212] to determine the similarity. The powder diffraction patterns of the samples of molecular complex **21** that transformed spontaneously and through heating, match the diffraction pattern of the ionic molecular complex **20** very well (Figure 5.34); this confirms that the neutral molecular complex (**21**) transforms to the known ionic form of the molecular complex (**20**).

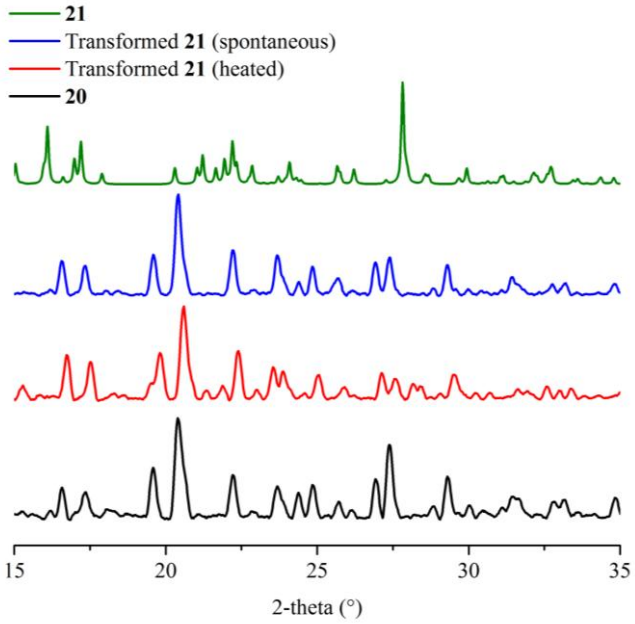

Figure 5.34 Powder diffraction patterns collected on a sample of molecular complex **20** (black), samples of **21** transformed by heating and spontaneously (red and blue, respectively), and a stable sample of molecular complex **21** (green)

Summary

The HSM and DSC experiments suggest that the red, neutral form of 4-I-2-MA 3,5-DNBA, **21**, undergoes a transformation to the ionic form of the molecular complex, **20**; this occurs either spontaneously or upon heating. A thermally-induced colour change from red to colourless was observed during HSM analysis over the temperature range 77 - 84 °C; a small exothermic peak

was also observed in the DSC thermogram of **21** at a slightly lower temperature, which was interpreted to correspond to the same phase transition. Following the transformation of **21** to the colourless phase, the sample melted at the same temperature as the pure sample of the ionic form, **20** (onset temperature of ~114 °C).

Powder X-ray diffraction confirmed that the transformation was to the known ionic form, **20**. The diffraction patterns of the samples of **21** that had transformed, both spontaneously and thermally, match the diffraction patterns of **20**. The phase transformation is therefore associated with a proton transfer from the carboxylic acid group of 3,5-DNBA to the amine group of 4-I-2-MA, resulting in a significant structural rearrangement and colour change. The transformation does not occur in a single crystal to single crystal manner due to the large structural differences between the neutral and ionic forms of the molecular complex.

5.3.5.2 4-bromo-2-methylaniline 3,5-dinitrobenzoic acid (22 and 23)

Thermal analysis

It was possible to carry out hot-stage microscopy analysis on a single crystal of molecular complex **23**. An orange single crystal of molecular complex **23** was heated between 30 °C and 150 °C at a rate of 5 °C/minute. A colour change from orange to colourless was observed over quite a broad temperature range of 61 - 83 °C; similarly to **21**, the transition moves across the crystal in a wave, with loss of single-crystallinity (Figure 5.35). Following the transformation, the colourless phase melts starts to melt at ~126 °C, forming an orange liquid, followed by immediate recrystallisation of colourless needles. The same HSM experiment was also carried out on a single crystal of the colourless, ionic form of the molecular complex, **20**. The crystal began to melt at ~127 °C, forming an orange liquid, with recrystallisation of colourless needles from the melt.

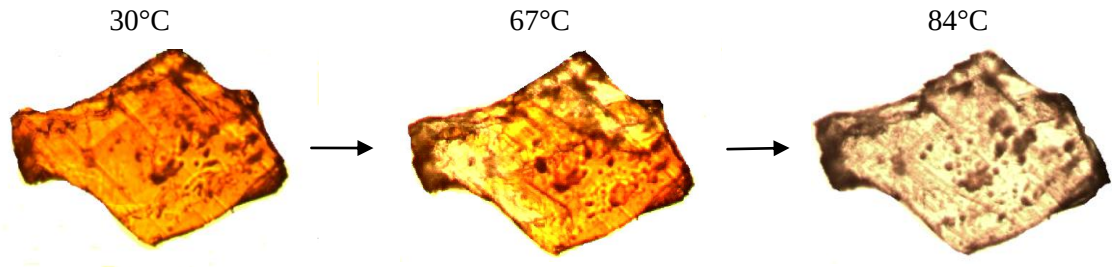

Figure 5.35 The thermally induced colour change in a crystal of molecular complex **23**, occurring as a wave across the crystal, shown at the start of the experiment (left), during the colour change (middle) and immediately following the transformation (right).

Although it was not possible to carry out DSC experiments on the neutral form, **23**, due to rapid transformation, experiments were conducted on samples of **22** and a transformed sample of **23**. Samples were heated between 40 °C and 150 °C at a rate of 5 °C/minute. The DSC thermogram obtained for the ionic form, **20**, has a sharp endothermic peak corresponding to the melt, with an onset temperature of 125.13 °C; there is also a small exothermic peak on cooling, with an onset temperature of 91.6 °C (Figure 5.36 (a)). The DSC thermogram for the transformed sample of **23** matches that of **22** very closely, there is a sharp endothermic peak with an onset temperature of 128.55 °C, corresponding to the melt, and a small endothermic peak on cooling, with an onset temperature of 102.72 °C (Figure 5.36 (b)).

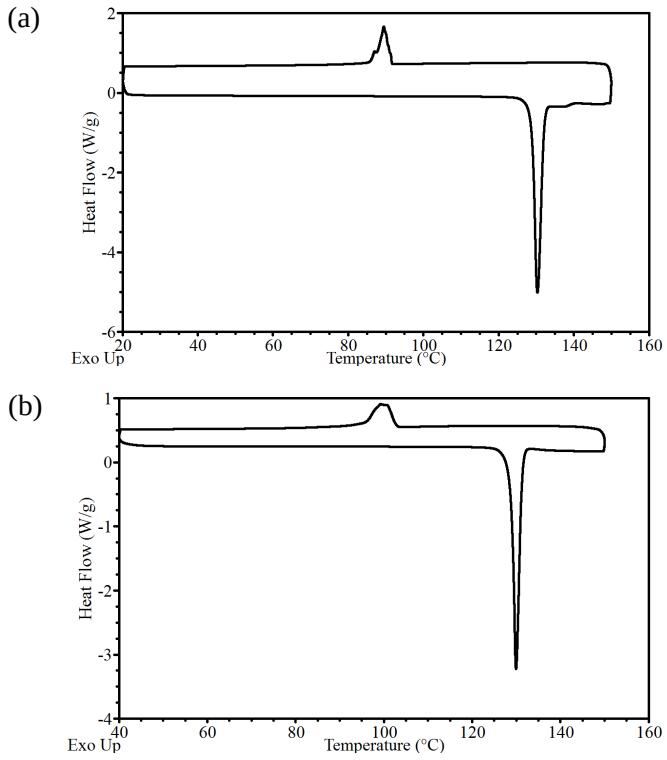

Figure 5.36 DSC thermograms of (a) molecular complex **22**, showing a large endothermic melt peak with an onset temperature of 125.13 °C, and (b) a transformed sample of molecular complex **23**, which matches that of **22** very closely.

Powder X-ray diffraction

Powder X-ray diffraction was carried out on samples of the ionic molecular complex, **22**, and samples of **23** that had spontaneously transformed to the colourless phase to investigate the phase transformation. It was not possible to carry out PXRD on the neutral complex, **23**, as all of the sample had spontaneously transformed. Powder diffraction patterns were compared against each other and against the simulated patterns for the molecular complexes, using the program PolySNAP[212] to determine the similarity. The peak positions in the powder diffraction

patterns of the transformed samples and the ionic molecular complex **22** match very well (Figure 5.37), suggesting that the neutral molecular complex, **23**, spontaneously transforms to the known ionic form of the molecular complex.

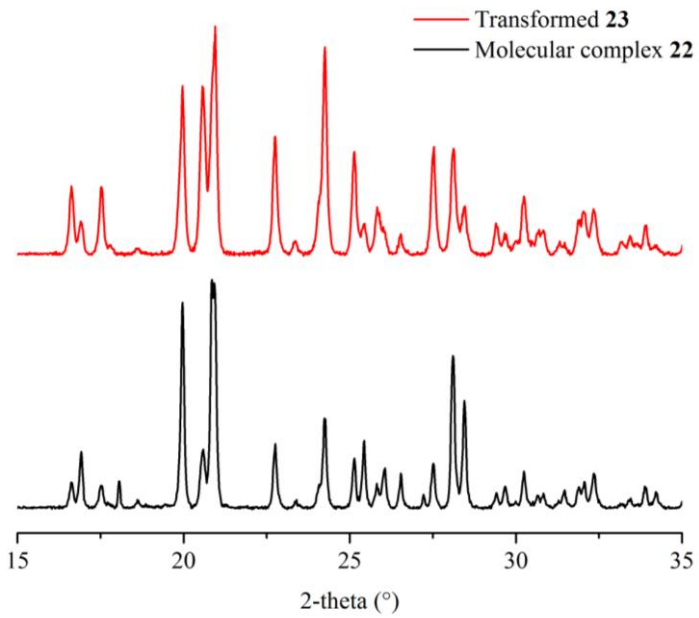

Figure 5.37 Powder diffraction patterns collected on a sample of molecular complex **22** (black) and a transformed sample of **23** (red).

Summary

The HSM and DSC experiments suggest that the orange, neutral form of 4-Br-2-MA 3,5-DNBA, **23**, undergoes a transformation to the ionic form of the molecular complex, **22**. A thermally induced colour change from orange to colourless was observed during HSM analysis over the temperature range 62 - 83 °C. Following the transformation, the crystal began to melt at ~126 °C, which matches the melting point of the ionic form, **22**. Although it was not possible to carry out DSC analysis on the neutral form, experiments were carried on the ionic form, **22**, and a spontaneously transformed sample of **23**, and both melt at approximately the same temperature.

Powder X-ray diffraction confirmed that the transformation was to the known ionic form, **22**. The diffraction patterns of the samples of **23** that transformed match the diffraction patterns of **21**. The phase transformation is therefore associated with a proton transfer from the carboxylic acid group of 3,5-DNBA to the amine group of 4-Br-2-MA, resulting in a significant structural rearrangement and colour change. As for the 4-I-2-MA complex, the transformation does not

occur in a single crystal to single crystal manner due to the large structural differences between the neutral and ionic forms of the molecular complex.

5.3.5.3 4-chloro-2-methylaniline 3,5-dinitrobenzoic acid (24)

Despite numerous attempts, it was not possible to obtain a neutral form of 4-Cl-2-MA 3,5-DNBA, with the ionic molecular complex, **24**, obtained in all of the crystallisation trials. HSM and DSC experiments were carried out on the molecular complex, and in each case heating was carried out between 40 °C and 150 °C at a rate of 5 °C/minute. A sharp endothermic peak was observed in the DSC thermogram with an onset temperature of 126.47 °C (Figure 5.38), which corresponds to the melt of the crystal observed at ~127 °C in the HSM experiment.

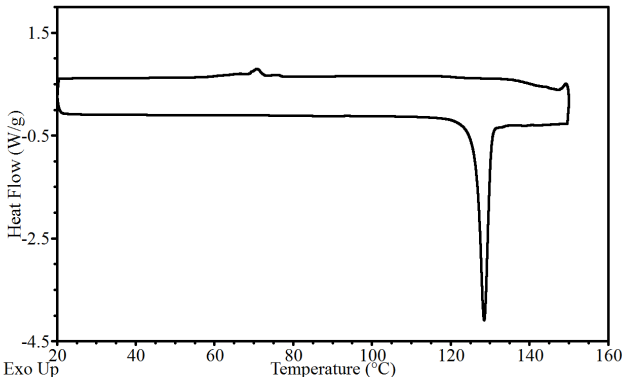

Figure 5.38 DSC thermogram of molecular complex **24**, showing a large endothermic melt peak with an onset temperature of 126.47 °C.

5.3.6 Summary and discussion

Five molecular complexes combining 4-I-2-MA, 4-Br-2-MA and 4-Cl-2-MA with 3,5-DNBA were obtained *via* slow evaporation, and structurally characterised by single crystal X-ray diffraction. In each molecular complex, the components have a 1:1 stoichiometry and, with the exception of 4-Cl-2-MA 3,5-DNBA, it was possible to obtain both neutral and ionic molecular complexes. The ΔpKa values for 4-I-2-MA, 4-Br-2-MA and 4-Cl-2-MA with 3,5-DNBA are 0.84, 0.89 and 1.03, respectively, which are all situated in the salt-cocrystal continuum. The neutral and ionic forms were easily distinguishable visually as, similarly to the 4-XA 3,5-DNBA complexes, the colour of the crystals was dependent on the protonation states of the molecules and associated crystal packing arrangement of the neutral or ionic molecules. In cases where the components were fully ionic (**20, 22** and **24**), the crystals were always colourless, and in each case the crystal structures were non-layered. Where the components were neutral (**21** and **23**),

the crystals were strongly coloured, and in each case the crystal structures were layered, with mixed stacks of alternating donors (4-X-2-MA) and acceptors (3,5-DNBA). The interactions between the stacked molecules dominated the packing arrangement, and the interactions within the planar sheets were only moderate to weak in strength.

With regards to the overall crystal packing the nature of the halogen was found to have very little effect in the ionic complexes. The ionic forms of the molecular complexes, **20**, **22** and **24**, were all isostructural, with the hydrogen bonding interactions of the tetrahedral NH_3^+ group dominating the packing arrangement. Similarly to 4-XA 3,5-DNBA, the crystal packing of the neutral forms, **21** and **23**, was similar although the complexes were not isostructural. The molecular orientations and intermolecular interactions within the planar sheets differed; the hydrogen bonds involving the amine and methyl groups are stronger in **21** than **23**, which may also play a role in the colour; there are also hydrogen bonds between 3,5-DNBA dimers in **21**, but not in **23**. However the overall structures consisted of columns of alternately stacked 4-X-2-MA and 3,5-DNBA molecules, with very similar interlayer distances. In terms of solid-state colour, 4-I-2-MA 3,5-DNBA and 4-Br-2-MA 3,5-DNBA were red and orange respectively; the colour may be attributed to $\pi\cdots\pi^*$ charge-transfer between the aromatic donor and acceptor. The intermolecular separation of the donor and acceptor in the stacking direction is approximately the same in the two complexes, thus, the difference in colour must be due to nature of the halogen and the relative orientations of the 4-X-2-MA and 3,5-DNBA molecules in the stacks. It is also possible that the strength of the hydrogen bonds in the sheets plays a role. There is less molecular overlap in the 4-I-2-MA complex than in the 4-Br-2-MA complex. In addition, iodine and bromine differ in electronegativity and therefore in their electron donating ability. This demonstrates how the simple exchange of the halogen substituent allows the solid-state colour to be tuned. Furthermore, the introduction of the electron donating methyl group substituent has a small influence on the crystal packing, altering the molecular overlap; there is a small shift of the absorbance in the visible region to longer wavelength (by ~20 nm), which is likely to be due to the change in the donating properties of the aniline component.

The crystallisation of the molecular complexes is complicated by the possibility of obtaining neutral and ionic forms. The neutral and ionic molecular complexes could be obtained under various crystallisation conditions, and it was not possible to predict which product would result; repeat crystallisation trials often resulted in a different molecular complex to the previous trial. In addition, the two neutral molecular complexes are metastable, and transform to a colourless phase; generally this occurred spontaneously under ambient conditions, although some crystals, in particular of **21**, remained stable for a significant period of time. However, the same transformation from coloured to colourless was observed upon heating single crystals of

4-I-2-MA 3,5-DNBA and 4-Br-2-MA 3,5-DNBA by HSM. The stability of the neutral forms appears to decrease with decreasing molecular weight i.e. I to Br to Cl, and it was not possible to obtain a neutral form of 4-Cl-2-MA 3,5-DNBA; the stability of the ionic forms increases with decreasing molecular weight. This is reflected in the increase in the melting point from I to Br to Cl, and reflects the strength of the halogen bonds formed.

The combination of thermal analysis and powder X-ray diffraction experiments all provide evidence that suggest that the neutral forms of the molecular complexes, **21** and **23**, are transforming to the ionic forms, **20** and **22**, respectively. The phase transformation would therefore be propagated by a proton transfer from the carboxylic acid group of 3,5-DNBA to the amine group of 4-X-2-MA, corresponding to a significant structural arrangement. Similarly to the 4-XA 3,5-DNBA complexes, the difference in the neutral and ionic forms is not simply in the location of the acidic proton in a hydrogen bond, and the transformation does not occur in a single crystal to single crystal manner.

5.4 Conclusions

Eleven molecular complexes of 4-haloanilines and 4-halo-2-methylanilines with the co-former 3,5-dinitrobenzoic acid have been synthesised and characterised. The results presented in this chapter firstly demonstrate the unusual possibility of obtaining a neutral and an ionic molecular complex of the same two components in the same 1:1 stoichiometry, under the same crystallisation conditions. Secondly, the structures provide insight into how the choice of suitable molecular components and their associated packing arrangements can induce colour in the solid-state; in addition, the tunability of colour is demonstrated through the simple exchange of the halogen substituent. Lastly, the systems provide an alternative mechanism for thermochromism in the solid-state, through proton transfer.

Crystallisation and phase transformations

The two series of molecular complexes reported in Chapter 5 are rare in that both neutral and ionic complexes can be formed from the same pair of co-molecules in the same stoichiometry. Typically, a multi-component crystallisation study of a particular co-former with a range of co-molecules will result in the formation of either an ionic or a neutral molecular complex for each molecular pair. The ΔpKa rule can be used to assess whether a neutral or ionic multi-component complex will be formed; in this case, the ΔpKa values sit in the salt-cocrystal continuum for each multi-component system, and based on this it is not possible to predict whether proton transfer will occur. Across both series of molecular complexes, the crystallisation of the

haloaniline molecule with the co-former 3,5-DNBA resulted in both a neutral and an ionic molecular complex, with the exception of 4-Cl-2-MA with which only an ionic form was obtained (Table 5.9). These systems are very interesting in terms of the ability to isolate and characterise a neutral and ionic form of the same molecular complex formed under the same slow evaporative crystallisation conditions.

Table 5.9 ΔpKa values for the multi-component crystallisations with 3,5-DNBA, and the resulting molecular complex(es) formed.

Co-molecule	ΔpKa	Neutral (N) or ionic (I) complex
4-iodoaniline	0.99	N, I
4-bromoaniline	1.07	N, I
4-iodo-2-methylaniline	0.84	N, I
4-bromo-2-methylaniline	0.89	N, I
4-chloro-2-methylaniline	1.03	I

Determining the crystallisation conditions required to obtain the different forms was complicated, and in some case not possible; in each system, both the neutral and ionic forms could be obtained from a range of crystallisation conditions and often repeat co-crystallisations would result in the opposite form to that obtained in the previous crystallisation. However, the ionic forms were formed more readily.

The neutral forms of the molecular complexes are all metastable and generally spontaneous conversion to a colourless phase occurred. In both series, the stability of the neutral form decreases with decreasing molecular weight (I>Br>Cl); the neutral 4-X-2-MA complexes appeared to be more stable than the corresponding 4-XA complexes, with more crystals remaining stable for a longer period of time. The iodine forms of each system are most stable, with some crystals of the complexes remaining stable for significant periods of time (up to one year at the time of writing); in the bromine forms, the transformation was very rapid. It was not possible to obtain a neutral form of 4-Cl-2-MA 3,5-DNBA, indicating that this complex has an even lower stability. The ionic forms of the molecular complexes are all very stable; the melting points of the ionic complexes increase with decreasing molecular weight (I<Br<Cl), which also relates to the relative stabilities of the neutral forms.

The trend in the ΔpKa values also reflects the stability of the neutral forms over the ionic forms, indicating that even very small changes in the pKa values of the molecular components can affect the nature of the complex formed and the stability. For the 4-XA and 4-X-2-MA systems, the higher the ΔpKa, the more stable the ionic form, and the more likely it is that a neutral

complex will be more unstable or will not form. In addition, the ΔpKa values for the 4-X-2-MA systems are lower than the corresponding 4-XA systems, reflected in the higher stability of the 4-X-2-MA 3,5-DNBA complex over that of the 4-IA 3,5-DNBA complex.

While the thermal behaviour of all the molecular complexes is complicated, a combination of thermal analysis and powder X-ray diffraction experiments provides evidence for the transformation of the neutral forms to an ionic form, corresponding to a colour change from either red or orange, to colourless. The melting points of the transformed neutral complexes correspond to the melting points of the ionic complexes. In the 4-X-2-MA 3,5-DNBA molecular complexes, the powder diffraction patterns of the transformed neutral molecular complexes match the patterns of the corresponding ionic complexes well. In the 4-XA 3,5-DNBA molecular complexes, the results are more complicated. A limited number of the transformed samples of 4-IA 3,5-DNBA correspond to one of the known ionic forms; however this is not the case for all. In 4-BrA 3,5-DNBA, the transformed samples do not match the known ionic form. It is possible, therefore, given the similarity of the behaviour and the colour change to the 4-X-2-MA series, that in these cases the transformation is to an unidentified ionic form of the molecular complex.

The phase transformation associated with the colour change is therefore propagated by a proton transfer from the carboxylic acid group of 3,5-DNBA to the amine group of the haloaniline, and this simple proton transfer between species is sufficient to initiate molecular rearrangement from the metastable neutral form to the more stable ionic form. This corresponds to a significant structural rearrangement, which results in a very distinct colour change, and this occurs either spontaneously or upon heating. The transition does not occur in a single crystal to single crystal manner and is irreversible. There is significant scope for further work on the crystallisation of the molecular complexes, in order to understand the complex nature of these systems, in terms of the crystallisation and phase transformations.

Crystal packing and colour

The eleven molecular complexes provide significant insights into the crystal packing and structural features that determine colour in the solid-state. All the starting components are colourless or pale coloured in nature, and colourless and coloured multi-component crystals are formed. From a crystal engineering perspective, the series of molecular complexes allow direct comparisons to be made between neutral and ionic complexes, between halogen types, and between substituted and non-substituted haloanilines.

In their ionic forms, the molecular complexes always form as colourless crystals; the hydrogen bonds of the tetrahedral NH_3^+ group direct the hydrogen bonding into a more three-dimensional form, with the same $R_4^3(10)$ hydrogen bonded rings formed between the amine group and the carboxylate groups of each 3,5-DNBA anion in each case. Overall, these interactions result in non-layered structures. The nature of the halogen does not impact the crystal packing arrangement; the ionic 4-X-2-MA 3,5-DNBA complexes are all isostructural, and the ionic 4-BrA 3,5-DNBA complex is isostructural with one of the 4-IA 3,5-DNBA polymorphs. The dominant interactions in the crystal packing are the charge-assisted hydrogen bonds involving the protonated amine group.

In their neutral forms, the molecular complexes always form as coloured crystals. The NH_2 group is generally coplanar with the benzene ring, and molecules of 3,5-DNBA form planar dimers. The interactions between these molecules result in layered structures, with mixed stacks of alternating planar 4-XA/4-X-2-MA and 3,5DNBA molecules. The interactions within the sheets are only moderate to weak in nature. The N-H···O hydrogen bonds involving the amine group are stronger in the I complexes than in the corresponding Br complex; furthermore, there are hydrogen bonds between dimers in the I complex, but not in the Br complex.

The crystal packing is dominated in each case by the interactions between the aromatic electron-rich donor (aniline) and electron-poor acceptor (3,5-DNBA) molecules. The colour may be attributed to $\pi\cdots\pi^*$ charge-transfer between the donor and acceptor. The overall crystal packing is quite similar in each 4-IA/4-BrA and 4-I-2-MA/4-Br-2-MA pair of complexes, but the complexes differ in the molecular orientation of the aniline component, which must be an effect of the halogen substituent. In terms of colour, the two neutral complexes of 4-IA 3,5-DNBA and 4-I-2-MA 3,5-DNBA both form as red crystals, whereas the equivalent bromine complexes form as orange crystals. The colours of charge-transfer complexes are dependent upon and sensitive to the electronic properties of the donor and acceptor and upon their relative orientations and overlap. The molecular separations in the stacking direction are similar across the complexes. However, the differences in the donating abilities of the halogen, and the relative molecular orientations of the stacked molecules, will affect the electronic properties of the systems. In addition, the hydrogen bonds involving the amine group may also play a role; the hydrogen bonds in the sheets are generally stronger in the iodine complexes, which are red in colour, than in the bromine complexes, which are orange in colour. Further work must be carried out in order to understand the exact nature of the charge-transfer and the differences between the I/Br complexes, through advanced solid-state calculations.

In addition to the ionic and neutral forms, 4-IA 3,5-DNBA also formed a methanol solvate form, which was structurally very different. The incorporation of methanol in the structure, providing an additional strong hydrogen bond donor group, results in a mixed ionisation complex with co-existing neutral and charged species. The molecular complex is layered and, similarly to the layered neutral complexes, it forms as coloured crystals. The structure consists of stacks of alternating 4-IA molecules and disordered 3,5-DNBA molecules. It is possible that the disorder in the structure plays a role in the colour. In order to investigate the methanol solvate complex, further interpretation of the diffuse scattering must first be carried out, which is not trivial.

Comparison of the crystal structures of the equivalent neutral and ionic 4-XA 3,5-DNBA and 4-X-2-MA 3,5-DNBA molecular complexes shows that the introduction of the methyl group substituent adjacent to the amine group has very little effect on the intermolecular interactions, overall crystal packing and resultant solid-state colour. The methyl group is not involved in any significant interactions in any of the molecular complexes. The ionic methyl-substituted complexes have very similar crystal structures to one of the 4-IA 3,5-DNBA salts, and the neutral methyl-substituted complexes have very similar crystal structures to the corresponding neutral 4-XA 3,5-DNBA complexes, with the only significant difference being the orientations of the haloanilines with respect to the 3,5-DNBA dimers. The corresponding substituted and non-substituted complexes have very similar solid-state colours; the absorbance spectra for the neutral 4-I-2-MA 3,5-DNBA complex displays a small shift (~20 nm) to longer wavelength relative to the 4-IA 3,5-DNBA complex, which may be due to the difference in the electron donating property of the aniline component.

In the context of the study on colour in multi-component molecular complexes, the systems provide key insight into the types of structure and molecular components required in order to induce colour in the solid-state. They also provide an alternative mechanism to thermochromism in haloaniline and dinitrobenzoic acid mutli-component systems. However, the difference between the neutral (coloured) and ionic (colourless) complexes is not simply in the location of the acidic proton, and there is a significant structural rearrangement upon transformation, which does not occur in a single-crystal to single-crystal manner. This further highlights how the extra crystal space in the 2-IA 3,4-DNBA complex in Chapter 4, through the formation of a 1:2 complex and the inclusion of disorder, enables the rearrangement to occur whilst maintaining the single crystal integrity.

CHAPTER 6

Colour in mixed stack

molecular complexes

6 Colour in mixed stack molecular complexes

Chapter 6 is concerned with the mixed stack donor···acceptor complexes of haloanilines and methyl-substituted haloanilines with dinitrosubstituted benzoic acid derivatives; related ionic molecular complexes are also reported for comparison. Unlike the molecular complexes presented in Chapters 4 and 5, the molecular complexes discussed here do not display temperature-dependent colour and are all stable under ambient conditions. The mixed stack complexes in this chapter are, however, all strongly coloured in the solid-state, which may be attributed to π-π* charge-transfer between the aromatic donor and acceptor components. In addition to the induction of colour in the solid-state through the formation of the multi-component complexes, comparison across the complexes presented in this chapter, and related complexes in Chapters 4 and 5, demonstrates that simple modifications to the molecular components can be made in order to tune the colour of the multi-component crystal. Such modifications include exchange of the halogen type and position, differing stoichiometries of the components, changing the ring positions of the substituents, and introduction of a methyl group substituent.

Multi-component crystallisation studies that are focused specifically on the tunability of colour are limited (§1.7.1), which is surprising given the potential that multi-component crystallisation offers for the modification of physical properties, for example in pigments. However, in terms of inducing colour in the solid-state, organic mixed stack complexes of aromatic donor and acceptor molecules are well known (§1.5). Such complexes typically have a 1:1 stoichiometric ratio of the donor and acceptor, but other ratios, such as 1:2 and 2:1, have been reported.[105] As observed in some of the complexes in this chapter, disorder has been found to occur in some of these systems;[115–117,224] the charge-transfer interactions and the formation of mixed stack columns take precedence over a close packing arrangement, resulting in an orientational disorder of one of the molecules due to an inefficient packing arrangement (discussed in Chapter 4).

In their neutral forms, the haloanilines can all act as aromatic electron donors and the dinitrosubstituted benzoic acid derivatives can all function as aromatic electron acceptors. However, there is also the possibility of proton transfer occurring between the acidic and basic moieties; whether charge-transfer or proton transfer dominates is dependent on the ΔpKa values (Figure 6.1). A search of the Cambridge Structural Database (CSD)[86] for neutral organic mixed stack complexes containing 2-, 3- and 4-substituted haloanilines and methyl-substituted haloanilines revealed that in the vast majority of haloaniline complexes a proton is transferred to the amine group. 4-iodoaniline trinitrobenzene[111] is the only example of a mixed stack

haloaniline complex in the CSD; the neutral charge-transfer molecular complex of 2-iodoaniline picric acid is known[171] but there is no crystal structure reported.

A series of multi-component crystallisations were conducted, choosing dinitrobenzoic acid and dinitrosalicylic acid co-formers (defined below) for their electron-accepting potential. In this chapter, the results of the following multi-component crystallisations are discussed: 2-iodoaniline (2-IA), 2-bromoaniline (2-BrA), 2-chloroaniline (2-ClA) with 3,5-dinitrobenzoic acid (3,5-DNBA); 2-iodo-4-methylaniline (2-I-4-MA), 2-bromo-4-methylaniline (2-Br-4-MA) and 2-chloro-4-methylaniline (2-Cl-4-MA) with 3,5-DNBA; 4-iodoaniline (4-IA) and 4-bromoaniline (4-BrA) with 3,5-dinitrosalicylic acid (3,5-DNSA); 3-bromoaniline (3-BrA) with 3,5-DNBA; 4-bromo-2-iodoaniline (4-Br-2-IA) with 3,4-dinitrobenzoic acid (3,4-DNBA) and 3,5-DNBA. The molecular components are shown in Figure 6.1; all are colourless or pale-coloured in their single component forms.

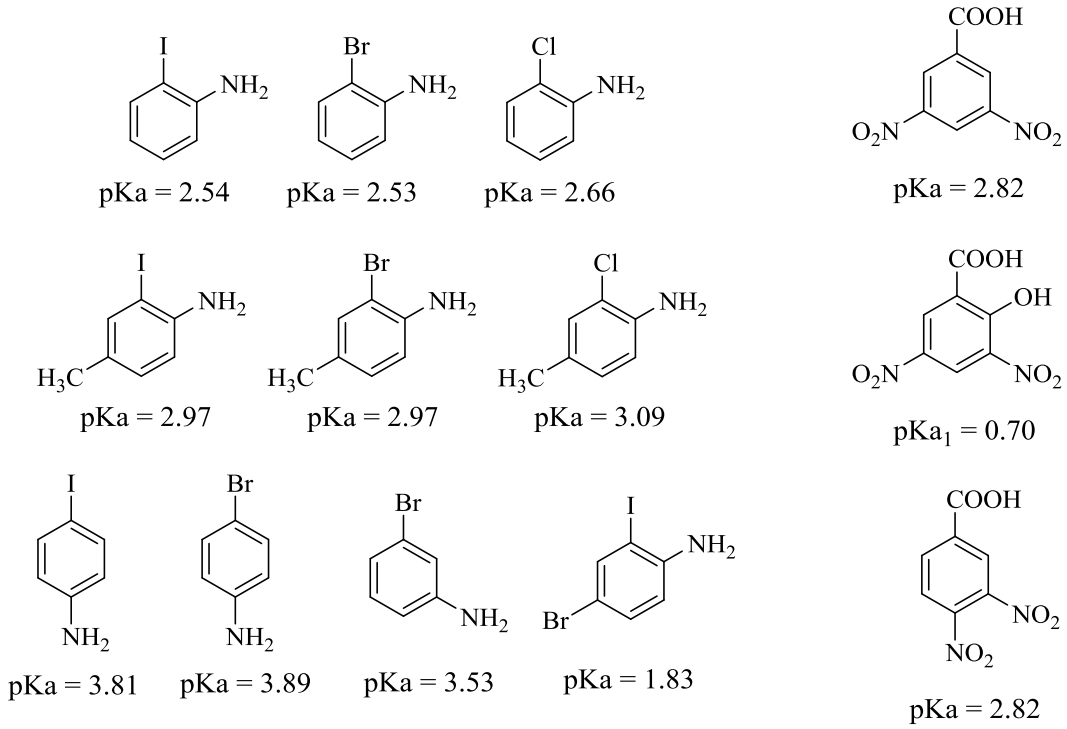

Figure 6.1 Chemical structures of the molecular components used in the multi-component crystallisation experiments in Chapter 6, and their pKa values.[227,228,240–242] Left, top:2-IA, 2-BrA, 2-ClA; left, middle: 2-I-4-MA, 2-Br-4-MA, 2-Cl-4-MA; left, bottom: 4-IA, 4-BrA, 3-BrA and 4-Br-2-IA. Right (top to bottom): 3,5-DNBA, 3,5-DNSA and 3,4-DNBA.

6.1 Molecular disorder in 2-haloaniline 3,5-dinitrobenzoic acid complexes

6.1.1 Experimental details

Molecular complexes **25** - **27** were synthesised *via* the method of slow evaporation (§3.1) using a 1:1 stoichiometric molar ratio of the 2-haloaniline and 3,5-dinitrobenzoic acid; crystallisation trials employed a range of solvents and evaporation temperatures. Single crystal X-ray diffraction experiments were carried out according to the procedures outlined in §3.2. Crystallographic data are given in Table 6.1 and refinement details are reported in Appendix A6.

2-iodoaniline 3,5-dinitrobenzoic acid (25)

Molecular complex **25** was synthesised from acetonitrile at ambient temperature; yellow/orange block crystals were obtained. Single crystal X-ray diffraction data were collected at 100 K using a Rigaku R-AXIS/RAPID image plate diffractometer. The structure was solved by direct methods using SHELXS-97[192] and refined using SHELXL-2014,[198] both within the WinGX program suite.[200]

2-bromoaniline 3,5-dinitrobenzoic acid (26)

Molecular complex **26** was synthesised from acetonitrile at ambient temperature; yellow/orange block crystals were obtained. Single crystal X-ray diffraction data were collected at 100 K using a Rigaku R-AXIS/RAPID image plate diffractometer. The structure was solved by direct methods using SHELXS-97[192] and refined using SHELXL-2014,[198] both within the WinGX program suite.[200]

2-chloroaniline 3,5-dinitrobenzoic acid (27)

Molecular complex **27** was synthesised from acetone at ambient temperature; bright yellow thin block crystals were obtained. Single crystal X-ray diffraction data were collected at 150 K using a Rigaku Oxford Diffraction SuperNova diffractometer (Cu Kα radiation). The structure was solved by direct methods using SHELXS-2013[192] and refined using SHELXL-2014,[198] both within the WinGX program suite. [200]

Table 6.1 Crystallographic data for molecular complexes **25- 27**

	25	**26**	**27**
Formula	(C_6H_6NI) $(C_7H_4N_2O_6)$	(C_6H_6NBr) $(C_7H_4N_2O_6)$	(C_6H_6NCl) $(C_7H_4N_2O_6)$
M/g mol^{-1}	431.14	384.15	339.69
T/K, Radiation	100(2), Mo Kα	100(2), Mo Kα	150(2), Cu Kα
Space Group	$P\bar{1}$	$P\bar{1}$	Fdd2
a/Å	6.9349(5)	6.917(4)	29.9152(3)
b/Å	7.7749(7)	7.522(4)	28.7388(2)
c/Å	14.7353(13)	14.081(8)	6.7407(1)
α/°	97.097(4)	99.804(12)	90
β/°	99.754(2)	98.867(12)	90
γ/°	100.632(3)	96.645(11)	90
V/Å	759.68(11)	705.7(7)	5795.16(11)
Z	2	2	16
ρ_{cal}/ g cm^{-3}	1.885	1.808	1.557
μ/mm^{-1}	2.143	2.950	2.694
θ Range/°	3.048 - 27.480	3.116 - 27.482	4.267 - 66.561
Ref Collected	18292	17531	14971
Independent	3459	3222	2371
Observed>2σ	2403	2432	2336
R(int)	0.0403	0.0505	0.0245
Completeness %	99.8	99.8	100.0
Parameters	180	200	194
Flack parameter	-	-	0.019(6)
GooF	1.175	1.121	1.071
R_1 (obs)	0.0874	0.0398	0.0389
R_1 (all)	0.1140	0.0587	0.0396
wR2 (all)	0.2317	0.1100	0.1071
$\rho_{max,min}$/e Å^{-3}	2.378, -2.438	0.560, -0.484	0.443, -0.372

6.1.2 2-haloaniline 3,5-dinitrobenzoic acid (25 - 27)

2-iodoaniline, 2-bromoaniline and 2-chloroaniline are light grey, light brown and light yellow, respectively; 3,5-dinitrobenzoic acid is a light yellow solid. Dissolution of the 2-haloaniline with 3,5-DNBA resulted in a pale yellow solution in each case. The molecular complexes of 2-IA 3,5-DNBA (**25**) and 2-BrA 3,5-DNBA (**26**) were yielded as yellow/orange block crystals, and 2-ClA 3,5-DNBA (**27**) formed as bright yellow thin block crystals. Single crystal UV-visible absorption spectra were collected on each of the molecular complexes at room temperature (Figure 6.2), according to the procedure outlined in §3.4.1. The spectra show a broad absorption band in the visible region, characteristic of a π···π* charge-transfer, with absorption below 550 nm in **25** and **26** and below 530 nm in **27**, which are consistent with the colour of the crystals.

(a)

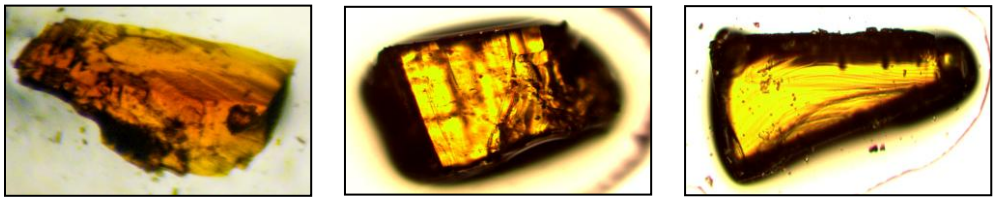

(b)

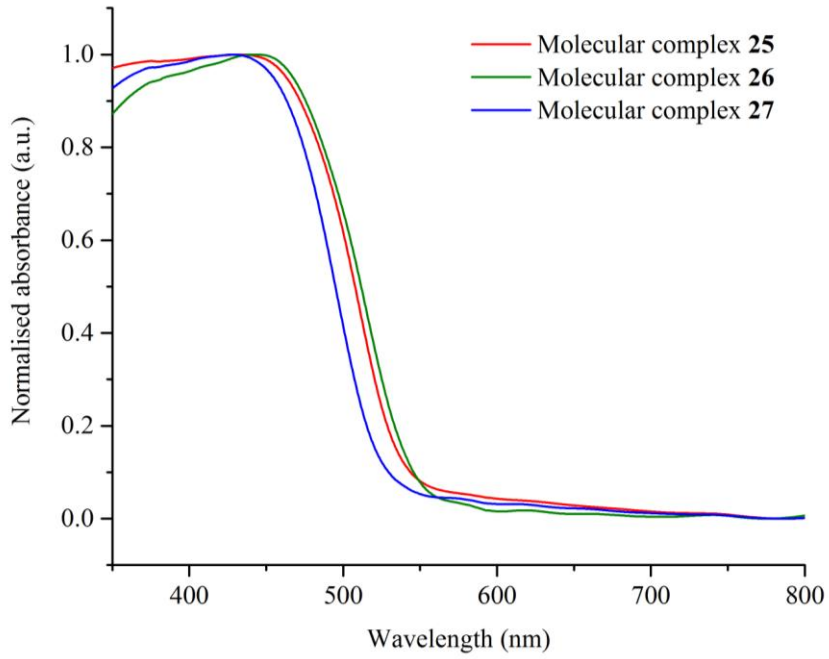

Figure 6.2 (a) Photographs of crystals of molecular complexes **25** (left), **26** (middle) and **27** (right); (b) single crystal UV-visible absorption spectra for molecular complexes **25**, **26** and **27** collected at room temperature.

The ΔpKa values for 2-IA 3,5-DNBA, 2-BrA 3,5-DNBA and 2-ClA 3,5-DNBA are −0.28, −0.29 and −0.16, respectively; on these grounds, proton transfer would not be expected to occur. Molecular complexes **25** and **26** both crystallise in the triclinic space group $P\bar{1}$, and molecular complex **27** in the orthorhombic space group Fdd2. In each of the molecular complexes, the 2-haloaniline and 3,5-dinitrobenzoic acid are present in a 1:1 ratio and both components are in their neutral forms; this contrasts with the 1:2 ratio of the 2-XA 3,4-DNBA complexes (Chapter 4). The asymmetric units contain one molecule of each component, and the 2-haloaniline molecules have whole molecule disorder over two positions. The crystal structures of the 2-IA and 2-BrA complexes are very similar, differing mainly in the orientations of the disordered 2-haloaniline molecules with respect to the dimers; the assembly of molecules in the 2-ClA complex is quite different, which must be due to the nature of the halogen.

In each complex, the molecules of 3,5-dinitrobenzoic acid form dimers *via* O-H···O hydrogen bonds of moderate strength between the carboxylic acid groups (Table 6.1); this acid dimer

synthon ($R_2^2(8)$ graph-set motif) is commonly observed for carboxylic acids.[40] The C-O bond lengths (1.252(7)/1.289(7) Å for molecular complex **25**; 1.251(3)/1.253(3) Å, for molecular complex **26**; 1.234(4)/1.298(4) Å for molecular complex **27**) are intermediate between distances expected for single and double bonds, which may indicate the presence of proton disorder.[37,39] However, due to the molecular disorder in the complexes, a model was employed with a single proton position, with the hydrogen atom located using Fourier difference maps and bound, with the use of a distance restraint, to the C-O group with the longer bond distance.

In molecular complexes **25** and **26**, the 3,5-DNBA dimer molecules are coplanar, but in molecular complex **27** there is an angle of ~13° between the mean ring planes of the dimer molecules. The carboxylic acid substituent groups are close to coplanar with the rings in each of the complexes (4° in molecular complex **25**, ~7° in molecular complex **26**, and ~2° in molecular complex **27**). As the nitro groups are not adjacent to any large substituents, they all have small torsion angles of less than 15° (~6°/11° in molecular complex **25**, ~0°/9° in molecular complex **26**, and ~5°/13° in molecular complex **27**); thus, the 3,5-DNBA molecules are all relatively planar.

Table 6.2 Hydrogen bond data (for bonds between 3,5-DNBA molecules) for molecular complexes **25** - **27** (N.B. hydrogen bonds involving 2-XA molecules are detailed in Table 6.3 due to the molecular disorder).

D-H···A	**D-H**	**H···A**	**D···A**	**<(DHA)**
Molecular complex **25**				
O2-H2···O1_#1	0.90(2)	1.71(2)	2.616(6)	177(10)
Molecular complex **26**				
O2-H2···O1_#1	0.92(2)	1.68(2)	2.584(3)	172(3)
C5-H5···O4_#2	0.93	2.66	3.560(4)	163
Molecular complex **27**				
O1-H1···O2_#1	0.88(3)	1.79(3)	2.649(3)	167(5)
C3-H3···O6_#2	0.93	2.725	3.338(4)	124

Molecular complex **25**: #1 -x+1,-y+1,-z

Molecular complex **26**: #1 -x,-y-1,-z+1 #2 -x,-y,-z

Molecular complex **27**: #1 -x+1/2,-y-1/2,z #2 x+1/4,-y-1/4,z-1/4

The 2-haloaniline molecules have whole-molecule disorder over two positions. The disorder models for each of the 2-haloaniline molecules are average models, and in each independent site in the crystal the molecule adopts one of the possible molecular orientations; the disorder is symmetry-independent in each case. In molecular complex **25**, the disordered sites have

occupancies of 0.539(2):0.461(2) (shown in purple and green, respectively, Figure 6.3 (a)); in molecular complex **26**, the disordered sites have occupancies of 0.692(1):0.308(1) (shown in pink and blue, respectively, in Figure 6.3 (b)); in molecular complex **27**, the disordered sites have occupancies of 0.796(3):0.204(3) (shown in blue and yellow, respectively, Figure 6.3 (c)). Across the three molecular complexes, the relative orientations of the disordered 2-haloaniline molecules are similar but not identical. The occupancy of the major site increases from 2-IA to 2-BrA to 2-ClA (~54% to ~69% to ~80%), which must be related to the nature of the halogen atom.

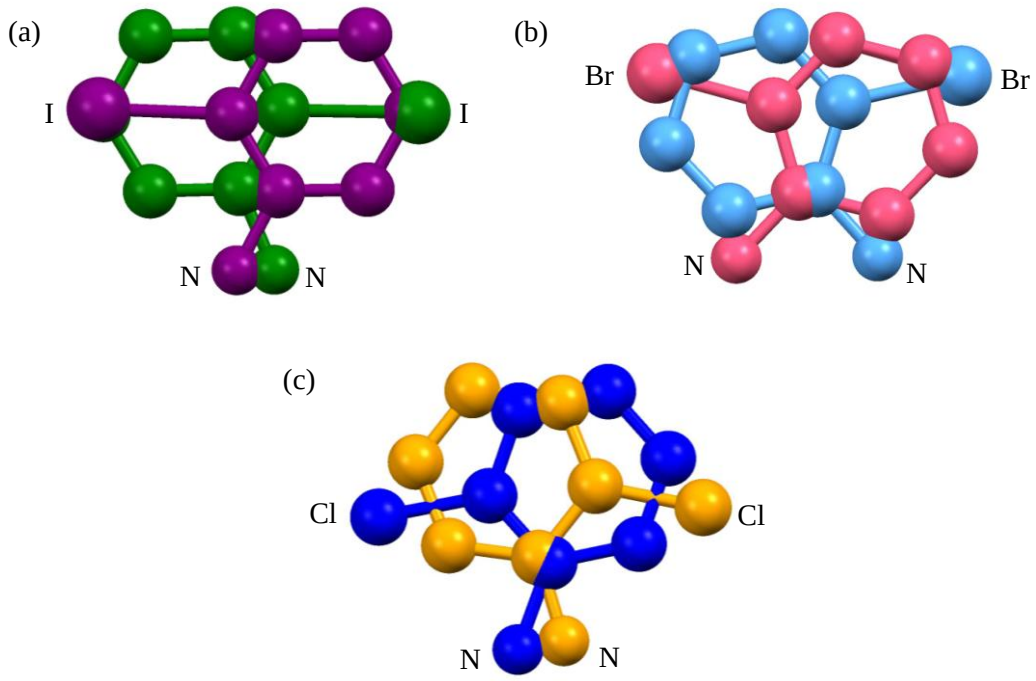

Figure 6.3 The molecular disorder of the 2-haloaniline molecules in (a) molecular complex **25**, where disorder occupancies of the 2-IA molecule are ~54:46 (purple/green); (b) molecular complex **26** where disorder occupancies of the 2-BrA molecule are ~69:31 (pink/blue); (c) molecular complex **27** where disorder occupancies of the 2-ClA molecules are ~80:20 (blue/yellow). Hydrogen atoms have been omitted for clarity.

The disordered 2-haloaniline molecules interact with the 3,5-DNBA dimers *via* a combination of hydrogen and halogen bonding interactions; the interactions vary depending on the nature of the halogen and the orientation adopted by the 2-haloaniline molecule in the site. Due to the disorder in the complexes, only the donor-acceptor distances are reported (Table 6.3). In molecular complex **25**, in both orientations the amine groups are in approximately the same position relative to the 3,5-DNBA chains, thus in both orientations the amine group is involved in three N-H···O hydrogen bonds to the nitro group O-atoms of two adjacent 3,5-DNBA molecules (**a** - **f**, Figure 6.4 (a), Table 6.3). There are no interactions between the iodine atoms

and the 3,5-DNBA molecules, but there are a number of weak C-H···O hydrogen bonds between the aromatic H-atoms of 2-IA and the carboxylic acid group O-atoms of the 3,5-DNBA dimer (Figure 6.4 (a)). The C-H···O hydrogen bonds are similar for both orientations of the 2-IA molecule, with C···O distances within the range ~3.3 - 3.5 Å. The similarity of the interactions in both orientations results in the occupancies of the disorder being close to 50:50, with the slightly stronger N-H···O bonds making the orientation shown in purple slightly more favourable.

In molecular complex **26**, when the 2-BrA molecule is in the orientation with the major occupancy (shown in pink, Figure 6.4 (b)) the amine group is involved in two N-H···O hydrogen bonds to the nitro group O-atom of a 3,5-DNBA molecule (**g** and **h**, Figure 6.4 (b), Table 6.3), and the Br atom is involved in a Br···O interaction with a nitro group O-atom (**j**, Figure 6.4 (b), Table 6.3), with a Br···O distance of 3.26(3) Å (less than the sum of the van der Waals radii of 3.37 Å). When the 2-BrA is in the orientation with the minor occupancy (shown in blue, Figure 6.4 (b)) the amine group is involved in a single N-H···O hydrogen bond with a nitro group O-atom (**i**, Figure 6.4 (b), Table 6.3). Similarly to **25**, there are C-H···O hydrogen bonds between the aromatic C-H groups of 2-BrA and the carboxylic acid group O-atoms of the 3,5-DNBA dimer with C···O distances within the range ~3.3 - 3.5 Å; there are two formed when the molecule is in the orientation with major occupancy and only one when the molecule is in the orientation with the minor occupancy. Overall, there are a greater number of interactions between the 2-BrA and 3,5-DNBA molecules when the 2-BrA is in the orientation with the major occupancy which offers an explanation for why it is more favourable.

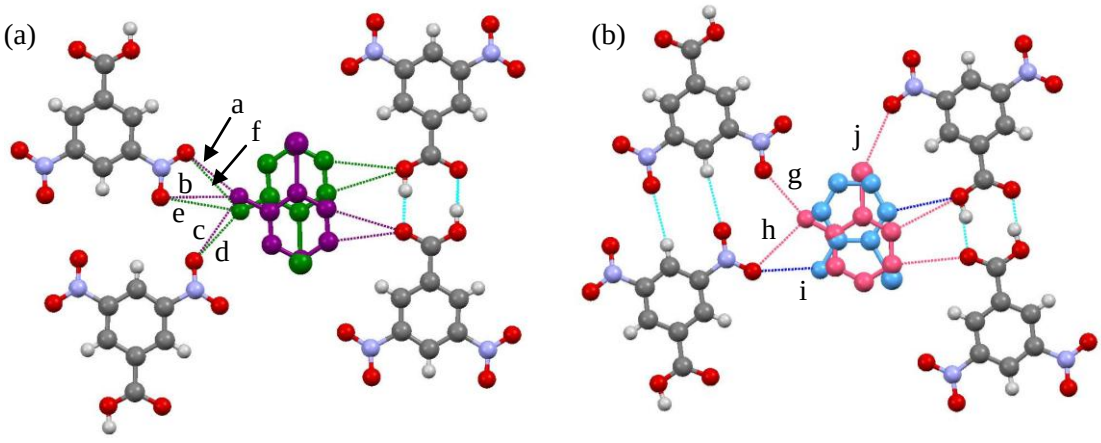

Figure 6.4 Intermolecular interactions between the 2-XA molecules and 3,5-DNBA molecules in (a) molecular complex **25** and (b) molecular complex **26**. Hydrogen atoms of 2-XA molecules have been omitted for clarity. Donor-acceptor distances for **a** - **j** are given in Table 6.3.

Table 6.3 Donor-acceptor distances for selected intermolecular interactions between 2-XA and the 3,5-DNBA molecules in molecular complexes **25** and **26** (refer to Figure 6.4 for labels **a**-**j**).

Bond type	**D-H···A or D···A**	**d(D···A)/ Å**
Molecular complex **25**		
a	N-H···O	2.95(2)
b	N-H···O	3.33(2)
c	N-H···O	3.51(2)
d	N-H···O	3.08(1)
e	N-H···O	3.40(1)
f	N-H···O	3.36(1)
Molecular complex **26**		
g	N-H···O	2.99(6)
h	N-H···O	3.20(6)
i	N-H···O	2.89(9)
j	Br···O	3.26(3)

In molecular complexes **25** and **26**, a similar planar two-dimensional sheet structure is formed, which consists of alternating channels of disordered 2-XA molecules and chains of 3,5-DNBA dimers. In **26**, the dimer units in the chains are linked through two equivalent weak C-H···O hydrogen bonds which form between an aromatic hydrogen (H5) and a nitro group oxygen (O4) molecules (Table 6.2). In **25**, there are no significant interactions linking the dimers in the chains.

Within the disordered channels of both complexes, there are interactions between pairs of 2-XA molecules (circled in Figure 6.5 (a)), which are dependent on whether the pair of molecules have the same orientation. In **25**, there is an I···I interaction (I···I = 3.854(3) Å c.f. the sum of the van der Waals radii of 3.96 Å) between molecules if they are in the same orientation (shown in purple); if they are in opposite orientations, there would be a C-H···I hydrogen bond (C···I = 3.879(8) Å). In **26**, there is a weak C-H···N hydrogen bond formed if the 2BrA molecules are in opposite orientations (C···N = 3.58(1) Å).

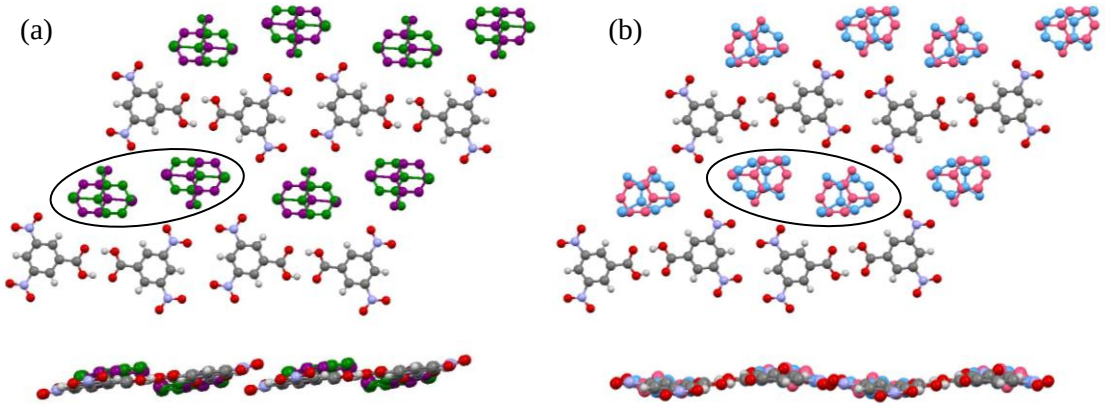

Figure 6.5 Planar two-dimensional sheet structures (viewed from above and side-on) formed in (a) molecular complex **25** and (b) molecular complex **26**. There are interactions between circled pairs of 2-XA molecules.

In molecular complex **27**, the structure is quite different, and the 2-ClA molecules interact with five surrounding 3,5-DNBA molecules. In both orientations, the amine group forms N-H···O hydrogen bonds to nitro group O-atoms (**a** - **e**, Figure 6.6, Table 6.4). When the 2-ClA molecule is in the orientation with major occupancy (shown in blue), the Cl atom is involved in a Cl···O interaction with a distance of 3.25(3) Å (marginally shorter than the sum of the van der Waals radii of 3.27 Å) (**f**, Figure 6.6, Table 6.4). When the 2-ClA molecule is in the orientation with the minor occupancy, there are no interactions involving the Cl atom that are shorter than the sum of the van der Waals radii. There are also a number of weak C-H···O hydrogen bonds between the aromatic H-atoms of 2-ClA and the carboxylic acid and nitro group O-atoms of the 3,5-DNBA molecules (Figure 6.6 (a)); the C···O distances are within the range ~3.3 - 3.6 Å. The greater strength of the N-H···O hydrogen bonds, and the Cl···O interaction, result in the higher occupancy of one orientation over the other.

The combination of interactions between 2-ClA molecules and 3,5-DNBA dimers results in a sheet structure (Figure 6.6 (b)). In molecular complex **27**, the dimers do not form linear chains and are rotated by ~60° with respect to each other; dimers are linked by O···O contacts (3.041(4) Å) between a nitro group O-atom and carboxylic acid group O-atoms, and a weak C-H···O hydrogen bond between an aromatic H-atom of one 3,5-DNBA molecule and a nitro group O-atom of an adjacent molecule (Table 6.2). Within the sheets, there is a single C-H···Cl (C···Cl = 3.564(3) Å) interaction between two 2-ClA molecules (circled in Figure 6.6 (b)) if the molecules are both in the orientation with the major occupancy (shown in blue). Unlike the 2-IA and 2-BrA complexes, the sheets are stepped (Figure 6.6 (c)).

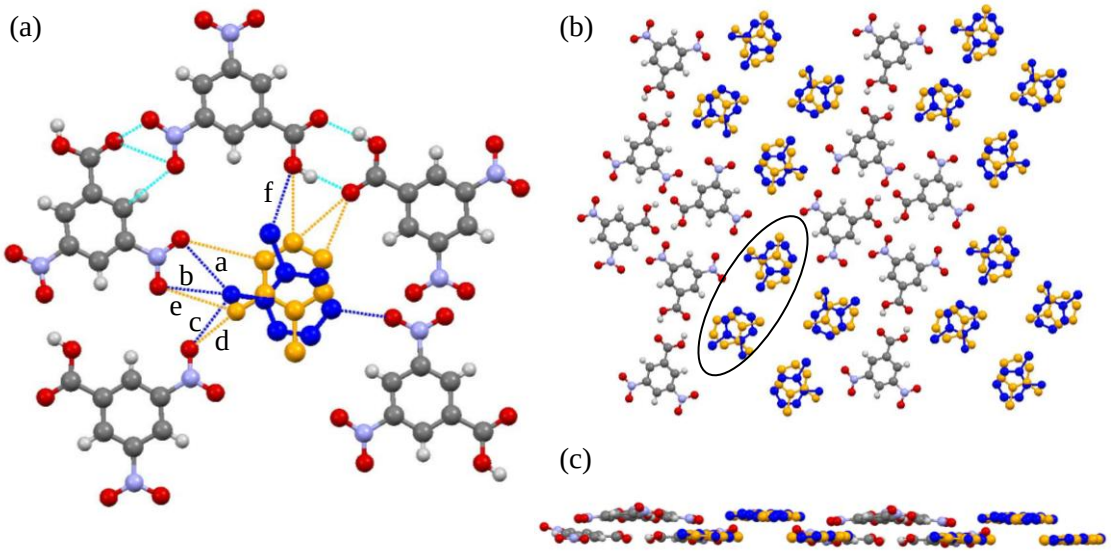

Figure 6.6 (a) Intermolecular interactions between the 2-ClA molecules and 3,5-DNBA molecules in molecular complex **27**. Hydrogen atoms of 2-ClA molecules have been omitted for clarity. Donor-acceptor distances for **a** - **e** (involving the amine and halogen substituents) are given in Table 6.4; (b) the sheet structure in molecular complex **27**, viewed perpendicular to the sheet. There are interactions between circled pairs of 2-ClA molecules. (c) The staggering of molecules within the sheets.

Table 6.4 Donor-acceptor distances for selected intermolecular interactions between 2-ClA and the 3,5-DNBA molecules in molecular complex **27** (refer to Figure 6.6 for labels **a**-**e**).

Bond type	D-H···A or D-H···A	d(D···A)/ Å
a	N-H···O	3.12(5)
b	N-H···O	3.04(6)
c	N-H···O	3.12(5)
d	N-H···O	2.82(2)
e	N-H···O	3.39(2)
f	Cl···O	3.25(3)

Within the sheets of each complex, the interactions between the 2-XA molecules and the hydrogen bonded 3,5-DNBA dimers are all weak or close to weak in nature (i.e. the hydrogen bonds are on the borderline between the moderate and weak classification, and the halogen bond distances are close to the sum of the van der Waals radii); this highlights the poor hydrogen bond donating ability of the NH_2 donor group. In each molecular complex, the planar sheets stack through aromatic donor···acceptor and halogen···π interactions, forming mixed stacks of alternating neutral aromatic donor (2-XA) and acceptor (3,5-DNBA) molecules, and these interactions dominate the packing arrangement. There are approximate intermolecular separations of ~3.40 Å, ~3.35 Å and ~3.35 Å between stacked 2-XA and 3,5-DNBA molecules in **25**, **26** and **27**, respectively; the ring planes of the stacked molecules are close to coplanar,

with angles of ~6°. There are two types of molecular overlap along the stack (shown by stacking types **i** and **ii**, Figure 6.7, left); the molecular overlap also differs with the orientation adopted by the disordered molecule, resulting in four possible types of molecular overlap (Figure 6.7, right).

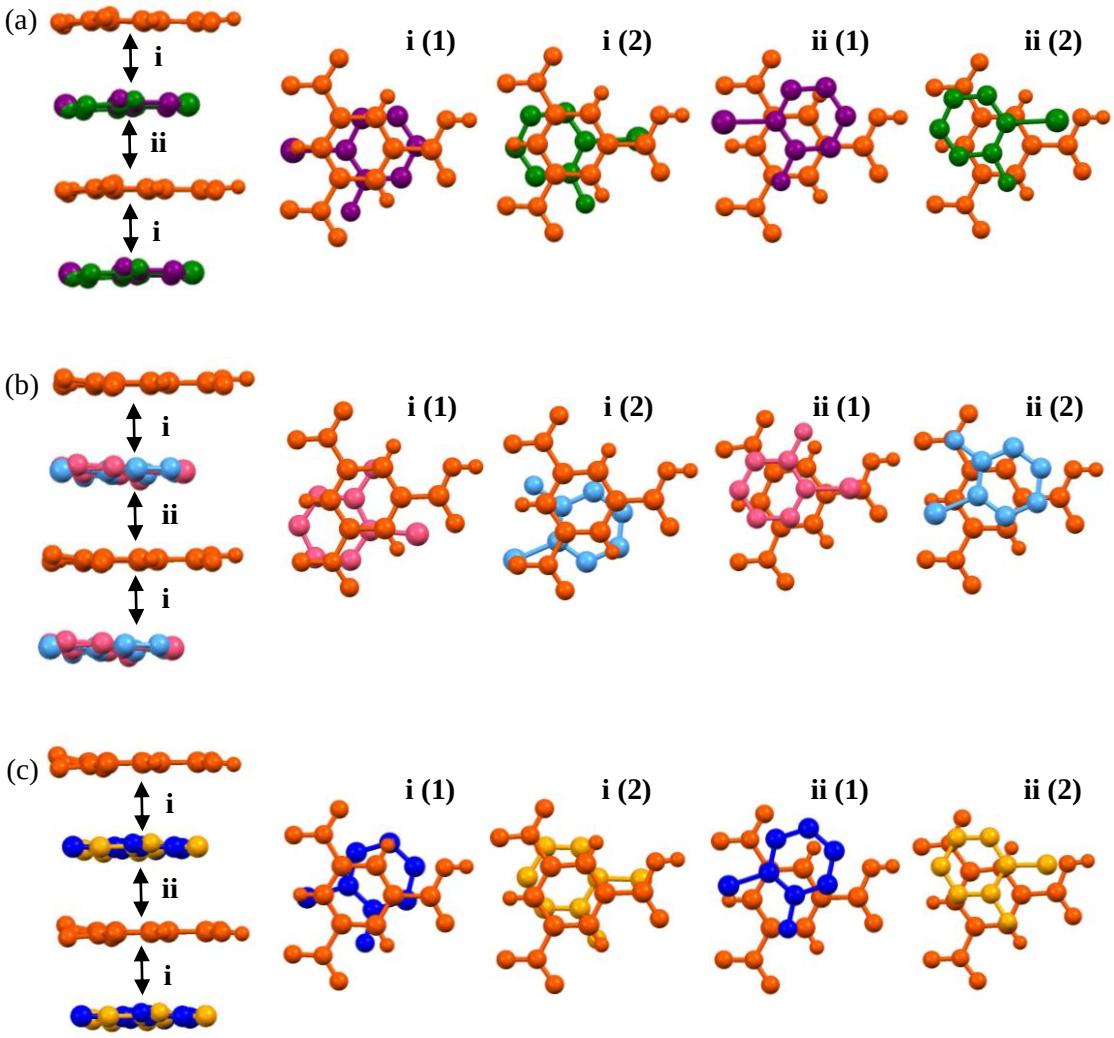

Figure 6.7 Stacking of alternate 2-XA and 3,5-DNBA molecules (left) and molecular overlap of 2-XA molecules above and below the dimer for both molecular orientations (right) in (a) molecular complex **25**, (b) molecular complex **26** and (c) molecular complex **27**. In each complex, the molecular overlap differs for the two possible orientations of the 2-XA (1 and 2). 3,5-DNBA molecules are shown in orange, and the disordered 2-XA molecules are shown in the colours according to Figure 6.3.

There is significant ring overlap between molecules in the stacks in each of the complexes; the amount of overlap and the stacking distances are similar across the complexes and for both molecular orientations. Halogen···π interactions are observed for both molecular orientations of the 2-XA molecule in each complex. In molecular complexes **25** and **27**, the stacking is very similar; the halogen sits directly in line with the carboxylic acid group of 3,5-DNBA when the molecule is in the orientation with the major occupancy. In **26**, there is also overlap of the

halogen and the carboxylic acid group, but in this complex it occurs when the molecule in the orientation with the minor occupancy.

The colours of the three complexes are very similar, seen visually and as shown in the visible absorption spectra (Figure 6.2). The crystal packing in the complexes is dominated by the aromatic donor···acceptor interactions, with the amount of molecular overlap similar for both possible orientations of the disordered 2-XA molecules; the hydrogen bonding between 2-XA and 3,4-DNBA in the sheets is only moderate to weak in nature. The colour in the solid-state can be attributed to $\pi\cdots\pi^*$ charge-transfer between the stacked neutral donor and acceptor molecules.

The 2-XA 3,5-DNBA molecular complexes do not exhibit temperature-dependent behaviour colour (unlike the 2-XA 3,4-DNBA complexes, Chapter 4, where the presence of space in the crystal packing allowing for molecular rearrangement). For comparison, the volume of crystal space available to the disordered 2-haloaniline molecules in **25** - **27** was calculated using Mercury,[201] similarly to those complexes in Chapter 4. In molecular complex **25**, the average volume available to each 2-IA molecule is 194.80 $Å^3$ compared to 166.93 $Å^3$ for an ordered 2-IA molecule; in molecular complex **26**, the average volume available to each 2-BrA molecule is 168.06 $Å^3$ compared to 158.20 $Å^3$ for an ordered 2-BrA molecule; in molecular complex **27**, the average volume available to each 2-ClA molecule is 167.41 $Å^3$ compared to 156.32 $Å^3$ for an ordered 2-ClA molecule. Thus in each molecular complex there is an increase in the volume of crystal space attributed to the 2-XA molecule compared to the fully ordered case. The percentage increases in volume for the disordered sites are 16.7%, 6.2% and 6.7% in **25**, **26** and **27** respectively which compare to 19.4%, 16.4% and 20.1% in the corresponding 2-XA 3,4-DNBA complexes. Therefore, there is less volume available to the 2-XA molecules in the 3,5-DNBA complexes, particularly in **26** and **27**, which will restrict reorientation of the disordered molecules. This can be attributed to the 1:1 stoichiometry of the 2-XA 3,5-DNBA complexes, compared to the 1:2 stoichiometry of the 2-XA 3,4-DNBA complexes. In the latter, as discussed in Chapter 4, the 3,4-DNBA molecules form a robust host framework; due to the 1:2 stoichiometry, there is only a single 2-XA molecule to each 3,4-DNBA dimer, thus stacking occurs between 2-XA and the centre of the 3,4-DNBA dimers to form a mixed stack. This has the effect of increasing the acceptor part of the mixed stack and the volume of space available to the donor. In contrast, in the 2-XA 3,5-DNBA complexes presented here, the 3,5-DNBA molecules do not form a robust dimer framework, and the 1:1 stoichiometry means that stacking occurs between 2-XA and 3,5-DNBA molecules, rather than with dimers, to form linear stacks. While disorder is observed in the mixed stacks due to the different sizes of the donor and

acceptor, their crystal packing is more efficient, thus there is less potential for molecular reorientation.

6.1.3 Summary and discussion

The co-crystallisation experiments of 2-iodoaniline, 2-bromoaniline and 2-chloroaniline with 3,5-dinitrobenzoic acid resulted in the formation of a single 1:1 molecular complex of each 2-haloaniline, each complex yielded as yellow crystals. In each molecular complex, the molecular components are in their neutral forms, as predicted from the negative ΔpKa values for each pair. The 2-haloaniline molecule is disordered over two well-defined positions, and the disorder is likely to be present due to competition between the hydrogen bond and halogen bond interactions and a greater number of acceptor atoms than donor atoms. The 3,5-DNBA molecules surrounding each 2-XA molecule mean there are O-atoms of at least four nitro groups with which to form hydrogen or halogen bonds, in addition to the carboxylic acid group O-atoms; this compares to two hydrogen bond donors (amine group) and a single halogen atom.
In general, crystal packing is driven to produce the most efficient and densely packed arrangement of molecules in a solid; however, molecular disorder has been observed in mixed stack CT complexes as a result of inefficient packing, particularly where there are no strong interactions to favour a single, ordered position. However, unlike the 2-XA 3,4-DNBA molecular complexes (**1**, **4** and **6**) described in Chapter 4, the complexes do not show temperature-dependent colour, which was related in the previous study to the availability of space within the crystal packing that allowed molecular rearrangement. There is less space available to the 2-XA molecules in the 3,5-DNBA complexes, and the environment around the disordered molecules differs considerably to that in the 3,4-DNBA complexes. The smaller amount of crystal space can be attributed to the difference in the stoichiometric ratios; in the 2-XA 3,5-DNBA complexes, the 1:1 ratio means that stacking occurs between 2-XA and 3,5-DNBA molecules (rather than mixed stacks of 2-XA and 3,4-DNBA dimers), resulting in a slightly more efficient crystal packing.

The carboxylic acid groups of the 3,5-DNBA molecules are all coplanar with the ring and the molecules form dimers, but they do not form a network as observed between 3,4-DNBA dimers in the complexes in Chapter 4. The 2-IA and 2-BrA complexes have very similar crystal structures, forming planar sheets of alternating 3,5-DNBA and disordered 2-XA channels; the two structures differ mainly by the orientations of the 2-XA molecules with respect to the 3,5-DNBA dimers. The 2-ClA complex is quite different, with the molecules in each sheet not coplanar. However, the molecular complexes all have layered structures, forming mixed stacks of alternating aromatic donor (2-XA) and acceptor (3,5-DNBA) molecules; the colour in the

solid-state can be attributed to $\pi\cdots\pi^*$ charge-transfer between the aromatic donor and acceptor. The stacking distances and molecular overlap are very similar across the series of complexes; in each case there is a similar amount of ring overlap, and the halogen atom sits above the carboxylic acid group. The comparable stacking is reflected in the similarity of the visible colour and absorption spectra of the single crystals, with the nature of the halogen not altering the optical properties. It is also possible that the molecular disorder present plays a role in lending these complexes their colour in the solid-state.

6.2 Molecular disorder and proton transfer in 2-halo-4-methylaniline 3,5-dinitrobenzoic acid complexes

6.2.1 Experimental details

Molecular complexes **28** - **30** were obtained *via* the method of slow evaporation (§3.1) using a 1:1 stoichiometric molar ratio of the 2-halo-4-methylaniline and 3,5-dinitrobenzoic acid; crystallisation trials employed a range of solvents and evaporation temperatures. Single crystal X-ray diffraction experiments were carried out according to the procedures outlined in §3.2. Crystallographic data are given in Table 6.5 and refinement details are reported in Appendix A6.

2-iodo-4-methylaniline 3,5-dinitrobenzoic acid (28)

Molecular complex **28** was synthesised from ethanol at ambient temperature; deep red block crystals were obtained. Single crystal X-ray diffraction data were collected at 150 K using a Rigaku Oxford Diffraction Xcalibur diffractometer. The structure was solved by direct methods using SHELXS-2013[192] and refined using SHELXL-2014,[198] both within the WinGX program suite.[200]

2-bromo-4-methylaniline 3,5-dinitrobenzoic acid (29)

Molecular complex **29** was synthesised from ethanol at ambient temperature; yellow plate crystals were obtained. Single crystal X-ray diffraction data were collected at 150 K using a Rigaku Oxford Diffraction Xcalibur diffractometer. The structure was solved by direct methods using SHELXS-2013[192] and refined using SHELXL-2014,[198] both within the WinGX program suite.[200]

2-chloro-4-methylanilinium 3,5-dinitrobenzoate (30)

Molecular complex **30** was synthesised from 2-propanol at ambient temperature; colourless needle crystals were obtained. Single crystal X-ray diffraction data were collected at 150 K using a Rigaku Oxford Diffraction Xcalibur diffractometer. The structure was solved by direct methods using SHELXS-2013[192] and refined using SHELXL-2014,[198] both within the WinGX program suite.[200]

Table 6.5 Crystallographic data for molecular complexes **28**- **30**

	28	**29**	**30**
Formula	(C_7H_8NI) $(C_7H_4N_2O_6)$	(C_7H_8NBr) $(C_7H_4N_2O_6)$	(C_8H_8NCl) $(C_7H_4N_2O_6)$
M/g mol^{-1}	445.17	384.15	353.72
T/K, Radiation	150(2), Mo Kα	150(2), Mo Kα	150(2), Mo Kα
Space Group	$P\bar{1}$	$P\bar{1}$	$P2_1$
a/Å	7.5367(7)	7.1526(4)	10.1511(5)
b/Å	8.3228(9)	7.2243(4)	5.7150(3)
c/Å	13.5151(15)	14.9898(16)	13.6754(7)
α/°	76.906(9)	95.730(6)	90
β/°	80.597(9)	90.402(6)	107.258(6)
γ/°	78.951(9)	91.404(4)	90
V/Å	804.00(15)	770.42(10)	757.64(7)
Z	2	2	2
ρ_{cal}/ g cm^{-3}	1.839	1.716	1.550
μ/mm^{-1}	2.028	2.706	0.290
θ Range/°	3.243 - 26.372	3.736 - 29.133	3.892 - 26.369
Ref Collected	8149	8196	15433
Independent	3295	3560	3087
Observed>2σ	2237	1837	2699
Rint	0.0379	0.0625	0.0474
Completeness %	99.8	99.1	99.6
Parameters	185	190	227
Flack parameter	-	-	0.02(4)
GooF	1.024	1.046	1.043
R_1 (obs)	0.0792	0.0830	0.0378
R_1 (all)	0.1187	0.1769	0.0485
wR2 (all)	0.1804	0.1508	0.0775
$\rho_{max,min}$/e Å^{-3}	2.153, -1.311	0.611, -0.392	0.189, -0.233

6.2.2 2-halo-4-methylaniline 3,5-dinitrobenzoic acid complexes (28 - 30)

2-I-4-MA is a light grey solid, 2-Br-4-MA and 2-Cl-4-MA are both light brown liquids, and 3,5-dinitrobenzoic acid is a light yellow solid; dissolution of the 2-X-4-MA with 3,5-DNBA resulted in pale yellow solutions in each case. ΔpKa values for 2-I-4-MA 3,5-DNBA, 2-Br-4-MA 3,5-DNBA and 2-Cl-4-MA 3,5-DNBA are 0.15, 0.15 and 0.27, respectively; these

values lie in the salt-cocrystal continuum (although very close to the lower limit), thus proton transfer may or may not occur.

The molecular complexes of 2-I-4-MA 3,5-DNBA (**28**) and 2-Br-4-MA 3,5-DNBA (**29**) form as deep red block and yellow plate crystals, respectively, and the molecular complexes are both neutral. The molecular complex of 2-Cl-4-MA 3,5-DNBA (**30**) is yielded as colourless needle crystals, and the molecular species are ionic. It was not possible to obtain a neutral form of 2-Cl-4-MA 3,5-DNBA, and similarly not possible to obtain ionic forms of 2-I-4-MA 3,5-DNBA and 2-Br-4-MA 3,5-DNBA. The solution colours are the same for all three materials, thus the origin of colour (or lack of colour) in the crystals therefore lies in the solid-state, with a dependence on the nature of the halogen and the ionisation states of the molecular components.

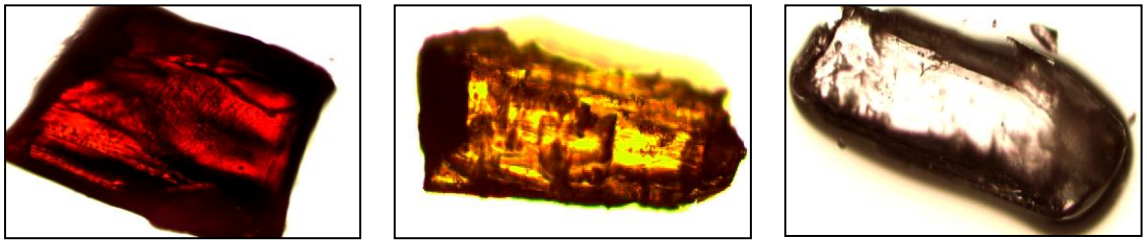

Figure 6.8 Photographs of crystals of molecular complexes **28** (left), **29** (middle) and **30** (right).

6.2.2.1 Neutral, disordered molecular complexes of 2-iodo-4-methylaniline and 2-bromo-4-methylaniline with 3,5-dinitrobenzoic acid (28 and 29)

Molecular complexes **28** and **29** both crystallise in the triclinic space group $P\bar{1}$. As for the 2-XA 3,5-DNBA complexes (§6.1.2), the 2-halo-methylaniline and 3,5-dinitrobenzoic acid are present in a 1:1 ratio and both molecular components are in their neutral forms; this contrasts with the 1:2 stoichiometry of the 2-X-4-MA 3,4-DNBA complexes. The asymmetric units contain one molecule of each component, and in both molecular complexes the 2-halo-methylaniline molecules have whole molecule disorder over two positions. The crystal structures of the 2-I-4-MA and 2-Br-4-MA complexes are very similar, differing mainly in the orientations of the haloaniline molecules with respect to the dimers; furthermore, the overall crystal packing is much like that observed in the corresponding 2-IA and 2-BrA complexes (**25** and **26**).

The 3,5-dinitrobenzoic acid molecules form dimers *via* O-H···O hydrogen bonds of moderate strength between the carboxylic acid groups (Table 6.6). The C-O bond lengths (1.253(8)/1.274(8) Å for molecular complex **28** and 1.251(7)/1.278(7) Å for molecular complex **29**) are intermediate between distances expected for single and double bonds, which

may indicate the presence of proton disorder.[37,39] However, due to the molecular disorder in the complexes, a model was employed with a single proton position, with the hydrogen atom located using Fourier difference maps and bound to the C-O group with the longer bond distance.

The molecules of the 3,5-DNBA dimers are equivalent and coplanar. In each molecular complex, the carboxylic acid substituent groups are close to coplanar with the benzene rings (~5° in molecular complex **28** and ~3° in molecular complex **29**). The nitro groups are twisted out of the ring planes by ~1°/8° in molecular complex **28** and ~5°/6° in molecular complex **29**; thus, the 3,5-DNBA molecules are relatively planar molecules. There are no hydrogen bonds formed between adjacent dimers in molecular complex **28**, and instead there are two equivalent short O···O contacts (O···O = 2.84(1) Å) linking dimers to form a chain, as observed in 2-IA 3,5-DNBA (**25**). In molecular complex **29**, there are two equivalent weak C-H···O hydrogen bonds (Table 6.6) formed between an aromatic hydrogen (H5) and a nitro group oxygen (O5) resulting in a hydrogen bonded chain of 3,5-DNBA molecules, as observed in 2-BrA 3,5-DNBA.

Table 6.6 Hydrogen bond data (for bonds between 3,5-DNBA molecules) for molecular complexes **28** and **29** (N.B. hydrogen bonds involving 2-X-4-MA molecules are detailed in Table 6.7 due to the molecular disorder).

D-H···A	**D-H**	**H···A**	**D···A**	**<(DHA)**
Molecular complex **28**				
O2-H2···O1_#1	0.89(2)	1.73(2)	2.621(6)	177(7)
Molecular complex **29**				
O2-H2···O1_#1	0.89(2)	1.73(2)	2.614(5)	174(5)
C5-H5···O5_#2	0.93	2.88	3.780(7)	165

Molecular complex **28**: #1 -x+1,-y+1,-z +1

Molecular complex **29**: #1 -x+2,-y+1,-z+1 #2 -x+1,-y+1,-z +1

The 2-I-4-MA and 2-Br-4-MA molecules are disordered over two positions and the disorder is symmetry-independent; in each site in the crystal that molecule can adopt one of the two possible orientations (Figure 6.9). In molecular complex **28**, the disorder has occupancies of 0.595(2):0.405(2) (shown in purple and green, respectively, Figure 6.9 (a)) and in molecular complex **29** the occupancies are 0.660(2):0.340(2) (shown in pink and blue, respectively, Figure 6.9 (b)). The relative orientations of the disordered 2-halo-4-methylaniline molecules are quite different in the two molecular complexes. The occupancy of the major site increases from 2-I-4-MA to 2-Br-4-MA (~60% to ~66%), which must be related to the halogen atom type.

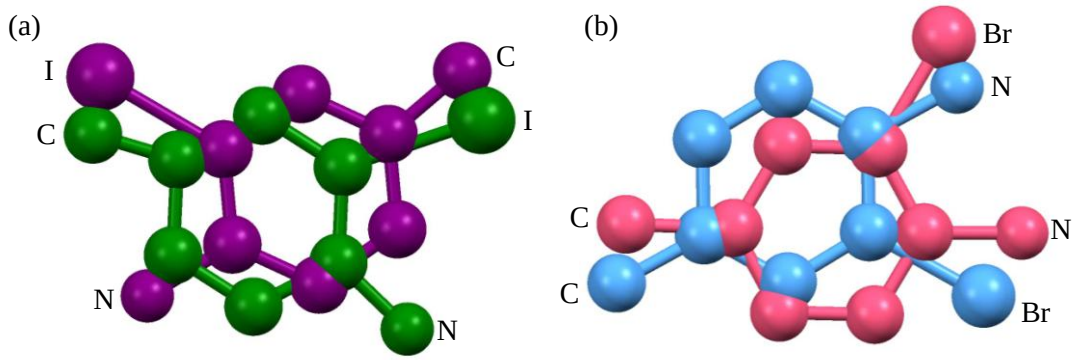

Figure 6.9 The molecular disorder of the 2-halo-4-methylaniline molecules in (a) molecular complex **28** where disorder occupancies of the 2-I-4-MA molecule are ~60:40 (purple/green); (b) molecular complex **29** where disorder occupancies of the 2-Br-4-MA molecule are ~66:34 (pink/blue). Hydrogen atoms have been omitted for clarity.

The disordered 2-halo-4-methylaniline molecules interact with the 3,5-DNBA dimers *via* a combination of hydrogen and halogen bonding interactions; as for 2-XA 3,5-DNBA, the interactions vary depending on both the nature of the halogen and the orientation adopted by the 2-halo-4-methylaniline molecule in the site. Due to the disorder in the complexes, only the donor-acceptor distances are reported (Table 6.7). In molecular complex **28**, in the orientation with the major occupancy (shown in purple, Figure 6.10 (a)) there are two N-H···O hydrogen bonds formed between the amine group and two O-atoms of the same nitro group (**a** and **b**, Figure 6.10 (a), Table 6.7); this compares to a single N-H···O hydrogen bond formed to a nitro group O-atom (**c**, Figure 6.10 (a), Table 6.7) when in the orientation with the minor occupancy (shown in green, Figure 6.10 (a)). In both orientations, a C-I···O halogen bond is formed between the iodine atom and a nitro group O-atom (**d** and **e**, Figure 6.10 (a), Table 6.7) with I···O distances of 3.201(6) Å and 3.480(7) Å for the major and minor orientations, respectively (c.f. the sum of the van der Waals radii of 3.50 Å). The methyl groups in both orientations are involved in weak C-H···O hydrogen bonds to either carboxylic acid or nitro group O-atoms (**f** - **h**, Figure 6.10 (a), Table 6.7). Two bonds are formed when in the orientation with the major occupancy, compared to a single bond in the alternate orientation. There are also weak C-H···O hydrogen bonds between the aromatic C-H groups of 2-I-4-MA and nitro group O-atoms of the 3,5-DNBA molecules, with C···O distances in the range ~3.5 - 3.7 Å. Overall, the interactions are very similar for the 2-I-4-MA molecule in either orientation, however the additional N-H···O and C-H···O hydrogen bonds and stronger I···O interaction for the orientation with the major occupancy (shown in purple) would account for it being slightly more favourable.

In molecular complex **29**, in both orientations a single N-H···O hydrogen bond is formed between the amine group and nitro group oxygen atoms (**i** and **j**, Figure 6.10 (b), Table 6.7); these are much weaker than those in **28**. The bromine atom is involved in a Br···O interaction

with a nitro group O-atom (**k** and **l**, Figure 6.10 (b), Table 6.7). The methyl groups in both orientations form a single weak C-H···O hydrogen bond to the same nitro group (**m** and **n**, Figure 6.10 (b), Table 6.7); there are also a number of weak C-H···O hydrogen bonds between the aromatic C-H groups of 2-Br-4-MA and nitro and carboxylic acid group O-atoms of the 3,5-DNBA molecules, with C···O distances in the range ~3.3 - 3.5 Å. Overall, the interactions are very similar in number and strength for both orientations, but the slightly stronger N-H···O hydrogen bond for the orientation shown in pink may account for it having the higher occupancy of the two.

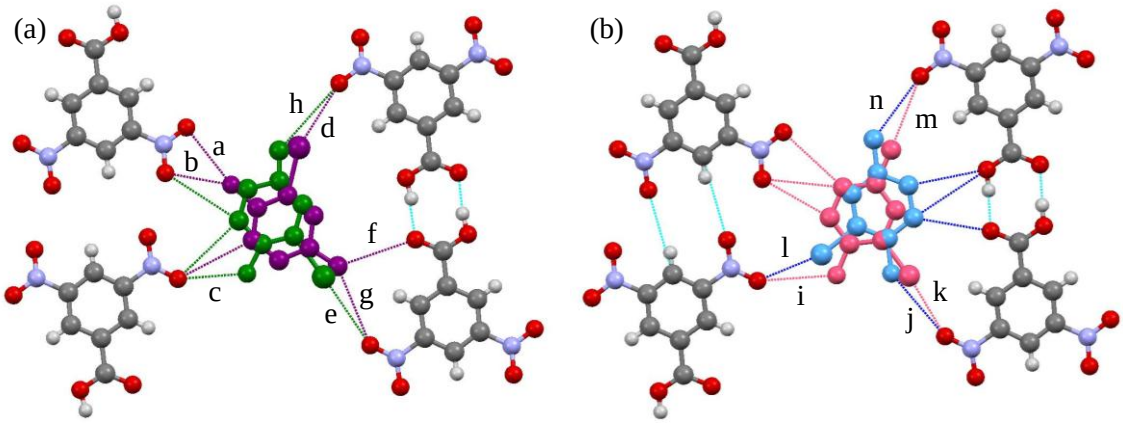

Figure 6.10 Intermolecular interactions between the 2-X-4-MA molecules and 3,5-DNBA molecules in (a) molecular complex **28** and (b) molecular complex **29**. Hydrogen atoms of 2-X-4-MA molecules have been omitted for clarity. Donor-acceptor distances for **a** - **n** are given in Table 6.7.

Despite the different disorder models in **28** and **29**, a similar two-dimensional sheet structure is formed in both molecular complexes, which is the same as that formed in the 2-IA and 2-BrA molecular complexes, **25** and **26**. The sheets are made up of alternating channels of disordered 2-X-4-MA molecules and chains of 3,5-DNBA dimers. Within the disordered channels of both complexes there are interactions between pairs of 2-X-4-MA molecules (circled in Figure 6.11). In **28**, there are N-H···I interactions if the two molecules are both in the orientation with the minor occupancy (N···I = 3.29(2) Å). In **29**, there are N-H···N interactions between adjacent amine groups if they are both in the orientation with the major occupancy (N···N = 3.26(1) Å) or if they are in opposite orientations (N···N = 3.32(2) Å). Similarly to the 2-XA 3,5-DNBA complexes, the interactions between the 2-X-4-MA molecules and the 3,5-DNBA dimers in the sheets are all weak or close to weak in nature (i.e. hydrogen bonds on the borderline between moderate and weak, and halogen bonds with distances close to the sum of the van der Waals radii); this highlights the poor hydrogen bond donating ability of the N-H donor groups.

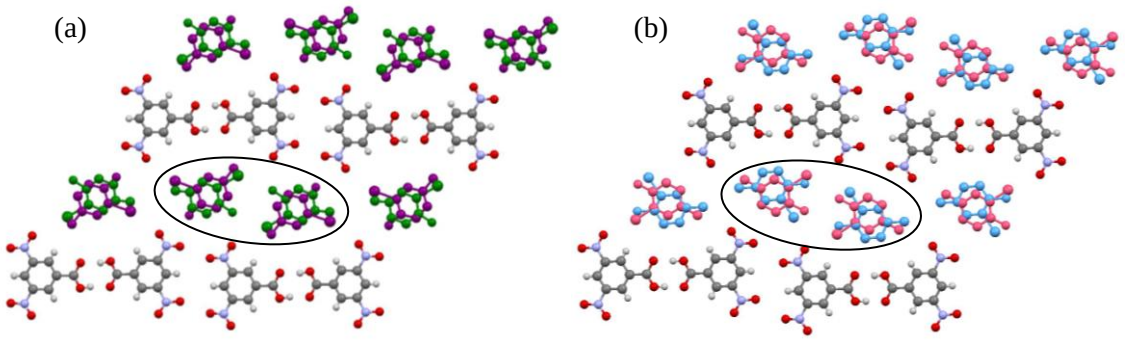

Figure 6.11 Planar two-dimensional sheet structures formed in (a) molecular complex **28** and (b) molecular complex **29**. There are interactions between circled pairs of 2-X-4-MA molecules.

Table 6.7 Donor-acceptor distances for selected intermolecular interactions between 2-X-4-MA and the 3,5-DNBA dimers in molecular complexes **28** and **29** (refer to Figure 6.10 for labels **a** - **n**).

Bond type	D-H···A or D···A	d(D···A)/ Å
Molecular complex **28**		
a	N-H···O	3.11(1)
b	N-H···O	2.86(1)
c	N-H···O	2.95(1)
d	I···O	3.201(6)
e	I···O	3.480(7)
f	C-H···O	3.48(1)
g	C-H···O	3.60(2)
h	C-H···O	3.80(2)
Molecular complex **29**		
i	N-H···O	3.34(1)
j	N-H···O	3.59(1)
k	Br···O	3.079(4)
l	Br···O	2.920(5)
m	C-H···O	3.41(1)
n	C-H···O	3.35(2)

In both molecular complexes, the planar sheets stack through aromatic donor···acceptor interactions, in addition to halogen···π interactions in **28**, forming mixed stacks of alternating donor (2-X-4-MA) and acceptor (3,5-DNBA) molecules. The planes of the stacked molecules are close to parallel, with an angle of ~3° between the mean ring planes; there is an approximate intermolecular separation of ~3.35 Å between stacked molecules in both **28** and **29**. There are two types of molecular overlap along the stack (shown by stacking types **i** and **ii**, Figure 6.12,

left); the molecular overlap also differs with the orientation adopted by the disordered molecule, resulting in four possible types of molecular overlap in each complex (Figure 6.12, left).

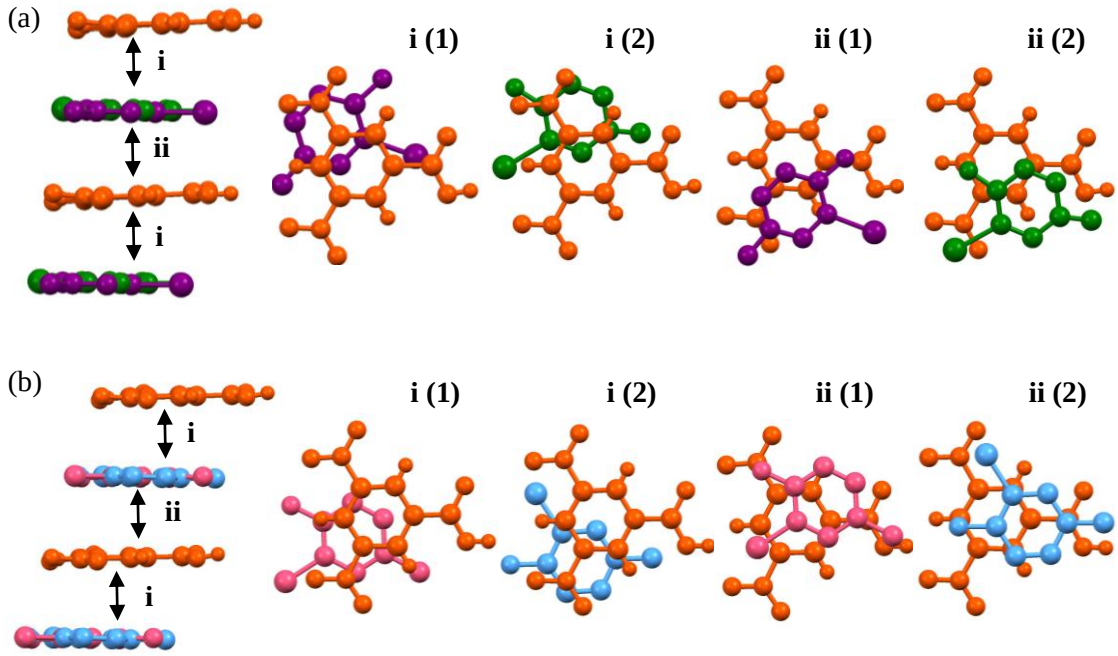

Figure 6.12 Stacking of alternate 2-X-4-MA and 3,5-DNBA molecules (left) and molecular overlap of 2-X-4-MA molecules above and below the dimer for both molecular orientations (right) in (a) molecular complex **28** and (b) molecular complex **29**. . In each complex, the molecular overlap differs for the two possible orientations of the 2-X-4-MA (1 and 2). 3,5-DNBA molecules are shown in orange, and the disordered 2-X-4-MA molecules are shown in the colours according to Figure 6.9.

There is a similar amount of ring overlap between stacked molecules in both molecular complexes, and the stacking distances are equal. However, unlike the 2-XA 3,5-DNBA complexes, the solid-state colour is dependent on the nature of the halogen (Figure 6.8). The stacks of molecular complex **28** are more linear than those in **29**, where the stacked molecules appear more offset. In molecular complex **28**, the iodine overlaps with the carboxylic acid group in one of the orientations (Figure 6.12 (a), **i(1)**); in molecular complex **29**, there are no interactions between the bromine atoms and the 3,5-DNBA molecules within the stacks.

The crystal packing in the complexes is dominated by the aromatic donor···acceptor interactions, and the colour can be attributed to π···π* charge-transfer between the stacked neutral donor and acceptor molecules. Charge-transfer is very sensitive to the electronic properties of the donor and acceptor moieties and to the relative orientations of the overlapping donor and acceptor molecules; thus the nature of halogen and the difference in the molecular orientations will affect the optical properties. In addition, it is possible that hydrogen bond strength plays a role; in **28**, the N-H···O hydrogen bonds are much stronger than in **29**. The pair

of complexes has demonstrated how simple exchange of the halogen substituent can tune the colour properties, however, further work is required in order to understand the electronic transitions involved and the difference in the colour.

6.2.2.2 Ionic molecular complex of 2-Cl-4-MA 3,5-DNBA (30)

The molecular complex of 2-Cl-4-MA 3,5-DNBA, **30**, has a very different structure and colour properties to the disordered 2-I-4-MA and 2-Br-4-MA complexes (**28** and **29**). Molecular complex **30** crystallises in the non-centrosymmetric monoclinic space group $P2_1$ and the two components are present in a 1:1 ratio; a proton is transferred from the carboxylic acid group of 3,5-DNBA to the amine group of 2-Cl-4-MA, thus both species are present in their ionic form. The asymmetric unit contains one of each of the ions. In the 3,5-dinitrobenzoate anion, the C-O distances of the carboxylate group are intermediate between those expected for single and double bonds, which is consistent with a delocalisation of the charge across the group (1.242(4) Å/1.271(3) Å). The carboxylate group is twisted out of the ring plane by ~13°, and the nitro groups have torsion angles of ~9° and ~12°. Three moderate strength N-H···O hydrogen bonds form between the NH_3^+ group of 2-Cl-4-MA and the O-atoms of the 3,5-DNBA carboxylate groups, resulting in $R_4^3(10)$ hydrogen bonded rings in which both of the carboxylate group oxygen atoms, O1 and O2, act as hydrogen bond acceptors, with O2 accepting two hydrogen bonds (Figure 6.13, Table 6.8). The N3-H3B···O1 hydrogen bond is supported by a weak hydrogen bond from an aromatic C-H group adjacent to the anilinium group (C···O distance = 3.282(4) Å).

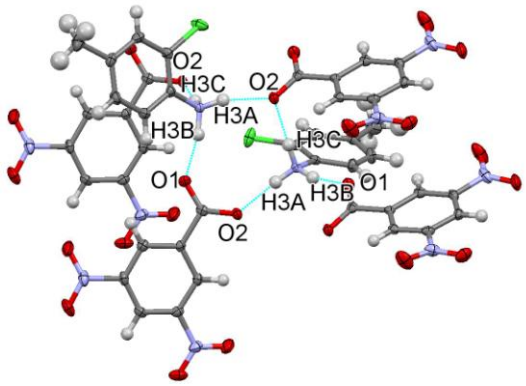

Figure 6.13 The hydrogen bonded ring in molecular complex **30**, formed through moderate strength N-H···O hydrogen bonds between the hydrogen atoms of NH_3^+ and carboxylate group oxygen atoms.

Table 6.8 Hydrogen bond data for molecular complex **30**

D-H···A	D-H	H···A	D···A	<(DHA)
N3-H3A···O2_#1	0.92(3)	1.86(3)	2.744(3)	162(3)
N3-H3B···O1_#2	0.97(4)	1.78(4)	2.722(4)	165(3)
N3-H3C···O2_#3	0.94(4)	1.82(4)	2.757(4)	171(3)

#1 x,y-1 z #2 -x+1,y-3/2,-z+2 #3 -x+1,y-1/2,-z+2

A weak C-H···Cl hydrogen bond is formed between an aromatic C-H of the 3,5-DNBA anion and the chlorine atom of 2-Cl-4-MA (C···Cl = 3.869(3) Å); in addition, one of the methyl C-H groups forms a weak C-H···Cl hydrogen bond with the chlorine atom of an adjacent 2-Cl-4-MA (C···Cl = 3.731(5) Å) and a weak C-H···O hydrogen bond with a carboxylate group O-atom of an adjacent 3,5-DNBA molecule (C···O = 3.590(4) Å). There are also O···O and O···π interactions between the nitro groups of adjacent 3,5-DNBA. Overall, the three-dimensional nature of the hydrogen bonding results in a non-layered structure with alternating sections of 2-Cl-4-MA and 3,5-DNBA molecules (Figure 6.14).

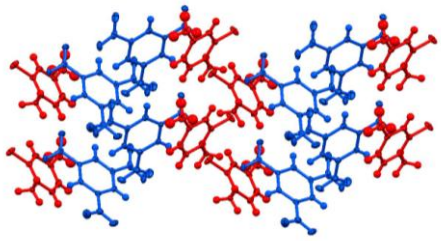

Figure 6.14 The non-layered crystal packing in molecular complex **30** with projection down the crystallographic *a*-axis. 2-Cl-4-MA molecules are shown in red and 3,5-DNBA molecules are shown in blue.

6.2.3 Summary and discussion

The co-crystallisation experiments of 2-iodo-4-methylaniline, 2-bromo-4-methyl-aniline and 2-chloro-4-methylaniline with 3,5-dinitrobenzoic acid resulted in the formation of a single 1:1 molecular complex of each 2-haloaniline. The ΔpKa values for all three 2-X-4-MA/3,5-DNBA pairs fall in the salt-cocrystal continuum, and therefore proton transfer may or may not occur; two neutral complexes and one ionic complex were formed. The slightly higher ΔpKa value for the 2-Cl-4-MA 3,5-DNBA complex may provide an explanation for the formation of an ionic complex. The three complexes demonstrate how solid-state colour may be tuned through simple exchange of the halogen, and through introduction of a methyl group. The 2-I-4-MA and 2-Br-4-MA complexes have very similar crystal structures to the corresponding 2-IA and 2-BrA complexes, and are yielded as red and yellow crystals, respectively; the molecular components

are neutral and there is disorder of the 2-halo-4-methylaniline over two well-defined positions which is likely to be present due to competition to form hydrogen bond and halogen bond interactions, and the weak nature of the interactions in the layers. The structures of the neutral complexes both consist of mixed stacks of alternating donor and acceptor molecules, with an equivalent intermolecular separation of ~3.35 Å; the aromatic electron donor···acceptor interactions dominate the packing arrangement. Despite the similarity of the overall structures, there is a significant difference in the optical properties of the two complexes, with the 2-I-4-MA complex forming as deep red crystals, in contrast to the yellow crystals of the 2-Br-4-MA complexes. The difference in colour between the two complexes must therefore be attributed to the exchange of the halogen and the differences in the molecular overlap, which will change the charge-transfer interaction. There is a similar amount of ring overlap in each complex; however, the halogen atom sits above the carboxylic acid in the iodine complex and interacts with the π-system of the 3,5-DNBA molecule, which is not observed in the bromine complex. It is also possible that hydrogen bond strength plays a role; the N-H···O hydrogen bonds are stronger in the 2-I-4-MA complex than in the 2-Br-4-MA complex.

In terms of the crystal packing in the neutral complexes, the introduction of the methyl group appears to have minimal influence on the overall assembly of molecules, with the 2-I-4-MA and 2-Br-4-MA structures both forming very similar sheet structures to the equivalent 2-XA complexes, consisting of alternating 3,5-DNBA chains and disordered 2-XA channels. This is in contrast to the equivalent 3,4-DNBA complexes, where the introduction of the methyl group changes the packing arrangement from planar to herringbone. The two structures differ mainly by the orientation of the 2-X-4-MA within the channels. However, the introduction of the methyl group substituent to the 2-IA molecule effectively tunes the solid-state colour, from yellow in 2-IA 3,5-DNBA to red in 2-I-4-MA 3,5-DNBA. The stacking distance between alternate molecules decreases from 3.44 Å to 3.35 Å with the introduction of the methyl group, which may provide an explanation for the colour change, in combination with changes to the donating properties of the donor and the molecular overlap.

The introduction of the methyl group to 2-ClA (to give 2-Cl-4-MA) has a great impact on both the crystal structure and the optical properties, through alteration of the ΔpKa. A proton is transferred from the 2-Cl-4-MA to the 3,5-DNBA resulting in ionic components, and the complex is yielded as colourless needle crystals. The charge-assisted three-dimensional hydrogen bonding of the protonated amine group locks the 2-Cl-4-MA molecule in a single position, and directs the packing into a non-layered form. It was not possible to obtain ionic forms of the I and Br complexes, and likewise not possible to obtain a neutral form of the Cl complex. The crystal structure of 2-Cl-4-MA 3,5-DNBA actually has a very similar crystal

packing arrangement to the ionic 4-Cl-2-MA 3,5-DNBA molecular complex (**24**) reported in Chapter 5 (§5.3.3). Thus in these ionic systems, the three dimensional hydrogen bonding involving the protonated amine group appears to have the greatest influence on the packing arrangement, and the positions of the halogen and methyl substituents have very little influence over the final structure.

6.3 Molecular disorder and proton transfer in 4-haloaniline 3,5-dinitrosalicylic acid complexes

6.3.1 Experimental details

Molecular complexes **31** - **34** were obtained *via* the method of slow evaporation (§3.1); crystallisation trials employed a range of solvents, evaporation temperatures and 1:1 and 2:1 stoichiometric ratios of the 4-haloaniline and 3,5-dinitrosalicylic acid. Single crystal X-ray diffraction experiments were carried out according to the procedures outlined in §3.2. Crystallographic data are given in Table 6.9; refinement details are reported in Appendix A6.

4-iodoaniline 4-iodoanilinium 3,5-dinitrosalicylate (1:2:2) (31)

Molecular complex **31** was synthesised from 2-propanol at ambient temperature, using a 2:1 stoichiometric ratio of 4-iodoaniline and 3,5-dinitrosalicylic acid; orange block crystals were obtained. Single crystal X-ray diffraction data were collected at 100 K using a Rigaku R-AXIS/RAPID image plate diffractometer. The structure was solved by direct methods using SHELXS-97[192] and refined using SHELXL-2014,[198] both within the WinGX program suite.[200]

4-bromoaniline 4-bromoanilinium 3,5-dinitrosalicylate (1:2:2) (32)

Molecular complex **32** was synthesised from ethanol at ambient temperature, using a 2:1 stoichiometric ratio of 4-bromoaniline and 3,5-dinitrosalicylic acid; orange block crystals were obtained. Single crystal X-ray diffraction data were collected at 100 K using a Rigaku R-AXIS/RAPID image plate diffractometer. The structure was solved by direct methods using SHELXS-97[192] and refined using SHELXL-2014,[198] both within the WinGX program suite.[200]

4-iodoaniline 3,5-dinitrosalicylic acid (1:1) (33)

Molecular complex **33** was synthesised from acetonitrile at 40 °C, using a 2:1 stoichiometric ratio of 4-iodoaniline and 3,5-dinitrosalicylic acid (N.B. the molecular components crystallised in a 1:1 ratio); colourless block crystals were obtained. Single crystal X-ray diffraction data were collected at 100 K using a Rigaku R-AXIS/RAPID image plate diffractometer. The

structure was solved by direct methods using SHELXS-97[192] and refined using SHELXL-2014,[198] both within the WinGX program suite.[200]

4-bromoaniline 3,5-dinitrosalicylic acid (1:1) (34)

Molecular complex **34** was synthesised from 2-propanol at 30 °C, using a 1:1 stoichiometric ratio of 4-bromoaniline and 3,5-dinitrosalicylic acid; pale yellow block crystals were obtained. Single crystal X-ray diffraction data were collected at 150 K using a Rigaku Oxford Diffraction Xcalibur diffractometer. The structure was solved by direct methods using SHELXS-2013[192] and refined using SHELXL-2014,[198] both within the WinGX program suite.[200]

Table 6.9 Crystallographic data for molecular complexes **31- 34**

	31	**32**	**33**	**34**
Formula	(C_6H_6NI) $2(C_6H_7NI)^+$ $2(C_7H_3N_2O_7)^-$	(C_6H_6NBr) $2(C_6H_7NBr)^+$ $2(C_7H_3N_2O_7)^-$	$(C_6H_7NI)^+$ $(C_7H_3N_2O_7)^-$	$(C_6H_7NBr)^+$ $(C_7H_3N_2O_7)^-$
M/g mol^{-1}	1113.30	972.10	447.14	400.15
T/K, Radiation	100(2), Mo Kα	100(2), Mo Kα	100(2), Mo Kα	150(2), Mo Kα
Space Group	$P\bar{1}$	$P\bar{1}$	$P\bar{1}$	$P\bar{1}$
a/Å	9.0879(11)	8.9236(14)	7.3806(15)	4.8161(3)
b/Å	9.9637(12)	9.7866(14)	9.3433(18)	11.1049(6)
c/Å	10.5749(12)	10.2414(13)	11.754(2)	14.2161(8)
α	94.099(4)	92.469(7)	80.602(5)	76.481(5)
β	103.810(4)	104.006(7)	71.795(5)	81.842(5)
γ	92.568(4)	93.163(7)	79.460(5)	83.531(5)
V/Å	925.59(19)	865.0(2)	752.1(3)	729.26(8)
Z	1	1	2	2
ρ_{cal}/ g cm^{-3}	1.997	1.866	1.974	1.822
μ/mm^{-1}	2.611	3.581	2.173	2.864
θ Range/°	2.994 - 27.485	3.013 - 27.484	3.047 - 27.479	3.749 - 26.369
Ref Collected	22287	20669	18894	5486
Independent	4221	3951	3419	2956
Observed>2σ	3036	3590	3209	2301
Rint	0.0356	0.0295	0.0327	0.0368
Completeness %	99.8	99.8	99.7	99.8
Parameters	253	253	229	229
GooF	1.195	1.073	1.085	1.029
R_1 (obs)	0.0392	0.0261	0.0191	0.0477
R_1 (all)	0.0657	0.0300	0.0212	0.0697
wR2 (all)	0.1110	0.0652	0.0473	0.0996
$\rho_{max,min}$/e Å^{-3}	1.208, -1.433	0.508, -0.610	0.510, -0.268	0.515, -0.614

6.3.2 Molecular complexes of 4-haloaniline and 3,5-dinitrosalicylic acid (31 - 34)

4-IA and 4-BrA are light purple and beige crystalline solids, respectively, and 3,5-dinitrosalicylic acid is a light yellow solid. Crystallisation trials were set up using 1:1 and

2:1 stoichiometric solutions of the 4-haloaniline and 3,5-dinitrosalicylic acid; dissolution of the two components resulted in pale orange and bright yellow solutions for 4-IA and 4-BrA, respectively. The ΔpKa values (using pKa_1 for 3,5-DNSA) are 3.11 and 3.19 for 4-IA 3,5-DNSA and 4-BrA 3,5-DNSA, respectively, thus the transfer of a single proton would be expected to occur from 3,5-DNSA to the 4-haloaniline.

Two molecular complexes of 4-IA 3,5-DNSA were obtained, both from 2:1 stoichiometric solutions.[239] In molecular complex **31**, the 4-IA and 3,5-DNSA components crystallised in a 3:2 ratio; in molecular complex **33**, the 4-IA and 3,5-DNSA crystallised in a 1:1 ratio. Thus the stoichiometry of the solution did not dictate the formation of a molecular complex of the same ratio; the composition of the molecular complex formed was dependent on the crystallisation solvent and the temperature of evaporation. Similarly, two molecular complexes of 4-BrA 3,5-DNSA, **32** and **34**, were formed, with 3:2 and 1:1 ratios of the 4-bromoaniline and 3,5-dinitrosalicylic acid components, respectively. Molecular complex **32** was obtained from a 2:1 stoichiometric solution of 4-BrA and 3,5-DNSA, while molecular complex **34** was obtained from a 1:1 stoichiometric solution.

The solution colours were not dependent on the stoichiometry of the solution, whereas the crystal colours are, thus the origin of the colour lies in the solid-state. The 3:2 molecular complexes of 4-IA 3,5-DNSA (**31**) and 4-BrA 3,5-DNSA (**32**) both formed as orange block crystals; the 1:1 molecular complexes of 4-IA 3,5-DNSA (**33**) and 4-BrA 3,5-DNSA (**34**) were yielded as colourless and pale yellow block crystals, respectively (Figure 6.15 (a)). Single crystal UV-visible absorption spectra were collected on each of the four molecular complexes at room temperature (Figure 6.15 (b)), according to the procedure outlined in §3.4.1. The absorption bands of the 3:2 complexes are red-shifted compared to the 1:1 complexes, and within each pair of complexes the absorption bands of the 4-BrA complexes are red-shifted relative to the absorption bands of the 4-IA complexes. The spectra of molecular complexes **31** and **32** exhibit broad charge-transfer absorption bands below 540 nm and 560 nm, which is consistent with the orange colour of the crystals. Molecular complexes **33** and **34** absorb at much shorter wavelength, with absorption maxima of 365 nm and 410 nm, respectively, which is consistent with the colourless nature of the crystals. Both spectra exhibit small shoulders with maxima at 420 nm and 490 nm for **33** and **34**, respectively.

(a)

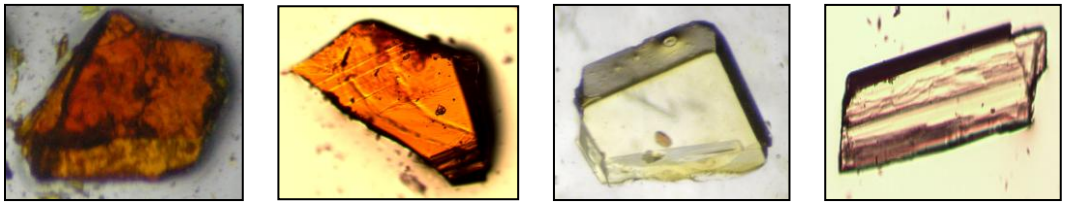

(b)

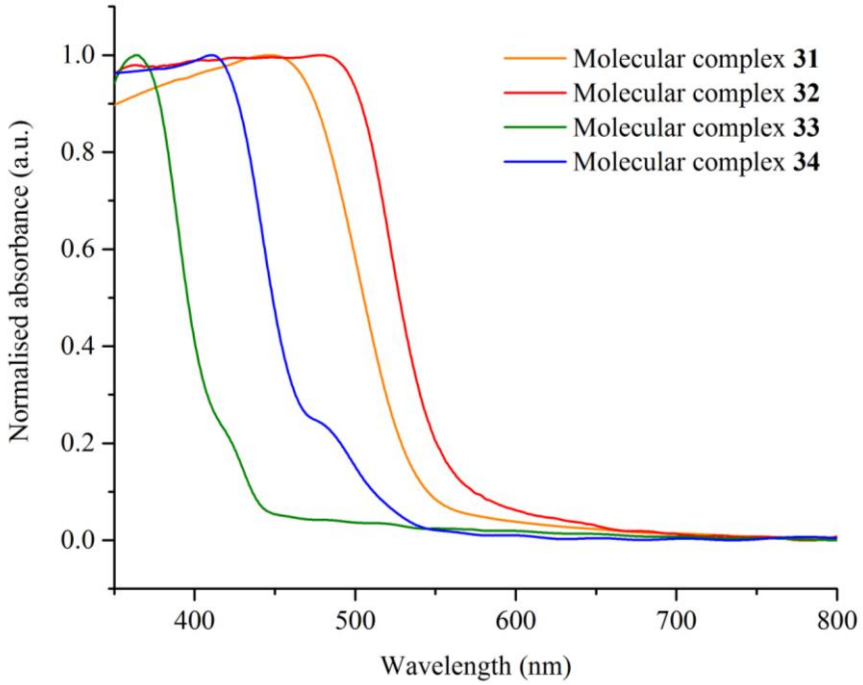

Figure 6.15 (a) Photographs of crystals of (from left to right) molecular complexes **31**, **32**, **33** and **34**; (b) single crystal UV-visible absorption spectra for molecular complexes **31**, **32**, **33** and **34** collected at room temperature.

6.3.2.1 4-haloaniline 4-haloanilinium 3,5-dinitrosalicylate (31 and 32)

Molecular complexes **31** and **32**, are isostructural and crystallise in the triclinic space group $P\bar{1}$; the components 4-haloaniline and 3,5-dinitrosalicylic acid are present in a 3:2 ratio. A proton is transferred from 3,5-dinitrosalicylic acid to one of the 4-haloaniline molecules; thus both neutral and ionic 4-XA molecules coexist but all 3,5-DNSA molecules are in their ionic form. The asymmetric unit contains one independent 3,5-dinitrosalicylate anion, one independent 4-haloanilinium cation, and a half-occupied neutral 4-haloaniline molecule. The anion and cation are both fully ordered, but the neutral 4-haloaniline molecule is disordered over two positions through an inversion centre; the two positions have occupancies of 50:50 (shown in purple and green, Figure 6.16).

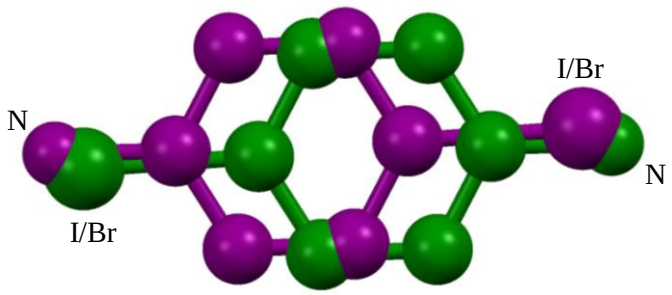

Figure 6.16 The molecular disorder of the 4-haloaniline in molecular complexes **31** and **32**, where disorder occupancies are 50:50. Hydrogen atoms have been omitted for clarity.

In the 3,5-dinitrosalicylate anion in both molecular complexes, an intramolecular O-H···O hydrogen bond is formed between the hydroxyl group and the carboxylic acid group (Table 6.10). In each case, the hydrogen atom resides closer to the carboxylate O atom, with O-H bond lengths of 0.88(7) Å and 0.95(2) Å in **31** and **32**, respectively. The carbonyl O-atom of the carboxylic acid group is clearly identifiable, with C-O bond lengths of 1.222(6) Å and 1.229(2) Å in **31** and **32**, respectively. The bond length of the C-O group to which the hydrogen atom is bound has a distance of 1.310(6) Å in **31** and 1.304(2) Å in **32**; this compares to slightly shorter C-O distances of 1.291(5) Å and 1.284(2) Å for the deprotonated hydroxyl groups in **31** and **32**, respectively. The formation of the intramolecular O-H···O hydrogen bond keeps the carboxylic acid group close to coplanar with the ring; the carboxylic acid groups have torsion angles of ~5° and ~4°. The nitro groups are twisted out of the ring plane by ~6°/~2° and ~5°/~3° in molecular complexes **31** and **32**, respectively. Pairs of 3,5-DNSA anions are linked *via* two equivalent weak C-H···O interactions between an aromatic H-atom and nitro group O-atom (C···O = 3.378(5) in **31** and 3.356(2) in **32**).

The NH_3^+ group of the 4-haloanilinium cation forms N-H···O hydrogen bonds to adjacent 3,5-DNSA anions, directing the hydrogen bonding into a three-dimensional form (Figure 6.17 (a), Table 6.10). Two hydrogen bonds form to carbonyl oxygen atoms of the carboxylic acid groups of two 3,5-DNSA anions and one to the deprotonated hydroxyl group O-atom of a third 3,5-DNSA. In addition, there are a number of weak C-H···O hydrogen bonds formed between aromatic C-H groups of the 4-XA cations and nitro group oxygen atoms of the 3,5-DNSA anions, with C···O distances in the range ~3.15 - 3.30 Å. The combination of these interactions forms a hydrogen bonded network which houses the disordered 4-XA molecules, with the disordered molecules isolated from one another; the 4-XA cations separate and link the columnar stacks (Figure 6.17 (b)).

(a) (b)

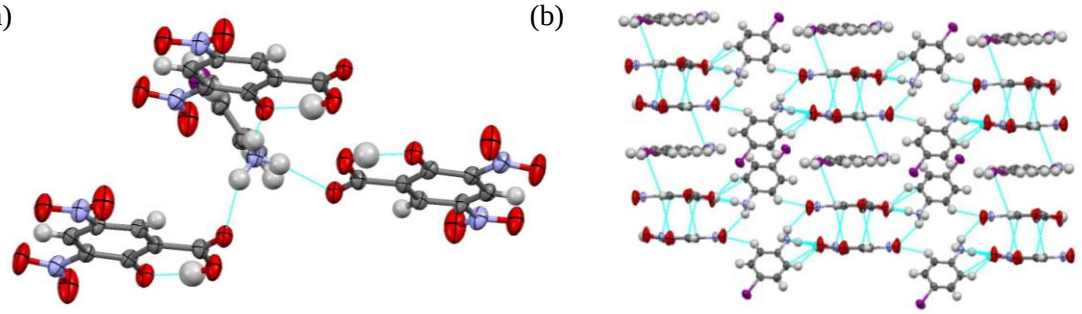

Figure 6.17 Hydrogen bonds formed between the NH_3^+ group of the 4-haloaniline cation and three 3,5-DNSA anions in molecular complexes **31** and **32** (shown for **31**); (b) hydrogen bonded network of 4-XA and 3,5-DNSA ions, housing the disordered neutral 4-XA molecules (shown for **31**).

Table 6.10 Hydrogen bond data for molecular complexes **31** and **32**

D-H···A	D-H	H···A	D···A	<(DHA)
Molecular complex **31**				
O2-H7···O3	0.87(7)	1.61(7)	2.442(5)	158(7)
N3-H3A···O1_#1	0.93(6)	2.21(6)	2.945(6)	136(5)
N3-H3B···O1_#2	0.83(6)	2.09(6)	2.903(5)	166(6)
N3-H3C···O3_#3	0.92(6)	1.96(6)	2.862(5)	165(5)
Molecular complex **32**				
O2-H7···O3	0.95(3)	1.52(3)	2.430(2)	160(2)
N3-H3A···O1	0.86(3)	2.18(3)	2.863(2)	137(2)
N3-H3B···O1_#1	0.87(3)	2.01(3)	2.865(2)	169(2)
N3-H3C···O3_#2	0.89(3)	1.94(3)	2.811(2)	164(2)

Molecular complex **31**: #1 x,y+1,z #2 -x,-y,-z #3 x-1,y+1,z

Molecular complex **32**: #1 -x+1,-y,-z #2 x-1,y,z

The neutral disordered molecules interact with the ordered network *via* a single weak N-H···O hydrogen bond between the amine group and nitro group oxygen atom of a 3,5-DNSA ion in an adjacent stack (N···O = 3.42(1) Å and 3.51(6) Å in **31** and **32**, respectively). This provides an explanation for the disorder, as there are no strong interactions to favour a single orientation. The only interaction involving the halogen atom is an X···π interaction to 3,5-DNSA molecules above and below; the same type of interaction is formed regardless of the orientation of the disordered 4-XA molecule.

The disordered neutral 4-XA molecules are stacked with 3,5-DNSA ions, with each spaced by pairs of stacked 3,5-DNSA molecules. There are π···π interactions between each 3,5-DNSA pair, with a distance of ~3.25 Å between the stacked 3,5-DNSA molecules in both complexes.

Between stacked 4-XA and 3,5-DNSA molecules, there are approximate intermolecular separations of ~3.55 Å and ~3.40 Å in **31** and **32**, respectively (**i**, Figure 6.18). The neutral 4-XA molecules are close to coplanar with the 3,5-DNSA anions, with angles of ~3° and 5° between the mean ring planes in **31** and **32**, respectively. The molecular overlap of the neutral 4-XA molecule and the planar 3,5-DNSA anion is identical in both molecular complexes and for both orientations. There is a small amount of ring overlap and the halogen atom overlaps directly with a nitro group of 3,5-DNSA in both possible orientations of the disordered molecule.

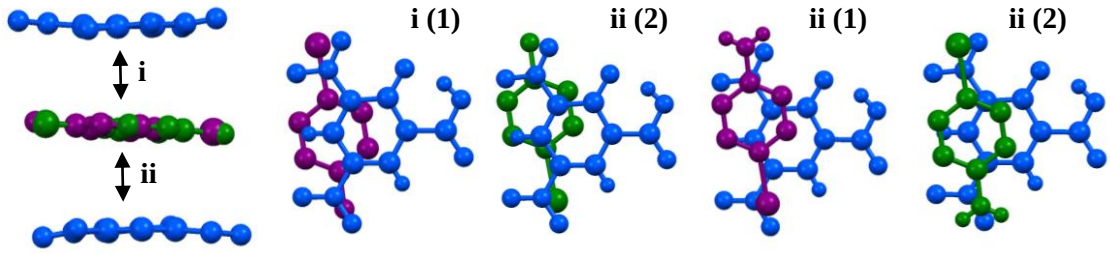

Figure 6.18 Stacking of alternate 4-XA and 3,5-DNSA in molecular complexes **31** and **32** (left); molecular overlap of the 3,5-DNSA cation and 4-XA for both molecular orientations (right). 3,5-DNSA molecules are shown in blue, and the disordered 4-XA molecules are shown in the colours according to Figure 6.16.

The colour of the 3:2 molecular complexes can be attributed to intermolecular π···π* charge-transfer between the neutral aromatic donor, 4-XA, and the planar aromatic acceptor, 3,5-DNSA; although the 3,5-DNSA has been deprotonated, the molecule can still act as an aromatic electron-acceptor due to the strongly withdrawing nitro groups. The stoichiometry of the complex means that one of the 4-XA molecules is neutral, thus a charge-transfer complex may still form. Given the identical molecular overlap, the different optical properties of the two complexes, as observed in the UV-visible absorption spectra (Figure 6.15), must be due to the difference in the stacking distance between the 4-XA and 3,5-DNSA (~3.55 Å vs. ~3.40 Å).

6.3.2.2 4-haloanilinium 3,5-dinitrosalicylate (33 and 34)

Molecular complexes **33** and **34** are not isostructural, but both crystallise in the triclinic space group $P\bar{1}$. The 4-haloaniline and 3,5-dinitrosalicylic acid components are present in a 1:1 ratio; a proton is transferred from the 3,5-DNSA to the 4-XA molecules, thus both species are present in their ionic form. The asymmetric unit contains one of each of the ions. In the 3,5-DNSA anion, an intramolecular O-H···O hydrogen bond is formed between the hydroxyl group and the carboxylate group (Table 6.11). In both molecular complexes, the hydrogen atom resides closer to the hydroxyl group O atom; both O-H distances are longer than standard (0.98(3) Å and

1.15(4) Å in **33** and **34**, respectively). The locations of the hydrogen atoms were determined from Fourier difference maps. The C-O bond lengths of the hydroxyl group are 1.321(2) Å (**33**) and 1.304(4) Å (**34**). The C-O distances of the carboxylate group are intermediate between those expected for single and double bonds, which is consistent with a delocalisation of the charge across the group (1.228(2) Å/1.282(2) Å in **33** and 1.247(4) Å/1.280(4) Å in **34**). In the 4-IA complex, **33**, the carboxylic acid group is close to coplanar with the ring (torsion angle of ~1°) and one of the nitro groups is also close to coplanar with a torsion angle of ~5°; however, the second nitro group is twisted out of the ring plane by ~41°. In the 4-BrA complex, **34**, the 3,5-DNSA molecule is approximately planar; the carboxylic acid group has a torsion angle of ~8°, and the nitro groups are rotated out of the ring plane by ~1°/~7°. Pairs of 3,5-DNSA anions are linked *via* two equivalent weak C-H···O interactions between an aromatic H-atom and nitro group O-atom (C···O = 3.277(2) in **33** and 3.362(4) in **34**).

In both molecular complexes, the NH_3^+ group of the 4-haloaniline cation forms N-H···O hydrogen bonds to adjacent 3,5-DNSA anions, directing the hydrogen bonding into a three-dimensional form (Figure 6.19, Table 6.11). In **33**, two hydrogen bonds form to carboxylate group oxygen atoms of two 3,5-DNSA anions, and a third forms to a nitro group O-atom. In **34**, two hydrogen bonds form to carboxylate group O-atoms, and one hydrogen atom (H3A) acts as bifurcated donor to hydroxyl and nitro group O-atoms. The anion and cation are not coplanar, with angles of ~28° and ~32° between the mean ring planes of the molecules in **33** and **34**, respectively.

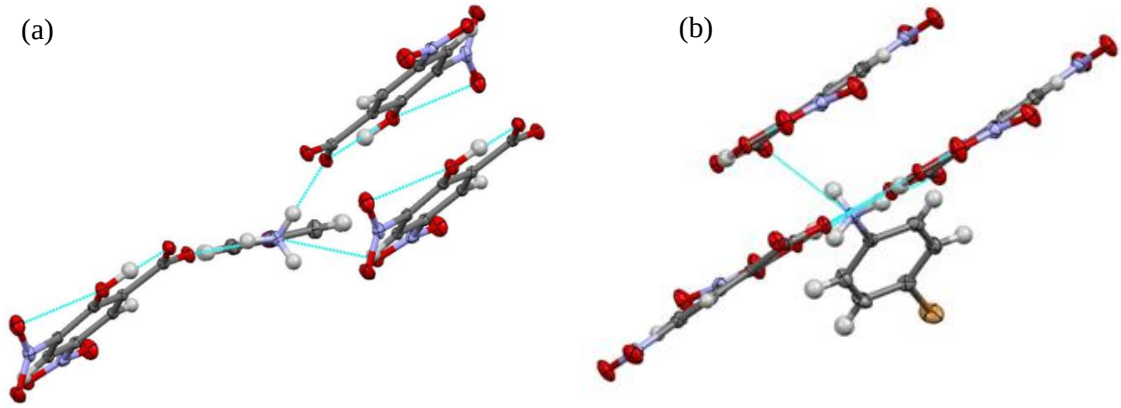

Figure 6.19 Hydrogen bonds formed between the NH_3^+ group of the 4-haloaniline cation and three 3,5-DNSA anions in (a) molecular complex **33** and (b) molecular complex **34**.

Table 6.11 Hydrogen bond data for molecular complexes **33** and **34**

D-H···A	D-H	H···A	D···A	<(DHA)
Molecular complex **33**				
O1-H1···O2	0.98(2)	1.52(2)	2.461(2)	159(2)
N3-H3A···O5_#1	0.86(3)	2.41(2)	2.950(2)	121(2)
N3-H3B···O3_#2	0.93(2)	1.80(2)	2.724(2)	168(2)
N3-H3C···O2_#3	0.90(2)	1.85(2)	2.744(2)	172(2)
Molecular complex **34**				
O1-H1···O2	1.15(4)	1.31(4)	2.423(3)	162(3)
N3-H3A···O7_#1	0.91(4)	2.24(4)	2.913(4)	131(3)
N3-H3A···O1_#2	0.91(4)	2.36(4)	3.117(4)	141(3)
N3-H3B···O3_#2	0.99(4)	1.82(4)	2.801(4)	174(3)
N3-H3C···O3_#3	0.86(4)	2.20(4)	2.976(4)	150(3)

Molecular complex **33**: #1 x+2,y,z-1 #2 x+1,y+1,z-1 #3 -x+1,-y,-z+1

Molecular complex **34**: #1 x+1,y,z #2 -x-1,-y+1,-z #3 -x,-y+1,-z

In molecular complex **33**, the iodine atom of the 4-IA cation is involved in two I···O halogen bonds to the oxygen atoms of adjacent hydroxyl and nitro groups (3.267(1) Å and 3.388(1) Å, compared to the sum of the van der Waals radii of 3.50 Å) ; the shorter of these two interactions is to the nitro group. In molecular complex **34**, the bromine atom of the 4-BrA cation is involved in two Br···π interactions to an adjacent 3,5-DNSA anion (with distances of 3.530(3) Å and 3.535(3) Å) (Figure 6.20 (c)). There are also weak C-H···O hydrogen bonds between aromatic H-atoms of 4-XA and nitro group O-atoms of 3,5-DNSA (C···O distances in the range 3.1 - 3.4 Å). In both complexes, the 3,5-DNSA anions are stacked through π···π interactions, however there are no π···π interactions between 4-XA cations due to a large parallel displacement. In **33**, the stacking of 3,5-DNSA is pairwise, and there is a separation of ~3.24 Å between molecules; in **34**, the stacking is continuous, with a separation of ~3.20 Å between the mean ring planes of the stacked 3,5-DNSA molecules (Figure 6.20 (a) and (c)). It is possible that the differences in the optical properties of the two complexes (as seen in the UV-visible absorption spectra, Figure 6.15) may be attributed to the differences in the 3,5-DNSA stacking and the present of halogen···π interactions in the 4-BrA complex. Furthermore, the nitro groups in **34** are both approximately coplanar with the 3,5-DNSA ring, whereas in **33** one of the nitro groups is twisted significantly out of the ring plane; this may have an effect on the extent of delocalisation and hence on the optical properties of the two complexes, with the absorption maximum of **33** shifted to shorter wavelength (by ~50 nm) compared to **34**.

In **33**, adjacent stacks are linked through an O···O interaction (2.917(2) Å) between a nitro group oxygen atom and a carboxylate group oxygen atom. In **34**, adjacent 3,5-DNSA stacked are linked through two equivalent O···O interactions (2.916(3) Å) between hydroxyl and carboxylate group O-atoms in the same plane. The crystal packing in the two complexes is quite different, which must be due to the nature of the halogen, but in each the crystal structures are not layered and there are no mixed stacks (Figure 6.20), thus the crystals formed are either colourless or pale yellow. This contrasts with the 3:2 molecular complexes where there is stacking between neutral 4-XA molecules and 3,5-DNSA anions (electron-donor-acceptor complex) and thus form as orange crystals.

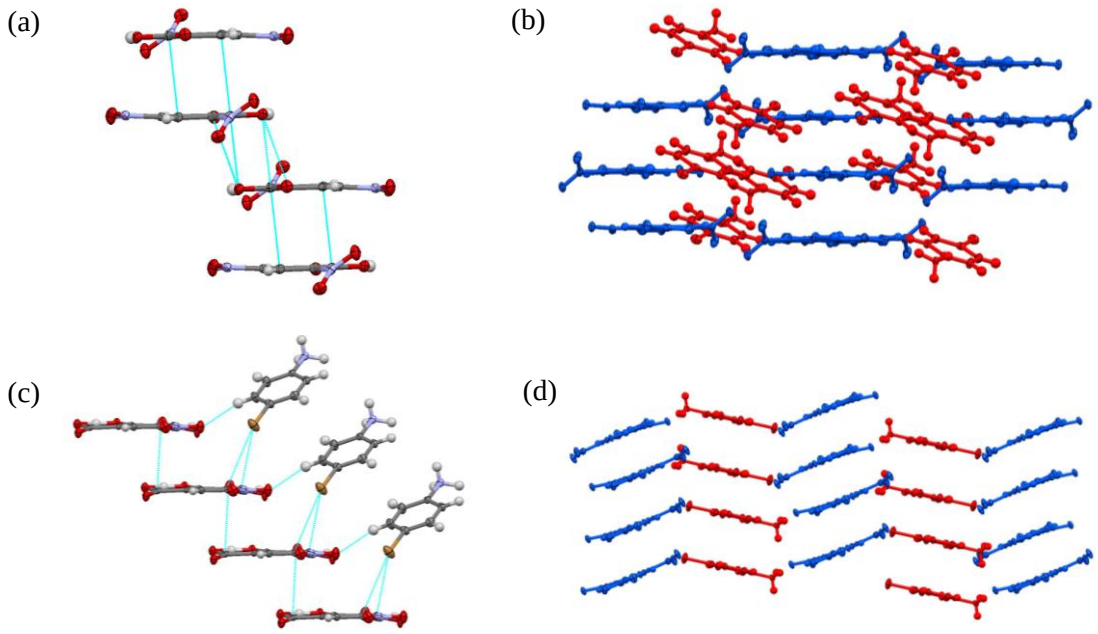

Figure 6.20 (a) Pairwise π···π interactions between stacked 3,5-DNSA molecules in molecular complex **33**; (b) crystal packing in molecular complex **33**; (c) π···π interactions between stacked 3,5-DNSA molecules, and Br···π interactions in molecular complex **34**; (d) crystal packing in molecular complex **34**. N.B. in (b) and (d), the 4-XA cations are shown in red and 3,5-DNSA anions are shown in blue.

6.3.3 Summary and discussion

A total of four molecular complexes, with two different stoichiometries, were obtained in the co-crystallisation of 4-IA and 4-BrA with 3,5-DNSA. The ΔpKa_1 values for each of 4-IA and 4-BrA with 3,5-DNSA were above 3, thus the transfer of a single proton was expected and subsequently observed in all of the complexes. Both 4-IA and 4-BrA formed a 3:2 complex with 3,5-DNSA, which were isostructural and consisted of an ionic pair and a neutral molecule of 4-XA disordered over two positions; the molecular complexes were yielded as orange crystals. Both 4-IA and 4-BrA also formed a 1:1 complex with 3,5-DNSA in which each molecular

component was in its ionic form; the molecular complexes were yielded as colourless (or very pale coloured) crystals. The solid-state colour is therefore dependent upon the stoichiometry of the complex formed and the ionisation states of the molecular components; the disorder may also play a role in the coloured complexes.

In both of the 3:2 complexes, the 3,5-DNSA anions are approximately planar; the ionic 4-XA and 3,5-DNSA components form an ordered hydrogen bonded framework which houses the neutral 4-XA molecules, which are disordered over two positions. The disorder arises as the NH_2 group of the additional 4-IA molecule has to compete with the significantly more basic NH_3^+ group for the strongest hydrogen bond acceptor atoms. This competition is evident in the fact there are no significant hydrogen bond acceptors remaining, and the 4-XA molecules are not fixed in a single position. In both of the complexes, the neutral 4-XA molecule stacks with the planar 3,5-DNSA anions. This type of molecular complex can be described as a 2:1 donor···acceptor complex, in which one of the donor molecules (4-XA) acts as a proton acceptor, and the second donor molecule acts as an electron donor and is involved in a charge-transfer interaction with the anion (3,5-DNSA); the anion acts as both an electron acceptor and a proton donor. The colour in the solid-state may be attributed to this charge-transfer interaction. The amount of molecular overlap in the stacks is identical in both the 4-IA and 4-BrA complexes, however the separation between the 4-XA and the 3,5-DNSA is greater in the 4-IA complex than the 4-BrA complex (3.55 Å vs. 3.40Å). This difference provides an explanation for the variation in the optical properties, with the absorption of the 4-BrA complex shifted to longer wavelength.

In the 1:1 complexes, both components are in their ionic forms, with the charge-assisted hydrogen bonds directing the hydrogen bonding arrangement into a three dimensional form. This results in non-layered crystal structures in which there is no stacking of alternate molecules thus forming colourless crystals; the stacking exists between equivalent molecules only. The 4-IA and 4-BrA complexes are not isostructural, and the absorption spectra of the 4-IA and 4-BrA show a shift in the absorption to longer wavelength for the 4-BrA complex. It is possible that this is due to the difference in stacking of the 3,5-DNSA molecules; in the 4-IA complex the stacking is pair-wise and one of the nitro groups is twisted significantly out of the ring plane. In the 4-BrA complex the $\pi\cdots\pi$ interactions are continuous along the stack.

6.4 Mixed ionisation state complex of 3-bromoaniline

6.4.1 Experimental details

Molecular complex **35** was synthesised *via* slow evaporation (§3.1) from ethanol at ambient temperature using a 1:1 stoichiometric molar ratio of 3-bromoaniline and 3,5-dinitrobenzoic acid; orange block crystals were obtained. Single crystal X-ray diffraction data were collected at 100 K, according to the procedures outlined in §3.2, using a Rigaku R-AXIS/RAPID image plate diffractometer. The structure was solved by direct methods using SHELXS-97[192] and refined using SHELXL-2014,[198] both within the WinGX program suite.[200] Crystallographic data are given in Table 6.12 and refinement details are reported in Appendix A6.

Table 6.12 Crystallographic data for molecular complex **35**

	35
Formula	(C_6H_6NBr) $(C_7H_4N_2O_6)$ $(C_6H_7NBr)^+$ $(C_7H_3N_2O_6)^-$
M/g mol^{-1}	768.30
T/K, radiation	100(2), Mo Kα
Space Group	$P\bar{1}$
a/Å	7.249(3)
b/Å	13.303(7)
c/Å	15.226(8)
α	95.778(7)
β	95.109(8)
γ	100.427(8)
V/Å	1428.1(12)
Z	2
ρ_{cal}/ g cm^{-3}	1.787
μ/mm^{-1}	2.916
θ Range/°	2.999 - 27.479
Ref Collected	32925
Independent	6484
Observed>2σ	4847
Rint	0.0867
Completeness %	99.6
Parameters	434
GooF	1.070
R_1 (obs)	0.0535
R_1 (all)	0.0765
wR2 (all)	0.1415
$\rho_{max,min}$/e Å^{-3}	0.765, -1.011

6.4.2 3-bromoaniline 3,5-dinitrobenzoic acid (35)

3-BrA is a light yellow liquid and 3,5-DNBA is a light yellow solid; dissolution of the two components resulted in a yellow solution. The ΔpKa value for 3-BrA with 3,5-DNBA is 0.71 which lies in the salt-cocrystal continuum, thus proton transfer may or may not occur. It should be noted that although a large range of crystallisation trials were conducted, it was not possible to form a molecular complex of the related 3-iodoaniline and 3,5-dinitrobenzoic acid; in all of the trials, the two molecular components crystallised individually.

The molecular complex 3-BrA 3,5-DNBA, **35**, is yielded as orange crystals (Figure 6.21), thus the origin of the colour lies in the solid-state. Molecular complex **35**, crystallises in the triclinic space group $P\bar{1}$. The asymmetric unit contains one neutral 3-BrA molecule, one neutral 3,5-DNBA molecule, one 3-bromoanilinium cation and one 3,5-dinitrobenzoate anion; thus, a proton has been transferred from one of the 3,5-DNBA molecules to one of the 3-BrA molecules, and the molecular complex is a mixed ionisation complex with co-existing neutral and charged species.

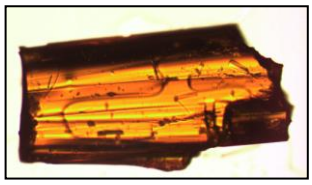

Figure 6.21 Photograph of a crystal of molecular complex **35**

In the neutral 3,5-DNBA molecule, the C-O bond lengths of the carboxylic acid group are characteristic of single and double bonds (1.230(5)/1.307(4) Å). The carboxylic acid group is close to coplanar with the ring plane, with a torsion angle of ~4°; the two nitro groups are rotated out of the ring plane by ~6° and ~9°. In the 3,5-DNBA anion, the C-O distances of the carboxylate group are approximately equidistant (1.255(5)/1.257(6) Å), which is consistent with a delocalisation of the charge across the group. The carboxylate group is twisted significantly out of the ring plane, with a torsion angle of ~39°; the two nitro groups have torsion angles of ~1° and ~10°.

The hydrogen atoms of the NH_3^+ group of the 3-BrA cation were located using electron density maps; the H-atoms are involved in N-H···O hydrogen bonds to four surrounding 3,5-DNBA molecules (two neutral and two charged). Two hydrogen bonds are formed through H1A and H1C, to an O-atom of the twisted carboxylate group and the carbonyl O-atom of a carboxylic acid group, respectively (Figure 6.22 (a), Table 6.13). The third hydrogen atom of the group,

H1B, acts as a bifurcated donor to a nitro group O-atom of the neutral 3,5-DNBA molecule, and to a carboxylate group O-atom (Figure 6.22 (a), Table 6.13). An O-H···O hydrogen bond is formed between the carboxylic acid group of a neutral 3,5-DNBA molecule and the carboxylate group of a 3,5-DNBA anion, and the NH_2 group of the neutral 3-BrA forms a single N-H···O hydrogen bond to the carboxylate group of a 3,5-DNBA anion. The combination of these hydrogen bonding interactions forms a pair of stacks; one stack contains alternating 3,5-DNBA anions and 3-BrA cations, and the second stack consists of alternating neutral 3-BrA and 3,5-DNBA molecules (Figure 6.22 (b)).

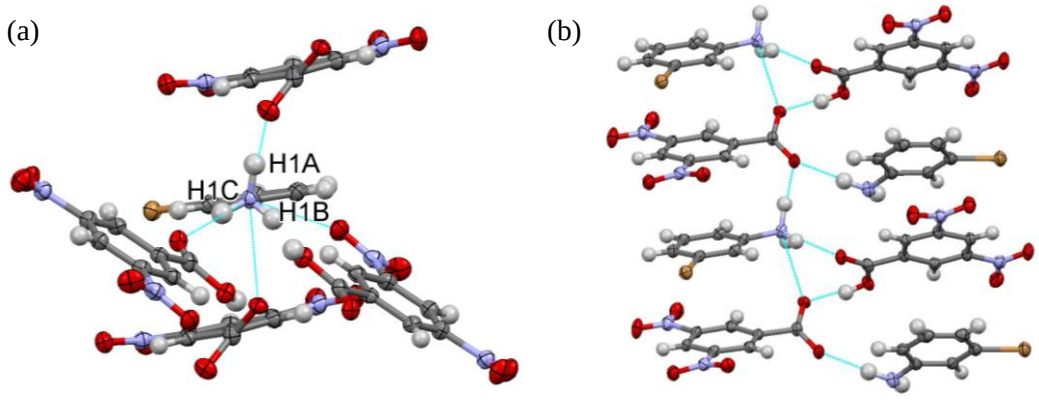

Figure 6.22 (a) Hydrogen bonding interactions **(b)** Hydrogen bonding between the neutral and ionic species in molecular complex **35**.

Table 6.13 Hydrogen bond data for molecular complexes **35**

D-H···A	D-H	H···A	D···A	<(DHA)
O1-H1O···O10_#1	0.91(2)	1.63(2)	2.533(4)	170(5)
N1-H1A···O9_#2	1.02(5)	1.69(5)	2.695(5)	170(4)
N1-H1B···O6_ #3	0.88(5)	2.00(5)	2.805(5)	152(5)
N1-H1B···O10	0.88(5)	2.40(5)	2.931(5)	120(4)
N1-H1C···O2_#4	0.89(6)	1.93(6)	2.772(5)	157(5)
N11-H11A···O9_#5	0.95(6)	2.07(6)	3.007(5)	170(5)

#1 x, y+1, z #2 x-1, y, z #3 -x+1, -y+1, -z+2 #4 x, y-1, z #5 -x+2, -y, -z+1

The bromine atoms of both the neutral and cationic 3-BrA molecules are involved in Br···O interactions. The bromine atom of the neutral molecules interacts with the nitro group oxygen of a neutral 3,5-DNBA molecule in an adjacent neutral stack (Br···O = 3.118(3) Å c.f. the sum of the van der Waals radii of 3.37 Å); the bromine atom of the cation interacts with the O-atom of the carbonyl group in an adjacent neutral stack (Br···O = 2.872(3) Å). In addition, there are number of weak C-H···O hydrogen bonds formed between aromatic C-H groups of the 3-BrA

components and O-atoms of nitro groups of the 3,5-DNBA components in adjacent stacks (C···O distances range between ~3.0 and ~3.5 Å).

The three-dimensional hydrogen bonding arrangement, in combination with the halogen interactions and weak C-H···O hydrogen bonds, link molecular stacks in three dimensions; the neutral and ionic stacks are tilted with respect to each other, by an angle of ~45°. Within each stack, the stacking molecules are approximately coplanar; in the ionic stack, there is an angle of ~3.80° between the mean ring planes of cations and anions, and in the neutral stack there is an angle of only ~1.87° between the ring planes of 3-BrA and 3,5-DNBA. There are π···π interactions between the molecules in both the neutral and ionic stacks, with approximate intermolecular separations of 3.40 Å and 3.28 Å in the neutral and ionic stacks, respectively. The neutral stacks are of the aromatic donor···acceptor type. There are two types of molecular overlap along the stack (shown by stacking types **i** and **ii**, Figure 6.23 (a) and (b)). In each stack there is a similar amount of ring overlap between the 3-BrA and 3,5-DNBA components, but the iodine atom does not overlap directly with the 3,5-DNBA in either stack. In the neutral stack (Figure 6.23 (b)), there is direct overlap of the amine group and the planar carboxylic acid group. The colour in the solid-state can be attributed to π···π* charge-transfer between the neutral, planar electron donor, 3-BrA, and electron acceptor, 3,5-DNBA.

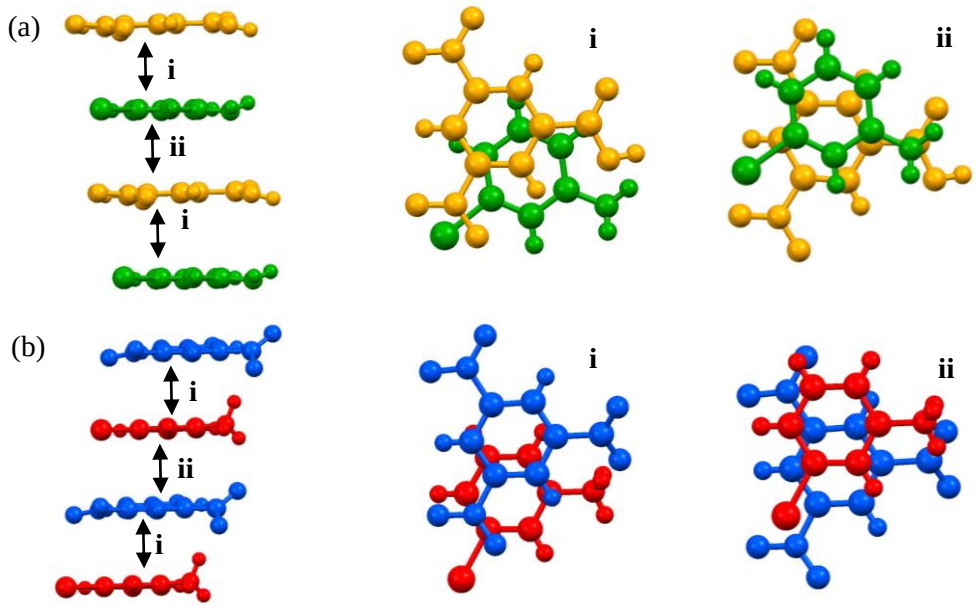

Figure 6.23 (a) Stacking of alternate neutral 3-BrA molecules (green) and 3,5-DNBA molecules (yellow), and molecular overlap of the two molecules in molecular complex **35**; (b) Stacking of alternate 3-BrA cations (red) and 3,5-DNBA anions (blue), and molecular overlap of the two ions in molecular complex **35**.

6.4.3 Summary and discussion

A single 1:1 molecular complex formed between 3-BrA and the co-former 3,5-DNBA, but it was not possible to obtain a complex of 3-IA with 3,5-DNBA. The ΔpKa value of the molecular complex 3-BrA 3,5-DNBA lies in the range of the salt-cocrystal continuum; 3-BrA 3,5-DNBA is a mixed ionisation complex which contains an ionic pair of molecules, whereby a proton is transferred from the carboxylic acid group of 3,5-DNBA to the NH_2 group of 3-BrA, and a neutral pair of molecules. Despite the proton transfer in one pair, the structure is formed of segregated stacks; one stack consists of alternating neutral molecules and one stack consists of alternating cations and anions. The colour can likely be attributed to charge-transfer between the neutral donor 3-BrA and acceptor 3,5-DNBA molecules.

6.5 Molecular complexes of 4-bromo-2-iodoaniline

6.5.1 Experimental details

Molecular complexes **36** and **37** were obtained *via* the method of slow evaporation (§3.1) using a 1:1 stoichiometric molar ratio of 4-bromo-2-iodoaniline and 3,5-dinitrobenzoic acid; crystallisation trials employed a range of solvents and evaporation temperatures. Single crystal X-ray diffraction experiments were carried out according to the procedures outlined in §3.2. Crystallographic data are given in Table 6.14 and refinement details are reported in Appendix A6.

4-bromo-2-iodoaniline 3,4-dinitrobenzoic acid (36)

Molecular complex **36** was synthesised from ethyl acetate at 30 °C; red block crystals were obtained. Single crystal X-ray diffraction data were collected at 100 K using a Rigaku Oxford Diffraction Gemini Ultra diffractometer (Mo Kα radiation). The structure was solved by direct methods using SHELXS-97[192] and refined using SHELXL-2014,[198] both within the WinGX program suite.[200]

4-bromo-2-iodoaniline 3,5-dinitrobenzoic acid (37)

Molecular complex **37** was synthesised from acetonitrile at ambient temperature; bright yellow block crystals were obtained. Single crystal X-ray diffraction data were collected at 100 K using a Rigaku R-AXIS/RAPID image plate diffractometer. The structure was solved by direct methods using SHELXS-97[192] and refined using SHELXL-2014,[198] both within the WinGX program suite.[200]

Table 6.14 Crystallographic data for molecular complexes **36** and **37**

	36	**37**
Formula	(C_6H_5NBrI) $(C_7H_4N_2O_6)$	(C_6H_5NBrI) $(C_7H_4N_2O_6)$
M/g mol^{-1}	510.04	510.04
T/K	100(2)	100(2)
Space Group	$P\bar{1}$	$P\bar{1}$
a/Å	7.4955(3)	6.454(8)
b/Å	7.8900(4)	7.700(8)
c/Å	14.5212(7)	15.914(2)
α	80.994(4)	80.684(6)
β	79.866(4)	87.807(6)
γ	67.832(5)	86.792(6)
V/Å	779.05(7)	778.9(8)
Z	2	2
ρ_{cal}/ g cm^{-3}	2.174	2.175
μ/mm^{-1}	4.657	4.658
θ Range/°	2.801 - 26.372	3.163 - 27.481
Ref Collected	13189	17620
Independent	3172	3543
Observed>2σ	2830	3231
Rint	0.0317	0.0277
Completeness %	99.8	99.8
Parameters	228	226
GooF	1.041	1.065
R_1 (obs)	0.0353	0.0236
R_1 (all)	0.0417	0.0271
wR2 (all)	0.0830	0.0563
$\rho_{max,min}$/e Å^{-3}	2.636, -1.106	1.195, -0.382

6.5.2 4-bromo-2-iodoaniline 3,4-dinitrobenzoic acid (36) and 4-bromoaniline 3,5-dinitrobenzoic acid (37)

Multi-component crystallisations were carried out using 4-Br-2-IA to investigate the effect of a second halogen substituent on the crystal packing and colour in the solid-state; the iodine atom and amine group are adjacent in the ring, as in the disordered complexes in Chapter 4 and in the disordered 2-IA 3,5-DNBA complex described in §6.1. The ΔpKa value for 4-Br-2-IA with both 3,4-DNBA and 3,5-DNBA is −0.99, thus neutral complexes were expected.

4-Br-2-IA is a light grey solid and 3,4-DNBA and 3,5-DNBA are both light yellow solids; dissolution of the two components in both co-crystallisations resulted in pale yellow solutions. The molecular complexes of 4-Br-2-IA 3,4-DNBA (**36**) and 4-Br-2-IA 3,5-DNBA (**37**) were yielded as red and bright yellow block crystals, respectively (Figure 6.24 (a)), thus the origin of the colour lies in the solid-state. Single crystal UV-visible absorption spectra were collected on

both of the molecular complexes at room temperature (Figure 6.24 (b)), according to the procedure outlined in 3.4.1. The broad absorbance bands are characteristic of $\pi\cdots\pi^*$ charge-transfer, with absorption below 630 nm and 530 nm in **36** and **37**, respectively, which is consistent with the colours of the crystals.

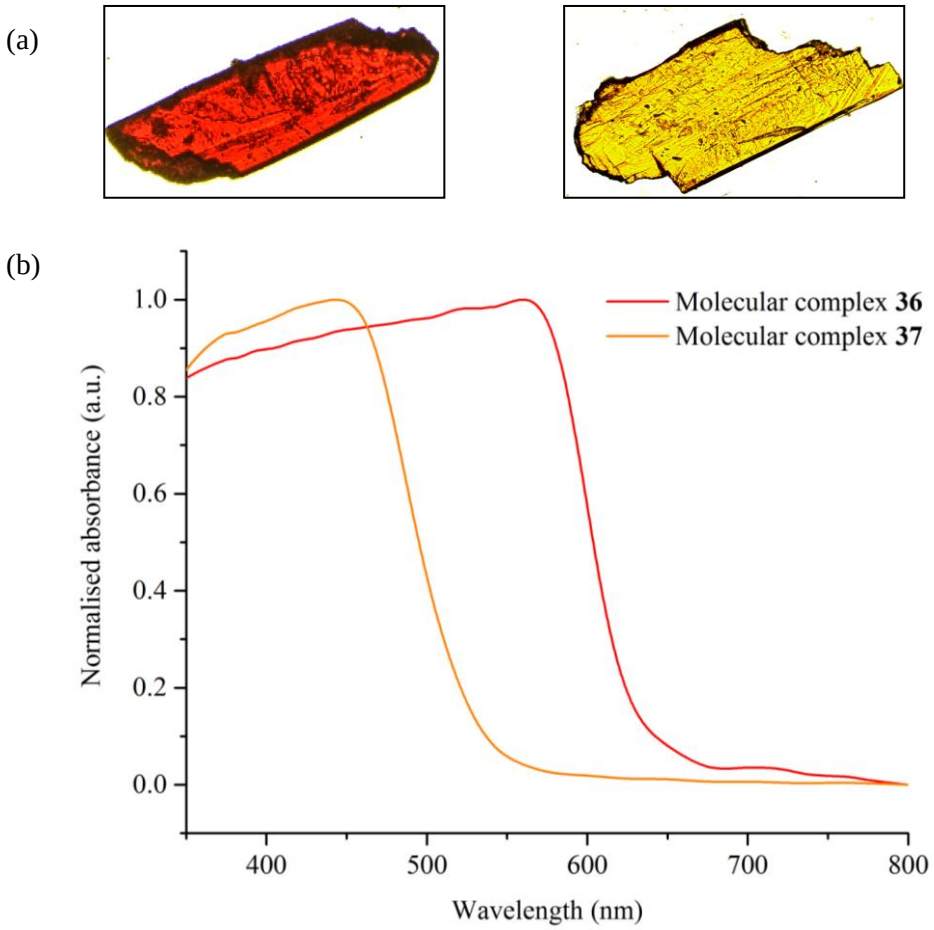

Figure 6.24 (a) Photographs of crystals of molecular complexes **36** (left) and **37** (right); (b) single crystal UV-visible absorption spectra for molecular complexes **36** and **37** collected at room temperature.

Molecular complexes **36** and **37** both crystallise in the triclinic space group $P\bar{1}$. The 4-bromo-2-iodoaniline and dinitrobenzoic acid components are present in a 1:1 ratio in their neutral forms; the asymmetric unit contains one molecule of 4-Br-2-IA and one molecule of the dinitrobenzoic acid in each case. The overall crystal packing is quite similar in both molecular complexes, in that both are formed of planar sheets, but the two are not isostructural. The introduction of the bromine substituent in the *para* position switches off the molecular disorder that is present in both 2-IA 3,4-DNBA (Chapter 4, §4.2) and 2-IA 3,5-DNBA (§6.1.2); in addition, the stoichiometry of the 4-Br-2-IA complex is 1:1, which contrasts with the 1:2 stoichiometry of the 2-IA 3,4-DNBA complex (Chapter 4).

In the neutral 3,4-DNBA molecule in **36**, the C-O bond lengths of the carboxylic group are characteristic of single and double bonds (1.220(5)/1.305(6) Å); the location of the proton was determined from the Fourier difference maps. The carboxylic acid group is close to coplanar with the ring, with a torsion angle of ~5°; the *m*-NO_2 and *p*-NO_2 groups have torsion angles of ~29° and ~55°, respectively. In molecular complex **37**, the C-O bond lengths of the carboxylic acid group of 3,5-DNBA are approximately equidistant (1.262(4)/1.278(3) Å), which may indicate the presence of proton disorder.[37,39] Due to the presence of heavy atoms, a model was employed with a single proton position, with the hydrogen atom located from the Fourier difference maps; the O-H distance was restrained to take a standard value and the displacement parameters of H fixed to be proportional to that of O. The carboxylic acid group is close to coplanar with the ring plane, with a torsion angle of ~3°; the two nitro groups are also close to coplanar with the ring (torsion angles of ~1° and ~8°). The 3,4-DNBA and 3,5-DNBA molecules in molecular complexes **36** and **37**, respectively, form dimers with an equivalent molecule *via* O-H···O hydrogen bonds of moderate strength between the carboxylic acid groups (Table 6.15); thus, the molecules of the dimer are coplanar. It is noteworthy that molecular complex **36** is the only 1:1 complex of 3,4-DNBA formed, and the hydrogen bonded tape of 3,4-DNBA dimers is not observed (as observed in all of the molecular complexes in Chapter 4), resulting in a very different structure.

In both molecular complexes, the dinitrobenzoic acid dimers and 4-Br-2-IA molecules interact *via* a number of hydrogen and halogen bonding interactions, resulting in a planar two-dimensional sheet structure; the construction of the sheets, and the interactions within the sheets, differ between **36** and **37** (Figure 6.25). In molecular complex **36**, each row of the sheet consists of alternating dimers and pairs of 4-Br-2-IA molecules (Figure 6.25 (a)). The hydrogen atoms of the amine group of 4-Br-2-IA, H1A and H1B, form hydrogen bonds to oxygen atoms of the *m*-NO_2 groups of two 3,4-DNBA molecules (Table 6.15). The iodine atom interacts with the carboxyl group O-atom of a 3,4-DNBA molecule *via* a short I···O contact (I···O = 3.294(3) Å c.f. the sum of the van der Waals radii of 3.50 Å); there is also a weak C-H···I hydrogen bond involving the aromatic H-atom adjacent to the *m*-NO_2 group (C···I = 4.012(4) Å, H···I = ~3.12 Å). The bromine is involved in a weak C-H···Br interaction (C···Br = 3.904(6) Å, H···Br = ~3.03 Å), and a pair of these interactions link two molecules of 4-Br-2-IA. There is also a weak bifurcated C-H···O hydrogen bond between an aromatic hydrogen of 4-Br-2-IA and O-atoms of the *m*- and *p*-NO_2 group of 3,4-DNBA (C···O = 3.301(6) Å and 3.373(6) Å).

In molecular complex **37**, the sheets consist of alternating rows of 3,5-DNBA dimers and 4-Br-2-IA molecules (Figure 6.25 (b)); there are weak C-H···O hydrogen bonds (C···O = 3.983(4) Å) between adjacent 3,5-DNBA dimers. The amine group of 4-Br-2-IA is

only involved in a single weak N-H···O hydrogen bond to a nitro group O-atom (Table 6.15) and the iodine atom interacts with a nitro group O-atom of a 3,5-DNBA molecule *via* a short I···O contact (I···O = 3.119(2) Å c.f. the sum of the van der Waals radii of 3.50 Å). The bromine atom is involved in a Br···O halogen bond with an O-atom of a 3,5-DNBA nitro group (I···O = 3.296(2) Å c.f. the sum of the van der Waals radii of 3.37 Å) and a Br···Br interaction between two 4-Br-2-IA molecules (Br···Br = 3.613(3) Å c.f. the sum of the van der Waals radii of 3.70 Å). There are two weak C-H···O hydrogen bonds between aromatic H-atoms of 4-Br-2-IA and the carboxylic acid group O-atoms of 3,5-DNBA (C···O = 3.453(4) Å and 3.445(4) Å). There is also a weak bifurcated C-H···O hydrogen bond between an aromatic H-atom of 4-Br-2-IA and O-atoms of one of the nitro groups of 3,5-DNBA (C···O = 3.613(4) Å and 3.680(4) Å).

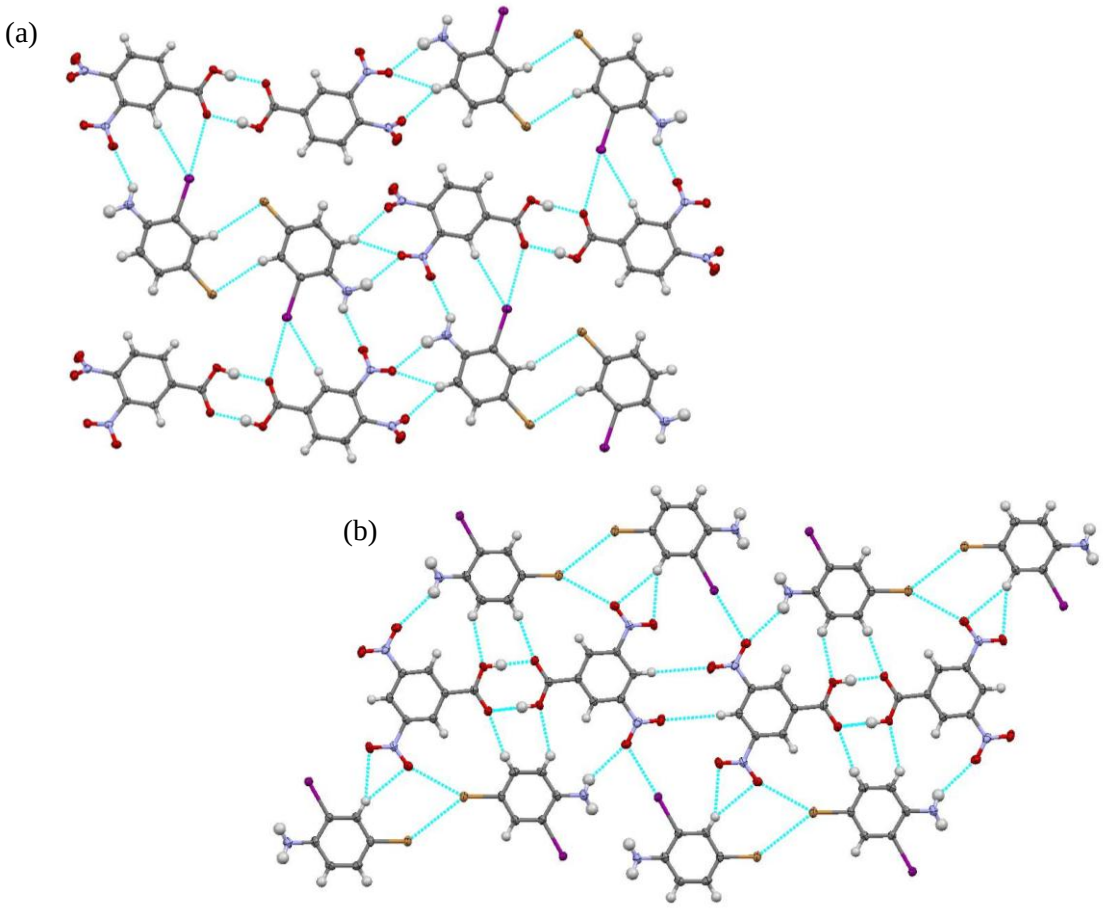

Figure 6.25 Planar two-dimensional sheet structure resulting from the combination of hydrogen bonds and halogen interactions in (a) molecular complex **36** and (b) molecular complex **37**.

Table 6.15 Hydrogen bond data for molecular complexes **36** and **37**

D-H···A	D-H	H···A	D···A	<(DHA)
Molecular complex **36**				
O1-H1···O2_#1	0.88(2)	1.80(2)	2.675(4)	174(6)
N1-H1A···O3	0.89(6)	2.48(6)	3.113(6)	129(5)
N1-H1B···O4_#2	1.00(7)	2.28(7)	3.217(6)	155(5)
Molecular complex **37**				
O1-H1···O2_#1	0.91(2)	1.72(2)	2.625(3)	177(4)
N1-H1A···O5_#2	0.88(4)	2.65(4)	3.386(4)	141(3)

Molecular complex **36**: #1 -x-1,-y,-z #2 -x+1,-y+1,-z+1

Molecular complex **37**: #1 -x+1,-y+2,-z #2 x+1,y,z

The sheets in each molecular complex stack through aromatic donor···acceptor interactions; there are approximate distances of 3.32 Å and 3.45 Å between stacked molecules in **36** and **37**, respectively. In both molecular complexes, the stacking is alternate between acceptor (DNBA) molecules and donor (4-Br-2-IA) molecules (Figure 6.26, (a) and (c)); the main differences are the rotation of the nitro groups in molecular complex **36** and the orientation of adjacent 4-Br-2-IA molecules with respect to each other. In **37**, the adjacent 4-Br-2-IA are further apart, with short contacts between bromine atoms; there is a centroid-centroid distance of ~9.67 Å between adjacent 4-Br-2-IA molecules in **37**, compared to a smaller distance of 6.99 Å in **36**.

The different orientations and distance between the molecules results in differing amounts and types of molecular overlap in the stacks of molecular complexes **36** and **37** (right, Figure 6.26); in both complexes the molecular overlap differs above and below the dimer, and this alternates along the stack (shown by stacking types **i** and **ii**, Figure 6.26 (a) and (c)). In molecular complex **36**, there is significant overlap between the rings of 4-Br-2-IA and 3,4-DNBA (**i**, Figure 6.26 (b)) and between the 4-Br-2-IA ring and the carboxylic acid group of 3,4-DNBA (**ii**, Figure 6.26 (b)). In molecular complex **37**, there is very little overlap between rings in one pair (**i**, Figure 6.26 (d)); in the second pair, there is partial ring overlap between molecules, and the bromine atom sits above the centre of the 3,5-DNBA dimer (**ii**, Figure 6.26 (d)).

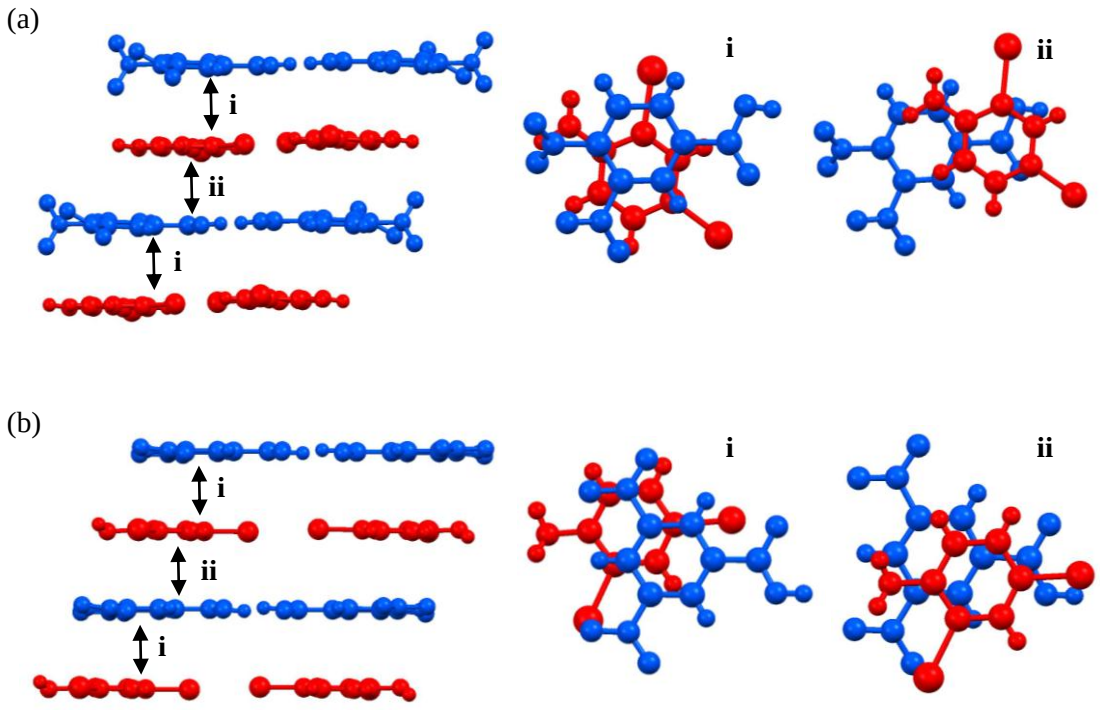

Figure 6.26 (a) Stacking of alternate 4-Br-2-IA and 3,4-DNBA molecules and molecular overlap of 4-Br-2-IA and 3,4-DNBA molecules in **36**; (b) Stacking of alternate 4-Br-2-IA and 3,5-DNBA molecules and molecular overlap of 4-Br-2-IA and 3,5-DNBA molecules in **37**. The 4-Br-2-IA is shown in red, and the dinitrobenzoic acid co-former in blue.

The colour in the solid-state can be attributed to $\pi\cdots\pi^*$ charge-transfer between the aromatic donor and acceptor molecules in the mixed stacks. However, despite both complexes consisting of the stacked, planar sheets with the same interlayer distance, the colour properties are quite different, with **36** forming as bright red crystals and **37** as bright yellow crystals. This must be due to the molecular overlap. In particular, there is a large amount of overlap between the 4-Br-2-IA ring and the carboxylic acid group in molecular complex **36**, which is not observed in **37**, and it is possible that the red colour of **36** can be attributed to this overlap with the centre of the dimer. In addition, the two hydrogen bonds involving the amine group in **36** are both stronger than the single hydrogen bond in **37**, which may also play a role in tuning the electronic structure that leads to the colour.

6.5.3 Summary and discussion

4-Br-2-IA forms a neutral 1:1 molecular complex with each of 3,4-dinitrobenzoic acid and 3,5-dinitrobenzoic acid. The carboxylic acid groups are coplanar with the rings and the dinitrobenzoic acid molecules form dimers through the carboxylic acid groups. Both molecular complexes are fully ordered, thus the introduction of the Br atom in the *para* position of the ring removes the disorder that was observed in the 2-IA 3,4-DNBA (§4.1) and 2-IA 3,5-DNBA

(§6.1) molecular complexes. This may be due to the more equivalent sizes of the 4-Br-2-IA and DNBA molecules in the mixed stack complexes (meaning more efficient packing and less molecular freedom). Furthermore, the additional halogen substituent is able to form halogen bonds, removing the competition for donors. The 4-Br-2-IA complex is also the only 3,4-DNBA complex which forms with a 1:1 stoichiometry (Chapter 4). The two structures further highlight the weakness of NH_2 as a hydrogen bond donor, since the hydrogen bonds involving this group have N···O distances that are characteristic of moderate to weak hydrogen bonds.

The structures of both molecular complexes are layered, with stacking of alternate molecules with similar intermolecular separations, however the optical properties of the two are quite different, as observed visually and in the UV-visible absorption spectra. Charge-transfer is sensitive to the molecular separation, molecular overlap and the nature of the donor and acceptor; thus, the stacking distances and the relative orientations of the molecules and the positions of the nitro groups will all contribute to the differences in the colour properties, in terms of the orbital overlap. In addition, the amine group hydrogen bonds are stronger in the 3,4-DNBA complex than in the 3,5-DNBA complex. The pair of complexes has demonstrated how changing the positions of the nitro group substituents of the co-former can effectively tune the colour properties; however, further work is required in order to understand the electronic transitions involved.

6.6 Conclusions

The systems in this chapter provide key insight into the types of structure and molecular components required in order to induce colour in the solid-state. Ten coloured molecular complexes, which do not display temperature-dependent colour, were obtained in the co-crystallisations of 2-, 3- and 4-substituted haloanilines and methyl-substituted haloanilines with 3,4-dinitrobenzoic acid, 3,5-dinitrobenzoic acid and 3,5-dinitrosalicylic acid. The colours range between yellow and red. Three colourless molecular complexes (**30**, **33** and **34**) are also reported, allowing structural comparison with the corresponding coloured complexes.

Neutral, ionic or mixed ionisation state complexes?

The 3,4-DNBA, 3,5-DNBA and 3,5-DNSA molecules all have the potential to act as proton donors and the NH_2 group of the aniline co-former is able to act as a proton acceptor. The ΔpKa rule can be used to assess whether a neutral or ionic multi-component complex likely to be formed (Table 6.16). The pKa_1 value of 3,5-DNSA is low and the molecule is highly acidic, and a single proton is always transferred from the 3,5-DNSA molecule to the aniline. The ΔpKa

values for 3,4- and 3,5-DNBA with the aniline co-formers were either negative or close to zero. All of the complexes formed with these co-formers were neutral, with the exception of 2-Cl-4-MA 3,5-DNBA, which is ionic and colourless, and 3-IA 3,5-DNBA, which is a coloured, mixed ionisation complex. For 2-Cl-4-MA 3,5-DNBA, the very small increase in the ΔpKa, compared to the I and Br complexes, results in full proton transfer.

Table 6.16 ΔpKa values for the multi-component crystallisations and the type of molecular complex(es) formed.

Co-molecule 1	Co-molecule 2	ΔpKa	Neutral (N), ionic (I) or mixed ionisation (M) complex
2-IA	3,5-DNBA	-0.28	N
2-BrA	3,5-DNBA	-0.29	N
2-ClA	3,5-DNBA	-0.16	N
2-I-4-MA	3,5-DNBA	0.15	N
2-Br-4-MA	3,5-DNBA	0.15	N
2-Cl-4-MA	3,5-DNBA	0.27	I
4-IA	3,5-DNSA	3.11	I (1:1), M (3:2)
4-BrA	3,5-DNSA	3.19	I (1:1), M (3:2)
3-BrA	3,5-DNBA	0.71	M
4-Br-2-IA	3,4-DNBA	-0.99	N
4-Br-2-IA	3,5-DNBA	-0.99	N

Colour in the solid-state

In their neutral forms, the aniline components can all act as aromatic electron-donors, and the nitro-substituted co-formers can all act as aromatic electron-acceptors, thus there is the potential to form mixed stack charge-transfer complexes. When there are no neutral molecules present in the structure, and all of the components in the molecular complexes are ionic (**30**, **33** and **34**), the three-dimensional hydrogen bonding arrangement results in non-layered structures. All of the coloured complexes have all or some of the molecules in their neutral forms. In the coloured 3,4-DNBA and 3,5-DNBA complexes, the carboxylic acid groups of the dinitrobenzoic acid molecules are always coplanar with the benzene ring and form dimers between the carboxylic acid substituents through O-H···O hydrogen bonds. In the coloured 3,5-DNSA complexes, although a proton is always transferred to the amine group of one 4-haloaniline molecule, the formation of an intramolecular O-H···O hydrogen bond between the adjacent hydroxyl and carboxylic acid groups, means that the carboxylic acid (or carboxylate) group remains coplanar with the benzene ring. All of the coloured molecular complexes feature mixed stacks of neutral

donor and acceptor molecules, with the exception of the 3:2 molecular complexes 4-XA 3,5-DNSA where the neutral 4-XA donor sits between two acceptor molecules. Due to the presence of neutral molecules in these 3:2 complexes, and in the 3-BrA 3,5-DNBA complex, charge-transfer can occur between the donor and acceptor. The colour in all of the neutral or mixed ionisation complexes can be attributed to $\pi\cdots\pi^*$ charge-transfer between the planar aromatic electron donor and acceptor molecules. The stacking distances between donor and acceptor molecules range between ~3.32 Å and ~3.55 Å (Table 6.17). Some corresponding pairs of molecular complexes show a trend, for example in the 4-Br-2-IA 3,4-DNBA and 4-Br-2-IA 3,5-DNBA complexes (**36** and **37**), the absorption band shifts to longer wavelength as the molecular separation between the donor and acceptor decreases. The same is true for the 4-XA 3,5-DNBA complexes (**31** and **32**).

Table 6.17 Relationship between the colour and the donor···acceptor stacking distance in the coloured molecular complexes.

Molecular complex	Colour	Absorbance (visible region)	Stacking distance between neutral D-A molecules
25	Yellow/orange	Below 550 nm	3.40 Å
26	Yellow/orange	Below 550 nm	3.35 Å
27	Yellow	Below 530 nm	3.35 Å
28	Red	-	3.35 Å
29	Yellow	-	3.35 Å
31	Orange	Below 540 nm	3.55 Å
32	Orange	Below 560 nm	3.40 Å
35	Orange	-	3.40 Å
36	Red	Below 630 nm	3.32 Å
37	Yellow	Below 530 nm	3.45 Å

The nature of charge-transfer is highly sensitive to the electronic properties of the donor and acceptor, their orientation and the relative molecular overlap of the two components, and these are all further factors to consider. The role of the molecular overlap and nature of the donor and acceptor molecules is evident in the neutral 2-X-4-MA 3,5-DNBA complexes (**28** and **29**); in these complexes, the molecular separation is the same, but the optical properties are very different. The hydrogen bonds involving the amine group may also play a role. Where the molecular complexes of a pair show significantly different colours (2-I-4-MA 3,5-DNBA (red) and 2-Br-4-MA (yellow), and 4-Br-2-IA 3,4-DNBA (red) and 4-Br-2-IA 3,5-DNBA (yellow)), the hydrogen bonds involving the NH_2 group are stronger in the sheets in the red complexes.

Molecular disorder

In addition to the presence of alternate stacking, seven of the ten coloured molecular complexes feature whole molecule disorder of the aniline component. Disorder has been shown to occur in weak CT mixed stack complexes such as those formed here, due to inefficient packing as a result of the requirement to form the aromatic donor···acceptor interactions, and the molecular freedom this gives. In these complexes, in addition to the inefficient packing and probable increased mobility, the disorder arises as a result of competition between the donor and acceptor groups, and the lack of strong interactions to favour a single position. In the neutral disordered complexes, the strongest hydrogen bond donor and acceptors form O-H···O hydrogen bonds through the carboxylic acid groups, leaving a number of weaker hydrogen bond acceptors, in the form of nitro groups, for the aniline co-molecule to interact with through the NH_2 or halogen substituents. In the 3:2 complexes of 4-XA 3,5-DNSA, the NH_2 group of the additional 4-IA molecule has to compete with the significantly more basic NH_3^+ group for the strongest hydrogen bond acceptor atoms. This competition is evident in the fact that there are no significant hydrogen bond acceptors remaining and thus no interactions involving the NH_2 group. The weakness of the NH_2 group as a hydrogen bond donor is indicated in complexes **36** and **37**, where the only hydrogen bonds involving this group are to the weak hydrogen bond acceptor O-atoms of the nitro groups with N···O distances more characteristic of moderate to weak hydrogen bonds. The presence of disorder may be considered to be a favourable attribute for colour, but an understanding of the subtle influences of the disorder on the inter-layer electronic effects requires further work.

In the 2-XA 3,5-DNBA complexes, the occupancy of the major site increases from 2-IA to 2-BrA to 2-ClA (i.e. ~54% to ~69% to ~80%); the 2-X-4-MA 3,5-DNBA complexes follow this trend with the occupancy of the major site increasing from 2-I-4-MA to 2-Br-4-MA (i.e. 60% to 66%). This trend must be the result of the halogen atom type, in terms of the intermolecular interactions and steric effects in the possible orientations.

In Chapter 4, the stoichiometry of the donor and acceptor is 1:2, and stacking occurs between the 2-XA molecule and the 3,4-DNBA dimer. This increases the freedom in the molecular plane by increasing the size of the 'acceptor' part (3,4-DNBA dimer); the crystal space around the donor molecules facilitates significant structural; rearrangement. In the mixed stack complexes in this chapter, the stoichiometry is 1:1, and stacking occurs between individual molecules, rather than with the dimer. Thus, the packing is more efficient, and no temperature-dependent colour is observed.

CHAPTER 7

Ionic molecular complexes

7 Ionic molecular complexes

7.1 Introduction

Chapter 7 is concerned with the ionic molecular complexes of haloanilines and methyl-substituted haloanilines with the nitro- and dinitrosubstituted benzoic acid derivatives 2,4-dinitrobenzoic acid (2,4-DNBA), 2,5-dinitrobenzoic acid (2,5-DNBA), 3,5-dinitrosalicylic acid (3,5-DNSA) and 2-nitrobenzoic acid (2-NBA); there are no previously reported molecular complexes of haloanilines with these co-formers in the CSD.[86] In their neutral forms, the haloanilines can all act as aromatic electron donors and the nitro- and dinitrosubstituted benzoic acid derivatives can all function as electron acceptors. However, there is also the possibility of proton transfer occurring between the acidic and basic moieties; whether charge-transfer or proton transfer dominates is dependent on the difference in the pKa values of the two components (Figure 7.1), and therefore on the acidity of the benzoic acid derivative. 2,4-DNBA, 2,5-DNBA, 2-NBA and 3,5-DNSA are all more acidic than 3,4- and 3,5-dinitrobenzoic acid. The presence of the *ortho* nitro group substituent on 2,4-DNBA, 2,5-DNBA and 2-NBA results in this higher acidity, due to steric effects and the electron-withdrawing nature of the NO_2 group adjacent to the carboxylic acid group (*ortho* effect). 3,5-dinitrosalicylic acid is highly acidic due to intramolecular hydrogen bonding between the adjacent carboxylic acid and hydroxyl groups.

The results of the following multi-component crystallisations, and the colour properties of resultant complexes, are discussed: 2-iodoaniline (2-IA), 2-bromoaniline (2-BrA), 2-chloroaniline (2-ClA), 3-iodoaniline (3-IA), 3-bromoaniline (3-BrA), 4-iodoaniline (4-IA), 4-bromoaniline (4-BrA) and 4-iodo-2-methylaniline (4-I-2-MA) with 2,4-DNBA; 3-IA and 4-IA with 2,5-DNBA; 2-IA, 2-BrA, 2-ClA, 3-IA, 3-BrA and 4-bromo-3-methylaniline (4-Br-3-MA) with 3,5-DNSA; and 4-IA with 2-NBA. The molecular components are shown in Figure 7.1. In each of the molecular complexes proton transfer dominates, and the molecular components are present in their ionic forms. As a result, the aromatic moieties cannot function as aromatic electron donors and acceptors; the molecular complexes are all colourless or very pale yellow in colour, and there is no change in colour on forming the multi-component crystal.

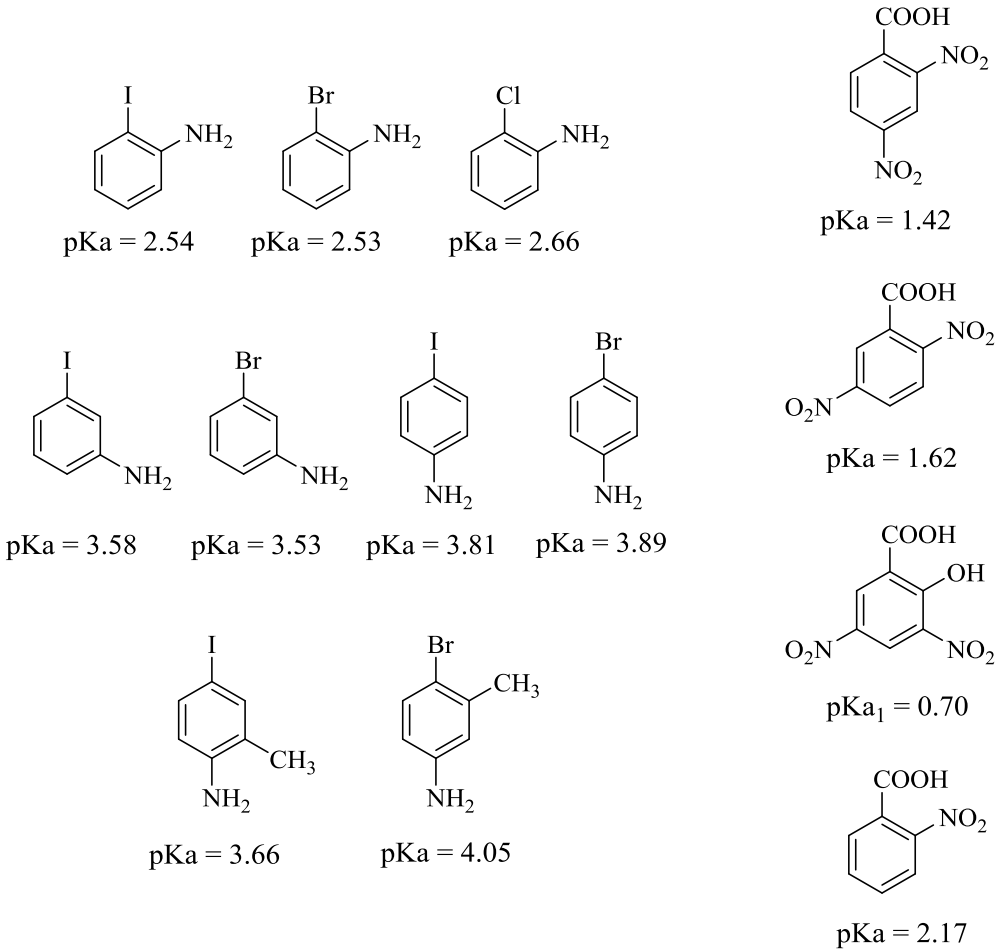

Figure 7.1 Chemical structures of the molecular components used in the multi-component crystallisation experiments in Chapter 7, and their pKa values.[227,228,240–243] Left, top:2-IA, 2-BrA, 2-ClA; left, middle: 3-IA, 3-BrA, 4-IA and 4-BrA; left, bottom: 4-I-2-MA and 4-Br-3-MA. Right (top to bottom): 2,4-DNBA, 2,5-DNBA, 3,5-DNSA and 2-NBA.

7.2 Molecular complexes of 2,4-dinitrobenzoic acid

The ΔpKa values for the systems comprising anilines with 2,4-dinitrobenzoic acid fall in the salt-cocrystal continuum, with ΔpKa ≥ 1. For 2-IA, 2-BrA and 2-ClA with 2,4-DNBA, the values are 1.12, 1.11 and 1.24, respectively; for 3-IA and 3-BrA with 2,4-DNBA the values are 2.16 and 2.11, respectively; for 4-IA, 4-BrA and 4-I-2-MA with 2,4-DNBA the values are 2.39, 2.47 and 2.24, respectively. In each of the molecular complexes of 2,4-dinitrobenzoic acid, the molecular components are present in a 1:1 stoichiometric ratio and a proton is transferred between the carboxylic acid group of 2,4-DNBA and the amine group of the aniline. In the 2,4-dinitrobenzoate anions, the C-O distances of the carboxylate groups are all intermediate between those expected for single and double bonds, which is consistent with a delocalisation of the charge across the group. The hydrogen atoms of the NH_3^+ groups of the aniline molecules were clearly identifiable in the electron density maps. As a result of the proton transfer, all the

molecular complexes are yielded as colourless crystals since the molecules cannot function as donors and acceptors.

7.2.1 Experimental details

Molecular complexes **38** - **45** were obtained *via* the method of slow evaporation (§3.1) using a 1:1 stoichiometric molar ratio of the haloaniline and 2,4-dinitrobenzoic acid; crystallisation trials employed a range of solvents and evaporation temperatures. Single crystal X-ray diffraction experiments were carried out according to the procedures outlined in §3.2. Crystallographic data is given in Table 7.1 and refinement details are reported in Appendix A7.

2-iodoanilinium 2,4-dinitrobenzoate (38)

Molecular complex **38** was synthesised from methanol at 40 °C; colourless needle crystals were obtained. Single crystal X-ray diffraction data were collected at 100 K using a Rigaku R-AXIS/RAPID image plate diffractometer. The structure was solved by direct methods using SHELXS-97[192] and refined using SHELXL-2014,[198] both within the WinGX program suite.[200]

2-bromoanilinium 2,4-dinitrobenzoate (39)

Molecular complex **39** was synthesised from ethanol at ambient temperature; colourless needle crystals were obtained. Single crystal X-ray diffraction data were collected at 150 K using a Rigaku Oxford Diffraction Gemini Ultra diffractometer (Mo Kα radiation). The structure was solved by direct methods using SHELXS-2013[192] and refined using SHELXL-2014,[198] both within the WinGX program suite.[200]

2-chloroanilinium 2,4-dinitrobenzoate (40)

Molecular complex **40** was synthesised from ethanol at ambient temperature; colourless needle crystals were obtained. Single crystal X-ray diffraction data were collected at 150 K using a Rigaku Oxford Diffraction Gemini Ultra diffractometer (Mo Kα radiation). The structure was solved by direct methods using SHELXS-2013[192] and refined using SHELXL-2014,[198] both within the WinGX program suite.[200]

3-iodoanilinium 2,4-dinitrobenzoate (41)

Molecular complex **41** was synthesised from 2-propanol at ambient temperature; colourless plate crystals were obtained. Single crystal X-ray diffraction data were collected at 100 K using a Rigaku R-AXIS/RAPID image plate diffractometer. The structure was solved by direct

methods using SHELXS-97[192] and refined using SHELXL-2014,[198] both within the WinGX program suite.[200]

3-bromoanilinium 2,4-dinitrobenzoate (42)

Molecular complex **42** was synthesised from acetone at ambient temperature; colourless plate crystals were obtained. Single crystal X-ray diffraction data were collected at 100 K using a Rigaku R-AXIS/RAPID image plate diffractometer. The structure was solved by direct methods using SHELXS-97[192] and refined using SHELXL-2014,[198] both within the WinGX program suite.[200]

4-iodoanilinium 2,4-dinitrobenzoate (43)

Molecular complex **43** was synthesised from acetone at ambient temperature; colourless needle crystals were obtained. Single crystal X-ray diffraction data were collected at 100 K using a Rigaku R-AXIS/RAPID image plate diffractometer. The structure was solved by direct methods using SHELXS-97[192] and refined using SHELXL-2014,[198] both within the WinGX program suite.[200]

4-bromoanilinium 2,4-dinitrobenzoate (44)

Molecular complex **44** was synthesised from acetonitrile at ambient temperature; colourless needle crystals were obtained. Single crystal X-ray diffraction data were collected at 100 K using a Rigaku R-AXIS/RAPID image plate diffractometer. The structure was solved by direct methods using SHELXS-97[192] and refined using SHELXL-2014,[198] both within the WinGX program suite.[200]

4-iodo-2-methylanilinium 2,4-dinitrobenzoate (45)

Molecular complex **45** was synthesised from ethyl acetate at ambient temperature; colourless block crystals were obtained. Single crystal X-ray diffraction data were collected at 100 K using a Rigaku Oxford Diffraction Gemini Ultra diffractometer (Mo Kα radiation). The structure was solved by direct methods using SHELXS-2013[192] and refined using SHELXL-2014,[198] both within the WinGX program suite.[200]

Table 7.1 Crystallographic data for molecular complexes **38** - **45**

	38	**39**	**40**	**41**	**42**	**43**	**44**	**45**
Formula	$(C_6H_7NI)^+$ $(C_7H_3N_2O_6)^-$	$(C_6H_7NBr)^+$ $(C_7H_3N_2O_6)^-$	$(C_6H_7NCl)^+$ $(C_7H_3N_2O_6)^-$	$(C_6H_7NI)^+$ $(C_7H_3N_2O_6)^-$	$(C_6H_7NBr)^+$ $(C_7H_3N_2O_6)^-$	$(C_6H_7NI)^+$ $(C_7H_3N_2O_6)^-$	$(C_6H_7NBr)^+$ $(C_7H_3N_2O_6)^-$	$(C_7H_9NI)^+$ $(C_7H_3N_2O_6)^-$
M/g mol^{-1}	431.14	384.15	339.69	431.14	384.15	431.14	384.15	445.17
T/K, radiation	100(2), Mo Kα	150(2), Mo Kα	150(2), Mo Kα	100(2), Mo Kα	100(2), Mo Kα	100(2), Mo Kα	100(2), Mo Kα	100(2), Mo Kα
Space Group	$P\bar{1}$	$P2_1/n$	$P2_1/n$	$P\bar{1}$	$P\bar{1}$	$Pca2_1$	$P2_1/c$	$P2_1/c$
a/Å	7.0475(7)	6.9840(2)	6.9429(3)	6.9143(15)	6.8978(14)	14.121(3)	15.7413(11)	15.233(5)
b/Å	7.9898(9)	26.6826(8)	27.4018(12)	7.3404(15)	7.2677(12)	6.6134(9)	7.0711(3)	7.992(5)
c/Å	13.556(2)	7.9941(2)	7.5038(3)	15.563(4)	15.400(3)	30.936(6)	13.3686(7)	13.631(5)
α	93.436(4)	90	90	90.477(11)	92.204(7)	90	90	90
β	94.064(4)	108.370(3)	103.143(4)	97.371(8)	96.781(7)	90	106.197(7)	109.432(5)
γ	104.491(3)	90	90	115.46(2)	115.638(8)	90	90	90
V/Å	734.8(2)	1413.80(7)	1390.19(10)	705.5	687.7	2889.0(9)	1428.97(15)	1564.9(12)
Z	2	4	4	2	2	8	4	4
ρ_{cal}/ g cm^{-3}	1.949	1.805	1.623	2.030	1.855	1.982	1.786	1.889
μ/mm^{-1}	2.216	2.945	0.313	2.307	3.027	2.254	2.914	2.084
θ Range/°	2.997 - 27.485	2.791 - 30.503	3.360 - 26.372	3.266 - 27.484	3.125 - 27.485	3.003 - 27.486	3.083 - 27.483	3.001 - 27.479
Ref Collected	17441	27991	6769	16771	15625	29597	34743	17993
Independent	3363	4032	2842	3223	3115	6579	3283	3579
Observed>2σ	3031	3233	2170	3139	2938	6189	3067	3217
Rint	0.0600	0.0443	0.0261	0.0247	0.0334	0.0450	0.0237	0.0420
Completeness %	99.8	100.0	99.8	99.8	99.8	99.7	99.9	99.8
Parameters	220	220	220	220	220	406	220	230
Flack parameter	-	-	-	-	-	0.011(11)	-	-
GooF	1.068	1.094	1.043	1.062	1.081	1.132	1.110	1.029
R_1 (obs)	0.0307	0.0378	0.0392	0.0153	0.0224	0.0299	0.0203	0.0223
R_1 (all)	0.0363	0.0561	0.0587	0.0159	0.0244	0.0319	0.0225	0.0267
wR2 (all)	0.0589	0.0768	0.0942	0.0393	0.0565	0.0675	0.0532	0.0537
$\rho_{max,min}$/e Å^{-3}	0.764, -0,735	0.555, -0.437	0.251, -0.291	0.404, -0.320	0.400, -0.297	0.710, -0.554	0.340, -0.267	0.671, -0.322

7.2.2 2-haloanilinium 2,4-dinitrobenzoate (38 - 40)

The ionic molecular complex 2-IA 2,4-DNBA (**38**) crystallises in the triclinic space group $P\bar{1}$ and 2-BrA 2,4-DNBA (**39**) and 2-ClA 2,4-DNBA (**40**) both crystallise in the monoclinic space group $P2_1/n$. The three molecular complexes have a 1:1 stoichiometric ratio of the 2-haloanilinium cation (2-XA) and 2,4-DNBA anion, with one of each ion in the asymmetric unit. The complexes have similar overall packing arrangements, with **39** and **40** isomorphous; all are yielded as colourless needle crystals. Due to steric effects, the carboxylate groups are twisted significantly out of the ring planes by ~89°, ~73° and ~88° in **38**, **39** and **40**, respectively; the *o*-NO_2 groups have torsion angles of ~7°, ~10° and ~7° and the *p*-NO_2 groups have torsion angles of 18°, ~11° and ~7° in **38**, **39** and **40**, respectively. Each hydrogen atom of the tetrahedral NH_3^+ groups of the 2-haloanilinium cations is involved in a moderate strength N-H···O hydrogen bond to a carboxylate group O-atom of an adjacent 2,4-dinitrobenzoate anion; hydrogen bonding data for **38 - 40** are given in Table 7.2.

Table 7.2 Hydrogen bond data for molecular complexes **38** - **40**

D-H···A	D-H	H···A	D···A	<(DHA)
Molecular complex **38**				
N3-H3A···O2_#1	0.89(4)	2.04(4)	2.870(3)	156(4)
N3-H3B···O1	0.83(4)	1.95(4)	2.745(4)	160(4)
N3-H3C···O2_#2	0.97(4)	1.76(4)	2.718(3)	169(3)
Molecular complex **39**				
N3-H3A···O1	0.93(3)	1.83(3)	2.762(2)	179(2)
N3-H3B···O2_#1	0.87(3)	1.99(3)	2.854(2)	177(3)
N3-H3C···O2_#2	0.92(3)	1.85(3)	2.765(2)	174(2)
Molecular complex **40**				
N3-H3A···O2_#1	0.87(2)	1.93(3)	2.790(2)	169(2)
N3-H3B···O2_#2	0.93(2)	1.83(2)	2.756(3)	174(2)
N3-H3C···O2_#3	0.97(3)	1.83(3)	2.793(2)	173(2)

Molecular complex **38**: #1 -x+1,-y+2,-z+1 #2 x-1,y,z #3 -x+1,-y+1,-z+2

Molecular complex **39**: #1 x-1/2,-y+1/2,z+1/2 #2 x+1/2,-y+1/2,z+1/2

Molecular complex **40**: #1 x-1/2,-y+1/2,z-3/2 #2x-1,y,z-1 #3 x,y,z-1

In molecular complex **38**, the three hydrogen bonds form a hydrogen bonded pair of stacks comprising alternating cations and anions, with two hydrogen bonds formed within a stack and one to an adjacent stack; the hydrogen bonds are saturated within the pair of stacks (Figure 7.2 (a)). This results in two hydrogen bonded rings with $R_4^2(8)$ and $R_4^4(12)$ graph-sets. The

cations and anions in the stack are close to parallel, with an angle of ~3° between the mean ring planes. The iodine atoms are involved in C-I···O halogen bonds (I···O = 2.960(2) Å, which are significantly less than the sum of the van der Waals radii of 3.50 Å) to carboxylate O-atoms perpendicular to the stacking direction, linking neighbouring pairs of stacks. In addition, two weak C-H···O hydrogen bonds (C···O = 3.250(4) Å and 3.250(4) Å) form between two aromatic H-atoms of 2-IA to a single nitro group O-atom in a bifurcated manner, extending the stacks in a direction perpendicular to the halogen bonds. The overall structure is layered (Figure 7.2 (a)) with an interlayer separation of ~3.5 Å.

In molecular complexes **39** and **40**, the hydrogen bonds also form stacks of alternating cations and anions; the ions are close to parallel, with an angle of ~2° between the mean ring planes. However, the 2-haloaniline molecules have differing orientations to the 2-IA complex, and the packing arrangement is constructed in a different manner (Figure 7.2 (b)), forming a large hydrogen bonded ring with a graph-set notation of $R_6^5(16)$. In the 2-IA 2,4-DNBA complex, **38**, the hydrogen bonds are saturated within the pair of stacks and only the I-atoms extend the structure perpendicular to the stacks (i.e. in and out of the plane of the page, Figure 7.2 (a)). In **39** and **40**, however, one hydrogen atom of the NH_3^+ group is available to form hydrogen bonds to neighbouring stacked pairs, perpendicular to the stacking direction. The Br/Cl atoms form halogen bonds with carboxylate O-atoms (Br···O = 3.130(2) Å and Cl···O = 3.107(1) Å, compared to the sum of the van der Waals radii of 3.37 Å and 3.27 Å, respectively) , effectively replacing one of the hydrogen bonds observed in **38**. This halogen bond extends the structure perpendicularly, in the opposite direction to the third hydrogen bond (i.e. out of the plane of the page, Figure 7.2 (b)). The halogen bonds involving Br/Cl are weaker than those involving I, and the hydrogen bonds are dominant in the overall assembly. Two weak C-H···O hydrogen bonds form between aromatic H-atoms of 2-BrA/2-ClA and two nitro group O-atoms in adjacent stacks (C···O = 3.322(3) Å and 3.276(3) Å in **39**; C···O = 3.322(3) Å and 3.276(3) Å in **40**). Despite the differences in the intermolecular interactions, the two molecular complexes have an almost identical layered packing arrangement to that in molecular complex **38** (Figure 7.2 (b)), with interlayer separations of ~3.5 Å.

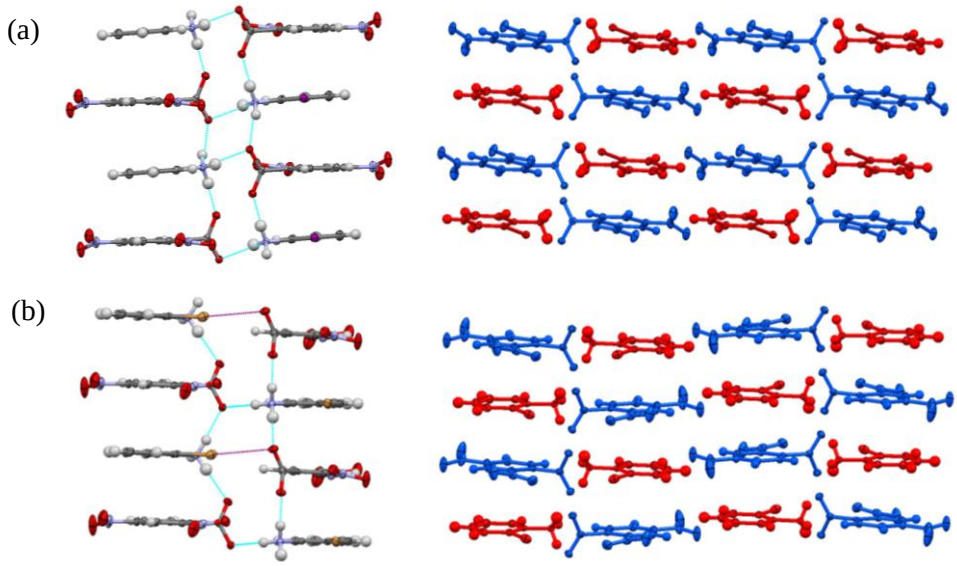

Figure 7.2 (a) Molecular complex **38**: hydrogen bonded pairs of stacks (left) and overall layered packing arrangement (right); (b) Molecular complexes **39** and **40**: hydrogen and halogen bonds within between two stacks (left, halogen bonds in purple), shown for **39**, and overall packing arrangement (right). 2-XA cations are shown in red and 2,4-DNBA anions are shown in blue.

7.2.3 3-haloanilinium 2,4-dinitrobenzoate (41 and 42)

The ionic molecular complexes of 3-IA 2,4-DNBA (**41**) and 3-BrA 2,4-DNBA (**42**) both crystallise in the triclinic space group $P\bar{1}$. The two molecular complexes have a 1:1 stoichiometric ratio of the 3-haloanilinium cation (3-XA) and 2,4-DNBA anion, with one of each ion in the asymmetric unit, and are isomorphous; both are yielded as colourless plate crystals. The carboxylate groups are rotated less significantly out of the ring plane than in the 2-XA complexes (~25° and ~22°, in **41** and **42**, respectively); however, due to steric effects the *o*-NO_2 groups are twisted by a greater degree, by ~69° and ~70° in **41** and **42**, respectively. The *p*-NO_2 groups in **41** and **42** are close to coplanar with the ring, with respective torsion angles of ~2° and ~6°.

Each hydrogen atom of the tetrahedral NH_3^+ groups of the 3-haloanilinium cations is involved in a moderate strength N-H···O hydrogen bond to adjacent carboxylate group O-atoms, forming a pair of stacks. Two of the hydrogen atoms act as bifurcated donors forming weak N-H···O hydrogen bonds to either the second carboxylate group O-atom or a twisted nitro group O-atom adjacent to the carboxylate group. The hydrogen bonding arrangement results in a similar stacking arrangement to the 2-XA 2,4-DNBA complexes (Figure 7.8 (a)). The hydrogen bonds are saturated within the stack, similarly to **38**, forming hydrogen bonded rings with $R_4^2(8)$ and $R_4^4(12)$ graph sets. Hydrogen bonding data for **41** and **42** are given in Table 7.3.

Table 7.3 Hydrogen bond data for molecular complexes **41** and **42**

D-H···A	D-H	H···A	D···A	<(DHA)
Molecular complex **41**				
N3-H3A···O2	0.86(2)	2.51(3)	2.933(2)	112(2)
N3-H3A···O4	0.86(2)	2.43(2)	3.241(2)	158(2)
N3-H3B···O1_#1	0.84(2)	1.98(2)	2.780(2)	160(2)
N3-H3C···O2_#2	0.88(2)	1.84(2)	2.720(2)	178(2)
N3-H3C···O1_#2	0.88(2)	2.65(2)	3.233(2)	125(2)
Molecular complex **42**				
N3-H3A···O2_#1	0.85(2)	2.48(2)	2.900(2)	111(2)
N3-H3A···O4_#1	0.85(2)	2.44(2)	3.225(2)	155(2)
N3-H3B···O1_#2	0.88(3)	1.93(3)	2.765(2)	157(2)
N3-H3C···O2	0.89(3)	1.83(3)	2.718(2)	178(2)
N3-H3C···O1	0.89(3)	2.63(3)	3.212(2)	124(2)

Molecular complex **41**: #1 x,y+1,z #2 -x+1,-y+1,-z

Molecular complex **42**: #1 -x+1,-y+1,-z #2 -x+1,-y+2,-z

The cations and anions in the stack are close to parallel with an angle of ~3° between the mean ring planes in both 3-XA complexes. In each complex, the halogen atom plays an identical role, forming a bifurcated halogen bond to the two O-atoms of the *p*-NO_2 group, connecting adjacent pairs of stacks perpendicular to the stacking direction (I···O = 3.247(2) Å and 3.497(2) Å in **41**, compared to the sum of the van der Waals radii of 3.50 Å; Br···O = 3.241(2) Å and 3.338(2) Å in **42**, compared to the sum of the van der Waals radii of 3.37 Å). There are also weak C-H···O hydrogen bonds (with C···O distances between 3.2 Å - 3.3 Å) between aromatic H-atoms of both molecules and carboxylate and nitro group O-atoms. The overall structure has a very similar layered structure to those seen in the 2-XA complexes (Figure 7.8 (b)), with an interlayer separation of ~3.5 Å.

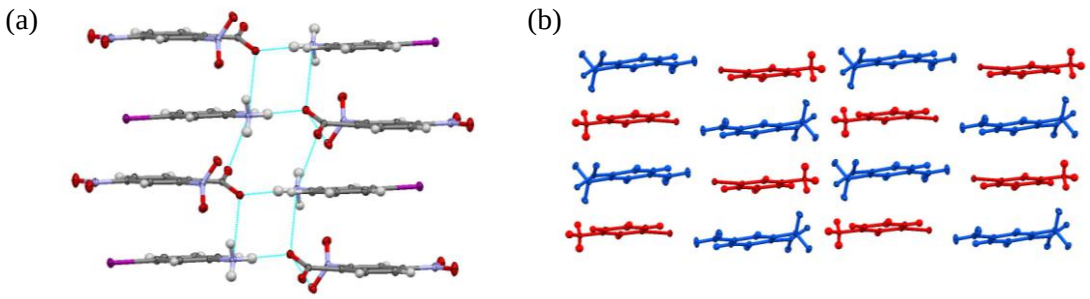

Figure 7.3 (a) N-H···O hydrogen bonds between the 3-XA cation and three 2,4-DNBA ions (shown for molecular complex **41**); (b) overall packing arrangement in molecular complexes **41** and **42**. 3-XA cations are shown in red and 2,4-DNBA anions are shown in blue.

7.2.4 4-haloanilinium and 4-iodo-2-methyanilinium 2,4-dinitrobenzoate (43 - 45)

The ionic molecular complex 4-IA 2,4-DNBA (**43**) crystallises in the orthorhombic space group $Pca2_1$; 4-BrA 2,4-DNBA (**44**) and 4-I-2-MA 2,4-DNBA (**45**) both crystallise in the monoclinic space group $P2_1/c$. All three molecular complexes have a 1:1 stoichiometry of the anilinium cation and 2,4-DNBA anion; molecular complex **43** has two independent cation/anion pairs in the asymmetric unit, while molecular complexes **44** and **45** have one of each of the ions in the asymmetric unit. The three molecular complexes all have similar layered packing arrangements (Figure 7.4), and are yielded as colourless crystals. Due to steric effects, the carboxylate groups are twisted significantly out of the ring plane, by ~83°/85°, ~80° and ~87° in **43**, **44** and **45** respectively; the *o*-NO_2 groups have torsion angles of ~3°/3°, ~13° and ~2° and the *p*-NO_2 groups have torsion angles of 12°/15°, ~1° and ~1° in **43**, **44** and **45**, respectively.

The hydrogen atoms of the NH_3^+ groups are each involved in moderate strength N-H···O hydrogen bonds with carboxylate group O-atoms, resulting in a stacked arrangement of molecules (Figure 7.4, Table 7.4). Two of the hydrogen bonds form within the same stack, and one of the hydrogen atoms acts as a bifurcated donor to the two carboxylate group O-atoms in an adjacent stack, forming a pair of stacks. Similarly to **39** and **40**, one H-atom of the NH_3^+ group is available to form a hydrogen bond with a neighbouring stack, extending the structure perpendicularly to the stacking direction. In **43**, a large hydrogen bonded ring is formed with a graph set of $R_6^5(16)$. In **44** and **45**, smaller hydrogen bonded rings are formed with $R_4^4(12)$ and $R_4^2(8)$ graph-sets, respectively (Figure 7.4). Hydrogen bonding data for **43** - **45** are given in Table 7.4.

In molecular complex **43**, there are two independent stacks with each comprising one of each of the independent cations and anions; the cations and anions in the stacks are all close to parallel, with an angle of ~3° between the mean ring planes (Figure 7.4 (a)). In molecular complexes **44** and **45**, there is a single independent stack; the cation and anion in a pair are close to parallel (angles of ~7° and ~1° between the mean ring planes in **44** and **45**, respectively). However, adjacent pairs are rotated with respect to one another (by ~20° and ~27° in **44** and **45**, respectively), forming a wave-like stack (Figure 7.4 (a)).

In addition to the N-H···O hydrogen bonds, the halogen atoms form halogen bonds to an O-atom of the *p*-NO_2 group, extending the structure perpendicularly to the stacking direction. In **43**, the halogen bonds have I···O distances of 3.067(9) Å and 3.141(9) Å (c.f. the sum of the van der Waals radii of 3.50 Å). In **44,** the Br···O distance is 3.085(1) Å (c.f. the sum of the van der Waals radii of 3.37 Å) and in **45**, the I···O distance is 3.148(2) Å. There are also weak

C-H···O hydrogen bonds in each molecular complex, formed between aromatic H-atoms of both ions and nitro group O-atoms of 2,4-DNBA, with C···O distances ranging between 3.2 - 3.4 Å. The methyl group of **45** is not involved in any intermolecular interactions. Each molecular complex has an overall layered arrangement (Figure 7.4), with approximate interlayer separations of 3.5 Å.

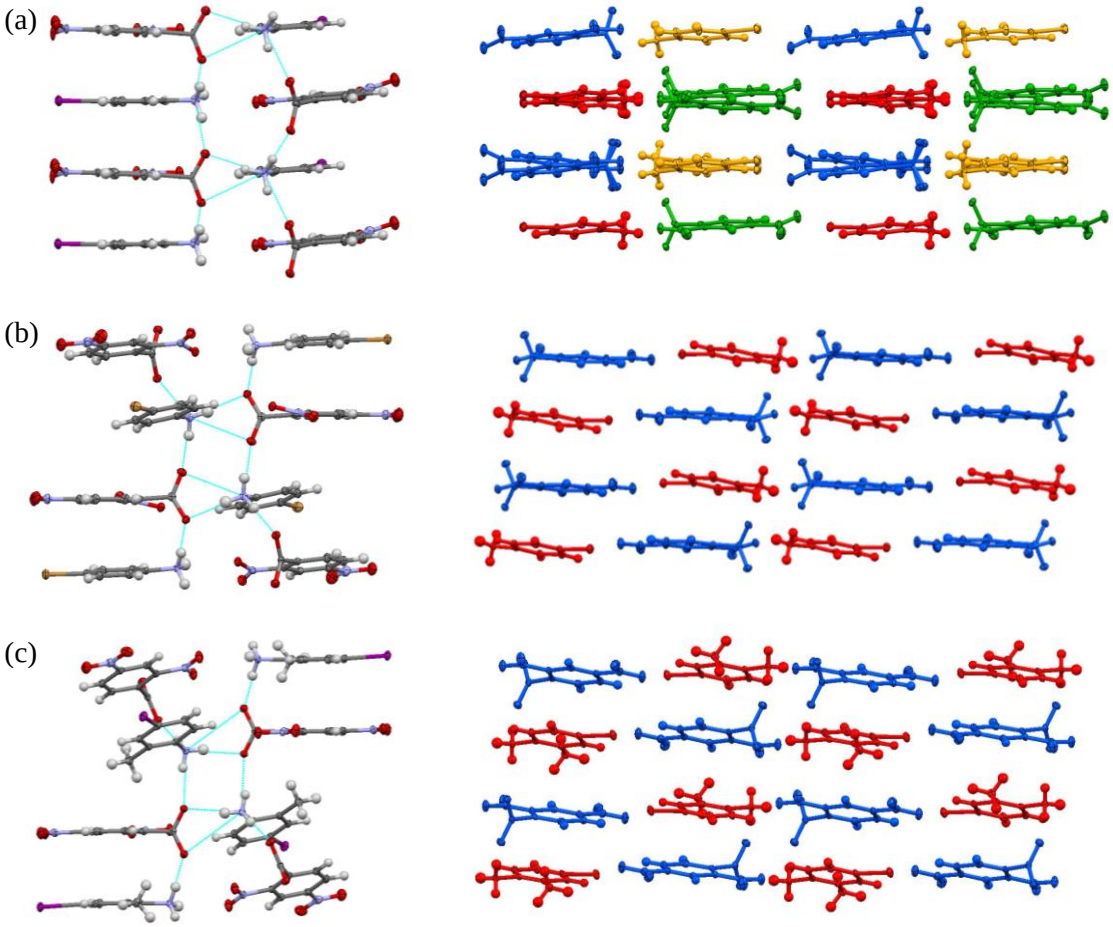

Figure 7.4 Hydrogen bonded stacks and overall packing arrangement in (a) molecular complex **43**, (b) molecular complex **44** and (c) molecular complex **45**. 4-IA cations are shown in red and yellow, 4-BrA and 4-I-2-MA cations are shown in red. 2,4-DNBA anions are shown in blue and green.

Table 7.4 Hydrogen bond data for molecular complexes **43 - 45**

D-H···A	D-H	H···A	D···A	<(DHA)
Molecular complex **43**				
N3-H5A···O8_#1	0.89	1.92	2.798(9)	169
N3-H5B···O1_#2	0.89	2.50	3.174(10)	133
N3-H5B···O2_#2	0.89	2.04	2.906(10)	165
N3-H5C···O7	0.89	1.94	2.790(8)	160
N3-H6A···O7	0.89	2.02	2.883(9)	163
N3-H6A···O8	0.89	2.61	3.277(9)	132
N3-H6B···O2_#1	0.89	1.89	2.778(8)	179
N3-H6C···O1	0.89	1.93	2.771(8)	158
Molecular complex **44**				
N3-H3A···O1_#1	0.86(2)	2.02(2)	2.878(2)	173(2)
N3-H3A···O2_#1	0.86(2)	2.53(2)	3.118(2)	126(2)
N3-H3B···O2_#2	0.88(2)	1.86(2)	2.740(2)	173(2)
N3-H3C···O2_#3	0.92(2)	1.89(2)	2.812(1)	174(2)
Molecular complex **45**				
N3-H3A···O1_#1	0.85(3)	1.99(3)	2.825(3)	167(2)
N3-H3B···O2	0.91(3)	1.84(3)	2.753(2)	175(2)
N3-H3C···O1_#2	0.84(3)	1.99(3)	2.823(2)	168(3)
N3-H3C···O2_#2	0.84(3)	2.83(3)	3.491(3)	137(3)

Molecular complex **43**: #1 x,y-1,z #2 x-1/2,-y,z

(Note: the bond distances and angles of the anilinium group were constrained to take standard values).

Molecular complex **44**: #1 -x+1,-y+1,-z+1 #2 x,y-1,z #3 x,-y+1/2,z-1/2

Molecular complex **44**: #1 x,-y+1/2,z+1/2 #2 -x+2,y-1/2,-z+3/2

7.3 Molecular complexes of 2,5-dinitrobenzoic acid

The ΔpKa values for 3-IA and 4-IA with 2,5-dinitrobenzoic acid are 1.96 and 2.19, respectively, which fall in the salt-cocrystal continuum. In both molecular complexes of 2,5-DNBA, the molecular components are present in a 1:1 stoichiometric ratio and a proton is transferred from the carboxylic acid group of 2,5-DNBA to the amine group of the haloaniline. In the 2,5-dinitrobenzoate anions, the C-O distances of the carboxylate groups are all intermediate between those expected for single and double bonds, which is consistent with a delocalisation of the charge across the group. The hydrogen atoms of the NH_3^+ groups of the 3-IA and 4-IA cations were clearly identifiable in the electron density maps. As a result of the proton transfer,

both molecular complexes are yielded as very pale yellow crystals (which corresponds to the solid-state colour of 2,5-DNBA), since the molecules cannot function as donors and acceptors.

7.3.1 Experimental details

Molecular complexes **46** and **47** were obtained *via* the method of slow evaporation (§3.1) using a 1:1 stoichiometric molar ratio of the haloaniline and 2,5-dinitrobenzoic acid; crystallisation trials employed a range of solvents and evaporation temperatures. Single crystal X-ray diffraction experiments were carried out according to the procedures outlined in §3.2. Crystallographic data is given in Table 7.5 and refinement details are reported in Appendix A7.

3-iodoanilinium 2,5-dinitrobenzoate (46)

Molecular complex **46** was synthesised from acetonitrile at ambient temperature; very pale yellow block crystals were obtained. Single crystal X-ray diffraction data were collected at 100 K using a Rigaku R-AXIS/RAPID image plate diffractometer. The structure was solved by direct methods using SHELXS-97[192] and refined using SHELXL-2014,[198] both within the WinGX program suite.[200]

4-iodoanilinium 2,5-dinitrobenzoate (47)

Molecular complex **47** was synthesised from acetonitrile at ambient temperature; very pale yellow block crystals were obtained. Single crystal X-ray diffraction data were collected at 100 K using a Rigaku R-AXIS/RAPID image plate diffractometer. The structure was solved by direct methods using SHELXS-97[192] and refined using SHELXL-2014,[198] both within the WinGX program suite.[200]

Table 7.5 Crystallographic data for molecular complexes **46** and **47**

	46	**47**
Formula	$(C_6H_7NI)^+ (C_7H_3N_2O_6)^-$	$(C_6H_7NI)^+ (C_7H_3N_2O_6)^-$
M/g mol^{-1}	431.14	431.14
T/K, radiation	100(2), Mo Kα	100(2), Mo Kα
Space Group	$P2_1/n$	$P2_1/c$
a/Å	6.9105(8)	16.164(6)
b/Å	30.274(5)	7.008(1)
c/Å	6.9379(12)	13.512(4)
α/°	90	90
β/°	100.387(5)	105.969(12)
γ/°	90	90
V/Å	1427.7(4)	1471.6(7)
Z	4	4
ρ_{cal}/ g cm^{-3}	2.006	1.946
μ/mm^{-1}	2.280	2.212
θ Range/°	3.060 - 27.486	3.048 - 27.485
Ref Collected	15082	17198
Independent	3157	3366
Observed>2σ	2839	3138
R(int)	0.0321	0.0312
Completeness %	97.3	99.9
Parameters	220	220
GooF	1.147	1.074
R_1 (obs)	0.0239	0.0208
R_1 (all)	0.0285	0.0230
wR2 (all)	0.0543	0.0489
$\rho_{max,min}$/e Å^{-3}	0.745, -0.384	0.535, -0.327

7.3.2 3-iodoanilinium 2,5-dinitrobenzoate (46) and 4-iodoanilinium 2,5-dinitrobenzoate (47)

The ionic molecular complexes of 3-IA 3,5-DNBA (**46**) and 4-IA 2,5-DNBA (**47**) crystallise in the monoclinic space groups $P2_1/n$ and $P2_1/c$, respectively. Both molecular complexes have a 1:1 stoichiometry of the haloanilinium cation and 3,5-DNBA anion, with one of each ion in the asymmetric unit; both are yielded as very pale yellow block crystals. The carboxylate groups are rotated significantly out of the ring plane due to steric effects, with torsion angles of ~75° and ~82°, in **46** and **47**, respectively; the *o*-NO_2 groups have torsion angles of ~20° and ~1° and the *m*-NO_2 groups have torsion angles of ~6° and ~1° in **46** and **47**, respectively. Each hydrogen atom of the tetrahedral NH_3^+ group is involved in a moderate strength N-H···O hydrogen bond to a carboxylate group O-atom of an adjacent 2,5-dinitrobenzoate anion, resulting in a stacked arrangement similar to the 2,4-DNBA complexes (Figure 7.5). Hydrogen bonding data for **46** and **47** are given in Table 7.6.

Table 7.6 Hydrogen bond data for molecular complexes 46 and 47

D-H···A	D-H	H···A	D···A	<(DHA)
Molecular complex **46**				
N3-H3A···O1_#1	0.85(3)	2.02(3)	2.854(4)	168(3)
N3-H3B···O2	0.83(4)	1.99(4)	2.814(3)	173(3)
N3-H3C···O2_#2	0.98(4)	1.81(4)	2.785(3)	179(3)
Molecular complex **47**				
N3-H3A···O2	0.83(3)	1.97(3)	2.783(2)	166(3)
N3-H3B···O1_#1	0.89(3)	1.88(3)	2.732(2)	160(2)
N3-H3C···O1_#2	0.88(3)	1.81(3)	2.683(2)	171(3)

Molecular complex **46**: #1 x+1,y,z #2 x+1/2,-y+1/2,z+1/2

Molecular complex **47**: #1 x,y+1,z #2 -x+1,y+1/2,-z+1/2

In molecular complex **46**, two of the hydrogen bonds form within the same stack, and the third hydrogen atom forms a hydrogen bond to a carboxylate group O-atom in an adjacent stack, forming a pair of stacks. Similarly to some of the 2,4-DNBA complexes, one H-atom of the NH_3^+ group is available to form a hydrogen bond with a neighbouring stacked pair, extending the structure perpendicularly to the stacking direction. A hydrogen bonded ring with a graph-set of $R_6^5(16)$ is formed, like that in **43** (Figure 7.5 (a)). The cation and anion are close to parallel, with an angle of only ~2° between the mean ring planes. The iodine atom forms halogen bonds to O-atoms of the *m*-nitro group which connects adjacent stacks in addition to the hydrogen bonds (I···O = 3.211(2) Å compared to the sum of the van der Waals radii of 3.50 Å). There are also weak C-H···O hydrogen bonds between aromatic H-atoms of both molecules with carboxylate and nitro group O-atoms of 2,5-DNBA anions, with C···O distances between 3.2 Å - 3.4 Å. The overall structure is layered with an interlayer separation of ~3.5 Å.

In **47**, a similar hydrogen bonded chain is formed to **46**, but the hydrogen bonds are saturated within a pair of stacks (Figure 7.5 (b)), forming $R_4^3(10)$ hydrogen bonded rings, unlike any of the 2,4-DNBA complexes. The cation and anion are rotated with respect to one another, by an angle of ~14°, forming a wave-like stack. The pairs of stacks are extended in the direction perpendicular to the stacking direction *via* C-I···O halogen bonds to *m*-NO_2 group O-atoms, with an I···O distance of 3.260(2) Å (compared to the sum of the van der Waals radii of 3.50 Å). In addition, there are weak C-H···π hydrogen bonds between aromatic H-atoms of both ions and the aromatic rings of the alternate ion, and C-H···O hydrogen bonds between the aromatic H-atoms of both ions and the nitro group O-atoms (interaction distances in the range 3.2 - 3.4 Å). The overall structure consists of rippled layers (Figure 7.5 (b)).

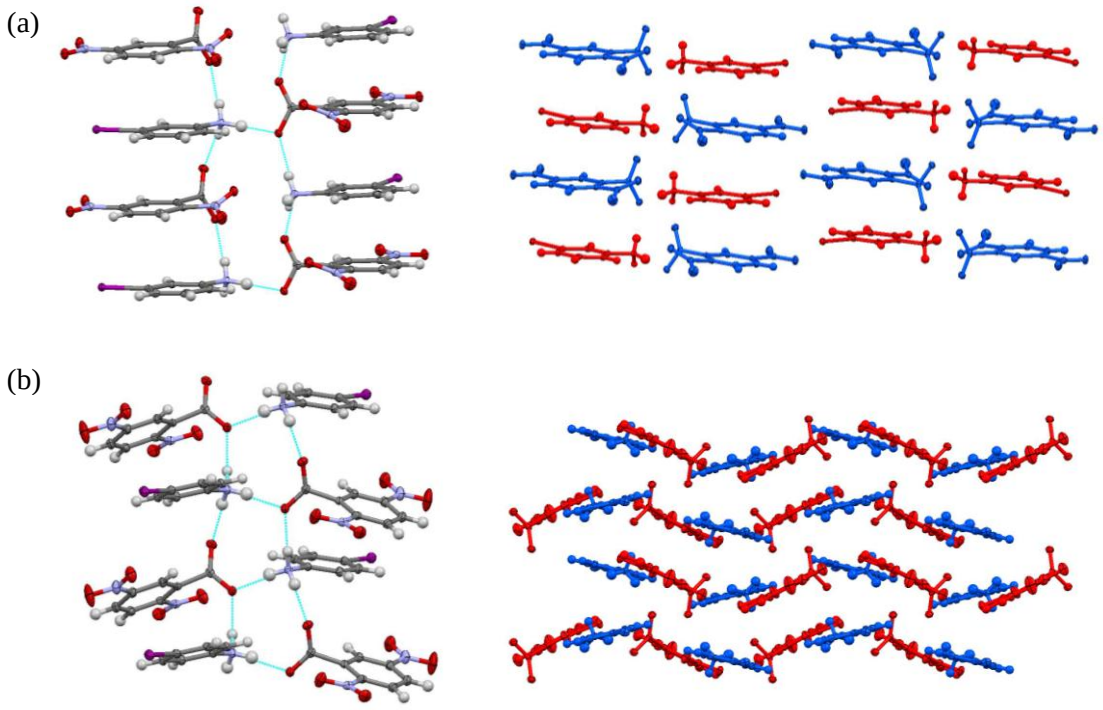

Figure 7.5 (a) Hydrogen bonded stacks and layered packing arrangement in molecular complex **46**; (b) hydrogen bonded stacks and rippled layer packing arrangement in molecular complex **47**. Haloanilinium cations are shown in red and 2,5-DNBA anions are shown in blue.

7.4 Molecular complexes of 3,5-dinitrosalicylic acid

The ΔpKa values for the anilines with 3,5-dinitrosalicylic acid fall in the salt-cocrystal continuum, with the exception of the 4-Br-3-MA complex which has a ΔpKa of greater than 3. For 2-IA, 2-BrA and 2-ClA with 3,5-DNSA, the values are 1.84, 1.83 and 1.96, respectively; for 3-IA and 3-BrA with 3,5-DNSA the values are 2.88 and 2.83, respectively; for 4-Br-3-MA the value is 3.35. In each of the molecular complexes of 3,5-dinitrosalicylic acid, the molecular components are present in a 1:1 stoichiometric ratio and a proton is transferred between 3,5-DNSA molecule and the amine group of the aniline. Note, the ionic 1:1 molecular complexes with the 4-haloanilines are reported in Chapter 6.

In each of the molecular complexes, an intramolecular O-H···O hydrogen bond is formed in the 3,5-dinitrosalicylate anion, between the carboxylic acid and hydroxyl groups, thus the carboxylic acid group is close to coplanar with the aromatic ring. The hydrogen atoms reside closer to the carboxylic acid group O-atom in each case; the C-O bond lengths of the carboxylic acid groups are consistent with those expected for single and double C-O bonds. The hydroxyl group C-O bonds have distances consistent with deprotonation. The hydrogen atoms of the NH_3^+ groups of the aniline molecules and the carboxylic acid groups were clearly identifiable in

the electron density maps. Despite the planarity of the 3,5-DNSA molecule, the proton transfer in the 1:1 complexes means there are no neutral molecules and the molecular complexes are all yielded as very pale yellow crystals (which corresponds to the solid-state colour of 3,5-DNSA), since the molecules cannot function as donors and acceptors.

7.4.1 Experimental details

Molecular complexes **48** - **53** were obtained *via* the method of slow evaporation (§3.1) using a 1:1 stoichiometric molar ratio of the haloaniline and 3,5-dinitrosalicylic acid; crystallisation trials employed a range of solvents and evaporation temperatures. Single crystal X-ray diffraction experiments were carried out according to the procedures outlined in §3.2. Crystallographic data are given in Table 7.7 and refinement details are reported in Appendix A7.

2-iodoanilinium 3,5-dinitrosalicylate (48)

Molecular complex **48** was synthesised from acetonitrile at 50 °C; pale yellow block crystals were obtained. Single crystal X-ray diffraction data were collected at 100 K using a Rigaku R-AXIS/RAPID image plate diffractometer. The structure was solved by direct methods using SHELXS-97[192] and refined using SHELXL-2014,[198] both within the WinGX program suite.[200]

2-bromoanilinium 3,5-dinitrosalicylate (49)

Molecular complex **49** was synthesised from ethyl acetate at ambient temperature; pale yellow block crystals were obtained. Single crystal X-ray diffraction data were collected at 100 K using a Rigaku R-AXIS/RAPID image plate diffractometer. The structure was solved by direct methods using SHELXS-97[192] and refined using SHELXL-2014,[198] both within the WinGX program suite.[200]

2-chloroanilinium 3,5-dinitrosalicylate (50)

Molecular complex **50** was synthesised from ethanol at ambient temperature; pale yellow block crystals were obtained. Single crystal X-ray diffraction data were collected at 100 K using a Rigaku Oxford Diffraction Gemini Ultra diffractometer (Mo Kα radiation). The structure was solved by direct methods using SHELXS-2013[192] and refined using SHELXL-2014,[198] both within the WinGX program suite.[200]

3-iodoanilinium 3,5-dinitrosalicylate (51)

Molecular complex **51** was synthesised from ethanol at ambient temperature; pale yellow block crystals were obtained. Single crystal X-ray diffraction data were collected at 100 K using a Rigaku R-AXIS/RAPID image plate diffractometer. The structure was solved by direct methods using SHELXS-97[192] and refined using SHELXL-2014,[198] both within the WinGX program suite.[200]

3-bromoanilinium 3,5-dinitrosalicylate (52)

Molecular complex **52** was synthesised from ethanol at ambient temperature; pale yellow block crystals were obtained. Single crystal X-ray diffraction data were collected at 100 K using a Rigaku R-AXIS/RAPID image plate diffractometer. The structure was solved by direct methods using SHELXS-97[192] and refined using SHELXL-2014,[198] both within the WinGX program suite.[200]

4-bromo-3-methylanilinium 3,5-dinitrosalicylate (53)

Molecular complex **53** was synthesised from 2-propanol at ambient temperature; pale yellow block crystals were obtained. Single crystal X-ray diffraction data were collected at 150 K using a Rigaku Oxford Diffraction Xcalibur diffractometer. The structure was solved by direct methods using SHELXS-2013[192] and refined using SHELXL-2014,[198] both within the WinGX program suite.[200]

Table 7.7 Crystallographic data for molecular complexes **48** - **53**

	48	**49**	**50**	**51**	**52**	**53**
Formula	$(C_6H_7NI)^+$ $(C_7H_3N_2O_7)^-$	$(C_6H_7NBr)^+$ $(C_7H_3N_2O_7)^-$	$(C_6H_7NCl)^+$ $(C_7H_3N_2O_7)^-$	$(C_6H_7NI)^+$ $(C_7H_3N_2O_7)^-$	$(C_6H_7NBr)^+$ $(C_7H_3N_2O_7)^-$	$(C_7H_9NBr)^+$ $(C_7H_3N_2O_7)^-$
M/g mol^{-1}	447.14	400.15	355.69	447.14	400.15	414.18
T/K, radiation	100(2), Mo Kα	100(2), Mo Kα	150(2), Mo Kα	100(2), Mo Kα	100(2), Mo Kα	150(2), Mo Kα
Space Group	$P\bar{1}$	$P\bar{1}$	$P\bar{1}$	$P\bar{1}$	$P\bar{1}$	$P\bar{1}$
a/Å	7.5943(7)	7.801(1)	7.8206(4)	7.5631(17)	7.4502(5)	7.4240(4)
b/Å	8.1263(8)	9.640(2)	9.6661(7)	8.908(2)	8.1486(5)	8.1183(4)
c/Å	13.3529(14)	10.533(2)	10.4579(7)	11.660(3)	12.6619(9)	13.7240(7)
α	91.082(4)	76.690(6)	76.938(6)	75.843(8)	80.999(6)	86.160(5)
β	102.125(4)	87.140(6)	87.126(5)	83.257(8)	87.551(6)	85.781(4)
γ	101.742(3)	68.069(5)	67.759(6)	77.224(7)	68.459(5)	69.063(5)
V/Å	787.2(2)	714.5(3)	712.26(9)	741.2(3)	706.10(9)	769.71(7)
Z	2	2	2	2	2	2
ρ_{cal}/ g cm^{-3}	1.886	1.860	1.658	2.003	1.882	1.787
μ/mm^{-1}	2.076	2.923	0.315	2.205	2.958	2.717
θ Range/°	3.089 - 27.485	3.284 - 27.478	2.816 - 30.496	3.202 - 27.485	3.193 - 27.482	3.368 - 26.369
Ref Collected	19025	16185	10731	18161	15883	9456
Independent	3591	3243	3826	3381	3228	3124
Observed>2σ	2378	3038	2785	3181	3094	2700
Rint	0.0305	0.0411	0.0389	0.0257	0.0304	0.0298
Completeness %	99.8	99.3	99.9	99.7	99.8	99.7
Parameters	188	232	232	233	233	250
GooF	1.200	1.103	1.045	1.140	1.055	1.057
R_1 (obs)	0.0620	0.0266	0.0471	0.0191	0.0226	0.0306
R_1 (all)	0.0914	0.0295	0.0764	0.0209	0.0239	0.0404
wR2 (all)	0.2267	0.0620	0.1034	0.0486	0.0563	0.0653
$\rho_{max,min}$/e Å^{-3}	2.466, -1.128	0.553, -0.362	0.360, -0.277	0.874, -0.295	0.476, -0.241	0.321, -0.301

7.4.2 2-haloanilinium 3,5-dinitrosalicylate (48 - 50)

The ionic molecular complexes of 2-IA 3,5-DNSA (**48**), 2-BrA 3,5-DNSA (**49**) and 2-ClA 3,5-DNSA (**50**) all crystallise in the triclinic space group $P\bar{1}$, and are yielded as pale yellow block crystals. The 2-haloanilinium (2-XA) and 3,5-dinitrosalicylate ions are present in a 1:1 ratio with one independent cation and anion in the asymmetric unit. Molecular complexes **49** and **50** are isomorphous, and **48** has a similar packing arrangement. An intramolecular O-H···O hydrogen bond is formed in the 3,5-dinitrosalicylate anion, between the carboxylic acid and hydroxyl groups (Table 7.9). The hydrogen atoms resides closer to the carboxylic acid group O atom in each case, with O-H distances of 0.93(9) Å, 0.74(3) Å and 0.92(2) Å in **48**, **49** and **50**, respectively. The C-O bond lengths of the carboxylic acid group are consistent with those expected for single and double C-O bonds (1.218(8) Å/1.303(8) Å (**48**), 1.221(3) Å/1.310(2) Å (**49**) and 1.226(3) Å/1.314(2) Å (**50**)). The C-O bond lengths of the deprotonated hydroxyl group are 1.286(7) Å, 1.294(2) Å and 1.297(2) Å in **48**, **49** and **50**, respectively, which is consistent with deprotonation. In each molecular complex, due to the formation of the intramolecular hydrogen bond, the carboxylic acid group is close to coplanar with the ring planes, with torsion angles of ~1°, ~2° and ~2° in molecular complexes **48**, **49** and **50**, respectively. The two nitro groups in each molecular complex are rotated out of the ring plane by ~8°/~30° in **48**, ~2°/~6° in **49**, and ~2°/~6° in **50**.

In an anisotropic refinement of the 2-IA 3,5-DNSA complex, **48**, the anisotropic displacement parameters of the 2-IA molecule implied rotation about a pivot amine group; the molecule has thus been modelled as disordered over two positions, with relative occupancies of 0.69(1) and 0.31(1) (shown in purple and green, respectively, Figure 7.6 (a)). In both modelled positions of the 2-IA cation, each hydrogen atom of the NH_3^+ group forms the same moderate strength N-H···O hydrogen bond. One H-atom forms a hydrogen bond with the deprotonated hydroxyl group, and one forms a hydrogen bond with the carbonyl group O-atom. The third H-atom acts as a bifurcated donor, forming hydrogen bonds with nitro group O-atoms of two adjacent 3,5-DNSA anions. In both modelled positions of the 2-IA cation, the iodine atom forms a halogen bond to an O-atom of an adjacent nitro group O-atom, with I···O distances of 3.07(7) Å and 3.36(8) Å for the major and minor orientations (shown in purple and green, respectively). There are also short O···O interactions between adjacent nitro and carboxylic acid groups. The cation and anion are rotated by ~57° with respect to each other, resulting in a non-layered packing arrangement (Figure 7.6 (c)); there are parallel offset π···π interactions between stacked 3,5-DNSA anions, with an approximate intermolecular separation of ~3.35 Å.

Table 7.8 Hydrogen bond data for molecular complexes **48 - 50**

D-H···A	D-H	H···A	D···A	<(DHA)
Molecular complex **48**				
O2-H2···O3	0.94(9)	1.64(9)	2.482(6)	147(8)
N3-H3A1···O1_#1	0.89	1.95	2.84(2)	178
N3-H3A2···O7	0.89	2.26	3.01(2)	142
N3-H3A2···O5_#2	0.89	2.65	3.12(2)	114
N3-H3A3···O3_#3	0.89	1.96	2.83(2)	165
N3-H3B1···O1_#1	0.89	2.04	2.84(3)	149
N3-H3B2···O7	0.89	2.40	3.10(3)	135
N3-H3B2···O5_#2	0.89	2.70	3.30(4)	126
N3-H3B3···O3_#3	0.89	1.87	2.68(3)	149
Molecular complex **49**				
O2-H2···O3	0.74(3)	1.79(3)	2.496(2)	159(3)
N3-H3A···O3_#1	0.87(3)	2.06(3)	2.892(2)	158(3)
N3-H3A···O4_#1	0.87(3)	2.57(3)	3.084(2)	118(2)
N3-H3B···O1_#2	0.87(3)	1.92(3)	2.786(2)	177(2)
N3-H3C···O3_#3	0.89(2)	2.01(3)	2.893(2)	174(2)
N3-H3C···O4_#3	0.89(2)	2.48(2)	2.925(2)	112(2)
Molecular complex **50**				
O2-H2···O3	0.92(2)	1.61(2)	2.499(2)	160(2)
N3-H3A···O3_#1	0.89(2)	2.10(2)	2.925(2)	154(2)
N3-H3A···O4_#1	0.89(2)	2.55(2)	3.108(2)	122(2)
N3-H3B···O1_#2	0.94(2)	1.83(2)	2.771(2)	180(2)
N3-H3C···O3_#2	0.96(3)	1.93(3)	2.890(3)	174(2)
N3-H3C···O4_#3	0.96(3)	2.45(2)	2.952(2)	112(2)

Molecular complex **48**: #1 x+1,y+1,z #2 -x+1,-y-1,-z+2 #3 -x,-y-1,-z+2

Note: the anilinium group H-atoms were placed in calculated positions; hydrogen bond data is given for both 2-IA positions.

Molecular complex **49**: #1 x,y,z-1 #2 -x+2,-y,-z+2 #3 -x+1,-y,-z+2

Molecular complex **50**: #1 x,y+1,z #2 x-1,y+1,z #3 x,y+1,z

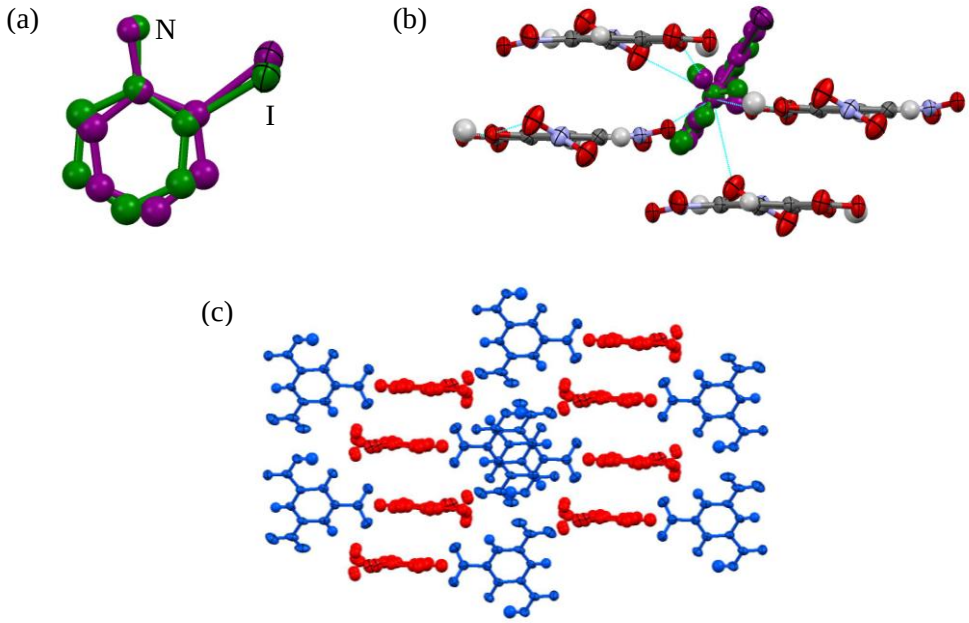

Figure 7.6 (a) Modeling of the disorder of the 2-IA molecule in molecular complex **48** over two positions about the pivot nitro group, with relative occupancies of 0.69(1) and 0.31(1), shown in purple and green, respectively. Hydrogen atoms have been omitted for clarity. (b) Hydrogen bonding between the 2-IA and 3,5-DNSA ions. (c) Overall packing arrangement in molecular complex **48**; 2-IA cations are shown in red and 3,5-DNSA anions are shown in blue.

In the isomorphous molecular complexes **49** and **50**, the molecules are fully ordered. Two hydrogen atoms of the NH_3^+ group of the 2-haloanilinium cations both form a bifurcated N-H···O hydrogen bond to hydroxyl and nitro group O-atoms of the same 3,5-DNSA anion. The third hydrogen atom forms a hydrogen bond to a carboxyl group O-atom of an adjacent anion (Figure 7.7 (a)). In molecular complex **49**, the bromine atoms form Br···Br halogen interactions (type I), with a distance of 3.517(5) Å (compared to the sum of the van der Waals radii of 3.70 Å); the corresponding Cl···Cl distance in molecular complex **50** is greater than the sum of the van der Waals radii. There are also a number of weak C-H···O hydrogen bonds between aromatic H-atoms of the 2-XA cations and the nitro group O-atoms of adjacent anions, with C···O distances in the range 3.3 - 3.5 Å; in addition, there are O···O and O···π interactions between anions, involving the nitro group O-atoms. The cation and anion are rotated by ~47° and 48° with respect to each other in molecular complexes **49** and **50**, respectively, resulting in a non-layered packing arrangement (Figure 7.7 (b)); there are no π···π interactions between pairs of cations or pairs of anions due to a large offset of the molecules in each case.

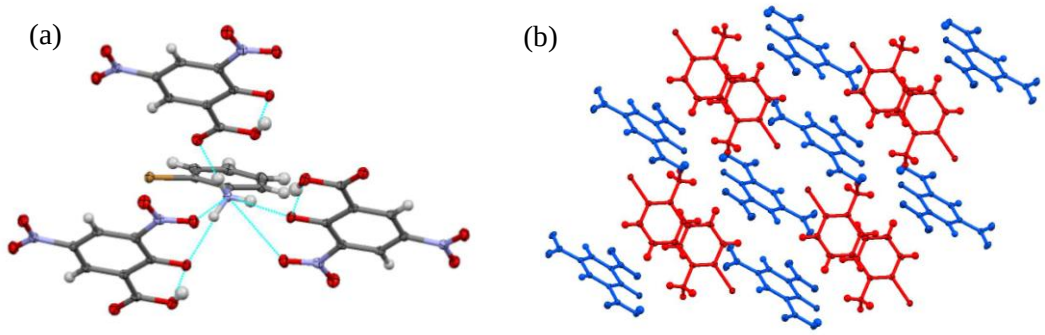

Figure 7.7 (a) Hydrogen bonding between the 2-XA cation and three adjacent 3,5-DNSA anions, shown for molecular complex **49**; (b) overall packing arrangement in molecular complexes **49** and **50**. 2-XA cations are shown in red and 3,5-DNSA anions are shown in blue.

7.4.3 3-haloanilinium 3,5-dinitrosalicylate (51 and 52)

The ionic molecular complexes of 3-IA 3,5-DNSA (**51**) and 3-BrA 3,5-DNSA (**52**) both crystallise in the triclinic space group $P\bar{1}$, and are yielded as pale yellow block crystals. The molecular components are present in a 1:1 ratio with one independent cation and anion in the asymmetric unit. The two molecular complexes are structurally similar, but they are not isostructural. An intramolecular O-H···O hydrogen bond is formed in the 3,5-dinitrosalicylate anion, between the carboxylic acid and hydroxyl groups (Table 7.9). The hydrogen atoms resides closer to the carboxylic acid group O atom in each case, with O-H distances of 0.72(3) Å and 0.84(2) Å in **51** and **52**, respectively. The C-O bond lengths of the carboxylic acid group (1.220(2) Å/1.315(2) Å (**51**) and 1.219(2) Å/1.317(2) Å (**52**)) are consistent with those expected for single and double C-O bonds. The C-O bond lengths of the deprotonated hydroxyl group are 1.287(2) Å and 1.285(2) Å in **51** and **52**, respectively, which is consistent with deprotonation. The carboxylic acid group is close to coplanar with the ring planes (~7° and ~1° in molecular complexes **51** and **52**, respectively), due to the formation of the intramolecular hydrogen bond; the nitro groups are rotated out of the ring plane by ~0°/~5° in **51** and by ~2° for both of the nitro groups in **52**.

The NH_3^+ groups of the 3-haloaniline cations form N-H···O hydrogen bonds to four 3,5-DNSA anions (Table 7.9). H3B and H3C are involved in hydrogen bonds to the carbonyl O-atom of the carboxylic acid group and O-atom of the deprotonated hydroxyl group, respectively; these two hydrogen bonds form between cations and anions in the same layer. The third hydrogen atom, H3A, acts as a bifurcated hydrogen bond donor to the nitro group O-atoms of two 3,5-DNSA anions in an adjacent layer (Figure 7.8).

Table 7.9 Hydrogen bond data for molecular complexes **51** and **52**

D-H···A	D-H	H···A	D···A	<(DHA)
Molecular complex **51**				
O2-H2A···O3	0.72(3)	1.81(3)	2.502(2)	161(3)
N3-H3A···O5_#1	0.87(3)	2.17(3)	2.975(2)	153(2)
N3-H3A···O7_#2	0.87(3)	2.37(2)	2.936(2)	122(2)
N3-H3B···O3_#3	0.89(3)	1.90(3)	2.777(2)	169(2)
N3-H3C···O1_#4	0.87(3)	1.93(3)	2.775(2)	165(3)
Molecular complex **52**				
O2-H2A···O3	0.84(2)	1.65(2)	2.470(2)	161(2)
N3-H3A···O5_#1	0.88(2)	2.39(2)	2.996(2)	126(2)
N3-H3A···O7_#2	0.88(2)	2.29(2)	3.000(2)	138(2)
N3-H3B···O3_#3	0.85(2)	1.92(2)	2.717(2)	156(2)
N3-H3C···O1_#4	0.83(2)	1.97(2)	2.799(2)	173(2)

Molecular complex **51**: #1 -x+1,-y-1,-z+1 #2 -x+1,-y,-z+1 #3 x+1,y+1,z-1 #4 x+1,y,z-1

Molecular complex **52**: #1 x+1,y,z #2 x,y+1,z #3 -x,-y+2,-z+1 #4 -x+1,-y+1,-z+1

A sheet structure is formed through the combination of the two hydrogen bonds involving H3B and H3C, and interactions between the halogen atom and an O-atom of a nitro group (I···O = 3.157(2) Å c.f. the sum of the van der Waals radii of 3.50 Å; Br···O = 3.333(1) Å c.f. the sum of the van der Waals radii of 3.37 Å) (Figure 7.8). The main difference in the sheet structures of the two molecular complexes is the tilt of the 3-XA cation with respect to the 3,5-DNSA anion; in **51**, there is an angle of ~13° of between the mean ring planes of the cation and anion, which contrasts with ~52° in **52**.

The bifurcated hydrogen bond involving H3A results in the formation of a pair of sheets. In **51**, there are parallel offset π···π interactions between pairs of 3-IA cations, separated by ~3.52 Å, and parallel offset π···π interactions between pairs of 3,5-DNSA anions, separated by ~3.31 Å. In **52**, there are parallel offset π···π interactions between pairs of 3-BrA cations, separated by ~3.35 Å, and parallel offset π···π interactions between pairs of 3,5-DNSA anions, separated by ~3.30 Å. In both complexes, pairs of sheets stack *via* offset π···π interactions between 3,5-DNSA anions. In **51**, the columns consist of alternating pairs of 3-IA and 3,5-DNSA (Figure 7.9 (a)), but there are no interactions between the cation and anion in adjacent layers. In molecular complex **52**, there are segregated stacks of 3-BrA cations and 3,5-DNSA anions (Figure 7.9 (b)).

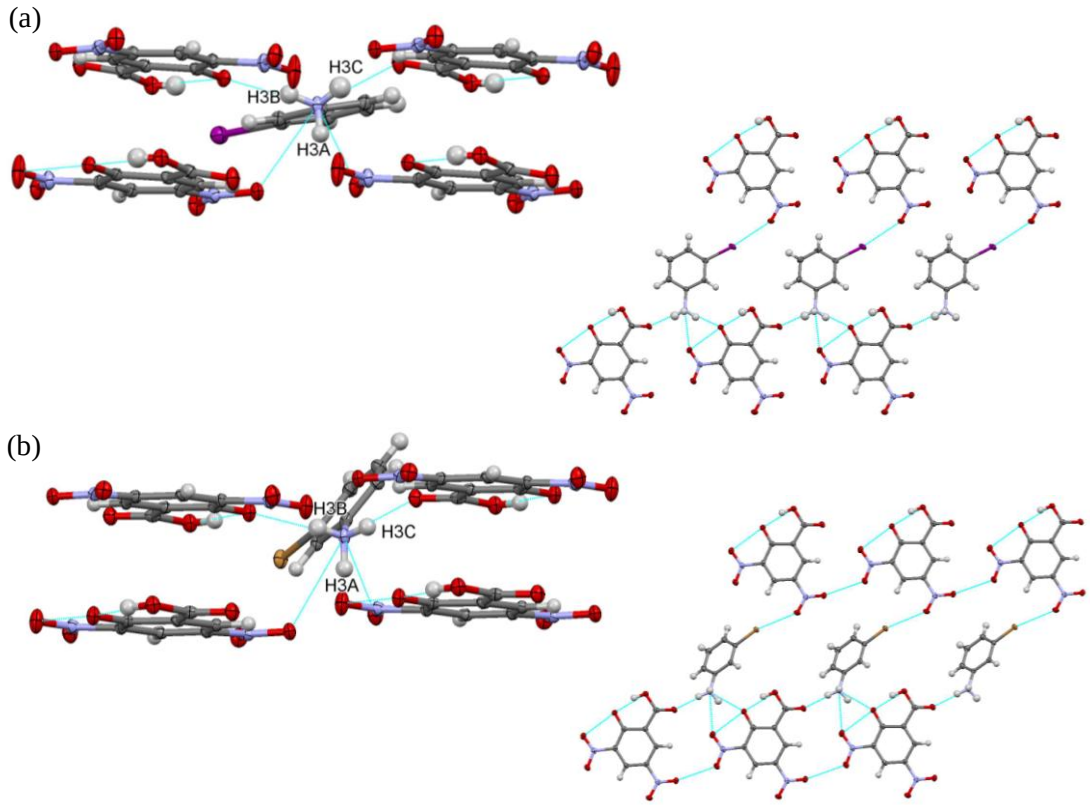

Figure 7.8 Hydrogen bonds formed between the NH_3^+ group of the 3-haloaniline cation and three 3,5-DNSA anions, and the formation of the sheet structure through two hydrogen bonds and a short X···O interaction, in (a) molecular complex **51** and (b) molecular complex **52**.

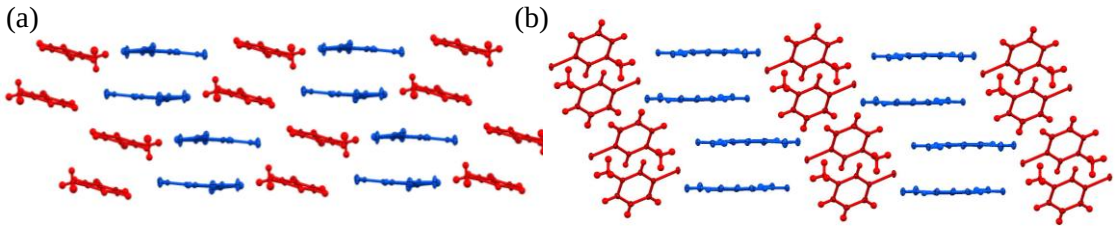

Figure 7.9 (a) Crystal packing in molecular complex **51** and (b) crystal packing and segregated stacks in molecular complex **52**. 3-XA cations are shown in red and 3,5-DNSA anions are shown in blue.

7.4.4 4-bromo-3-methylanilinium 3,5-dinitrosalicylate (53)

The ionic molecular complex of 4-Br-3-MA 3,5-DNSA (**53**) crystallises in the triclinic space group $P\bar{1}$, forming as pale yellow block crystals. The molecular components crystallise in a 1:1 ratio with one cation and anion in the asymmetric unit. An intramolecular O-H···O hydrogen bond is formed in the 3,5-dinitrosalicylate anion, between the carboxylic acid and hydroxyl groups (Table 7.10). The hydrogen atom resides closer to the carboxylic acid group O-atom in each case, with an O-H distance of 0.88(3) Å (Table 7.10). The C-O bond lengths of the carboxylic acid group (1.220(2) Å/1.313(3) Å) are consistent with those expected for single and

double C-O bonds. The carboxylic acid group is close to coplanar with the ring planes, with a torsion angle of ~2°, and the nitro groups are rotated out of the ring plane by ~1° and ~6°.

The 4-Br-3-MA cation has disorder of the methyl group (approximately 50:50) over the two *meta*-positions, with relative occupancies of 0.518(6) and 0.482(6) for the two sites (shown in purple and green, respectively, Figure 7.10 (a)). The NH_3^+ group of the cation forms N-H···O hydrogen bonds to four 3,5-DNSA anions (Table 7.10, Figure 7.10 (b)). H3B forms moderate strength bifurcated hydrogen bonds to nitro group O-atoms of two 3,5-DNSA anions and H3C forms moderate strength bifurcated hydrogen bonds to nitro group and hydroxyl group O-atoms on the same 3,5-DNSA anion. The third hydrogen atom, H3A, forms a moderate strength hydrogen bond to a carboxyl O-atom.

Table 7.10 Hydrogen bond data for molecular complex **53**

D-H···A	**D-H**	**H···A**	**D···A**	**<(DHA)**
Molecular complex **53**				
O2-H2···O3	0.88(3)	1.66(3)	2.498(2)	159(3)
N3-H3A···O1_#1	0.86(3)	1.94(3)	2.795(3)	178(3)
N3-H3B···O5_#2	0.88(3)	2.37(3)	2.989(3)	128(2)
N3-H3B···O7_#3	0.88(3)	2.25(3)	2.978(3)	140(2)
N3-H3C···O3_#4	0.94(3)	1.83(3)	2.737(3)	162(2)
N3-H3C···O4_#4	0.94(3)	2.25(3)	2.797(3)	116(2)

#1 x-1,y+1,z+1 #2 -x,-y+1,-z+2 #3 -x+1,-y,-z+2 #4 x,y,z+1

A sheet structure is formed, similar to that in the 3-XA 3,5-DNSA complexes (**51** and **52**), through a combination of the hydrogen bonds involving H3A and H3C, and halogen bonds between the bromine and O-atom of a nitro group (Br···O = 3.157(2) Å c.f. the sum of the van der Waals radii of 3.37 Å) (Figure 7.10 (c)). There is an angle of ~42° of between the mean ring planes of the cation and anion. The interaction of the third hydrogen atom, H3B, with two anions in an adjacent layer results in the formation of a pair of sheets, with parallel offset π···π interactions between pairs of 3,5-DNSA anions, separated by ~3.29 Å, extending the structure perpendicular to the sheets; there are no interactions between anions. The methyl group is not involved in any interactions. The overall packing arrangement is non-layered with segregated cations and anions (Figure 7.10 (d)), similar to that of 3-BrA 3,5-DNSA (**52**); however, the packing is quite different to the corresponding non-methyl substituted 1:1 complex of 4-BrA 3,5-DNSA (**34**) discussed in Chapter 6, which must be a consequence of the extra space required to accommodate the methyl group.

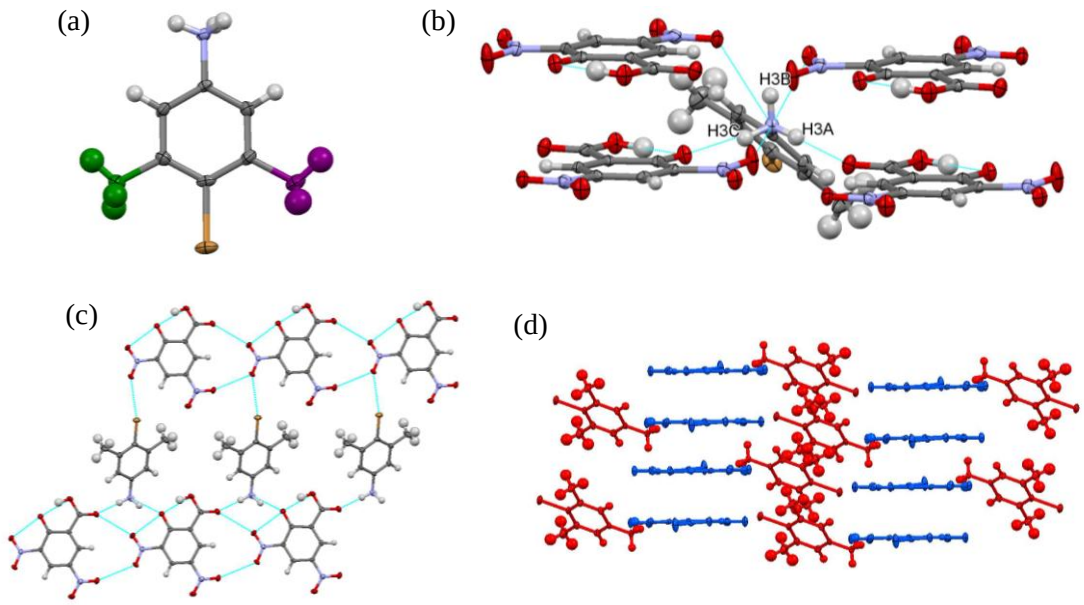

Figure 7.10 (a) Disorder of the methyl group over two positions (shown in purple and green) in the 4-Br-3-MA cation; (b) hydrogen bonding between the 4-Br-3-MA cation and four 3,5-DNSA anions in molecular complex **53**; (c) formation of a sheet structure through two hydrogen bonds and a Br···O halogen bond; (d) overall packing arrangement in **53**, with 4-Br-3-MA cations shown in red and 3,5-DNSA anions shown in blue. Note: both possible positions of the disordered methyl group are shown.

7.5 Molecular complex of 2-NBA

It was possible to form only a single molecular complex with a singly nitro-substituted benzoic acid co-former in this study, that of 4-iodoanilinium 2-nitrobenzoate; the ΔpKa value for the complex is 1.64, falling in the salt-cocrystal continuum. Proton transfer occurs between the carboxylic acid group of 2-NBA and the amine group of the 4-IA. The C-O distances of the carboxylate group are intermediate between those expected for single and double bonds, which is consistent with a delocalisation of the charge across the group. The hydrogen atoms of the NH_3^+ groups of the aniline molecules were clearly identifiable in the electron density maps. As a result of the proton transfer, the molecular complex is yielded as colourless crystals since the molecules cannot function as donors and acceptors.

7.5.1 Experimental details

4-iodoanilinium 2-nitrobenzoate (54)

Molecular complex **54** was synthesised *via* slow evaporation (§3.1) from acetone at 4 °C using a 1:1 stoichiometric molar ratio of 4-iodoaniline and 2-nitrobenzoic acid; colourless block crystals were obtained. Single crystal X-ray diffraction data were collected at 100 K, according to the procedures outlined in §3.2, using a Rigaku R-AXIS/RAPID image plate diffractometer. The

structure was solved by direct methods using SHELXS-97[192] and refined using SHELXL-97,[198] both within the WinGX program suite.[200] Crystallographic data are given in Table 7.11 and refinement details are reported in Appendix A7.

Table 7.11 Crystallographic data for molecular complex **54**

	54
Formula	$(C_6H_7NI)^+$ $(C_7H_4NO_4)^-$
M/g mol^{-1}	386.14
T/K, radiation	100(2), Mo Kα
Space Group	$P2_1/c$
a/Å	14.5446(8)
b/Å	5.8800(4)
c/Å	15.9960(13)
α/°	90
β/°	95.857(3)
γ/°	90
V/Å	1360.9(2)
Z	4
ρ_{cal}/ g cm^{-3}	1.885
μ/mm^{-1}	2.368
θ Range/°	3.045 - 27.480
Ref Collected	16463
Independent	3132
Observed>2σ	2904
R(int)	0.0251
Completeness %	99.8
Parameters	190
GooF	1.067
R_1 (obs)	0.0213
R_1 (all)	0.0241
wR2 (all)	0.0494
$\rho_{max,min}$/e Å^{-3}	0.663, -0.323

7.5.2 4-iodoanilinium 2-nitrobenzoate (54)

The ionic molecular complex of 4-IA 2-NBA (**54**) crystallises in the triclinic space group $P\bar{1}$ and is yielded as colourless block crystals. The complex has a 1:1 stoichiometry of the 4-iodoanilinium cation and 2-nitrobenzoate anion, with one of each ion in the asymmetric unit. The carboxylate group is twisted significantly out of the ring plane, by ~25° due to steric effects; the *o*-NO_2 group has a torsion angle of ~69°. Each hydrogen atom of the NH_3^+ group forms a moderate strength N-H···O hydrogen bond to an adjacent carboxylate group O-atom, resulting in a hydrogen bonded chain of cations and anions (Figure 7.11 (a)). The cation and anion are rotated with respect to one another by ~57°, resulting in a non-layered packing arrangement (Figure 7.11 (b)). Within the chains there are also weak C-H···O hydrogen bonds

(C···O = 3.378(2) Å and 3.483(2) Å) between adjacent aromatic H-atoms of 4-IA and the two O-atoms of the nitro group of 2-NBA.

Table 7.12 Hydrogen bond data for molecular complex **54**

D-H···A	D-H	H···A	D···A	<(DHA)
N2-H2A···O2_#1	0.92(3)	1.81(3)	2.725(2)	175(2)
N2-H2B···O1_#2	0.86(3)	2.02(3)	2.856(2)	166(2)
N2-H2C···O1_#3	0.85(3)	1.97(3)	2.808(2)	168(2)

#1 x-1,y,z #2 -x+1, y+1/2,-z+1/2 #3 x-1,y+1,z

The chains are extended in the direction perpendicular to the chain through C-I···O halogen bonds to nitro group O-atoms, with an I···O distance of 3.143(1) Å, compared to the sum of the van der Waals radii of 3.50 Å. Above and below the chains, weak C-H···π hydrogen bonds form between the aromatic H-atoms of the anion and the π-system of the cation, with an interaction distance of ~3.5 Å; there are also weak C-H···O hydrogen bonds between an aromatic H-atom of one anion and an O-atom of an adjacent twisted carboxylate group (C···O = 3.378(2) Å).

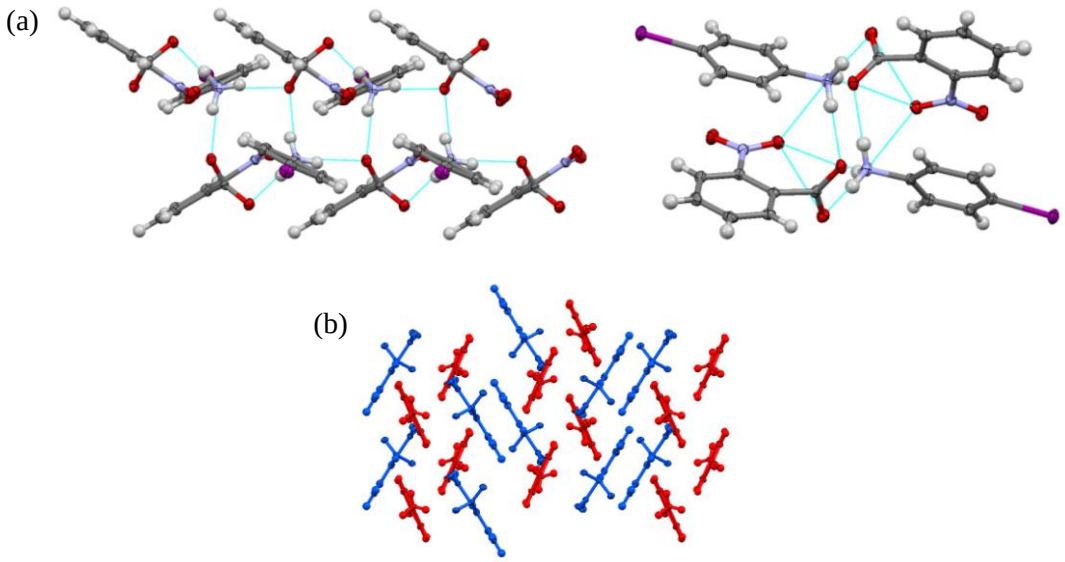

Figure 7.11 (a) Hydrogen bonded chain of cations and anions in molecular complex **54**, viewed side-on (left) and along the chain (right); (b) non-layered packing arrangement, with 4-IA cations shown in red and 2-NBA anions shown in blue.

7.6 Conclusions

The seventeen molecular complexes discussed in this chapter are all fully ionic, with a 1:1 stoichiometry of the aniline and nitro/dinitrosubstituted benzoic acid derivative.

2,4-dinitrobenzoic acid, 2,5-dinitrobenzoic acid, 2-nitrobenzoic acid and 3,5-dinitrosalicylic acid are all more acidic than 3,4-dinitrobenzoic acid and 3,5-dinitrobenzoic acid (§7.1), and the ΔpKa values for each multi-component system all lie in the region of the salt-cocrystal continuum with $1 \leq \Delta pKa \geq 3$ (with the exception of 4-Br-3-MA 3,5-DNSA which has a value greater than 3) (Table 7.13). In each multi-component crystallisation, a proton is fully transferred from the carboxylic acid group or hydroxyl group of the acidic component to the amine group of the aniline component. With proton transfer dominating in the formation of the complexes, all of the molecular complexes are colourless or pale coloured, with no new colour observed upon complexation. Aromatic donor···acceptor interactions, thus charge-transfer, are not expected in these complexes; it is found throughout this work that the presence of proton transfer, and hence ionic moieties, means these interactions are not present.

Table 7.13 ΔpKa values for the multi-component crystallisations in Chapter 7, which all result in ionic molecular complexes.

Co-molecule 1	**Co-molecule 2**	**Molecular complex number**	**ΔpKa**
2-IA	2,4-DNBA	**38**	1.12
2-BrA	2,4-DNBA	**39**	1.11
2-ClA	2,4-DNBA	**40**	1.24
3-IA	2,4-DNBA	**41**	2.16
3-BrA	2,4-DNBA	**42**	2.11
4-IA	2,4-DNBA	**43**	2.39
4-BrA	2,4-DNBA	**44**	2.47
4-I-2-MA	2,4-DNBA	**45**	2.24
3-IA	2,5-DNBA	**46**	1.96
4-IA	2,5-DNBA	**47**	2.19
2-IA	3,5-DNSA	**48**	1.84
2-BrA	3,5-DNSA	**49**	1.83
2-ClA	3,5-DNSA	**50**	1.96
3-IA	3,5-DNSA	**51**	2.88
3-BrA	3,5-DNSA	**52**	2.83
4-Br-3-MA	3,5-DNSA	**53**	3.35
4-IA	2-NBA	**54**	1.64

In the 2,4-DNBA, 2,5-DNBA and 2-NBA complexes (**38** - **47** and **54**), the carboxylate group has C-O bond lengths which are consistent with a delocalisation of the charge across the group. The carboxylate group has a significant rotation out of the ring plane (> 70°) due to steric effects; this is with the exception of the two 3-XA 2,4-DNBA complexes (**41** and **42**) which instead have a significant rotation of the *o*-NO2 group (~70°).

In all of the 2,4-DNBA and 2,5-DNBA complexes, the tetrahedral NH_3^+ group directs a stacked arrangement of alternate cations and anions, with each cation and anion pair close to parallel (less than 10° angle between the mean ring planes). The stacks form through moderate strength N-H···O hydrogen bonds to the twisted carboxylic acid (or nitro) groups. The halogen atoms play a similar role in each complex, connecting hydrogen bonded stacks in the direction perpendicular to the stacking direction, through formation of C-X···O halogen bonds to nitro group O-atoms. All of the complexes have weak C-H···O hydrogen bonds between aromatic H-atoms of both ions and nitro/carboxylate group O-atoms. In the 2-NBA complex, the packing is slightly different. The structure is formed through N-H···O hydrogen bonds involving the tetrahedral NH_3^+ group, however there is a much greater angle between the mean ring planes of the cation and anion, thus stacks are not formed. The iodine atom plays a similar role in linking the hydrogen bonded chains through formation of hydrogen bonds.

In each of the 3,5-DNSA complexes (**48** - **53**), a proton is transferred from the hydroxyl group of the 3,5-DNSA molecule; the hydrogen atom resides closer to the carboxylic acid group and the C-O bond lengths are consistent with those expected for single and double bonds. An intramolecular hydrogen bond is formed between the carboxylic acid group and deprotonated hydroxyl group, thus the carboxylic acid group is coplanar, or close to coplanar, with the aromatic ring. As a result, the structures are quite different to those of the nitro/dinitrobenzoic acid complexes. The structures are all formed through N-H···O hydrogen bonds involving the tetrahedral NH_3^+ group; however, with the exception of 3-IA 3,5-DNSA (**51**), there is an angle of greater than 40° between the mean ring planes of the cation and anion, thus there is no stacking, and the cation and anion are segregated. In four of the six complexes, there are offset π···π interactions between the parallel, planar 3,5-DNSA anions which play a key role in the packing. In the 2-IA, 3-IA, 3-BrA and 4-Br-3-MA 3,5-DNSA complexes, the halogen atom of the cation is influential in the structure, forming C-X···O halogen bonds with adjacent nitro group O-atoms. However, in the 2-BrA and 2-ClA 3,5-DNSA complexes, this interaction is not formed, and the halogen atom does not play a significant role. Br···Br interactions are observed in 2-BrA 3,5-DNSA; there are no halogen interactions in the isostructural 2-ClA 3,5-DNSA complex, due to the separation of the chlorine atoms, indicating that halogen interactions are not the main driving force in the crystal packing.

With the exception of the pair of 3-IA 2,4-DNBA and 3-BrA 2,4-DNBA complexes (**41** and **42**) which are isostructural, the iodine-containing complexes in a series have different crystal structures to the isostructural bromine/chlorine-containing complexes in the same series. The structural differences must be a consequence of the halogen type, related to the strength of the halogen bonds as well as steric effects, due to the larger size of iodine compared to bromine and chlorine. In the 2-XA 2,4-DNBA complexes (**38** - **40**), the iodine atom plays a more significant role in the packing arrangement than either the bromine or the chlorine atoms; in the 2-BrA and 2-ClA complexes, the packing is dominated by hydrogen bonding. In the 2-XA 3,5-DNSA complexes (**48** - **50**), the bromine and chlorine atoms are not influential in directing the packing arrangement.

CHAPTER 8

Conclusions and Future Work

8 Conclusions and Future Work

The research presented in this thesis has demonstrated the application of multi-component crystallisation as a route to tuneable and switchable colour properties, in a series of molecular complexes of haloanilines with nitro- and dinitro-substituted benzoic acid derivatives. The series of molecular complexes highlights the key properties required for colour, the tunability of colour, and two possible mechanisms for thermochromism. Furthermore, a salt-cocrystal continuum has been established for the series, based on ΔpKa values, and a number of conclusions can be drawn in relation to the principles of crystal engineering which will be applicable in moving forward with this work.

8.1 Temperature-dependent and switchable colour

Two mechanisms for thermochromism have been identified in the series of haloaniline-dinitrobenzoic acid complexes: disorder-facilitated structural rearrangement and proton transfer, which were discussed in Chapters 4 and 5, respectively. There is also a further example demonstrating a combination of the two mechanisms. The disordered molecular complexes of 2-XA 3,4-DNBA (where X = I, Br, Cl) (Chapter 4) all undergo phase transitions upon heating. The phase transitions in the 2-IA complex are irreversible, and those in the 2-BrA and 2-ClA complexes are fully reversible. The first phase transition is associated with a reorientation of the disordered molecules, with no changes in the overall packing arrangement or colour. However, the second phase transition in 2-IA 3,4-DNBA is associated with a colour change from red to yellow; this is associated with a significant structural rearrangement, with survival of the single crystal (Figure 8.1).

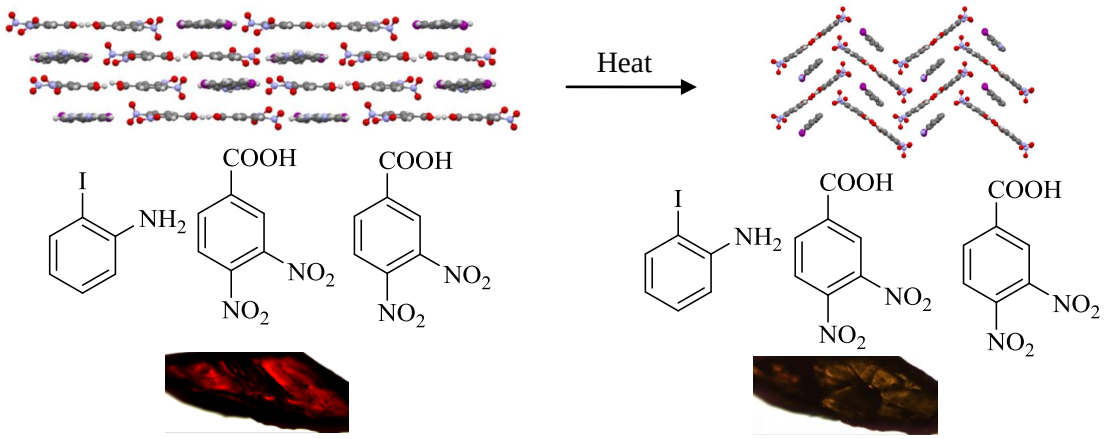

Figure 8.1 Single-crystal to single-crystal thermochromism in the molecular complex of 2-IA 3,4-DNBA, where the thermochromism upon heating is associated with a significant structural rearrangement, facilitated through the additional crystal space due to the molecular disorder.

In the presence of molecular disorder, inefficient packing is inherent in the crystal lattice. In the 2-XA 3,4-DNBA complexes, the disorder arises as a result of competition between hydrogen/halogen bond donor and acceptor groups, and a lack of strong interactions to favour a single position. The average structure shows two possible molecular positions, but only one of these is occupied in any one site, which means there is additional crystal space surrounding the molecule. Void space calculations were conducted with the donor 2-XA molecule removed from the model, to determine the volume of crystal space available to accommodate the donor in the stack. When compared to the volume of an ordered 2-XA molecule, there is an increase of 16 - 20% in each of the 2-XA 3,4-DNBA complexes. The greater volume of crystal space (or 'reorientation pockets') associated with each 2-haloaniline molecule may allow the structure the flexibility to rearrange, thereby allowing the massive structural rearrangement observed (from planar to herringbone, Figure 8.1) to occur in a single-crystal to single-crystal manner. For 2-IA 3,4-DNBA, the thermochromic properties can therefore be attributed to the disorder present in the system and the structural changes which the disorder facilitates.

The molecular complex 2-FA 3,4-DNBA displays different behaviour, despite having a very similar solid-state packing arrangement under ambient conditions. No phase transitions were observed upon heating, however a SCSC phase transition was observed upon cooling to below ambient temperature *in situ*; this was associated with a change in the unit cell parameters and a change in colour from red to colourless. Structural analysis revealed that a proton had been transferred between the carboxylic acid group of one of the 3,4-DNBA molecules and the 2-FA molecule, with an associated switching off of the colour (Figure 8.2). The ΔpKa values for the 2-IA, 2-BrA and 2-ClA systems are negative, suggesting neutral complexes should prevail. Moving to the 2-FA complex shifts the ΔpKa value into the salt-cocrystal continuum and therefore opens up the possibility of this second, proton-transfer-mediated mechanism.

In forming halogen bonds, fluorine has quite different characteristics to those of the other halogen atoms, and in addition the 2-FA molecule is smaller in size than the other 2-XA molecules. However, the same 3,4-DNBA network persists in the 2-FA 3,4-DNBA complex, hosting the 2-FA molecule, and this is essentially maintained upon proton transfer, enabled through the 1:2 stoichiometry of the 2-FA and 3,4-DNBA. The recurrence of the 3,4-DNBA host framework means that the crystal space available to the 2-FA donor molecule is even greater, due to the smaller size of the molecule (~34% increase compared to an ordered 2-FA molecule). The phase transition and survival of the single crystal may again be facilitated through the increased volume of void space in the crystal due to disorder; this allows rearrangement of the molecules to accommodate the proton transfer and the resultant three-dimensional hydrogen bonded network, without disintegration of the single crystal. The single-

crystal to single-crystal thermochromic transition may be therefore be attributed to a combination of two mechanisms i.e. disorder-facilitated proton transfer.

In the series of 4-XA 3,5-DNBA and 4-X-2-MA 3,5-DNBA molecular complexes (Chapter 5), the neutral molecular complexes undergo a colour-switching phase transition associated with a proton transfer; in some cases this occurs spontaneously, but some of the crystals remain stable under ambient conditions, allowing full structural characterisation, and the phase transition occurs upon heating and is thus thermochromic. The neutral molecular complexes exhibit different solid-state colours depending on the nature of the halogen, with the iodine complexes red in colour and the bromine complexes orange in colour; upon proton transfer a colour change to colourless is observed (Figure 8.3). Unlike the disordered 2-XA 3,4-DNBA complexes, the phase transition does not occur in a single-crystal to single-crystal manner due to the large structural rearrangement that occurs upon the transfer of a proton, and the vast change in the hydrogen bonding interactions, with the loss of the 3,5-DNBA dimer motif, which is a consequence of the 1:1 stoichiometry.

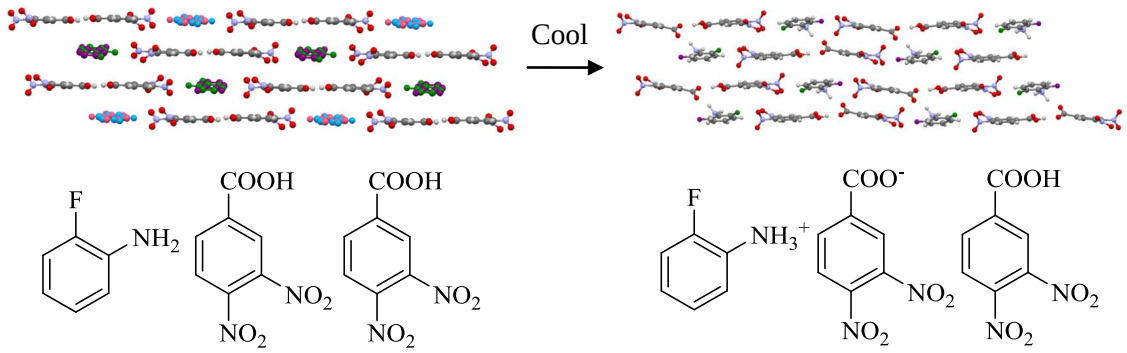

Figure 8.2 Single-crystal to single-crystal phase transition in the molecular complex of 2-FA 3,4-DNBA, where the thermochromism upon cooling is associated with a proton transfer, facilitated through the additional crystal space due to the molecular disorder.

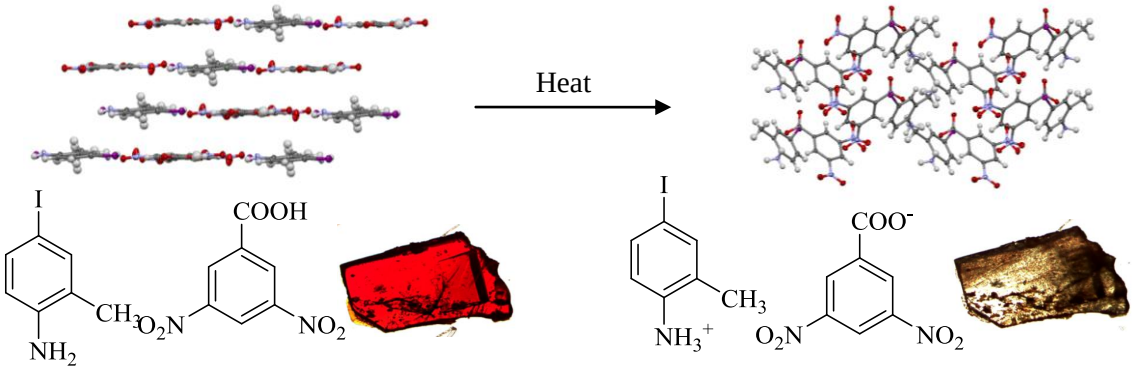

Figure 8.3 Thermochromism due to proton transfer, and an associated structural rearrangement, upon heating the molecular complex of 4-I-2-MA 3,5-DNBA; this is not a single-crystal to single-crystal transition, with the single-crystallinity being lost on undergoing the transition.

Modification of the thermal behaviour, and the associated thermochromic properties of both systems, can be achieved through exchange of the halogen. In the series of 2-XA 3,4-DNBA molecular complexes, the phase transition temperatures (and reversibility of the transitions) are tuneable through changing the nature of the halogen substituent; there is an increase in the phase transition temperature with decreasing molecular weight i.e. I < Br < Cl. The phase transitions from Form I to Form II occur at 52 °C, 65 °C and 90 °C for the 2-IA, 2-BrA and 2-ClA complexes, respectively; the phase transition to Form III occurs at 85 °C and 95 °C for the 2-IA and 2-BrA complexes, respectively. Exchanging the halogen substituent for fluorine results in very different thermochromic behaviour, with a phase transition observed on cooling (between 298 K and 220 K). In the series of 4-XA/4-X-2-MA 3,5-DNBA molecular complexes, there is also a dependence on the nature of the halogen; this is reflected in the colour of the molecular complexes i.e. red or orange, and in the temperature at which proton transfer occurs. For the single crystals, the phases transitions occur between 98 - 108 °C for 4-IA 3,5-DNBA, and between 77 - 84 °C and 61 - 83 °C for 4-I-2-MA 3,5-DNBA and 4-Br-2-MA 3,5-DNBA, respectively. Related to this trend is the stability of the molecular complex which also changes with the halogen; the neutral I complexes generally seem to have a higher stability than the neutral Br complexes, and it was not possible to obtain a neutral 4-Cl-2-MA complex. Based on the melting points, this is likely due to the relative stabilities of the ionic forms, which increase with decreasing molecular weight.

The stoichiometry of the donor and acceptor is of great importance in governing the phase transitions and associated structural rearrangements. In the 4-XA/4-X-2-MA 3,5-DNBA systems, the 1:1 stoichiometry of the donor and acceptor means that the intermolecular interactions change dramatically upon proton transfer, with loss of the 3,5-DNBA dimer; thus, the transition does not occur in a single-crystal to single-crystal manner. The 1:2 stoichiometry and the persistence of the 3,4-DNBA host framework is key to the very different properties of the 2-XA 3,4-DNBA systems. The overall framework persists across the range of 2-haloaniline molecules and remains intact on undergoing the massive structural arrangement. Furthermore, in contrast with the disordered 1:1 2-XA 3,5-DNBA complexes in Chapter 6, where no temperature-dependent behaviour is observed, the robust 3,4-DNBA host framework and the 1:2 stoichiometry of the donor and acceptor very effectively increases the size of the acceptor part of the stack, resulting in a more inefficient packing and increased space for rearrangement.

8.2 Inducing and tuning colour in the solid-state

Of the 54 molecular complexes reported in this thesis, 25 exhibit deep colour upon formation of the solid-state molecular complex, that differs from that of either of the individual components

(which individually are colourless or pale coloured in the solid-state). The colour of each molecular complex may be attributed to π-π* charge-transfer between the donor and acceptor. Where a UV-visible absorption spectrum has been obtained, the charge-transfer interaction gives rise to a broad charge-transfer absorbance band in the visible region; visually, the colours of the molecular complexes range between red and yellow (Table 8.2). Each of the coloured molecular complexes include suitable planar π-electron donor (D) and π-electron acceptor (A) moieties; in the systems studied, the donor is the aniline component due to the electron-donating nature of the NH_2 group, and the acceptor is the nitro- or dinitrosubstituted benzoic acid derivative, due to the strongly electron-withdrawing nature of the NO_2 groups. The donor and acceptor molecules are all in their neutral forms, with the exceptions of the 3:2 molecular complexes of 4-XA 3,5-DNSA (**31** and **32**), where only one of the 4-haloaniline molecules is neutral, and the mixed ionisation state complex of 4-IA 3,5-DNBA MeOH (**17**). The crystal structures consist of mixed stacks of the donor and acceptor; in the vast majority of cases there is continuous D-A stacking, but six of the molecular complexes have stacking within a three-molecule (A-D-A) unit, demonstrating that continuous stacking is not essential for the generation of the solid-state colour properties. In the 2-XA 3,4-DNBA complexes, the donor and acceptor crystallise in a 1:2 ratio; all other molecular complexes crystallise in a 1:1 ratio of the donor and acceptor, with the exception of the 3:2 4-XA 3,5-DNSA complexes. In this latter case, one of the 4-XA molecules remains neutral as a result of the stoichiometry, and is therefore an electron-donor. The neutral molecule is sandwiched between two 3,5-DNSA anions, resulting in an A-D-A stack. The 3,5-DNSA can still function as an electron acceptor in its anionic form, since OH and O^- are both electron-donating; in addition, the molecule remains planar through formation of an intramolecular hydrogen bond between the carboxylic acid group and deprotonated hydroxyl group.

The nature of the charge transfer is highly sensitive to the electronic properties of the donor and acceptor, their orientation and the relative molecular overlap of the two components; the solid-state colour can thus be tuned through modification of either co-former. The approximate separation of the donor and acceptor was measured in each of the molecular complexes (Table 8.2). The majority of the intermolecular donor⋯acceptor separations fall within the range 3.30 Å - 3.50 Å. Some corresponding pairs of molecular complexes show a trend; for example, the red 4-Br-2-IA 3,4-DNBA (**36**) has a smaller stacking distance and absorbance at longer wavelength than the corresponding yellow 4-Br-2-IA 3,5-DNBA complex (**37**); this is also true for the pair of 4-XA 3,5-DNSA complexes. However, there is no apparent overall relationship between the colour and the stacking distance. In terms of molecular overlap, trends are observed within a particular series; for example in the red 2-XA 3,4-DNBA molecular complexes (Chapter 4), the stacking is continuous between the 2-XA donor and the 3,4-DNBA dimer, and

molecular overlap typically occurs between the aromatic ring of the donor and the carboxylic acid group or centre of the dimer. However, the same trend, in terms of overlap, is not observed across all complexes of the same colour.

Table 8.1 The colour of the molecular complex and the approximate donor⋯acceptor (D⋯A) stacking distance; the colour reported is that of the single crystal observed visually under the microscope.

Molecular complex	**Single crystal colour**	**Absorbance (visible region)**	**Stacking distance between D and A**
2-IA 3,4-DNBA (**1**)	Red	Below 570 nm	3.40 Å
2-IA 3,4-DNBA (**2**)	Red	Below 570 nm	3.35 Å
2-BrA 3,4-DNBA (**4**)	Red	Below 590 nm	3.35 Å
2-BrA 3,4-DNBA (**5**)	Red	Below 590 nm	3.34 Å
2-ClA 3,4-DNBA (**6**)	Red	Below 610 nm	3.35 Å
2-FA 3,4-DNBA (**7**)	Red	-	3.35 Å
4-IA 3,5-DNBA (**16**)	Red	Below 600 nm	3.36 Å
4-IA 3,5-DNBA MeOH (**17**)	Red	Below 540 nm	3.30 Å
4-I-2-MA 3,5-DNBA (**21**)	Red	Below 620 nm	3.23 Å
2-I-4-MA 3,5-DNBA (**28**)	Red	-	3.35 Å
4-Br-2-IA 3,4-DNBA (**36**)	Red	Below 630 nm	3.32 Å
2-I-4-MA 3,4-DNBA (**10**)	Orange	-	3.40 Å
2-Br-4-MA 3,4-DNBA (**11**)	Orange	-	3.40 Å
2-Cl-4-MA 3,4-DNBA (**12**)	Orange	-	3.40 Å
4-BrA 3,5-DNBA (**19**)	Orange	-	3.32 Å
4-Br-2-MA 3,5-DNBA (**23**)	Orange	-	3.30 Å
4-IA 3,5-DNSA (**31**)	Orange	Below 540 nm	3.55 Å
4-BrA 3,5-DNSA (**32**)	Orange	Below 560 nm	3.40 Å
3-BrA 3,5-DNBA (**35**)	Yellow/orange	-	3.40 Å
2-IA 3,5-DNBA (**25**)	Yellow/orange	Below 550 nm	3.40 Å
2-BrA 3,5-DNBA (**26**)	Yellow/orange	Below 550 nm	3.35 Å
2-IA 3,4-DNBA (**3**)	Yellow	Below 540 nm	3.38 Å
2-ClA 3,5-DNBA(**27**)	Yellow	Below 530 nm	3.35 Å
2-Br-4-MA 3,5-DNBA (**29**)	Yellow	-	3.35 Å
4-Br-2-IA 3,5-DNBA (**37**)	Yellow	Below 530 nm	3.45 Å

18 of the 25 molecular complexes exhibit molecular disorder of one of the components (this is of the haloaniline component, with the exception of molecular complex **17**). The presence of disorder may be considered to be a favourable attribute for the generation of colour in the solid-state, given the high propensity for it observed in this thesis, and the colour properties will be determined by the local, short-range structure rather than the global average; however, an understanding of the subtle influences of the disorder on the inter-layer electronic effects requires further work.

The most significant factor for the colour properties is the nature of the donor and acceptor molecules, with the ring substituents and their locations on the aromatic ring playing a vital role (as demonstrated for a number of pairs of molecular complexes discussed below). The effect of the intermolecular interactions between the donor and acceptor molecules within the layers is another factor to consider; this was noted in Chapter 6 for corresponding red and yellow molecular complexes, where the hydrogen bonds within the layers are stronger for those complexes that are red in colour.

It has been demonstrated across the series of molecular complexes that tunability of colour can be achieved through several routes including: exchange of the halogen atom, variation in substituent positions on the donor and acceptor molecules, introduction of a methyl group substituent on the donor, and variation of the stoichiometric ratio of the donor and acceptor. The effect of the halogen is clear in several pairs of molecular complexes, including the 4-X-2-MA 3,5-DNBA complexes (**21** and **23**) and the 2-X-4-MA 3,5-DNBA complexes (**28** and **29**). Here, different colours are observed between corresponding I and Br complexes; the iodine complex is red and the bromine complex is orange/yellow (Figure 8.4). In each case, the difference in colour may be a combination of the differing electronic properties of the donor molecules and varying molecular overlap as an effect of the alteration in packing arrangement, both a result of the exchange of the halogen. However, it should be noted that the nature of the halogen does not have a significant effect in all systems, evident through the identical red colour of each of the 2-XA 3,4-DNBA complexes and the yellow colour of each of the 2-XA 3,5-DNBA complexes.

The colour can also be tuned through changing the positions of one of more of the nitro groups on the acceptor moiety, or by changing the position of the halogen relative to the amine group on the donor; the effect of these variations is evident in a number of complexes. The molecular complexes of 2-XA 3,4-DNBA and 2-XA 3,5-DNBA are red and yellow in colour, respectively (Figure 8.5), which is achieved through transferring one of the nitro group substituents between the *para* and *ortho* ring sites of the benzoic acid derivative; this also results in a different stoichiometric ratio of the donor and acceptor. With regards to the position of the halogen

substituent relative to the amine group, the effect on colour is clearly demonstrated in the 4-IA 3,5-DNBA complex (red) and 2-IA 3,5-DNBA complex (yellow) (Figure 8.5).

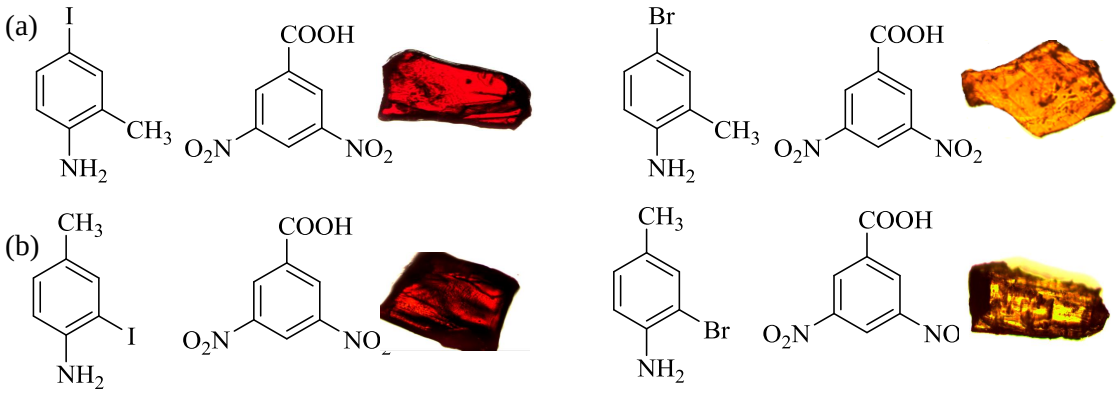

Figure 8.4 Tunability of colour through exchange of the halogen atom, demonstrated in the pairs of molecular complex (a) 4-I-2-MA 3,5-DNBA (**21**) and 4-Br-2-MA (**23**) and (b) 2-I-4-MA 3,5-DNBA (**28**) and 2-Br-4-MA 3,5-DNBA (**29**).

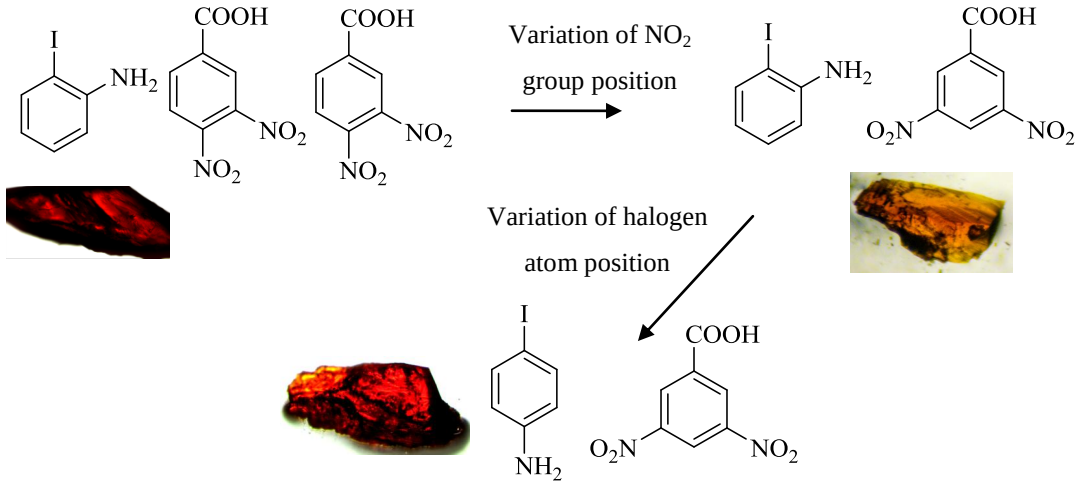

Figure 8.5 Tunability of colour through variation of the location of one of the nitro group substituents on the acceptor molecule and the halogen atom on the donor molecule.

The introduction of a methyl group substituent was found to tune the colour significantly in only one example, in the pair of 2-IA 3,5-DNBA (**25**) (shown in Figure 8.5 (b), right) and 2-I-4-MA 3,5-DNBA (**28**) (shown in Figure 8.4 (b), left) molecular complexes. This may be a result of the differing donor properties or relative orientations of the donor and acceptor. In the 4-XA 3,5-DNBA and 4-X-2-MA 3,5-DNBA complexes in Chapter 5, the introduction of the methyl group substituent does not have a significant influence on the colour observed, with both iodine complexes red in colour and the bromine complexes orange. Finally, as shown by the 4-XA 3,5-DNSA complexes (Chapter 6, **31** - **34**), the stoichiometry of the donor and acceptor in the final complex is also important; the presence of an additional donor molecule results in the

formation of a charge-transfer complex which is orange in colour; the molecular components in the 1:1 molecular complexes are in their ionic forms and the complexes lack colour.

8.3 Proton transfer and the salt-cocrystal continuum

Proton transfer in the molecular complexes is key to the generation of both colour and switchable colour. For colour in the solid-state, at least some of the molecular components must be in their neutral forms for charge-transfer interactions. Proton transfer in these systems switches off colour, thus in the design of coloured multi-component crystals, proton transfer is disfavoured. It is also unfavourable in the design of disordered systems, since the molecular disorder can only occur in neutral mixed-stack charge transfer crystals, where the aromatic donor···acceptor interactions dominate the packing arrangement, and there are a lack of strong interactions (e.g. hydrogen bonds) within the layers; where proton transfer occurs, the three-dimensional hydrogen bonding arrangement between ions dominates the crystal packing. However, for some switchable colour properties, as in the case of some of the thermochromic materials, proton transfer provides the mechanism for the colour change and is thus favourable.

In assessing the likelihood of proton transfer in molecular complexes such as those studied, it is possible to make correlations between the ΔpKa value and the final ionisation state of the molecular complex; Table 8.2 shows the molecular complexes of anilines with nitro- and dinitrosubstituted benzoic acid derivatives. Where $\Delta pKa \leq 0.15$, neutral molecular complexes are formed, and where $\Delta pKa \geq 1.10$, ionic molecular complexes are formed (with the exception of the mixed ionisation 4-XA 3,5-DNSA complexes, where the ionisation states result from the 3:2 stoichiometry). Of particular interest are those complexes which fall in the region $0.27 \leq \Delta pKa \leq 1.10$, which may be defined as the 'salt-cocrystal continuum' for these systems. It is notable that this range is considerably smaller than the commonly used ΔpKa rule, which has the continuum between 0 and 3, emphasising the empirical nature of the rule.

In the region identified in this study, it is not possible to predict whether a neutral or ionic form will be obtained, and in some cases a mixed ionisation state complex is obtained, not always as a result of stoichiometry. Furthermore, only a very small increase in the ΔpKa, as a result of the halogen atom, can have a significant effect, as shown for the 2-X-4-MA 3,5-DNBA complexes (**28** - **30**), where the I and Br complexes are neutral but the Cl complex is ionic, as a result of an increase of only 0.12 in the ΔpKa value. The uncertainty in the continuum region is clearly evident in the 4-XA 3,5-DNBA and 4-X-2-MA 3,5-DNBA complexes (**14** - **24**). For these molecular complexes, it is possible to obtain both neutral and ionic forms under the same conditions, which is unusual and unexpected behaviour. The trend in the ΔpKa values also

reflects the stability of the neutral forms over the ionic forms of these complexes, indicating that even very small changes in the pKa values of the molecular components can affect the nature of the complex formed and the stability. The higher the ΔpKa, the more stable the ionic form, and the more likely it is that a neutral complex will be more unstable or will not form. This clear region of uncertainty thus provides an interesting area in which to investigate potential metastable materials with colour-switching capabilities.

Table 8.2 In ascending values of ΔpKa, the molecular complexes of anilines with nitro- and dinitrosubstituted benzoic acid derivatives, the stoichiometries and the ionisation state(s) of the molecular complexes.

Molecular complex	**Stoichiometry**	**ΔpKa**	**Neutral (N), ionic (I) or mixed ionisation (M)**
4-Br-2-IA 3,4-DNBA (**36**)	1:1	-0.99	N
4-Br-2-IA 3,5-DNBA (**37**)	1:1	-0.99	N
2-BrA 3,4-DNBA (**4**, **5**)	1:2	-0.29	N
2-BrA 3,5-DNBA (**26**)	1:1	-0.29	N
2-IA 3,4-DNBA (**1** - **3**)	1:2	-0.28	N
2-IA 3,5-DNBA (**25**)	1:1	-0.28	N
2-ClA 3,4-DNBA (**6**)	1:2	-0.16	N
2-ClA 3,5-DNBA (**27**)	1:1	-0.16	N
2-Br-4-MA 3,4-DNBA (**11**)	1:2	0.15	N
2-Br-4-MA 3,5-DNBA (**29**)	1:1	0.15	N
2-I-4-MA 3,4-DNBA (**10**)	1:2	0.15	N
2-I-4-MA 3,5-DNBA (**28**)	1:1	0.15	N
2-Cl-4-MA 3,4-DNBA (**12**)	1:2	0.27	N
2-Cl-4-MA 3,5-DNBA (**30**)	1:1	0.27	I
2-FA 3,4-DNBA (**7**, **8**)	1:2	0.43	N, M
3-BrA 3,5-DNBA (**35**)	1:1	0.71	M
4-I-2-MA 3,5-DNBA (**20**, **21**)	1:1	0.84	I, N
4-Br-2-MA 3,5-DNBA (**22**, **23**)	1:1	0.89	I, N
4-IA 3,5-DNBA (**14** - **16**)	1:1	0.99	I, N
4-IA 3,5-DNBA MeOH (**17**)	2:2:1	0.99	M
4-Cl-2-MA 3,5-DNBA (**24**)	1:1	1.03	I
4-BrA 3,5-DNBA (**18**, **19**)	1:1	1.07	I, N
2-BrA 2,4-DNBA (**39**)	1:1	1.11	I
2-IA 2,4-DNBA (**38**)	1:1	1.12	I

Table 8.2 continued

Molecular complex	Stoichiometry	ΔpKa	Neutral (N), ionic (I) or mixed ionisation (M)
2-ClA 2,4-DNBA (**40**)	1:1	1.24	I
4-IA 2-NBA (**54**)	1:1	1.64	I
2-IA 3,5-DNSA (**49**)	1:1	1.83	I
2-BrA 3,5-DNSA (**48**)	1:1	1.84	I
2-ClA 3,5-DNSA (**50**)	1:1	1.96	I
3-IA 2,5-DNBA (**46**)	1:1	1.96	I
3-BrA 2,4-DNBA (**41**)	1:1	2.11	I
3-IA 2,4-DNBA (**42**)	1:1	2.16	I
4-IA 2,5-DNBA (**47**)	1:1	2.19	I
4-I-2-MA 2,4-DNBA (**45**)	1:1	2.24	I
4-IA 2,4-DNBA (**43**)	1:1	2.39	I
4-BrA 2,4-DNBA **(44**)	1:1	2.47	I
3-BrA 3,5-DNSA (**52**)	1:1	2.83	I
3-IA 3,5-DNSA (**51**)	1:1	2.88	I
4-IA 3,5-DNSA (**31**, **33**)	2:1, 1:1	3.11	M, I
4-BrA 3,5-DNSA (**32**, **34**)	2:1, 1:1	3.19	M, I
4-Br-3-MA 3,5-DNSA (**53**)	1:1	3.35	I

8.4 Crystal engineering

8.4.1 Intermolecular interactions

Hydrogen bonds, halogen bonds and π···π (or aromatic donor···acceptor) interactions all play a significant role in the assembly of the molecular complexes, and the combination, and competition, of the interactions is vital to structure and function. Where proton transfer has occurred, the N-H···O hydrogen bonds that form between the tetrahedral NH_3^+ group and carboxylate group O-atoms dominate the packing arrangement due to their charged nature. In the neutral molecular complexes, hydrogen bonded dimers, with graph-set notation $R_2^2(8)$, consistently form between two dinitrobenzoic acid molecules *via* moderate strength O-H···O hydrogen bonds. The remaining hydrogen bonds are much weaker in nature, forming between the NH_2 group of the haloaniline and nitro group O-atoms of the dinitrobenzoic acid molecules. Weaker hydrogen bonds such as C-H···O are also observed in the structures of many of the molecular complexes, and are particularly important in the 3,4-DNBA complexes

(Chapter 4, **1 - 13**), where they play an important role in the formation of the 3,4-DNBA host framework (§8.4.2).

In the molecular complexes of methyl-substituted haloanilines, the methyl group tends not to be involved in any significant or structure-directing intermolecular interactions; however, the group can influence the crystal packing due to its size, and as a result, none of the molecular complexes of methyl-substituted haloanilines are isostructural with those of the corresponding non-substituted haloanilines. However, the influence on the overall packing arrangement is minimal. The effect of the methyl group in crystal packing is demonstrated in the neutral molecular complexes of 4-XA 3,5-DNBA and 4-X-2-MA 3,5-DNBA (**16** and **21**, **19** and **23**); the orientation of the aniline component within the sheets differs between the 4-XA complex and the corresponding 4-X-2-MA complex which must be a result of the presence of the methyl group, but the overall packing arrangements are very closely related.

Halogen bonding plays a key role in the crystal packing of many of the complexes. Modification of the aniline component through exchange of the halogen substituent can influence the crystal packing through both steric effects and halogen bond strength, and also has an impact on the tunability of colour properties and temperature-dependent behaviour (§8.1, §8.2). The effect of the halogen-type is particularly evident in many of the neutral mixed stack complexes, where the orientations of the disordered haloaniline molecules differ across the series. In the 2-XA 3,4-DNBA complexes (**1 - 6**), the Form I 2-IA complex has a different orientation of the haloaniline molecules to those in the isostructural 2-BrA and 2-ClA complexes. In the 2-XA and 2-X-4-MA 3,5-DNBA complexes, the 2-IA/2-BrA and 2-I-4-MA/2-Br-4-MA complexes (**25** and **26**, **28** and **29**) differ in the orientations of the haloaniline molecules, and the 2-ClA complex (**27**) has a different overall packing arrangement. In the ordered neutral 4-XA 3,5-DNBA and 4-X-2-MA complexes (**16** and **19**, **21** and **23**), similar observations are made, with the orientations of the haloaniline molecules in the I complexes different to those in the Br complexes. These differences must be due to a combination of the differing halogen bond strengths and halogen atom sizes. Only two of the haloaniline molecular complexes include fluorine as the halogen atom (2-FA 3,4-DNBA, **7** and **8**); as a halogen bond donor, fluorine is quite different to the other halogen atoms. The neutral 2-FA 3,4-DNBA complex features the same packing arrangement as the other 2-XA 3,4-DNBA complexes, but the fluorine atom is not involved in any interactions with the 3,4-DNBA framework. Where proton transfer occurs, the structure is dominated by the hydrogen bonds between the NH_3^+ group. The fluorine atom is disordered over the two *ortho* sites, due to its small size and lack of significant interactions.

In general, the exchange of the halogen in the ionic complexes has little influence, and in many cases the molecular complexes are isostructural, as for the series of ionic 4-X-2-MA 3,5-DNBA complexes (**20**, **22** and **24**). In the ionic molecular complexes, the structures are typically directed by the hydrogen bonds between the cations and anions. This is also true of many of the ionic molecular complexes in Chapter 7, where the 2,4-DNBA complexes all display a very similar overall packing arrangement, dominated by the hydrogen bonds between the NH_3^+ group and the carboxylate group O-atoms of the anion. Where there are differences in the interactions, the halogen is generally more structure-directing in the complexes of I-substituted anilines than those of Br and Cl.

In the neutral molecular complexes, the interactions between the aromatic electron donor and electron acceptor dominate the packing, forming mixed stack arrangements. As discussed in §8.1, this typically results in an increased volume of crystal space available to the donor molecules. The intermolecular interactions within the layers of the mixed stack molecular complexes are relatively weak i.e. the hydrogen bonds involving the NH_2 group are at the borderline between classification of moderate and weak, and the halogen bonds have distances close to the sum of the van der Waals radii, often resulting in molecular disorder (§8.4.3).

8.4.2 Recurrent motifs

The carboxylic acid dimer (graph-set notation $R_2^2(8)$) is observed across all of the neutral molecular complexes of dinitrobenzoic acids, formed through the strongest hydrogen bond donor and acceptor groups. In the 3,4-DNBA complexes in Chapter 4, the robust 3,4-DNBA host framework is recurring across the series; the carboxylic acid dimers are connected *via* weak C-H···O hydrogen bonds between aromatic H-atoms and the carboxylic acid group O-atoms, forming a hydrogen bonded tape (Figure 8.6).

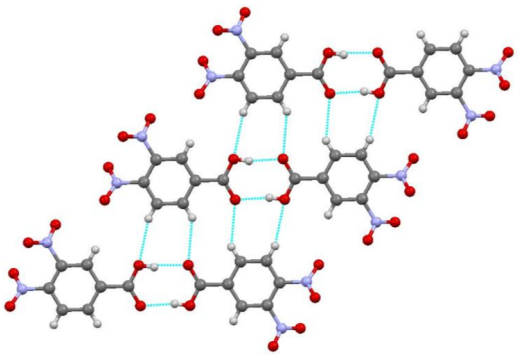

Figure 8.6 The recurring 3,4-DNBA hydrogen bonded tape in the 1:2 molecular complexes with 3,4-DNBA (Chapter 4).

The formation of this host framework is significant in the disorder-facilitated thermochromic mechanism, and is maintained through the phase transitions. The 3,4-DNBA framework persists with the methyl-substituted haloanilines as donor molecules, and with the introduction of a host molecule with a different functional group, as seen, for example, with 2-iodophenol.

8.4.3 Molecular disorder

Many of the neutral molecular complexes exhibit molecular disorder of the haloaniline molecule over two or more positions. In each case, the donor haloaniline molecule is a bi-functional hydrogen and halogen bond donor, providing the potential for competition between the NH_2 and halogen substituents for the acceptor groups. Such competition can give rise to molecular disorder, especially where there is a lack of strong interactions to favour a single position. The NH_2 group is a relatively poor hydrogen bond donor, evidenced across the neutral ordered complexes, where the majority of the hydrogen bonds involving the amine group are at the border between the classification of moderate and weak. In the formation of the carboxylic acid dimer motif in the molecular complexes of dinitrobenzoic acids, this leaves only the nitro group O-atoms of the dinitrobenzoic acid molecules available to act as hydrogen/halogen bond acceptors; the O-atoms of nitro groups are relatively poor acceptors when compared to O-atoms bound to carbon. In the 3:2 complexes of 4-XA 3,5-DNSA, which exhibit disorder of the neutral 4-XA molecule, the NH_2 group of the additional 4-IA molecule has to compete with the significantly more basic NH_3^+ group for the strongest hydrogen bond acceptor atoms. This competition is evident in the fact that there are no significant hydrogen/halogen bond acceptors remaining and thus only one weak interaction between the hosted disordered molecule and the ordered, ionic framework.

Exchanging the NH_2 group of 2-iodoaniline for an OH group, to give 2-iodophenol, was found to eliminate molecular disorder, in the molecular complex of 2-iodophenol 3,4-dinitrobenzoic acid (**13**). The molecular complex has a very similar overall packing arrangement to the corresponding disordered 2-iodoaniline complex, consisting of alternating channels of 3,4-DNBA dimers and 2-iodophenol, maintaining the 3,4-DNBA hydrogen bonded framework. However, the hydroxyl group is a stronger hydrogen bond donor than the amine group, and the formation of a hydrogen bond involving this group resulted in only a single possible orientation, effectively locking the 2-iodophenol molecule in place and removing competition.

Where molecular disorder is present, there is an increased volume of space available to the molecule than in the fully ordered case (Table 8.3), which can in some cases facilitate structural rearrangement or proton transfer (§8.1). As a crystal engineering design tool, molecular

disorder, and the associated increased crystal space, may be utilised. The relative occupancies of the disordered molecular orientations differ across the molecular complexes of 2-IA, 2-BrA and 2-ClA with 3,4-DNBA and 3,5-DNBA (Table 8.3). In general, the relative occupancies of the two possible orientations in the 2-IA complexes are more similar (i.e. closer to 50:50), than in the 2-BrA and 2-ClA complexes, where one molecular site becomes increasingly favoured. The reasons for this are not completely clear, but must be due to the nature of the halogen, and a combination of steric and bond strength effects.

Table 8.3 The % increase in the volume available to the disordered 2-haloaniline molecule compared to an ordered molecule, and the relative occupancies of the two possible orientations.

Molecular complex	% increase in volume	Relative occupancies
2-IA 3,4-DNBA (**1**)	19.40	50:50, 50:50
2-IA 3,4-DNBA (**2**)	9.17	77:23, 52:48
2-IA 3,4-DNBA (**3**)	22.66	56:44
2-BrA 3,4-DNBA (**4**)	16.36	50:50, 90:10
2-BrA 3,4-DNBA (**5**)	8.98	90:10
2-ClA 3,4-DNBA (**6**)	20.09	50:50, 90:10
2-FA 3,4-DNBA (**7**)	34.82	50:50, 57:43
2-IA 3,5-DNBA (**25**)	16.70	54:46
2-BrA 3,5-DNBA (**26**)	6.23	69:31
2-ClA 3,5-DNBA (**27**)	7.09	80:20

8.5 Future work

8.5.1 Probing the existing molecular complexes

In terms of the molecular complexes discussed in this thesis, there are a number of directions in which to proceed. The modeling of periodic systems is challenging since the description of the molecular species must also take into account the influence of the crystalline environment. However, solid-state calculations are necessary for an understanding of the origin of colour; this will involve determining the electronic properties of the molecular components, through calculation of the HOMO and LUMO of the aromatic electron donor and electron acceptor, respectively, in order to establish the exact nature of the charge-transfer interaction in the molecular complexes. The UV-visible absorption spectra can then be calculated and directly compared to the experimental measurements. This will enable a clearer understanding of how colour may be tuned, through modification of the molecular components.

For an improved understanding of the temperature-dependent behaviour of the disordered molecular complexes (2-XA 3,4-DNBA, Chapter 4), insight must first be gained into the nature of the disorder. Firstly, calculations may be conducted in order to determine the relative energies of the possible configurations of the molecular disorder giving an idea of the statistical populations that should be found at a given temperature and also providing further evidence for the experimentally determined disorder models. Energy barriers for switching between the multiple positions could also be calculated. At present, only the average crystal structure is known, thus interpretation of the diffuse scattering will aid understanding of the local order in these complexes, and the possible influence of the molecular disorder on the optical properties. This, however, requires very high quality diffraction patterns which are not available at present. Computational modeling can also be applied to evaluate the likelihood of local order models. With a further focus on the disordered molecular complexes of 2-XA 3,4-DNBA, additional work must be carried out on the characterisation of the unknown forms using the results of the variable temperature powder X-ray diffraction experiments. In particular, the reasons behind the reversibility of the 2-BrA and 2-ClA complexes but the irreversibility of the 2-IA complex is not understood; an understanding of how reversibility (or lack of) could be designed into materials such as these, could lead to a highly versatile set of materials which could be used as temperature sensors, for example.

The thermochromic 4-XA 3,5-DNBA and 4-X-2-MA complexes are a highly interesting series on which to focus attention, due to their colour-switching properties. However, there are difficulties in preserving the metastable neutral forms, thus a deeper understanding of the crystallisation of these systems, and maintenance of the neutral form, would be valuable. Furthermore, it may be possible to stabilise the metastable form through incorporation into a host system such as polymers or zeolites. At present, the transition is not reversible so methods, such as the application of an electric field, which may drive the proton backwards and forwards would be desirable in the production of a potential device.

In terms of properties, the focus of this work has been on colour and temperature-dependent colour; however, charge-transfer crystals are also interesting for other properties, for example ferroelectricity. The additional space in the disordered 2-XA 3,4-DNBA molecular complexes, and the inherent breaking of centrosymmetry on short-length scales (the disorder breaks the inversion symmetry in these systems), makes these ideal systems to examine the effect of external fields both on the polarisability, but also, more broadly, on the optical properties.

8.5.2 Designing new systems

In terms of the design of new multi-component systems, there are three key areas on which to focus. The first is the use of molecular disorder as a crystal engineering design tool, as a means of incorporating crystal space, for the facilitation of structural or molecular rearrangement, as discussed in Chapter 4. This may be for the development of thermochromic systems, or systems that switch in response to another external stimulus, and for which the properties may not be limited to colour (e.g. solubility, gas storage, NLO, ferroelectricity). To this end, the recurring 3,4-dinitrobenzoic acid framework may be exploited as a host system; of particular interest is the molecular complex 2-FA 3,4-DNBA, which combines disorder and proton-transfer for colour switching, and through appropriate choice of co-molecules it may be possible to generate this combination in further systems. Secondly, the metastable systems discussed in Chapter 5 are a key class of systems to develop; working in the salt-cocrystal continuum established in this work may identify new functional metastable materials with switchable properties which can be driven by proton transfer. Finally, with regards to tuning colour, the incorporation of a third planar, aromatic molecular component into the materials may be investigated, to form ternary molecular complexes with the potential for generating new colour properties.

8.6 Concluding remarks

While it is clear that a deeper understanding of these materials and their properties is required, the work described in this thesis has provided a strong basis upon which to build, in terms of inducing and tuning colour and switchable colour. There is enormous potential for the development of the class of multi-component systems already identified, in addition to the design of new related systems, using the principles established in this research. Future efforts will likely focus on the following key areas: molecular disorder (and increased crystal space) and metastable systems as a route to switchable properties, and the design of ternary molecular complexes of the current systems with the potential to display new colour properties and thus increased tunability.

REFERENCES

References

1 C. B. Aakeröy, N. R. Champness and C. Janiak, *CrystEngComm*, 2010, **12**, 22–43.

2 D. Braga, G. R. Desiraju, J. S. Miller, A. G. Orpen and S. L. Price, *CrystEngComm*, 2002, **4**, 500–509.

3 G. R. Desiraju, *J. Chem. Sci.*, 2010, **122**, 667–675.

4 G. M. J. Schmidt, *Pure Appl. Chem.*, 1971, **27**, 647–678.

5 O. Almarsson and M. J. Zaworotko, *Chem. Commun.*, 2004, 1889–1896.

6 T. Friščić and W. Jones, *J. Pharm. Pharmacol.*, 2010, **62**, 1547–1559.

7 P. Vishweshwar, J. A. Mcmahon, J. A. Bis and M. J. Zaworotko, *J. Pharm. Sci.*, 2006, **95**, 499–516.

8 E.-Y. Choi, M. Jazbinsek, S.-H. Lee, P. Günter, H. Yun, S. W. Lee and O.-P. Kwon, *CrystEngComm*, 2012, **14**, 4306–4311.

9 M. Gryl, S. Cenedese and K. Stadnicka, *J. Phys. Chem. C*, 2015, **119**, 590–598.

10 O. Bolton and A. J. Matzger, *Angew. Chem. Int. Ed.*, 2011, **50**, 8960–8963.

11 K. B. Landenberger, O. Bolton and A. J. Matzger, *Angew. Chem. Int. Ed.*, 2013, **52**, 6468–6471.

12 S. L. James, *Chem. Soc. Rev.*, 2003, **32**, 276–288.

13 K. Biradha, *CrystEngComm*, 2003, **5**, 374–384.

14 B. K. Saha, A. Nangia and M. Jaskólski, *CrystEngComm*, 2005, **7**, 355–358.

15 R. Taylor, *CrystEngComm*, 2014, **16**, 6852–6865.

16 J.-M. Lehn, *Angew. Chem. Int. Ed.*, 1988, **27**, 89–112.

17 G. R. Desiraju, *Angew. Chem. Int. Ed.*, 1995, **34**, 2311–2327.

18 E. Arunan, G. R. Desiraju, R. A. Klein, J. Sadlej, S. Scheiner, I. Alkorta, D. C. Clary, R. H. Crabtree, J. J. Dannenberg, P. Hobza, H. G. Kjaergaard, A. C. Legon, B. Mennucci and D. J. Nesbitt, *Pure Appl. Chem.*, 2011, **83**, 1637–1641.

19 G. A. Jeffrey, *An Introduction to Hydrogen Bonding*, Oxford University Press, 1997.

20 T. Steiner, *Angew. Chem. Int. Ed.*, 2002, **41**, 48–76.

21 L. C. Gilday, S. W. Robinson, T. A. Barendt, M. J. Langton, B. R. Mullaney and P. D. Beer, *Chem. Rev.*, 2015, **115**, 7118–7195.

22 M. Metrangolo and G. Resnati, *Cryst. Growth Des.*, 2012, **12**, 5835–5838.

23 P. Politzer and J. S. Murray, *ChemPhysChem*, 2013, **14**, 278–294.

24 C. A. Hunter and J. K. M. Sanders, *J. Am. Chem. Soc.*, 1990, **112**, 5525–5534.

25 C. B. Aakeröy, J. Desper, B. A. Helfrich, P. Metrangolo, T. Pilati, G. Resnati and A. Stevenazzi, *Chem. Commun.*, 2007, 4236–4238.

26 C. B. Aakeröy, M. Fasulo, N. Schultheiss, J. Desper and C. Moore, *J. Am. Chem. Soc.*, 2007, **129**, 13772–13773.

27 B. Ji, W. Wang, D. Deng, Y. Zhang, L. Cao, L. Zhou, C. Ruan and T. Li, *CrystEngComm*, 2013, **15**, 769–774.

28 G. R. Desiraju, *Angew. Chem. Int. Ed.*, 2011, **50**, 52–59.

29 P. Gilli, V. Bertolasi, V. Ferretti, G. Gilli and P. Giui, *J. Am. Chem. Soc.*, 1994, **116**, 909–915.

30 M. D. Ward, *Chem. Commun.*, 2005, 5838–5842.

31 G. R. Desiraju, *Acc. Chem. Res.*, 2002, **35**, 565–573.

32 L. Brammer, E. A. Bruton and P. Sherwood, *Cryst. Growth Des.*, 2001, **1**, 277–290.

33 I. Rozas, I. Alkorta and J. Elguero, *J. Phys. Chem. A.*, 1998, **102**, 9925–9932.

34 C. J. Marsden, B. J. Smith, J. A. Pople, H. F. Schaefer III and L. Radom, *J. Chem. Phys.*, 1991, **95**, 1825–1828.

35 C. L. Perrin, *Acc. Chem. Res.*, 2010, **43**, 1550–1557.

36 C. L. Perrin and J. B. Nielson, *Annu. Rev. Phys. Chem*, 1997, **48**, 511–544.

37 C. C. Wilson, N. Shankland and A. J. Florence, *J. Chem. Soc., Faraday Trans.*, 1996, **92**, 5051–5057.

38 C. C. Wilson, N. Shankland and A. J. Florence, *Chem. Phys. Lett.*, 1996, **253**, 103–107.

39 A. O. F. Jones, N. Blagden, G. J. Mcintyre, A. Parkin, C. C. Seaton, L. H. Thomas and C. C. Wilson, *Cryst. Growth Des.*, 2013, **13**, 497–509.

40 M. C. Etter, *Acc. Chem. Res.*, 1990, **23**, 120–126.

41 P. Metrangolo, H. Neukirch, T. Pilati and G. Resnati, *Acc. Chem. Res.*, 2005, **38**, 386–395.

42 A. Mukherjee, S. Tothadi and G. R. Desiraju, *Acc. Chem. Res.*, 2014, **47**, 2514–2524.

43 G. R. Desiraju, P. S. Ho, L. Kloo, A. C. Legon, R. Marquardt, P. Metrangolo, P. Politzer, G. Resnati and K. Rissanen, *Pure Appl. Chem.*, 2013, **85**, 1711–1713.

44 J. P. M. Lommerse, A. J. Stone, R. Taylor and F. H. Allen, *J. Am. Chem. Soc.*, 1996, **118**, 3108–3116.

45 T. Clark, M. Hennemann, J. S. Murray and P. Politzer, *J. Mol. Model*, 2007, **13**, 291–296.

46 C. Wang, D. Danovich, Y. Mo and S. Shaik, *J. Chem. Theory Comput.*, 2014, **10**, 3726–3737.

47 K. E. Riley and P. Hobza, *J. Chem. Theory Comput.*, 2008, **4**, 232–242.

48 K. E. Riley and P. Hobza, *Phys. Chem. Chem. Phys.*, 2013, **15**, 17742–17751.

49 L. Brammer, G. Mínguez Espallargas and S. Libri, *CrystEngComm*, 2008, **10**, 1712–1727.

50 D. Cincic, T. Friščić and W. Jones, *Chem. Mater.*, 2008, **20**, 6623–6626.

51 A. Priimagi, G. Cavallo, P. Metrangolo and G. Resnati, *Acc. Chem. Res.*, 2013, **46**, 2686–2695.

52 M. Saccone, G. Terraneo, T. Pilati, G. Cavallo, A. Priimagi, P. Metrangolo and G. Resnati, *Acta Crystallogr. Sect. B*, 2014, **70**, 149–156.

53 G. R. Desiraju and R. Parthasarathy, *J. Am. Chem. Soc.*, 1989, **111**, 8725–8726.

54 P. Metrangolo and G. Resnati, *IUCrJ*, 2013, **1**, 5–7.

55 A. Mukherjee and G. R. Desiraju, *IUCrJ*, 2013, **1**, 49–60.

56 F. F. Awwadi, R. D. Willett, K. A. Peterson and B. Twamley, *Chem. Eur. J.*, 2006, **12**, 8952–8960.

57 P. Metrangolo, F. Meyer, T. Pilati, G. Resnati and G. Terraneo, *Angew. Chem. Int. Ed.*, 2008, **47**, 6114–6127.

58 J.-L. Syssa-Magal, K. Boubekeur, P. Palvadeau, A. Meerschaut and B. Schollhorn, *CrystEngComm*, 2005, **7**, 302.

59 P. Metrangolo, J. S. Murray, T. Pilati, P. Politzer, G. Resnati and G. Terraneo, *CrystEngComm*, 2011, **13**, 6593.

60 R. W. Troff, T. Mäkelä, F. Topič, A. Valkonen, K. Raatikainen and K. Rissanen, *Eur. J. Org. Chem.*, 2013, 1617–1637.

61 K. E. Riley, J. S. Murray, J. Fanfrlík, J. Řezáč, R. J. Solá, M. C. Concha, F. M. Ramos and P. Politzer, *J. Mol. Model.*, 2013, **19**, 4651–4659.

62 C. Janiak, *J. Chem. Soc., Dalt. Trans.*, 2000, 3885–3896.

63 C. A. Hunter, K. R. Lawson, J. Perkins and C. J. Urch, *J. Chem. Soc., Perkin Trans. 2*, 2001, 651–669.

64 C. R. Martinez and B. L. Iverson, *Chem. Sci.*, 2012, **3**, 2191–2201.

65 S. Grimme, *Angew. Chem. Int. Ed.*, 2008, **47**, 3430–3434.

66 M. Etter, *J. Phys. Chem.*, 1991, **95**, 4601–4610.

67 C. B. Aakeröy, K. Epa, S. Forbes, N. Schultheiss and J. Desper, *Chem. Eur. J.*, 2013, **19**, 14998–15003.

68 C. A. Hunter, *Angew. Chem. Int. Ed.*, 2004, **43**, 5310–5324.

69 C. B. Aakeröy, M. Baldrighi, J. Desper, P. Metrangolo and G. Resnati, *Chem. Eur. J.*, 2013, **19**, 16240–16247.

70 C. Aakeroy, P. Chopade and J. Desper, *Cryst. Growth Des.*, 2013, **13**, 4145–4150.

71 C. B. Aakeröy, S. Panikkattu, P. D. Chopade and J. Desper, *CrystEngComm*, 2013, **15**, 3125–3136.

72 A. Takemura, L. J. McAllister, P. B. Karadakov, N. E. Pridmore, A. C. Whitwood and D. W. Bruce, *CrystEngComm*, 2014, **16**, 4254–4264.

73 L. H. Thomas, C. Wales, L. Zhao and C. C. Wilson, *Cryst. Growth Des.*, 2011, **11**, 1450–1452.

74 C. B. Aakeröy and D. J. Salmon, *CrystEngComm*, 2005, **7**, 439–448.

75 J. D. Dunitz, *CrystEngComm*, 2003, **5**, 506.

76 G. R. Desiraju, *CrystEngComm*, 2003, **5**, 466–467.

77 A. D. Bond, *CrystEngComm*, 2007, **9**, 833–834.

78 C. B. Aakeröy, M. E. Fasulo and J. Desper, *Mol. Pharm.*, 2007, **4**, 317–322.

79 S. L. Childs, G. P. Stahly and A. Park, *Mol. Pharm.*, 2007, **4**, 323–338.

80 C. B. Aakeroy, J. Desper and B. A. Helfrich, *CrystEngComm*, 2004, **6**, 19–24.

81 E. E. Simanek, M. Mammen, D. M. Gordon, D. Chin, J. P. Mathias, C. T. Seto and G. M. Whitesides, *Tetrahedron*, 1995, **51**, 607–619.

82 C. B. Aakeroy, A. M. Beatty and B. A. Helfrich, *Angew. Chem. Int. Ed.*, 2001, **40**, 3240–3242.

83 B. R. Bhogala, S. Basavoju and A. Nangia, *CrystEngComm*, 2005, **7**, 551–562.

84 C. B. Aakeröy, J. Desper, B. a. Helfrich, P. Metrangolo, T. Pilati, G. Resnati and A. Stevenazzi, *ChemComm*, 2007, 4236–4238.

85 C. B. Aakeröy, A. M. Beatty and B. A. Helfrich, *J. Am. Chem. Soc.*, 2002, **124**, 14425–14432.

86 F. H. Allen, *Acta Crystallogr. Sect. B*, 2002, **58**, 380–388.

87 N. Schultheiss and A. Newman, *Cryst. Growth Des.*, 2009, **9**, 2950–2967.

88 A. Sarkar and S. Rohani, *J. Pharm. Biomed. Anal.*, 2015, **110**, 93–99.

89 A. O. Surov, A. N. Manin, A. P. Voronin, K. V. Drozd, A. A. Simagina, A. V. Churakov and G. L. Perlovich, *Eur. J. Pharm. Sci.*, 2015, **77**, 112–121.

90 E. Nauha, E. Kolehmainen and M. Nissinen, *CrystEngComm*, 2011, **13**, 6531–6537.

91 E. Nauha and M. Nissinen, *J. Mol. Struct.*, 2011, **1006**, 566–569.

92 D. I. A. Millar, H. E. Maynard-Casely, D. R. Allan, A. S. Cumming, A. R. Lennie, A. J. Mackay, I. D. H. Oswald, C. C. Tang and C. R. Pulham, *CrystEngComm*, 2012, **14**, 3742–3749.

93 K. B. Landenberger and A. J. Matzger, *Cryst. Growth Des.*, 2010, **10**, 5341–5347.

94 S. Horiuchi and Y. Tokura, *Nat. Mater.*, 2008, **7**, 357–366.

95 A. S. Tayi, A. K. Shveyd, A. C.-H. Sue, J. M. Szarko, B. S. Rolczynski, D. Cao, T. J. Kennedy, A. A. Sarjeant, C. L. Stern, W. F. Paxton, W. Wu, S. K. Dey, A. C. Fahrenbach, J. R. Guest, H. Mohseni, L. X. Chen, K. L. Wang, J. F. Stoddart and S. I. Stupp, *Nature*, 2012, **488**, 485–489.

96 D. A. Haynes, W. Jones and W. D. S. Motherwell, *CrystEngComm*, 2006, **8**, 830–840.

97 D. A. Haynes and L. K. Pietersen, *CrystEngComm*, 2008, **10**, 518–524.

98 C. C. Seaton, T. Munshi, S. E. Williams and I. J. Scowen, *CrystEngComm*, 2013, **15**, 5250–5260.

99 D. M. S. Martins, D. S. Middlemiss, C. R. Pulham, C. C. Wilson, M. T. Weller, P. F. Henry, N. Shankland, K. Shankland, W. G. Marshall, R. M. Ibberson, K. Knight, S. Moggach, M. Brunelli and C. A. Morrison, *J. Am. Chem. Soc.*, 2009, **131**, 3884–3893.

100 S. Horiuchi, R. Kumai and Y. Tokura, *Angew. Chem. Int. Ed.*, 2007, **46**, 3497–3501.

101 K.-S. Huang, D. Britton, L. Margaret, T. C. Etter and S. R. Byrn, *J. Mater. Chem.*, 1997, **7**, 713–720.

102 A. J. Cruz-Cabeza, *CrystEngComm*, 2012, **14**, 6362–6365.

103 T. R. Shattock, K. K. Arora, P. Vishweshwar and M. J. Zaworotko, *Cryst. Growth Des.*, 2008, **8**, 4533–4545.

104 S. Mohamed, D. A. Tocher, M. Vickers, P. G. Karamertzanis and S. L. Price, *Cryst. Growth Des.*, 2009, **9**, 3–7.

105 F. H. Herbstein, *Crystalline Molecular Complexes and Compounds*, Oxford University Press, 2005.

106 R. S. Mulliken, *J. Am. Chem. Soc.*, 1952, **74**, 811–824.

107 R. Foster, *J. Phys. Chem.*, 1980, **84**, 2135–2141.

108 K. P. Goetz, D. Vermeulen, M. E. Payne, C. Kloc, L. E. McNeil and O. D. Jurchescu, *J. Mater. Chem. C*, 2014, **2**, 3065–3076.

109 A. Das and S. Ghosh, *Angew. Chem. Int. Ed.*, 2014, **53**, 2038–2054.

110 F. H. Herbstein and M. Kaftory, *Acta Crystallogr. Sect. B*, 1976, **32**, 387–396.

111 H. M. Powell, G. Huse and P. W. Cooke, *J. Chem. Soc.*, 1943, 153–157.

112 C. C. Seaton, N. Blagden, T. Munshi and I. J. Scowen, *Chem. Eur. J.*, 2013, **19**, 10663–10671.

113 W. Zhu, R. Zheng, X. Fu, H. Fu, Q. Shi, Y. Zhen, H. Dong and W. Hu, *Angew. Chem. Int. Ed.*, 2015, **54**, 6785–6789.

114 W. Zhu, R. Zheng, Y. Zhen, Z. Yu, H. Dong, H. Fu, Q. Shi and W. Hu, *J. Am. Chem. Soc.*, 2015, **137**, 11038–11046.

115 J. Harada, M. Ohtani, Y. Takahashi and T. Inabe, *J. Am. Chem. Soc.*, 2015, **137**, 4477–4486.

116 J. Lefebvre, G. Odou, M. Muller, A. Mierzejewski and T. Luty, *Acta Crystallogr. Sect. B*, 1989, **45**, 323–336.

117 J. Lefebvre, K. Rohleder, A. Mierzejewski and T. Luty, *J. Chem. Phys.*, 1995, **102**, 2165–2173.

118 W. C. McCrone, *In: Physics and Chemistry of the Organic Solid State*, Interscience, 1965.

119 J. Bernstein, *Polymorphism in Molecular Crystals*, Clarendon Press, 2002.

120 A. L. Grzesiak, M. Lang, K. Kim and A. J. Matzger, *J. Pharm. Sci.*, 2003, **92**, 2260–2271.

121 F. P. A. Fabbiani and C. R. Pulham, *Chem. Soc. Rev.*, 2006, **35**, 932–942.

122 I. G. Goldberg and J. A. Swift, *Cryst. Growth Des.*, 2012, **12**, 1040–1045.

123 E. F. Paulus, F. J. J. Leusen and M. U. Schmidt, *CrystEngComm*, 2007, **9**, 131–143.

124 L. Yu, *Acc. Chem. Res.*, 2010, **43**, 1257–1266.

125 J. Bernstein, R. Davey and J. Henck, *Angew. Chem. Int. Ed.*, 1999, **38**, 3440–3461.

126 D.-K. Bučar, R. W. Lancaster and J. Bernstein, *Angew. Chem. Int. Ed.*, 2015, **54**, 6972–6993.

127 P. H. Toma, M. P. Kelley, T. B. Borchardt, R. Stephen and B. Kahr, *Chem. Mater.*, 1994, **6**, 1317–1324.

128 C. Kitamura, T. Ohara, N. Kawatsuki, A. Yoneda, T. Kobayashi, H. Naito, T. Komatsu and T. Kitamura, *CrystEngComm*, 2007, **9**, 644–647.

129 T. Kinuta, T. Sato, N. Tajima, Y. Matsubara, M. Miyazawa and Y. Imai, *CrystEngComm*, 2012, **14**, 1016–1020.

130 G. Klebe, F. Graser, E. Hädicke and J. Berndt, *Acta Crystallogr. Sect. B*, 1989, **45**, 69–77.

131 P. M. Kazmaier and R. Hoffmann, *J. Am. Chem. Soc.*, 1994, **116**, 9684–9691.

132 C. Kitamura, Y. Abe, T. Ohara, A. Yoneda, T. Kawase, T. Kobayashi, H. Naito and T. Komatsu, *Chem. Eur. J.*, 2010, **16**, 890–898.

133 K. J. Fujimoto and C. Kitamura, *J. Chem. Phys.*, 2013, **139**, 1–12.

134 J. R. G. Sander, D.-K. Bučar, R. F. Henry, J. Baltrusaitis, G. G. Z. Zhang and L. R. MacGillivray, *J. Pharm. Sci.*, 2010, **99**, 3676–3683.

135 B. B. Koleva, T. Kolev, R. W. Seidel, H. Mayer-Figge, M. Spiteller and W. S. Sheldrick, *J. Phys. Chem. A.*, 2008, **112**, 2899–2905.

136 T. Kolev, B. B. Koleva, R. W. Seidel, M. Spiteller and W. S. Sheldrick, *Cryst. Growth Des.*, 2009, **9**, 3348–3352.

137 B. B. Koleva, T. Kolev, R. W. Seidel, M. Spiteller, H. Mayer-Figge and W. S. Sheldrick, *J. Phys. Chem. A.*, 2009, **113**, 3088–3095.

138 P. Erk, H. Hengelsberg, M. F. Haddow and R. Van Gelder, *CrystEngComm*, 2004, **6**, 474–483.

139 D.-K. Bučar, S. Filip, M. Arhangelskis, G. O. Lloyd and W. Jones, *CrystEngComm*, 2013, **15**, 6289–6291.

140 R. Kuroda, Y. Imai and N. Tajima, *ChemComm*, 2002, 2848–2849.

141 R. Kuroda, T. Sato and Y. Imai, *CrystEngComm*, 2008, **10**, 1881–1890.

142 J. Lee, Y. Y. Yuan, Y. Kang, W. L. Jia, Z. H. Lu and S. Wang, *Adv. Funct. Mater.*, 2006, **16**, 681–686.

143 C. A. Strassert, C.-H. Chien, M. D. Galvez Lopez, D. Kourkoulos, D. Hertel, K. Meerholz and L. De Cola, *Angew. Chem. Int. Ed.*, 2011, **50**, 946–950.

144 F. Gao, Q. Liao, Z.-Z. Xu, Y.-H. Yue, Q. Wang, H.-L. Zhang and H.-B. Fu, *Angew. Chem. Int. Ed.*, 2010, **49**, 732–735.

145 D. Yan, J. Lu, J. Ma, M. Wei, D. G. Evans and X. Duan, *Angew. Chem. Int. Ed.*, 2011, **50**, 720–723.

146 D. Yan, J. Lu, M. Wei, S. Qin, L. Chen, S. Zhang, D. G. Evans and X. Duan, *Adv. Funct. Mater.*, 2011, **21**, 2497–2505.

147 Z.-P. Deng, L.-H. Huo, H. Zhao and S. Gao, *Cryst. Growth Des.*, 2012, **12**, 3342–3355.

148 Q. Feng, M. Wang, B. Dong, C. Xu, J. Zhao and H. Zhang, *CrystEngComm*, 2013, **15**, 3623–3629.

149 Q. J. Shen, H. Q. Wei, W. S. Zou, H. L. Sun and W. J. Jin, *CrystEngComm*, 2012, **14**, 1010–1015.

150 D. Yan, A. Delori, G. O. Lloyd, T. Friščić, G. M. Day, W. Jones, J. Lu, M. Wei, D. G. Evans and X. Duan, *Angew. Chem. Int. Ed.*, 2011, **50**, 12483–12486.

151 D. Yan, A. Delori, G. O. Lloyd, B. Patel, T. Friščić, G. M. Day, D.-K. Bučar, W. Jones, J. Lu, M. Wei, D. G. Evans and X. Duan, *CrystEngComm*, 2012, **14**, 5121–5123.

152 D. Yan and D. G. Evans, *Mater. Horiz.*, 2014, **1**, 46–57.

153 M. Papadopoulos, A. Sadlej and J. Leszczynski, *Non-Linear Optical Properties of Matter: From Molecules to Condensed Phases*, Springer, 2006.

154 C. C. Evans, M. Bagieu-Beucher, R. Masse and J.-F. Nicoud, *Chem. Mater.*, 1998, **10**, 847–854.

155 B. B. Ivanova and M. Spiteller, *Cryst. Growth Des.*, 2010, **10**, 2470–2474.

156 B. B. Ivanova and M. Spiteller, *Struct. Chem.*, 2010, **21**, 989–993.

157 D. J. Williams, *Angew. Chem. Int. Ed.*, 1984, **23**, 690–703.

158 V. Nalla, R. Medishetty, Y. Wang, Z. Bai, H. Sun, J. Wei and J. J. Vittal, *IUCrJ*, 2015, **2**, 317–321.

159 Y. Le Fur, M. Bagieu-Beucher, R. Masse, J.-F. Nicoud and J.-P. Lévy, *Chem. Mater.*, 1996, **8**, 68–75.

160 F. Pan, M. S. Wong, V. Gramlich, C. Bosshard and P. Gu, *J. Am. Chem. Soc.*, 1996, **118**, 6315–6316.

161 M. Gryl, T. Seidler, K. Stadnicka, I. Matulkova, I. Nemec, N. Tesarova and P. Nemec, *CrystEngComm*, 2014, **16**, 5765–5768.

162 M. A. White and M. LeBlanc, *J. Chem. Educ.*, 1999, **76**, 1201–1205.

163 J. H. Day, *Chem. Rev.*, 1963, **63**, 65–80.

164 M. Irie, *Chem. Rev.*, 2000, **100**, 1685–1716.

165 E. L. Harty, A. R. Ha, M. R. Warren, A. L. Thompson, D. R. Allan, A. L. Goodwin and N. P. Funnell, *Chem. Commun.*, 2015, **51**, 10608–10611.

166 T. Mizutani, H. Takagi, Y. Ueno, T. Horiguchi, K. Yamamura and H. Ogoshi, *J. Phys. Org. Chem.*, 1998, **11**, 737–742.

167 S. C. Lee, Y. G. Jeong, W. H. Jo, H.-J. Kim, J. Jang, K.-M. Park and I. H. Chung, *J. Mol. Struct.*, 2006, **825**, 70–78.

168 P. Naumov, S. C. Lee, N. Ishizawa, Y. G. Jeong, I. H. Chung and S. Fukuzumi, *J. Phys. Chem. A.*, 2009, **113**, 11354–11366.

169 J. H. Day, *Chem. Rev.*, 1970, **227**, 419–419.

170 K. Ogawa, T. Fujiwara and J. Harada, *Mol. Cryst. Liq. Cryst. Sci. Technol., Sec. A*, 2000, **344**, 169–178.

171 M. Tanaka, H. Matsui, J. Mizoguchi and S. Kashino, *Bull. Chem. Soc. Jpn.*, 1994, **67**, 1572–1579.

172 M. T. Reetz, S. Hoger and K. Harms, *Angew. Chem. Int. Ed.*, 1994, **33**, 181–183.

173 T. Kinuta, T. Sato, N. Tajima, R. Kuroda, Y. Matsubara and Y. Imai, *J. Mol. Struct.*, 2010, **982**, 45–49.

174 P. Muller, R. Herbst-Irmer, A. L. Spek, T. R. Schneider and M. R. Sawaya, *Crystal Structure Refinement: A Crystallographer's Guide to SHELXL*, Oxford University Press, 2006.

175 C. C. Wilson, *Crystallogr. Rev.*, 2009, **15**, 3–56.

176 V. M. Nield and D. A. Keen, *Diffuse Neutron Scattering from Crystalline Materials*, Oxford University Press, 2001.

177 T. R. Welberry and D. J. Goossens, *IUCrJ*, 2014, **1**, 550–62.

178 A. D. Bond, R. Boese and G. R. Desiraju, *Angew. Chem. Int. Ed.*, 2007, **46**, 618–622.

179 A. D. Bond, *CrystEngComm*, 2012, **14**, 2363–2366.

180 T. R. Welberry, *Diffuse X-Ray Scattering and Models of Disorder*, Oxford University Press, 2010.

181 L. H. Thomas, T. R. Welberry, D. J. Goossens, A. P. Heerdegen, M. J. Gutmann, S. J. Teat, P. L. Lee, C. C. Wilson and J. M. Cole, *Acta Crystallogr. Sect. B*, 2007, **63**, 663–673.

182 W. Clegg, *Crystal Structure Determination*, Oxford University Press, 1998.

183 W. Massa, *Crystal Structure Determination*, Springer, 2004.

184 A. J. Blake, W. Clegg, J. M. Cole, J. S. O. Evans, P. Main, S. Parsons and D. J. Watkin, *Crystal Structure Analysis: Principles and Practice*, Oxford University Press, 2009.

185 T. Hahn, *International Tables for Crystallography A: Space-group symmetry*, Springer, 2005.

186 W. C. Röntgen, *Nature*, 1896, **53**, 274–277.

187 W. Friedrich, P. Knipping and M. Laue, *Sitzungsber. K. Bayer. Akad. Wiss.*, 1912, 303–322.

188 W. H. Bragg and W. L. Bragg, *Proc. R. Soc. Lond. A*, 1913, **88**, 428–438.

189 W. H. Bragg, *Proc. R. Soc. Lond. A*, 1913, **89**, 246–248.

190 D. Sayre, *Acta Crystallogr. Sect. A*, 1952, **5**, 60–65.

191 G. Oszlányi and A. Sütó, *Acta Crystallogr. Sect. A*, 2008, **64**, 123–134.

192 G. M. Sheldrick, *Acta Crystallogr. Sect. A*, 2008, **64**, 112–122.

193 R. E. Dinnebier and S. J. L. Billinge, *Powder Diffraction: Theory and Practice*, 2008.

194 G. W. H. Hohne, W. F. Hemminger and H.-J. Flammersheim, *Differential Scanning Calorimetry*, Springer, 2003.

195 C. N. R. Rao, *Ultra-Violet and Visible Spectroscopy: Chemical Applications*, Butterworth & Co. (Publishers) Ltd., 3rd edn., 1975.

196 Cambridge Reactor Design, *http://www.cambridgereactordesign.com/*, Accessed 02/09/2015.

197 Diamond Light Source, *http://www.diamond.ac.uk/Home.html*, Accessed 02/09/2015.

198 G. M. Sheldrick, *Acta Crystallogr. Sect. C*, 2015, **71**, 3–8.

199 A. L. Spek, *J. Appl. Crystallogr.*, 2003, **36**, 7–13.

200 L. J. Farrugia, *J. Appl. Crystallogr.*, 1999, **32**, 837–838.

201 C. F. Macrae, P. R. Edgington, P. McCabe, E. Pidcock, G. P. Shields, R. Taylor, M. Towler and J. Van De Streek, *J. Appl. Crystallogr.*, 2006, **39**, 453–457.

202 Rigaku Oxford Diffraction, *http://www.rigaku.com/en/smc*, Accessed 03/09/2015.

203 Rigaku Corporation, *http://www.rigaku.com/en/smc*, Accessed 03/09/2015.

204 *CrysAlisPro*, Rigaku Oxford Diffraction, Kent, UK.

205 *CrystalClear 2.0*, Rigaku Corporation, Tokyo, Japan.

206 Oxford Cryosystems Ltd, *http://www.oxcryo.com/*, Accessed 02/09/2015.

207 H. Nowell, S. A. Barnett, K. E. Christensen, S. J. Teat and D. R. Allan, *J. Synch. Rad.*, 2012, **19**, 435–441.

208 Advanced Light Source, *http://www-als.lbl.gov/*, Accessed 02/09/2015.

209 Bruker AXS, *https://www.bruker.com/products/x-ray-diffraction-and-elemental-analysis/about-bruker-axs.html*, Accessed 07/09/2015.

210 Dectris, *https://www.dectris.com/pilatus3-r-s-and-x.html*, Accessed 07/09/2015.

211 *APEX2*, Bruker AXS Inc., Madison, Wisconsin, USA.

212 G. Barr, W. Dong and C. J. Gilmore, *J. Appl. Crystallogr.*, 2009, **42**, 965–974.

213 Mettler Toledo, *http://uk.mt.com/gb/en/home.html*, Accessed 07/09/2015.

214 Studio86Designs, *http://www.studio86designs.co.uk/index.html*, Accessed 07/09/2015.

215 TA Instruments, *http://www.tainstruments.com/*.

216 *TA Universal Analysis 2000*, TA Instruments, Hertfordshire, UK.

217 *Bio-Kine32*, BioLogic, Claix, France.

218 PerkinElmer Inc., *http://www.perkinelmer.co.uk/lab-solutions/default.xhtml*, Accessed 07/09/2015.

219 K. Biradha and R. Santra, *Chem. Soc. Rev.*, 2013, **42**, 950–967.

220 V. Stilinovic and B. Kaitner, *Cryst. Growth Des.*, 2013, **13**, 1703–1711.

221 D. Kitagawa and S. Kobatake, *Chem. Asian J.*, 2014, **9**, 289–293.

222 G. Liu, J. Liu, Y. Liu and X. Tao, *J. Am. Chem. Soc.*, 2014, **136**, 590–593.

223 B. P. Krishnan and K. M. Sureshan, *J. Am. Chem. Soc.*, 2015, **137**, 1692–6.

224 K. Rohleder, T. Luty and B. Kuchta, *J. Chem. Phys.*, 1994, **100**, 1573.

225 T. Akutagawa, H. Koshinaka, D. Sato, S. Takeda, S. Noro, H. Takahashi, R. Kumai, Y. Tokura and T. Nakamura, *Nat. Mater.*, 2009, **8**, 342–347.

226 Z. Liu, K. Kubo, S. Noro, T. Akutagawa and T. Nakamura, *Cryst. Growth Des.*, 2014, **14**, 537–543.

227 P. D. Bolton and F. M. Hall, *J. Chem. Soc.*, 1969, **B**, 1047–1051.

228 J. F. J. Dippy, S. R. C. Hughes and J. W. Laxton, *J. Chem. Soc.*, 1956, 2995–3000.

229 W. F. Baitinger, P. vo. R. Schleyer, T. S. S. R. Murty and L. Robinson, *Tetrahedron*, 1964, **20**, 1635–1647.

230 J. M. A. Robinson, D. Philp, K. D. M. Harris and B. M. Kariuki, *New J. Chem.*, 2000, **24**, 799–806.

231 M. Zeller, J. L. Stouffer, V. C. Solomon and L. S. Curtin, *Acta Crystallogr. Sect. C*, 2011, **67**, 397–404.

232 A. Parkin, C. K. Spanswick, C. R. Pulham and C. C. Wilson, *Acta Crystallogr. Sect. E*, 2005, **61**, 1087–1089.

233 S. K. Nayak, S. J. Prathapa and T. N. Guru Row, *J. Mol. Struct.*, 2009, **935**, 156–160.

234 D. Chopra, V. Thiruvenkatam and T. N. G. Row, *Cryst. Growth Des.*, 2006, **6**, 843–845.

235 K. Prout, J. Fail, R. M. Jones, R. E. Warner and J. C. Emmett, *J. Chem. Soc., Perkin Trans. 2*, 1988, 265.

236 H. Szatyłowicz, *J. Phys. Org. Chem.*, 2008, **21**, 897–914.

237 A. Lemmerer, S. Govindraju, M. Johnston, X. Motloung and K. L. Savig, *CrystEngComm*, 2015, **17**, 3591–3595.

238 D. Wiechert and D. Mootz, *Angew. Chem. Int. Ed.*, 1999, **80**, 1974–1976.

239 C. L. Jones, C. C. Wilson and L. H. Thomas, *CrystEngComm*, 2014, **16**, 5849–5858.

240 P. D. Bolton and F. M. Hall, *J. Chem. Soc.*, 1969, **B**, 259–263.

241 L. G. Bray, J. F. J. Dippy, S. R. C. Hughes and L. W. Laxton, *J. Chem. Soc*, 1957, 2405–2408.

242 P. D. Bolton and F. M. Hall, *Austral. J. Chem.*, 1968, **21**, 939.

243 A. de Courville, *Comp. Kend. Acad. Sci. Paris, Ser. C.*, 1966, **262**, 1196.

APPENDICES

Appendix A4 (Chapter 4)

A4.1: Crystal structure refinement details

Note: all crystal structures were refined using SHELXL-2014.

2-iodoaniline 3,4-dinitrobenzoic acid, Form I (1)

3,4-dinitrobenzoic acid molecules: The anisotropic displacement parameters for the non-hydrogen atoms were allowed to refine freely. The aromatic hydrogen atoms of the 3,4-DNBA molecules were placed in calculated positions and refined as riding on the atoms to which they were bonded. The hydrogen atoms of the carboxylic acid groups were located using Fourier difference maps and the positions refined using a distance restraint (0.9 Å); the U_{iso} of the H-atoms were constrained to $1.5U_{eq}$ of the O-atom to which it is bonded.

2-iodoaniline molecules: Both 2-IA molecules are 50:50 disordered over an inversion centre. Both are half-occupied in the asymmetric unit so the site occupancy factors for the atoms of these molecules were set to 0.5. With the exception of the I atoms, the non-hydrogen atoms of the 2-IA molecules were refined only isotropically. In order to ensure chemically sensible bond lengths and angles were obtained, the benzene rings of the disordered molecules were constrained to take a standard geometry in each case using an AFIX 66 command. The isotropic displacement parameters for the carbon atoms in each ring (C15-C20 and C21-C26) were constrained to take the same values using the EADP command; relaxation of this constraint resulted in unreasonable isotropic displacement parameters for these atoms. Aromatic hydrogen atoms and the hydrogen atoms of the NH_2 groups were placed in calculated positions and refined as riding on the atoms to which they were bonded.

2-iodoaniline 3,4-dinitrobenzoic acid, Form II (2)

3,4-dinitrobenzoic acid molecules: The anisotropic displacement parameters for the non-hydrogen atoms were allowed to refine freely. The aromatic hydrogen atoms of the 3,4-DNBA molecules were placed in calculated positions and refined as riding on the atoms to which they were bonded. The hydrogen atoms of the carboxylic acid groups were located using Fourier difference maps and the positions refined using a distance restraint (0.9 Å); the U_{iso} of the H-atoms were constrained to $1.5U_{eq}$ of the O-atoms to which they are bonded.

2-iodoaniline molecules: Both 2-IA molecules are disordered over two possible positions which were identified in a Fourier difference map. The two molecular sites were allowed to refine freely against each other, giving occupancies of 0.768(2):0.231(2) and 0.526(1):0.474(1) for the two independent 2-IA sites. With the exception of the I atoms, the non-hydrogen atoms were refined only isotropically. In order to ensure chemically sensible bond lengths and angles were

obtained, the benzene rings of the disordered molecules were constrained to take a standard geometry in each case using an AFIX 66 command. Due to the overlapping regions of electron density, the isotropic displacement parameters for the carbon atoms in each ring (C29A-C34A, C29B-C34B, C35A-C40A, C35B-C40B) were constrained to take the same values using the EADP command; relaxation of this constraint resulted in unreasonable isotropic displacement parameters for these atoms. Aromatic hydrogen atoms and the hydrogen atoms of the NH_2 groups were placed in calculated positions and refined as riding on the atoms to which they were bonded.

2-iodoaniline 3,4-dinitrobenzoic acid, Form III (3)

3,4-dinitrobenzoic acid molecules: The anisotropic displacement parameters for the non-hydrogen atoms were allowed to refine freely. The aromatic hydrogen atoms of the 3,4-DNBA molecules were placed in calculated positions and refined as riding on the atoms to which they were bonded. The hydrogen atoms of the carboxylic acid groups were located using Fourier difference maps and the positions refined using a distance restraint (0.9 Å); the U_{iso} of the H-atoms were constrained to $1.5U_{eq}$ of the O-atoms to which they are bonded.

2-iodoaniline molecule: The 2-IA molecule is disordered over two possible positions which were identified in a Fourier difference map. The two molecular orientations were allowed to refine freely against each other, giving occupancies of 0.56(2):0.44(2). With the exception of the I atoms, the non-hydrogen atoms were refined only isotropically. In order to ensure chemically sensible bond lengths and angles were obtained, the benzene rings of the disordered molecules were constrained to take a standard geometry in each case using an AFIX 66 command. Due to the overlapping regions of electron density, the isotropic displacement parameters for the carbon atoms in each ring (C15A-C20A, C15B-C20B) were constrained to take the same values using the EADP command; relaxation of this constraint resulted in unreasonable isotropic displacement parameters for these atoms. The anisotropic displacement parameters of the iodine atoms, I1A and I1B, were also constrained to take the same values using the EADP command. Aromatic hydrogen atoms and the hydrogen atoms of the NH_2 groups were placed in calculated positions and refined as riding on the atoms to which they were bonded.

2-bromoaniline 3,4-dinitrobenzoic acid, Form I (4)

3,4-dinitrobenzoic acid molecules: The anisotropic displacement parameters for the non-hydrogen atoms were allowed to refine freely. The aromatic hydrogen atoms of the 3,4-DNBA molecules were placed in calculated positions and refined as riding on the atoms to which they were bonded. The hydrogen atoms of the carboxylic acid groups were located using

Fourier difference maps and the positions refined using a distance restraint (0.9 Å); the U_{iso} of the H-atoms were constrained to $1.5U_{eq}$ of the O-atom to which it is bonded.

2-bromoaniline molecule disordered over the inversion centre: The molecule is half-occupied in the asymmetric unit, so the site occupancy factors for the atoms of this molecule were set to 0.5. With the exception of the Br atoms, the non-hydrogen atoms were refined only isotropically. In order to ensure chemically sensible bond lengths and angles were obtained, the benzene ring of the was constrained to take a standard geometry using an AFIX 66 command. The isotropic displacement parameters for the carbon atoms in the ring (C28-C33) were constrained to take the same values using the EADP command' relaxation of this constraint resulted in unreasonable isotropic displacement parameters for these atoms. There are other significant peaks in the residual electron density observable in the region of this 2-BrA molecule suggesting a more complex disorder model. These are likely to correspond to a second 2-BrA position but, due to the very low occupation, only the heavier Br atom can be modelled. The PART instruction was used, and a free variable was introduced, and the two bromine atoms were allowed to refine freely against each other to give approximate 85:15 occupancies. Aromatic hydrogen atoms and the hydrogen atoms of the NH_2 groups were placed in calculated positions and refined as riding on the atoms to which they were bonded.

2-bromoaniline molecule with symmetry-independent disorder: The molecule has two possible positions which were identified in a Fourier difference map. The two molecular sites were allowed to refine freely against each other, giving occupancies of 0.905(1):0.095(1). With the exception of the two Br atoms, the non-hydrogen atoms were refined only isotropically. In order to ensure chemically sensible bond lengths and angles were obtained, the benzene ring of the disordered molecules were constrained to take a standard geometry in each case using an AFIX 66 command. Due to the overlapping regions of electron density, the isotropic displacement parameters for the carbon atoms in each ring (C22-C27 and C22A-C27A) were constrained to take the same values using the EADP command; relaxation of this constraint resulted in unreasonable isotropic displacement parameters for these atoms. The C23-N7A distance was restrained to take a standard length (1.4 Å) using a distance restraint; due to overlapping regions of electron density, the isotropic displacement parameters for the two nitrogen atoms, N7 and N7A, were constrained to take the same values using the EADP command. Aromatic hydrogen atoms and the hydrogen atoms of the NH_2 groups were placed in calculated positions and refined as riding on the atoms to which they were bonded.

2-bromoaniline 3,4-dinitrobenzoic acid, Form II (5)

3,4-dinitrobenzoic acid molecules: The two nitro groups of one 3,4-DNBA molecule are disordered over two possible positions; an initial anisotropic refinement showed elongated parameters for the N and O atoms. Due to steric effects, the positions adopted by the two nitro

groups are influenced by each other resulting in just two possible arrangements. The additional sites were identified from the Fourier difference map. The two possible orientations were allowed to refine freely against each other, giving approximate 50:50 occupancies. The anisotropic displacement parameters for the non-hydrogen atoms were allowed to refine freely. The thermal parameters of the ring C-atoms are slightly elongated in the direction perpendicular to the ring plane, reflecting the two possible nitro group positions lying either side of the plane. The aromatic hydrogen atoms of the 3,4-DNBA molecules were placed in calculated positions and refined as riding on the atoms to which they were bonded. The hydrogen atoms of the carboxylic acid groups were located using Fourier difference maps and the positions refined using a distance restraint (0.9 Å); the U_{iso} of the H-atoms were constrained to $1.5U_{eq}$ of the O-atom to which it is bonded.

2-bromoaniline molecule: The 2-BrA molecule is disordered over two possible positions which were identified from the Fourier Difference map. The two sites were allowed to refine freely against each other, giving 0.923(2):0.077(2) occupancies. With the exception of the Br atoms, the non-hydrogen atoms were refined only isotropically. In order to ensure chemically sensible bond lengths and angles were obtained, the benzene rings of the disordered molecules were constrained to take a standard geometry in each case using an AFIX 66 command. Due to the overlapping regions of electron density, the isotropic displacement parameters for the carbon atoms in each ring (C15A-C20A, C15B-C20B) were constrained to take the same values using the EADP command; relaxation of this constraint resulted in unreasonable isotropic displacement parameters for these atoms. . The C20B-N1B distance was restrained to take a standard length (1.4 Å) using a distance restraint. Aromatic hydrogen atoms and the hydrogen atoms of the NH_2 groups were placed in calculated positions and refined as riding on the atoms to which they were bonded.

2-chloroaniline 3,4-dinitrobenzoic acid, Form I (6)

3,4-dinitrobenzoic acid molecules: The anisotropic displacement parameters for the non-hydrogen atoms were allowed to refine freely. The aromatic hydrogen atoms of the 3,4-DNBA molecules were placed in calculated positions and refined as riding on the atoms to which they were bonded. The hydrogen atoms of the carboxylic acid groups were located using Fourier difference maps and the positions refined using a distance restraint (0.9 Å); the U_{iso} of the H-atoms were constrained to $1.5U_{eq}$ of the O-atom to which it is bonded.

2-ClA molecule disordered over the inversion centre: The molecule is half-occupied in the asymmetric unit, so the site occupancy factors for the atoms of this molecule were set to 0.5. With the exception of the Cl atom, the non-hydrogen atoms were refined only isotropically. In order to ensure chemically sensible bond lengths and angles were obtained, the benzene ring of the was constrained to take a standard geometry using an AFIX 66 command. The isotropic

displacement parameters for the carbon atoms in the ring (C28-C33) were constrained to take the same values using the EADP command; relaxation of this constraint resulted in unreasonable isotropic displacement parameters for these atoms. Aromatic hydrogen atoms and the hydrogen atoms of the NH_2 groups were placed in calculated positions and refined as riding on the atoms to which they were bonded.

2-ClA molecule with symmetry-independent disorder: The molecule has two possible positions which were identified from the Fourier difference map. The two molecular sites were allowed to refine freely against each other, giving 0.876(2):0.124(2) occupancies. With the exception of the two Cl atoms, the non-hydrogen atoms were refined only isotropically. In order to ensure chemically sensible bond lengths and angles were obtained, the benzene ring of the disordered molecules were constrained to take a standard geometry in each case using an AFIX 66 command. Due to overlapping regions of electron density, the isotropic displacement parameters for the carbon atoms in each ring (C22-C27 and C22A-C27A) were constrained to take the same values using the EADP command; relaxation of this constraint resulted in unreasonable isotropic displacement parameters for these atoms. The C23-N7A distance was restrained to take a standard length (1.4 Å) using a distance restraint; the isotropic displacement parameters for the corresponding nitrogen atoms, N7 and N7A, were constrained to take the same values using the EADP command. Aromatic hydrogen atoms and the hydrogen atoms of the NH_2 groups were placed in calculated positions and refined as riding on the atoms to which they were bonded.

2-fluoroaniline 3,4-dinitrobenzoic acid (7)

3,4-dinitrobenzoic acid molecules: The anisotropic displacement parameters for the non-hydrogen atoms were allowed to refine freely. The aromatic hydrogen atoms of the 3,4-DNBA molecules were placed in calculated positions and refined as riding on the atoms to which they were bonded. The hydrogen atoms of the carboxylic acid groups were located using Fourier difference maps and the positions refined using a distance restraint (0.9 Å); the U_{iso} of the H-atoms were constrained to $1.5U_{eq}$ of the O-atom to which it is bonded.

2-fluoroaniline molecule disordered over the inversion centre: The molecule is half-occupied in the asymmetric unit, so the site occupancy factors for the atoms of this molecule were set to 0.5. All the atoms of the molecule were refined only isotropically. In order to ensure chemically sensible bond lengths and angles were obtained, the benzene ring of the was constrained to take a standard geometry using an AFIX 66 command. The isotropic displacement parameters for the carbon atoms in the ring (C34-C39) were constrained to take the same values using the EADP command; relaxation of this constraint resulted in unreasonable isotropic displacement parameters for these atoms. The C39-F3 distance was restrained to take a standard length (1.35 Å) using a distance restraint. The C38-N9 distance was restrained to take a standard length

(1.4 Å) using a distance restraint. Aromatic hydrogen atoms and the hydrogen atoms of the NH_2 groups were placed in calculated positions and refined as riding on the atoms to which they were bonded.

2-fluoroaniline molecule with symmetry-independent disorder: The molecule has two possible positions which were identified in a Fourier difference map. The two molecular sites were allowed to refine freely against each other, giving 0.568(8):0.432(8) occupancies. All of the non-hydrogen atoms were refined only isotropically. In order to ensure chemically sensible bond lengths and angles were obtained, the benzene ring of the disordered molecules were constrained to take a standard geometry in each case using an AFIX 66 command. Due to the overlapping regions of electron density, the isotropic displacement parameters for the carbon atoms in each ring (C22-C27 and C28-C33) were constrained to take the same values using the EADP command. The isotropic displacement parameters of N7 and N8 were constrained to take the same values using the EADP command; this was also done for F1 and F2. Relaxation of these EADP constraints resulted in unreasonable isotropic displacement parameters for these atoms. The C26-N7 and C28-N8 distances were restrained to take a standard length (1.4 Å) using a distance restraint; the C33-F2 distance was restrained to take a standard length (1.35 Å) using a distance restraint. The C25-N7 and C27-N7 distances were restrained to be equal using the SADI restraint. Aromatic hydrogen atoms and the hydrogen atoms of the NH_2 groups were placed in calculated positions and refined as riding on the atoms to which they were bonded.

2-fluoroanilinium 3,4-dinitrobenzoate 3,4-dinitrobenzoic acid (8)

3,4-dinitrobenzoic acid/3,4-dinitrobenzoate molecules: The anisotropic displacement parameters for the non-hydrogen atoms were allowed to refine freely. The aromatic hydrogen atoms were placed in calculated positions and refined as riding on the atoms to which they were bonded. The hydrogen atom of the carboxylic acid group was located using Fourier difference maps and its position and anisotropic displacement parameters allowed to freely refine.

2-fluoroanilinium cation: The non-hydrogen atoms were refined anisotropically. The fluorine atom has two possible positions which were identified in a Fourier difference map, *ortho* to the amine group (bound to C15 and C19). The two sites were allowed to refine freely against each other, giving 0.696(5):0.304(5) occupancies. The C15-F2 and C19-F1 distances were refined to take standard a standard length (1.35 Å) using a distance restraint. The aromatic hydrogen atoms were placed in calculated positions and refined as riding on the atoms to which they were bonded. The hydrogen atoms of the NH_3^+ group were located using Fourier difference maps; H-atom positions were allowed to freely refine, but the U_{iso} of the H-atoms was constrained to $1.5U_{eq}$ of the N-atom to which they are bonded.

2-fluoro-4-[(1E)-2-(2-fluorophenyl)diazenyl]-benzenamine 3,4-dinitrobenzoic acid (9)

The anisotropic displacement parameters for the non-hydrogen atoms were allowed to refine freely, with the exception of the disordered nitro groups of one 3,4-DNBA molecule. The two nitro groups of one 3,4-DNBA molecule are disordered over two possible positions. The additional sites were identified in a Fourier difference map. The two possible orientations for each of the nitro groups were allowed to refine freely against each other, giving approximate 56:44 ratios for each nitro group. The aromatic hydrogen atoms were placed in calculated positions and refined as riding on the atoms to which they were bonded. The hydrogen atoms of the carboxylic acid groups were located using Fourier difference maps and the positions refined using a distance restraint (0.9 Å). The hydrogen atoms of the NH_2 group were located using Fourier difference maps; the H-atom positions and the isotropic displacement parameters were allowed to freely refine.

2-iodo-4-methylaniline 3,4-dinitrobenzoic acid (10)

3,4-dinitrobenzoic acid molecules: The anisotropic displacement parameters for the non-hydrogen atoms were allowed to refine freely. The aromatic hydrogen atoms of the 3,4-DNBA molecules were placed in calculated positions and refined as riding on the atoms to which they were bonded. The hydrogen atom of the carboxylic acid group was also placed in a calculated position and refined as riding on the O-atom to which it was bonded.

2-iodo-4-methylaniline molecule: The 2-I-4-MA molecule is modelled as disordered over an inversion centre and over two symmetry-independent positions which were identified in a Fourier Difference map. The occupancies of the symmetry-independent disorder positions were allowed to refine freely against each other, giving approximate occupancies of 38.5:38.5:11.5:11.5 for the four possible positions. It was not possible to locate the methyl or amine groups. With the exception of the I atoms, the non-hydrogen atoms were refined only isotropically. In order to ensure chemically sensible bond lengths and angles were obtained, the benzene rings of the disordered molecules were constrained to take a standard geometry in each case using an AFIX 66 command. Due to the overlapping regions of electron density, the isotropic displacement parameters for the carbon atoms in each ring (C15-C20, C15A-C20A) were constrained to take the same values using the EADP command; relaxation of this constraint resulted in unreasonable isotropic displacement parameters for these atoms. The anisotropic displacement parameters of the iodine atoms, I1 and I1A, were also constrained to take the same values using the EADP command. The I1-C16 and I1-C20, and I1A C19A and I1A C15A distances were restrained to take similar values using the SADI restraint. The I1-C15 and I1A-C20A distances were restrained to take a standard length (2.1 Å) using a distance restraint. All of the atoms of the disordered 2-I-4-MA molecules were constrained to lie in the same plane using the FLAT command. No hydrogen atoms were assigned to the molecule.

2-bromo-4-methylaniline 3,4-dinitrobenzoic acid (11)

3,4-dinitrobenzoic acid molecules: The anisotropic displacement parameters for the non-hydrogen atoms were allowed to refine freely. The aromatic hydrogen atoms of the 3,4-DNBA molecules were placed in calculated positions and refined as riding on the atoms to which they were bonded. The hydrogen atom of the carboxylic acid group was also placed in a calculated position and refined as riding on the O-atom to which it was bonded.

2-bromo-4-methylaniline molecule: The 2-Br-4-MA molecule is modelled as disordered over an inversion centre and over two symmetry-independent positions which were identified in a Fourier difference map. The occupancies of the symmetry-independent disorder positions were allowed to refine freely against each other, giving approximate occupancies of 33.5:33.5:16.5:16.5 for the four possible positions. It was not possible to locate the methyl or amine groups. All non-hydrogen atoms were refined only isotropically. In order to ensure chemically sensible bond lengths and angles were obtained, the benzene rings of the disordered molecules were constrained to take a standard geometry in each case using an AFIX 66 command. Due to the overlapping regions of electron density, the isotropic displacement parameters for the carbon atoms in each ring (C15-C20, C15A-C20A) were constrained to take the same values using the EADP command; relaxation of this constraint resulted in unreasonable isotropic displacement parameters for these atoms. The isotropic displacement parameters of the bromine atoms, Br1 and Br1A, were also constrained to take the same values using the EADP command. The Br1-C16 and Br1-C20, and Br1A C19A and Br1A C15A distances were restrained to be similar using the SADI restraint. The Br1-C15 and Br1A-C20A distances were restrained to take a standard length (1.9 Å) using a distance restraint. All of the atoms of the disordered 2-Br-4-MA molecules were constrained to lie in the same plane using the FLAT command. It was not possible to assign hydrogen atoms to the molecule.

2-chloro-4-methylaniline 3,4-dinitrobenzoic acid (12)

3,4-dinitrobenzoic acid molecules: The anisotropic displacement parameters for the non-hydrogen atoms were allowed to refine freely. The aromatic hydrogen atoms of the 3,4-DNBA molecules were placed in calculated positions and refined as riding on the atoms to which they were bonded. The hydrogen atom of the carboxylic acid group was also placed in a calculated position and refined as riding on the O-atom to which it was bonded.

2-chloro-4-methylaniline molecule: The 2-Cl-4-MA molecule is modelled as disordered over an inversion centre and over two symmetry-independent positions which were identified in a Fourier difference map. The occupancies of the symmetry-independent disorder positions were allowed to refine freely against each other, giving approximate occupancies of 33.5:33.5:16.5:16.5 for the four possible positions. It was not possible to locate the methyl or amine groups. All non-hydrogen atoms were refined only isotropically. In order to ensure

chemically sensible bond lengths and angles were obtained, the benzene rings of the disordered molecules were constrained to take a standard geometry in each case using an AFIX 66 command. Due to the overlapping regions of electron density, the isotropic displacement parameters for the carbon atoms in each ring (C15-C20, C15A-C20A) were constrained to take the same values using the EADP command; relaxation of this constraint resulted in unreasonable isotropic displacement parameters for these atoms. The isotropic displacement parameters of the chlorine atoms, Cl1 and Cl1A, were also constrained to take the same values using the EADP command. The Cl1-C16 and Cl1-C20, and Cl1A C16A and Cl1A C15A distances were restrained to be similar using the SADI restraint. The Cl1-C15 and Cl1A-C20A distances were restrained to take a standard length (1.75 Å) using a distance restraint. All of the atoms of the disordered 2-Cl-4-MA molecules were constrained to lie in the same plane using the FLAT command. No hydrogen atoms were assigned to the molecule.

2-iodophenol 3,4-dinitrobenzoic acid (13)

All non-hydrogen atoms were refined anisotropically. Aromatic hydrogen atoms were placed in calculated positions and refined as riding on the atoms to which they were bonded. The hydrogen atoms of the carboxylic acid and hydroxyl groups were identified using Fourier difference maps; the positions were refined using a distance restraint (0.9 Å) and the U_{iso} of the H-atoms were constrained to $1.5U_{eq}$ of the O-atoms to which they are bonded.

A4.2: PXRD experiment, Beamline I11, Diamond Light Source

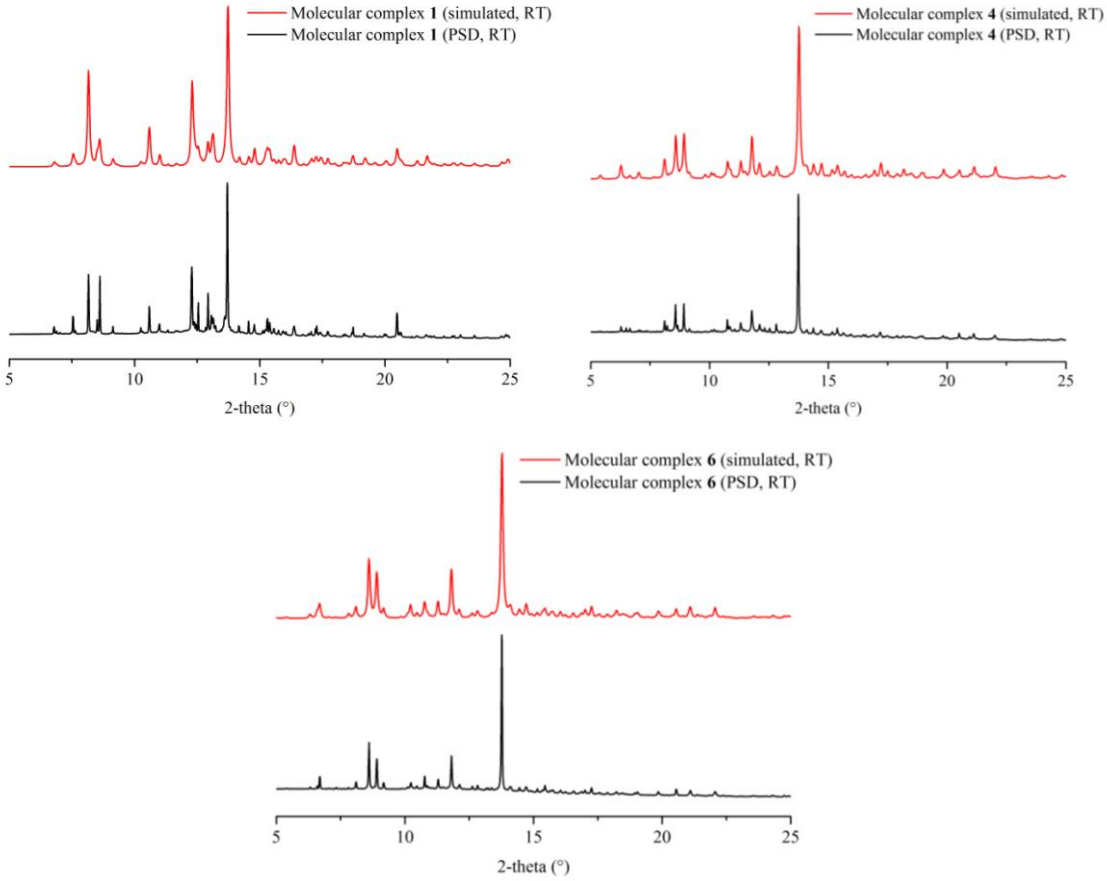

Figure A4.1 The simulated powder diffraction patterns and the room temperature diffraction patterns of molecular complexes **1**, **4** and **6**.

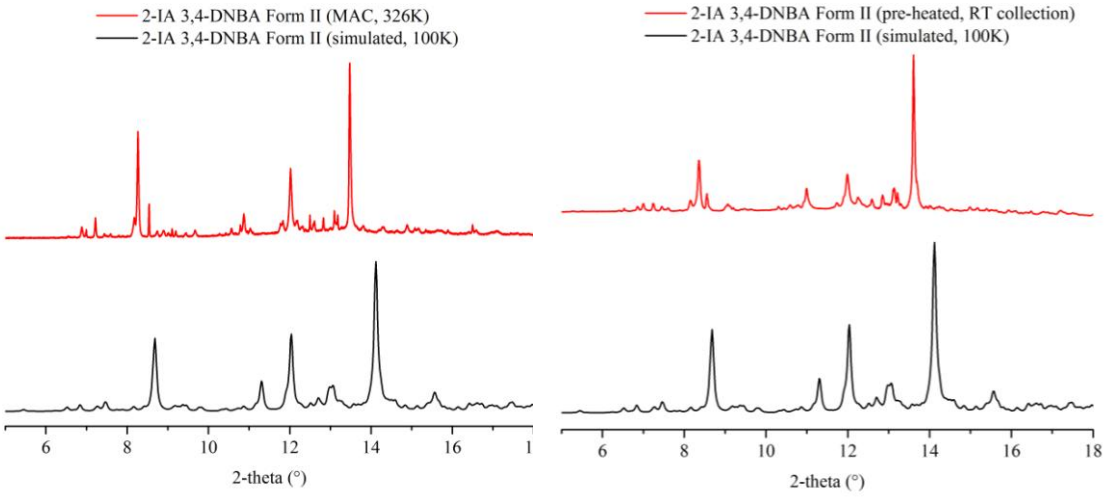

Figure A4.2 Left: the simulated powder diffraction pattern of 2-IA 3,4-DNBA Form II (**2**) and phase II in the variable temperature MAC data (326 K). Right: the simulated powder diffraction pattern of 2-IA 3,4-DNBA Form II (**2**) and the sample pre-heated past the first phase transition.

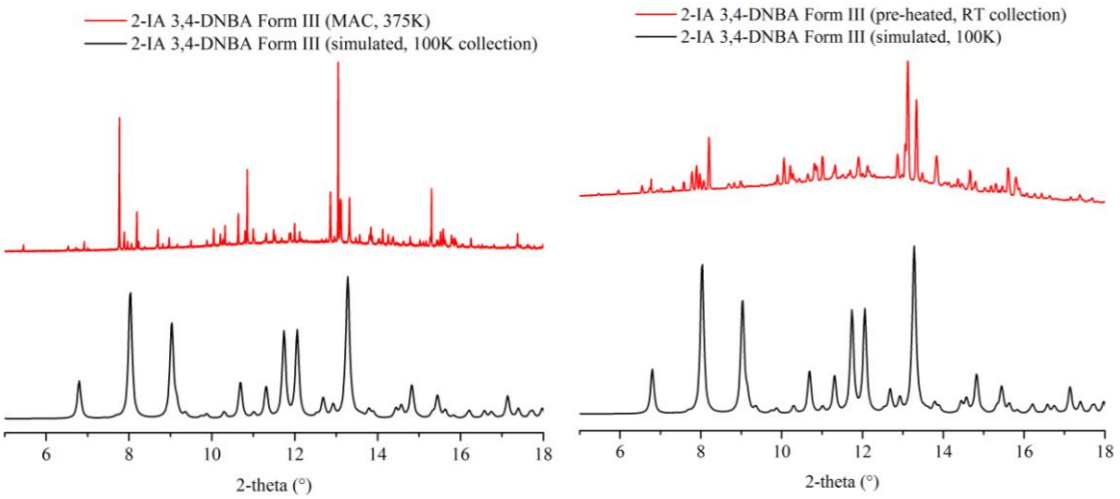

Figure A4.3 Top: The simulated powder diffraction pattern of 2-IA 3,4-DNBA Form III (**3**) and phase III in the variable temperature MAC data. Bottom: The simulated powder diffraction pattern of 2-IA 3,4-DNBA Form III (**3**) and the sample pre-heated past the first phase transition.

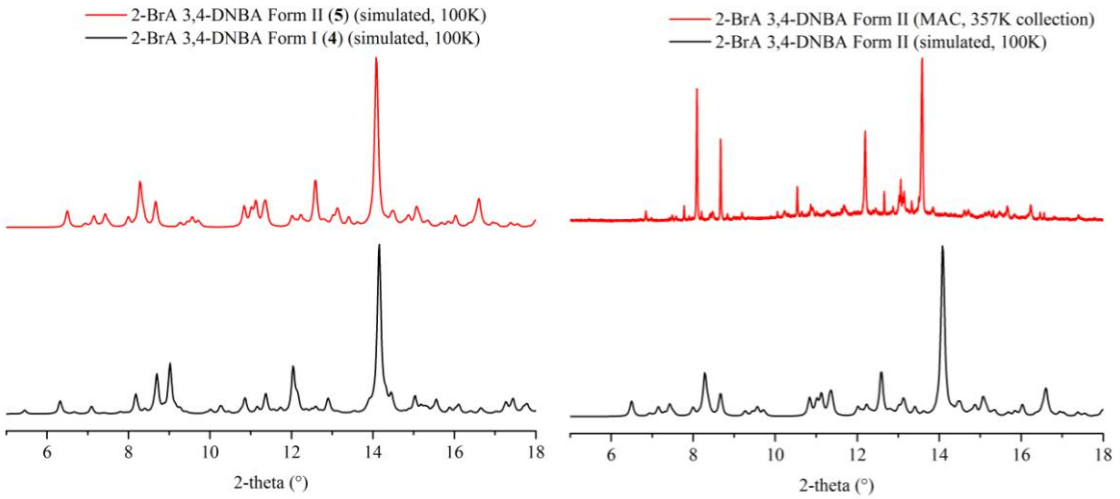

Figure A4.4 Left: the simulated powder diffraction patterns of Forms I and II of the molecular complex 2-BrA 3,4-DNBA (**4** and **5**). Right: the simulated powder diffraction pattern of 2-BrA 3,4-DNBA Form II (**5**) and phase II in the variable temperature MAC data (357 K).

A4.3: 2-fluoroaniline 3,4-dinitrobenzoic acid analysis

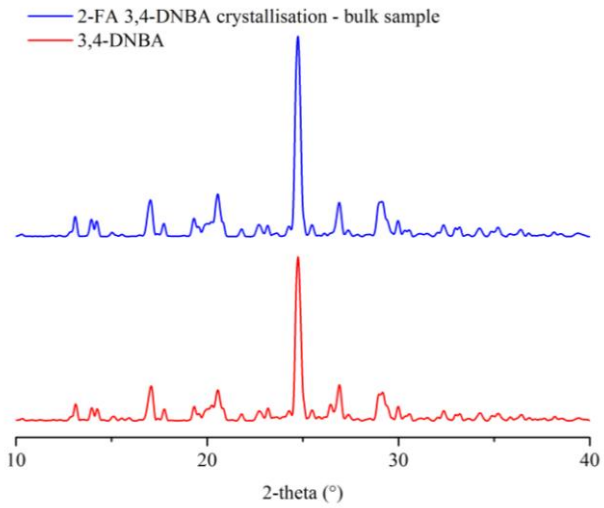

Figure A4.5 Comparison of the powder diffraction pattern of the colourless bulk sample of the 2-FA 3,4-DNBA crystallisation and the powder diffraction pattern of pure 3,4-DNBA.

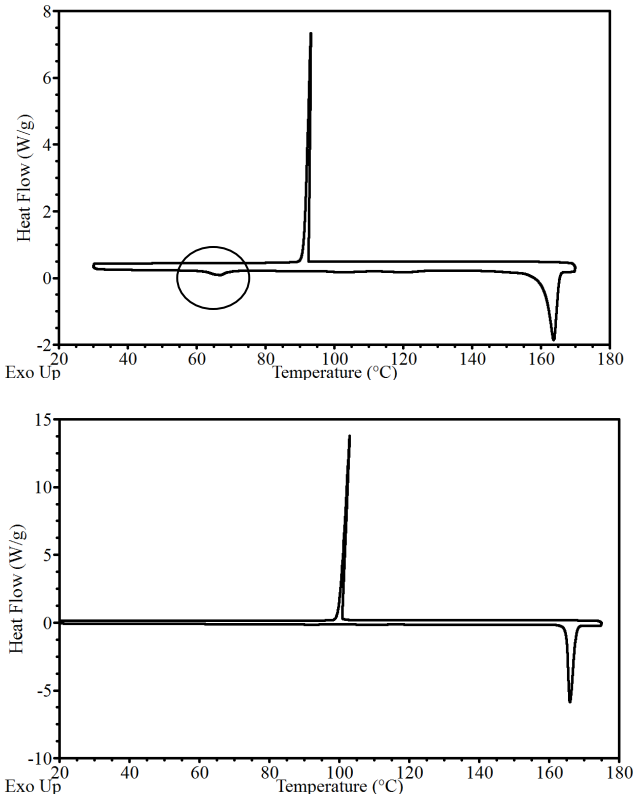

Figure A4.6 Top: DSC thermogram of the bulk sample of the 2-FA 3,4-DNBA crystallisation, showing the thermal event at ~66 °C (circled); Bottom: DSC thermogram of pure 3,4-DNBA.

Appendix A5 (Chapter 5)

A5.1 Crystal structure refinement details

Note: all crystal structures were refined using SHELXL-2014.

4-iodoanilinium 3,5-dinitrobenzoate Form I (14)

All non-hydrogen atoms were refined anisotropically. Aromatic hydrogen atoms were placed in calculated positions and refined as riding on the atoms to which they were bonded. The hydrogen atoms of the two NH_3^+ groups were located using Fourier difference maps; H-atom positions were allowed to freely refine, but the U_{iso} of the H-atoms was constrained to $1.5U_{eq}$ of the N-atom to which they are bonded.

4-iodoanilinium 3,5-dinitrobenzoate Form II (15)

All non-hydrogen atoms were refined anisotropically. Aromatic hydrogen atoms were placed in calculated positions and refined as riding on the atoms to which they were bonded. The hydrogen atoms of the NH_3^+ group were located using Fourier difference maps and allowed to freely refine.

4-iodoaniline 3,5-dinitrobenzoic acid (16)

All non-hydrogen atoms were refined anisotropically. Aromatic hydrogen atoms were placed in calculated positions and refined as riding on the atoms to which they were bonded. The hydrogen atoms of the NH_2 group were identified using Fourier difference maps; the positions were allowed to freely refine, but the U_{iso} of the H-atoms was constrained to $1.5U_{eq}$ of the N-atom to which they are bonded. The hydrogen atom of the carboxylic acid group was located using Fourier difference maps and the position refined using a distance restraint (0.9 Å); the U_{iso} of the H-atom was constrained to $1.5U_{eq}$ of the O-atom to which it is bonded.

4-iodoaniline 3,5-dinitrobenzoic acid methanol solvate (17)

4-iodoaniline molecules: The 4-IA molecules are well-described and the positions and anisotropic displacement parameters (ADPs) for the non-hydrogen atoms were allowed to refine freely. The aromatic hydrogen atoms of the 4-iodoaniline molecules were placed in calculated positions and refined as riding on the atoms to which they were bonded. The hydrogen atoms on the amine group could not be determined due to an ambiguity of the protonation state of this molecule and were therefore omitted from the model.

3,5-dinitrobenzoic acid molecules: The Q-peaks corresponding to the atoms of the two independent 3,5-DNBA molecules were easily assigned, but when the positions and ADPs were

allowed to refine freely, there was significant elongation of the ADPs. One of the assigned nitro groups in both molecules showed bond lengths and angles which were characteristic of a well-described nitro group. However, the C-N or C-C distances and N-O or C-O distances of the second nitro or carboxylic acid groups, respectively, took values in between those expected for the two groups. A model was therefore adopted where the molecules could adopt two positions around the well-defined pivot nitro group but with the carboxylic acid or nitro groups flipped. The PART instruction was used to divide the atoms for each independent molecule into two groups and a free variable was introduced. Due to the close positions of these two orientations, significant constraints had to be applied for a chemically meaningful refinement. With the exception of the pivot nitro group, corresponding pairs of C/N/O (A and B) atoms for the whole molecule were constrained to be equal using the EADP command to ensure sensible isotropic displacement parameters were obtained; all atoms except the pivot nitro group were refined only isotropically. The benzene rings were restrained to take a standard geometry using an AFIX 66 command. The C-C distances of the carboxylic acid groups and C-N distances of the disordered nitro groups were restrained to take standard values of 1.51 Å and 1.47 Å, respectively using a DFIX command. The N-O distances were constrained to take values of 1.22 Å using a DFIX command. The C-O distances of the carboxylic acid groups were not restrained due to the ambiguity about the protonation state (these groups are 50:50 disordered between a carboxylic acid group and a carboxylate group). The occupancies of the two positions for each independent 3,5-DNBA molecule were allowed to freely refine and these converged at approximately 50:50 in each case. The aromatic hydrogen atoms of the 3,5-dinitrobenzoic acid molecules were placed in calculated positions and refined as riding on the atoms to which they were bonded. It was not possible to assign hydrogen atoms to the carboxyl groups due to an ambiguity of the protonation states of the two molecules, so these hydrogen atoms were omitted from the model.

Methanol molecule: The methanol molecule was also found to be disordered over two positions; the atoms of two positions were divided using the PART instruction and a free variable was introduced. The two positions were allowed to freely refine to approximately 50:50, and due to the close proximity of the two positions the atoms were only refined isotropically. The hydrogen atoms of the methyl groups were placed on calculated positions and refined as riding on the atoms to which they were bonded. It was not possible to identify the hydrogen atoms of the hydroxyl groups in a Fourier difference map due to the disorder so these hydrogen atoms were omitted from the model.

4-bromoanilinium 3,5-dinitrobenzoate (18)

All non-hydrogen atoms were refined anisotropically. Aromatic hydrogen atoms were placed in calculated positions and refined as riding on the atoms to which they were bonded. The

hydrogen atoms of the two NH_3^+ groups were located using Fourier difference maps; H-atom positions were allowed to freely refine, but the U_{iso} of the H-atoms was constrained to $1.5U_{eq}$ of the N-atom to which they are bound.

4-bromoaniline 3,5-dinitrobenzoic acid (19)

All non-hydrogen atoms were refined anisotropically. Aromatic hydrogen atoms were placed in calculated positions and refined as riding on the atoms to which they were bonded. The hydrogen atoms of the NH_2 group were identified using Fourier difference maps; the positions were allowed to freely refine, but the U_{iso} of the H-atoms was constrained to $1.5U_{eq}$ of the N-atom to which they are bonded. The hydrogen atoms of the carboxylic acid groups were located using Fourier difference maps and the positions refined using a distance restraint (DFIX 0.9 Å); the U_{iso} of the H-atom was constrained to $1.5U_{eq}$ of the O-atom to which it is bonded.

4-iodo-2-methylanilinium 3,5-dinitrobenzoate (20)

All non-hydrogen atoms were refined anisotropically. Aromatic hydrogen atoms were placed in calculated positions and refined as riding on the atoms to which they were bonded. The hydrogen atoms of the NH_3^+ group were identified using Fourier difference maps, and the positions and isotropic displacement parameters allowed to freely refine. The methyl group H-atoms were located initially using Fourier difference maps and the bond distances and angles constrained to take standard values; the U_{iso} of the H-atoms was constrained to $1.5U_{eq}$ of the C-atom to which they are bonded.

4-iodo-2-methylaniline 3,5-dinitrobenzoic acid (21)

All non-hydrogen atoms were refined anisotropically. Aromatic hydrogen atoms were placed in calculated positions and refined as riding on the atoms to which they were bonded. The hydrogen atoms of the NH_2 group were located using Fourier difference maps and the positions and isotropic displacement parameters allowed to freely refine. The hydrogen atom of the carboxylic acid group was located using Fourier difference maps; the position was refined using a distance restraint (DFIX 0.9 Å) and the isotropic thermal parameters allowed to freely refine. The methyl group H-atoms were located initially using Fourier difference maps and the bond distances and angles constrained to take standard values; the U_{iso} of the H-atoms was constrained to $1.5U_{eq}$ of the C-atom to which they are bonded.

4-bromo-2-methylanilinium 3,5-dinitrobenzoate (22)

All non-hydrogen atoms were refined anisotropically. Aromatic hydrogen atoms were placed in calculated positions and refined as riding on the atoms to which they were bonded. The hydrogen atoms of the NH_3^+ group were identified using Fourier difference maps, and the

positions and isotropic displacement parameters allowed to freely refine. The methyl group H-atoms were located initially using Fourier difference maps and the bond distances and angles constrained to take standard values; the U_{iso} of the H-atoms was constrained to $1.5U_{eq}$ of the C-atom to which they are bonded.

4-bromo-2-methylaniline 3,5-dinitrobenzoic acid (23)

All non-hydrogen atoms were refined anisotropically. Aromatic hydrogen atoms were placed in calculated positions and refined as riding on the atoms to which they were bonded. The hydrogen atoms of the NH_2 group were located using Fourier difference maps and the positions and isotropic displacement parameters allowed to freely refine. The hydrogen atom of the carboxylic acid group was located using Fourier difference maps; the position was refined using a distance restraint (DFIX 0.9 Å) and the isotropic thermal parameters allowed to freely refine. The methyl group H-atoms were located initially using Fourier difference maps and the bond distances and angles constrained to take standard values; the U_{iso} of the H-atoms was constrained to $1.5U_{eq}$ of the C-atom to which they are bonded.

4-chloro-2-methylanilinium 3,5-dinitrobenzoate (24)

All non-hydrogen atoms were refined anisotropically. Aromatic hydrogen atoms were placed in calculated positions and refined as riding on the atoms to which they were bonded. The hydrogen atoms of the NH_3^+ group were identified using Fourier difference maps, and the positions and isotropic displacement parameters allowed to freely refine. The methyl group H-atoms were located initially using Fourier difference maps and the bond distances and angles constrained to take standard values; the U_{iso} of the H-atoms was constrained to $1.5U_{eq}$ of the C-atom to which they are bonded.

A5.2: IR spectra relating to molecular complex 17

Molecular complex **17** has significant molecular disorder resulting in ambiguity in the assignment of protonation states of the 4-iodoaniline (4IA) and 3,5-dinitrobenzoic acid (3,5-DNBA) molecules; the geometry around the molecules was consistent with either neutral molecules, protonated 4IA molecules or deprotonated 3,5-DNBA molecules and it was not possible to resolve any H atom positions due to the disorder. Spectra were recorded for the single component 4IA (Figure A5.1); the features corresponding to an NH_2 group in 4IA could be clearly identified in the 3500-3000 cm^{-1} region.

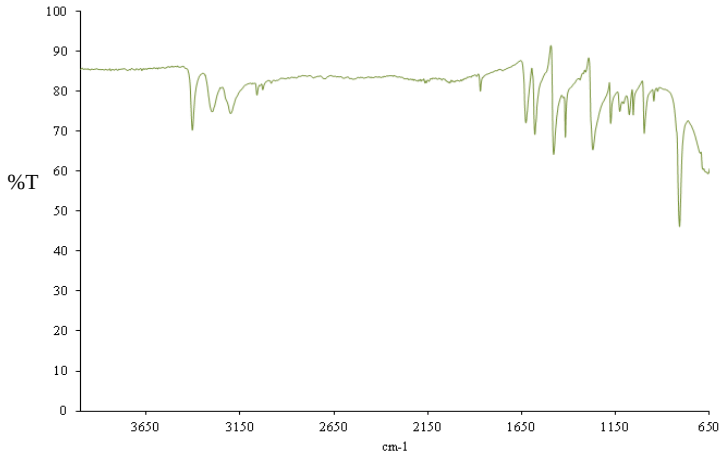

Figure A5.1 IR spectrum for 4-iodoaniline

The IR spectrum of molecular complex **17** (Figure A5.2) was compared to those of the 4IA complexes **33** (Figure A5.3) and **31** (Figure A5.4) in which the protonation states of the 4-IA molecules could clearly be resolved from single crystal X-ray diffraction. Complex **33** contains only protonated 4IA molecules (with NH_3^+ groups) and the region 3500-3000 cm^{-1} shows significant differences to that of neutral 4IA consistent with a lowering of symmetry. Complex **31** contains a mixture of neutral and ionic 4IA molecules (and therefore a mixture of NH_2 and NH_3^+ groups). The IR spectra of molecular complex **17** shows similarities to that of complex **31** and shows a pattern which has characteristics of both 4IA and complex **33**. Combined with crystallographic arguments, this is consistent with molecular complex **17** being comprised of both neutral and ionic 4IA molecules.

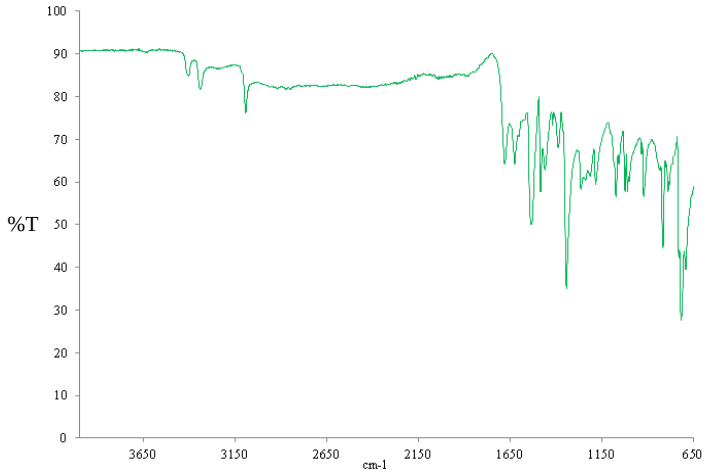

Figure A5.2 IR spectrum for molecular complex **17**

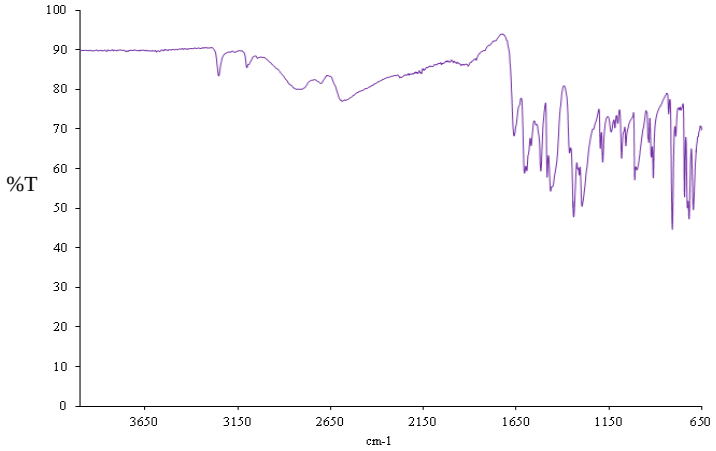

Figure A5.3 IR spectrum for molecular complex **33** (containing only ionic 4-IA molecules).

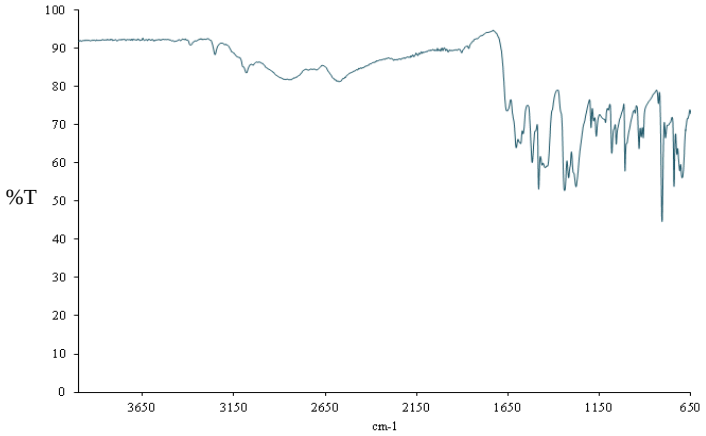

Figure A5.4 IR spectrum for molecular complex **31** (containing 4-IA molecules with mixed ionisation states).

Appendix A6 (Chapter 6)

A6.1 Crystal structure refinement details

Note: all crystal structures were refined using SHELXL-2014.

2-iodoaniline 3,5-dinitrobenzoic acid (25)

3,5-dinitrobenzoic acid molecule: The anisotropic displacement parameters for the non-hydrogen atoms were allowed to refine freely. The aromatic hydrogen atoms of the 3,5-DNBA molecule were placed in calculated positions and refined as riding on the atoms to which they were bonded. The hydrogen atom of the carboxylic acid group was located using Fourier difference maps and the position refined using a distance restraint (0.9 Å); the U_{iso} of the H-atom was constrained to $1.5U_{eq}$ of the O-atom to which it was bonded.

2-iodoaniline molecule: The 2-IA molecule is disordered over two possible positions which were identified in a Fourier difference map. The two molecular sites were allowed to refine freely against each other, giving occupancies of 0.539(2):0.461(2). With the exception of the I atoms, the non-hydrogen atoms were refined only isotropically. In order to ensure chemically sensible bond lengths and angles were obtained, the benzene rings of the disordered molecules were constrained to take a standard geometry in each case using an AFIX 66 command. Due to the overlapping regions of electron density, the isotropic displacement parameters for the carbon atoms in each ring (C8A-C13A, C8B-C13B) were constrained to take the same values using the EADP command; relaxation of this constraint resulted in unreasonable displacement parameters for these atoms. The C8A-I1A and C8B-I1B distances were restrained to take a standard length (2.1 Å) using a distance restraint. Aromatic hydrogen atoms and the hydrogen atoms of the NH_2 groups were placed in calculated positions and refined as riding on the atoms to which they were bonded.

2-bromoaniline 3,5-dinitrobenzoic acid (26)

3,5-dinitrobenzoic acid molecule: The anisotropic displacement parameters for the non-hydrogen atoms were allowed to refine freely. The aromatic hydrogen atoms of the 3,5-DNBA molecules were placed in calculated positions and refined as riding on the atoms to which they were bonded. The hydrogen atom of the carboxylic acid group was located using Fourier difference maps and the position refined using a distance restraint (0.9 Å); the U_{iso} of the H-atom was constrained to $1.5U_{eq}$ of the O-atom to which it was bonded.

2-bromoaniline molecule: The 2-BrA molecule is disordered over two possible positions which were identified in a Fourier difference map. The two molecular sites were allowed to refine freely against each other, giving occupancies of 0.692(1):0.308(1). All atoms were refined only isotropically. In order to ensure chemically sensible bond lengths and angles were obtained, the

benzene rings of the disordered molecules were constrained to take a standard geometry in each case using an AFIX 66 command. Due to the overlapping regions of electron density, the isotropic displacement parameters for the carbon atoms in each ring (C8A-C13A, C8B-C13B) were constrained to take the same values using the EADP command; relaxation of this constraint resulted in unreasonable displacement parameters for these atoms. Aromatic hydrogen atoms and the hydrogen atoms of the NH_2 groups were placed in calculated positions and refined as riding on the atoms to which they were bonded.

2-chloroaniline 3,5-dinitrobenzoic acid (27)

3,5-dinitrobenzoic acid molecule: The anisotropic displacement parameters for the non-hydrogen atoms were allowed to refine freely. The aromatic hydrogen atoms of the 3,5-DNBA molecules were placed in calculated positions and refined as riding on the atoms to which they were bonded. The hydrogen atom of the carboxylic acid group was located using Fourier difference maps and the position refined using a distance restraint (0.9 Å); the U_{iso} of the H-atom was constrained to $1.5U_{eq}$ of the O-atom to which it was bonded.

2-chloroaniline molecule: The 2-ClA molecule is disordered over two possible positions which were identified in a Fourier difference map. The two molecular sites were allowed to refine freely against each other, giving occupancies of 0.796(3):0.204(3). All non-hydrogen atoms were refined anisotropically. In order to ensure chemically sensible bond lengths and angles were obtained, the benzene rings of the disordered molecules were constrained to take a standard geometry in each case using an AFIX 66 command. Due to the overlapping regions of electron density, the anisotropic displacement parameters for the carbon atoms in each ring (C8A-C13A, C8B-C13B) were constrained to take the same values using the EADP command; relaxation of this constraint resulted in unreasonable displacement parameters for these atoms. The anisotropic displacement parameters of N3A and N3B were also constrained to take the same values using the EADP command. Aromatic hydrogen atoms and the hydrogen atoms of the NH_2 groups were placed in calculated positions and refined as riding on the atoms to which they were bonded.

2-iodo-4-methylaniline 3,5-dinitrobenzoic acid (28)

3,5-dinitrobenzoic acid molecule: The anisotropic displacement parameters for the non-hydrogen atoms were allowed to refine freely. The aromatic hydrogen atoms of the 3,5-DNBA molecule were placed in calculated positions and refined as riding on the atoms to which they were bonded. The hydrogen atom of the carboxylic acid group was located using Fourier difference maps and the position refined using a distance restraint (0.9 Å); the U_{iso} of the H-atom was constrained to $1.5U_{eq}$ of the O-atom to which it was bonded.

2-iodo-4-methylaniline molecule: The 2-I-4-MA molecule is disordered over two possible positions which were identified in a Fourier difference map. The two molecular sites were allowed to refine freely against each other, giving occupancies of 0.595(2):0.405(2). With the exception of the I atoms, the non-hydrogen atoms were refined only isotropically. In order to ensure chemically sensible bond lengths and angles were obtained, the benzene rings of the disordered molecules were constrained to take a standard geometry in each case using an AFIX 66 command. Due to the overlapping regions of electron density, the isotropic displacement parameters for the carbon atoms in each ring and the methyl carbon atom (C8A-C14A, C8B-C14B) were constrained to take the same values using the EADP command; relaxation of this constraint resulted in unreasonable displacement parameters for these atoms. The C8A-I1A and C8B-I1B distances were restrained to take a standard length (2.1 Å) using a distance restraint; the N3A-C9A and N3B-C9B distances were also restrained to take a standard length (1.4 Å) using a distance restraint. SADI restraints were applied to ensure the C-C-C angles for the methyl substituents were chemically sensible; the C14A-C11A distance was constrained to be similar to the C14A-C13A distance, and the C14B-C11B distance was constrained to be similar to the C14B-C13B distance. Aromatic hydrogen atoms, the hydrogen atoms of the NH_2 groups, and the methyl group hydrogen atoms were placed in calculated positions and refined as riding on the atoms to which they were bonded.

2-bromo-4-methylaniline 3,5-dinitrobenzoic acid (29)

3,5-dinitrobenzoic acid molecule: The anisotropic displacement parameters for the non-hydrogen atoms were allowed to refine freely. The aromatic hydrogen atoms of the 3,5-DNBA molecule were placed in calculated positions and refined as riding on the atoms to which they were bonded. The hydrogen atom of the carboxylic acid group was located using Fourier difference maps and the position refined using a distance restraint (0.9 Å); the U_{iso} of the H-atom was constrained to $1.5U_{eq}$ of the O-atom to which it was bonded.

2-bromo-4-methylaniline molecule: The 2-Br-4-MA molecule is disordered over two possible positions which were identified in a Fourier difference map. The two molecular sites were allowed to refine freely against each other, giving occupancies of 0.661(2):0.339(2). With the exception of the Br and N atoms, the non-hydrogen atoms were refined only isotropically. In order to ensure chemically sensible bond lengths and angles were obtained, the benzene rings of the disordered molecules were constrained to take a standard geometry in each case using an AFIX 66 command. Due to the overlapping regions of electron density, the isotropic displacement parameters for the carbon atoms in each ring and the methyl carbon atom (C8A-C14A, C8B-C14B) were constrained to take the same values using the EADP command; relaxation of this constraint resulted in unreasonable displacement parameters for these atoms. The anisotropic displacement parameters of N3A and N3B were also constrained to take the

same values using the EADP command. Aromatic hydrogen atoms, the hydrogen atoms of the NH_2 groups, and the methyl group hydrogen atoms were placed in calculated positions and refined as riding on the atoms to which they were bonded.

2-chloro-4-methylaniline 3,5-dinitrobenzoic acid (30)

All non-hydrogen atoms were refined anisotropically. Aromatic hydrogen atoms were placed in calculated positions and refined as riding on the atoms to which they were bonded. The hydrogen atoms of the NH_3^+ group of 2-Cl-4-MA were identified using Fourier difference maps, and the positions allowed to freely refine; the U_{iso} of the H-atoms were constrained to $1.5U_{eq}$ of the N-atom to which they are bound. The methyl group H-atoms were located initially using Fourier difference maps and the bond distances and angles constrained to take standard values; the U_{iso} of the H-atoms were constrained to $1.5U_{eq}$ of the C-atom to which they are bound.

4-iodoaniline 4-iodoanilinium 3,5-dinitrosalicylic acid (1:2:2) (31)

3,5-dinitrosalicylate molecule: The anisotropic displacement parameters for the non-hydrogen atoms were allowed to refine freely. The aromatic hydrogen atoms were placed in calculated positions and refined as riding on the atoms to which they were bonded. The hydrogen atom of the carboxylic acid group was located using Fourier difference maps and the position allowed to freely refine; the U_{iso} of the H-atom was constrained to $1.5U_{eq}$ of the O-atom to which it was bonded.

4-iodoanilinium molecule: The anisotropic displacement parameters for the non-hydrogen atoms were allowed to refine freely. The aromatic hydrogen atoms were placed in calculated positions and refined as riding on the atoms to which they were bonded. The hydrogen atoms of the NH_3^+ group of 2-Cl-4-MA were identified using Fourier difference maps, and the positions allowed to freely refine; the U_{iso} of the H-atoms were constrained to $1.5U_{eq}$ of the N-atom to which they are bound.

4-iodoaniline molecule: The neutral 4-IA molecule is 50:50 disordered over an inversion centre; the molecule is half-occupied in the asymmetric unit so the site occupancy factors for the atoms of this molecule were set to 0.5. All non-hydrogen atoms were refined anisotropically. In order to ensure chemically sensible bond lengths and angles were obtained, the benzene rings of the disordered molecules were constrained to take a standard geometry in each case using an AFIX 66 command. Due to the overlapping regions of electron density, the anisotropic displacement parameters for the carbon atoms in the ring (C14-C19) were constrained to take the same values using the EADP command; relaxation of this constraint resulted in unreasonable displacement parameters for these atoms. The two positions for the 4IA molecule are displaced such that the I and N positions are very close and a series of constraints and restraints had to be applied. The EADP command was used to constrain the anisotropic

displacement parameters of N4 and I2 to be the same due to the close proximity of the two positions. SADI restraints were applied to ensure the C-C-I/N angles were chemically sensible. The C17-I2 bond length was restrained to be similar to the ordered C11-I1 bond length; the C14-N4 bond length was restrained to be similar to the ordered C8-N3 bond length. The C-CI and C-C-N bond angles on either side of the iodine/amine groups were restrained to be similar i.e. the C16-I2 distance should be the same as the C18-I2 distance and the C15-N4 distance should be the same as the C19-N4 distance. All H-atoms were placed in calculated positions and refined as riding on the atoms to which they were bonded.

4-bromoaniline 4-bromoanilinium 3,5-dinitrosalicylic acid (1:2:2) (32)

3,5-dinitrosalicylate molecule: The anisotropic displacement parameters for the non-hydrogen atoms were allowed to refine freely. The aromatic hydrogen atoms were placed in calculated positions and refined as riding on the atoms to which they were bonded. The hydrogen atom of the carboxylic acid group was located using Fourier difference maps and the position allowed to freely refine; the U_{iso} of the H-atom was constrained to $1.5U_{eq}$ of the O-atom to which it was bonded.

4-bromoanilinium molecule: The anisotropic displacement parameters for the non-hydrogen atoms were allowed to refine freely. The aromatic hydrogen atoms were placed in calculated positions and refined as riding on the atoms to which they were bonded. The hydrogen atoms of the NH_3^+ group of 4-BrA were identified using Fourier difference maps, and the positions allowed to freely refine; the U_{iso} of the H-atoms were constrained to $1.5U_{eq}$ of the N-atom to which they are bound.

4-bromoaniline molecule: The neutral 4-BrA molecule is 50:50 disordered over an inversion centre; the molecule is half-occupied in the asymmetric unit so the site occupancy factors for the atoms of this molecule were set to 0.5. All non-hydrogen atoms were refined anisotropically. In order to ensure chemically sensible bond lengths and angles were obtained, the benzene rings of the disordered molecules were constrained to take a standard geometry in each case using an AFIX 66 command. Due to the overlapping regions of electron density, the anisotropic displacement parameters for the carbon atoms in the ring (C14-C19) were constrained to take the same values using the EADP command; relaxation of this constraint resulted in unreasonable displacement parameters for these atoms. All H-atoms were placed in calculated positions and refined as riding on the atoms to which they were bonded.

4-iodoaniline 3,5-dinitrosalicylic acid (1:1) (33)

All non-hydrogen atoms were refined anisotropically. Aromatic hydrogen atoms were placed in calculated positions and refined as riding on the atoms to which they were bonded. The hydrogen atoms of the NH_3^+ group and hydroxyl group were located using Fourier difference

maps; their positions were allowed to freely refine, but the U_{iso} of the H-atoms were constrained to $1.5U_{eq}$ of the N- or O-atom to which they were bonded.

4-bromoaniline 3,5-dinitrosalicylic acid (1:1) (34)

All non-hydrogen atoms were refined anisotropically. Aromatic hydrogen atoms were placed in calculated positions and refined as riding on the atoms to which they were bonded. The hydrogen atoms of the NH_3^+ group and hydroxyl group were located using Fourier difference maps; their positions were allowed to freely refine, but the U_{iso} of the H-atoms were constrained to $1.5U_{eq}$ of the N- or O-atom to which they were bonded.

3-bromoaniline 3,5-dinitrobenzoic acid (35)

All non-hydrogen atoms were refined anisotropically. Aromatic hydrogen atoms were placed in calculated positions and refined as riding on the atoms to which they were bonded. The hydrogen atoms of the NH_2 and NH_3^+ groups and were located using Fourier difference maps; their positions were allowed to freely refine, but the U_{iso} of the H-atoms were constrained to $1.5U_{eq}$ of the N-atom to which they were bonded. The hydrogen atom of the carboxylic acid group was located using Fourier difference maps and the position refined using a distance restraint (0.9 Å); the U_{iso} of the H-atom was constrained to $1.5U_{eq}$ of the O-atom to which it is bonded.

4-bromo-2-iodoaniline 3,4-dinitrobenzoic acid (36)

All non-hydrogen atoms were refined anisotropically. Aromatic hydrogen atoms were placed in calculated positions and refined as riding on the atoms to which they were bonded. The hydrogen atoms of the NH_2 group were located using Fourier difference maps and allowed to freely refine. The hydrogen atom of the carboxylic acid group was located using Fourier difference maps and the position refined using a distance restraint (0.9 Å); the U_{iso} of the H-atom was constrained to $1.5U_{eq}$ of the O-atom to which it is bonded.

4-bromo-2-iodoaniline 3,5-dinitrobenzoic acid (37)

All non-hydrogen atoms were refined anisotropically. Aromatic hydrogen atoms were placed in calculated positions and refined as riding on the atoms to which they were bonded. The hydrogen atoms of the NH_2 and carboxylic acid groups were located using Fourier difference maps; their positions were allowed to freely refine, but the U_{iso} of the H-atoms were constrained to $1.5U_{eq}$ of the N- or O-atom to which they were bonded.

Appendix A7 (Chapter 7)

A7-1 Crystal structure refinement details

Note: all crystal structures were refined using SHELXL-2014.

2-iodoanilinium 2,4-dinitrobenzoate (38)

All non-hydrogen atoms were refined anisotropically. Aromatic hydrogen atoms were placed in calculated positions and refined as riding on the atoms to which they were bonded. The hydrogen atoms of the NH_3^+ group were located using Fourier difference maps and allowed to freely refine.

2-bromoanilinium 2,4-dinitrobenzoate (39)

All non-hydrogen atoms were refined anisotropically. Aromatic hydrogen atoms were placed in calculated positions and refined as riding on the atoms to which they were bonded. The hydrogen atoms of the NH_3^+ group were located using Fourier difference maps and allowed to freely refine.

2-chloroanilinium 2,4-dinitrobenzoate (40)

All non-hydrogen atoms were refined anisotropically. Aromatic hydrogen atoms were placed in calculated positions and refined as riding on the atoms to which they were bonded. The hydrogen atoms of the NH_3^+ group were located using Fourier difference maps and allowed to freely refine.

3-iodoanilinium 2,4-dinitrobenzoate (41)

All non-hydrogen atoms were refined anisotropically. Aromatic hydrogen atoms were placed in calculated positions and refined as riding on the atoms to which they were bonded. The hydrogen atoms of the NH_3^+ group were located using Fourier difference maps and allowed to freely refine.

3-bromoanilinium 2,4-dinitrobenzoate (42)

All non-hydrogen atoms were refined anisotropically. Aromatic hydrogen atoms were placed in calculated positions and refined as riding on the atoms to which they were bonded. The hydrogen atoms of the NH_3^+ group were located using Fourier difference maps and allowed to freely refine.

4-iodoanilinium 2,4-dinitrobenzoate (43)

All non-hydrogen atoms were refined anisotropically. Aromatic hydrogen atoms were placed in calculated positions and refined as riding on the atoms to which they were bonded. The amine group H-atoms were located initially using Fourier difference maps and the bond distances and angles constrained to take standard values; the U_{iso} of the H-atoms was constrained to $1.5U_{eq}$ of the C-atom to which they are bonded.

4-bromoanilinium 2,4-dinitrobenzoate (44)

All non-hydrogen atoms were refined anisotropically. Aromatic hydrogen atoms were placed in calculated positions and refined as riding on the atoms to which they were bonded. The hydrogen atoms of the NH_3^+ group were located using Fourier difference maps and allowed to freely refine.

4-iodo-2-methylanilinium 2,4-dinitrobenzoate (45)

All non-hydrogen atoms were refined anisotropically. Aromatic hydrogen atoms were placed in calculated positions and refined as riding on the atoms to which they were bonded. The hydrogen atoms of the NH_3^+ group were located using Fourier difference maps and allowed to freely refine. The methyl group H-atoms were located initially using Fourier difference maps and the bond distances and angles constrained to take standard values; the U_{iso} of the H-atoms was constrained to $1.5U_{eq}$ of the C-atom to which they are bonded.

3-iodoanilinium 2,5-dinitrobenzoate (46)

All non-hydrogen atoms were refined anisotropically. Aromatic hydrogen atoms were placed in calculated positions and refined as riding on the atoms to which they were bonded. The hydrogen atoms of the NH_3^+ group were located using Fourier difference maps and allowed to freely refine.

4-iodoanilinium 2,5-dinitrobenzoate (47)

All non-hydrogen atoms were refined anisotropically. Aromatic hydrogen atoms were placed in calculated positions and refined as riding on the atoms to which they were bonded. The hydrogen atoms of the NH_3^+ group were located using Fourier difference maps and allowed to freely refine.

2-iodoanilinium 3,5-dinitrosalicylate (48)

2-iodoanilinium cation: The 2-IA molecule is disordered over two possible positions which were identified in a Fourier difference map. The two molecular sites were allowed to refine freely against each other, giving occupancies of 0.69(1):0.31(1). With the exception of the

I-atoms, the non-hydrogen atoms were refined only isotropically. In order to ensure chemically sensible bond lengths and angles were obtained, the benzene rings of the disordered molecules were constrained to take a standard geometry in each case using an AFIX 66 command. All atoms were refined isotropically. Due to the overlapping regions of electron density, the isotropic displacement parameters for corresponding pairs of carbon atoms were constrained to take the same values using the EADP command, as were the N and I-atoms; relaxation of this constraint resulted in unreasonable isotropic displacement parameters for these atoms. The C8A-N3A and C8B-N3B distances were restrained to take a standard length (1.4 Å) using a distance restraint. Aromatic hydrogen atoms and the hydrogen atoms of the NH_3^+ groups were placed in calculated positions and refined as riding on the atoms to which they were bonded.

3,5-dinitrosalicylate anion: All non-hydrogen atoms were refined anisotropically. Aromatic hydrogen atoms were placed in calculated positions and refined as riding on the atoms to which they were bonded. The hydrogen atom of the carboxylic acid group was located using Fourier difference maps and the position allowed to freely refine; the U_{iso} of the H-atom was constrained to $1.5U_{eq}$ of the O-atom to which it was bonded.

2-bromoanilinium 3,5-dinitrosalicylate (49)

All non-hydrogen atoms were refined anisotropically. Aromatic hydrogen atoms were placed in calculated positions and refined as riding on the atoms to which they were bonded. The hydrogen atoms of the NH_3^+ group were located using Fourier difference maps and allowed to freely refine. The hydrogen atom of the carboxylic acid group was located using Fourier difference maps and the position allowed to freely refine; the U_{iso} of the H-atom was constrained to $1.5U_{eq}$ of the O-atom to which it was bonded.

2-chloroanilinium 3,5-dinitrosalicylate (50)

All non-hydrogen atoms were refined anisotropically. Aromatic hydrogen atoms were placed in calculated positions and refined as riding on the atoms to which they were bonded. The hydrogen atoms of the NH_3^+ group were located using Fourier difference maps and allowed to freely refine. The hydrogen atom of the carboxylic acid group was located using Fourier difference maps and the position allowed to freely refine; the U_{iso} of the H-atom was constrained to $1.5U_{eq}$ of the O-atom to which it was bonded.

3-iodoanilinium 3,5-dinitrosalicylate (51)

All non-hydrogen atoms were refined anisotropically. Aromatic hydrogen atoms were placed in calculated positions and refined as riding on the atoms to which they were bonded. The hydrogen atoms of the NH_3^+ group and carboxylic acid group were located using Fourier difference maps and allowed to freely refine.

3-bromoanilinium 3,5-dinitrosalicylate (52)

All non-hydrogen atoms were refined anisotropically. Aromatic hydrogen atoms were placed in calculated positions and refined as riding on the atoms to which they were bonded. The hydrogen atoms of the NH_3^+ group and carboxylic acid group were located using Fourier difference maps and allowed to freely refine.

4-bromo-3-methylanilinium 3,5-dinitrosalicylate (53)

4-bromo-3-methylanilinium cation: All non-hydrogen atoms were refined anisotropically. The methyl group of the 4-Br-3-MA molecule has two possible positions which were identified in a Fourier difference map, *meta* to the amine group (bound to C9 and C13). The two sites were allowed to refine freely against each other, giving 0.518(6):0.482(6) occupancies. Aromatic hydrogen atoms were placed in calculated positions and refined as riding on the atoms to which they were bonded. The hydrogen atoms of the NH_3^+ group were located using Fourier difference maps and their positions allowed to freely refine; the U_{iso} of the H-atoms was constrained to $1.5U_{eq}$ of the N-atom to which they are bonded. The methyl group H-atoms were located initially using Fourier difference maps and the bond distances and angles constrained to take standard values; the U_{iso} of the H-atoms was constrained to $1.5U_{eq}$ of the C-atom to which they are bonded.

3,5-dinitrosalicylate anion: All non-hydrogen atoms were refined anisotropically. Aromatic hydrogen atoms were placed in calculated positions and refined as riding on the atoms to which they were bonded. The hydrogen atom of the carboxylic acid group was located using Fourier difference maps and the position allowed to freely refine; the U_{iso} of the H-atom was constrained to $1.5U_{eq}$ of the O-atom to which it was bonded.

4-iodoanilinium 2-nitrobenzoate (54)

All non-hydrogen atoms were refined anisotropically. Aromatic hydrogen atoms were placed in calculated positions and refined as riding on the atoms to which they were bonded. The hydrogen atoms of the NH_3^+ group were located using Fourier difference maps and allowed to freely refine.